TURNING UP THE HEAT:
ROLE OF BROWN ADIPOSE TISSUE IN METABOLIC DISEASE

MARIËTTE BOON

Turning up the heat:
Role of brown adipose tissue in metabolic disease
Cover design & Layout: Mirjam de Bruin
Printing: Gildeprint Drukkerijen, Enschede
ISBN: 978-94-6108-682-2

Turning up the heat:
Role of brown adipose tissue in metabolic disease

Proefschrift

ter verkrijging van
de graad van Doctor aan de Universiteit Leiden,
op gezag van Rector Magnificus prof. mr. C.J.J.M. Stolker,
volgens besluit van het College van Promoties
te verdediging op donderdag 12 juni 2014
klokke 12.30 uur

door

Mariëtte Rebecca Boon

geboren te Alkmaar
in 1988

PROMOTIECOMMISSIE

Promotor Prof. dr. P.C.N. Rensen

Copromotor Dr. I.M. Jazet

Overige leden Prof. dr. ir. L.M. Havekes
Prof. dr. J.W. Jukema
Prof. dr. M. Yazdanbakhsh
Prof. dr. W. van Marken Lichtenbelt (MUMC, Maastricht)
Prof. dr. J. Heeren (University of Hamburg, Hamburg)

The work described in this thesis was performed at the department of Endocrinology and Metabolic Diseases at the Leiden University Medical Center, Leiden, the Netherlands, and at the Einthoven Laboratory for Experimental Vascular Medicine, Leiden, the Netherlands.

Mariëtte Boon was supported by the Board of Directors of the LUMC and the Dutch Diabetes Research Foundation (grant 2012.11.1500).

The printing of this thesis was kindly supported by Sanofi, Novo Nordisk B.V. and TSE systems.

TABLE OF CONTENTS

PART 1	**General introduction and outline**	9
CHAPTER 1	Physiological aspects of brown adipose tissue	11
CHAPTER 2	Involvement of brown adipose tissue in metabolic disease	23
CHAPTER 3	South Asians: a population with a disadvantageous metabolic phenotype	37
	Outline	49
PART 2	**Animal studies on role of brown adipose tissue in metabolism and obesity**	51
CHAPTER 4	Brown adipose tissue internalizes fatty acids by selective delipidation of lipoproteins rather than by uptake of lipoproteins	53
CHAPTER 5	BMP7 activates brown adipose tissue and reduces diet-induced obesity only at subthermoneutrality	69
CHAPTER 6	Metformin lowers plasma triglycerides by promoting VLDL-triglyceride clearance by brown adipose tissue	95
CHAPTER 7	Cannabinoid receptor 1 blockade diminishes dyslipidemia via peripheral activation of brown adipose tissue	123
CHAPTER 8	Inhibition of the central melanocortin system decreases brown adipose tissue activity	149
CHAPTER 9	Central role for brown adipose tissue in dyslipidemia and atherosclerosis development	167
PART 3	**Human studies on role of brown adipose tissue in metabolism and obesity**	189
CHAPTER 10	Short-term high-fat diet increases macrophage markers in skeletal muscle accompanied by impaired insulin signaling in healthy male subjects	191
CHAPTER 11	E-selectin is elevated in cord blood of South Asian compared to Caucasian neonates	209
CHAPTER 12	South Asians exhibit disturbed HDL functionality as compared to white Caucasians	221
CHAPTER 13	Brown adipose tissue volume is markedly lower in healthy lean adolescents from South Asian compared to white Caucasian origin	239
CHAPTER 14	Supraclavicular skin temperature as a measure of ^{18}F-fluorodeoxyglucose uptake by brown adipose tissue in human subjects	257
PART 4	**General discussion, summary and curriculum vitae**	273
CHAPTER 15	General discussion and future perspectives	275
CHAPTER 16	Summary en Nederlandse samenvatting	297
	List of publications	309
	Curriculum vitae	313

PART 1

GENERAL INTRODUCTION AND OUTLINE

PHYSIOLOGICAL ASPECTS OF BROWN ADIPOSE TISSUE

MARIËTTE R. BOON
LEONTINE E.H. BAKKER
WOUTER D. VAN MARKEN LICHTENBELT
GEERTJE VAN DER HORST
GABRI VAN DER PLUIJM
JOUKE T. TAMSMA
JOHANNES W.A. SMIT
A.EDO MEINDERS
INGRID M. JAZET
PATRICK C.N. RENSEN

MODIFIED FROM:

Bruin vet: een lichaamseigen mechanisme in de strijd tegen obesitas? Ned Tijdschr Geneeskd. 2013; 157: A5502.

Bone Morphogenetic Protein-7: a broad-spectrum agent with therapeutic potential in obesity. Cytokine & Growth Factor Reviews 2011; 22: 221-9.

1

ANATOMY AND ORIGIN OF BROWN ADIPOSE TISSUE

In 1551, the Swiss naturalist Konrad Gessner first described brown adipose tissue (BAT) as being "neither fat, nor flesh *(nec pinguitudo, nec caro),* but something in between" (1,2). Now, some 460 years later, we know that Gessner had guessed the origin of brown adipocytes correctly – they are not typical fat-storing cells or flesh (muscle cells), but rather have characteristics of both white adipocytes and muscle cells, as well as several characteristics unique to brown fat cells.

Brown and white adipocytes form separate tissues that are histologically and functionally distinct **(TABLE 1)**, although both cell types are sometimes found intermingled (3). While the amount of white adipose tissue (WAT) is roughly 20% of total body weight, adult humans are estimated to have only 100-200 grams of BAT. Furthermore, a white adipocyte contains a large vacuole filled with triglycerides (TG), which is fully compatible with its function to store lipids, surrounded by a thin layer of cytoplasm. The cytoplasm contains the nucleus and cell organelles, including a few mitochondria that mediate the formation of ATP, the main energy supplier of cells. In contrast, a brown adipocyte contains several small lipid droplets that are surrounded by a large number of mitochondria that mediate its energy-combusting function in the cytoplasm (see below). The iron-containing proteins in mitochondria, which are part of the respiratory chain, give BAT its brownish color.

Brown adipocytes are present in (at least) two forms. They may form brown fat pads, which are located in neonates in the subscapular area and in adults along the aorta and in the supraclavicular region (4). In addition, individual brown adipocytes are also found scattered within other tissues, such as WAT and muscle, there forming a pool of 'peripheral

TABLE 1 - Comparison between white and brown adipose tissue

	White adipose tissue	Brown adipose tissue
Microscopic image	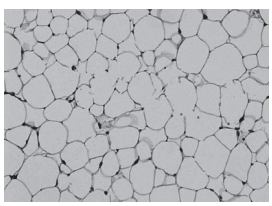	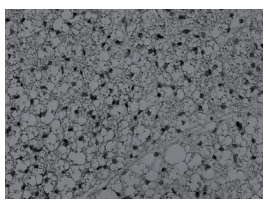
Amount in body	Approx. 12 - 35 kg	Approx. 100 - 200 g
Morphology	Cells filled with a large lipid droplet Low number of mitochondria	Cells filled with multiple small lipid droplets High number of mitochondria
Location	Throughout the whole body	In specific fat pads mainly located between the shoulders and along the great vessels; groups of cells within white adipose tissue and muscle
Function	Storage of fat	Combustion of fat toward heat

brown adipocytes' (5,6). These cells are also called 'beige adipocytes', since their phenotype lies between white and brown adipocytes. The two types of brown adipocytes have different origins **(FIGURE 1)**.

Brown adipocytes present in the brown fat pads derive from Myf5$^+$ precursor cells; these precursor cells can differentiate into both brown adipocytes and skeletal muscle cells, depending on the presence of stimuli such as bone morphogenetic protein 7 (BMP7) (5,7,8). Thus, the brown adipocytes in fat pads and muscle cells share a common precursor cell and, therefore, brown adipocytes are much more 'flesh-like' than previously suspected (3).

The existence of peripheral brown adipocytes (or beige adipocytes) was initially discovered in the WAT depot from animals that were chronically exposed to cold, resulting in a

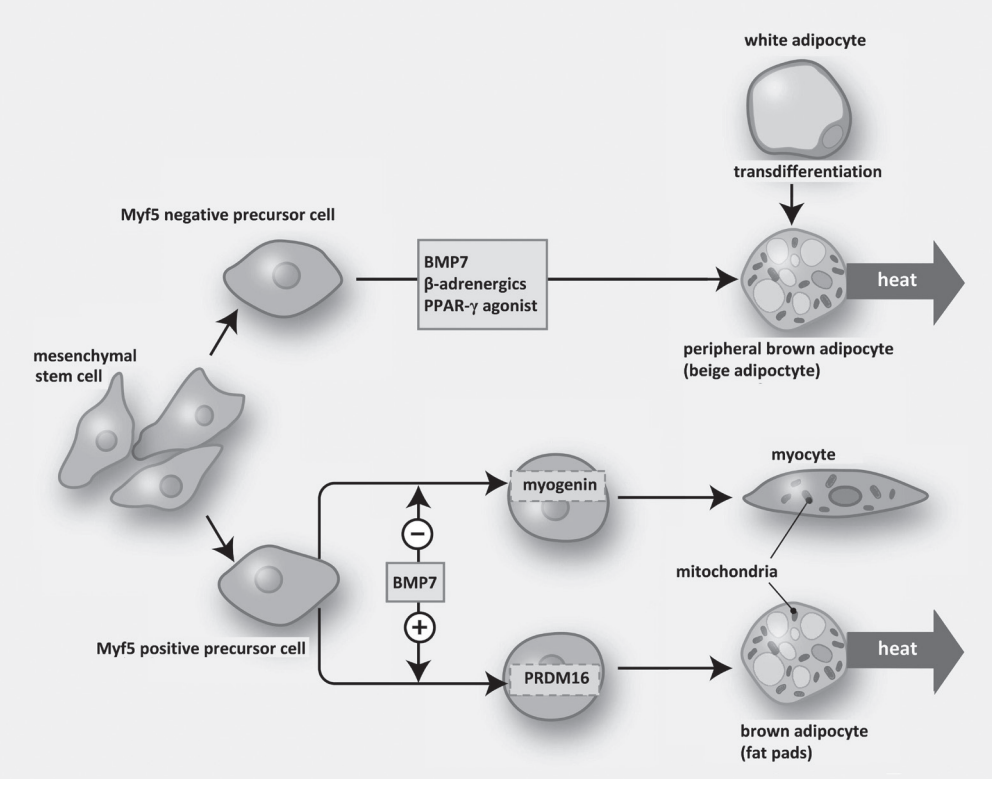

FIGURE 1 - Differentiation of mesenchymal stem cells towards brown adipocytes. Myf5-positive precursor cells can differentiate towards muscle cells or brown adipocytes, depending on the presence of BMP7. Muscle cells express myogenin, and brown adipocytes PRDM16. This type of brown adipocyte is present in fat pads. Myf5-negative precursor cells differentiate toward peripheral brown adipocytes ('beige adipocytes') under influence of, amongst other factors, BMP7, cold stimulation (= ß-adrenergic stimulation) and PPAR-γ agonists. Myf5, myogenic factor 5; BMP7, bone morphogenetic protein-7; PRDM16, PR domain containing 16; PPAR-γ, peroxisome proliferator-activated receptor-γ.

Adapted from: Boon et al, NTvG 2013 (14).

shift in color from white to brownish (9). The precise origin of these peripheral brown adipocytes is currently a topic of intensive study. Cell fate tracking studies have shown that peripheral brown adipocytes that emerge in WAT in response to cold exposure do not express Myf5, and are therefore Myf5$^-$ precursor cells (5). More specifically, in both WAT and muscle, a subpopulation of Myf5$^-$ precursor cells called the Sca1$^+$ adipose progenitors have been identified that are capable of differentiating into peripheral brown adipocytes (10). It is likely that also other, yet to be discovered, types of precursor cells are present in WAT and muscle that can give rise to peripheral brown adipocytes. In addition, peripheral brown adipocytes may arise from transdifferentiation of white adipocytes (11).

Several factors can stimulate the differentiation of Myf5$^+$ precursor cells in the brown fat pads into brown adipocytes (e.g. BMP7), as well as the differentiation of Myf5$^-$ precursor cells into peripheral brown adipocytes (e.g. BMP7, cold induction, and peroxisome proliferator-activated receptor-γ (PPARγ)-agonists) (8,10-13). These stimuli are, therefore, considered interesting therapeutic targets to activate BAT by enhancing its differentiation.

HEAT PRODUCTION BY BROWN ADIPOSE TISSUE

While the main function of WAT is the storage of energy in the form of TG, BAT burns TG-derived fatty acids (FA) toward heat. This results from the process of 'uncoupling', in which energy is released as heat instead of being used for generation of ATP, leading to increased energy expenditure. A detailed description of the physiology of the brown adipocyte is explained below and shown in **FIGURE 2** (14).

Each brown adipocyte is individually innervated by a sympathetic nerve (15,16). The most well-known stimulus resulting in activation of BAT by the sympathetic nervous system is cold. All sensory input on temperature is coordinated in the temperature center within the preoptic chiasma/anterior hypothalamic nuclei of the brain, located in front of the third ventricle (17). This area receives input from sensory nerve fibers in the skin. Upon stimulation, the sympathetic nerve locally releases noradrenalin, which binds to adrenergic receptors on the brown adipocyte. Activation of these receptors results in a fast induction of intracellular lipolysis, induced by activation of adipose triglyceride lipase (ATGL) and hormone sensitive lipase (HSL) through phosphorylation, resulting in release of FA from TG-filled lipid droplets. FA are directed to the mitochondria where they either allosterically activate uncoupling protein 1 (UCP1) present in the inner membrane of the mitochondrion or can undergo oxidation. In addition, adrenergic stimulation enhances transcription and synthesis of UCP1 to enhance the total mitochondrial content of UCP1 (3). Of note, while it has been irrefutably proven that in rodents, the ß3-adrenergic receptor is the main receptor by which BAT is sympathetically activated (3), the dominant adrenergic receptor in humans (i.e., α or ß) remains to be identified (see **CHAPTER 2)**.

The synthesis of ATP that is required as energy source in tissues such as the heart and skeletal muscle, e.g. to mediate muscle contraction, starts with the conversion of FA, and to

a lesser extent glucose, into acetyl coenzyme A that participates in the citric acid cycle in the mitochondrion. The cytric acid cycle generates energy-rich complexes, such as NADH and $FADH_2$, which donate their electrons during oxidative phosphorylation to the electron transport chain, thereby creating a gradient of H^+-ions from the matrix toward the inner membrane space across the inner mitochondrial membrane. The energy stored in this gradient is then used by the enzyme ATP synthase to convert ADP into energy-rich ATP, while protons are transported back into the mitochondrial matrix. However, brown/beige adipocytes express UCP1 that forms pores in the inner mitochondrial membrane causing leakage of protons back to the matrix. Therefore, the energy created by the proton gradient is not used

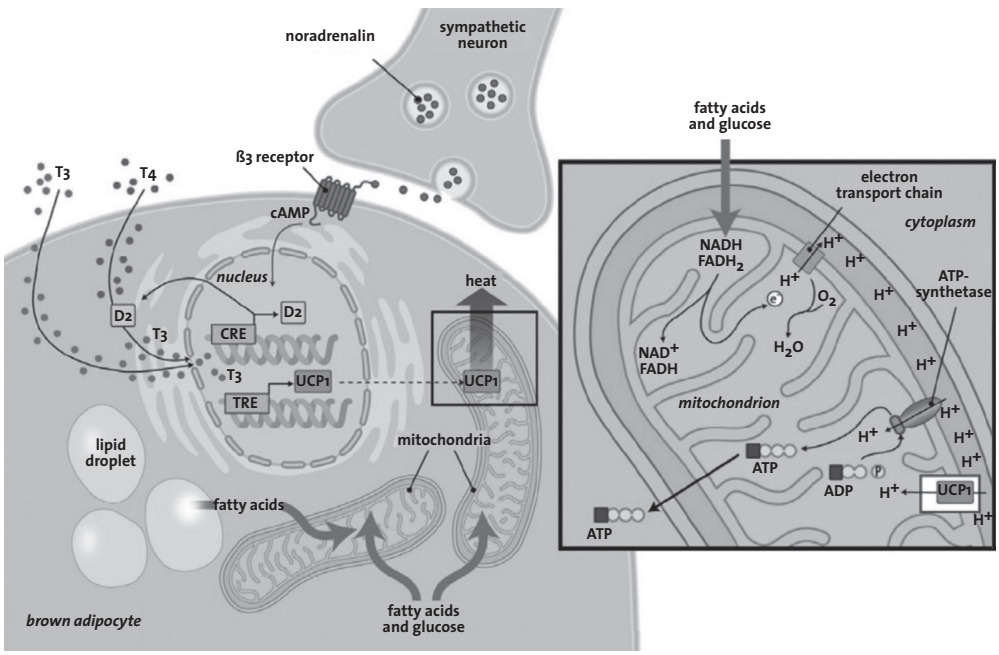

FIGURE 2 - Activation of brown adipose tissue. In the resting state, the energy-rich complexes NADH and FADH2 that are generated from the citric acid cycle in the mitochondrial matrix during combustion of glucose and fatty acids, release their energy in the form of electrons to the electron transport chain in the inner membrane of the mitochondrion. This results in build-up of an H^+-gradient across the inner membrane (see right panel). In cell types such as myocytes, the energy of this H^+-gradient is used by the enzyme ATP synthase to convert ADP into ATP. However, in the mitochondria of brown adipocytes UCP-1 proteins are present in the inner membrane that uncouple the H^+-gradient from ATP synthesis. This occurs when a sympathetic neuron activates the brown adipocyte by secretion of noradrenalin, which binds to adrenergic receptors on the brown adipocyte membrane (see left figure). This results in formation of cAMP and eventually activation and synthesis of UCP-1. Leakage of H^+ across the inner membrane via UCP-1 results in production of heat instead of ATP. The synthesis of UCP-1 is also stimulated by the active thyroid hormone T3. cAMP, cyclic AMP; UCP-1, uncoupling protein-1; T3, tri-iodothyronine; T4, thyroxine; D2, type 2 deiodinase.
Adapted from: Boon et al, NTvG 2013 (14).

for generation of ATP, but rather dissipates as heat, a process called 'nonshivering thermogenesis' (3,18). The greater the density of mitochondria (or the amount or activity of UCP-1) in BAT, the more FA will be burnt and released as heat when BAT is activated. Of note, FA derived from intracellular TG stores (rather than those directly taken up from the plasma) are the main activators of UCP1 and substrates for mitochondrial uncoupling, as thermogenesis is defective in mice that lack ATGL (19), indicating that FA taken up by brown adipocytes are not directly used for combustion. Therefore, maintenance of intracellular TG stores is essential for BAT non-shivering thermogenesis.

Accordingly, after intracellular lipolysis, the intracellular TG stores of the brown adipocyte need to be replenished. This is mediated via three mechanisms: 1) uptake of glucose followed by de *novo* lipogenesis, 2) uptake of albumin-bound free FA, and 3) uptake of TG-derived FA from very-low-density lipoproteins and chylomicrons in the plasma (3,20,21). While uptake of glucose by the brown adipocyte is mediated by the glucose transporters GLUT-1 and GLUT-4, uptake of FA is mainly mediated by the FA transporter CD36. Of note, a previous study of Bartelt et al (20) suggested that, upon cold exposure, BAT takes up TG-derived FA from chylomicron-sized (~250 nm) lipoprotein-like particles via whole particle uptake. However, this is in contrast to TG-derived FA uptake by WAT and muscle and is not in line with the increased expression of LPL and CD36 that occurs upon cold exposure in BAT. Thus, whether the uptake of chylomicron-derived FA by BAT truly occurs via whole particle uptake and by which mechanism VLDL-derived FA are taken up, remains to be investigated.

In addition to cold, thyroid hormone is also involved in the activation of BAT. After uptake of T3 and T4 by the brown adipocyte and intracellular conversion of T4 into T3 by the enzyme type-2-deiodinase (D2), the active thyroid hormone T3 is translocated into the nucleus and binds to a thyroid hormone responsive element located on the promoter of the UCP1 gene (22). This leads to increased transcription of UCP1 and consequently to increased conversion of energy into heat. Furthermore, T3 is able to stabilize the UCP1 mRNA, thereby reducing its degradation in the cell (3). During cold-induction, the activity of D2 is increased in BAT, leading to locally increased amounts of T3. This is an additional and necessary mechanism to stimulate thermogenesis by BAT (23).

PRESENCE OF FUNCTIONAL BROWN ADIPOSE TISSUE IN ADULT HUMANS

In mammals, the primary function of BAT thus is the production of heat to prevent a decrease in core body temperature. Production of heat by active BAT during cold exposure is called 'non-shivering thermogenesis' (NST), which is distinct from 'shivering thermogenesis' resulting from skeletal muscle contractions. In neonates, NST is particularly important, since they have a relatively large body surface area and little capacity to shiver due to underdevelopment of their muscles (3). Although BAT remains present in large quantities in rodents and other mammals, in humans the amount of BAT declines fast after infancy.

Although in adult humans skeletal muscle contributes largely to heat production, BAT is still present. Already in 1981, Huttunen et al (24) demonstrated in a post-mortem study that adults who lived in cold environments had significant amounts of BAT, suggesting a role for NST in humans under cold circumstances. However, it was only in the last decade that BAT has been shown to be functionally active in human adults. This was the direct consequence of the evolvement of new imaging techniques, particularly the ^{18}F-fluorodeoxyglucose (^{18}F-FDG) positron emission tomography-computed tomography (PET-CT) scan. ^{18}F-FDG is an analogue of glucose that is taken up by metabolically active tissues without being metabolized. Accordingly, ^{18}F-FDG PET-CT scans are widely used as a diagnostic tool in the field of oncology to visualize tumors, as they take up high amounts of FDG. Interestingly, it was frequently observed that FDG uptake occurred at sites other than tumor tissue and the brain, specifically in anatomical areas that were described earlier to contain BAT (24,25). FDG uptake in regions corresponding to BAT occurred especially in patients feeling cold at the timing of FDG administration and warming of patients prior to scanning or administration

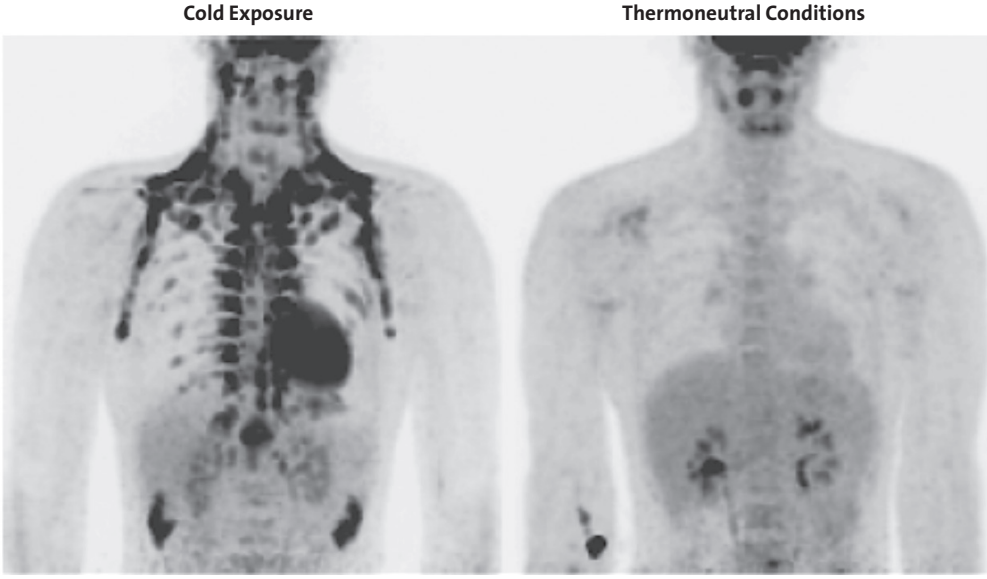

FIGURE 3 - ^{18}F-fluorodeoxyglucose (FDG)-PET-CT scan visualizing brown adipose tissue in adult humans after exposure to cold and under thermoneutral conditions. Brown adipose tissue (BAT) can be visualized by use of an FDG-PET-CT scan. To this end, the subject (left) is exposed to cold (16°C) for 2 hours in order to activate BAT. After 1 hour of cold induction, the radioactive tracer ^{18}F-FDG is injected intravenously. ^{18}F-FDG, a glucose-analog, is taken up by organs which have a high glucose metabolism, especially the brain, heart and BAT. After 2 hours of cold induction, the uptake of ^{18}F-FDG is visualized by means of a low-dose-CT-scan, immediately followed by a PET-scan. The CT-scan is used for localization of the uptake areas. The activity and volume of the BAT are quantified by autocontouring the areas of FDG uptake, by use of a previously set threshold. The right figure shows FDG uptake after 2 hours of exposure to thermoneutral temperature (22°C).
Images were reproduced from van Marken Lichtenbelt et al. (29), with permission.

of the ß blocker propranolol prevented the uptake in those areas (26,27). The presence of active BAT in adult humans was confirmed in 2009, when the FDG-positive areas in the BAT regions were shown to histologically resemble murine BAT and furthermore express high levels of UCP1, the bona fide marker of BAT (28-30).

Currently, the cold-induced ^{18}F-FDG PET-CT scan is the 'gold standard' for determination of BAT volume and BAT activity in human subjects. Exposing subjects to a cold environment before FDG administration is of crucial importance, as under thermoneutral conditions generally no FDG uptake by BAT can be seen due to lack of sympathetic stimulation of BAT (29) **(FIGURE 3)**. Thus, to visualize BAT, subjects are usually cooled for approximately 2 hours at a temperature just above their shivering temperature, followed by infusion of ^{18}F-FDG and performance of the PET-CT scan (29-32). The method of cooling differs between research institutes and may either consist of water (e.g. water-perfused mattresses) or air cooling (e.g. air-climated room). Furthermore, the environmental temperature may remain fixed (approximately 15-17°C) or a personalized cooling protocol may be used in which every subject is cooled slightly above his/her own shivering temperature. At the moment, no consensus consists as to which cooling protocol is superior since they all have their pros and cons. However, that cooling is crucial for proper BAT visualization is no matter of debate. Of note, research by Van Marken Lichtenbelt and others with ^{18}F-FDG PET-CT scans showed that, after cold induction, BAT is present in nearly 100% of young adults (29).

A recent topic of debate is on how 'brown' human BAT actually is. Distinction between classical brown and beige adipocytes cannot be simply made on the basis of an FDG PET-CT scan, as both types of brown adipocytes take up high amounts of glucose when stimulated (33). Recent genotyping of human BAT biopsies, obtained from the supraclavicular area from subjects who showed FDG uptake in this area, demonstrated that human BAT more closely resembles the beige fat found in WAT depots in mice rather than the classical murine BAT (6). Therefore, a former vision was that human BAT solely consists of 'beige' adipocytes. A recent study by Cypess et al (34) refuted this vision. Different depots of neck adipose tissue were isolated from adult human volunteers and gene expression, differentiation capacity and basal oxygen consumption were compared to different mouse adipose depots. Although the variation in the properties of human neck adipose tissue was substantial between subjects, they showed that some human samples have many similarities with the classical BAT found in rodents. Intriguingly, it appeared that the unstimulated energy expenditure of the human BAT samples is similar to that of mouse interscapular BAT, underscoring the energy-combusting potential of this adipose tissue in humans.

REFERENCES

1 Cannon B, Nedergaard J. Developmental biology: Neither fat nor flesh. Nature 2008; 454: 947-948.
2 Gesner C, Rondelet G, Belon P, et al. Historiae Animalium; De Quadrupedibus viuiparis; Liber Primus 1620; Editio secunda: 744.
3 Cannon B, Nedergaard J. Brown adipose tissue: function and physiological significance. Physiol Rev 2004; 84: 277-359.
4 van Marken Lichtenbelt WD, Vanhommerig JW, Smulders NM, et al. Cold-activated brown adipose tissue in healthy men. N Engl J Med 2009; 360: 1500-1508.
5 Seale P, Bjork B, Yang W, et al. PRDM16 controls a brown fat/skeletal muscle switch. Nature 2008; 454: 961-967.
6 Wu J, Bostrom P, Sparks LM, et al. Beige adipocytes are a distinct type of thermogenic fat cell in mouse and human. Cell 2012; 150: 366-376.
7 Kajimura S, Seale P, Kubota K, et al. Initiation of myoblast to brown fat switch by a PRDM16-C/EBP-beta transcriptional complex. Nature 2009; 460: 1154-1158.
8 Tseng YH, Kokkotou E, Schulz TJ, et al. New role of bone morphogenetic protein 7 in brown adipogenesis and energy expenditure. Nature 2008; 454: 1000-1004.
9 Cousin B, Cinti S, Morroni M, et al. Occurrence of brown adipocytes in rat white adipose tissue: molecular and morphological characterization. J Cell Sci 1992; 103: 931-942.
10 Schulz TJ, Huang TL, Tran TT, et al. Identification of inducible brown adipocyte progenitors residing in skeletal muscle and white fat. Proc Natl Acad Sci U S A 2011; 108: 143-148.
11 Barbatelli G, Murano I, Madsen L, et al. The emergence of cold-induced brown adipocytes in mouse white fat depots is determined predominantly by white to brown adipocyte transdifferentiation. Am J Physiol Endocrinol Metab 2010; 298: E1244-E1253.
12 Ohno H, Shinoda K, Spiegelman BM, et al. PPARgamma agonists induce a white-to-brown fat conversion through stabilization of PRDM16 protein. Cell Metab 2012; 15: 395-404.
13 Qiang L, Wang L, Kon N, et al. Brown remodeling of white adipose tissue by SirT1-dependent deacetylation of Ppargamma. Cell 2012; 150: 620-632
14 Boon MR, Bakker LE, Meinders AE, et al. Bruin vet: een lichaamseigen middel in de strijd tegen obesitas? Ned Tijdschr Geneeskd 2013; 157: A5502.
15 Norman D, Mukherjee S, Symons D, et al. Neuropeptides in interscapular and perirenal brown adipose tissue in the rat: a plurality of innervation. J Neurocytol 1988; 17: 305-311.
16 Watanabe J, Mishiro K, Amatsu T, et al. Absence of paravascular nerve projection and cross-innervation in interscapular brown adipose tissues of mice. J Auton Nerv Syst 1994; 49: 269-276.
17 Boulant JA. Role of the preoptic-anterior hypothalamus in thermoregulation and fever. Clin Infect Dis 2000; 31 Suppl 5: S157-S161.
18 Heaton GM, Wagenvoord RJ, Kemp A, et al. Brown-adipose-tissue mitochondria: photoaffinity labelling of the regulatory site of energy dissipation. Eur J Biochem 1978; 82: 515-521.
19 Zimmermann R, Strauss JG, Haemmerle G, et al. Fat mobilization in adipose tissue is promoted by adipose triglyceride lipase. Science 2004; 306: 1383-1386.
20 Bartelt A, Bruns OT, Reimer R, et al. Brown adipose tissue activity controls triglyceride clearance. Nat Med 2011; 17: 200-205.
21 Festuccia WT, Blanchard PG, Deshaies Y. Control of Brown Adipose Tissue Glucose and Lipid Metabolism by PPARgamma. Front Endocrinol (Lausanne) 2011; 2: 84.
22 Rabelo R, Reyes C, Schifman A, et al. Interactions among receptors, thyroid hormone response elements, and ligands in the regulation of the rat uncoupling protein gene expression by thyroid hormone. Endocrinology 1996; 137: 3478-3487.
23 de Jesus AR, Magalhaes A, Miranda DG, et al. Association of type 2 cytokines with hepatic fibrosis in human Schistosoma mansoni infection. Infect Immun 2004; 72: 3391-3397.

24 Huttunen P, Hirvonen J, Kinnula V. The occurrence of brown adipose tissue in outdoor workers. Eur J Appl Physiol Occup Physiol 1981; 46: 339-345.

25 Garcia CA, Van ND, Majd M, et al. Benzodiazepine-resistant "brown fat" pattern in positron emission tomography: two case reports of resolution with temperature control. Mol Imaging Biol 2004; 6: 368-372.

26 Garcia CA, Van ND, Atkins F, et al. Reduction of brown fat 2-deoxy-2-[F-18]fluoro-D-glucose uptake by controlling environmental temperature prior to positron emission tomography scan. Mol Imaging Biol 2006; 8: 24-29.

27 Jacobsson H, Bruzelius M, Larsson SA. Reduction of FDG uptake in brown adipose tissue by propranolol. Eur J Nucl Med Mol Imaging 2005; 32: 1130.

28 Cypess AM, Lehman S, Williams G, et al. Identification and importance of brown adipose tissue in adult humans. N Engl J Med 2009; 360: 1509-1517.

29 van Marken Lichtenbelt WD, Vanhommerig JW, Smulders NM, et al. Cold-activated brown adipose tissue in healthy men. N Engl J Med 2009; 360: 1500-1508.

30 Virtanen KA, Lidell ME, Orava J, et al. Functional brown adipose tissue in healthy adults. N Engl J Med 2009; 360: 1518-1525.

31 Vijgen GH, Bouvy ND, Teule GJ, et al. Brown adipose tissue in morbidly obese subjects. PLoS One 2001; 6: e17247.

32 Vosselman MJ, Brans B, van der Lans AA, et al. Brown adipose tissue activity after a high-calorie meal in humans. Am J Clin Nutr 2013; 98: 57-64.

33 Bartelt A, Heeren J. Adipose tissue browning and metabolic health. Nat Rev Endocrinol 2013, *in press.*

34 Cypess AM, White AP, Vernochet C, et al. Anatomical localization, gene expression profiling and functional characterization of adult human neck brown fat. Nat Med 2013; 19: 635-639.

INVOLVEMENT OF BROWN ADIPOSE TISSUE IN METABOLIC DISEASE

MARIËTTE R. BOON
LEONTINE E.H. BAKKER
JANINE J. GEERLING
SANDER KOOIJMAN
EDWIN T. PARLEVLIET
LOUIS M. HAVEKES
JOHANNES A. ROMIJN
ILLIANA M. MEURS
WOUTER D. VAN MARKEN LICHTENBELT
A. EDO MEINDERS
INGRID M. JAZET
PATRICK C.N. RENSEN

MODIFIED FROM:

Bruin vet: een lichaamseigen mechanisme in de strijd tegen obesitas? Ned Tijdschr Geneeskd. 2013; 157: A5502.

Sympathetic nervous system control of triglyceride metabolism: physiology and novel therapeutic insights. J Lipid Res 2014; 55: 180-9.

2

METABOLISM OF TRIGLYCERIDE-RICH LIPOPROTEINS

Triglycerides (TG) and cholesterol, the most common lipids in our diet, are essential for the human body by serving various functions. TG, esters composed of a glycerol backbone and three fatty acids, are the main source of energy in the body: TG-derived fatty acids (FA) can be combusted in the heart and skeletal muscle to generate adenosine triphosphate (ATP), and in brown adipose tissue (BAT) to generate heat. In case of a positive energy balance, FA are stored as TG in white adipose tissue (WAT), which can subsequently be lipolyzed and combusted elsewhere toward ATP in times of need. Cholesterol does not provide energy but rather is an essential constituent of cell membranes as well as the precursor for the synthesis of bile acids and steroid hormones.

Since lipids are hydrophobic and thus not soluble in blood, they are transported in so-called lipoproteins. A lipoprotein consists of a lipid-rich core containing TG and esterified cholesterol (i.e., cholesteryl esters), surrounded by a shell composed of phospholipids and unesterified cholesterol. In the shell, various apolipoproteins are embedded that can function as building blocks for the synthesis of lipoproteins within cells including enterocytes and hepatocytes, and in plasma as cofactors and modulators of enzyme activity, (phospho)lipid transfer factors, and receptor ligands. Apolipoproteins thus regulate the intracellular synthesis of lipoproteins, their metabolism in the circulation and their uptake by peripheral tissues. Lipoproteins can be divided in different classes based on their density, namely (from lowest to highest density) chylomicrons, very low density lipoproteins (VLDL), intermediate density lipoprotein (IDL), low density lipoprotein (LDL) and high density lipoprotein (HDL). The lipoproteins in these classes not only differ in their density, but also in size, and have a different combination of apolipoproteins embedded in their shell, mediating different functions.

In the blood, cholesterol is primarily transported within the cholesterol-rich lipoproteins LDL and HDL. In contrast, dietary and endogenously derived TG are carried in chylomicrons and VLDL, which are therefore called TG-rich lipoproteins (TRLs) (1). After a meal, dietary TG and cholesterol are taken up by enterocytes the intestine, assembled into chylomicrons and subsequently released via the lymph into the circulation. During fasting, the liver ensures a supply of TG to peripheral tissues by secretion of TG-rich VLDL particles, which are assembled by hepatocytes from exogenous lipids derived from chylomicrons or endogenous lipids derived from de novo lipogenesis (2). Once chylomicrons and VLDL arrive in the circulation, lipoprotein lipase (LPL) that is present on the capillary beds of adipose tissue and muscle hydrolyzes TG into glycerol and free fatty acids (FFA). The liberated FFA can subsequently be taken up by white adipocytes to be stored as TG or by muscle cells and brown adipocytes to be combusted towards ATP and heat, respectively (3,4). Cellular uptake of FFA is mediated by various cell surface receptors, including FA transport proteins (FATP) and CD36 (5). During lipolysis, the TRL becomes enriched with the apolipoprotein apoE. The TRL remnant is either rapidly cleared by the liver via binding of apoE to mainly the LDL receptor or LDL-related protein (LRP) (6), or is further hydrolyzed to generate LDL. Therefore, there is a continuous flux of FA from the intestine and liver *(i.e.* TG production) towards organs for storage (i.e.,

liver and WAT) or combustion (i.e., liver, muscle and BAT), followed by clearance of cholesterol-enriched TRL remnants by the liver and subsequent re-initiation of this cycle **(FIGURE 1)** (7). In addition, lipolysis of intracellular TG in WAT, *e.g.* under conditions of fasting, contributes to a flux of FA from WAT to liver *(e.g.* for VLDL-TG synthesis), muscle and BAT *(i.e.* combustion).

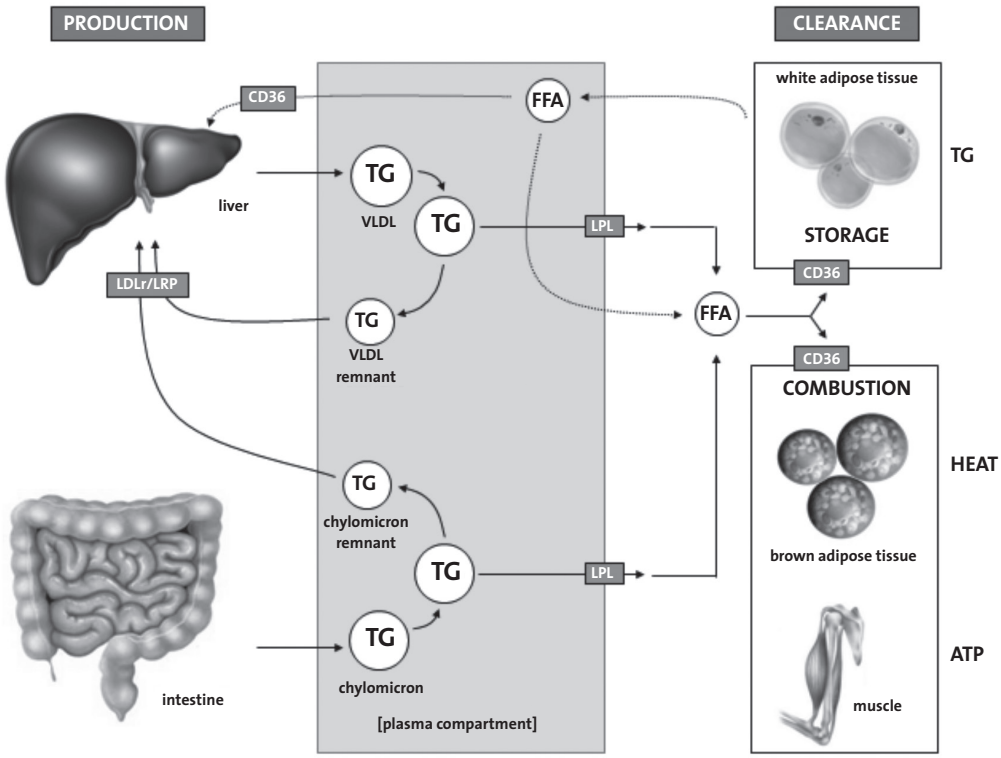

FIGURE 1 - Schematic representation of TG-rich lipoprotein metabolism. Following a meal, dietary triglycerides (TG) and cholesterol are taken up by the intestine and assembled within chylomicrons, which are released in the circulation. The liver assembles endogenous lipids to form very low-density lipoproteins (VLDL), the predominant carrier of circulating TG under low food supply. TG from both types of TG-rich lipoproteins are rapidly hydrolyzed into glycerol and free fatty acids (FFA) by lipoprotein lipase (LPL), present on the capillary bed, resulting in formation of chylomicron remnants and VLDL remnants. These remnants are rapidly cleared by the liver mainly via the LDL receptor (LDLr) or LDL related protein (LRP). FFA can be taken up by peripheral organs via cellular FA transporters such as CD36 and subsequently be stored by white adipose tissue or combusted by brown adipose tissue and muscle. Finally, TG stores within the white adipose tissue can be lipolyzed and released in the bloodstream as FFA, which can subsequently be transported to the liver to be assembled into new VLDL-TG particles, or be combusted by the brown adipose tissue and muscle.
Adapted from: Boon and Geerling et al., 2013 (7).

INVOLVEMENT OF BAT IN TG METABOLISM

As briefly mentioned in **CHAPTER 1,** BAT may contribute to clearance of plasma FA by two mechanisms; uptake of albumin-bound FA as well as uptake of FA derived from TG within from VLDL and chylomicrons, the latter likely being dependent on the presence of endothelium-bound LPL in BAT (8). The magnitude of the TG clearance capacity of BAT became clear only recently when Bartelt et al (8) demonstrated that mice that are housed at 4°C for 24 hours, a major trigger for BAT activation, show a massive lowering of plasma TG levels. Furthermore, BAT activation by means of cold exposure is able to correct hyperlipidemia in hyperlipidemic ApoA5 knockout mice (8). In contrast, animals in which BAT is surgically denervated become rapidly obese and hypertriglyceridemic (9). These findings underscore the involvement of BAT in total energy expenditure and TG clearance, at least in mice.

Also in humans, BAT likely substantially contributes to TG metabolism. In a recent study by Ouellet et al (10), human subjects were cooled for 2 hours followed by infusion of the FA tracer ^{18}F-fluoro-thiaheptadecanoic acid (^{18}F-FTHA) and performance of a PET-CT scan. Indeed, cold exposure resulted in enhanced FA uptake by BAT as compared to muscle and WAT. It is likely that human BAT also utilizes FA from circulating lipoproteins, though this has not been investigated yet. Furthermore, 2 hours of cold exposure results in a rapid increase in BAT CT radio density, suggestive of lowering of intracellular TG stores in BAT. Indeed, as mentioned in **CHAPTER 1,** intracellular TG are the main fuel for BAT thermogenesis in animal models (11). In room temperature-acclimated rats, short-term acute cold exposure leads to a massive depletion of intracellular lipid droplets in BAT (12). A similar depletion of intracellular lipid in BAT was found at necropsy in newborn infants and adults who died from hypothermia (13). Thus, a fast initial combustion of intracellular TG upon acute BAT activation may well explain why short-term cold exposure does not result in acute lowering of plasma TG in human subjects (10). Likely, prolonged BAT activation will result in lowering of plasma TG levels in human subjects as a consequence of increased clearance from the plasma towards BAT.

INVOLVEMENT OF BAT IN NON-SHIVERING THERMOGENESIS

When mammals are exposed to a cold environment, various physiological responses occur in order to maintain core body temperature. First, blood perfusion will be redirected. This is marked by peripheral vasoconstriction and consequently less blood flow towards the skin and other distally located tissues in order to retain the heat in the core, a response called 'insulation' (14,15). Furthermore, thermogenesis will be enhanced so that additional heat is produced (15,16). This cold-induced thermogenesis can globally be divided into two components, 'shivering thermogenesis' (e.g. heat production due to muscle contractions) and 'non-shivering thermogenesis' (NST) (15). In rodents, NST occurs in BAT as a consequence of uncoupling of ATP synthesis by UCP1, as described in **CHAPTER 1,** and results in increased

resting energy expenditure (REE) (4). Of note, UCP1 knockout mice that lack the capacity to produce heat by NST rely on shivering thermogenesis in the cold (17).

In adult humans, short-term well-controlled cold exposure may enhance REE by as much as 30% (10,18-21). Since shivering does not occur in these cooling protocols (see **CHAPTER 1)**, the increase in REE is likely due to increased uncoupling by BAT. Indeed, cold acclimation increases NST, BAT volume and activity but not uncoupling in muscle in human subjects, supporting the vision that muscle is likely not involved in NST in humans (22).

Interestingly, REE correlates with BAT activity in several studies (22,23) and lean subjects with BAT activity have significantly higher levels of NST than those that do not show BAT activity (24). Lastly, using PET with ^{11}C-acetate, cold-induced oxidative metabolism in BAT in human subjects has been demonstrated, confirming the contribution of BAT in NST in humans (10).

INVOLVEMENT OF BAT IN PATHOLOGY

Pheochromocytomas

Pheochromocytomas are neuroendocrine tumors that secrete excessive amounts of noradrenalin, an important activator of BAT. Indeed, on ^{18}F-FDG-PET-CT-scans in patients with this tumor, an increased mass and activity of BAT is seen, accompanied by increased energy expenditure (25,26). Moreover, after resection of the tumor FDG uptake as well as energy expenditure decrease dramatically (27), supporting that the increased energy expenditure typical for this condition is likely due to increased BAT-mediated NST. Furthermore, pheochromocytoma patients exhibit increased browning of visceral WAT (28), which may also contribute to the enhanced energy expenditure. Whether this browning is due to increased transdifferentiation of white into brown adipocytes or differentiation of brown preadipocytes present in the visceral WAT towards mature brown adipocytes (see **CHAPTER 1)** remains to be determined.

Hyperthyroidism/hypothyroidism

Mouse studies have shown that thyroid hormone may activate BAT both directly (via the T3 receptor in BAT) and indirectly (via the sympathetic nervous system) (29,30). Interestingly, energy expenditure is increased in patients with hyperthyroidism and decreased in patients with hypothyroidism. A recent study showed that hyperthyroidism in human patients increases glucose uptake in BAT independently of BAT perfusion (31). Therefore, the weight loss and excessive transpiration in hyperthyroidism, and the weight gain and reduced cold tolerance in hypothyroidism, can at least be partly attributed to an increased and decreased activity of BAT, respectively.

Obesity, dyslipidemia and type 2 diabetes

When energy intake exceeds energy expenditure (i.e. positive energy balance), TG is stored in WAT. In addition, TG may be stored ectopically in organs such as skeletal muscle and liver, resulting in malfunction of these organs. A prolonged positive energy balance may result in development of overweight and obesity. Currently, over 50% of the Dutch population is overweight (25 < BMI < 30 kg/m^2) and more than 10% is already obese (BMI > 30 kg/m^2) (32). Obesity is strongly associated with development of other disorders and diseases, such as dyslipidemia, type 2 diabetes, cardiovascular disease and cancer (33).

Interestingly, recent studies point towards a role of disturbed BAT function in development of obesity and related disorders. In human adults, the amount of BAT is inversely correlated with BMI and percentage of body fat (23). More specifically, BAT volume is inversely correlated with parameters of central obesity, such as visceral fat volume on CT-scan and waist circumference (34). These findings suggest that obesity is associated with a low level of BAT activity. Indeed, excision of BAT or sympathetic denervation of BAT in mice results in hypertriglyceridemia and obesity (9). Thus, in humans, a reduced activity of BAT may predispose to obesity and obesity-related diseases such as dyslipidemia and type 2 diabetes by accumulation of TG in the blood and subsequent storage in WAT as well as in ectopic fat depots such as skeletal muscle and the liver. This is associated with reduced insulin sensitivity of these organs and eventually type 2 diabetes. Furthermore, since BAT is also involved in clearance of plasma glucose *(i.e.* for *de novo* lipogenesis, see **CHAPTER 1)** (35), BAT could also contribute to glucose homeostasis, particularly in resting conditions when glucose utilization by skeletal muscle is minimal. A low activity of BAT might thus not only predispose to T2DM via the above described relation to obesity, but also via reduced glucose uptake at rest (36). However, the lower BAT activity found in overweight and obese human subjects may also at least in part be a consequence of their increased subcutaneous white fat layer, which may substantially contribute to the maintenance of body temperature, making active BAT redundant (37).

MANIPULATING ACTIVITY AND VOLUME OF BAT

The incidence of obesity is rapidly increasing, resulting in concomitantly enhanced morbidity and mortality. Therefore, novel therapeutic as well as preventive strategies are highly warranted. Current strategies to combat obesity are mostly aimed at targeting the energy intake side of the energy balance (e.g. caloric restriction), but these have not proven to be effective on the long term (38). Thus, identifying methods to increase activity of resident BAT or to induce growth of new BAT is of particular interest, since this will result in increased REE and consequently lowering of plasma TG and glucose levels as well as weight loss. Theoretically, BAT volume and activity can be increased in different ways. Generally, a distinction is made between methods that activate already present brown adipocytes, and methods that stimulate the recruitment of new BAT.

1 Stimulation of existing BAT

Stimulation of sympathetic nervous system

BAT is strongly innervated by the sympathetic nervous system (see **CHAPTER 1, FIGURE 2)** (4). The main activator of this pathway is cold. Several studies have shown a relation between the volume and activity of BAT and the outdoor temperature, with the highest activity during the coldest month of the year (39). Therefore, the simplest method to activate BAT is cold induction, for instance via creating a colder living and/or working environment. Indeed, a recent study by Van der Lans et al (22) showed that cold acclimation of healthy adult humans for 10 days results in increased BAT activity and volume, accompanied by increased NST. Whether this will result in weight loss and lowering of plasma TG and glucose in obese human subjects remains to be determined.

In addition to indirect activation of adrenergic receptors by cold, sympathicomimetics could also be used. In mouse models, activating the ß3 adrenergic receptor was very successful with respect to inducing weight loss (40). Unfortunately, no weight loss was observed in humans treated with a ß3 adrenergic receptor agonist (41,42). However, a recent study suggests that the α1 or α2 adrenergic receptor may be of superior importance in humans (Sondergaard et al., unpublished). Therefore, novel studies should focus on further identification and targeting of the relevant receptors for clinical purposes.

Furthermore, sympathetic outflow towards BAT may be manipulated by targeting brain regions that control these sympathetic outflow neurons. The major brain region involved in the regulation of sympathetic outflow towards BAT is the hypothalamus (4). Lowering of hypothalamic AMP-activated protein kinase (AMPK), a cellular energy sensor, has been shown to enhance sympathetic outflow towards BAT (43). Interestingly, nicotine, the main constituent of cigarette smoke, lowers hypothalamic AMPK activation and enhances BAT activation and energy expenditure in mice (44). This may well explain why cessation of smoking results in weight gain in human subjects (45). Future studies should thus be directed at identifying novel compounds that may activate BAT via lowering of hypothalamic AMPK.

Stimulation of non-adrenergic receptors in BAT

Next to adrenergic receptors, a variety of other receptor types are present in BAT. As mentioned, the T3 receptor is highly expressed within the nucleus of the brown adipocyte and activation of this receptor markedly enhances BAT activation (29). In addition, the bone morphogenetic protein (BMP) receptor is well expressed on brown adipocytes and *in vitro* treatment of brown adipocytes with BMP7 results in massive activation, at least in part via the intracellular p38 mitogen-activated protein (MAP) kinase pathway (46). Of note, the cardiac natriuretic peptides ANP and BNP have been shown to activate BAT via the same intracellular mechanism, resulting in massively enhanced energy expenditure, and this effect was mediated via the NP clearance receptor in BAT (47). Our current knowledge on the receptor types present in BAT and their functions is far from complete. Therefore, future studies may reveal new receptors that could provide novel therapeutic handles to activate BAT.

Stimulation of AMP-activated protein kinase in BAT

One strategy to identify novel mechanisms for BAT activation is to study compounds that are already in clinical use and result in lowering of body weight and plasma TG levels. These compounds may, at least in part, exert their effects via activation of BAT. For instance, metformin is one of the most widely used glucose-lowering agents for the treatment of type 2 diabetes and is now considered as the first-line drug therapy for patients (48,49). Besides its glucose-lowering effect, metformin also markedly reduces plasma TG levels (50), the mechanism of which is currently unknown. In addition, metformin is among the few anti-diabetic drugs that does not result in weight gain, but even evokes a mild decrease in body weight. Interestingly, metformin is a well-known activator of the cellular energy sensor AMP-activated protein kinase (AMPK) in various tissues (51) and recent studies point towards a role for AMPK in BAT differentiation, and likely also activation, as it stimulates mitochondrial biogenesis and UCP-1 activation (52). Future studies should unravel whether the TG-lowering effect of metformin is indeed mediated by BAT activation and whether the mechanism involves activation of intracellular AMPK in BAT.

Furthermore, the cannabinoid 1 receptor (CB1R) inverse agonist rimonabant has been shown to result in long-term maintained weight loss and reduction of dyslipidemia in obese patients (53-56). Rimonabant was considered one of the most promising therapeutic drugs to treat obesity, until the appearance of central psychiatric side effects resulted in its removal from the market in 2008. Nevertheless, several lines of evidence indicate that the effect of CB1R blockade is not restricted to a central mode of action, especially since the CB1R has been shown to be present in several peripheral tissues including the liver (57), skeletal muscle (58) and white adipocytes (59). Interestingly, treatment of rodents with rimonabant resulted in enhanced thermogenesis and energy expenditure (60), suggesting a role for BAT in the beneficial effects of CB1R blockade. Furthermore, in liver and white adipose tissue, CB1R blockade activated intracellular AMPK (61,62). Thus, BAT may be involved in the beneficial effects of rimonabant on obesity and dyslipidemia and this is possibly mediated by activation of intracellular AMPK.

2 Recruitment of new BAT

Stimulating differentiation

Irisin is a recently discovered hormone that, at least in mice, is secreted by skeletal muscle during exercise. Of note, exogenous administration of irisin in mice was able to induce 'browning' of subcutaneous WAT. This resulted in an increase in energy expenditure, a lowering in body weight and an improvement in glucose tolerance (63). Therefore, irisin was regarded a novel and promising anti-obesity hormone that acted via recruitment of peripheral, beige adipocytes. However, a recent study provided evidence against a possible beneficial effect of irisin in humans (64). FNDC5, the gene encoding the precursor of irisin, shows a mutation in humans resulting in only 1% of the full-length protein. Thus, the beneficial effect of irisin in mice can likely not be translated to humans and the search for other compounds that may enhance recruitment of BAT is highly warranted.

One of the key regulators in the differentiation of adipocytes is PPARγ. Animal studies have shown that PPARγ agonists can recruit precursor cells of BAT and, in addition, can induce browning of white adipocytes, thereby obtaining UCP-1 (65). PPARγ agonists are already used in the treatment of T2DM: the thiazolinediones (TZDs). Research has shown that the improvement in insulin sensitivity with TZDs is partly caused by an accelerated clearance of glucose by BAT (66). Remarkably, though, use of TZDs leads to weight gain (partly due to fluid retention) and a different (disadvantageous) fat distribution, making their use as a weight loss agent less likely. Moreover, prescription of these agents is limited due to side effects such as heart failure and osteoporotic fractures (67,68).

In addition, as mentioned in **CHAPTER 1,** BMP7 is a potent inducer of BAT growth both *in vitro* and *in vivo,* resulting in enhanced energy expenditure and prevention of weight gain (46). The importance of BMP7 in BAT development appeared from BMP7 knock-out mice, which exhibit marked BAT paucity (46). Of note, BMP7 plays a pivotal role not only in the differentiation of BAT, but also in the development of bone (69,70), cartilage (71) and kidney (72). As such, BMP7 may be used in the treatment of several other pathological conditions besides obesity, such as incomplete fracture healing, osteoarthritis and renal fibrosis (73). Although the role of BMP7 in recruitment of brown adipocytes in the brown fat pads has been well-established, the precise mechanism by which BMP7 exerts this effect (i.e., direct effect or involvement of sympathetic activation by the hypothalamus) and the efficiency of BMP7 to recruit beige adipocytes *in vivo* are currently unknown and elucidation of the mechanism may provide interesting directions for future studies.

REFERENCES

1 Williams KJ. Molecular processes that handle -- and mishandle -- dietary lipids. J Clin Invest 2008; 118: 3247-3259.

2 Tessari P, Coracina A, Cosma A, et al. Hepatic lipid metabolism and non-alcoholic fatty liver disease. Nutr Metab Cardiovasc Dis 2009; 19: 291-302.

3 Bonora M, Patergnani S, Rimessi A, et al. ATP synthesis and storage. Purinergic Signal 2012; 8: 343-357.

4 Cannon B, Nedergaard J. Brown adipose tissue: function and physiological significance. Physiol Rev 2004; 84: 277-359.

5 Glatz JF, Luiken JJ, Bonen A. Membrane fatty acid transporters as regulators of lipid metabolism: implications for metabolic disease. Physiol Rev 2010; 90: 367-417.

6 Heeren J, Niemeier A, Merkel M, et al. Endothelial-derived lipoprotein lipase is bound to postprandial triglyceride-rich lipoproteins and mediates their hepatic clearance in vivo. J Mol Med (Berl) 2002; 80: 576-584.

7 Geerling JJ, Boon MR, Kooijman S, et al. Sympathetic nervous system control of triglyceride metabolism: novel concepts derived from recent studies. J Lipid Res 2013, *in press*.

8 Bartelt A, Bruns OT, Reimer R, et al.Brown adipose tissue activity controls triglyceride clearance. Nat Med 2011; 17: 200-205.

9 Dulloo AG, Miller DS. Energy balance following sympathetic denervation of brown adipose tissue. Can J Physiol Pharmacol 1984; 62: 235-240.

10 Ouellet V, Labbe SM, Blondin DP, et al. Brown adipose tissue oxidative metabolism contributes to energy expenditure during acute cold exposure in humans. J Clin Invest 2012; 122: 545-552.

11 Festuccia WT, Blanchard PG, Deshaies Y. Control of Brown Adipose Tissue Glucose and Lipid Metabolism by PPARgamma. Front Endocrinol (Lausanne) 2011; 2: 84.

12 Baba S, Jacene HA, Engles JM, et al. CT Hounsfield units of brown adipose tissue increase with activation: preclinical and clinical studies. J Nucl Med 2010; 51: 246-250.

13 Aherne W, Hull D. Brown adipose tissue and heat production in the newborn infant. J Pathol Bacteriol 1966; 91: 223-234.

14 Charkoudian N. Skin blood flow in adult human thermoregulation: how it works, when it does not, and why. Mayo Clin Proc 2003; 78: 603-612.

15 van Marken Lichtenbelt WD, Schrauwen P. Implications of nonshivering thermogenesis for energy balance regulation in humans. Am J Physiol Regul Integr Comp Physiol 2011; 301: R285-R296.

16 Davis TR. Chamber cold acclimatization in man. J Appl Physiol 1961; 16: 1011-1015.

17 Feldmann HM, Golozoubova V, Cannon B, et al. UCP1 ablation induces obesity and abolishes diet-induced thermogenesis in mice exempt from thermal stress by living at thermoneutrality. Cell Metab 2009; 9: 203-209.

18 Celi FS, Brychta RJ, Linderman JD, et al. Minimal changes in environmental temperature result in a significant increase in energy expenditure and changes in the hormonal homeostasis in healthy adults. Eur J Endocrinol 2010; 163: 863-872.

19 Claessens-van Ooijen AM, Westerterp KR, Wouters L, et al. Heat production and body temperature during cooling and rewarming in overweight and lean men. Obesity (Silver Spring) 2006; 14: 1914-1920.

20 Warwick PM, Busby R. Influence of mild cold on 24 h energy expenditure in 'normally' clothed adults. Br J Nutr 1990; 63: 481-488.

21 Wijers SL, Saris WH, van Marken Lichtenbelt WD. Cold-induced adaptive thermogenesis in lean and obese. Obesity (Silver Spring) 2010; 18: 1092-1099.

22 van der Lans AA, Hoeks J, Brans B, et al. Cold acclimation recruits human brown fat and increases nonshivering thermogenesis. J Clin Invest 2013; 123: 3395-3403.

23 van Marken Lichtenbelt WD, Vanhommerig JW, Smulders NM, et al. Cold-activated brown adipose tissue in healthy men. N Engl J Med 2009; 360: 1500-1508.

24 Yoneshiro T, Aita S, Matsushita M, et al. Brown adipose tissue, whole-body energy expenditure, and thermogenesis in healthy adult men. Obesity (Silver Spring) 2011; 19: 13-16.

25 Dong A, Wang Y, Lu J, et al. Hypermetabolic Mesenteric Brown Adipose Tissue on Dual-Time Point FDG PET/CT in a Patient With Benign Retroperitoneal Pheochromocytoma. Clin Nucl Med 2013, *in press*

26 Petrak O, Haluzikova D, Kavalkova P, et al. Changes in energy metabolism in pheochromocytoma. J Clin Endocrinol Metab 2013; 98: 1651-1658.

27 Kuji I, Imabayashi E, Minagawa A, et al. Brown adipose tissue demonstrating intense FDG uptake in a patient with mediastinal pheochromocytoma. Ann Nucl Med 2008; 22: 231-235.

28 Frontini A, Vitali A, Perugini J, et al. White-to-brown transdifferentiation of omental adipocytes in patients affected by pheochromocytoma. Biochim Biophys Acta 2013; 1831: 950-959.

29 Branco M, Ribeiro M, Negrao N, et al. 3,5,3'-Triiodothyronine actively stimulates UCP in brown fat under minimal sympathetic activity. Am J Physiol 1999; 276: E179-E187.

30 Lopez M, Varela L, Vazquez MJ, et al. Hypothalamic AMPK and fatty acid metabolism mediate thyroid regulation of energy balance. Nat Med 2010; 16: 1001-1008.

31 Lahesmaa M, Orava J, Schalin-Jantti C, et al. Hyperthyroidism increases brown fat metabolism in humans. J Clin Endocrinol Metab 2013, *in press*.

32 www.cbs.nl. 2013.

33 Obesity: preventing and managing the global epidemic. Report of a WHO consultation. World Health Organ Tech Rep Ser 2000; 894: 1-253.

34 Wang Q, Zhang M, Ning G, et al. Brown adipose tissue in humans is activated by elevated plasma catecholamines levels and is inversely related to central obesity. *PLoS One* 2011; 6: e21006.

35 Stanford KI, Middelbeek RJ, Townsend KL, et al. Brown adipose tissue regulates glucose homeostasis and insulin sensitivity. J Clin Invest 2013; 123: 215-223.

36 Nedergaard J, Cannon B. The changed metabolic world with human brown adipose tissue: therapeutic visions. Cell Metab 2010; 11: 268-272.

37 Vijgen GH, Bouvy ND, Teule GJ, et al. Brown adipose tissue in morbidly obese subjects. *PLoS One* 2011; 6: e17247.

38 Simpson SA, Shaw C, McNamara R. What is the most effective way to maintain weight loss in adults? BMJ 2011; 343: d8042.

39 Saito M, Okamatsu-Ogura Y, Matsushita M, et al. High incidence of metabolically active brown adipose tissue in healthy adult humans: effects of cold exposure and adiposity. Diabetes 2009; 58: 1526-1531.

40 Subramanian S, Vollmer RR. Sympathetic activation by fenfluramine depletes brown adipose tissue norepinephrine content in rats. Pharmacol Biochem Behav 2002; 73: 639-645.

41 Larsen TM, Toubro S, van Baak MA, et al. Effect of a 28-d treatment with L-796568, a novel beta(3)-adrenergic receptor agonist, on energy expenditure and body composition in obese men. Am J Clin Nutr 2002; 76: 780-788.

42 Redman LM, de JL, Fang X, et al. Lack of an effect of a novel beta3-adrenoceptor agonist, TAK-677, on energy metabolism in obese individuals: a double-blind, placebo-controlled randomized study. J Clin Endocrinol Metab 2007; 92: 527-531.

43 Lockie SH, Heppner KM, Chaudhary N, et al. Direct control of brown adipose tissue thermogenesis by central nervous system glucagon-like peptide-1 receptor signaling. Diabetes 2012; 61: 2753-2762.

44 Martinez de Morentin PB, Whittle AJ, Ferno J, et al. Nicotine induces negative energy balance through hypothalamic AMP-activated protein kinase. Diabetes 2012; 61:807-817.

45 Filozof C, Fernandez Pinilla MC, Fernandez-Cruz A. Smoking cessation and weight gain. Obes Rev 2004; 5: 95-103.

46 Tseng YH, Kokkotou E, Schulz TJ, et al. New role of bone morphogenetic protein 7 in brown adipogenesis and energy expenditure. Nature 2008; 454: 1000-1004.

47 Bordicchia M, Liu D, Amri EZ, et al. Cardiac natriuretic peptides act via p38 MAPK to induce the brown fat thermogenic program in mouse and human adipocytes. J Clin Invest 2012; 122: 1022-1036.

48 Goodarzi MO, Bryer-Ash M. Metformin revisited: re-evaluation of its properties and role in the pharmacopoeia of modern antidiabetic agents. Diabetes Obes Metab 2005; 7: 654-665.

49 Nathan DM, Buse JB, Davidson MB, et al. Medical management of hyperglycaemia in type 2 diabetes mellitus: a consensus algorithm for the initiation and adjustment of therapy: a consensus statement from the American Diabetes Association and the European Association for the Study of Diabetes. Diabetologia 2009; 52: 17-30.

50 Salpeter SR, Buckley NS, Kahn JA, et al. Meta-analysis: metformin treatment in persons at risk for diabetes mellitus. Am J Med 2008; 121: 149-157.

51 Zhou G, Myers R, Li Y, et al. Role of AMP-activated protein kinase in mechanism of metformin action. J Clin Invest 2001; 108: 1167-1174.

52 Shan T, Liang X, Bi P, et al. Myostatin knockout drives browning of white adipose tissue through activating the AMPK-PGC1alpha-Fndc5 pathway in muscle. FASEB J 2013; 27: 1981-1989.

53 Addy C, Wright H, Van LK, et al. The acyclic CB1R inverse agonist taranabant mediates weight loss by increasing energy expenditure and decreasing caloric intake. Cell Metab 2008; 7: 68-78.

54 Despres JP, Golay A, Sjostrom L. Effects of rimonabant on metabolic risk factors in overweight patients with dyslipidemia. N Engl J Med 2005; 353: 2121-2134.

55 Pi-Sunyer FX, Aronne LJ, Heshmati HM, et al. Effect of rimonabant, a cannabinoid-1 receptor blocker, on weight and cardiometabolic risk factors in overweight or obese patients: RIO-North America: a randomized controlled trial. JAMA 2006; 295: 761-775.

56 Van Gaal LF, Rissanen AM, Scheen AJ, et al. Effects of the cannabinoid-1 receptor blocker rimonabant on weight reduction and cardiovascular risk factors in overweight patients: 1-year experience from the RIO-Europe study. Lancet 2005; 365: 1389-1397.

57 Osei-Hyiaman D, DePetrillo M, Pacher P, et al. Endocannabinoid activation at hepatic CB1 receptors stimulates fatty acid synthesis and contributes to diet-induced obesity. J Clin Invest 2005; 115: 1298-1305.

58 Eckardt K, Sell H, Taube A, et al. Cannabinoid type 1 receptors in human skeletal muscle cells participate in the negative crosstalk between fat and muscle. Diabetologia 2009; 52: 664-674.

59 Cota D, Marsicano G, Tschop M, et al. The endogenous cannabinoid system affects energy balance via central orexigenic drive and peripheral lipogenesis. J Clin Invest 2003; 112: 423-431.

60 Verty AN, Allen AM, Oldfield BJ. The effects of rimonabant on brown adipose tissue in rat: implications for energy expenditure. Obesity (Silver Spring) 2009; 17: 254-261.

61 Tedesco L, Valerio A, Cervino C, et al. Cannabinoid type 1 receptor blockade promotes mitochondrial biogenesis through endothelial nitric oxide synthase expression in white adipocytes. Diabetes 2008; 57: 2028-2036.

62 Wu HM, Yang YM, Kim SG. Rimonabant, a cannabinoid receptor type 1 inverse agonist, inhibits hepatocyte lipogenesis by activating liver kinase B1 and AMP-activated protein kinase axis downstream of Galpha i/o inhibition. Mol Pharmacol 2011; 80: 859-869.

63 Bostrom P, Wu J, Jedrychowski MP, et al. A PGC1-alpha-dependent myokine that drives brown-fat-like development of white fat and thermogenesis. Nature 2012; 481: 463-468.

64 Raschke S, Elsen M, Gassenhuber H, et al. Evidence against a beneficial effect of irisin in humans. PLoS One 2013; 8: e73680.
65 Petrovic N, Shabalina IG, Timmons JA, et al. Thermogenically competent nonadrenergic recruitment in brown preadipocytes by a PPARgamma agonist. Am J Physiol Endocrinol Metab 2008; 295: E287-E296.
66 Teruel T, Hernandez R, Rial E, et al. Rosiglitazone up-regulates lipoprotein lipase, hormone-sensitive lipase and uncoupling protein-1, and down-regulates insulin-induced fatty acid synthase gene expression in brown adipocytes of Wistar rats. Diabetologia 2005; 48: 1180-1188.
67 Iqbal MB, Fisher NG, Lyne JC, et al. Thiazolinediones and heart failure: the potential to precipitate irreversible cardiac dysfunction. Int J Cardiol 2008; 123: e35-e37.
68 Mazziotti G, Canalis E, Giustina A. Drug-induced osteoporosis: mechanisms and clinical implications. Am J Med 2010; 123: 877-884.
69 Sampath TK, Maliakal JC, Hauschka PV, et al. Recombinant human osteogenic protein-1 (hOP-1) induces new bone formation in vivo with a specific activity comparable with natural bovine osteogenic protein and stimulates osteoblast proliferation and differentiation in vitro. J Biol Chem 1992; 267: 20352-20362.
70 Vukicevic S, Luyten FP, Reddi AH. Stimulation of the expression of osteogenic and chondrogenic phenotypes in vitro by osteogenin. Proc Natl Acad Sci U S A 1989; 86: 8793-8797.
71 Fan Z, Chubinskaya S, Rueger DC, et al. Regulation of anabolic and catabolic gene expression in normal and osteoarthritic adult human articular chondrocytes by osteogenic protein-1. Clin Exp Rheumatol 2004; 22: 103-106.
72 Vukicevic S, Kopp JB, Luyten FP, et al. Induction of nephrogenic mesenchyme by osteogenic protein 1 (bone morphogenetic protein 7). Proc Natl Acad Sci U S A 1996; 93: 9021-9026.
73 Boon MR, van der Horst G, van der Pluijm G, et al. Bone morphogenetic protein 7: a broad-spectrum growth factor with multiple target therapeutic potency. Cytokine Growth Factor Rev 2011; 22: 221-229.

SOUTH ASIANS: A POPULATION WITH A DISADVANTAGEOUS METABOLIC PHENOTYPE

MARIËTTE R. BOON
LEONTINE E.H. BAKKER
RIANNE A.D. VAN DER LINDEN
ANTOINETTE VAN OUWEKERK
PAULINE L. DE GOEJE
JACQUELINE COUNOTTE
INGRID M. JAZET
PATRICK C.N. RENSEN

MODIFIED FROM:

High prevalence of cardiovascular disease in South Asians: central role for brown adipose tissue?

Submitted.

EPIDEMIOLOGY OF CVD IN SOUTH ASIANS

The South Asian population originally descends from the Indian subcontinent (India, Pakistan, Bangladesh, Nepal and Sri Lanka) and comprises approximately 20% of the total world population. Currently, over 200,000 South Asians are living in the Netherlands, especially in The Hague. The burden and mortality of cardiovascular diseases (CVD) are significantly higher among both native and migrant South Asians in comparison to subjects of white Caucasian descent (1-3). The age standardized mortality rate for CVD is around 50% higher in South Asian countries than in Western countries (3). Furthermore, individuals are affected by CVD at a younger age and as a result India suffers the highest loss in potentially productive years of life due to cardiovascular deaths (2;4;5). In 2030, this loss is estimated to be ten times higher than in the United States, whereas the population size is only three times larger (2). CVD risk is also higher in migrant South Asians living in Western countries. Studies consistently show that the risk of CVD among South Asian immigrants is at least two-fold increased compared to native populations as well as other immigrant groups. In Canada, the prevalence of CVD among South Asian immigrants is 10.7%, compared to 5.4% and 2.4% for people from European and Chinese descent, respectively (4). Furthermore, South Asians in the UK show a 40-60% higher mortality rate from coronary heart disease compared to European whites (1;6;7). In addition, in all of these studies South Asian immigrants were affected at a younger age than control groups.

The exceptionally high CVD risk in South Asians poses a major health and socioeconomic burden. Therefore, it is important to gain more insight in the pathogenesis of CVD in this population. It is likely that at least part of the excess risk is explained by genetic factors, since both South Asians in native countries as well as migrated South Asians are at increased risk. In addition, environmental factors, such as changes secondary to urbanization and migration, may play a role. Indeed, the risk of CVD appears to increase as South Asians move from rural India to urban India to immigrant populations (8).

When considering underlying causes for the increased CVD risk in the South Asian population, the pathogenesis of CVD should be discussed first.

PATHOGENESIS OF CARDIOVASCULAR DISEASE

The major cause of CVD is atherosclerosis, which is present many years before any clinical symptoms of CVD become manifest, including ischemic heart disease, cerebrovascular accident and peripheral arterial occlusive disease.

Atherosclerosis development starts with endothelial damage and dysfunction, often promoted by inflammatory mediators or shear stress induced by nonlaminar blood flow. This results in enhanced recruitment of inflammatory leukocytes such as monocytes and T-lymphocytes towards the damaged site, and migration of monocytes into the subendothelial intima followed by transformation into macrophages. At the same time, low-density lipo-

protein (LDL) particles may infiltrate into the vessel wall and become oxidized (e.g. due to release of reactive oxygen species or cigarette smoke). Macrophages within the vessel wall can take up oxidized LDL via receptors such as scavenger receptor A (SRA) and CD36, and become lipid-laden foam cells (9). What follows is an inflammatory status in which leukocytes and local endothelial cells excrete pro-inflammatory cytokines, including interferon γ (IFN-γ), tumor-necrosis factor-α (TNF-α) and growth factors, further stimulating leukocyte recruitment, accumulation of macrophages as well as proliferation of smooth muscle cells in the vascular intima, which produce elastin and collagen (10). This all sequentially leads to plaque formation, plaque expansion and formation of a fibrous cap. High-density lipoprotein (HDL) supposedly has an atheroprotective role, primarily by removing cholesterol from atherosclerotic plaques and transporting it back to the liver for excretion via the bile. Furthermore, it prevents LDL from oxidation and has anti-inflammatory properties (11).

From the above-mentioned pathophysiology it becomes clear that the development of atherosclerosis may be promoted by metabolic as well as inflammatory risk factors. Metabolic or 'classical' risk factors include dyslipidemia (marked by elevated LDL-C and decreased HDL-C levels), hypertension (resulting in nonlaminar blood flow), and smoking (resulting in endothelial dysfunction) (12). Furthermore, insulin resistance and central obesity are metabolic risk factors that are associated with increased CVD risk (13-15). Most of these classical cardiovascular risk factors are highly present in South Asians. In addition, although the precise mechanism is still under debate, also inflammatory or 'nonclassical' risk factors may contribute to development of CVD. Among these are systemic inflammation (marked by elevated C-reactive protein and/or TNF-α levels), as well as HDL dysfunction and endothelial dysfunction which can both give rise to inflammation (16).

Next, we will discuss the classical (metabolic) and nonclassical (inflammatory) risk factors for CVD in South Asian subjects.

CLASSICAL CVD RISK FACTORS IN SOUTH ASIANS

Dyslipidemia

Dyslipidemia, often comprising increased levels of LDL-C and triglycerides and decreased levels of HDL-C, is one of the main risk factors for CVD. South Asians were consistently shown to have higher triglyceride and lower HDL-C levels (7;17;18). Some studies also reported higher LDL-C levels in South Asian subjects compared to white Caucasians (4;19).

Obesity

South Asians have a disadvantageous fat distribution pattern with relatively thin extremities and higher abdominal adiposity (20;21). Furthermore, at a similar level of BMI, body fat percentage is higher in South Asians compared to white Caucasians (20;22). South Asians also have a tendency for higher deposition of fat within cells of non-adipose tissues such as

muscle and liver, so called "ectopic" sites. Petersen *et al.* (23) showed that in healthy lean South Asians hepatic triglyceride content was two-fold higher than in healthy lean white Caucasians. This higher triglyceride content was associated with hepatic insulin resistance and increased levels of pro-inflammatory cytokines. Storage of fat in these ectopic sites has a disruptive effect on glucose metabolism and it is now increasingly recognized that hepatic steatosis may be causally related to hepatic insulin resistance, the metabolic syndrome, systemic inflammation and even CVD (23-26).

Insulin resistance

Insulin resistance and elevated fasting glucose levels are more prevalent in non-diabetic South Asians compared to non-diabetic white Caucasians (7;18). In South Asians, the high rate of type 2 diabetes (T2D) is most striking. In 35-60 year old South Asian males living in the UK, diabetes prevalence was 16% compared with only 4% among European whites (7;18;27). Other studies, amongst which one conducted in the Netherlands, have reported an even higher prevalence of up to 25.4% for both South Asian men and women (28;29). Furthermore, the onset of diabetes is over 10 years earlier in South Asians (28), and diabetes occurs at a lower BMI compared to white Caucasians: the risk of developing T2D of a South Asian with a BMI of 21 kg/m^2 is comparable to the risk of a white Caucasian with a BMI of 30 kg/m^2 (3;19). Finally, South Asians often develop more diabetes-related complications, such as diabetic nephropathy and retinopathy (30).

Thus, in South Asians a disadvantageous metabolic profile consisting of central obesity, insulin resistance, and dyslipidemia, is highly prevalent. It is commonly assumed that an ethnic susceptibility towards a disturbed energy homeostasis *(e.g.* lower oxidation of glucose and fatty acids by mitochondria) might underlie this phenotype (31). In line with this, South Asian subjects have lower energy expenditure (32). As no efficient treatment is available for their disadvantageous phenotype, unravelling its cause is of great importance and may be beneficial in preventing, at least in part, the development of T2D and CVD in the South Asian population.

Excess risk

Studies have shown that after correction for the above-mentioned classical risk factors, ethnicity still remains an independent determinant of cardiovascular events in the South Asian population (1;4;7). Thus, residual risk is present suggesting that additional factors *(i.e.* nonclassical cardiovascular risk factors) may play a role. Aberrancies in several pathways may contribute to these nonclassical risk factors which are shortly summarized as 'inflammatory' factors. These factors will be shortly discussed in the following section; inflammation, HDL dysfunction and endothelial activation.

NON-CLASSICAL CVD RISK FACTORS IN SOUTH ASIANS

C-reactive protein

As mentioned above, inflammation is a well-recognized key player in the pathogenesis of atherosclerosis and may, therefore, be considered a risk factor for CVD. Besides promoting initiation of atherosclerosis development through monocyte attraction, it may lead to instability of the fibrous cap of the atherosclerotic plaque, resulting in rupture of the plaque and a subsequent cardiovascular event. C-reactive protein (CRP), which is synthesized by the liver in response to inflammatory factors released by macrophages and adipocytes (33;34), is a sensitive marker of inflammation (35). In a study of Chambers et al (17), CRP levels were found to be significantly higher in South Asians compared with Europeans even after adjustment for conventional risk factors such as age, smoking and body mass index, suggesting a chronic state of low grade inflammation in this population. However, in their study the difference in CRP levels was predominantly explained by greater central obesity and insulin resistance in South Asians. Visceral adipose tissue has been found to be a major source of cytokine release into the circulation (17;36). Intriguingly, the increased risk of CVD in South Asians was associated with a larger amount of visceral adipose tissue (37). Not only do South Asians have more visceral adipose tissue, their adipocytes appear to be more inflammatory as well. Several studies reported that South Asian adipocytes release higher levels of pro-inflammatory cytokines, such as CRP, interleukin 6 (IL-6) and TNF-α in comparison to white Caucasians (23;38), indicating a chronic inflammatory state.

HDL dysfunction

Multiple studies have consistently shown lower HDL-C levels in South Asians compared to white Caucasians (6;17;21;39-42). The cardiovascular protective effects of HDL have been attributed to several atheroprotective properties. Firstly, HDL stimulates cholesterol efflux from foam cells present in atherosclerotic plaques by acting as cholesterol acceptor and transporting cholesterol back to the liver for excretion into the bile (43). Secondly, HDL prevents LDL from oxidation (44-46). Thirdly, HDL has anti-inflammatory properties; during the early phase of atherosclerosis development, HDL may prevent leukocyte adhesion to endothelial cells by lowering expression of monocyte chemotactic protein 1 (MCP-1) and vascular cell adhesion molecule (VCAM-1) and by counteracting platelet-activating factor (PAF) induced adhesion of leukocytes (44-47). Fourthly, HDL induces vasodilatation through stimulation of nitric oxide (NO) release by endothelial cells (54). This results in lower endothelial shear stress and thereby slows down initiation of atherosclerosis development. Thus, dysfunction of HDL may not only directly aggrevate atherosclerosis development as a consequence of lower cholesterol uptake from the vascular wall, but also indirectly through induction of inflammation as well as endothelial dysfunction.

Recent evidence suggests that HDL functionality may be more importantly linked to CVD than plasma HDL-C levels *per se* (48;49). In trials that aimed at raising HDL-C levels, *e.g.* with dalcetrapib (50) or niacin (51) on top of statin, no decrease in the occurrence of cardio-

vascular endpoints was observed. Furthermore, several studies showed that HDL is dysfunctional in patients with coronary atherosclerosis, in men with cardiovascular risk factors, and in patients with an acute phase response after surgery (52-55).

Remarkably, little is known about HDL functionality in South Asians. To date only one cross-sectional, uncontrolled pilot study assessed the anti-oxidative capacity of HDL in South Asian immigrants living in the USA. They found dysfunctional HDL in 50% of the participants, which was significantly correlated with carotid intima media thickness, a surrogate marker of atherosclerosis (56). However, they lacked a control group of another ethnicity, so no statements could be made on the implication of this percentage for their increased risk of CVD. Future studies in this direction are, therefore, highly warranted.

Endothelial activation

Endothelial activation is regarded an important initiating factor in the pathogenesis of atherosclerosis and CVD (57). Endothelial activation is characterized by a proadhesion, proinflammatory, and procoagulatory milieu that favours all stages of atherogenesis. A hallmark of endothelial activation is a reduction in the bioavailability of endothelium-derived NO. An impaired NO-mediated vasodilatory response has been demonstrated in patients with cardiac risk factors or established atherosclerosis (58;59). Furthermore, the degree of impairment is related to the severity and extent of coronary artery disease (60).

Interestingly, previous studies have demonstrated reduced flow-mediated vasodilatation in South Asians compared to white Caucasians, pointing to endothelial activation and lower NO bioavailability (27;61). Of note, NO is mainly produced by the endothelium as a consequence of an interaction with HDL (62;63). Hence, besides a susceptibility for endothelial activation, dysfunctionality of HDL with respect to its ability to induce endothelial NO production is another possible explanation for the lower NO bioavailability in South Asians.

Circulating endothelial progenitor cells (EPCs), mobilized from the bone marrow, have an important role in the repair and regeneration of the endothelium (64-66). The number of circulating EPCs is lower in patients with established coronary artery disease, is predictive of future cardiovascular events, and is positively correlated with measures of endothelial function (67;68). Intriguingly, South Asians have lower circulating numbers of EPCs compared to white Caucasians, which may lead to a reduced capacity for endothelial repair (61;69). Furthermore, exercise-induced EPC mobilization was reduced in South Asian men (69). Interestingly, NO appears to be critical for EPC mobilization in response to exercise (69). Hence, the reduced exercise mediated EPC mobilization in South Asians may be secondary to their reduced NO bioavailability. Future studies should be directed at further investigating endothelial activation in this population and at developing strategies that enhance EPC mobilization by augmenting NO bioavailability.

CONCLUDING REMARKS

In conclusion, South Asians are more liable to develop CVD at an early age, and classical risk factors associated with CVD, including dyslipidemia, central obesity and insulin resistance, are more prevalent in this ethnicity compared to subjects of white Caucasian origin. The underlying cause for this highly prevalent disadvantageous metabolic phenotype is currently unknown. Of note, these 'metabolic' risk factors seem to account for only part of the increased risk in South Asians as ethnicity remains an independent determinant of cardiovascular events. Nonclassical 'inflammatory' risk factors, i.e. higher levels of inflammation, HDL dysfunction, and endothelial activation may be involved in the residual CVD risk in South Asians (see **FIGURE 1)**, although the presence of these risk factors requires further investigation as it has not always been properly studied. Furthermore, which of these factors plays a dominant role and is therefore the most promising therapeutic target to lower the excess CVD risk in South Asians remains to be investigated.

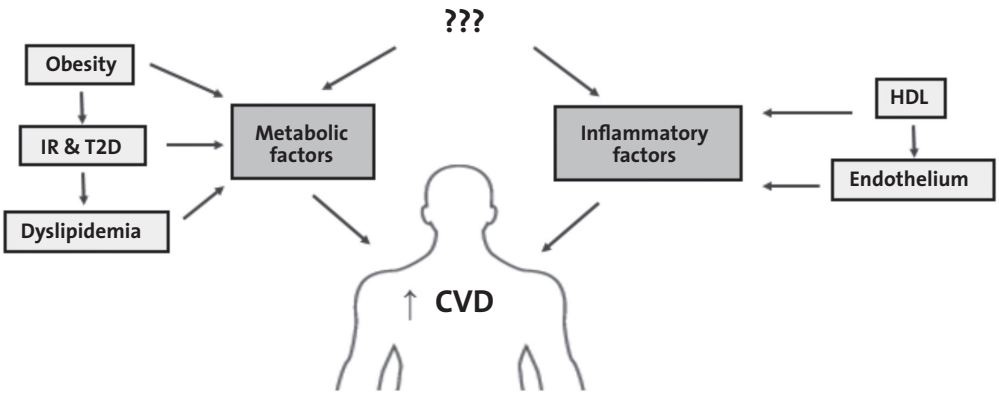

FIGURE 1 - **Proposed underlying mechanisms in the high cardiovascular risk in the South Asian population.** Classical (metabolic) risk factors, i.e. central obesity, insulin resistance and type 2 diabetes, and dyslipidemia are highly prevalent in the South Asian population. Furthermore, dysfunctional HDL and endothelium may enhance inflammation and these nonclassical risk factors may contribute to the 'residual' CVD risk of the South Asian population. Whether the high prevalence of metabolic and inflammatory factors in the South Asian population is due to a common (disadvantageous) factor remains to be determined. *CVD,* cardiovascular disease; *IR,* insulin resistance; *HDL,* high-density lipoprotein; *T2D,* type 2 diabetes.

REFERENCES

1 Forouhi N, Sattar N, Tillin T, et al. Do known risk factors explain the higher coronary heart disease mortality in South Asians compared with European men? Prospective follow-up of the Southall and Brent studies, UK. Diabetologia 2006; 49: 2580-1588.

2 Srinath R, Shah B, Varghese C, et al. Responding to the threat of chronic diseases in India. Lancet 2005; 366: 1744-1749.

3 Turin TC, Shahana N, Wangchuk LZ, et al. Burden of Cardio- and Cerebro-vascular Disease and the Conventional Risk Factors in South Asian Population. Global Health 2005; 8: 121-130.

4 Anand SS, Yusuf S, Vuksan V, et al. Differences in risk factors, atherosclerosis and cardiovascular disease between ethnic groups in Canada: the study of health assessment and risk in ethnic groups (SHARE). Lancet 2000; 356: 279-284.

5 Joshi P, Islam S, Pais P, et al. Risk factors for early myocardial infarction in South Asians compared with individuals in other countries. JAMA 2007; 297: 286-294.

6 McKeigue PM, Shah B, Marmot MG. Relation of central obesity and insulin resistance with high diabetes prevalence and cardiovascular risk in South Asians. Lancet 1991; 337: 382-386.

7 McKeigue PM, Ferrie JE, Pierpoint T, et al. Association of early-onset coronary heart disease in South Asian men with glucose intolerance and hyperinsulinemia. Circulation 1993; 87: 152-161.

8 Gupta R, Gupta R, Agrawal A, et al. Migrating husbands and changing cardiovascular risk factors in the wife: a cross sectional study in Asian Indian women. J Epidemiol Community Health 2012; 66: 881-889.

9 Steinberg D. Atherogenesis in perspective: hypercholesterolemia and inflammation as partners in crime. Nat Med 2002; 8: 1211-1217.

10 Hansson GK, Libby P. The immune response in atherosclerosis: a double-edged sword. Nat Rev Immunol 2006; 6: 508-519.

11 Nisoli E, Clementi E, Paolucci C, et al. Mitochondrial biogenesis in mammals: the role of endogenous nitric oxide. Science 2003; 299: 896-899.

12 Third Report of the National Cholesterol Education Program (NCEP) Expert Panel on Detection, Evaluation, and Treatment of High Blood Cholesterol in Adults (Adult Treatment Panel III) final report. Circulation 2002; 106: 3143-3421.

13 Haffner SM, Lehto S, Ronnemaa T, et al. Mortality from coronary heart disease in subjects with type 2 diabetes and in nondiabetic subjects with and without prior myocardial infarction. N Engl J Med 1998; 339: 229-234.

14 Lee CD, Folsom AR, Pankow JS, et al. Cardiovascular events in diabetic and nondiabetic adults with or without history of myocardial infarction. Circulation 2004; 109: 855-860.

15 Malmberg K, Yusuf S, Gerstein HC, et al. Impact of diabetes on long-term prognosis in patients with unstable angina and non-Q-wave myocardial infarction: results of the OASIS (Organization to Assess Strategies for Ischemic Syndromes) Registry. Circulation 2000; 102: 1014-1019.

16 Bloomgarden ZT. Inflammation, atherosclerosis, and aspects of insulin action. Diabetes Care 2005; 28: 2312-2319.

17 Chambers JC, Eda S, Bassett P, et al. C-reactive protein, insulin resistance, central obesity, and coronary heart disease risk in Indian Asians from the United Kingdom compared with European whites. Circulation 2001; 104: 145-150.

18 Tziomalos K, Weerasinghe CN, Mikhailidis DP, et al. Vascular risk factors in South Asians. Int J Cardiol 2008; 128: 5-16.

19 Razak F, Anand SS, Shannon H, et al. Defining obesity cut points in a multiethnic population. Circulation 2007; 115: 2111-2118.

20 Lear SA, Humphries KH, Kohli S, et al. The use of BMI and waist circumference as surrogates of body fat differs by ethnicity. Obesity (Silver Spring) 2007; 15: 2817-2824.

21 Raji A, Gerhard-Herman MD, Warren M, et al. Insulin resistance and vascular dysfunction in nondiabetic Asian Indians. J Clin Endocrinol Metab 2004; 89: 3965-3972.

22 Chandalia M, Lin P, Seenivasan T, et al. Insulin resistance and body fat distribution in South Asian men compared to Caucasian men. PLoS One 2007; 2: e812.
23 Petersen KF, Dufour S, Feng J, et al. Increased prevalence of insulin resistance and nonalcoholic fatty liver disease in Asian-Indian men. Proc Natl Acad Sci U S A 2006; 103: 18273-18277.
24 Bajaj S, Nigam P, Luthra A, et al. A case-control study on insulin resistance, metabolic co-variates & prediction score in non-alcoholic fatty liver disease. Indian J Med Res 2009; 129: 285-292.
25 Ndumele CE, Nasir K, Conceicao RD, et al. Hepatic steatosis, obesity, and the metabolic syndrome are independently and additively associated with increased systemic inflammation. Arterioscler Thromb Vasc Biol 2011; 31: 1927-1932.
26 Targher G, Bertolini L, Padovani R, et al. Prevalence of nonalcoholic fatty liver disease and its association with cardiovascular disease among type 2 diabetic patients. Diabetes Care 2007; 30: 1212-1218.
27 Chambers JC, McGregor A, Jean-Marie J, et al. Abnormalities of vascular endothelial function may contribute to increased coronary heart disease risk in UK Indian Asians. Heart 1999; 81: 501-504.
28 Mukhopadhyay B, Forouhi NG, Fisher BM, et al. A comparison of glycaemic and metabolic control over time among South Asian and European patients with Type 2 diabetes: results from follow-up in a routine diabetes clinic. Diabet Med 2006; 23: 94-98.
29 Middelkoop BJ, Kesarlal-Sadhoeram SM, Ramsaransing GN, et al. Diabetes mellitus among South Asian inhabitants of The Hague: high prevalence and an age-specific socioeconomic gradient. Int J Epidemiol 1999; 28: 1119-1123.
30 Chandie Shaw PK, Vandenbroucke JP, Tjandra YI, et al. Increased end-stage diabetic nephropathy in Indo-Asian immigrants living in the Netherlands. Diabetologia 2002; 45: 337-341.
31 Hall LM, Moran CN, Milne GR, et al. Fat oxidation, fitness and skeletal muscle expression of oxidative/lipid metabolism genes in South Asians: implications for insulin resistance? PLoS One 2010; 5: e14197.
32 Bakker LE, van Schinkel LD, Guigas B, et al. A 5-day high-fat, high-calorie diet impairs insulin sensitivity in healthy, young South Asian men but not in Caucasian men. Diabetes 2014; 63: 248-258.
33 Lau DC, Dhillon B, Yan H, et al. Adipokines: molecular links between obesity and atheroslcerosis. Am J Physiol Heart Circ Physiol 2005; 288: H2031-H2041.
34 Pepys MB, Hirschfield GM. C-reactive protein: a critical update. J Clin Invest 2003; 111: 1805-1812.
35 Madjid M, Willerson JT. Inflammatory markers in coronary heart disease. Br Med Bull 2011; 100: 23-38.
36 Kissebah AH. Intra-abdominal fat: is it a major factor in developing diabetes and coronary artery disease? Diabetes Res Clin Pract 1996; 30 Suppl: 25-30.
37 Lear SA, Chockalingam A, Kohli S, et al. Elevation in cardiovascular disease risk in South Asians is mediated by differences in visceral adipose tissue. Obesity (Silver Spring) 2012; 20: 1293-1300.
38 Peters MJ, Ghouri N, McKeigue P, et al. Circulating IL-6 concentrations and associated anthropometric and metabolic parameters in South Asian men and women in comparison to European whites. Cytokine 2013; 61: 29-32.
39 Ajjan R, Carter AM, Somani R, et al. Ethnic differences in cardiovascular risk factors in healthy Caucasian and South Asian individuals with the metabolic syndrome. J Thromb Haemost 2007; 5: 754-760.
40 Chandalia M, Abate N, Garg A, et al. Relationship between generalized and upper body obesity to insulin resistance in Asian Indian men. J Clin Endocrinol Metab 1999; 84: 2329-2335.
41 Ehtisham S, Crabtree N, Clark P, et al. Ethnic differences in insulin resistance and body composition in United Kingdom adolescents. J Clin Endocrinol Metab 2005; 90: 3963-3969.

42 McKeigue PM, Marmot MG, Syndercombe Court YD, et al. Diabetes, hyperinsulinaemia, and coronary risk factors in Bangladeshis in east London. Br Heart J 1988; 60: 390-396.
43 Barter PJ, Baker PW, Rye KA. Effect of high-density lipoproteins on the expression of adhesion molecules in endothelial cells. Curr Opin Lipidol 2002; 13: 285-288.
44 Navab M, Hama SY, Cooke CJ, et al. Normal high density lipoprotein inhibits three steps in the formation of mildly oxidized low density lipoprotein: step 1. J Lipid Res 2000; 41: 1481-1494.
45 Navab M, Ananthramaiah GM, Reddy ST, et al. The double jeopardy of HDL. Ann Med 2005; 37: 173-178.
46 von EA, Hersberger M, Rohrer L. Current understanding of the metabolism and biological actions of HDL. Curr Opin Clin Nutr Metab Care 2005; 8: 147-152.
47 Sugatani J, Miwa M, Komiyama Y, et al. High-density lipoprotein inhibits the synthesis of platelet-activating factor in human vascular endothelial cells. J Lipid Mediat Cell Signal 1996; 13: 73-88.
48 Corsetti JP, Gansevoort RT, Sparks CE, et al. Inflammation reduces HDL protection against primary cardiac risk. Eur J Clin Invest 2010; 40: 483-489.
49 deGoma EM, deGoma RL, Rader DJ. Beyond high-density lipoprotein cholesterol levels evaluating high-density lipoprotein function as influenced by novel therapeutic approaches. J Am Coll Cardiol 2008; 51: 2199-2211.
50 Schwartz GG, Olsson AG, Abt M, et al. Effects of dalcetrapib in patients with a recent acute coronary syndrome. N Engl J Med 2012; 367: 2089-2099.
51 Sharma M. Combination therapy for dyslipidemia. Curr Opin Cardiol 2011; 26:420-423.
52 Ansell BJ, Navab M, Hama S, et al. Inflammatory/antiinflammatory properties of high-density lipoprotein distinguish patients from control subjects better than high-density lipoprotein cholesterol levels and are favorably affected by simvastatin treatment. Circulation 2003; 108: 2751-2756.
53 Navab M, Hama SY, Hough GP, et al. A cell-free assay for detecting HDL that is dysfunctional in preventing the formation of or inactivating oxidized phospholipids. J Lipid Res 2001; 42: 1308-1317.
54 Roberts CK, Ng C, Hama S, et al. Effect of a short-term diet and exercise intervention on inflammatory/anti-inflammatory properties of HDL in overweight/obese men with cardiovascular risk factors. J Appl Physiol 2006; 101: 1727-1732.
55 Van Lenten BJ, Hama SY, de Beer FC, et al. Anti-inflammatory HDL becomes pro-inflammatory during the acute phase response. Loss of protective effect of HDL against LDL oxidation in aortic wall cell cocultures. J Clin Invest 1995; 96: 2758-2767.
56 Dodani S, Kaur R, Reddy S, et al. Can dysfunctional HDL explain high coronary artery disease risk in South Asians? Int J Cardiol 2008; 129: 125-132.
57 Bonetti PO, Lerman LO, Lerman A. Endothelial dysfunction: a marker of atherosclerotic risk. Arterioscler Thromb Vasc Biol 2003; 23: 168-175.
58 Celermajer DS, Sorensen KE, Gooch VM, et al. Non-invasive detection of endothelial dysfunction in children and adults at risk of atherosclerosis. Lancet 1992; 340: 1111-1115.
59 Schachinger V, Britten MB, Zeiher AM. Prognostic impact of coronary vasodilator dysfunction on adverse long-term outcome of coronary heart disease. Circulation 2000; 101: 1899-1906.
60 Neunteufl T, Katzenschlager R, Hassan A, et al. Systemic endothelial dysfunction is related to the extent and severity of coronary artery disease. Atherosclerosis 1997; 129: 111-118.
61 Murphy C, Kanaganayagam GS, Jiang B, et al. Vascular dysfunction and reduced circulating endothelial progenitor cells in young healthy UK South Asian men. Arterioscler Thromb Vasc Biol 2007; 27: 936-942.
62 Jin RC, Loscalzo J. Vascular Nitric Oxide: Formation and Function. J Blood Med 2010; 2010: 147-162.

63 Nofer JR, van der Giet M, Tolle M, et al. HDL induces NO-dependent vasorelaxation via the lysophospholipid receptor S1P3. J Clin Invest 2004; 113: 569-581.
64 Aicher A, Zeiher AM, Dimmeler S. Mobilizing endothelial progenitor cells. Hypertension 2005; 45: 321-325.
65 Griese DP, Ehsan A, Melo LG, et al. Isolation and transplantation of autologous circulating endothelial cells into denuded vessels and prosthetic grafts: implications for cell-based vascular therapy. Circulation 2003; 108: 2710-2715.
66 Peichev M, Naiyer AJ, Pereira D, et al. Expression of VEGFR-2 and AC133 by circulating human CD34(+) cells identifies a population of functional endothelial precursors. Blood 2000; 95: 952-958.
67 Hill JM, Zalos G, Halcox JP, et al. Circulating endothelial progenitor cells, vascular function, and cardiovascular risk. N Engl J Med 2003; 348: 593-600.
68 Vasa M, Fichtlscherer S, Aicher A, et al. Number and migratory activity of circulating endothelial progenitor cells inversely correlate with risk factors for coronary artery disease. Circ Res 2001; 89: E1-E7.
69 Cubbon RM, Murgatroyd SR, Ferguson C, et al. Human exercise-induced circulating progenitor cell mobilization is nitric oxide-dependent and is blunted in South Asian men. Arterioscler Thromb Vasc Biol 2010; 30: 878-884.

OUTLINE OF THESIS

As is evident from **CHAPTER 1** and **2** described in the first part of the thesis, brown adipose tissue (BAT) is a recently identified player in energy metabolism in human adults and a promising new target to treat obesity and related diseases. Interestingly, as described in **CHAPTER 3**, South Asians have lower energy expenditure, which may thus theoretically be caused by a reduction in BAT activity. Therefore, the studies of which the results are described in this thesis were aimed at 1) gaining more insight in the physiology of BAT, 2) identifying novel targets that may activate BAT, and 3) investigating the involvement of BAT in metabolism in humans with a focus on potential differences between South Asians and white Caucasians.

In the second part of this thesis, the role of BAT in metabolism and obesity is investigated using mouse studies. Since fatty acids (FA) are the main fuel for thermogenesis in BAT, and intracellular FA stores rapidly diminish upon BAT activation, BAT is required to take up FA from the plasma. It has been previously suggested that BAT takes up FA by uptake of whole lipoproteins *(i.e.* chylomicrons and VLDL), but this is in contrast to selective TG-derived FA uptake as exerted by white adipose tissue and muscle. Therefore, in **CHAPTER 4**, we aimed to investigate the mechanism by which BAT takes up lipoprotein-TG-derived FA by performing kinetic studies using glycerol tri[^{3}H]oleate and [^{14}C]cholesteryl oleate double-labeled lipoprotein-mimicking particles. Next, we focused on novel tools and targets that may activate BAT, thereby enhancing clearance of plasma TG and increasing energy expenditure. Based on the discovery that BMP7 can activate BAT, in **CHAPTER 5**, we investigated the mechanism by which BMP7 activates BAT, with focus on the role of the sympathetic nervous system, by treating high-fat fed lean mice and diet-induced obese mice with BMP7 under regular room temperature and thermoneutral temperature. In **CHAPTER 6**, the mechanism by which the anti-diabetic drug metformin lowers plasma TG was investigated. To this end, we performed VLDL-TG production and TG clearance experiments in dyslipidemic APOE*3-Leiden.CETP transgenic mice, as well as mechanistic studies *in vitro* using a brown adipocyte line, and put special focus on activation of intracellular AMPK. In **CHAPTER 7**, we investigated whether the TG-lowering effect of systemic cannabinoid 1 receptor blockade that was previously found in patients treated with rimonabant was mediated by activation of BAT in diet-induced obese APOE*3-Leiden.CETP transgenic mice. We further explored the underlying mechanism by performing experiments at thermoneutrality as well as using a strictly peripheral cannabinoid 1 receptor blocker. The brain is an important activator of BAT, especially in case of cold exposure. In **CHAPTER 8** we aimed to gain more insight in mediators that modulate BAT activity via the brain by studying the role of the melanocortin system on BAT function. To this end, we antagonized the central melanocortin 3 and 4 receptor in APOE*3-Leiden.CETP mice and studied BAT function and activity. To investigate whether BAT activation could protect against atherosclerosis development, in **CHAPTER 9**, we treated dyslipidemic APOE*3-Leiden.CETP mice with the ß3-adrenergic agonist CL316243 and studied energy expenditure, lipid metabolism and atherosclerosis development.

In the third part of the thesis, human studies on the role of BAT in metabolism and

obesity are described. A well-known cause of obesity is long term high-fat feeding, which may result in development of insulin resistance and eventually type 2 diabetes. To gain more insight in underlying mechanisms responsible for the development of high-fat diet induced insulin resistance, in **CHAPTER 10** we studied the effects of short-term high fat feeding on macrophage markers in skeletal muscle in healthy male subjects. The South Asian population is especially prone to develop obesity and related disorders, such as type 2 diabetes and cardiovascular disease (CVD). In **CHAPTER 11**, we investigated whether the high CVD risk in the South Asian population may be due to an ethnic susceptibility to develop endothelial activation. To this end, we measured markers for endothelial activation in cord blood of South Asian and white Caucasian neonates. In **CHAPTER 12**, we investigated whether HDL dysfunction may be present in the South Asian population by measuring different measures of HDL functionality in 3 cohorts of South Asian subjects and matched white Caucasian subjects *(i.e.,* neonates, adolescents and adults). The highly prevalent disadvantageous metabolic phenotype consisting of obesity, dyslipidemia and insulin resistance likely also underlies the high CVD risk in the South Asian population. Therefore, in **CHAPTER 13** we investigated whether a lower BAT volume or activity may be present in the South Asian population by performing cold-induced ^{18}F-FDG PET-CT scans in healthy lean Dutch South Asian and matched white Caucasian subjects. Since the ^{18}F-FDG PET-CT scan is currently the 'gold standard' to determine BAT volume and activity, but its use is limited by cost and radiation exposure, in **CHAPTER 14** we investigated whether supraclavicular skin temperature, the location at which most BAT is located, may serve as a quantitative measure of ^{18}F-FDG uptake in human subjects by use of wireless iButtons.

Finally in the fourth part of the thesis, the results from these studies and their implications are discussed in **CHAPTER 15** and summarized in **CHAPTER 16**.

PART 2

ANIMAL STUDIES ON ROLE OF BROWN ADIPOSE TISSUE IN METABOLISM AND OBESITY

BROWN ADIPOSE TISSUE INTERNALIZES FATTY ACIDS BY SELECTIVE DELIPIDATION OF LIPOPROTEINS RATHER THAN BY UPTAKE OF LIPOPROTEINS

MARIËTTE R. BOON
P. PADMINI S.J. KHEDOE
GEERTE HOEKE
SANDER KOOIJMAN
WIENEKE DIJK
SANDER KERSTEN
LOUIS M. HAVEKES
PIETER S. HIEMSTRA
JIMMY F.P. BERBÉE
PATRICK C.N. RENSEN

In preparation.

ABBREVATIONS

[^{3}H]TO	glycerol tri[^{3}H]oleate
[^{14}C]CO	[^{14}C]cholesteryl oleate
ATGL	adipose triglyceride lipase
BAT	brown adipose tissue
FA	fatty acid
HSL	hormone sensitive lipase
LPL	lipoprotein lipase
MGL	monoglyceride lipase
TG	triglyceride
TRL	triglyceride-rich lipoprotein
UCP1	uncoupling protein 1
(g,s)WAT	(gonadal, subcutaneous) white adipose tissue

ABSTRACT

The ability of brown adipose tissue (BAT) to produce heat upon cold and other stimuli is dependent on burning of intracellular triglyceride (TG) stores that need to be replenished by the uptake of TG-derived fatty acids (FA) from plasma. According to the current dogma, BAT takes up TG-rich lipoproteins (TLRs) as whole particles. However, the demonstrated critical involvement of LPL and CD36 would be more consistent with selective uptake of TG-derived FA by BAT. Therefore, the aim of the present study was to assess which mechanism prevails in the uptake of FA by BAT. Glycerol tri[^{3}H]oleate ([^{3}H]TO) and [^{14}C]cholesteryl oleate ([^{14}C]CO) labeled lipoprotein-mimicking TRLs with a mean diameter of 45, 80 and 150 nm (ranging from VLDL to chylomicrons) were synthesized and intravenously injected (0.2 mg TG/mouse) into male C57Bl/6J mice. The distribution of the radiolabels over the various organs was determined at 15 min after injection. For particles of 45, 80 and 150 nm, the uptake of ^{3}H-activity by BAT exceeded that of all other organs, and was much higher (28, 28, and 20% of injected dose/g) than the uptake of ^{14}C-activity (2, 3 and 4% of injected dose/g), indicating highly selective uptake of TG-derived FA by BAT as compared to the uptake of the particle core. Under conditions of increased BAT activity (housing for 24 h at 7°C), the uptake of both ^{3}H-activity (67, 57, and 47% of injected dose/g) and ^{14}C-activity (6, 8, and 24% of injected dose/g) by BAT increased, while retaining the selectivity for uptake of FA over CO. In conclusion, BAT takes up TRL-derived TG by means of selective FA uptake and this is consistent for TRLs ranging from small VLDL to small chylomicrons.

INTRODUCTION

Brown adipose tissue (BAT) is an important player in energy homeostasis due to its ability to combust energy towards heat by virtue of the presence of uncoupling protein 1 (UCP1), a process called non-shivering thermogenesis (1). The most well-known trigger for activation of BAT is cold, which increases sympathetic outflow from the hypothalamic temperature centre towards BAT. Here, nerve endings release noradrenalin that binds to adrenergic receptors on the brown adipocyte membrane (2). Activation of an intracellular signalling cascade subsequently leads to a fast induction of intracellular lipolysis, mediated by adipose triglyceride lipase (ATGL), hormone sensitive lipase (HSL) and monoglyceride lipase (MGL), resulting in release of fatty acids (FA) from triglyceride (TG)-filled lipid droplets (3). FA are directed to the mitochondria where they either allosterically activate UCP1 present in the inner membrane of the mitochondrion or undergo oxidation in the mitochondrial matrix (2). UCP1 dissipates the proton gradient across the inner mitochondrial membrane that is generated by the respiratory chain, resulting in production of heat. Of note, FA used for activation of UCP1 and oxidation are mainly derived from intracellular TG stores as mice that lack ATGL exhibit defective thermogenesis (4). Therefore, maintenance of intracellular TG stores is essential for BAT non-shivering thermogenesis.

Replenishment of intracellular TG stores within the brown adipocyte is mediated via three mechanisms; uptake of glucose followed by *de novo* lipogenesis, or uptake of albumin-bound FA and lipoprotein-derived FA from the plasma followed by incorporation of FA within TG (2;3;5). Circulating TG-rich lipoproteins (TRLs), *i.e.* very-low-density lipoproteins (VLDL) and chylomicrons, are the main source of FA for TG stores in BAT (3). These types of TRLs differ in their apolipoprotein composition as well as their size (VLDL: 30-80 nm and chylomicrons: 100-500 nm).

Only recently, BAT appeared as a major player in plasma TG clearance. Bartelt et al. (5) showed that 24 h of cold exposure markedly enhanced clearance of glycerol tri[^{3}H]oleate-labeled TRLs which was specifically mediated by BAT (5;6). The authors suggested that upon cold exposure, BAT took up TG from chylomicron-sized (~250 nm) TRL-like particles via whole particle uptake. However, they also demonstrated that BAT activation by cold was accompanied by enhanced expression of LPL and CD36, the presence of both appeared critical for TG uptake (5;6), which is in line with selective uptake of TG-derived FA by CD36 after liberation via LPL as occurs in skeletal muscle, heart and WAT.

Therefore, the aim of the present study was to investigate the mode of FA uptake by BAT in mice while modulating BAT activity using various ambient temperatures (7°C-28°C), by using glycerol tri[^{3}H]oleate and cholesteryl [^{14}C]oleate double-labeled TRL-mimicking particles with diameters ranging from VLDL to chylomicrons (45-150 nm). These emulsion particles have been previously shown to acquire apolipoproteins including apoCs and apoE in the circulation (7), thereby truly mimicking the TRL metabolism *in vivo*.

MATERIALS AND METHODS

Animals and diet

For all studies described in this manuscript, 8-10 week old male C57Bl/6J mice (Jackson Laboratory, Bar Harbor, ME) were used. Mice were housed in conventional cages with a 12:12-h light-dark cycle and had free access to chow food and water. All mouse experiments were performed in accordance with the Institute for Laboratory Animal Research Guide for the Care and Use of Laboratory Animals and have received approval from the Departmental Ethical Review Board (Leiden University Medical Center, Leiden, The Netherlands).

Acclimation to ambient temperature

Mice were single-housed one week prior to the experiment at an environmental temperature of 21°C, and randomized based on fasting plasma triglyceride (TG) levels, total cholesterol (TC) levels and body weight in two groups that were exposed to an ambient temperature of 7°C or 21°C for 24 h while being fasted the last 4 h before performing a terminal kinetic experiment with TG-rich emulsion particles (see below). In a second experiment, mice were randomized into two groups that were exposed for 4 h to an ambient temperature of 21°C or 28°C, while being fasted, prior to the kinetic experiment. For each temperature group, mice were divided into three groups that received lipoprotein-mimicking TG-rich emulsion particles of different size (average 45, 80 or 150 nm, n=6 per group).

Plasma parameters

At randomisation and after exposure to different ambient temperatures (prior to the clearance experiment), a blood sample was collected from the tail vein of 4 h fasted mice into capillaries. Capillaries were placed on ice and centrifuged, and plasma was assayed for TG and TC using commercially available enzymatic kits from Roche Diagnostics (Mannheim, Germany).

Preparation of labeled TRL-mimicking emulsion particles

TRL-mimicking emulsion particles were prepared from 100 mg of total lipid including triolein (70 mg), egg yolk phosphatidylcholine (22.7 mg), lysophosphatidylcholine (2.3 mg), cholesteryl oleate (3.0 mg) and cholesterol (2.0 mg) (7;8). For preparation of double-labeled TRL-mimicking emulsion particles, before sonification the radioactive tracers glycerol tri[^{3}H]oleate ([^{3}H]TO) (100 µCi) and [^{14}C]cholesteryl oleate ([^{14}C]CO) (10 µCi) were added. Sonification was performed using a Soniprep 150 (MSE Scientific Instruments, UK) that is equipped with a water bath for temperature (54°C) maintenance, at 10 µm output (8). The emulsion was fractionated by consecutive density gradient ultracentrifucation steps in a Beckman SW 40 Ti rotor. After centrifugation for 27 min at 20,000 rpm at 20°C, an emulsion fraction containing chylomicron-like particles (average size 150 nm) was removed from the top of the tube by aspiration and replaced by NaCl buffer of similar density *(i.e.* 1.006 g/mL). After a subsequent centrifugation step for 27 min at 40,000 rpm large VLDL-like particles (average size 80 nm) were obtained in a similar manner. A third centrifugation step for 3 h at 40,000 rpm yielded small VLDL-like particles (average size 45 nm). Characterization of

emulsion fractions was done by determination of TG concentration (as described under *Plasma parameters)* and radioactivity or fluorescence for radioactively or fluorescently labeled emulsion particles, respectively. Emulsions were stored at 4°C under argon and used for *in vivo* kinetic experiments within 5 days following preparation.

***In vivo* clearance of labeled TRL-mimicking emulsion particles**

To study the *in vivo* clearance of labeled TRL-mimicking emulsion particles, mice were fasted for 4 h and injected intravenously with 200 µL of emulsion particles (0.2 mg TG per mouse). Blood samples were taken from the tail vein at 2, 5, 10 and 15 min after injection to determine the serum decay of [^{3}H]TO and [^{14}C]CO. Plasma volumes were calculated as 0.04706 × body weight (g) (9). After taking the last blood sample, mice were cervically dislocated and perfused with ice-cold PBS containing 10 U/mL heparin via the heart to remove blood from the organs. Subsequently, the liver, heart, spleen, hindlimb muscle, gonadal white adipose tissue (gWAT), subcutaneous WAT (sWAT) and interscapular brown adipose tissue (BAT) were collected. Organs were dissolved overnight at 55°C in Tissue Solubilizer (Amersham Biosciences, Rosendaal, The Netherlands), and ^{3}H and ^{14}C activity were quantified. Uptake of [^{3}H]TO- and [^{14}C]CO-derived radioactivity by the organs was expressed per gram wet tissue weight.

Statistical analysis

Differences between groups were determined using unpaired two-tailed Student's tests with the SPSS 20.0 software package for Windows (SPSS, Chicago, United States). Probability values less than 0.05 were considered statistically significant. Data are presented as mean ± SEM.

RESULTS

BAT selectively takes up fatty acids from TRL-mimicking particles at 21°C

To study the mode of FA uptake by BAT, we generated [^{3}H]TO and [^{14}C]CO double-labeled TRL-mimicking particles with a diameter of 45, 80 and 150 nm *(i.e.* representing small VLDL, large VLDL and chylomicrons). These particles allow us to follow the uptake of FA ([^{3}H]oleate) and the remnant core ([^{14}C]CO]) simultaneously. The clearance and distribution of the radiolabels was determined in mice that were exposed to regular room temperature (21°C), cold (7°C) or thermoneutrality (28°C) prior to the kinetic experiment.

In mice exposed at the regular temperature of 21°C, the plasma clearance of [^{3}H]TO was faster **(FIGURE 1A-C)** than that of [^{14}C]CO **(FIGURE 1D-F)**, for particles of 45, 80 and 150 nm, respectively. This indicates that for all particles the uptake of FA by organs precedes the uptake of CO, suggestive of initial peripheral LPL-mediated TG hydrolysis followed by the uptake of core remnants by the liver. Indeed, in metabolic tissues that express LPL (i.e., muscle, WAT and BAT) the uptake of ^{3}H-activity **(FIGURE 2A-C)** was higher than that of ^{14}C-activity

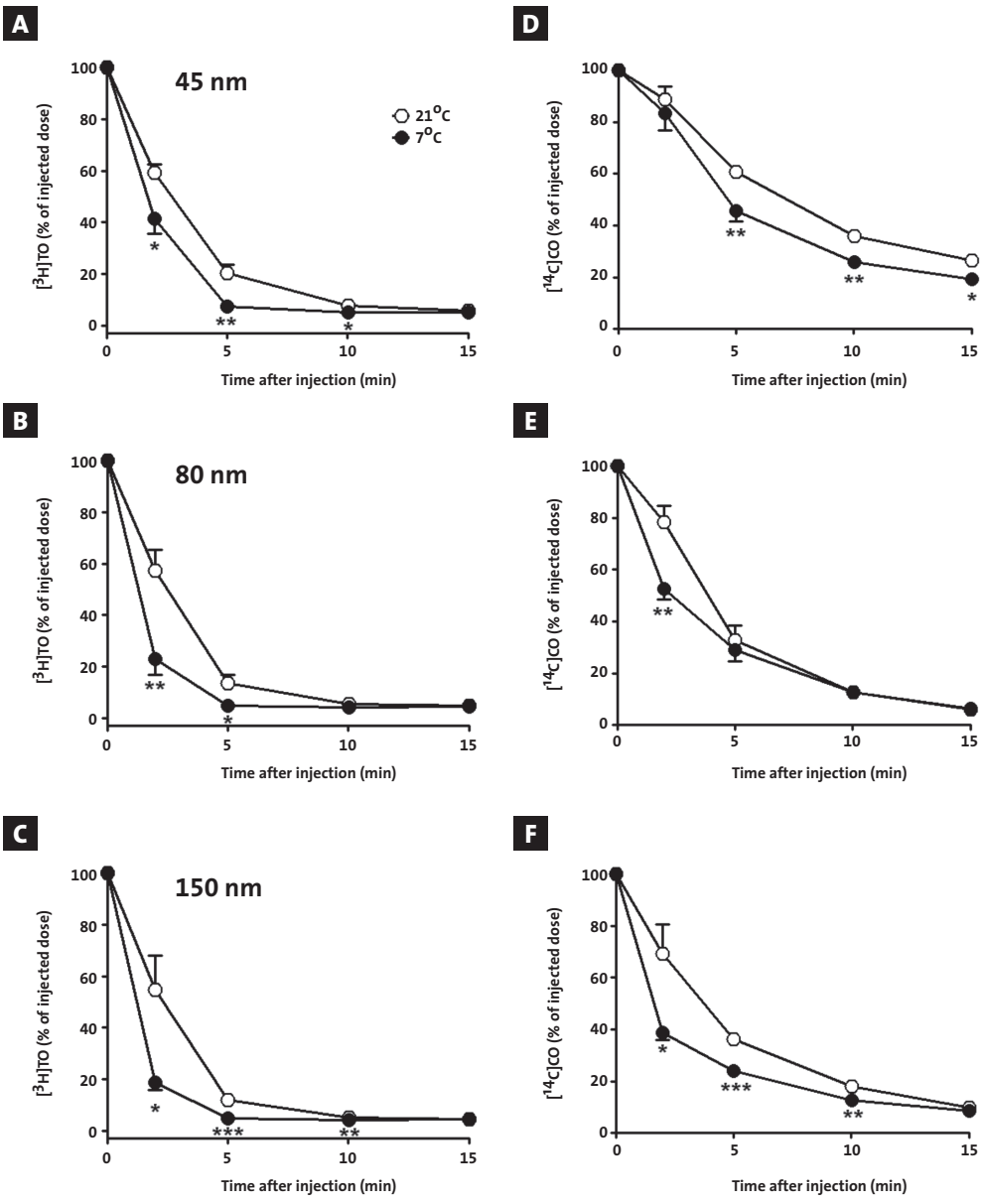

FIGURE 1 - Cold exposure enhances serum clearance of double-labeled TRL-mimicking particles. Glycerol tri[^{3}H]oleate ([^{3}H]TO) and [^{14}C]cholesteryl oleate ([^{14}C]CO) labeled TRL-mimicking particles of different size (45, 80 and 150 nm) were injected intravenously into 4-hour fasted mice that had been exposed to an ambient temperature of 21°C (open symbols) or 7°C (closed symbols) for 24 h prior to the experiment. Blood was collected at the indicated time points and [^{3}H]TO activity **A-C** as well as [^{14}C]CO activity **D-F** were measured in plasma.

Values are means ± SEM (n=6) *P<0.05, **P<0.01, ***P<0.001 compared to the 21°C group. *TRL*, triglyceride-rich lipoprotein.

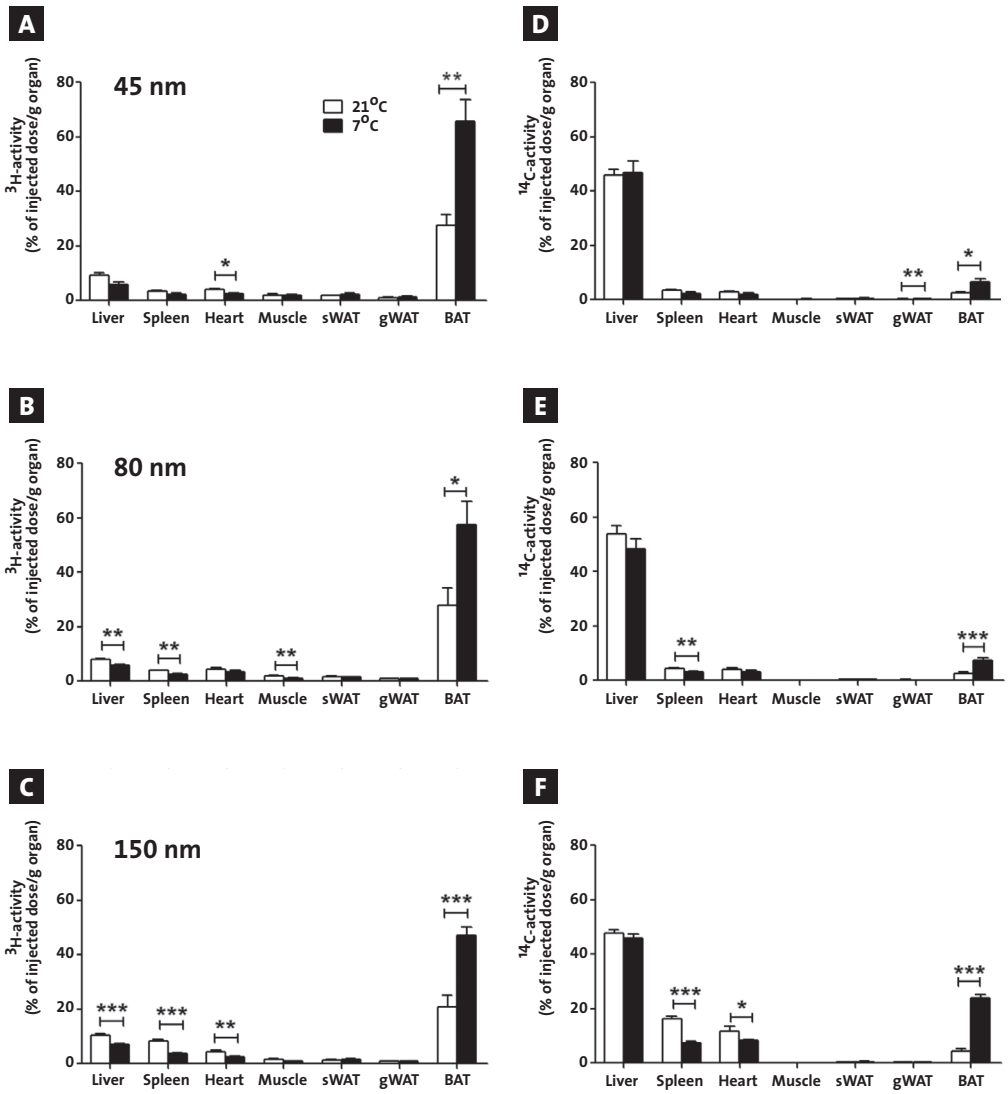

FIGURE 2 - Cold exposure enhances fatty acid uptake from double-labeled TRL-mimicking particles by BAT. Glycerol tri[^{3}H]oleate ([^{3}H]TO) and [^{14}C]cholesteryl oleate ([^{14}C]CO) labeled TRL-mimicking particles of different size (45, 80 and 150 nm) were injected intravenously into 4-hour fasted mice that had been exposed to an ambient temperature of 21°C (open symbols) or 7°C (closed symbols) for 24 h prior to the experiment. After 15 min, mice were sacrificed and uptake of [^{3}H]TO-derived activity **A-C** and [^{14}C]CO activity **D-F** was determined in various organs, and expressed as percentage of the injected dose per gram wet tissue weight.

Values are means ± SEM (n=6) *P<0.05, **P<0.01, ***P<0.001 compared to the 21°C group. BAT, brown adipose tissue; *TRL*, triglyceride-rich lipoprotein; *(s,g)WAT*, subcutaneous, gonadal white adipose tissue.

(FIGURE 2D-F), whereas the uptake of ^{14}C-activity by the liver was much higher than that of ^{3}H-activity. Remarkably, the uptake of ^{3}H-activity by BAT exceeded that of all other organs, and was much higher (28, 28, and 20% of injected dose/g) **(FIGURE 2A-C)** than the uptake of ^{14}C-activity (2, 3 and 4% of injected dose/g) **(FIGURE 2D-F)**, indicating highly selective uptake of TG-derived FA without substantial uptake of core remnants by BAT.

Cold exposure enhances selective fatty acid uptake from TRL-mimicking particles by BAT

Housing mice for 24 h at 7°C accelerated the plasma clearance of [^{3}H]TO for particles of 45, 80 and 150 nm **(FIGURE 1A-C)**, due to a selective, markedly enhanced uptake of ^{3}H-activity by BAT (+139%, P<0.01; +111%, P<0.05, and +150%, P<0.001) **(FIGURE 2A-C)**. Accordingly, 24 h of cold exposure resulted in a -43% reduction in plasma TG levels (0.58 ± 0.05 vs. 0.33 ± 0.02, P<0.001). Likewise, the plasma decay of [^{14}C]CO was accelerated **(FIGURE 1D-F)** which was accompanied by an increased retention of ^{14}C-label by BAT (+168%, P<0.05; +181%, P<0.001, and +464%, P<0.001) **(FIGURE 2D-F)**. Despite the increased retention of ^{14}C-label in BAT, the selectivity of uptake of ^{3}H-label over ^{14}C-label was still retained, especially for the 45 and 80 nm sized particles. In fact, the majority of [^{3}H]TO-depleted [^{14}C]CO-containing core remnants were still taken up by the liver **(FIGURE 2)**. In contrast, [^{14}C]CO uptake by BAT was low for both the 45 nm particle (2% per g and 6% per g for 21°C and 7°C, respectively) and the 80 nm particle (3% per g and 7% per g for 21°C and 7°C, respectively) **(FIGURE 2)**, pointing to selective FA uptake by BAT with minimal remnant particle retention.

As a measure for the selective retention of FA versus core remnants, we calculated the lipolysis index for all organs as the ratio of ^{3}H-activity (%/g) and ^{14}C-activity (%/g) **(FIGURE 3)**. This index indicates whether the organs primarily take up TG-depleted particles (lipolysis index < 1), unmodified particles (lipolysis index = 1), or FA derived from particles (lipolysis index > 1). For particles of 45, 80 and 150 nm, the lipolysis index of the liver was far below 1, confirming its primary role in the uptake of core remnants. Albeit that the uptake by the spleen increased with particle size, the lipolysis index approximated 1 for all particle sizes, consistent with its recognized involvement in uptake of whole particles through phagocytosis (10;11). For all particles sizes, the lipolysis index of classical organs involved in the selective uptake of lipoprotein TG-derived FA (i.e., skeletal muscle, WAT) exceeded 1, consistent with highly selective uptake of FA over CO. In analogy, BAT showed a similarly high lipolysis index for particles of all sizes. The lipolysis index of BAT for the 150 nm-sized particles was lower than that of the 45 nm and 80 nm-sized particles, but this was also found for skeletal muscle and WAT. Thus, these data suggest that TG-derived FA from different sized TRLs (ranging from small VLDL to small chylomicrons) are taken up by skeletal muscle, WAT and BAT mainly by selective FA uptake.

The lipolysis index did not differ much between housing at 21°C and 7°C. For particles of all sizes, the lipolysis index in the liver was lower upon cold exposure, indicating internalization of remnants after further TG depletion. Cold exposure reduced the lipolysis index in muscle and BAT with respect to uptake of the 150 nm-sized particles, indicating relatively more retention and/or uptake of the particle core compared to 21°C.

Exposure to thermoneutral temperature lowers selective fatty acid uptake from TRL-mimicking particles by BAT

To investigate the mode of VLDL and chylomicron-derived FA uptake by BAT in case of reduced sympathetic input towards BAT (2), we repeated the clearance experiments with double-labeled TRL-mimicking particles of all sizes in mice that were exposed to regular room temperature (21°C) versus thermoneutrality (28°C) for 4 hours prior to the experiment. For particles of 45, 80 and 150 nm, plasma [^{3}H]TO clearance was attenuated at 28°C **(FIGURE 4A-C)**, mainly due to lower uptake of ^{3}H-activity by BAT (-66%, P<0.01, -74%, P<0.01 and -76%, P<0.001, respectively) **(FIGURE 4D-F)**. Accordingly, 4 h of thermoneutrality increased plasma

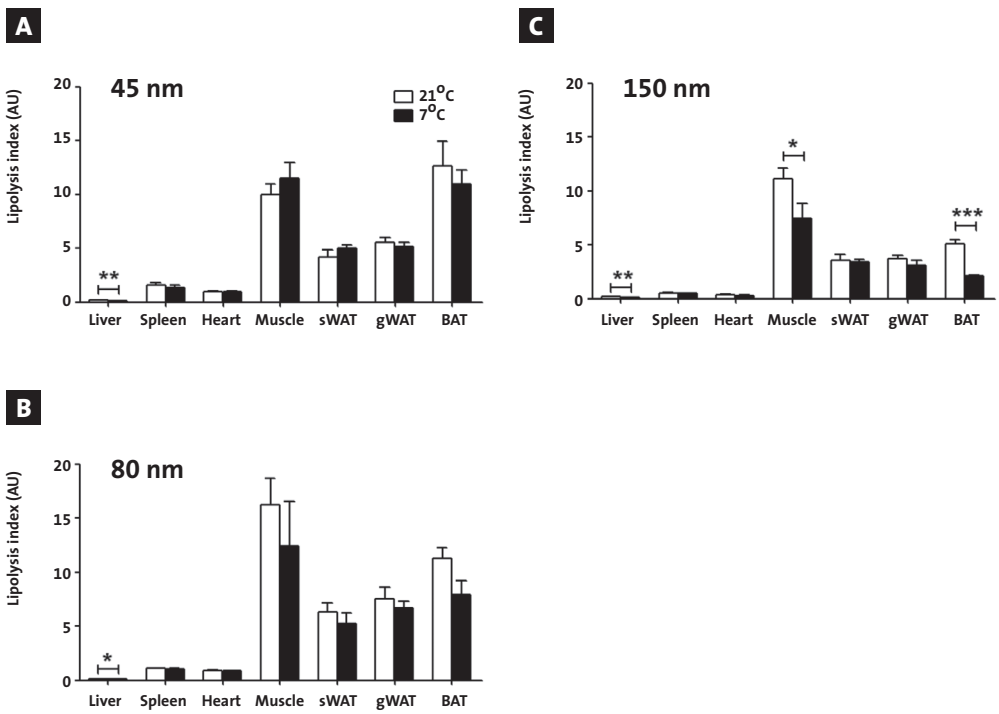

FIGURE 3 - Lipolysis index in muscle, WAT and BAT points to selective FA uptake at 21°C and 7°C. Glycerol tri[^{3}H]oleate ([^{3}H]TO) and [^{14}C]cholesteryl oleate ([^{14}C]CO) labeled TRL-mimicking particles of different size (45, 80 and 150 nm) were injected intravenously into 4-hour fasted mice that had been exposed to an ambient temperature of 21°C (open symbols) or 7°C (closed symbols) for 24 h prior to the experiment. After 15 min, mice were sacrificed and uptake of [3H]TO-derived activity and [^{14}C]CO activity was determined in various organs, and expressed as percentage of the injected dose per gram wet tissue weight. Lipolysis index was calculated for all organs as the ratio of ^{3}H-activity (%/g) and ^{14}C-activity (%/g) for particles of 45 nm **A**, 80 nm **B** and 150 nm **C**.

Values are means ± SEM (n=6) *P<0.05, **P<0.01, ***P<0.001 compared to the 21°C group. *BAT*, brown adipose tissue; *TRL*, triglyceride-rich lipoprotein; *(s,g)WAT*, subcutaneous, gonadal white adipose tissue.

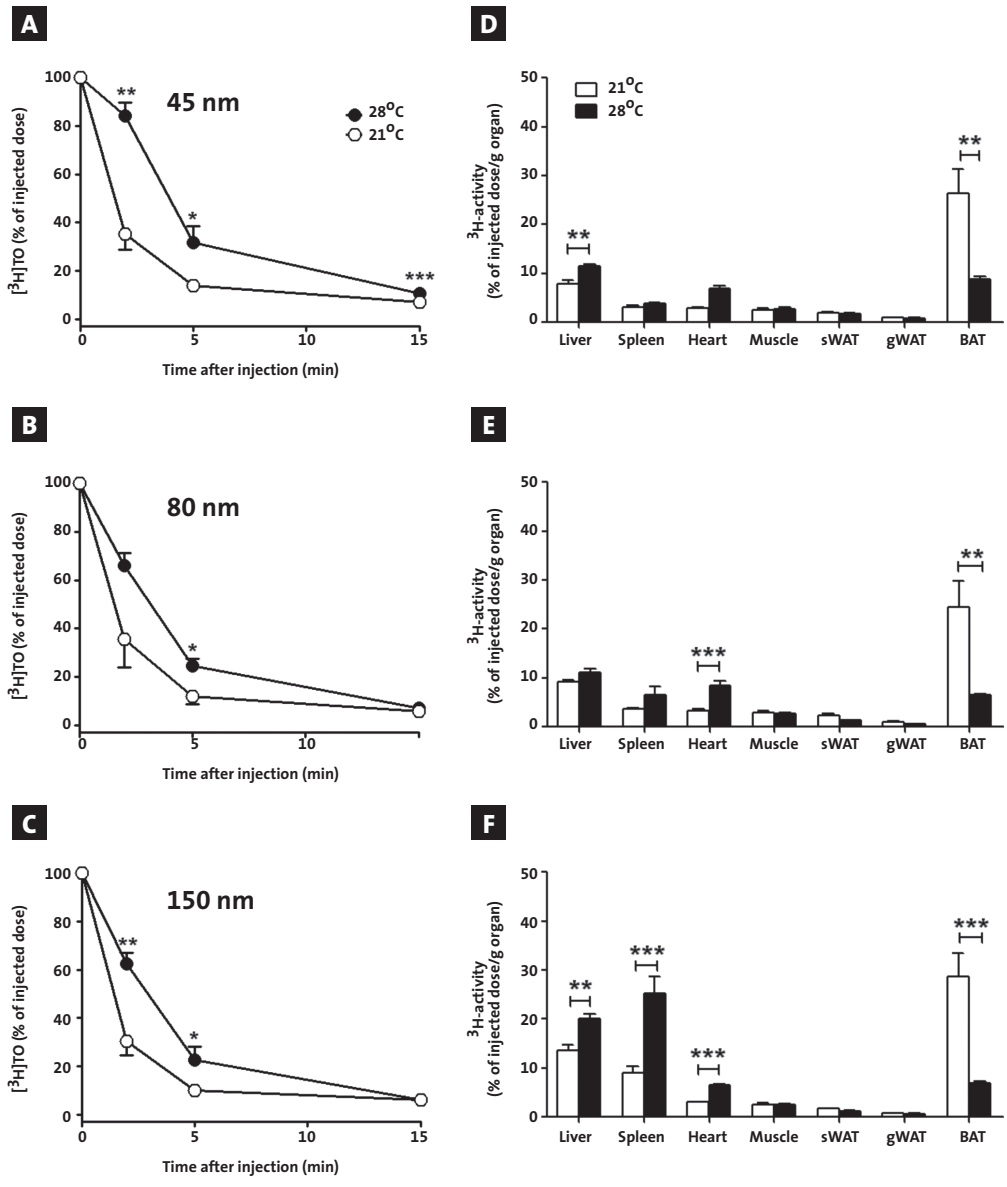

FIGURE 4 - Thermoneutrality attenuates serum [^{3}H]TO clearance of double-labeled TRL-mimicking particles accompanied by lower uptake of [^{3}H]TO-derived activity by BAT. Glycerol tri[^{3}H]oleate ([^{3}H]TO) and [^{14}C] cholesteryl oleate ([^{14}C]CO) labeled TRL-mimicking particles of different size (45, 80 and 150 nm) were injected intravenously into 4-hour fasted mice that had been exposed to an ambient temperature of 21°C (open symbols) or 28°C (closed symbols) for 4 h prior to the experiment. Blood was collected at the indicated time points and [^{3}H]TO activity was measured in plasma **A-C**. In addition, uptake of [^{3}H]TO-derived activity was determined in various organs, and expressed as percentage of the injected dose per gram wet tissue weight **D-F**.

Values are means ± SEM (n=6) *P<0.05, **P<0.01, ***P<0.001 compared to the 21°C group. *BAT*, brown adipose tissue; *TRL*, triglyceride-rich lipoprotein; *(s,g)WAT*, subcutaneous, gonadal white adipose tissue.

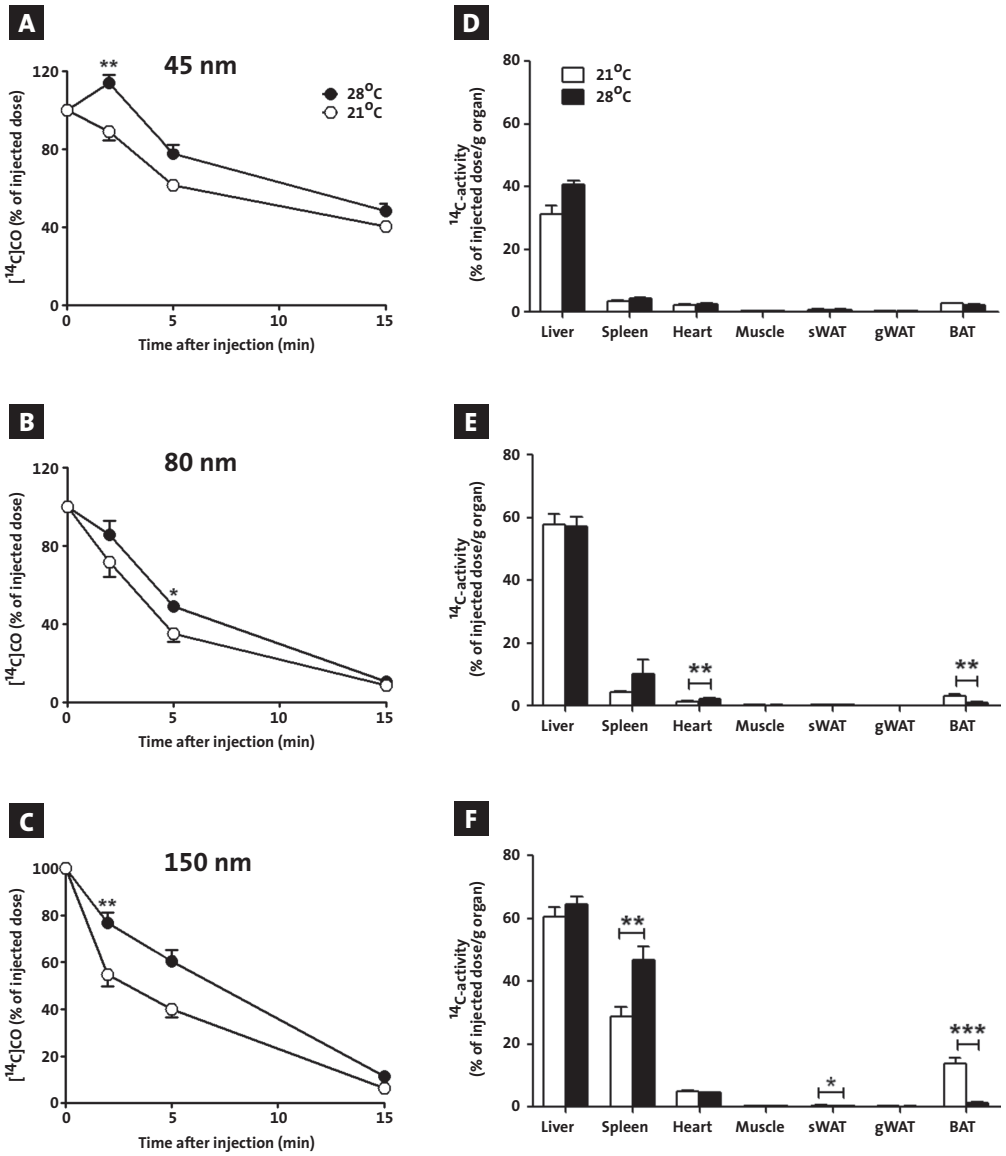

FIGURE 5 - Thermoneutrality attenuates serum [^{14}C]CO clearance of double-labeled TRL-mimicking particles accompanied by lower [^{14}C]CO uptake by BAT. Glycerol tri[^{3}H]oleate ([^{3}H]TO) and [^{14}C]cholesteryl oleate ([^{14}C]CO) labeled TRL-mimicking particles of different size (45, 80 and 150 nm) were injected intravenously into 4-hour fasted mice that had been exposed to an ambient temperature of 21°C (open symbols) or 28°C (closed symbols) for 4 h prior to the experiment. Blood was collected at the indicated time points and [^{14}C]CO activity was measured in plasma **A-C**. In addition, uptake of [^{14}C]CO-derived radioactivity was determined in various organs, and expressed as percentage of the injected dose per gram wet tissue weight **D-F**.

Values are means ± SEM (n=6) *P<0.05, **P<0.01, ***P<0.001 compared to the 21°C group. *BAT*, brown adipose tissue; *TRL*, triglyceride-rich lipoprotein; *(s,g)WAT*, subcutaneous, gonadal white adipose tissue.

TG levels by a marked +88% (0.42 ± 0.02 vs. 0.79 ± 0.04, P<0.001). Again, plasma [^{14}C]CO clearance was slower for all particle sizes as compared to [^{3}H]TO clearance **(FIGURE 5A-C)** and the liver was the main contributor of [^{14}C]CO uptake **(FIGURE 5D-F)**. Thermoneutrality had an opposite effect on [^{14}C]CO uptake by BAT as compared to cold exposure, resulting in lower uptake and a lipolysis index comparable to WAT and muscle, even for the 150 nm sized particle. In addition, thermoneutrality enhanced [^{3}H]oleate uptake by liver, resulting in an increase in lipolysis index. Thus, these data demonstrate that, also at thermoneutral temperature, TRL-derived FA from different sized TRLs are taken up through selective FA uptake by BAT.

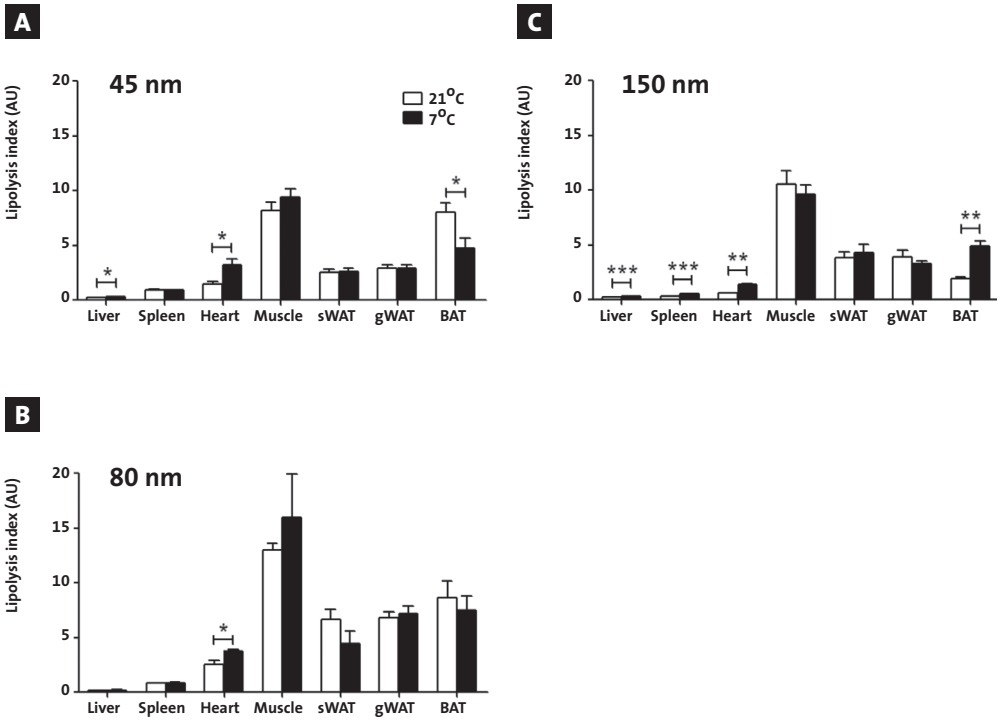

FIGURE 6 - Lipolysis index in muscle, WAT and BAT points to selective FA uptake at thermoneutrality. Glycerol tri[^{3}H]oleate ([^{3}H]TO) and [^{14}C]cholesteryl oleate ([^{14}C]CO) labeled TRL-mimicking particles of different size (45, 80 and 150 nm) were injected intravenously into 4-hour fasted mice that had been exposed to an ambient temperature of 21°C (open symbols) or 28°C (closed symbols) for 4 h prior to the experiment. After 15 min, mice were sacrificed and uptake of [^{3}H]TO-derived radioactivity and [^{14}C]CO radioactivity was determined in various organs, and expressed as percentage of the injected dose per gram wet tissue weight. Lipolysis index was calculated for all organs as the ratio of ^{3}H-activity (%/g) and ^{14}C-activity (%/g) for particles of 45 nm **A**, 80 nm **B** and 150 nm **C**.

Values are means ± SEM (n=6) *P<0.05, **P<0.01, ***P<0.001 compared to the 21°C group. *BAT*, brown adipose tissue; *TRL*, triglyceride-rich lipoprotein; *(s,g)WAT*, subcutaneous, gonadal white adipose tissue.

DISCUSSION

BAT has recently been identified as a major player in TG metabolism (5), but the mechanism by which BAT takes up FA from TG-rich VLDL and chylomicrons had not been fully established yet. In the present study, by performing kinetic studies with [^{3}H]TO and [^{14}C]CO double-labeled TRL-mimicking particles of different size (ranging from VLDL to chylomicrons), we provide strong evidence that BAT takes up FA by selective delipidation of the TRL, followed by uptake of the remnant particle by the liver. This mechanism is independent of environmental temperature, as it was evident at thermoneutrality, room temperature as well as after cold induction.

Lipoprotein lipase (LPL), expressed on endothelial cells of the capillary bed of metabolically active tissues, is crucially involved in hydrolysis of TG-rich lipoproteins, resulting in release of FA and subsequent uptake by the adjacent tissue (12). Cellular uptake of FA is mediated by various cell surface receptors, including FA transport proteins and CD36 (13). BAT activation has repeatedly been shown to result in massive enhancement of LPL activity as well as increased CD36 expression (5;6). In fact, the LPL/CD36 route is required for TRL-derived FA uptake by BAT as inhibition of local LPL activity in BAT through injection of tetrahydrolipstatin abolished uptake of [3H]oleate and CD36-/- mice show cold intolerance due to inability to take up FA by BAT (5). Therefore, it would make physiological sense if in BAT, as in muscle and WAT, VLDL and chylomicron-derived TG are taken up after LPL-mediated delipidation of the particle, resulting in the generation of core remnants that can subsequently been taken up by the liver.

Besides for muscle and WAT, the present study supports that this mechanism also holds true for BAT, as we found high uptake of [^{3}H]TO-derived activity and low [^{14}C]CO uptake in BAT following injection of emulsion particles with sizes ranging from VLDL to chylomicrons. Accordingly, lipolysis indices in BAT were high as compared to liver and comparable to those found in WAT and muscle. As these results were found both at thermoneutrality, room temperature and upon cold exposure, it is suggested that the mode of TRL-derived FA uptake is independent of BAT activation status. Accordingly, a study by Laplante et al (6) showed that BAT activation by means of PPARγ agonism resulted in enhanced uptake of [^{3}H] oleate from VLDL-like emulsion particles. However, as no non-releasable core label was used in their study, no definitive statements could be made on whether the uptake truly represented selective FA uptake. However, in their study [^{3}H]oleate uptake in BAT highly correlated with the enhanced LPL activity that occurred in the tissue, suggesting that clearance of VLDL-TG and uptake of the radiolabeled FA was mainly determined by LPL-mediated hydrolysis of TG.

A remarkable finding of the present study was that the uptake of ^{3}H-activity per gram organ was higher in BAT as compared to all other organs. This supports the importance of BAT in TG metabolism even at normal room temperature. Considering the uncovered mechanism of FA uptake by BAT, this may suggest that LPL activity and/or CD36 expression in BAT exceeds that of other metabolic organs, such as WAT. Future studies are needed to confirm this hypothesis.

Furthermore, upon cold exposure we found somewhat higher ^{14}C-activity in BAT after injection of the 150 nm sized TRL-mimicking particles as compared to the smaller (45 and 80 nm) VLDL-like particles. This is in line with the previous study of Bartelt et al (5) in which retention of chylomicron-like particles of ~250 nm was found in BAT. This may suggest that chylomicron-like particles remain bound to the capillaries in BAT during lipolysis. On the underlying mechanism for the specific retention of larger particles we can only speculate. As larger chylomicron-like particles have a higher surface area than VLDL-like particles through which they can bind to heparan sulfate proteoglycans on endothelial cells through electrostatic interactions, the avidity for binding may be higher than for smaller particles. It could be hypothesized that cold induction further enhances HSPG expression on endothelium to further maximize interaction of the TG-rich particles with LPL resulting in enhanced lipolysis. This may thus be an efficient mechanism to maximize FA uptake by BAT. Future studies should focus on elucidating this mechanism, for instance by measuring HSPG expression in BAT upon cold exposure.

The magnitude of the TG clearance capacity of BAT became clear only recently when Bartelt et al (5) demonstrated that mice that are housed at 4°C for 24 h show a massive lowering of plasma TG levels. These data are in full accordance with the present study in which we found that cold exposure for 24 h resulted in 43% reduction in plasma TG levels. The findings that metabolically active BAT stores exist in adult humans (14-16) and that BAT volume and activity are lower in obese subjects (15), have increased interest in the therapeutic potential of BAT to combat obesity and related disorders, such as dyslipidemia. Also in humans, BAT likely substantially contributes to TG metabolism. In a recent study by Ouellet et al (17), human subjects were cooled for 2 h followed by infusion of the FA tracer ^{18}F-fluoro-thiaheptadecanoic acid (^{18}F-FTHA) and performance of a PET-CT scan. Indeed, cold exposure enhanced FA uptake by BAT as compared to muscle and WAT. Based on our studies, it is likely that human BAT also utilizes FA from circulating lipoproteins, though this has not been investigated yet.

In conclusion, we show that, in mice, BAT takes up lipoprotein-derived FA by means of selective FA uptake rather than uptake of lipoproteins. Future studies should elucidate whether this is also the primary mechanism of FA uptake by BAT in humans.

REFERENCES

1 van Marken Lichtenbelt WD, Schrauwen P. Implications of nonshivering thermogenesis for energy balance regulation in humans. Am J Physiol Regul Integr Comp Physiol 2011; 301: R285-R296.

2 Cannon B, Nedergaard J. Brown adipose tissue: function and physiological significance. Physiol Rev 2004; 84: 277-359.

3 Festuccia WT, Blanchard PG, Deshaies Y. Control of Brown Adipose Tissue Glucose and Lipid Metabolism by PPARgamma. Front Endocrinol (Lausanne) 2011; 2: 84.

4 Zimmermann R, Strauss JG, Haemmerle G, et al. Fat mobilization in adipose tissue is promoted by adipose triglyceride lipase. Science 2004; 306: 1383-1386.

5 Bartelt A, Bruns OT, Reimer R, et al. Brown adipose tissue activity controls triglyceride clearance. Nat Med 2011; 17: 200-205.

6 Laplante M, Festuccia WT, Soucy G, et al. Tissue-specific postprandial clearance is the major determinant of PPARgamma-induced triglyceride lowering in the rat. Am J Physiol Regul Integr Comp Physiol 2009; 296: R57-R66.

7 Rensen PC, Herijgers N, Netscher MH, et al. Particle size determines the specificity of apolipoprotein E-containing triglyceride-rich emulsions for the LDL receptor versus hepatic remnant receptor in vivo. J Lipid Res 1997; 38: 1070-1084.

8 Rensen PC, van Dijk MC, Havenaar EC, et al. Selective liver targeting of antivirals by recombinant chylomicrons--a new therapeutic approach to hepatitis B. Nat Med 1995; 1: 221-225.

9 Jong MC, Rensen PC, Dahlmans VE, et al. Apolipoprotein C-III deficiency accelerates triglyceride hydrolysis by lipoprotein lipase in wild-type and apoE knockout mice. J Lipid Res 2001; 42: 1578-1585.

10 Hultin M, Carneheim C, Rosenqvist K, et al. Intravenous lipid emulsions: removal mechanisms as compared to chylomicrons. J Lipid Res 1995; 36: 2174-2184.

11 Hussain MM, Mahley RW, Boyles JK, et al. Chylomicron-chylomicron remnant clearance by liver and bone marrow in rabbits. Factors that modify tissue-specific uptake. J Biol Chem 1989; 264: 9571-9582.

12 Geerling JJ, Boon MR, Kooijman S, et al. Sympathetic nervous system control of triglyceride metabolism: novel concepts derived from recent studies. J Lipid Res 2013, in press.

13 Glatz JF, Luiken JJ, Bonen A. Membrane fatty acid transporters as regulators of lipid metabolism: implications for metabolic disease. Physiol Rev 2010; 90: 367-417.

14 Cypess AM, Lehman S, Williams G, et al. Identification and importance of brown adipose tissue in adult humans. N Engl J Med 2009; 360: 1509-1517.

15 van Marken Lichtenbelt WD, Vanhommerig JW, Smulders NM, et al. Cold-activated brown adipose tissue in healthy men. N Engl J Med 2009; 360: 1500-1508.

16 Virtanen KA, Lidell ME, Orava J, et al. Functional brown adipose tissue in healthy adults. N Engl J Med 2009; 360: 1518-1525.

17 Ouellet V, Labbe SM, Blondin DP, et al. Brown adipose tissue oxidative metabolism contributes to energy expenditure during acute cold exposure in humans. J Clin Invest 2012; 122: 545-552.

BMP7 ACTIVATES BROWN ADIPOSE TISSUE AND REDUCES DIET-INDUCED OBESITY ONLY AT SUBTHERMONEUTRALITY

MARIËTTE R. BOON
SJOERD A.A. VAN DEN BERG
YANAN WANG
JAN VAN DEN BOSSCHE
SOFIA KARKAMPOUNA
MATTHIAS BAUWENS
MARIJKE DE SAINT-HUBERT
GEERTJE VAN DE HORST
SLOBODAN VUKICEVIC
MENNO P.J. DE WINTHER
LOUIS M. HAVEKES
J. WOUTER JUKEMA
JOUKE T. TAMSMA
GABRI VAN DER PLUIJM
KO WILLEMS VAN DIJK
PATRICK C.N. RENSEN

PLoS One 2013; 8:e74083.

ABBREVATIONS

ATGL	Adipose triglyceride lipase
BAT	Brown adipose tissue
BMP7	Bone morphogenetic protein 7
DEXA	Dual-energy X-ray absorptiometry
EE	Energy expenditure
FDG	Fluorodeoxyglucose
HSL	Hormone-sensitive lipase
LPL	Lipoprotein lipase
PET	Positron emission tomography
Q-RT-PCR	Quantitative real-time PCR
TC	Total cholesterol
TG	Triglyceride
UCP-1	Uncoupling protein-1
WAT	White adipose tissue

ABSTRACT

Brown adipose tissue (BAT) dissipates energy stored in triglycerides as heat via the uncoupling protein UCP-1 and is a promising target to combat hyperlipidemia and obesity. BAT is densely innervated by the sympathetic nervous system, which increases BAT differentiation and activity upon cold exposure. Recently, Bone Morphogenetic Protein 7 (BMP7) was identified as an inducer of BAT differentiation. We aimed to elucidate the role of sympathetic activation in the effect of BMP7 on BAT by treating mice with BMP7 at varying ambient temperature, and assessed the therapeutic potential of BMP7 in combating obesity. High-fat diet fed lean C57Bl6/J mice were treated with BMP7 via subcutaneous osmotic minipumps for 4 weeks at 21°C or 28°C, the latter being a thermoneutral temperature in which sympathetic activation of BAT is largely diminished. At 21°C, BMP7 increased BAT weight, increased the expression of Ucp1, Cd36 and hormone-sensitive lipase in BAT, and increased total energy expenditure. BMP7 treatment markedly increased food intake without affecting physical activity. Despite that, BMP7 diminished white adipose tissue (WAT) mass, accompanied by increased expression of genes related to intracellular lipolysis in WAT. All these effects were blunted at 28°C. Additionally, BMP7 resulted in extensive 'browning' of WAT, as evidenced by increased expression of BAT markers and the appearance of whole clusters of brown adipocytes via immunohistochemistry, independent of environmental temperature. Treatment of diet-induced obese C57Bl6/J mice with BMP7 led to an improved metabolic phenotype, consisting of a decreased fat mass and liver lipids as well as attenuated dyslipidemia and hyperglycemia. In conclusion, together, these data show that BMP7-mediated recruitment and activation of BAT only occurs at subthermoneutral temperature, and is thus likely dependent on sympathetic activation of BAT, and that BMP7 may be a promising tool to combat obesity and associated disorders.

INTRODUCTION

Human adipose tissue is broadly classified as either white adipose tissue (WAT) or brown adipose tissue (BAT). WAT functions as an energy storage depot characterized by a large intracellular lipid droplet per adipocyte and is furthermore a prominent endocrine organ, producing hormones that regulate appetite and satiety (1). In contrast, BAT is an energy dissipation depot characterized by multi-locular lipid droplets per adipocyte and a wealth of densely packed mitochondria. Uncoupling protein-1 (UCP-1) in these mitochondria uncouples respiration from ATP synthesis, leading to heat production (2).

The most well-known trigger for activation of BAT is cold, which increases sympathetic outflow from the hypothalamic temperature centre towards BAT, leading to release of noradrenalin and increased thermogenesis. Recently, a second alternative pathway was demonstrated to control thermogenesis, in which alternatively activated (M2) macrophages release noradrenalin to activate BAT locally (3).

Fatty acids are an important substrate for BAT thermogenesis. The fatty acids originate from triglyceride (TG)-rich lipoproteins and are released upon local lipoprotein lipase (LPL) activity (4). Mouse studies have shown that BAT has a great clearance capacity for TG. Cold exposure drastically accelerates plasma TG clearance as a result of increased uptake into BAT and thereby corrects hyperlipidemia in pathophysiological settings (5).

The recent findings that metabolically active BAT stores exist in adult humans and that BAT volume and activity are lower in obese subjects (6-8), have increased interest in the therapeutic potential of BAT to combat obesity and related disorders, such as dyslipidemia. In both rodents and humans, brown adipocytes are present in well-localized fat pads, as well as scattered in other tissues, such as WAT and muscle, there forming a 'peripheral' pool of brown adipocytes (9). The latter are also called 'brite' cells because their phenotypic characteristics lie between those of white and brown adipocytes (10). Mouse studies demonstrate that cold exposure and other triggers like PPARγ agonism induce bright cell formation (11-13). Identification of signalling pathways that regulate differentiation of the two types of brown adipocytes could lead to the development of novel therapies for obesity and related disorders.

Bone Morphogenetic Protein 7 (BMP7) is an important inducer of brown adipocyte differentiation. *In vitro* treatment of a variety of precursor cells, such as C3H10T1/2 mesenchymal cells and Myf5+ precursor cells, with BMP7 resulted in the development of fully differentiated brown adipocytes with high UCP-1 expression (14, 15). Moreover, short-term adenoviral overexpression of BMP7 in different mouse models confirmed the ability of BMP7 to increase interscapular brown fat mass and oxygen consumption (14). However, the potential of BMP7 to induce BAT activity in a more therapeutic regimen is currently unknown. Moreover, the role of ambient temperature in the effects of BMP7 on brown fat function and energy metabolism, and the therapeutic potential of BMP7 to treat dyslipidemia and obesity has not been reported yet.

Therefore, the aim of the present study was to elucidate the role of ambient temperature, which determines the sympathetic output to BAT, in the effect of BMP7 on BAT and

to asses the therapeutic potential of BMP7 in combating obesity and related disorders. We show here that treatment of C57Bl6/J mice with BMP7 via osmotic minipumps for 4 weeks effectively increased BAT differentiation, BAT activity and total energy expenditure, and decreased white fat mass. These effects were blunted at 28°C (thermoneutral temperature) and are thus likely dependent on the degree of sympathetic activation. Furthermore, BMP7 markedly enhanced brite cell formation in WAT independent of environmental temperature. Of note, treatment of diet-induced obese C57Bl6/J mice with BMP7 diminished fat mass and liver lipid content and attenuated dyslipidemia and hyperglycemia. Together, our results show that that low subthermoneutral ambient temperature, at which sympathetic activation is present, is required for BMP7-mediated recruitment and activation of BAT and suggest that BMP7 may be a therapeutic tool to ameliorate obesity, and related disorders.

RESEARCH DESIGN AND METHODS

Animals

Male C57Bl/6J mice (Jackson Laboratory, Bar Harbor, ME) were housed in conventional cages with a 12:12-h light-dark cycle and had free access to food and water. All animal experiments were approved by the institutional ethics committee on animal care and experimentation at Leiden University Medical Center.

Mechanistic studies on the effect of BMP7 on BAT

4-week old C57Bl/6J mice were randomized according to their body weight and plasma triglyceride (TG) and total cholesterol (TC) levels into 6 groups (n=9). Mice were housed at 21°C or at 28°C (i.e. thermoneutral temperature) and received soluble recombinant BMP7 (obtained from the Vukicevic lab, Zagreb, Croatia) (33 µg/kg/day or 100 µg/kg/day) or vehicle (saline) for 4 weeks while being fed a high-fat diet (45% energy as lard, D12451, Research Diet Services). BMP7 or saline was administered at a constant rate via an osmotic minipump (model 1004, Alzet DURECT Corp), which was implanted subcutaneously in the left back region. Mice were weighed twice a week.

^{18}F-FDG PET scans

After 7 days of treatment, mice underwent an ^{18}F-fluorodeoxyglucose (FDG) positron emission tomography (PET) scan to quantify the metabolic volume of different BAT depots (interscapular, neck and back). After 2 h fasting, mice were anesthetized using isoflurane and i.p. injected with ^{18}F-FDG (20 MBq). Then, mice were allowed to awake, and were placed in their cage for 1 h (phase of tracer uptake). Scans were performed with the microPET system (uPET Focus 120, Siemens). Data for accumulation of ^{18}F-FDG on the PET images were determined on the basis of radioactive counts per volume, corrected for the injected dose per gram of animal weight. A volume of interest was manually drawn around the different BAT depots, with a cut-off value of 50% of the maximum inside the volume, to determine BAT metabolic volume.

Indirect calorimetry

Indirect calorimetry was performed in fully automatic metabolic cages (LabMaster System, TSE Systems, Bad Homburg, Germany) during the fourth week of treatment. After 20 h acclimatization, oxygen uptake ($V^{\cdot} O_2$), carbon dioxide production ($V^{\cdot} CO_2$) and caloric intake were measured for 5 consecutive days. Carbohydrate and fat oxidation rates were calculated from V˙ O2 and V˙ CO2 as described previously (16). Total energy expenditure (EE) was calculated from the sum of carbohydrate and fat oxidation. Physical activity was measured using infrared sensor frames.

RNA isolation and Q-RT-PCR analysis

Total RNA was isolated with the Nucleospin® RNA II Kit (Macherey-Nagel) according to the manufacturer's instructions. 1 µg of total RNA was reverse-transcribed with iScript cDNA synthesis kit (Bio-Rad), and the obtained cDNA was purified with Nucleospin Extract II kit (Macherey-Nagel). Real-time PCR was carried out on the IQ5 PCR machine (Bio-Rad) using the Sensimix SYBR Green RT-PCR mix (Quantace). Melt curve analysis was included to assure a single PCR product was formed. Expression levels were normalized using *ß2-microglobulin* and *36b4* as housekeeping genes. Primer sequences are listed in **TABLE 1**.

Histology

Interscapular BAT and gonadal WAT were removed and fixed directly in 4% paraformaldehyde, dehydrated and embedded in paraffin. Sections (5 µm) were dewaxed in xylene, rehydrated in ethanol and treated with 3% H_2O_2 (Sigma) in absolute methanol for 30 min. Next, sections were immersed in 10 mM citrate buffer (pH=6.0), boiled for 10 min and cooled down at room temperature. Slides were blocked during 60 min with normal goat serum (1:75 in PBS) and incubated overnight at 4°C with rabbit monoclonal anti-UCP-1 antibodies (Abcam) diluted 1:300 in normal goat serum (1:75). Next, sections were incubated for 60 min with biotinylated goat α-rabbit secondary antibodies (Vector Labs) diluted 1:600 in normal goat serum (1:75). Immunostaining was amplified using Vector Laboratories Elite ABC kit (Vector Labs) and the immunoperoxidase complex was visualized with Nova Red (Vector Labs). Counterstaining was performed with Mayer's hematoxylin (1:4).

Isolation of peritoneal macrophages

Mouse peritoneal cells were collected by flushing the peritoneal cavity with 10 ml sterile ice-cold PBS, as previously described (17). Cells were centrifuged at 1,200 rpm for 5 min at 4°C and resuspended in RPMI1640 medium supplemented with 10% heat-inactivated fecal calf serum. Total leukocyte counts were determined using a Beckman Counter. Cells were plated overnight at $1x10^6$ cells/ml in 500 µl in a 24 wells plate. Cells were subsequently lysed in buffer with ß-mercaptoethanol (100:1) and RNA was isolated as described above.

Studies on BMP7 in a diet-induced obesity model

8-week old C57Bl/6J mice were fed a high-fat diet (45% energy, D12451, Research Diet Services) for 12 weeks to induce obesity. Mice were then randomized according to their body

weight and plasma TG, TC and glucose levels into groups that received soluble recombinant BMP7 (100 µg/kg/day) or vehicle (saline) for 4 weeks via subcutaneous osmotic minipumps while being fed a high-fat diet. Mice were weighed twice a week.

Dual-energy X-ray absorptiometry (DEXA) scan

After 4 weeks treatment, body composition was measured by DEXA using the Norland pDEXA Sabre X-ray Bone Densitometer. Mice were anaesthetized intraperitoneally with a combination of 6.25 mg/kg acepromazine (Alfasan), 6.25 mg/kg midazolam (Roche) and 0.31 mg/kg fentanyl (Janssen-Cilag). The total body of the mice was scanned, yet the heads were excluded from the analyses.

Plasma parameters

At baseline and after 4 weeks of treatment, plasma was obtained via tail vein bleeding after 4 h fasting and assayed for TC, TG, and phospholipids using the commercially available enzymatic kits from Roche Molecular Biochemicals. Plasma glucose levels were measured using a commercially available kit and standardized according to the instructions of the manufacturer (Instruchemie, Delfzijl, The Netherlands).

Liver lipid extraction

Lipids were extracted from livers consistent with a modified protocol from Bligh and Dyer (18). In short, a small piece of liver was homogenized in ice-cold methanol. Lipids were removed after centrifugation by adding 1,800 µl of CH_3OH-$CHCl_3$ (3:1 vol/vol) to 45 µl of homogenate. The $CHCl_3$ phase was dried and suspended in 2% Triton X-100. Hepatic triglyceride (TG), total cholesterol (TC) and phospholipid (PL) concentrations were measured using commercial kits, as explained above. Liver lipids were expressed per milligram of protein, which was determined using the BCA protein assay kit (Pierce).

***In vitro* treatment of bone-marrow derived macrophages with BMP7**

Bone marrow-derived macrophages were obtained from C57Bl6/J mice and cultured for 8 days in LCM (RPMI1640 medium, supplemented with 10% FCS and 15% L929-conditioned medium). Then, cells were rinsed with PBS, lifted with a warm Lidocain/EDTA/PBS solution, washed in RPMI1640 and plated in LCM at 10^6 cells/ml in 500 µl in a 24 wells plate. Cells were either stimulated with soluble recombinant BMP7 (8.3 nM) or vehicle for 24 hours or with BMP7 or vehicle for 18 hours + 6 hours LPS treatment (10 ng/ml). The supernatant was collected for measurement of IL-6, IL-12 and TNF by commercial ELISA (Invitrogen) and NO_2- by Griess assay, as described before (19). RNA was isolated with the Roche RNA isolation kit as described by the suppliers.

Statistical analysis

All data are represented as means ± SEM unless indicated otherwise. Data were analyzed with SPSS 17.0 using one-way ANOVA (when three groups were compared) Student T-tests (when two groups were compared) or, in case the data were not normally distributed, using

nonparametric tests. Statistical analysis for the indirect calorimetry data were performed on 12-hour averages per parameter, based on the light-dark cycle. Data were generated for the light period between 7:00 AM and 7:00 PM and for the dark period between 7:00 PM and 7:00 AM. Normality checks were performed and comparisons were made using either one-way ANOVA or nonparametric tests. Probability values less than 0.05 were considered statistically significant.

RESULTS

BMP7 increases BAT volume and UCP-1 expression at 21°C, but not at thermoneutrality

To investigate whether BMP7 administered via constant low-dose release by osmotic minipumps is capable of increasing BAT volume and activity *in vivo,* 4-week old C57Bl6/J mice (n=9 per group) were treated with BMP7 at 33 µg/kg/day, 100 µg/kg/day or saline for 4 weeks. Mice were housed at either 21°C or 28°C, the latter being a thermoneutral temperature at which sympathetic activity towards BAT is virtually absent (20). At 21°C, BMP7 significantly and dose-dependently increased interscapular BAT weight, both at 33 µg/kg/

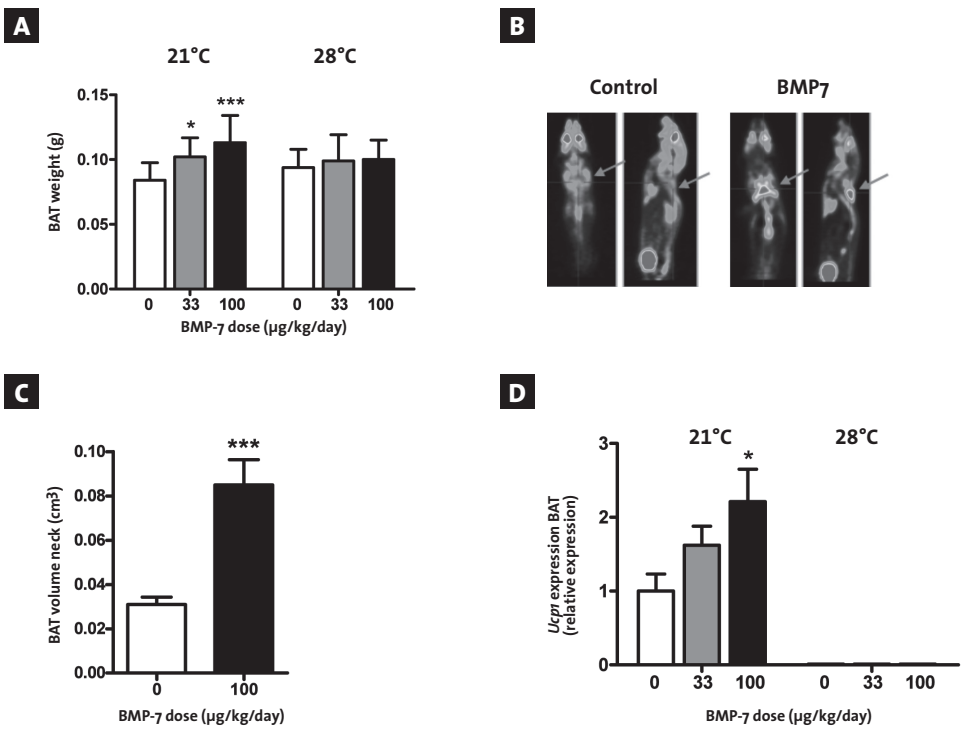

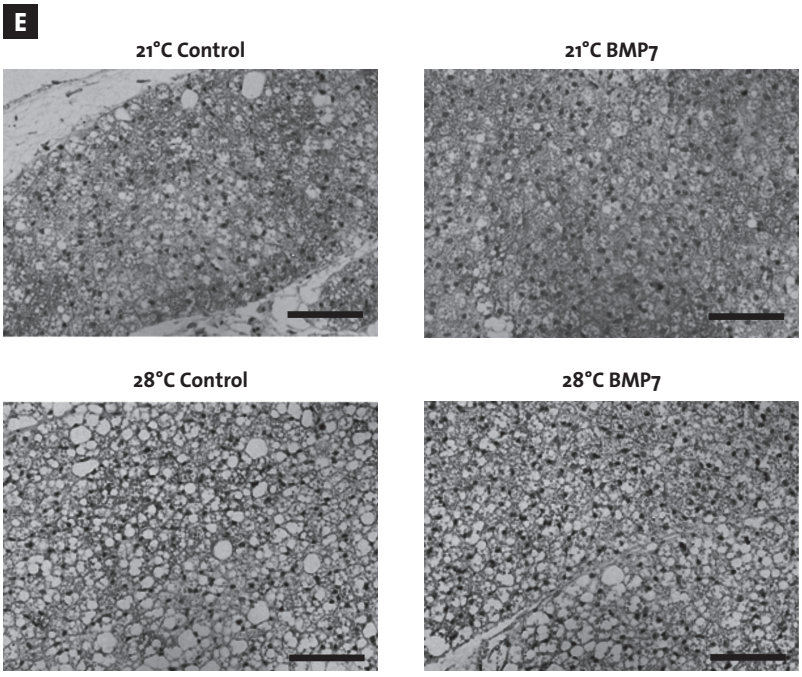

FIGURE 1 - Systemic administration of BMP7 increases BAT volume and UCP-1 expression in mice at 21°C, but not at thermoneutrality. 4-week-old C57Bl/6J mice were treated for 4 weeks with BMP7 (33 or 100 µg/kg/day) or saline via a subcutaneously located osmotic minipump at an environmental temperature of 21°C or 28°C. **A** Weight of the interscapular brown fat pads, after quantitative removal, of mice housed at 21°C (left) and 28°C (right). **B** Representative pictures of ^{18}F-FDG PET scans that were taken in control and BMP7 (100 µg/kg/day) treated animals (housed at 21°C) after one week of treatment, from which BAT metabolic volume **C** was determined. Arrows indicate neck BAT depots. **D** Expression of *Ucp1* in BAT measured by Q-RT-PCR of mice housed at 21°C (left) and 28°C (right). **E** Representative pictures of immunohistochemical UCP-1 stainings of BAT in control and BMP7 (100 µg/kg/day) treated animals housed at 21°C (top) and 28°C (bottom). Arrows point to UCP-1 positive cells.

Values are means + SEM (n=9) and expression of genes was corrected for the housekeeping genes *ß2-microglobulin* and 36b4. *P<0.05, ***P<0.001 compared to the control group.

day (+20%, P<0.05) and at 100 µg/kg/day (+30%, P<0.01), while at 28°C no effects of BMP7 were seen **(FIGURE 1A)**. ^{18}F-FDG PET-scans acquired one week after BMP7 treatment (100 µg/kg/day) in mice that were housed at 21°C, showed that BAT metabolic volume in the neck region had already increased by +175% (P<0.001, **FIGURES 1B-C)**. Furthermore, 100 µg/kg/day of BMP7 increased expression of *Ucp1* in BAT as measured by qPCR (+115%, P<0.05, **FIGURE 1D)**. and increased UCP-1 protein judged from immunohistochemistry **(FIGURE 1E)**. At 28°C, expression of *Ucp1* was markedly downregulated compared to 21°C (-97%, P<0.001), consistent with virtually absent sympathetic activity **(FIGURE 1D)**. Moreover, lipid droplet size was markedly increased, pointing to less active BAT **(FIGURE 1E)**. Importantly, at 28°C the effect of BMP7 on *Ucp1* expression was completely abolished **(FIGURES 1D-E)**.

BMP7 dose-dependently increases energy expenditure, related to increased fat oxidation at 21°C, but not at thermoneutrality

After three weeks of treatment with BMP7, whole body energy metabolism and food intake of mice was assessed with a metabolic cage system. At 21°C, BMP7 significantly and dose-dependently increased energy expenditure, fatty acid and carbohydrate oxidation (up to +45%, +37% and +26% respectively, P<0.05), while physical activity levels were unaltered **(FIGURE 2A)**. Because fatty acid and carbohydrate oxidation were both increased, respiratory exchange ratio did not change upon BMP7 treatment (data not shown). Of note, BMP7 treatment resulted in a marked increase in food intake, both at 33 µg/kg/day (+28%, P<0.05) and at 100 µg/kg/day (+37%, P<0.01) **(FIGURE 2B)**. At 28°C, these effects were fully absent **(SUPPLEMENTARY FIGURES 1A-B)**. As fatty acids are an important substrate for energy expenditure in BAT, we determined the expression of the scavenger receptor *Cd36,* hormone-sensitive lipase *(Hsl),* and adipose triglyceride lipase *(Atgl),* the latter two involved in intracellular lipolysis. At 21°C, BMP7 increased expression of *Cd36* (up to +95%, P<0.05, **FIGURE 2C)**. and *Hsl* (up to +82%, P<0.05, **FIGURE 2D)** but not of *Atgl* **(FIGURE 2E)** in BAT, suggesting increased cellular uptake of fatty acids via CD36 and liberation of intracellular fatty acids from TG via HSL for oxidation purposes. At 28°C, basal expression of *Cd36, Hsl* and *Atgl* was lower and unaffected by BMP7 **(FIGURES 2C-E).**

BMP7 decreases gonadal white fat weight and increases expression of genes related to lipolysis at 21°C, but not at thermoneutrality

Despite the increased energy expenditure, BMP7 treatment did not affect body weight development, not at thermoneutrality **(SUPPLEMENTARY FIGURE 1C)** nor at 21°C **(SUPPLEMENTARY**

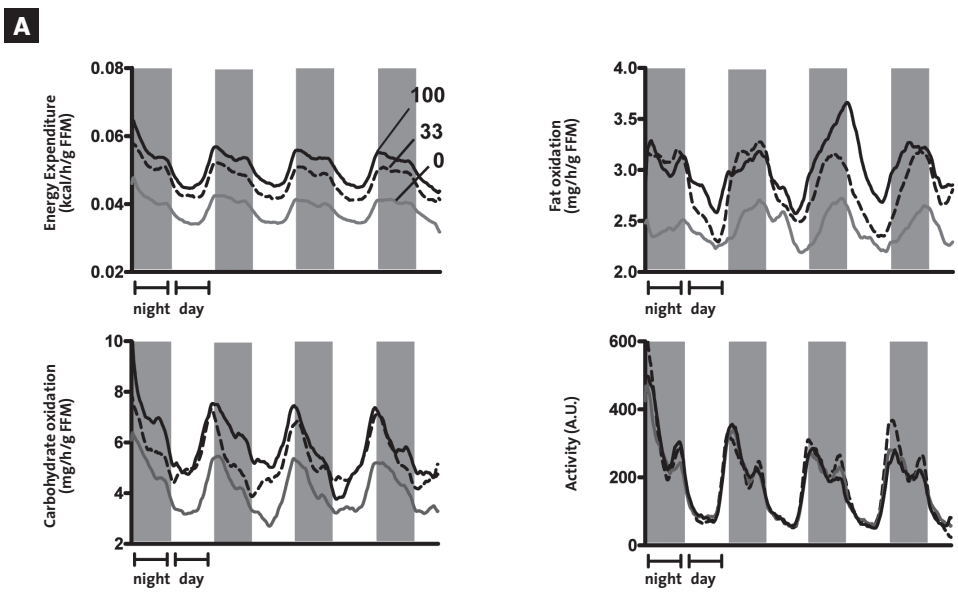

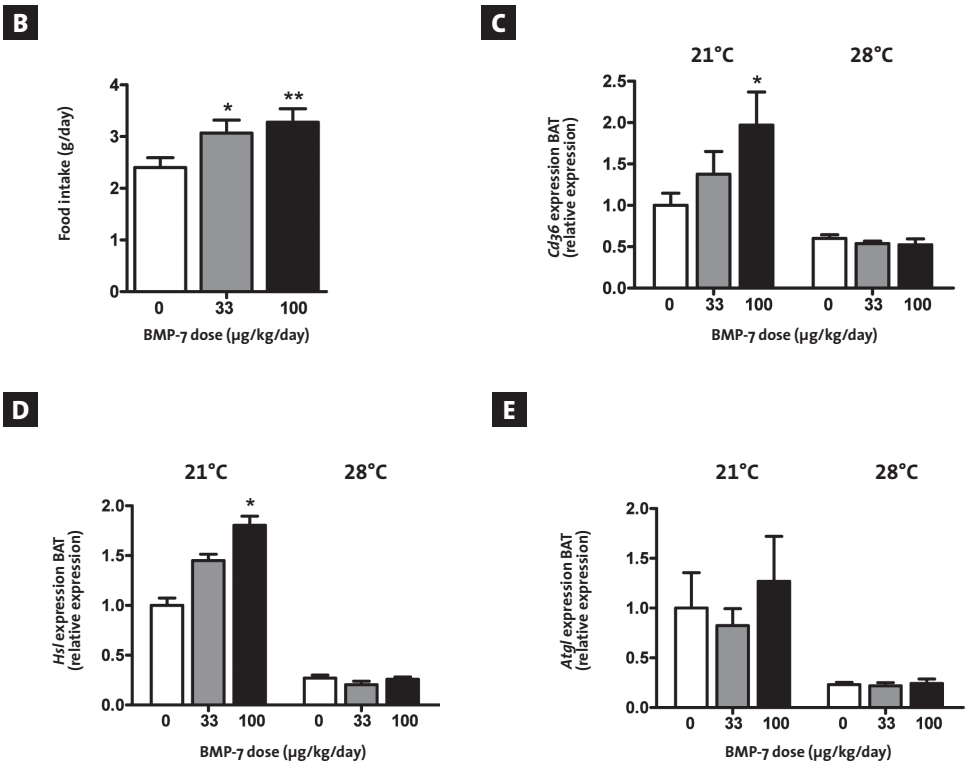

FIGURE 2 – BMP7 increases energy expenditure and fat oxidation at 21°C. 4-week-old C57Bl/6J mice were treated for 4 weeks with BMP7 (33 or 100 µg/kg/day) or saline via a subcutaneously located osmotic minipump at an environmental temperature of 21°C or 28°C. **A** Energy expenditure, activity levels and fat and carbohydrate oxidation measured during 5 consecutive days in the fourth week of treatment via fully automatic metabolic cages in mice housed at 21°C. Measurements were corrected for free fat mass (FFM) **B** Food intake measured during the fourth week of treatment in mice housed at 21°C. **C-E** Expression of *Cd36* **C**, *Hsl* **D** and *Atgl* **E** in BAT measured by Q-RT-PCR of mice housed at 21°C (left) or 28°C (right).

Values are means + SEM (n=9) and expression of genes was corrected for the housekeeping genes *ß2-microglobulin* and *36b4*. *P<0.05, ** P<0.01 compared to the control group.

FIGURE 2A). This might in part be explained by an increase in bone mineral content induced by BMP7 treatment (+20%, P<0.05) **(SUPPLEMENTARY FIGURE 2B)**, a well-known effect of BMP7 (21). To investigate whether BMP7 treatment affected white fat content in vivo, we quantitatively removed and weighed the right gonadal white fat pad (gWAT). In line with our calorimetric data **(FIGURE 2A)**, BMP7 decreased gWAT weight at 21°C (-12%, P<0.05), but not at 28°C **(FIGURE 3A)**. To gain more insight into the underlying mechanism, we studied expression of genes related to lipolysis in this fat pad. Indeed, BMP7 increased gene expression of both *Hsl* (+150%, P<0.05, **FIGURE 3B)** and *Atgl* (+50%, P<0.05, **FIGURE 3C)** at 21°C, suggesting increased TG breakdown in WAT, but not at 28°C.

BMP7 induces brite cell formation independent of environmental temperature

In WAT, brite cells are present that contribute to total energy expenditure through uncoupling by UCP-1 (22). Therefore, we studied if BMP7 treatment induced brite cell formation. Indeed, BMP7 markedly increased UCP-1 expression in gWAT, both at 21°C (+920%, P<0.05) and 28°C (+760%, P<0.05) **(FIGURE 3D)**. Moreover, immunohistochemical staining of UCP-1 in gWAT confirmed that, at both temperatures, BMP7 induced the appearance of fields of UCP-1 positive cells with brown cell-like morphology, so-called 'browning' of white fat **(FIGURE 3E)**.

BMP7 alters M1/M2 balance in BAT and WAT at 21°C, but not at thermoneutrality

Recently, M2 macrophages were shown to be crucial for BAT function via release of noradrenalin (3). Recruitment and activation of these macrophages is induced by sympathetic stimulation of BAT (3). Therefore, we investigated whether BMP7 could influence the presence of M2 macrophages in BAT, thereby possibly contributing to BMP7-induced BAT activation. Indeed, after 4 weeks of BMP7 treatment, expression of the M2 markers *Mrc1* tended to and *Cd163* was increased in BAT (+94%, P=0.068 and + 232%, P<0.05 respectively) **(FIGURES 4A-B)**, while the M1 markers *Nos2* and *Tnf* **(FIGURES 4C-D)** were unaltered. Interestingly, at 28°C, basal expression of all tested macrophage markers was largely diminished, which is in line with diminished sympathetic activation, and expression was not influenced by BMP7

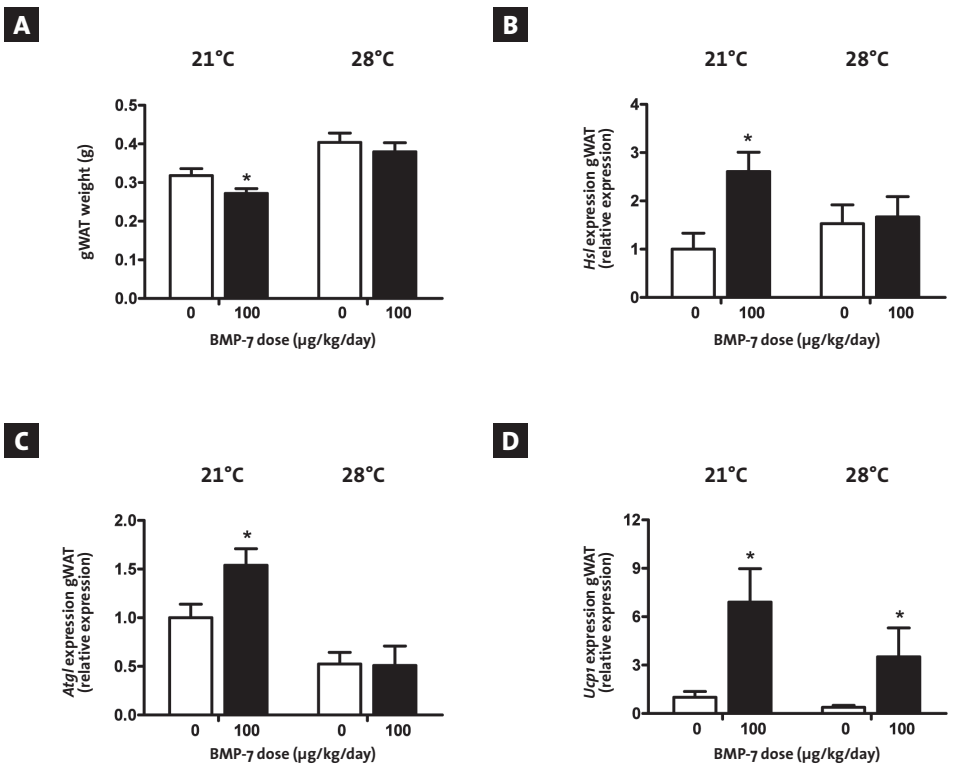

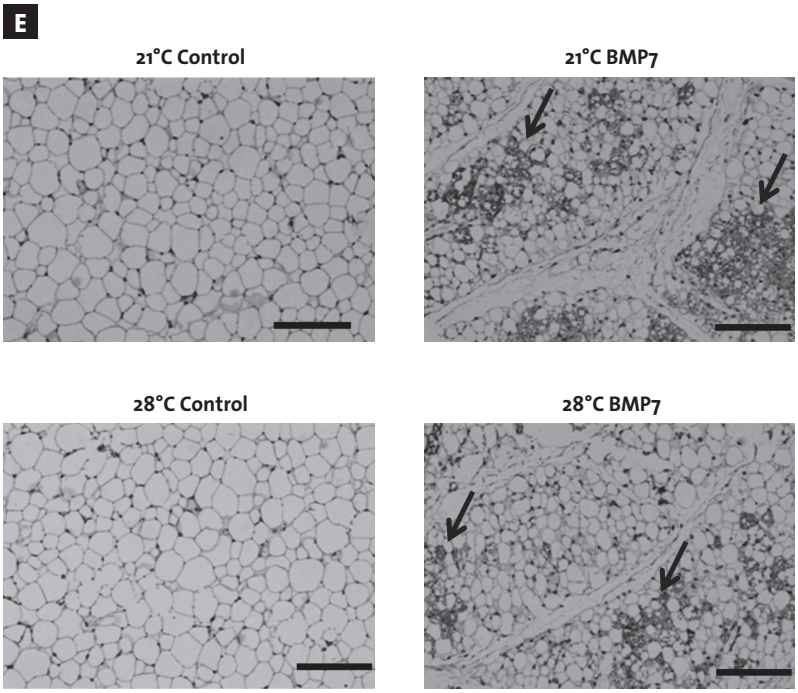

FIGURE 3 – BMP7 reduces white fat weight and induces browning of white adipose tissue. 4-week-old C57Bl/6J mice were treated for 4 weeks with BMP7 (33 or 100 µg/kg/day) or saline via a subcutaneously located osmotic minipump at an environmental temperature of 21°C or 28°C. **A** Weight of the right gonadal white fat pad, after quantitative removal, after which expression of *Hsl* **B**, *Atgl* **C** and *Ucp1* **D** was measured by Q-RT-PCR of mice housed at 21°C (left) or 28°C (right). (E) Representative pictures of immunohistochemical UCP-1 stainings of WAT in the control and BMP7 (100 µg/kg/day) animals housed at 21°C (top) and 28°C (bottom). Values are means + SEM (n=9) and expression of genes was corrected for the housekeeping genes *ß2-microglobulin* and *36b4*. *P<0.05 compared to the control group.

treatment **(FIGURES 4B,D)**. Moreover, mice that received BMP7 treatment showed increased expression of M2 markers in gWAT, but only at 21°C **(SUPPLEMENTARY FIGURES 3A-C)**. In addition, isolated peritoneal macrophages from mice that had been treated with BMP7 (100 µg/kg/day) at 21°C showed increased expression of the M2 markers *Mrc1* and *Cd163*, while expression of the M1 markers *Tnf* and *Nos2* was markedly diminished **(FIGURE 4E)**. Thus, both in the adipose tissue and in the peritoneal cavity, the M1/M2 balance was altered towards M2 after *in vivo* BMP7 treatment at 21°C.

To investigate whether BMP7 directly affects macrophage polarisation, we treated bone-marrow derived macrophages with BMP7 for 24 h *in vitro*. However, no effect was seen on expression of M1 or M2 markers as measured via Q-RT-PCR **(FIGURE 4F)**, nor on cytokine production by macrophages after stimulation with LPS **(SUPPLEMENTARY FIGURES 4A-D)**, suggesting that BMP7 alters M1/M2 balance *in vivo* via an indirect mechanism.

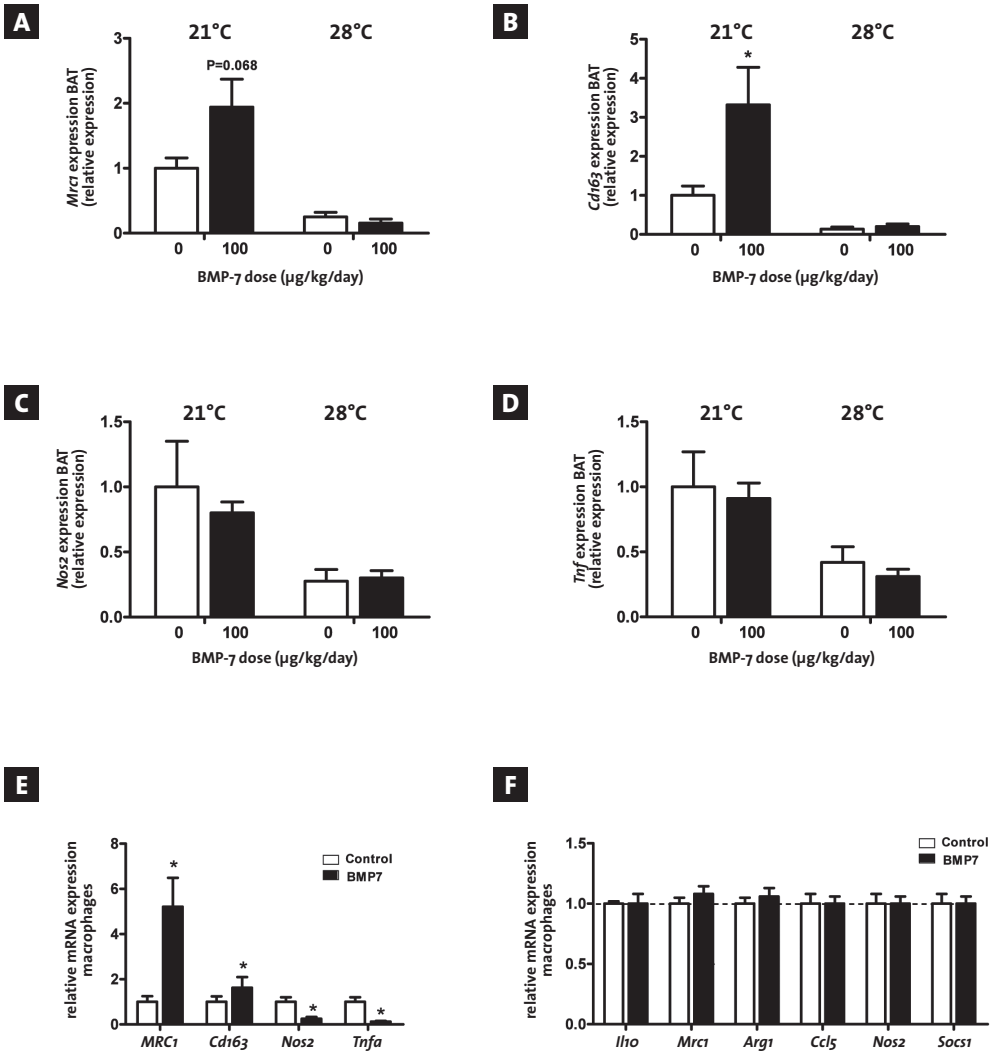

FIGURE 4 - **BMP7 results in altered M1/M2 balance in BAT and peritoneal macrophages.** 4-week-old C57Bl/6J mice were treated for 4 weeks with BMP7 (33 or 100 µg/kg/day) or saline via a subcutaneously located osmotic minipump at an environmental temperature of 21°C or 28°C. Expression of the M2 markers *Mrc1* **A** and *Cd163* **B** and the M1 markers *Nos2* **C** and *Tnf* **D** was measured in BAT by Q-RT-PCR of mice housed at 21°C (left) and 28°C (right). **E** After 4 weeks of treatment, peritoneal macrophages were isolated and markers of M2 and M1 macrophages were measured by Q-RT-PCR of mice housed at 21°C. **F** Bone-marrow derived macrophages were isolated from untreated C57Bl/6J mice and treated *ex vivo* with BMP7 (8.3 nM) for 24 hrs. The expression of markers for M2 and M1 macrophages was measured via Q-RT-PCR.

Values are means + SEM (n=9 for *in vivo* and n=3 for *in vitro)* and expression of genes was corrected for the housekeeping genes *ß2-microglobulin* and *36b4*. *P<0.05 compared to the control group.

BMP7 decreases obesity and attenuates liver lipid accumulation, dyslipidemia, and hyperglycemia in diet-induced obese mice

To investigate if BMP7 could improve the metabolic phenotype in diet-induced obesity, C57Bl6/J mice were fed a high-fat diet for 12 weeks and then treated with BMP7 (100 µg/kg/day) or saline for four weeks via subcutaneous osmotic minipumps in the presence of a high-fat diet. After 4 weeks of treatment, BMP7 tended to decrease body weight (-7%, P=0.09) **(FIGURE 5A)** but significantly reduced total fat mass (-7%, P<0.05) as measured by DEXA analysis **(FIGURE 5B)**. Furthermore, in liver, BMP7 markedly reduced triglyceride (TG) accumulation (-40%, P<0.01) as well as phospholipids (-21%, P<0.05), but not total cholesterol (TC). In addition, BMP7 lowered plasma TG (-25%, P<0.05) and total cholesterol levels (-10%, P<0.05) **(FIGURE 5D)**, and diminished hyperglycemia (-27%, P<0.01). Overall, these data are in full accordance with increased fatty acid and carbohydrate oxidation induced by BMP7 treatment and underscore the therapeutic potential of BMP7 to diminish diet-induced obesity and related disorders.

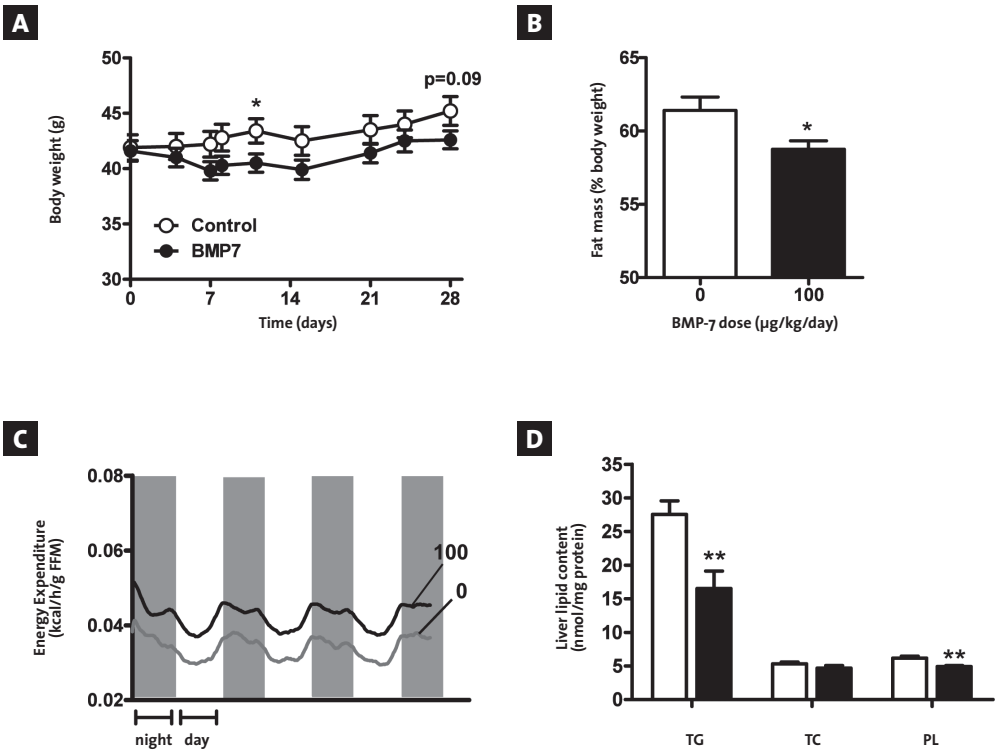

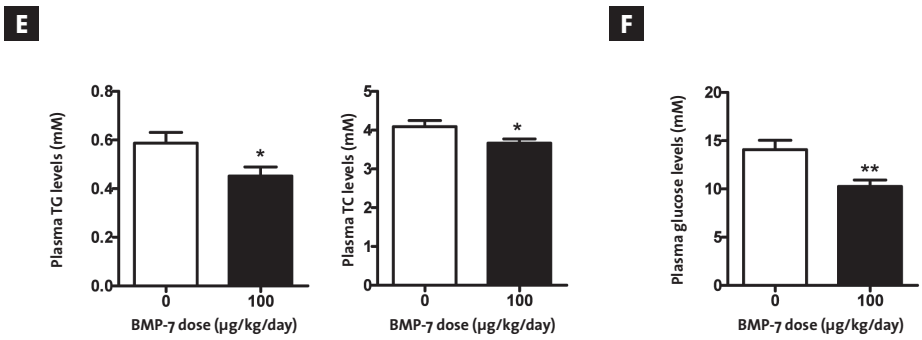

FIGURE 5 - BMP7 decreases obesity and attenuates liver lipid accumulation, dyslipidemia and hyperglycemia in diet-induced obese mice. 8-week-old C57Bl/6J mice were fed a high-fat diet for 12 weeks and then treated for 4 weeks with BMP7 (100 µg/kg/day) or saline via a subcutaneous osmotic minipump at an environmental temperature of 21°C while feeding a high-fat diet **A** Body weight development (gram) **B** Total fat mass as measured via DEXA-scan (expressed as percentage of body weight) **C** Liver content of triglycerides (TG), total cholesterol (TC) and phospholipids (PL) **D** Plasma triglyceride (TG) and total cholesterol (TC) levels. **E** Plasma glucose levels.

Values are means + SEM (n=9). *P<0.05, **P<0.01 compared to the control group.

DISCUSSION

Given its potential to dissipate energy instead of storing it, BAT is considered a promising target to treat obesity and related disorders, such as dyslipidemia and hyperglycemia (23). In this study, we show that 4 weeks treatment of mice with the endogenous growth factor BMP7 effectively increased BAT volume and formation of brite cells in WAT and boosted whole-body metabolism. We furthermore demonstrate that at thermoneutral temperature nearly all effects of BMP7 on BAT were absent, suggesting that sympathetic activation importantly contributes to the effect of BMP7 on BAT differentiation and activity. Moreover, BMP7 was able to diminish white fat content, liver lipid accumulation as well as to reduce dyslipidemia and hyperglycemia in diet-induced obese mice, underscoring the therapeutic potential of BMP7 in combating obesity and related disorders.

Our data are in line with a previous study performed by Tseng et al. (14), in which transient adenoviral overexpression of BMP7 increased BAT volume and oxygen consumption. We show that BMP7 markedly stimulates BAT volume and activity in mice only at subthermoneutral temperature, accompanied by a reduction in diet-induced obesity, liver lipid accumulation, dyslipidemia and hyperglycemia, and an altering of the M1/M2 balance in BAT and WAT towards increased anti-inflammatory M2 macrophages.

Interestingly, we found that treating mice for 4 weeks with BMP7 not only diminished white fat content in diet-induced obese mice, but also markedly lowered liver lipid accumu-

lation, plasma TG levels and, to a lesser extent, plasma cholesterol levels. The lowering in plasma lipid levels is probably the direct consequence of the increased BAT activity induced by BMP7. That is, fatty acids derived from LPL-mediated hydrolysis of TG-rich lipoproteins form an important substrate for BAT thermogenesis (2). Indeed, expression of CD36 in BAT, a scavenger receptor that is rate-limiting for the uptake of fatty acids from plasma into BAT (24), was significantly upregulated in BAT of BMP7 treated mice. Moreover, a recent study by Bartelt et al. (5) shows that BAT has a tremendous capacity to clear plasma TG. 4 h of cold induction (4°C) normalized plasma TG levels in severely hypertriglyceridemic apoA5 knock-out mice (5). Since increased plasma TG levels are an independent risk factor for cardio-vascular disease in both men and women (25) BMP7 might thus be an interesting treatment modality to manage cardiovascular disease through attenuating dyslipidemia via targeting BAT.

Despite an improved metabolic phenotype in both lean and diet-induced obese mice upon BMP7 treatment, we did not observe effects on body weight development. This might in part be due to the fact that BMP7 is capable of inducing bone formation (21). Indeed, in our study, BMP7 treated mice exhibited increased bone mineral content as measured via DEXA-scan. In addition, part of the beneficial effect of BMP7 on energy expenditure might be offset by the increase in food intake (up to +37%) we observed. This is probably rather a consequence of the increased uncoupling due to BAT activation (26) then a direct effect of BMP7 on food intake, since we did not observe this effect at thermoneutrality. Moreover, a recent study by Townsend et al (27) showed that intracerebral infusion of BMP7 resulted in a decrease in food intake rather than an increase.

A striking finding in our study is that at thermoneutrality, BMP7 exerted virtually no effect on BAT, suggesting that sympathetic activation of BAT is a prerequisite for the effects of BMP7 on BAT differentiation and activity.

A first explanatory mechanism for this finding may involve the intracellular signaling route by which BMP7 induces UCP-1 upregulation in brown adipocytes. The pathway involves binding of BMP7 to the BMP-receptor II subtype and induction of the p38 MAPK route, in which the accessory proteins TAB1 an XIAP1 modulate downstream signaling. Via binding to and activation of still unknown transcription factors, this leads to upregulation of UCP-1 expression (28,29). Interestingly, protein kinase A (PKA), a downstream target of the thermogenic ß3-adrenergic receptor, also induces p38 MAPK (29). Thus, via p38 MAPK, the ß3-adrenergic and BMP7 signaling routes are intertwined. Possibly, p38 MAPK should be activated above a certain threshold before BMP7 can induce its downstream effects on UCP-1 expression This might explain why at thermoneutrality, in which sympathetic activity and thus ß3 signalling towards BAT are largely diminished, BMP7 was unable to increase BAT volume and activity.

A second mechanism that could explain the ineffectiveness of BMP7 at thermoneutral temperature may involve a central mode of action of BMP7. A central player involved in BAT activation is the hypothalamus, which projects onto sympathetic nerves that densely innervate BAT (2). Various circulating peptides have been shown to be capable of activating BAT via the hypothalamus, such as GLP-1 (30) and BMP8B, another member of the BMP family

(31). In addition, Townsend et al. (27) showed that central administration of BMP7 resulted in reduced food intake, confirming that BMP7 is at least capable of exerting central effects. However, it remains to be determined whether subcutaneously administered BMP7 is able to enter the hypothalamus to subsequently exert central actions.

Interestingly, we showed that treatment of mice with BMP7 resulted in an altered M1/M2 macrophage balance in both BAT, gWAT and the peritoneal cavity, with increased expression of M2 markers. M2 macrophages have recently been shown to importantly contribute to BAT thermogenesis by releasing noradrenalin (3). Possibly the increased presence of M2 macrophages in BAT in response to BMP7 treatment contributed to the increased BAT activity found in these mice. However, since the initial paper describing the involvement of M2 macrophages in BAT function has been under debate recently, future studies should further explore the necessity of M2 macrophages in mediating the effects of BMP7 on BAT. Furthermore, whether the effect of BMP7 on macrophage polarisation is either direct or indirect, in response to changes in BAT, remains to be determined. Although we could not show in our *in vitro* experiments a direct effect of BMP7 on M1/M2 skewing in bone-marrow derived macrophages, a recent study in which human THP-1 monocytes were treated with BMP7 demonstrated significant polarization of monocytes into M2 macrophages (32). However, since the change in M1/M2 balance did not happen at thermoneutral temperature suggests that environmental factors are at least in part involved in the effects of BMP7 on macrophage polarisation.

In this study, we show that BMP7 not only increased the volume of the interscapular brown fat pad, but also show for the first time that BMP7 markedly induced appearance of brite cells in WAT, so-called 'browning' of WAT. This could have been caused by either transdifferentiation of white fat cells into brite adipocytes, or differentiation of brite precursor cells that are present in WAT towards brite adipocytes. Both mechanisms are plausible. White fat cells have been shown to be capable of transdifferentiating towards brite adipocytes and they furthermore have the BMP-II receptor (21,33). Moreover, in WAT, Myf5- precursor cells are present that can differentiate into brite cells *in vitro* (9, 34). Future studies are needed to elucidate the mechanism by which BMP7 induces 'browning' of WAT in more detail. However, since we found that brown fat cells obviously appeared as clusters in WAT, it is more plausible that BMP7 primarily acted on precursor cells resulting in proliferation and subsequent differentiation. Intriguingly, browning happened independent of environmental temperature. This could be explained by the fact that WAT, in contrast to BAT, is less dense innervated by the sympathetic nervous system and thus probably less dependent on its activation (2). In addition, UCP-1 expression might be differentially regulated in bright cells compared to the brown adipocytes present in the brown fat pads.

Brite cells have been suggested to contribute importantly to total energy expenditure, as these cells are more abundant in obesity-resistant strains of mice (35,36). In our study, mice that were treated with BMP7 at 28°C displayed an increase of brite fat cells without activating brown fat pads. This was however not sufficient to raise total energy expenditure. Interestingly, the recently indentified hormone irisin, which is released from muscle after exercise, selectively induced browning of subcutaneous WAT depots, without affecting

differentiation or activity of brown fat pads, and did lead to an increase in total energy expenditure (21).

In conclusion, BMP7 stimulates BAT volume, activity and total energy expenditure only at subthermoneutrality, suggesting that intact sympathetic activation is a prerequisite for the effects of BMP7 on BAT. Furthermore, we found that BMP7 diminishes obesity and liver lipid accumulation, and attenuates dyslipidemia and hyperglycemia in diet-induced obese mice. We anticipate that BAT may be a promising novel treatment goal, and BMP7 a treatment modality, in fighting obesity and related disorders.

ACKNOWLEDGEMENTS

We thank Peter ten Dijke (Molecular Cell Biology, LUMC, Leiden) for valuable input and critical reading our manuscript and Amanda Pronk (Human Genetics, LUMC, Leiden) and Lianne van der Wee (Endocrinology, LUMC, Leiden) for excellent technical assistance.

REFERENCES

1 Rosen ED, Spiegelman BM (2006) Adipocytes as regulators of energy balance and glucose homeostasis. Nature 444: 847-853.

2 Cannon B, Nedergaard J (2004) Brown adipose tissue: function and physiological significance. Physiol Rev 84: 277-359.

3 Nguyen KD, Qiu Y, Cui X, et al (2011) Alternatively activated macrophages produce catecholamines to sustain adaptive thermogenesis. Nature 480: 104-108.

4 Goldberg IJ, Eckel RH, Abumrad NA (2009) Regulation of fatty acid uptake into tissues: lipoprotein lipase- and CD36-mediated pathways. J Lipid Res 50: S86-S90

5 Bartelt A, Bruns OT, Reimer R, et al (2011) Brown adipose tissue controls triglyceride clearance. Nature Medicine 17: 200-205

6 Cypess AM, Lehman S, Williams G, et al (2009) Identification and importance of brown adipose tissue in adult humans. N Engl J Med 360: 1509-1517.

7 van Marken Lichtenbelt WD, Vanhommerig JW, Smulders NM, et al (2009) Cold-activated brown adipose tissue in healthy men. N Engl J Med 360: 1500-1508.

8 Virtanen KA, Lidell ME, Orava J, et al (2009) Functional brown adipose tissue in healthy adults. N Engl J Med 360: 1518-1525.

9 Seale P, Bjork B, Yang W, et al (2008) PRDM16 controls a brown fat/skeletal muscle switch. Nature 454: 961-967.

10 Wu J, Bostrom P, Sparks LM, et al (2012) Beige adipocytes are a distinct type of thermogenic fat cell in mouse and human. Cell 150: 366-76.

11 Cousin B, Cinti S, Morroni M, et al (1992) Occurrence of brown adipocytes in rat white adipose tissue: molecular and morphological characterization. J Cell Sci 103: 931-942.

12 Fukui Y, Masui S, Osada S, Umesono K, Motojima K (2000) A new thiazolidinedione, NC-2100, which is a weak PPAR-gamma activator, exhibits potent antidiabetic effects and induces uncoupling protein 1 in white adipose tissue of KKAy obese mice. Diabetes 49: 759-767.

13 Sell H, Berger JP, Samson P, et al (2004) Peroxisome proliferator-activated receptor gamma agonism increases the capacity for sympathetically mediated thermogenesis in lean and ob/ob mice. Endocrinology 145: 3925-3934.

14 Tseng YH, Kokkotou E, Schulz TJ, et al (2008) New role of bone morphogenetic protein 7 in brown adipogenesis and energy expenditure. Nature 454: 1000-1004.

15 Schulz TJ, Huang TL, Tran TT, et al (2011) Identification of inducible brown adipocyte progenitors residing in skeletal muscle and white fat. Proc Natl Acad Sci U S A 108: 143-148.

16 Van Klinken JB, Van den Berg SAA, Havekes LM, Willems van Dijk K (2012) Estimation of activity related energy expenditure and resting metabolic rate in freely moving mice from indirect calorimetry data. PLoS ONE 7(5):e36162. doi:10.1371/journal.pone.0036162

17 Kanters E, Pasparakis M, Gijbels MJ, et al (2003) Inhibition of NF-kappaB activation in macrophages increases atherosclerosis in LDL receptor-deficient mice. J Clin Invest 112: 1176-1185

18 Bligh EG, Dyer WJ. (1959) A rapid method of total lipid extraction and purification. Can J Biochem Physiol 37: 911-9177.

19 Goossens P, Gijbels MJ, Zernecke A, et al (2010) Myeloid type I interferon signaling promotes atherosclerosis by stimulating macrophage recruitment to lesions. Cell Metab 2: 142-153.

20 Castillo M, Hall JA, Correa-Medina M, et al (2011) Disruption of thyroid hormone activation in type 2 deiodinase knockout mice causes obesity with glucose intolerance and liver steatosis only at thermoneutrality. Diabetes 60: 1082-1089.

21 Boon MR, van der Horst G, van der Pluijm G, et al (2011) Bone morphogenetic protein 7: a broad-spectrum growth factor with multiple target therapeutic potency. Cytokine Growth Factor Rev.22: 221-229.

22 Boström P, Wu J, Jedrychowski MP, et al (2012) A PGC1-alpha-dependent myokine that drives brown-fat-like development of white fat and thermogenesis. Nature 481: 463-468.
23 Frühbeck G, Becerril S, Sáinz N, Garrastachu P, Garciá-Velloso MJ (2008) BAT: a new target for human obesity? Cell Press 30: 387-396.
24 Bartelt A, Merkel M, Heeren J (2012) A new, powerful player in lipoprotein metabolism: brown adipose tissue. J Mol Med 90: 887-893.
25 Hokanson JE, Ausin MA (1996) Plasma triglyceride level is a risk factor for cardiovascular disease independent of high-density lipoprotein cholesterol level: a meta-analysis of population-based prospective studies. J Cardiovasc Risk 3: 213-219.
26 Cannon B, Nedergaard J (2009) Thermogenesis challenges the adipostat hypothesis for body-weight control. Proc. Nutr. Soc 64: 401-407.
27 Townsend KL, Suzuki R, Huang TL, et al (2012) Bone morphogenetic protein 7 (BMP7) reverses obesity and regulates appetite through a central mTOR pathway. FASEB J 26: 2187-2196.
28 Schulz TJ, Tseng YH (2009) Emerging role of Bone Morphogenetic Proteins in adipogenesis and energy metabolism. Cytokine Growth Factor Rev;20: 523-531.
29 Cao W, Medvedev AV, Daniel KW, Collins C (2001) ß-adrenergic activation of p38 MAP Kinase in adipocytes. cAMP induction of the uncoupling protein 1 (UCP1) gene requires p38 MAP kinase. The Journal of Biological Chemistry 276: 27077-27082.
30 Lockie SH, Heppner KM, Chaudhary N, et al (2012) Direct control of brown adipose tissue thermogenesis by central nervous system glucagon-like peptide-1 receptor signaling. Diabetes;61: 2753-2762.
31 Whittle AJ, Carobbio S, Martins L, et al (2012) BMP8B increases brown adipose tissue thermogenesis through both central and peripheral actions. Cell 149: 871-885.
32 Rocher C, Singla R, Singla PK, Parhasarathy S, Singla DK (2012) Bone morphogenetic protein 7 polarizes THP-1 cells into M2 macrophages. Can J Physiol Pharmacol 7: 947-951.
33 Barbatelli G, Murano I, Madsen L, et al (2010) The emergence of cold-induced brown adipocytes in mouse white fat depots is determined predominantly by white to brown adipocyte transdifferentiation. Am J Physiol Endocrinol Metab 298: E1244-E1253.
34 Timmons JA, Wennmalm K, Larsson O, et al (2007) Myogenic gene expression signature establishes that brown and white adipocytes originate from distinct cell lineages. Proc Natl Acad Sci U S A 104: 4401-4406.
35 Almind K, Manieri M, Sivitz WI, Cinti S, Kahn CR (2007) Ectopic brown adipose tissue in muscle provides a mechanism for differences in risk of metabolic syndrome in mice. Proc Natl Acad Sci U S A 104: 2366-2371.
36 Xue B, Rim JS, Hogan JC, Coulter AA, Koza RA, Kozak LP (2007) Genetic variability affects the development of brown adipocytes in white fat but not in interscapular brown fat. J Lipid Res 48: 41-51.

SUPPLEMENTARY APPENDIX

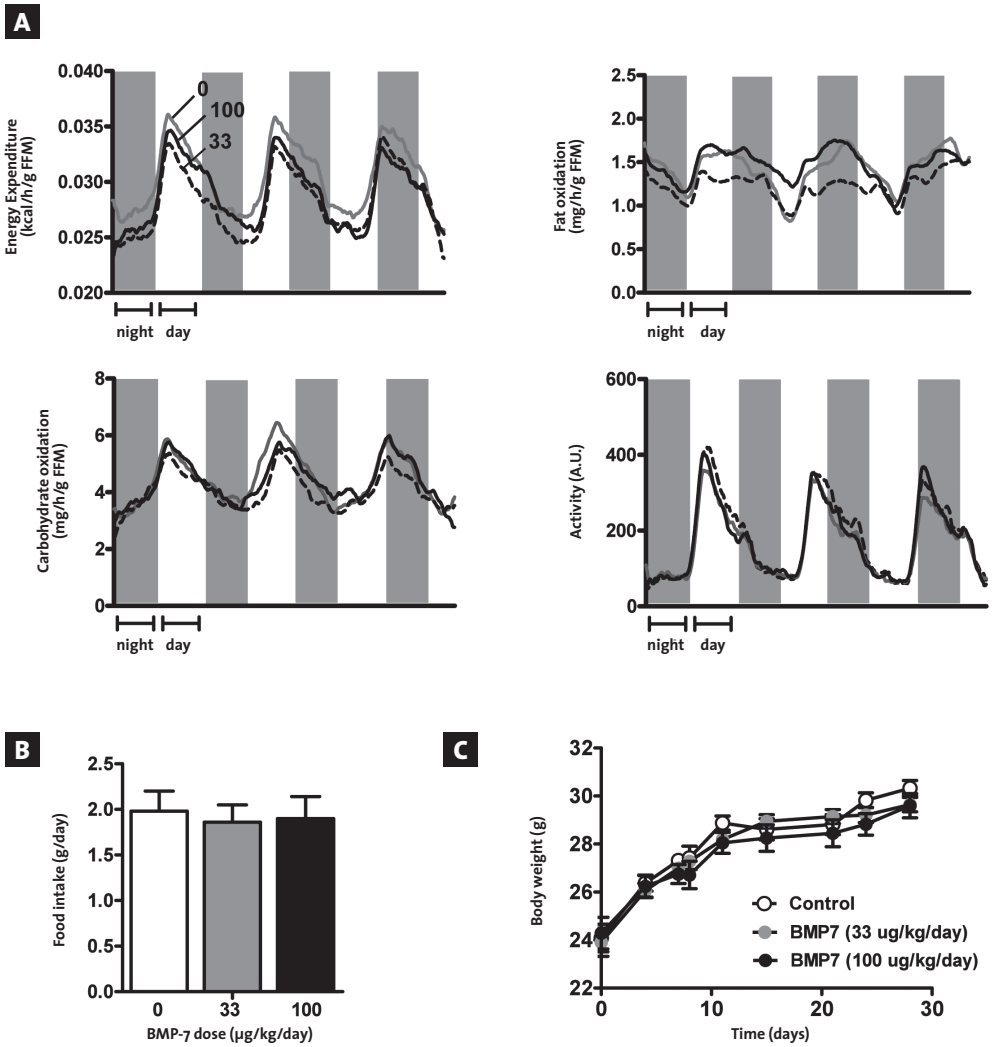

SUPPLEMENTARY FIGURE 1 – BMP7 does not affect energy expenditure, fat oxidation, food intake and weight development at thermoneutrality. 4-week-old C57Bl/6J mice were treated for 4 weeks with BMP7 (33 or 100 µg/kg/day) or saline via a subcutaneously located osmotic minipumps at an environmental temperature of 21°C or 28°C. **A** Energy expenditure, fat and carbohydrate oxidation and activity levels measured during 5 consecutive days in the fourth week of treatment via fully automatic metabolic cages in mice housed at 28°C. Measurements were corrected for free fat mass (FFM). **B** Food intake measured during the fourth week of treatment in mice housed at 28°C. **C** Body weight (gram) development during treatment at 28°C.
Values are means + SEM (n=9).

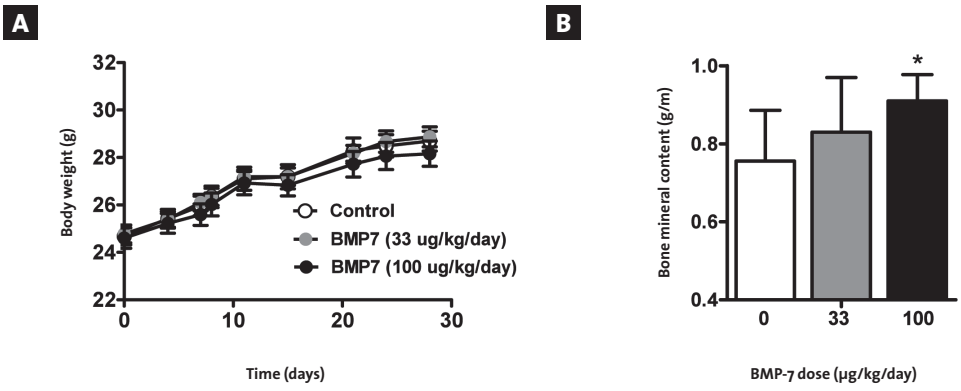

SUPPLEMENTARY FIGURE 2– BMP7 does not affect weight development but increases bone mineral content at 21°C. 4-week-old C57Bl/6J mice were treated for 4 weeks with BMP7 (33 or 100 µg/kg/day) or saline via a subcutaneously located osmotic minipumps at an environmental temperature of 21°C or 28°C. **A** Body weight development (gram) during treatment at 21°C **B** Bone mineral content as measured via DEXA scan after 4 weeks of treatment at 21°C.

Values are means + SEM (n=9) *P<0.05 compared to the control group.

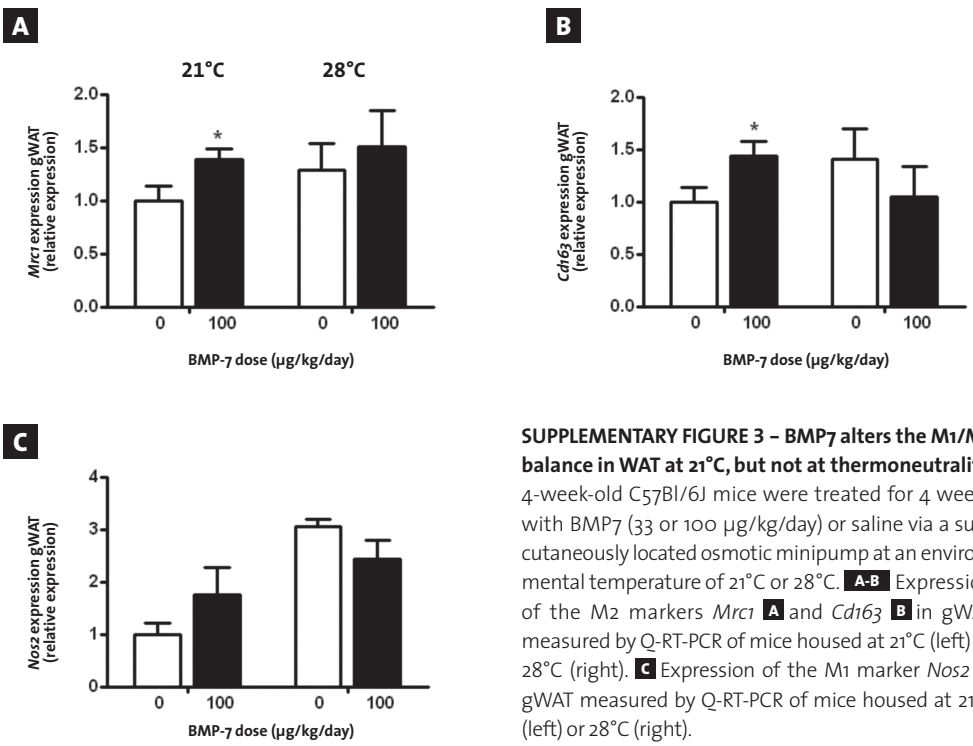

SUPPLEMENTARY FIGURE 3 – BMP7 alters the M1/M2 balance in WAT at 21°C, but not at thermoneutrality. 4-week-old C57Bl/6J mice were treated for 4 weeks with BMP7 (33 or 100 µg/kg/day) or saline via a subcutaneously located osmotic minipump at an environmental temperature of 21°C or 28°C. **A-B** Expression of the M2 markers *Mrc1* **A** and *Cd163* **B** in gWAT measured by Q-RT-PCR of mice housed at 21°C (left) or 28°C (right). **C** Expression of the M1 marker *Nos2* in gWAT measured by Q-RT-PCR of mice housed at 21°C (left) or 28°C (right).

Values are means + SEM (n=9) and expression of genes was corrected for the housekeeping genes *ß2-microglobulin* and *36b4*. *P<0.05 compared to the control group.

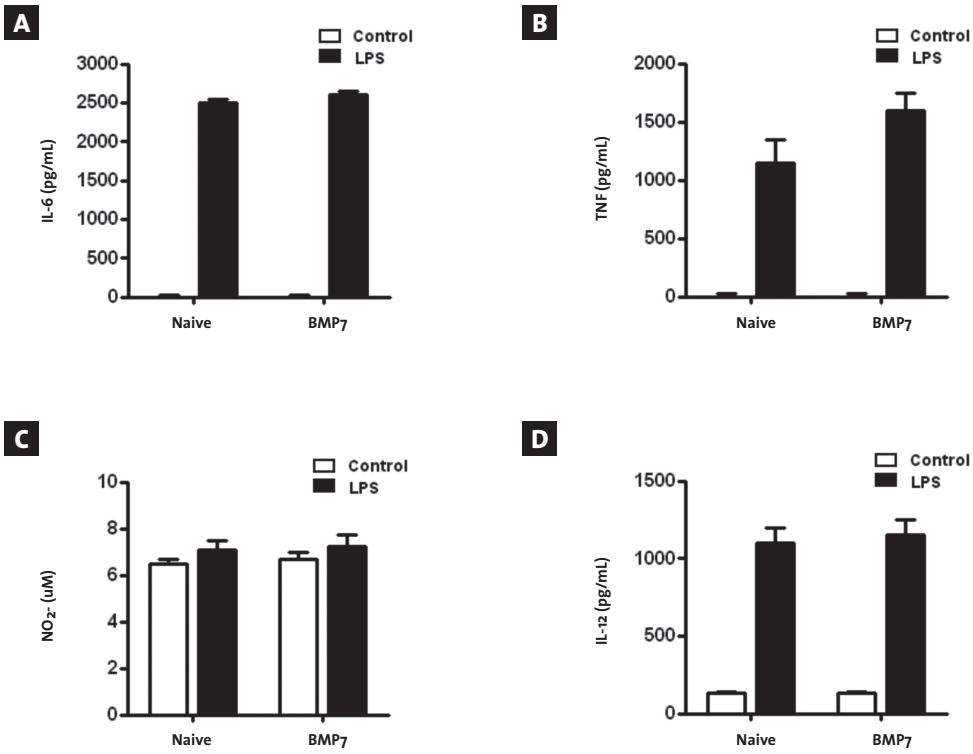

SUPPLEMENTARY FIGURE 4 – BMP7 does not alter cytokine secretion by bone-marrow derived macrophages. Bone-marrow derived macrophages were isolated from untreated C57BL6/J mice, plated in a 24-well plate (10^6 cells/mL) and stimulated with BMP7 (8.3 nM) or vehicle for 24 hours or with BMP7 (8.3 nM) or vehicle for 18 hours + 6 hours LPS (10 ng/mL). The concentration of IL-6 **A**, TNF **B**, NO_2- **C** and IL-12 **D** in the supernatant was measured.

Values are means + SEM (n=3).

TABLE 1 - **Primers used for quantitative real-time PCR analysis**

Gene	Forward primer	Reverse primer
36b4	GGACCCGAGAAGACCTCCTT	GCACATCACTCAGAATTTCAATGG
Arg1	CATGGGCAACCTGTGTCCTT	CGATGTCTTTGGCAGATATGCA
Atgl	ACAGTGTCCCCATTCTCAGG	TTGGTTCAGTAGGCCATTCC
ß2-microglobulin	TGACCGGCTTGTATGCTATC	CAGTGTGAGCCAGGATATAG
Ccl5	GGAGTATTTCTACACCAGCAGCAA	GCGGTTCCTTCGAGTGACA
Cd163	CTCAGGAAACCAATCCCAGA	CAAGAGCCCTCGTGGTAGAC
Cd36	GCAAAGAACAGCAGCAAAATC	CAGTGAAGGCTCAAAGATGG
Hsl	AGACACCAGCCAACGGATAC	ATCACCCTCGAAGAAGAGCA
Il10	TTTGAATTCCCTGGGTGAGAA	CTCCACTGCCTTGCTCTTATTTTC
Mrc1	GAGAGCCAAGCCATGAGAAC	GTCTGCACCCTCCGGTACTA
Nos2	CGGGCATCTGGTAGCCAGCG	TGGCAACATCAGGTCGGCCAT
Soc1	CCGTGGGTCGCGAGAAC	AAGGAACTCAGGTAGTCACGGAGTA
Tnf	GGCAGGTCTACTTTGGAGTCATTGC	ACATTCGAGGCTCCAGTGAATTCGG
Ucp1	TCAGGATTGGCCTCTACGAC	TGCATTCTGACCTTCACGAC

Arg1 arginase 1
A*tgl* adipose triglyceride lipase
Ccl5 Chemokine (C-C motif) ligand 5
Hsl hormone-sensitive lipase
Il10 interleukin-10
Mrc1 mannose receptor 1
Nos2 nitric oxide synthase 2
Tnf tumor necrosis factor-α
Ucp-1 uncoupling protein-1

METFORMIN LOWERS PLASMA TRIGLYCERIDES BY PROMOTING VLDL-TRIGLYCERIDE CLEARANCE BY BROWN ADIPOSE TISSUE IN MICE

MARIËTTE R. BOON*
JANINE J. GEERLING*
GERARD C. VAN DER ZON
SJOERD A.A. VAN DEN BERG
ANITA M. VAN DEN HOEK
MARC LOMBÈS
HANS M.G. PRINCEN
LOUIS M. HAVEKES
PATRICK C.N. RENSEN
BRUNO GUIGAS

* Both authors contributed equally

Diabetes 2014; 63: 1-12.

ABSTRACT

Metformin is the first-line drug for the treatment of type 2 diabetes. Besides its well-characterized antihyperglycemic properties, metformin also lowers plasma VLDL triglycerides (TGs). In this study, we investigated the underlying mechanisms in APOE*3-Leiden.CETP mice, a well-established model for human-like lipoprotein metabolism. We found that metformin markedly lowered plasma total cholesterol and TG levels, an effect mostly due to a decrease in VLDL-TG, whereas HDL was slightly increased. Strikingly, metformin did not affect hepatic VLDL-TG production, VLDL particle composition, and hepatic lipid composition but selectively enhanced clearance of glycerol tri[3H] oleate-labeled VLDL-like emulsion particles into brown adipose tissue (BAT). BAT mass and lipid droplet content were reduced in metformin-treated mice, pointing to increased BAT activation. In addition, both AMP-activated protein kinase α1 (AMPKα1) expression and activity and HSL and mitochondrial content were increased in BAT. Furthermore, therapeutic concentrations of metformin increased AMPK and HSL activities and promoted lipolysis in T37i differentiated brown adipocytes. Collectively, our results identify BAT as an important player in the TG-lowering effect of metformin by enhancing VLDL-TG uptake, intracellular TG lipolysis, and subsequent mitochondrial fatty acid oxidation. Targeting BAT might therefore be considered as a future therapeutic strategy for the treatment of dyslipidemia.

INTRODUCTION

Metformin is one of the most widely used glucose-lowering agents for the treatment of type 2 diabetes (1) and is now considered the first-line drug therapy for patients (2). This antidiabetic drug from the biguanides family is prescribed for its effective antihyperglycemic action, mostly achieved through a potent reduction of hepatic glucose production secondary to inhibition of gluconeogenesis (3). Interestingly, another important but often overlooked property of metformin relies on its beneficial. effect on the blood lipid profile, which is characterized by a significant reduction in circulating triglycerides (TGs) and VLDL cholesterol and increased HDL cholesterol levels (4). This metabolic feature might partly be involved in its cardioprotective effect observed in obese patients treated with the drug (5). Despite extensive efforts during the last years (6), the exact molecular mechanism (s) of action of metformin still remains incompletely understood, especially the one by which the drug exerts its lipid-lowering action. In 2001, Zhou et al. (7) were the first to report that metformin activates hepatic AMPactivated protein kinase (AMPK), emphasizing the putative role of this energy-sensing kinase in the mechanism of action of the drug.

AMPK is a well-conserved serine/threonine protein kinase that plays a crucial role in the regulation of catabolic/anabolic pathways by acting as a cellular energy and nutrient sensor (8,9). AMPK consists of a heterotrimeric complex containing a catalytic a subunit and two regulatory ß and γ subunits. Each subunit has several isoforms (α1, α2; ß1, ß2; γ1, γ2, γ3) that are encoded by distinct genes, giving multiple heterotrimeric combinations with tissue-specific distribution (8,9). The ß subunit contains a threonine residue (Thr 172) whose phosphorylation by upstream kinases, such as the liver kinase B (LKB1), is required for AMPK activation. The b subunit acts as a scaffold to which the two other subunits are bound and also allows AMPK to sense energy reserves in the form of glycogen (8,9). Binding of AMP and/or ADP to selective domains on the γ subunit leads to AMPK activation via a complex mechanism involving direct allosteric activation, phosphorylation on Thr172 by AMPK upstream kinases, and inhibition of dephosphorylation of this residue by specific protein phosphatases that remain to be identified (8,9). Interestingly, the mechanism by which metformin activates AMPK, involving specific inhibition of the mitochondrial respiratory chain complex 1 (10,11), was recently clarified (12,13), although the contribution of the LKB1/AMPK axis in its hepatic effects still remains controversial (14–18).

The objective of this study was to investigate the molecular mechanisms underlying the effects of metformin on lipoprotein metabolism by using APOE*3-Leiden. CETP (E3L.CETP) transgenic mice, a well-established model of human-like lipoprotein metabolism (19) that also responds to lipid-lowering pharmacological interventions (20–23). Collectively, our data show that treatment of E3L.CETP mice with metformin is able to recapitulate the lipid-lowering effect of the drug evidenced in humans, i.e., causing a reduction in plasma VLDL-TG associated with a parallel mild increase in HDL cholesterol. Remarkably, this effect is not mediated by apparent changes in hepatic VLDL-TG production but rather by a selective increase in VLDL-TG clearance by the brown adipose tissue (BAT). At the molecular level, we found an increase in AMPKα1 activity and protein expression of both hormone-sensitive

lipase (HSL) and mitochondrial respiratory chain complexes, suggesting that metformin, on top of increasing VLDL-TG uptake, also promotes intracellular TG lipolysis and subsequent mitochondrial fatty acid (FA) oxidation in BAT.

RESEARCH DESIGN AND METHODS

Materials
All chemicals were purchased from Sigma-Aldrich (St. Louis, MO).

Ethics
All mouse experiments were performed in accordance with the Institute for Laboratory Animal Research Guide for the Care and Use of Laboratory Animals and have received approval from the university ethical review boards (Leiden University Medical Center).

Animals, Diet, and Metformin Treatment
Homozygous human CETP transgenic mice were crossbred with hemizygous APOE*3-Leiden (E3L) mice at our Institutional Animal Facility to obtain E3L.CETP mice, as previously described (19). In this study, 12-week-old E3L. CETP female mice, housed under standard conditions in conventional cages with ad libitum access to food and water, were fed a Western-type diet containing 0.1% (weight for weight [w/w]) cholesterol (Hope Farms, Woerden, the Netherlands) for 4 weeks. Upon randomization according to body weight, plasma total cholesterol (TC), and TG levels, mice next received Western-type diet with or without 200 mg/kg body weight/day (0.2%, w/w) metformin for 4 weeks. Unless otherwise mentioned, experiments were performed after 4 h of fasting at 1:00 P.M. with food withdrawn at 9:00 A.M.

Plasma Lipid and Lipoprotein Analysis
Plasma was obtained via tail vein bleeding and assayed for TC, TG, and phospholipid (PL) using the commercially available enzymatic kits 236691, 11488872, and 1001140 (Roche Molecular Biochemicals, Indianapolis, IN), respectively. Free FAs were measured using the NEFA-C kit from Wako Diagnostics (Instruchemie, Delfzijl, the Netherlands). The distribution of lipids over plasma lipoprotein fractions was determined using fast protein liquid chromatography. Plasma was pooled per group, and 50 µL of each pool was injected onto a Superose 6 PC 3.2/30 column (Akta System, Amersham Pharmacia Biotech, Piscataway, NJ) and eluted at a constant flow rate of 50 µL/min in 1 mmol/L EDTA in PBS, pH 7.4. Fractions of 50 µL were collected and assayed for TC and TG as described above.

Hepatic VLDL-TG and VLDL-apoB Production
Mice were fasted for 4 h prior to the start of the experiment. During the experiment, mice were sedated with 6.25 mg/kg acepromazine (Alfasan, Woerden, the Netherlands), 6.25 mg/kg

midazolam (Roche, Mijdrecht, the Netherlands), and 0.31 mg/kg fentanyl (Janssen-Cilag, Tilburg, the Netherlands). At t = 0 min, blood was taken via tail bleeding and mice were intravenously injected with 100 µL PBS containing 100 µCi Trans^{35}S label (ICM Biomedicals, Irvine, CA) to measure de novo total apolipoprotein B (apoB) synthesis. After 30 min, the animals received 500 mg tyloxapol (Triton WR-1339; Sigma- Aldrich) per kilogram body weight as a 10% (w/w) solution in sterile saline, to prevent systemic lipolysis of newly secreted hepatic VLDL-TG. Additional blood samples were taken at t = 15, 30, 60, and 90 min after tyloxapol injection and used for determination of plasma TG concentration. After 90 min, the animals were killed and blood was collected by orbital bleeding for isolation of VLDL by density-gradient ultracentrifugation, as previously described (19–23). ^{35}S-apoB was measured in the VLDL fraction, and VLDL-apoB production rate was calculated as dpm.h-1, as previously reported (19–23).

In Vivo Clearance of VLDL-Like Emulsion Particles

Mice were fasted overnight with food withdrawn at 6:00 P.M. During the experiment, mice were sedated as described above. At t = 0 min, blood was taken via tail bleeding and mice received a continuous intravenous infusion of glycerol tri[^{3}H]oleate-labeled emulsion particles mixed with albumin-bound [^{14}C]oleic acid (4.4 µCi [^{3}H]TG and 1.2 µCi [^{14}C]FA; both from GE Healthcare Life Sciences, Little Chalfont, U.K.) at a rate of 100 µL/h for 2.5 h, as previously described (24,25). Blood samples were taken using chilled paraoxoncoated capillaries by tail bleeding at 90 and 120 min of infusion to ensure that steady-state conditions had been reached. Subsequently, mice were killed and organs were quickly harvested and snap frozen in liquid nitrogen. Retention of radioactivity in the saponified tissues was measured per milligram of tissue and corrected for the corresponding plasma-specific activities of [^{3}H]FA and [^{14}C]FA, as previously described (24).

Hepatic Lipid Composition

Liver lipids were extracted as previously described (20). In brief, small liver pieces were homogenized in ice-cold methanol. After centrifugation, lipids were extracted by addition of 1,800 µL CH_3OH:$CHCl_3$ (1:3 volume for volume [v/v]) to 45 µL homogenate, followed by vigorous vortexing and phase separation by centrifugation (14,000 rpm; 15 min at room temperature). The organic phase was dried and dissolved in 2% Triton X-100 in water. TG, TC, and PL concentrations were measured using commercial kits as described above. Liver lipids were expressed as nanomoles per milligram protein, which was determined using the BCA protein assay kit (Pierce, Rockford, IL).

Histology

Interscapular BAT was removed and fixed directly in 4% paraformaldehyde, dehydrated, and embedded in paraffin. Hematoxylin and eosin staining was performed using standard protocols. The area of intracellular lipid vacuoles in BAT was quantified using Image J (NIH).

Cell Culture and Brown Adipocyte Differentiation

T37i cells were cultured and differentiated as described previously (26). Cells were next treated with metformin or vehicle (PBS) for 8 h. Then, supernatant was collected for determination of glycerol (Instruchemie, Delfzijl, the Netherlands) and cells were harvested in ice-cold lysis buffer, as described below.

Western Blot Analysis

Snap-frozen liver and BAT samples (~50 mg) or T37i cells were lysed in ice-cold buffer containing the following: 50 mmol/L HEPES (pH 7.6), 50 mmol/L NaF, 50 mmol/L KCl, 5 mmol/L NaPPi, 1 mmol/L EDTA, 1 mmol/L EGTA, 1 mmol/L dithiothreitol, 5 mmol/L ß-glycerophosphate, 1 mmol/L sodium vanadate, 1% NP40, and protease inhibitor cocktail (Complete; Roche). Western blots were performed as previously described (13). All the primary antibodies used are listed in **SUPPLEMENTARY TABLE 1**. Bands were visualized by enhanced chemiluminescence and quantified using Image J (NIH).

AMPK Assay

AMPK activity was assayed after immunoprecipitation with specific antibodies directed against α1- or α2-AMPK catalytic subunits (Kinasource, Dundee, Scotland), as previously described (14).

RNA/DNA Purification and qRT-PCR

RNA was extracted from snap-frozen liver or BAT samples (~25 mg) using Tripure RNA Isolation Reagent (Roche). Total RNA (1–2 µg) was reverse transcribed, and quantitative real-time PCR was then performed with SYBR Green Core Kit on a MyIQ thermal cycler (Bio-Rad). mRNA expression was normalized to CypD mRNA content and expressed as fold change compared with control mice using the ΔΔCT method. Genomic DNA was extracted using the Qiagen Tissue and Blood Kit (Qiagen, Hilden, Germany). For mitochondrial DNA copy number, ND1 (mitochondrial) and LPL (nuclear) copy numbers were quantified by qRT-PCR. All the primer sequences are listed in **SUPPLEMENTARY TABLE 1**.

Statistical Analysis

All data are expressed as mean ± SEM. Statistical analysis was performed using SPSS 17.0 software package for Windows (SPSS, Chicago, IL) with two-tailed unpaired Student *t* test. Differences between groups were considered statistically significant at $P < 0.05$.

RESULTS

Metformin Reduces Plasma Cholesterol and TG Levels

To investigate the effect of metformin on lipoprotein metabolism, E3L.CETP mice were first fed a cholesterolrich (0.1%) Western-type diet for 4 weeks and next treated with or without

metformin (200 mg/kg body weight/day) added to the diet for another 4 weeks. As compared with the control group, metformin did not affect body weight and composition, food intake and plasma glucose, and insulin and FA levels throughout the intervention period **(SUPPLEMENTARY FIGURE 1)**. However, metformin rapidly reduced both plasma TC (227 and 236% at weeks 2 and 4, respectively; $P < 0.05$) and TGs (226 and 238% at weeks 2 and 4, respectively; $P < 0.05$) in a time-dependent manner **(FIGURES 1A** and **C)**. Plasma lipoprotein profile analysis showed that this lipidlowering effect mostly resulted from a reduction of VLDL particles. In addition, a slight shift in plasma cholesterol profile, from VLDL-C to HDL-C (237 and +37%, respectively), was evidenced **(FIGURES 1B** and **D)**.

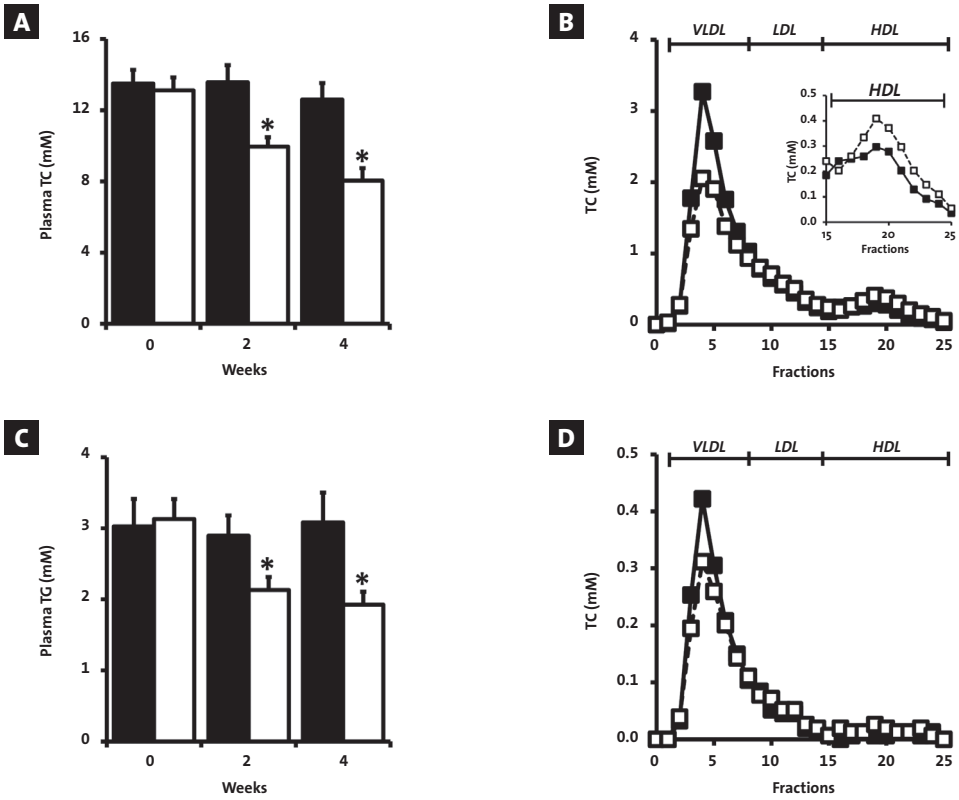

FIGURE 1 - Effect of metformin on plasma cholesterol and TG levels and lipoprotein distribution. Blood samples from 4 h–fasted control (black bars) and metformin-treated (open bars) mice were collected by tail bleeding using chilled paraoxon-coated capillaries at different time points. Plasma TC **A** and TGs **C** levels were determined. The plasma samples collected after 4 weeks of treatment were pooled groupwise and size fractionated by fast protein liquid chromatography. The individual fractions were analyzed for cholesterol **B** and TGs **D**. Data are means ± SEM ($n = 9$ per group).

*$P < 0.05$ vs. control.

Metformin Does Not Affect Hepatic VLDL-TG Production

Plasma VLDL-TG levels are determined by the balance between VLDL-TG production by the liver and VLDL-TG clearance by peripheral organs. Therefore, we first assessed the effect of metformin on hepatic VLDL-TG and -apoB production by injecting Trans^{35}S and tyloxapol in 4 h–fasted control and metformin-treated E3L.CETP mice. Despite the significantly lower basal plasma TG levels (1.72 ± 0.26 vs. 2.65 ± 0.36 mmol/L, $P < 0.05$; data not shown), metformin did not affect the time-dependent accumulation of plasma TG after tyloxapol injection when compared with control E3L.CETP mice **(FIGURE 2A)**. Therefore, the VLDL-TG production

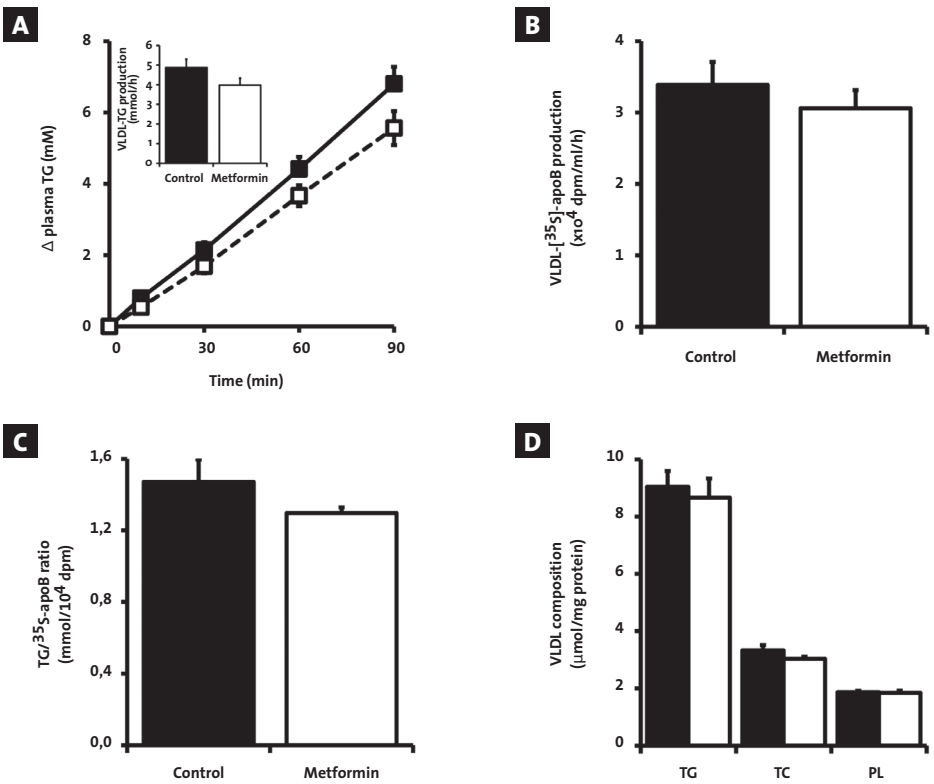

FIGURE 2 - Effect of metformin on hepatic VLDL-TG production. After 4 weeks of treatment, 4 h–fasted control (black squares/bars) and metformin-treated mice (open squares/bars) were injected with Trans^{35}S label ($t = -30$ min) and tyloxapol ($t = 0$ min), and blood samples were drawn up to 90 min after tyloxapol injection. Plasma TG concentrations were determined and plotted as the increase in plasma TG as compared with baseline **A**. The rate of TG production was calculated from the slopes of the curves from the individual mice (**A**, *inset)*. After 120 min, mice were exsanguinated and the total VLDL fraction was isolated by ultracentrifugation. The rate of newly synthesized VLDL-^{35}S-apoB **B**, the TG-to–^{35}S-apoB ratio **C**, as well as the amount of TGs, TC, and PLs per mg VLDL protein **D** were measured. Data are means ± SEM ($n = 5$–8 per group).

*$P < 0.05$ vs. control.

rate, calculated from the slope of the curve, was not significantly different **(FIGURE 2A,** inserted panel), although a trend for a slight decrease can eventually be suggested. The rate of VLDL-apoB production **(FIGURE 2B)**, the ratio of TG-apoB **(FIGURE 2C)**, as well as the composition of the VLDL particles secreted **(FIGURE 2D)** were not significantly altered, indicating that metformin did not affect the hepatic lipidation of VLDL particles. In line with these results, the TG, TC, and PL content in the liver from E3L.CETP mice did not significantly differ between the control and metformin groups, although hepatic TC content tended to be decreased in the metformin-treated group (221%, $P = 0.07$) **(SUPPLEMENTARY FIGURE 2)**. Furthermore, in our experimental conditions, metformin treatment did not affect hepatic AMPK activity, as

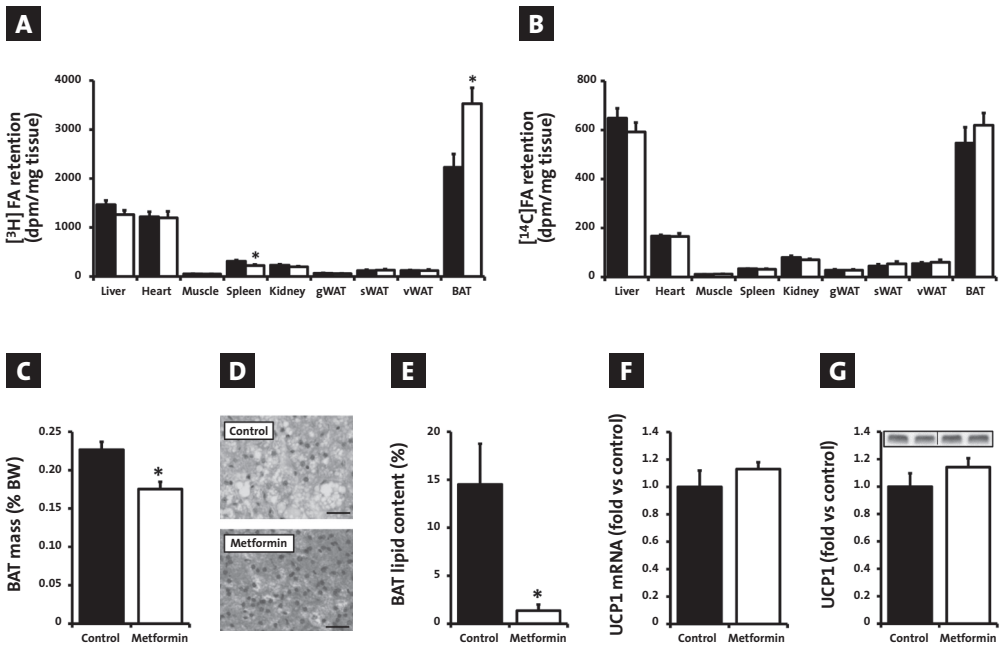

FIGURE 3 - Effect of metformin on peripheral VLDL-TG clearance and BAT. Four hour–fasted control (black bars) and metformin-treated (open bars) mice were continuously infused with [^{3}H]TG-labeled VLDL-like emulsion particles mixed with albumin-bound [^{14}C]FA for 2.5 h. Blood samples were taken using chilled paraoxon-coated capillaries by tail bleeding at 90 and 120 min of infusion to ensure that steadystate conditions had been reached. Subsequently, mice were killed and organs were quickly harvested and snap frozen in liquid nitrogen. Plasma levels of TGs and FAs were determined in plasma, and uptake of the radioactively [^{3}H]TG-labeled emulsion particles **A** and albumin-bound [^{14}C]FA **B** was determined in the organs. In separate experiments, BAT from control and metformin-treated mice were collected and weighed **C**. Hematoxylin and eosin staining of BAT sections was performed, and representative pictures are shown **D**. Relative content of lipid vacuoles in BAT tissue sections ($n = 3–4$ per group) were quantified **E**. mRNA **F** and protein **G** expression of UCP1 were determined by qRT-PCR and Western blot, respectively. Data are means ± SEM ($n = 7–8$ per group).

*$P < 0.05$ vs. control. BW, body weight. (A high-quality color representation of this figure is available in the online issue.)

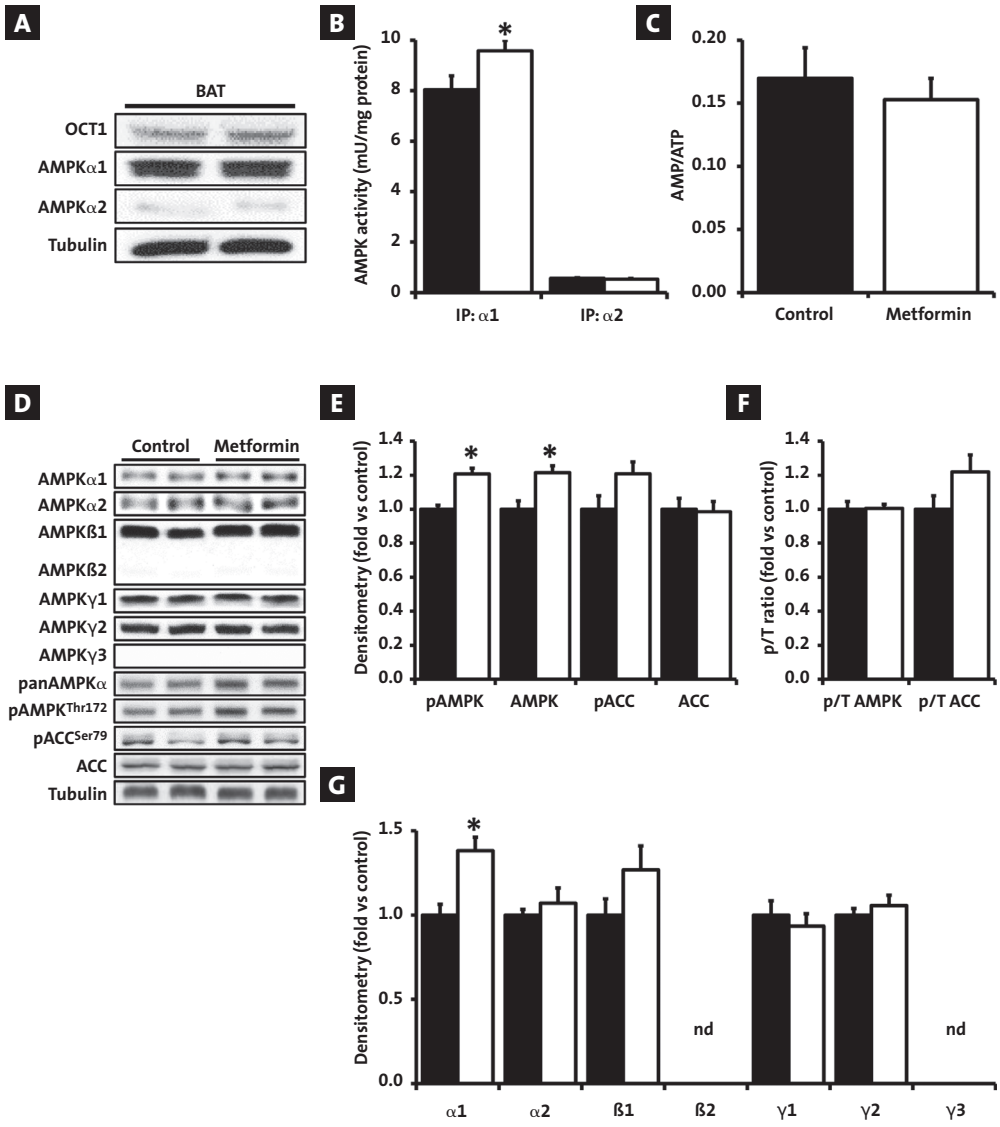

FIGURE 4 - Effect of metformin on AMPK expression, activity, and downstream signaling in BAT. BAT from 4 h–fasted mice was collected after 4 weeks of treatment with (open bars) or without metformin (control, black bars) and immediately snap frozen in liquid nitrogen. The protein expression of OCT1, AMPKα1, and AMPKα2 was determined by Western blot in BAT from control mice **A**. AMPK activity was measured by kinase assay after immunoprecipitation of either AMPKα1 or -α2 catalytic subunits with specific antibodies **B**. Adenine nucleotide concentrations in BAT were measured by high-performance liquid chromatography, and the AMP-to-ATP ratio was calculated **C**. The protein expression of BAT AMPK catalytic (α) and regulatory (ß and γ) subunits, ACC, and the phosphorylation states of Thr172- AMPK and Ser79-ACC were assessed by Western blot **D**, followed by densitometric quantification **E-G**. Tubulin expression was used as internal housekeeping protein. Data are means ± SEM (*n* = 8 per group).

*P < 0.05 vs. control. ND, not detectable.

assessed by phosphorylation of Thr172-AMPK and Ser79-acetyl-CoA carboxylase (ACC), the main downstream target of AMPK **(SUPPLEMENTARY FIGURE 2)**. Finally, we found that hepatic expression of key genes involved in FA/TG uptake, synthesis, and oxidation were not affected, whereas *Lrp1* and *Scarp1,* both involved in cholesterol uptake, were significantly downregulated by metformin **(SUPPLEMENTARY TABLE 1)**. In addition, the expression of *Abca1, Lcat,* and *Pltp* was also found to be significantly downregulated by metformin, suggesting that part of the HDL-enhancing effect of the drug could result from subtle changes in hepatic lipoprotein metabolism.

Metformin Promotes VLDL-TG Clearance by BAT and Influences BAT Mass and Composition

As clearance of TG from plasma is the other major determinant of TG metabolism, the effect of metformin on whole-body lipid partitioning was investigated next. For this purpose, the tissue-specific retention of FA derived from both [^{3}H]TG-labeled VLDL-like emulsion particles and albumin-bound [^{14}C]FA was determined after continuous tracer infusion for 2.5 h. Strikingly, metformin did not affect the uptake of [^{3}H]TG-derived FA by liver, heart, skeletal

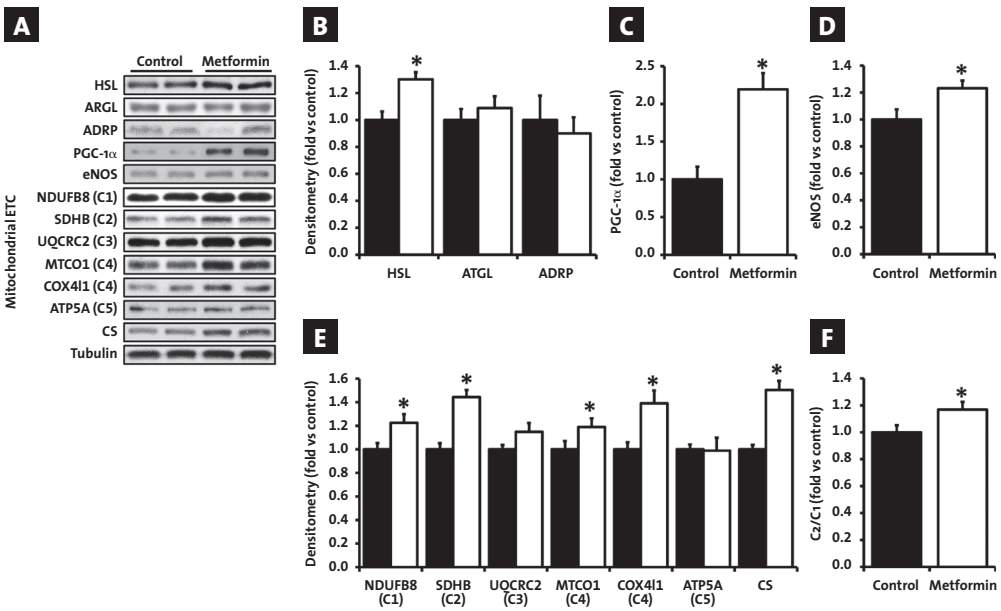

FIGURE 5 - Effect of metformin on expression of key lipolytic and mitochondrial proteins in BAT. BAT was collected in control (black bars) and metformin-treated (open bars) mice, as described in **FIGURE 4**. The protein expression of HSL, ATGL, ADRP, eNOS, PGC-1α, and CS and of various mitochondrial respiratory chain subunits (C1, NDUFB8; C2, SDHB; C3, UQCRC2; C4, MTCO1 and COX4I1; C5, ATP5A) was assessed by Western blot **A**, followed by densitometric quantification **B-E**. Tubulin expression was used as internal housekeeping protein. The ratio of mitochondrial respiratory chain complex 2 to complex 1 was calculated **F**. Data are means ± SEM (n = 8 per group).

*P < 0.05 vs. control. ETC, electron transport chain.

muscle, and various WAT depots but markedly increased ^{3}H retention in BAT (+58%, $P < 0.05$) **(FIGURE 3A)**. The uptake of albumin-bound [^{14}C]FA was not different for any of the organs studied **(FIGURE 3B)**, suggesting that metformin does not affect FA uptake per se but rather promotes lipoprotein lipase (LPL)–mediated VLDL-TG hydrolysis in BAT. Interestingly, BAT mass (–29%) and intracellular lipid droplet content (–91%) were found to be reduced in metformin-treated mice **(FIGURES 3C–E)**, both pointing toward more active BAT (27). However, neither UCP1 mRNA expression nor protein content was significantly affected **(FIGURES 3F** and **G)**.

Metformin Increases AMPK Activity, Lipolytic Machinery, and Mitochondrial Content in BAT

To further investigate the molecular mechanism by which metformin increased VLDL-TG clearance by BAT, we first showed that the organic cation transporter 1 (OCT1), which is crucial for intracellular transport of metformin (28), was expressed in BAT at both transcript (data not shown) and protein levels **(FIGURE 4A)**. We next determined the mRNA expression of genes involved in FA/lipoprotein uptake, FA metabolism, mitochondrial functions, and BAT differentiation but did not find any significant effect of metformin treatment in our

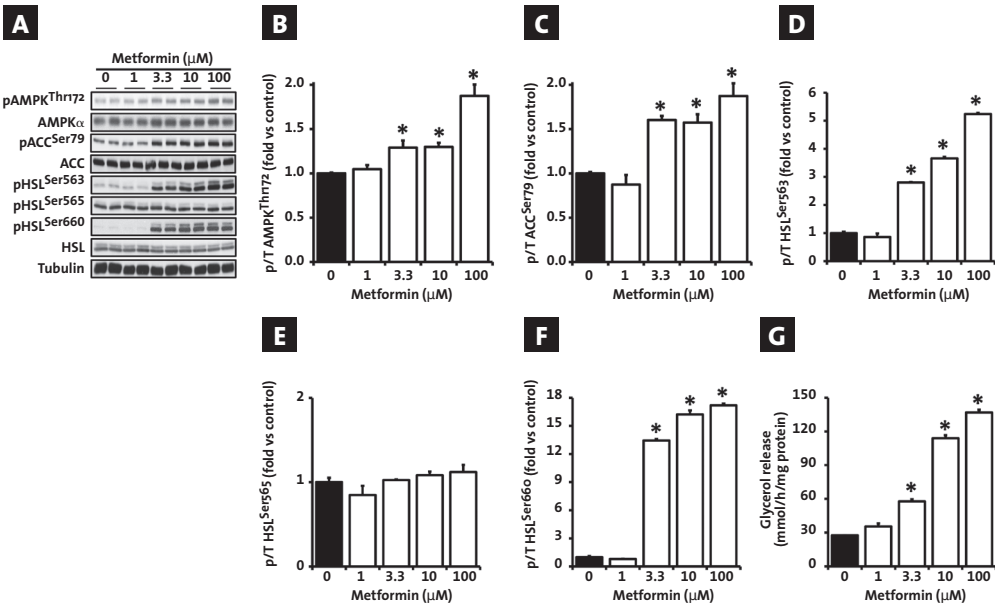

FIGURE 6 - Effect of metformin on AMPK signaling and lipolysis in T37i brown adipocytes. T37i cells were cultured and differentiated in brown adipocytes as described in RESEARCH DESIGN AND METHODS and next treated with increasing concentrations of metformin for 8 h. The protein expression and phosphorylation states of AMPKα, ACC, and HSL on various residues were assessed by Western blot **A** and the phospho-to-total ratios were calculated after densitometric quantification **B-F**. Tubulin expression was used as internal housekeeping protein. The lipolysis rate was assessed by measuring the time-dependent accumulation of glycerol in the culture medium **G** and expressed as μmol/h/mg protein. Data are means ± SEM *(n* = 3).

*$P < 0.05$ vs. control.

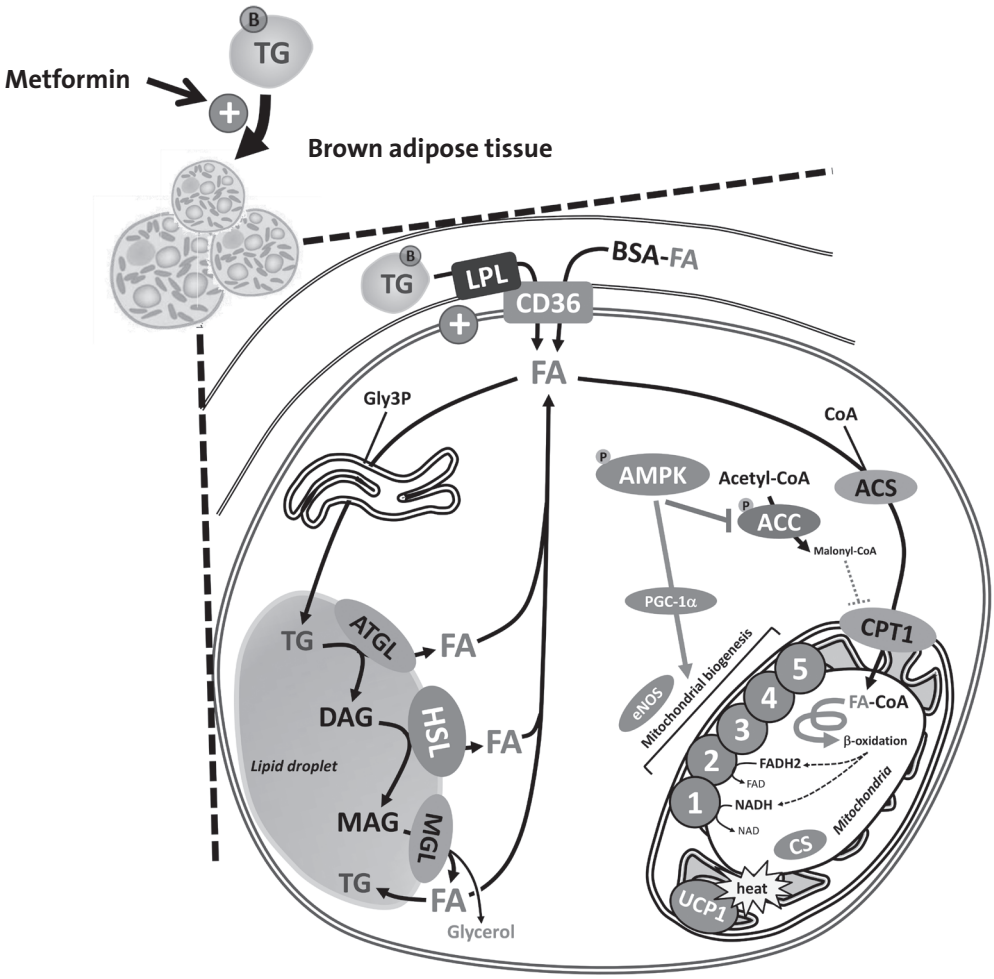

FIGURE 7 - Proposed mechanism for the BAT-mediated TG-lowering effect of metformin. Metformin exerts a beneficial effect on circulating lipids by lowering plasma TG, through a selective increase in TG-derived FA uptake by BAT. In addition, metformin also improves intracellular lipolytic capacity by increasing HSL expression and activity, thereby enhancing FA release from TG stored in lipid droplets. We propose that metformin next promotes FA oxidation in BAT by multiple (path)ways. First, metformin activates AMPK, leading to the subsequent phosphorylation and inactivation of its downstream target ACC. This relieves the inhibition exerted by malonyl-CoA on CPT1, ultimately promoting mitochondrial FA transport and oxidation. Second, metformin increases the tissue mitochondrial content, an effect that might be due to AMPK-mediated stimulation of mitochondrial biogenesis, as reflected by higher expression of eNOS and PGC-1α. Finally, by changing the qualitative composition of the mitochondrial respiratory chain, metformin can enhance respiratory chain complex 2–mediated FA oxidation and UCP1-independent metabolic uncoupling of oxidative phosphorylation.

experimental condition **(SUPPLEMENTARY TABLE 1)**. We confirmed that BAT mostly expressed AMPKα1 **(FIGURE 4A)**, as previously reported (29,30). Interestingly, we found that metformin selectively increased the activity of α1- (+19%, $P < 0.05$) but not of α2-containing AMPK heterotrimers in BAT **(FIGURE 4B)** without affecting the whole-tissue energy state, as assessed by the AMP-ATP ratio **(FIGURE 4C)**. This was associated with a significant increase in both Thr172 phosphorylation (+21%, $P < 0.05$) and expression of the AMPKα catalytic subunits (+21%, $P < 0.05$), whereas the phospho-to-total ratio was not affected **(FIGURES 4D–F)**. However, a trend for increased phosphorylation of the AMPK downstream target ACC was evidenced (+22%, $P = 0.07$) **(FIGURES 4D–F)**. The only AMPK subunit significantly increased by metformin was the α1 isoform (+38%, $P < 0.05$), whereas the other subunits were not affected **(FIGURE 4G)**, suggesting that the higher AMPK activity in BAT from metformin-treated mice was mostly due to an increase in AMPKα1 content. We next examined whether some of the key players involved in the regulation of TG lipolysis and FA oxidation in BAT were affected by metformin. Interestingly, the protein expression of the lipolytic enzyme HSL, but not that of adipose TG lipase (ATGL) and adipose differentiation– related protein (ADRP), was significantly increased by metformin in BAT (+30%, $P < 0.05$) **(FIGURES 5A** and **B)**. In addition, although the mitochondrial DNA content was not affected (data not shown), we found a marked increase in protein expression of two of the main regulators of mitochondrial biogenesis, endothelial nitric oxide synthase (eNOS) and PGC-1α (+23 and +127%, respectively; $P < 0.05$), together with a significantly higher content of citrate synthase (CS) and of most of the mitochondrial electron transport chain complexes in BAT from metformin-treated E3L.CETP mice **(FIGURES 5A** and **C–E)**. Of note, the ratio of mitochondrial respiratory chain complex 2 to complex 1 expression was also increased by metformin in BAT (+17%, $P < 0.05$) **(FIGURE 5F)**.

Metformin Induces AMPK Activation and Lipolysis in T37i Brown Adipocytes

To investigate whether metformin can directly affect AMPK activity and lipid metabolism in BAT, we used T37i cells, a well-established in vitro model of differentiated brown adipocytes (26). Interestingly, we showed that therapeutic concentrations of metformin dose-dependently increased phosphorylation states of AMPK, ACC, and HSL **(FIGURES 6A–F)**, as well as glycerol release into the medium, pointing toward enhanced intracellular lipolysis **(FIGURE 6G)**. Taken together, our results show that metformin not only promotes VLDL-TG uptake by BAT but also enhances both intracellular lipolytic and mitochondrial FA ß-oxidation capacity in this tissue **(FIGURE 7)**.

DISCUSSION

Metformin not only improves glycemic control in type 2 diabetic patients but also exerts beneficial effects on plasma lipid profiles (4) by a mechanism that has remained, so far, poorly understood. In the current study, we have therefore investigated the molecular mechanism(s) underlying this lipid-lowering property of metformin using E3L.CETP mice, a

well-characterized transgenic model displaying a human-like lipoprotein metabolism and human-like responses to lipid-modulating drugs when fed a Western-type diet (19–23). Our results show that chronic treatment of E3L.CETP mice with metformin recapitulates the effects on circulating lipoproteins observed in patients treated with the drug, i.e., reduction in plasma TG associated with significant reduction in VLDL (31). We next demonstrated that metformin does not affect hepatic VLDL-TG production but instead selectively promotes VLDL-TG clearance by BAT, an effect associated with elevated components of intracellular lipolytic and mitochondrial FA oxidation machinery in this highly active metabolic tissue. To the best of our knowledge, this study is the first one reporting that BAT is involved in the lipid-lowering effect of metformin, and therefore constitutes an important target tissue for the drug.

Plasma TG levels are determined by the balance between production of chylomicron-TG and VLDL-TG in intestine and liver, respectively, and their LPL-mediated TG clearance in peripheral tissues. In our study, all the experiments were performed in fasted mice, thereby excluding any significant contribution of intestine-derived chylomicrons to the change observed in circulating TG concentrations. Furthermore, metformin treatment did not affect the postprandial response to an oral lipid load **(SUPPLEMENTARY FIGURE 3)**, suggesting that impaired intestinal TG absorption is not involved in the TG-lowering effect of the drug. Besides its central role in glucose homeostasis, the liver plays a key role in lipid metabolism, notably by regulating synthesis and secretion of apoB-containing VLDL-TG particles (32). Hepatic VLDLTG production is mostly driven by intracellular substrate availability resulting from both FA uptake from the circulation and the balance between de novo lipogenesis and mitochondrial FA ß-oxidation in the liver (33). In our study, we found that metformin did not significantly affect plasma FA levels; hepatic lipid content; AMPK activity; expression of genes involved in FA/TG uptake, synthesis, and oxidation; VLDL-TG and VLDL-apoB secretion rates; and composition of the excreted VLDL particles. Although we did not find an apparent contribution of the liver to the TG-reducing effect of metformin, we cannot completely exclude that some of its hepatic effects were lowered or masked due to our experimental conditions, e.g., fasting state, and the pharmacokinetic features of the drug. Of note, we found that expression of some genes involved in hepatic HDL uptake *(Lrp1* and *Scarb1)* and remodeling *(Abca1* and *Pltp)* was decreased by metformin, suggesting that part of the mild HDL-raising effect of the drug might be partly due to subtle changes in cholesterol metabolism in the liver. Future studies are required for clarifying the exact underlying molecular mechanism.

Plasma VLDL-TG clearance is driven by LPL-mediated lipolysis in the capillaries of peripheral tissues (34). The most striking result of our present study was that metformin induced a potent and selective increase in VLDLglycerol tri[^{3}H]oleate-derived [^{3}H]oleate retention in BAT without affecting VLDL-TG uptake by heart, muscle, and various white adipose tissues. Recently, Bartelt et al. (35) were the first to identify BAT as a major organ involved in plasma VLDL-TG clearance in rodents. In this elegant study confirming previous observations (36), they reported that BAT constitutes a quantitatively relevant lipid-clearing organ displaying very high rates of VLDL-TG uptake (35) by a mechanism that still remains to be fully charac-

terized. In the current study, our observation that metformin promotes VLDL-[^{3}H]TG–derived FA but not albumin-bound [^{14}C]FA retention in BAT suggests that the TG-lowering effect of the drug is mediated by a tissue-specific increase in LPL-mediated VLDL-TG hydrolysis with subsequent retention of the liberated FA in BAT. At the molecular level, it remains to be clarified whether increases in endothelial LPL expression and/or subtle changes in apolipoproteins and angiopoietin-like proteins regulating local LPL activity (37) are involved in the BAT-specific VLDL-derived TG hydrolysis induced by metformin.

Owing to its high mitochondrial and oxidative enzyme content, BAT has a marked ability to oxidize both glucose and FA, the latter being derived from either LPL-mediated hydrolysis of VLDL-TG or intracellular TG that is stored in lipid droplets. Once released, FAs are rapidly reesterified in TG or directed to mitochondria for oxidation or activation of UCP1, leading to dissipation of the proton gradient across the inner mitochondrial membrane and heat production (38). At the molecular level, we found that metformin, both in vivo and in vitro, increased AMPK activity and Ser79-ACC phosphorylation, an effect that is expected to promote mitochondrial FA transport and oxidation by relieving the inhibition of CPT1α by malonyl-CoA (9). AMPK activation is known to trigger mitochondrial biogenesis, at least in skeletal muscle (39) and liver (40). Interestingly, the expression of key proteins of the mitochondrial respiratory chain complexes and CS was increased by metformin in BAT, indicating enhanced mitochondrial content in this tissue. Mechanistically, the expression of PGC-1α and eNOS, which are both recognized as important regulators of mitochondrial biogenesis (41,42), were found to be higher in BAT from metformin-treated mice, suggesting activation of the AMPK-PGC1α-eNOS pathway by metformin in this tissue. Finally, we found that metformin affected the qualitative composition of the mitochondrial respiratory chain in BAT, leading to an increase in complex 2 relative to complex 1. This effect might also contribute to enhanced FA oxidation by promoting electron supply to the respiratory chain complex 2. Interestingly, modulating the ratio of $FADH_2$ to NADH oxidation will also affect the stoichiometry of oxidative phosphorylation and promote UCP1-independent metabolic uncoupling, with the yield of ATP synthesis being lowered by ~40% when $FADH_2$ is oxidized as compared with NADH (43). Taken together, we propose that secondary to its tissue-specific increase in VLDL-TG uptake, metformin promotes FA oxidation in BAT by enhancing both intracellular lipolytic capacity and mitochondrial oxidative machinery. It is important to underline that we do not exclude that another AMPKindependent mechanism(s) in BAT might also contribute to the TG-lowering effect of metformin in vivo.

The recent discovery of metabolically active BAT in adult humans (44–46) has caused a revival interest in this potential new therapeutic target for the treatment of obesity and metabolic disorders (47,48). Although the precise role of BAT in TG metabolism remains to be established, it has been recently shown that FA uptake and oxidation in BAT significantly contributes to energy expenditure in humans (49). Thus, it is tempting to speculate that part of the weight-lowering property of metformin might be secondary to enhanced lipid oxidation and energy dissipation in BAT. Further studies allowing imaging of lipid metabolism in BAT from metformin- treated patients, for instance using ^{18}F-labeled FA incorporated into VLDL-TG coupled to position emission tomography scanning (50), would be crucial to

specifically address this point.

In summary, we show that metformin exerts a beneficial effect on circulating lipids by lowering plasma TG, through a selective BAT-mediated increase in VLDL-TG uptake/lipolysis **(FIGURE 7)**. The current study is the first identifying BAT as a new important mechanistic player in the lipid-lowering action of metformin, suggesting that targeting this tissue, on top of being interesting for body weight management, might also be of therapeutic importance in the treatment of dyslipidemia.

ACKNOWLEDGMENTS

The authors are grateful to Elsbet Pieterman, Chris van der Bent, Linda Switzar, and Amanda Pronk (Leiden University Medical Center) for their valuable technical assistance.

REFERENCES

1 Goodarzi MO, Bryer-Ash M. Metformin revisited: re-evaluation of its properties and role in the pharmacopoeia of modern antidiabetic agents. Diabetes Obes Metab 2005;7:654–665.

2 Nathan DM, Buse JB, Davidson MB, et al.; American Diabetes Association; European Association for the Study of Diabetes. Medical management of hyperglycaemia in type 2 diabetes mellitus: a consensus algorithm for the initiation and adjustment of therapy: a consensus statement from the American Diabetes Association and the European Association for the Study of Diabetes. Diabetologia 2009;52:17–30.

3 Natali A, Ferrannini E. Effects of metformin and thiazolidinediones on suppression of hepatic glucose production and stimulation of glucose uptake in type 2 diabetes: a systematic review. Diabetologia 2006;49:434–441.

4 Salpeter SR, Buckley NS, Kahn JA, Salpeter EE. Meta-analysis: metformin treatment in persons at risk for diabetes mellitus. Am J Med 2008;121: 149–157.e2.

5 UK Prospective Diabetes Study (UKPDS) Group. Effect of intensive bloodglucose control with metformin on complications in overweight patients with type 2 diabetes (UKPDS 34). Lancet 1998a;352:854–865.

6 Viollet B, Guigas B, Sanz Garcia N, Leclerc J, Foretz M, Andreelli F. Cellular and molecular mechanisms of metformin: an overview. Clin Sci (Lond) 2012;122:253–270.

7 Zhou G, Myers R, Li Y, et al. Role of AMP-activated protein kinase in mechanism of metformin action. J Clin Invest 2001; 108:1167–1174.

8 Carling D, Thornton C, Woods A, Sanders MJ. AMP-activated protein kinase: new regulation, new roles? Biochem J 2012;445:11–27.

9 Hardie DG, Ross FA, Hawley SA. AMPK: a nutrient and energy sensor that maintains energy homeostasis. Nat Rev Mol Cell Biol 2012;13:251–262.

10 El-Mir MY, Nogueira V, Fontaine E, Avéret N, Rigoulet M, Leverve X. Dimethylbiguanide inhibits cell respiration via an indirect effect targeted on the respiratory chain complex I. J Biol Chem 2000;275:223–228.

11 Owen MR, Doran E, Halestrap AP. Evidence that metformin exerts its antidiabetic effects through inhibition of complex 1 of the mitochondrial respiratory chain. Biochem J 2000;348:607–614.

12 Hawley SA, Ross FA, Chevtzoff C, et al. Use of cells expressing gamma subunit variants to identify diverse mechanisms of AMPK activation. Cell Metab 2010;11:554–565.

13 Stephenne X, Foretz M, Taleux N, et al. Metformin activates AMP-activated protein kinase in primary human hepatocytes by decreasing cellular energy status. Diabetologia 2011;54:3101–3110.

14 Guigas B, Bertrand L, Taleux N, et al. 5-Aminoimidazole-4-carboxamide-1-beta-D-ribofuranoside and metformin inhibit hepatic glucose phosphorylation by an AMP-activated protein kinase-independent effect on glucokinase translocation. Diabetes 2006;55:865–874.

15 Foretz M, Hébrard S, Leclerc J, et al. Metformin inhibits hepatic gluconeogenesis in mice independently of the LKB1/AMPK pathway via a decrease in hepatic energy state. J Clin Invest 2010;120:2355–2369.

16 Shaw RJ, Lamia KA, Vasquez D, et al. The kinase LKB1 mediates glucose homeostasis in liver and therapeutic effects of metformin. Science 2005; 310:1642–1646.

17 Kalender A, Selvaraj A, Kim SY, et al. Metformin, independent of AMPK, inhibits mTORC1 in a rag GTPase-dependent manner. Cell Metab 2010;11: 390–401.

18 Miller RA, Chu Q, Xie J, Foretz M, Viollet B, Birnbaum MJ. Biguanides suppress hepatic glucagon signalling by decreasing production of cyclic AMP. Nature 2013;494:256–260.

19 Westerterp M, van der Hoogt CC, de Haan W, et al. Cholesteryl ester transfer protein decreases high-density lipoprotein and severely aggravates atherosclerosis in APOE*3-Leiden mice. Arterioscler Thromb Vasc Biol 2006;26:2552–2559.
20 Bijland S, Pieterman EJ, Maas AC, et al. Fenofibrate increases very low density lipoprotein triglyceride production despite reducing plasma triglyceride levels in APOE*3-Leiden.CETP mice. J Biol Chem 2010; 285: 25168–25175.
21 Bijland S, van den Berg SA, Voshol PJ, et al. CETP does not affect triglyceride production or clearance in APOE*3-Leiden mice. J Lipid Res 2010;51:97–102.
22 de Haan W, van der Hoogt CC, Westerterp M, et al. Atorvastatin increases HDL cholesterol by reducing CETP expression in cholesterol-fed APOE*3-Leiden.CETP mice. Atherosclerosis 2008;197:57–63
23 van der Hoorn JW, de Haan W, Berbée JF, et al. Niacin increases HDL by reducing hepatic expression and plasma levels of cholesteryl ester transfer protein in APOE*3Leiden.CETP mice. Arterioscler Thromb Vasc Biol 2008; 28:2016–2022.
24 Coomans CP, Geerling JJ, Guigas B, et al. Circulating insulin stimulates fatty acid retention in white adipose tissue via KATP channel activation in the central nervous system only in insulin-sensitive mice. J Lipid Res 2011;52:1712–1722.
25 Teusink B, Voshol PJ, Dahlmans VE, et al. Contribution of fatty acids released from lipolysis of plasma triglycerides to total plasma fatty acid flux and tissue-specific fatty acid uptake. Diabetes 2003;52:614–620.
26 Zennaro MC, Le Menuet D, Viengchareun S, Walker F, Ricquier D, Lombès M. Hibernoma development in transgenic mice identifies brown adipose tissue as a novel target of aldosterone action. J Clin Invest 1998; 101:1254–1260.
27 Ortega-Molina A, Efeyan A, Lopez-Guadamillas E, et al. Pten positively regulates brown adipose function, energy expenditure, and longevity. Cell Metab 2012;15:382–394.
28 Shu Y, Sheardown SA, Brown C, et al. Effect of genetic variation in the organic cation transporter 1 (OCT1) on metformin action. J Clin Invest 2007;117:1422–1431.
29 Pulinilkunnil T, He H, Kong D, et al. Adrenergic regulation of AMP-activated protein kinase in brown adipose tissue in vivo. J Biol Chem 2011;286: 8798–8809.
30 Mulligan JD, Gonzalez AA, Stewart AM, Carey HV, Saupe KW. Upregulation of AMPK during cold exposure occurs via distinct mechanisms in brown and white adipose tissue of the mouse. J Physiol 2007;580:677–684.
31 Jonker JT, Wang Y, de Haan W, et al. Pioglitazone decreases plasma cholesteryl ester transfer protein mass, associated with a decrease in hepatic triglyceride content, in patients with type 2 diabetes. Diabetes Care 2010; 33:1625–1628.
32 Xiao C, Hsieh J, Adeli K, Lewis GF. Gut-liver interaction in triglyceride-rich lipoprotein metabolism. Am J Physiol Endocrinol Metab 2011;301:E429–E446.
33 Nielsen S, Karpe F. Determinants of VLDL-triglycerides production. Curr Opin Lipidol 2012;23:321–326.
34 Dallinga-Thie GM, Franssen R, Mooij HL, et al. The metabolism of triglyceride-rich lipoproteins revisited: new players, new insight. Atherosclerosis 2010;211:1–8.
35 Bartelt A, Bruns OT, Reimer R, et al. Brown adipose tissue activity controls triglyceride clearance. Nat Med 2011;17:200–205.
36 Hagberg CE, Falkevall A, Wang X, et al. Vascular endothelial growth factor B controls endothelial fatty acid uptake. Nature 2010;464:917–921.
37 Davies BS, Beigneux AP, Fong LG, Young SG. New wrinkles in lipoprotein lipase biology. Curr Opin Lipidol 2012;23:35–42.

38 Festuccia WT, Blanchard PG, Deshaies Y. Control of brown adipose tissue glucose and lipid metabolism by PPARg. Front Endocrinol (Lausanne) 2011;2:84.
39 Zong H, Ren JM, Young LH, et al. AMP kinase is required for mitochondrial biogenesis in skeletal muscle in response to chronic energy deprivation. Proc Natl Acad Sci USA 2002;99:15983–15987.
40 Guigas B, Taleux N, Foretz M, et al. AMP-activated protein kinase-independent inhibition of hepatic mitochondrial oxidative phosphorylation by AICA riboside. Biochem J 2007;404:499–507.
41 Jornayvaz FR, Shulman GI. Regulation of mitochondrial biogenesis. Essays Biochem 2010;47:69–84.
42 Lira VA, Brown DL, Lira AK, et al. Nitric oxide and AMPK cooperatively regulate PGC-1 in skeletal muscle cells. J Physiol 2010;588:3551–3566.
43 Leverve XM, Taleux N, Favier R, et al. Cellular energy metabolism and integrated oxidative phosphorylation. In *Molecular System Bioenergetics: Energy for Life*. Saks V, Ed. Weinheim, WILEY-VCH Verlag GmbH & Co., 2007, p. 11–27.
44 Cypess AM, Lehman S, Williams G, et al. Identification and importance of brown adipose tissue in adult humans. N Engl J Med 2009;360:1509–1517.
45 van Marken Lichtenbelt WD, Vanhommerig JW, Smulders NM, et al. Coldactivated brown adipose tissue in healthy men. N Engl J Med 2009;360: 1500–1508.
46 Virtanen KA, Lidell ME, Orava J, et al. Functional brown adipose tissue in healthy adults. N Engl J Med 2009;360:1518–1525.
47 Ravussin E, Galgani JE. The implication of brown adipose tissue for humans. Annu Rev Nutr 2011;31:33–47.
48 Seale P, Kajimura S, Spiegelman BM. Transcriptional control of brown adipocyte development and physiological function—of mice and men. Genes Dev 2009;23:788–797.
49 Ouellet V, Labbé SM, Blondin DP, et al. Brown adipose tissue oxidative metabolism contributes to energy expenditure during acute cold exposure in humans. J Clin Invest 2012;122:545–552.
50 Labbé SM, Grenier-Larouche T, Croteau E, et al. Organ-specific dietary fatty acid uptake in humans using positron emission tomography coupled to computed tomography. Am J Physiol Endocrinol Metab 2011;300:E445–E453.

SUPPLEMENTARY DATA

SUPPLEMENTARY TABLE 1 - **Primary antibodies for Western blots**

Primary antibody	Residue	Supplier	Reference	Dilution
ACC	-	Cell Signaling	#3662	1:2000
ACC	Ser79	Cell Signaling	#3661	1:2000
ADRP	-	AbCam	Ab108323	1:1000
AMPKα	-	Cell Signaling	#2532	1:1000
AMPKα	Thr172	Cell Signaling	#2535	1:1000
AMPKα1	-	Kinasource	AB-140	1:2500
AMPKα2	-	Kinasource	AB-141	1:2500
ATGL	-	Cell Signaling	#2439	1:1250
ATP5A (C5)	-	AbCam	ab110413	1:1000
COX4I1 (C4)	-	Aviva Systems Biology	ARP42784	1:500
CS	-	AbCam	Ab96600	1:1000
HSL	-	Cell Signaling	#4107	1:2000
HSL	Ser563	Cell Signaling	#4139	1:2000
HSL	Ser565	Cell Signaling	#4137	1:1000
HSL	Ser660	Cell Signaling	#4126	1:1000
MTCO1 (C4)	-	AbCam	ab110413	1:1000
NDUFB8 (C1)	-	AbCam	ab110413	1:1000
eNOS (NOS3)	-	Santa Cruz	sc-654	1:1000
OCT1	-	Santa Cruz	sc-133866	1:500
PGC1α	-	AbCam	ab54481	1:1000
UCP1	-	Sigma	U6382	1:2500
UQCRC2 (C3)	-	AbCam	ab110413	1:1000
SDHB (C2)	-	AbCam	ab110413	1:1000
Tubulin	-	Cell Signaling	#2148	1:2000

SUPPLEMENTARY TABLE 2 - **Primer sequences for qRT-PCR**

Gene	Accession number	Forward primer	Reverse primer
Abca1	NM_013454.3	CCCAGAGCAAAAAGCGACTC	GGTCATCATCACTTTGGTCCTTG
Abcg5	NM_031884	TGTCCTACAGCGTCAGCAACC	GGCCACTCTCGATGTACAAGG
Abcg8	NM_026180	TCCTGTGAGCTGGGCATCCGA	CCCGCAGCCTGAGCTCCCTAT
Acaca	NM_133360.2	CAGCTGGTGCAGAGGTACCG	TCTACTCGCAGGTACTGCCG
Acacb	NM_133904.2	GCGCCTACTATGAGGCCCAGCA	ACAAACTCGGCTGGGGACGC
Acly	NM_134037.2	TGTGGACGGCTTCATCGGCG	ATGTCATCCCAGGGGTGACG
Acox1	NM_015729	GGGACCCACAAGCCTCTGCCA	GTGCCGTCAGGCTTCACCTGG
Apoa1	NM_009692	TGCGGTCAAAGACAGCGGCA	AGATTCAGGTTCAGCTGTTGGCCC
Apob	NM_009693	CAGCTGCAAGTGTCCTCGTC	GACACAGAGGGCTTTGCCAC

Gene	Accession number	Forward primer	Reverse primer
Atp5a1	NM_007505.2	CCAAGCAGGCTGTCGCTTACCG	TCTCCAGCAGGCGGGAGTGT
Cd36	NM_001159558	GCAAAGAACAGCAGCAAAATC	CAGTGAAGGCTCAAAGATGG
Cidea	NM_007702	CTCGGCTGTCTCAATGTCAA	CCGCATAGACCAGGAACTGT
Cidec	NM_178373	CCATCAGAACAGCGCAAGAAG	AGAGGGTTGCCTTCACGTTC
Cox7a1	NM_009944.3	AAAACCGTGTGGCAGAGAAG	CCAGCCCAAGCAGTATAAGC
Cpt1a	NM_013495	AGGAGACAAGAACCCCAACA	AAGGAATGCAGGTCCACATC
Creb1	NM_133828	AGCTGCCACTCAGCCGGGTA	TCGCCTGAGGCAGCTTGAACA
Cs	NM_026444.3	GCTAAGTACTGGGAGCTCATCTAT	GCCTAGAGTCAATGGCTCCG
Dgat1	NM_010046.2	CTAGTGAGCGTTCCCCTGCG	GGGCATCGTAGTTGAGCACG
Dio2	NM_010050	CGCTCCAAGTCCACTCGCGG	CGGCCCCATCAGCGGTCTTC
Fabp1	NM_017399.4	GCCACCATGAACTTCTCCGGCA	GGTCCTCGGGCAGACCTATTGC
Fasn	NM_007988	CACAGGCATCAATGTCAACC	TTTGGGAAGTCCTCAGCAAC
*Fdft*1	NM_010191.2	CCAACTCAATGGGTCTGTTCCT	TGGCTTAGCAAAGTCTTCCAACT
Fdps	NM_134469.4	ATGGAGATGGGCGAGTTCTTC	CCGACCTTTCCCGTCACA
Gpam	NM_008149.3	TCATACCCGTGGGCATCTCG	AATCCACTCGGACGTAGCCG
Gpihbp1	NM_026730	AGTGGACAGCCAGGGAGTGGC	GCTCTCCCCGCTGTGAAGCAC
Hmgcr	NM_008255	CTTGTGGAATGCCTTGTGATTG	AGCCGAAGCAGCACATGAT
Hmgcs1	NM_145942.4	GGACTGGAAGCCTTTGGGGACG	TGCCAGGACAGAAGCCAGGGA
Hmgcs2	NM_008256.4	CATCGCAGGAAGTATGCCCG	GCTGTTTGGGTAGCAGCTCG
Idi1	NM_145360.2	TGGGAATACCCTTGGAAGAGGTTGA	CCCCAGATACCATCAGATTGGGCCT
Lcat	NM_008490.2	GGCAAGACCGAATCTGTTGAG	ACCAGATTCTGCACCAGTGTGT
Ldlr	NM_010700	GCATCAGCTTGGACAAGGTGT	GGGAACAGCCACCATTGTTG
Lipe	NM_010719	AGCCTCATGGACCCTCTTCT	GCCTAGTGCCTTCTGGTCTG
Lpl	NM_008509	CAGGGGGTCACCTGGTCGAAGT	AGCTGGTCCACGTCTCCGAGT
Lrp1	NM_008512	GGAACTCCAGTCGCTGCAAC	TAGCACAGGGATGTCCGCTC
Mttp	NM_008642	GCCTGTGGCTTTGCCACCCA	TCCACCACTGCCTTGAGCTTGC
ND1	NP_904328.1	CTACAACCATTTGCAGACGC	GGAACTCATAGACTTAATGC
Ndufb8	NM_026061.2	GAGGCACGGAGAGCCTTCCA	GGGAGCATCGGGTAGTCGCC
Nr1h3	NM_013839.4	CTGCACGCCTACGTCTCCAT	AAGTACGGAGGCTCACCAGCT
Pltp	NM_011125.2	GGCCGTCTCAGTGCTAAGTT	CGAAGTTGATACCCTCAGGAA
Pnpla2	NM_001163689	TTCGCAATCTCTACCGCCTC	TGGTTCAGTAGGCCATTCCTC
Plin2	NM_007408.3	CAGGATGGAGGAAAGACTGC	CTTATCCACCACCCCTGAGA
Plin4	NM_020568.3	TGCCCCCTCATCTAAAGTGTC	AGGCATCTTCACTGCTGGTC
Plin5	NM_001077348.1	TGTCCAGTGCTTACAACTCGG	CAGGGCACAGGTAGTCACAC
Ppara	NM_011144	CAACCCGCCTTTTGTCATAC	CCTCTGCCTCTTTGTCTTCG
Pparg	NM_011146	CCTGCGGAAGCCCTTTGGTGA	AGCCTGGGCGGTCTCCACTG
Ppargc1a	NM_008904.2	TGCTAGCGGTTCTCACAGAG	AGTGCTAAGACCGCTGCATT
Ppargc1b	NM_133249	CTTGCTTTTCCCAGATGAGG	CCCTGTCCGTGAGGAACG
Prkaa1	NM_001013367	TGGTGGGAAAAATCCGCCGGG	CGGCTTTCCTTTTCGTCCAACCTTC
Prkaa2	NM_178143	ACCGAGCTATGAAGCAGCTGGGTT	CCTCTGCTCCACCACCTCATCATC
Scarb1	NM_016741	TCGCTTCACGGCCCCCGATA	ACAGAGGCGCACCAAACCTGC

Gene	Accession number	Forward primer	Reverse primer
Scd1	NM_009127.4	GCTCTACACCTGCCTCTTCGGGAT	TCCAGAGGCGATGAGCCCCG
Sdha	NM_023281.1	GGGACAGGTGCTGAAGCATGTGAAT	GCAATGCTCAGGGCACAGGCT
Sdhb	NM_023374.3	CGACGGTCGGGGTCTCCTTGA	CCTGAAACTGCAGGCCGACTC
Sqle	NM_009270.3	TCGTTCGTGACGGACCCGGA	ACTGTATCTCCAAGGCCCAGCTCC
Srebf1	NM_011480	GGCCGAGATGTGCGAACT	TTGTTGATGAGCTGGAGCATGT
Srebf1	NM_011480	CTGGCTGAGGCGGGATGA	TACGGGCCACAAGAAGTAGA
Tfam	NM_009360	CTTCCTGGGTTCACCCGCAC	ATGGGCACTATGGCTCCGTC
Ucp1	NM_009463	TCAGGATTGGCCTCTACGAC	TGCATTCTGACCTTCACGAC
Vldlr	NM_013703	TCTTGAGCAGTGTGGCCGTC	TTGCAGTCAGGGTCTCCGTC

SUPPLEMENTARY TABLE 3 - **Effect of metformin on hepatic expression of genes involved in FA/TG and lipoprotein metabolism.** Livers were isolated from 4 h-fasted mice treated with or without metformin for 4 weeks. mRNA expression of the indicated genes were quantified by RT-PCR relative to CypD gene and expressed as fold difference compared with the control group. Data are means ± SEM (n=8). *, p<0.05.

Genes by function	Protein	Fold change	
		Control	Metformin
FA uptake			
Fabp1	**FABP1**	1.00 ± 0.16	1.16 ± 0.14
Cd36	**CD36**	1.00 ± 0.13	0.89 ± 0.06
Lpl	**LPL**	1.00 ± 0.07	0.83 ± 0.10
FA/TG synthesis			
Srebf1	**SREBP-1A**	1.00 ± 0.14	0.84 ± 0.16
Srebf1	**SREBP-1C**	1.00 ± 0.06	0.94 ± 0.09
Nr1h3	**LXRα**	1.00 ± 0.06	0.97 ± 0.04
Fasn	**FAS**	1.00 ± 0.16	0.97 ± 0.25
Scd1	**SCD1**	1.00 ± 0.22	0.82 ± 0.16
Dgat1	**DGAT1**	1.00 ± 0.13	0.89 ± 0.10
FA oxidation			
Pparagc1a	**PGC1α**	1.00 ± 0.10	0.72 ± 0.16
Ppara	**PPARα**	1.00 ± 0.10	0.93 ± 0.06
Cpt1a	**CPT1α**	1.00 ± 0.05	0.94 ± 0.06
Acaca	**ACC1**	1.00 ± 0.12	0.83 ± 0.14
Acacb	**ACC2**	1.00 ± 0.22	1.07 ± 0.13
Acox1	**ACOX1**	1.00 ± 0.06	0.92 ± 0.09
Lipoprotein uptake			
Ldlr	**LDLr**	1.00 ± 0.10	0.96 ± 0.12
Lrp1	**LRP1**	1.00 ± 0.09	**0.85 ± 0.07***
Scarb1	**SRB1**	1.00 ± 0.05	**0.86 ± 0.05***

Genes by function	Protein	Fold change	
		Control	Metformin
VLDL synthesis			
Apob	**ApoB**	1.00 ± 0.05	0.88 ± 0.07
Mttp	**MTP**	1.00 ± 0.10	0.95 ± 0.12
Cholesterol synthesis			
Srbp2	**SRBP2**	1.00 ± 0.06	1.07 ± 0.11
Hmgcr	**HMG CoA-R**	1.00 ± 0.15	1.13 ± 0.21
Hmgcs1	**HMG CoA-S1**	1.00 ± 0.10	1.04 ± 0.18
Hmgcs2	**HMG CoA-S2**	1.00 ± 0.06	0.99 ± 0.06
Sqle	**SQLE**	1.00 ± 0.20	1.07 ± 0.21
Idi1	**IDI1**	1.00 ± 0.10	**1.30 ± 0.10***
Fdps	**FDPS**	1.00 ± 0.23	1.21 ± 0.17
Fdft1	**FDFT1**	1.00 ± 0.09	0.87 ± 0.14
Cholesterol excretion			
Abcg5	**ABCG5**	1.00 ± 0.10	0.82 ± 0.09
Abcg8	**ABCG8**	1.00 ± 0.07	0.83 ± 0.12
HDL metabolism			
Apoa1	**ApoA1**	1.00 ± 0.10	0.96 ± 0.15
Lipe	**HL**	1.00 ± 0.30	0.70 ± 0.16
Pltp	**PLTP**	1.00 ± 0.11	**0.78 ± 0.10***
Abca1	**ABCA1**	1.00 ± 0.07	**0.78 ± 0.09***
Lcat	**LCAT**	1.00 ± 0.04	**0.87 ± 0.06***
CETP	**CETP**	1.00 ± 0.17	0.73 ± 0.20

SUPPLEMENTARY TABLE 4 - **Effect of metformin on BAT expression of genes involved in tissue differentiation, lipoprotein/FA uptake, TG synthesis, FA oxidation and mitochondrial functions.** Brown adipose tissues were isolated from 4 h-fasted mice treated with or without metformin for 4 weeks. mRNA expression of the indicated genes were quantified by RT-PCR relative to CypD gene and expressed as fold difference compared with the control group. Data are means +/- SEM (n=7-8).

Genes by function	Protein	Fold change	
		Control	Metformin
BAT differentiation			
Prdm16	**PRDM16**	1.00 ± 0.27	1.14 ± 0.35
Cidea	**CIDEA**	1.00 ± 0.20	1.09 ± 0.20
Dio2	**DIO2**	1.00 ± 0.16	1.00 ± 0.20
Essra	**ESSR**α	1.00 ± 0.36	1.03 ± 0.43

Genes by function	Protein	Fold change	
		Control	Metformin
Lipoprotein/FA uptake			
CD36	**CD36**	1.00 ± 0.11	0.90 ± 0.12
Ldlr	**LDLr**	1.00 ± 0.20	1.19 ± 0.29
Lrp1	**LRP1**	1.00 ± 0.09	1.34 ± 0.34
Vldlr	**VLDLr**	1.00 ± 0.12	0.96 ± 0.11
Gpihbp1	**GPIHBP1**	1.00 ± 0.05	1.17 ± 0.13
Lpl	**LPL**	1.00 ± 0.16	0.96 ± 0.22
FA/TG synthesis			
Scd1	**SCD1**	1.00 ± 0.17	0.94 ± 0.26
Fasn	**FAS**	1.00 ± 0.14	1.25 ± 0.22
Acly	**ACLY**	1.00 ± 0.23	0.94 ± 0.18
Dgat1	**DGAT1**	1.00 ± 0.16	1.10 ± 0.13
Pck1	**PEPCK**	1.00 ± 0.18	1.18 ± 0.26
Gpam	**GPAT**	1.00 ± 0.23	1.03 ± 0.31
FA oxidation			
Ppara	**PPARα**	1.00 ± 0.23	1.15 ± 0.25
Pparg	**PPARγ**	1.00 ± 0.06	1.06 ± 0.08
Cpt1a	**CPT1α**	1.00 ± 0.20	0.98 ± 0.31
Prkaa1	**AMPKα1**	1.00 ± 0.12	1.11 ± 0.14
Prkaa2	**AMPKα2**	1.00 ± 0.20	1.09 ± 0.14
Acaca	**ACC1**	1.00 ± 0.19	1.12 ± 0.19
Acacb	**ACC2**	1.00 ± 0.19	1.25 ± 0.26
Lipid droplets			
Cidea	**CIDEA**	1.00 ± 0.20	1.09 ± 0.20
Cidec	**FSP27**	1.00 ± 0.23	1.05 ± 0.28
Pnpla2	**ATGL**	1.00 ± 0.24	1.04 ± 0.36
Plin2	**ADRP/Perilipin 2**	1.00 ± 0.13	1.03 ± 0.16
Plin4	**S3–12/Perilipin 4**	1.00 ± 0.17	0.94 ± 0.19
Plin5	**PAT-1/Perilipin 5**	1.00 ± 0.23	1.04 ± 0.31
Mitochondria			
Pparagc1a	**PGC1α**	1.00 ± 0.25	1.01 ± 0.21
Tfam	**Tfam**	1.00 ± 0.13	0.96 ± 0.17
Cs	**CS**	1.00 ± 0.19	0.96 ± 0.24
Ucp1	**UCP1**	1.00 ± 0.12	1.13 ± 0.05
Cox7a1	**COX7**	1.00 ± 0.11	1.05 ± 0.07
Atp5a1	**ATP5A1**	1.00 ± 0.09	0.99 ± 0.09
Ndufb8	**NDUFB8**	1.00 ± 0.13	0.98 ± 0.13
Sdha	**SDHA**	1.00 ± 0.10	1.06 ± 0.21
Sdhb	**SDHB**	1.00 ± 0.12	0.90 ± 0.10
Uqcrc2	**UQCRC2**	1.00 ± 0.08	1.04 ± 0.07

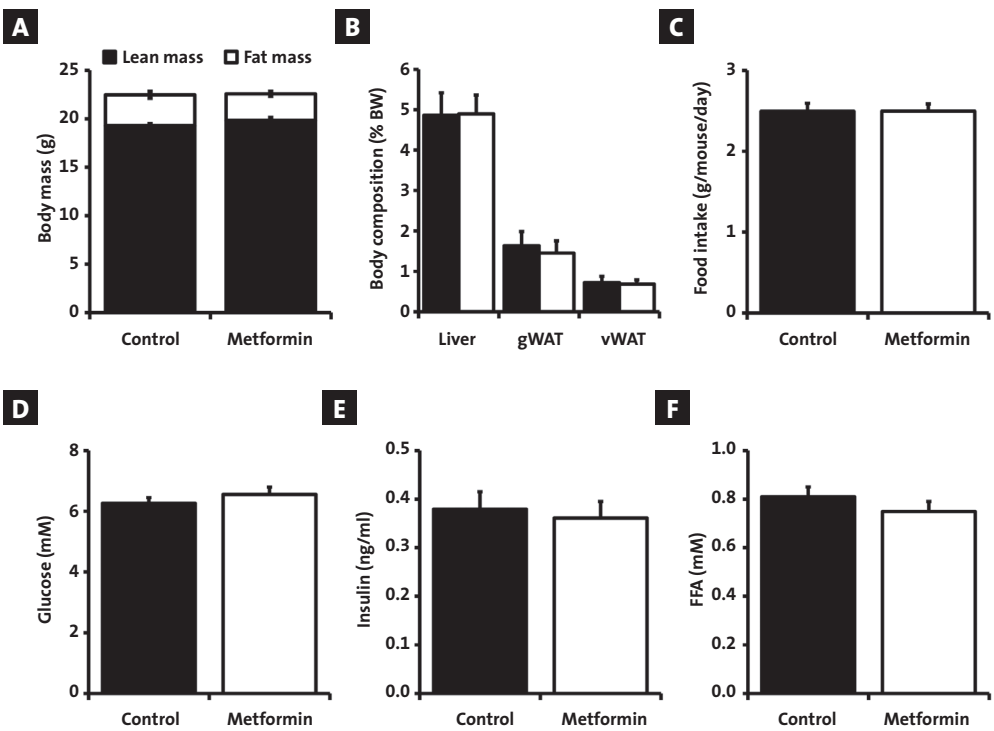

SUPPLEMENTARY FIGURE 1 - Effect of metformin on body weight and composition, food intake and various plasma parameters. Body weight and composition **A-B** and mean food intake **C** were measured throughout the study in control (black bars) and metformin-treated (open bars) mice. Blood samples were collected as described in **FIGURE 1** and plasma glucose **D**, insulin **E** and free fatty acids (FFA; **F** levels were determined.
Values are means ± SEM (n=9/group).

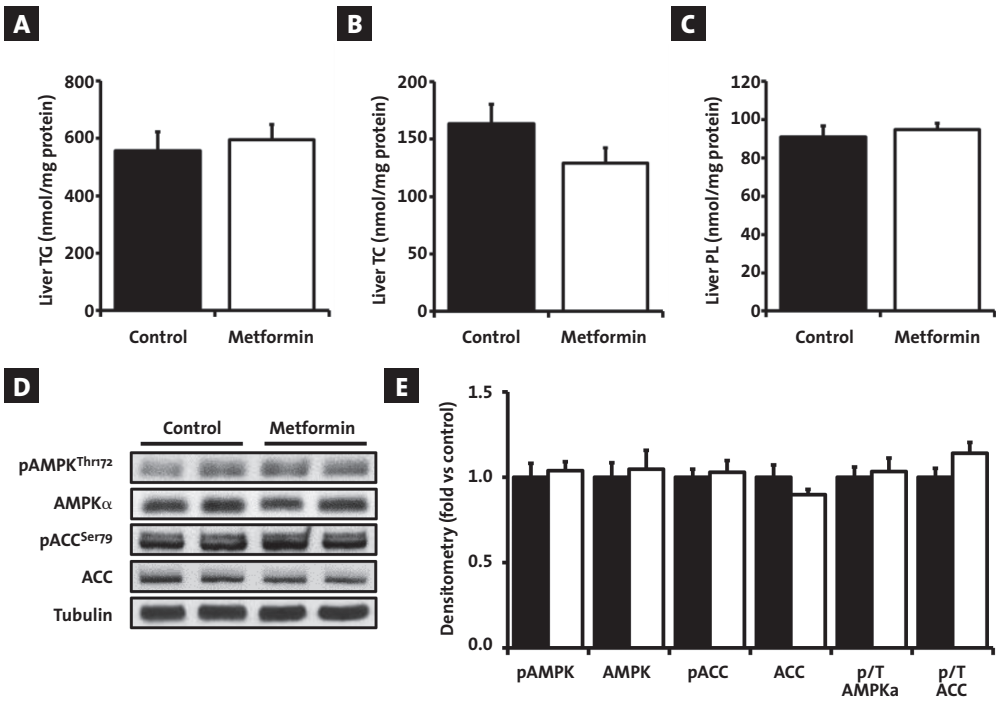

SUPPLEMENTARY FIGURE 2 - Effect of metformin on hepatic lipid composition and AMPK signalling. Livers from 4 h-fasted mice were collected after 4 weeks of treatment with (open bars) or without metformin (control, black bars) and immediately snap-frozen in liquid nitrogen. Hepatic TG **A**, TC **B** and PL **C** content were measured after lipid extraction. The phosphorylation state of Thr172-AMPK and Ser79-ACC, and AMPKα and ACC protein expression were assessed by Western blot **D**, followed by densitometric quantification **E**. Tubulin expression was used as internal housekeeping protein. Data are means ± SEM (n=5-8 per group).

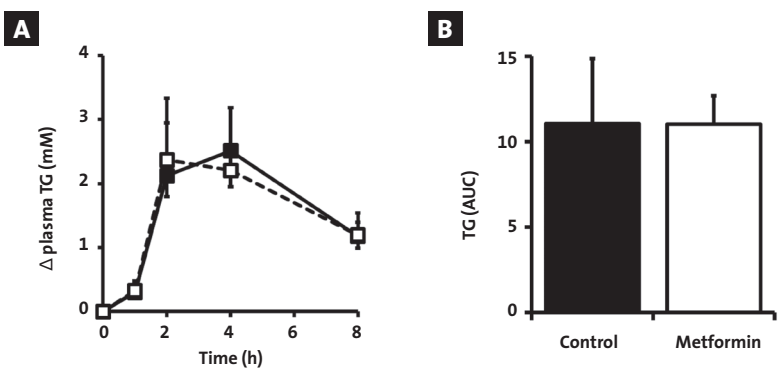

SUPPLEMENTARY FIGURE 3 - Effect of metformin on postprandial TG response. Overnightfasted control (closed squares) and metformin-treated (open squares) mice were given an intragastric bolus of 200 µl of olive oil. Blood samples were drawn at 0, 1, 2, 4, and 8 h. TG concentrations were determined in plasma and corrected for their respective values at time 0 **A**. The areas under the curse were calculated **B**. Data are means ± SEM (n=9-10/group).

CANNABINOID 1 RECEPTOR BLOCKADE DIMINISHES OBESITY AND DYSLIPIDEMIA VIA PERIPHERAL ACTIVATION OF BROWN ADIPOSE TISSUE

MARIËTTE R. BOON
SANDER KOOIJMAN
ANDREA D. VAN DAM
LEONARD R. PELGROM
JIMMY F.P. BERBÉE
CHERYL A.R. VISSEREN
ROBIN C. VAN AGGELE
ANITA M. VAN DEN HOEK
HETTY C.M. SIPS
MARC LOMBÈS
LOUIS M. HAVEKES
JOUKE T. TAMSMA
BRUNO GUIGAS
ONNO C. MEIJER
J. WOUTER JUKEMA
PATRICK C.N. RENSEN

FASEB J, revision invited.

ABBREVATIONS

ACC2	acetyl-CoA carboxylase 2
ACSL1	long-chain-fatty-acid-CoA ligase 1
BAT	brown adipose tissue
CB1R	cannabinoid type 1 receptor
CHO	carbohydrate
DIO	diet-induced obesity
E3L.CETP	APOE*3-Leiden.CETP
FASN	fatty acid synthase
(F)FA	(free) fatty acids
HSL	hormone-sensitive lipase
LPL	lipoprotein lipase
PL	phospholipids
SCD-1	stearoyl-CoA desaturase
TC	total cholesterol
TG	triglyceride
UCP-1	uncoupling protein-1
SNS	sympathetic nervous system
VLDL	very-low density lipoprotein
(g,s)WAT	(gonadal, subcutaneous) white adipose tissue

ABSTRACT

The endocannabinoid system is an important player in energy metabolism by regulating appetite, lipolysis and energy expenditure. Chronic blockade of the cannabinoid 1 receptor (CB1R) leads to long-term maintained weight loss and reduction of dyslipidemia in experimental and human obesity. The molecular mechanism by which CB1R blockade reverses dyslipidemia in obesity has not been clarified yet. In this study, we show that systemic CB1R blockade by rimonabant in a diet-induced obese mouse model for human-like lipoprotein metabolism reversed obesity, increased energy expenditure and lowered plasma VLDL-triglycerides (TG). Mechanistic studies showed that rimonabant selectively increased VLDL-TG clearance by brown adipose tissue (BAT) accompanied by decreased lipid droplet size in BAT. Of note, the mechanism involved peripheral activation of BAT since the effects were still present at thermoneutral temperature at which sympathetic output towards BAT is negligible and could be fully recapitulated by using the strictly peripheral CB1R antagonist AM6545. In support, we demonstrate that the CB1R is highly expressed in BAT and that *in vitro* blockade of the CB1R in cultured brown adipocytes increased UCP-1 content and lipolysis. Our data indicate that selective targeting of the peripheral CB1R in BAT has therapeutic potential in attenuating dyslipidemia and obesity.

INTRODUCTION

The endocannabinoid system regulates a broad range of physiological functions (1) and consists of G-protein coupled cannabinoid receptors, its endogenous lipid ligands (endocannabinoids) and the enzymes involved in the biosynthesis and degradation of endocannabinoids (2,3). The cannabinoid type 1 receptor (CB1R) is expressed at high levels in the brain but also at functionally relevant concentrations in various peripheral tissues (1). In contrast, the cannabinoid type 2 receptor is mainly expressed on immune cells (4). CB1R knockout mice display reduced adiposity and are resistant to diet-induced obesity (5). Moreover, overweight and obese humans exhibit an overactive endocannabinoid system (6,7), suggesting a role of the endocannabinoid system in energy metabolism.

Chronic systemic blockade of the CB1R with the inverse agonist rimonabant leads to long-term maintained weight loss and reduction of dyslipidemia in obese rodents (8,9) and humans (10-13). Rimonabant was considered one of the most promising therapeutic drugs to treat obesity, until the appearance of central psychiatric side effects resulted in its removal from the market in 2008. Nevertheless, several lines of evidence indicate that the effect of CB1R blockade is not restricted to a central mode of action, especially since the CB1R has been shown to be present in peripheral tissues including the liver (14), skeletal muscle (15) and adipocytes (16). More specifically, Tam et al (17) recently showed that the strictly peripheral CB1R antagonist AM6545 induced weight loss and diminished hepatic steatosis in a mouse model. Thus, it seems plausible that psychiatric side effects can be avoided by strict peripheral blockade of the CB1R, while retaining the beneficial anti-obesity and lipid-lowering effects.

Despite clear evidence that pharmacological CB1R antagonism improves dyslipidemia, the exact mechanisms and the peripheral tissues involved have not yet been elucidated. Recently, brown adipose tissue (BAT) emerged as an important player in triglyceride (TG) clearance (18). In contrast to white adipose tissue (WAT), which stores excess TG as fat, BAT dissipates energy into heat, a process mediated by the mitochondrial uncoupling protein-1 (UCP-1) (19). The best known trigger for activation of BAT is cold, which increases sympathetic outflow from the hypothalamic temperature centre towards BAT, leading to release of noradrenalin and increased thermogenesis (19). Metabolically active BAT stores exist in adult humans (20-22), and BAT volume and activity are lower in obese subjects (22). In addition, BAT volume and activity are lower in South Asians, a population prone to develop type 2 diabetes mellitus and cardiovascular disease (23). Together, these findings have increased interest in the therapeutic potential of BAT to combat obesity and related disorders, such as dyslipidemia.

In this study, we aimed at elucidating the molecular mechanism by which CB1R blockade attenuates dyslipidemia in diet-induced obesity by using a mouse model for human-like lipoprotein metabolism.

MATERIALS AND METHODS

Animals and diet

Homozygous human cholesteryl ester transfer protein (CETP) transgenic mice were crossbred with hemizygous APOE*3-Leiden (E3L) mice at our Institutional Animal Facility to obtain E3L.CETP mice, as previously described (24). We chose to perform our studies in this specific mouse model, since these mice are a well-established model for human-like lipoprotein metabolism and respond to lipid-lowering pharmacological interventions (24-26). In all the studies described below, 10 week-old E3L.CETP male mice were housed under standard conditions in conventional cages in a 12:12 h light: dark cycle with *ad libitum* access to food and water, and were fed a high-fat diet (HFD; Research diets, New Brunswick, USA, 60% lard fat) for 12 weeks to induce obesity. From the 7th week onwards, the drinking water was supplied with 10% fructose. All mouse experiments were performed in accordance with the Institute for Laboratory Animal Research Guide for the Care and Use of Laboratory Animals and have received approval from the Departmental Ethical Review Board (Leiden University Medical Center, Leiden, The Netherlands).

Pharmacological intervention

After 12 weeks of HFD, diet-induced obese (DIO) mice were randomised according to their body weight and plasma total cholesterol (TC) and triglyceride (TG) levels into four groups. Subsequently, mice were housed at either 21°C (subthermoneutral) or 28°C (thermoneutral), and received 60% HFD with or without 10 mg/kg body weight/day (0.00885%, w/w) rimonabant (Axon Medchem, Groningen, the Netherlands) or AM6545 (Sigma-Aldrich, St. Louis, USA) for 4 weeks.

Body weight and food intake

In all experiments, mice were housed individually during the 4 week treatment period. Food intake was recorded daily by weighing the food that was left in the cage or was recorded automatically in metabolic cages (see below). Body weight was measured twice a week.

Indirect calorimetry and physical activity

Indirect calorimetry was performed in fully automatic metabolic cages (LabMaster System, TSE Systems, Bad Homburg, Germany) during the fourth week of treatment. After 20 h acclimatization, oxygen uptake ($V^{\cdot} O_2$), carbon dioxide production ($V^{\cdot} CO_2$) and caloric intake were measured for 5 consecutive days. Carbohydrate (CHO) and fat oxidation rates were calculated from $V^{\cdot} O_2$ and $V^{\cdot} CO_2$ as described previously (27). Total energy expenditure (EE) was calculated from $V^{\cdot} O_2$ and $V^{\cdot} CO_2$ using the Weir equation (28). Physical activity was measured using infrared sensor frames.

Dual-energy X-ray absorptiometry (DEXA) scan

After 4 weeks treatment, body composition was measured by DEXA using the Norland pDEXA Sabre X-ray Bone Densitometer. Mice were anaesthetized intraperitoneally with a

combination of 6.25 mg/kg acepromazine (Alfasan), 6.25 mg/kg midazolam (Roche) and 0.31 mg/kg fentanyl (Janssen-Cilag). The total body of the mice was scanned, yet the heads were excluded from the analyses.

Plasma parameters

Blood was collected from the tail vein of 4-6 hour fasted mice into chilled capillaries that were coated with paraoxon (Sigma, St. Louis, MO) to prevent ongoing lipolysis (29). Capillaries were placed on ice and centrifuged, and plasma was assayed for TG, TC, and phospholipids (PL) using commercially available enzymatic kits from Roche Diagnostics (Mannheim, Germany for TG and TC) and Instruchemie (Delfzijl, the Netherlands for PL). Free fatty acids (FFA) were measured using NEFA C kit from Wako Diagnostics (Instruchemie, Delfzijl, The Netherlands).

Lipoprotein profiles

To determine lipid distribution over plasma lipoproteins, pooled plasma was used for fast performance liquid chromatography (FPLC). Plasma was injected onto a Superose 6 column (ÄKTA System, Amersham Pharmacia Biotech, Piscataway, NJ) and eluted at a constant flow rate of 50 µL/min with PBS pH 7.4. TG and TC were measured as described above in collected fractions of 50 µL.

In vivo clearance of labeled VLDL-like emulsion particles

VLDL-like TG-rich emulsion particles (80 nm) labeled with glycerol tri[^{3}H]oleate (triolein, TO) were prepared and characterized as described previously (30). To study the *in vivo* clearance of the VLDL-like particles, mice were fasted for 4 h and injected (t = 0) via the tail vein with 200 µL of emulsion particles (1.0 mg TG per mouse). Blood samples were taken from the tail vein at 2, 10, 20 and 30 min after injection to determine the serum decay of [^{3}H]TO. Plasma volumes were calculated as 0.04706 × body weight (g) as determined from ^{125}I-BSA clearance studies as described previously (31). After taking the last blood sample, mice were cervically dislocated and perfused with ice-cold PBS via the heart to remove blood from the organs. Subsequently, the liver, heart, spleen, hindlimb muscle, gonadal WAT (gWAT), subcutaneous WAT (sWAT) and brown adipose tissue (BAT) were collected. Organs were dissolved overnight at 60°C in Tissue Solubilizer (Amersham Biosciences, Rosendaal, The Netherlands), and ^{3}H activity was quantified. Uptake of [^{3}H]TO-derived radioactivity by the organs was expressed per gram wet tissue weight.

In vivo hepatic VLDL-TG and VLDL-apoB production

To measure VLDL production *in vivo,* mice were fasted for 4 h and anesthetized by intraperitoneal injection of 6.25 mg/kg acepromazine (Alfasan), 6.25 mg/kg midazolam (Roche) and 0.31 mg/kg fentanyl (Janssen-Cilag). Mice were injected intravenously with Tran[^{35}S] label (150 µCi/mouse) (MP Biomedicals, Eindhoven, The Netherlands) to label newly produced apolipoprotein B (apoB). After 30 min, at t=0 min, Triton WR-1339 (Sigma-Aldrich) was injected intravenously (0.5 mg/g body weight, 10% solution in PBS) to block serum

VLDL-TG clearance. Blood samples were drawn before (t = 0) and at 15, 30, 60, and 90 min after injection of Triton WR-1339 and used for determination of plasma TG concentration as described above. After 90 min, mice were exsanguinated via the retro-orbital plexus. VLDL was isolated from serum after density gradient ultracentrifugation at d<1.006 g/mL by aspiration (32) and examined for incorporated ^{35}S-activity.

RNA isolation and qRT-PCR analysis

Total RNA was isolated with the Nucleospin® RNA II Kit (Macherey-Nagel) according to the manufacturer's instructions. 1 µg of total RNA was reverse-transcribed with iScript cDNA synthesis kit (Bio-Rad), and the obtained cDNA was purified with Nucleospin Extract II kit (Macherey-Nagel). Real-time PCR was carried out on the IQ5 PCR machine (Bio-Rad) using the Sensimix SYBR Green RT-PCR mix (Quantace). Melt curve analysis was included to assure a single PCR product was formed. Expression levels were normalized using glyceraldehyde-3-phosphate dehydrogenase *(Gapdh), ß2-microglobulin* and *36b4* as housekeeping genes. Primer sequences are listed in **TABLE 1.**

Histology

Interscapular BAT, liver and sWAT were removed and fixed directly in 4% paraformaldehyde, dehydrated and embedded in paraffin. For UCP-1 staining in BAT, sections (5 µm) were dewaxed in xylene, rehydrated in ethanol and treated with 3% H_2O_2 (Sigma) in absolute methanol for 30 min. Next, sections were immersed in 10 mmol/L citrate buffer (pH 6.0), boiled for 10 min and cooled down at room temperature. Slides were blocked during 60 min with normal goat serum (1:75 in PBS) and incubated overnight at 4°C with rabbit monoclonal anti-UCP-1 antibodies (Abcam) diluted 1:400 in normal goat serum (1:75). Next, sections

TABLE 1 - **List of primer sequences for RT-PCR**

Gene	Forward primer	Reverse primer
36b4	GGACCCGAGAAGACCTCCTT	GCACATCACTCAGAATTTCAATGG
Acc2	AGATGGCCGATCAGTACGTC	GGGGACCTAGGAAAGCAATC
Acsl1	TGCCAGAGCTGATTGACATTC	GGCATACCAGAAGGTGGTGAG
Atgl	ACAGTGTCCCCATTCTCAGG	TTGGTTCAGTAGGCCATTCC
ß2-microglobulin	TGACCGGCTTGTATGCTATC	CAGTGTGAGCCAGGATATAG
Cd36	GCAAAGAACAGCAGCAAAATC	CAGTGAAGGCTCAAAGATGG
Fasn	GCGCTCCTCGCTTGTCGTCT	TAGAGCCCAGCCTTCCATCTCCTG
Hsl	AGACACCAGCCAACGGATAC	ATCACCCTCGAAGAAGAGCA
Lpl	CCCTAAGGACCCCTGAAGAC	GGCCCGATACAACCAGTCTA
Pgc1a	TGCTAGCGGTTCTCACAGAG	AGTGCTAAGACCGCTGCATT
Prdm16	ACTTTGGATGGGAGCAGATG	CTCCAGGCTCGATGTCCTTA
Scd1	GCGATACACTCTGGTGCTCA	CCCAGGGAAACCAGGATATT
Ucp1	TCAGGATTGGCCTCTACGAC	TGCATTCTGACCTTCACGAC

were incubated for 60 min with biotinylated goat α-rabbit secondary antibodies (Vector Labs) diluted 1:600 in normal goat serum (1:75). Immunostaining was amplified using Vector Laboratories Elite ABC kit (Vector Labs) and the immunoperoxidase complex was visualized with Nova Red (Vector Labs). Counterstaining was performed with Mayer's hematoxylin (1:4). Haematoxylin and Eosin stainings of liver and sWAT sections were done using standard protocols. Intracellular lipid content in BAT was quantified by use of ImageJ (version 1.47).

Liver lipid extraction

Lipids were extracted from livers consistent with a modified protocol from Bligh and Dyer (33). Small liver samples (approx. 50 mg) were homogenized in 10 µL of ice-cold methanol per mg tissue. Lipids were extracted into an organic phase by adding 1800 µL of CH_3OH: $CHCl_3$ (3:1, vol/vol) to 45 µL of homogenate and subsequent centrifugation. The lower, organic phase was dried and suspended in 2% Triton X-100. Hepatic TG and TC concentrations were measured using commercial kits, as explained (see: *Plasma parameters)*. Liver lipids were expressed per milligram of protein, which was determined using the BCA protein assay kit (Thermo Scientific, Rockford, IL, USA).

In vitro experiments with brown adipocytes

The murine brown preadipocyte cell line T37i (34) was cultured in HAM'S-F12 medium (Gibco-Invitrogen) supplemented with 10% fetal calf serum, 2 mM HEPES, 100 U/mL penicillin and 100 µg/mL streptomycin (Gibco-Invitrogen). For experiments, T37i cells were seeded in 6-wells plates and grown towards confluence. Two days after reaching confluence, cells were differentiated using normal culture medium supplemented with 2 nM triiodothyronine (T3) (Sigma) and 112 ng/mL bovine insulin (Sigma). The differentiation medium was replaced every 2 or 3 days. After 9 days of differentiation, cells were stimulated for 8 h with rimonabant (Axon Medchem) at 0.1 µM or 1 µM or with vehicle (DMSO). Then, 500 µL of supernatant was collected and snap-frozen in liquid nitrogen. Cells were washed twice with ice-cold PBS and cells were harvested in ice-cold lysis buffer as described below.

Protein isolation and Western Blot

T37i cells or snap-frozen tissue samples were lysed in ice-cold buffer containing 50 mM Hepes (pH 7.6), 50 mM NaF, 50 mM KCl, 5 mM NaPPi, 1 mM EDTA, 1 mM EGTA, 1 mM DTT, 5 mM ß-glycerophosphate, 1 mM sodium vanadate, 1% NP40 and protease inhibitors using cocktail tablets (Roche). Homogenates were centrifuged at 13,000 rpm for 15 min at 4°C and the protein content of the supernatant was determined using the BCA Protein Assay Kit from Thermo Scientific. Proteins (20 µg) were separated by 10% SDS-PAGE followed by transfer to a polyvinylidene fluoride transfer membrane (Merck, Amsterdam, The Netherlands). Membranes were blocked for 1 h at room temperature in Tris-buffered saline tween-20 buffer with 5% non-fat dry milk followed by an overnight incubation with specific primary antibodies. Primary antibodies specific for cannabinoid type 1 receptor (CB1R), E2-F, AMPK, P-AMPK, ACC, P-ACC and tubulin were purchased from Cell Signaling (Leiden, The Netherlands). A primary antibody specific for uncoupling protein 1 (UCP1) was purchased from

Sigma-Aldrich. All antibodies were diluted 1:1000. Blots were incubated with horseradish peroxidase-conjugated secondary antibodies for 1 h at room temperature. Bands were visualized with SuperSignal West Pico Chemiluminescent Substrate (Pierce) and quantified using ImageJ (version 1.47).

Statistical analysis

All data are expressed as mean ± SEM. Statistical analysis using the unpaired two-tailed Student's test was performed with the SPSS 20.0 software package for Windows (SPSS, Chicago, United States) to determine differences between vehicle- and compound-treated groups. A P-value < 0.05 was considered statistically significant.

RESULTS

Systemic CB1R blockade by rimonabant in DIO mice reduces obesity and dyslipidemia and increases energy expenditure. To investigate the effect of systemic CB1R blockade on body composition and energy balance, E3L.CETP transgenic mice were fed a HFD for 12 weeks to render them obese (mean body weight: 53.2 ± 0.9 g) and treated with rimonabant or vehicle for 4 weeks. Rimonabant elicited a profound decrease in body mass (-25%, P<0.001; **FIGURE 1A)** which was not due to a decrease in lean mass but rather to a massive decrease in fat mass (-32%, P<0.001; **FIGURE 1B)**. Rimonabant decreased caloric intake transiently (i.e. until day 6) **(FIGURE 1C)**, in accordance with previous observations (35, 36), while it persistently induced weight loss throughout the treatment period (i.e. 4 weeks). Furthermore, rimonabant markedly diminished plasma TG levels (-59%, P<0.05) and TC levels (-40%, P<0.01) **(FIGURE 1D)**, which is in line with previous human studies (10-12). Rimonabant tended to reduce plasma phospholipid (PL) levels (-31%, P=0.05) and had no effect on plasma free fatty acid (FFA) levels. Lipoprotein profiling showed that the marked decrease in plasma TG mostly resulted from a reduction in VLDL-TG (AUC -62%) **(FIGURE 1E)**. The persistent reduction in body weight despite the transient decrease in food intake following rimonabant treatment suggests increased energy expenditure. Indeed, rimonabant increased substrate utilization reflected by increased fat oxidation (+18%, P<0.05; **FIGURE 1F)**, carbohydrate (CHO) oxidation (+18%, P<0.05; **FIGURE 1G)**, and consequently total energy expenditure (+17%, P<0.05; **FIGURE 1H)**, as measured via indirect calorimetry, without increasing locomotor activity **(FIGURE 1I)**.

Systemic CB1R blockade by rimonabant attenuates dyslipidemia by activating brown adipose tissue. Plasma VLDL-TG levels are determined by the balance between hepatic VLDL-TG production and VLDL-TG clearance by lipoprotein lipase (LPL)-expressing peripheral organs. Therefore, to gain insight into the mechanism by which systemic CB1R antagonism reduces plasma VLDL-TG, we first assessed the effect of rimonabant on VLDL production. DIO mice were treated with rimonabant or vehicle for 4 weeks and then sequentially injected with Trans^{35}S and Triton WR1339 resulting in linear accumulation of VLDL in which newly synthe-

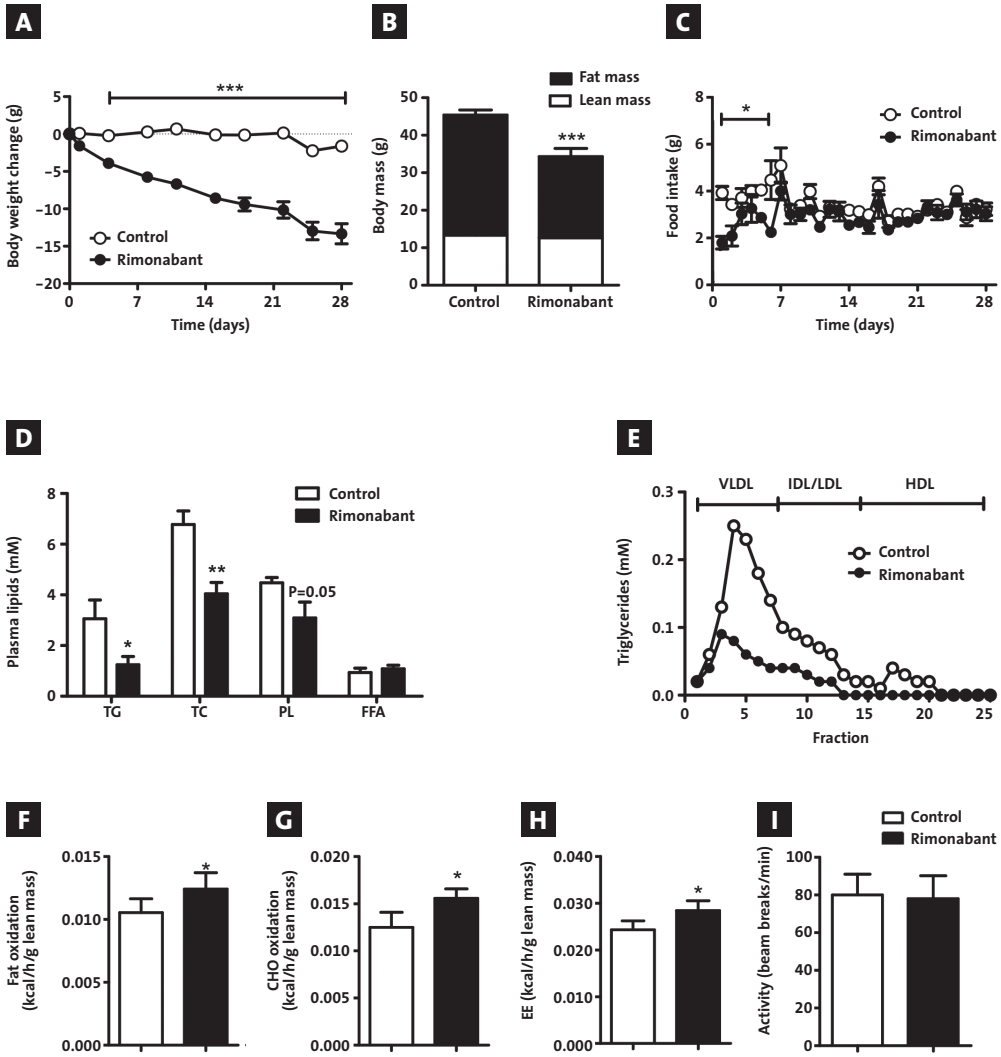

FIGURE 1 – Systemic CB1R blockade by rimonabant in DIO mice reduces obesity and dyslipidemia and increases energy expenditure. Male E3L.CETP mice were fed a HFD for 12 weeks to induce DIO and were then treated with rimonabant or vehicle for 4 weeks while housed at 21°C. **A** Body weight change (g) during the treatment period. **B** Lean and fat mass (g) as measured via DEXA-scan after 4 weeks of treatment. **C** Mean daily food intake (g) during the treatment period. **D** Plasma triglyceride (TG), total cholesterol (TC), phospholipid (PL), and free fatty acid (FFA) levels in 4-hour fasted mice after 4 weeks of treatment. **E** TG distribution over lipoproteins after separation from pooled plasma (n=9) by FPLC. **F** Fat oxidation, **G**) carbohydrate (CHO) oxidation, **H** energy expenditure (EE), and **I** activity levels as measured during 5 consecutive days in the fourth week of treatment via fully automatic metabolic cages. **F-H** Measurements were corrected for lean mass.

Values are means ± SEM (n=9) *P<0.05, **P<0.01, ***P<0.001 compared to the control group.

sized apolipoproteins are radiolabeled. Rimonabant did not affect the time-dependent accumulation of plasma TG following Triton injection **(FIGURE 2A)**. Therefore, the VLDL-TG production rate, as determined from the slope of the curve, was not significantly different. In addition, the rate of VLDL-apoB production did not change **(FIGURE 2B)**. In line with these observations, hepatic expression of lipogenic genes such as fatty acid synthase *(Fasn)* and stearoyl-CoA desaturase *(Scd1)* was unchanged **(FIGURE 2C)**. All together, these data demonstrate that global CB1R antagonism does not diminish dyslipidemia by lowering hepatic VLDL-TG production.

To investigate whether rimonabant increases VLDL-TG clearance, we determined the kinetics of i.v. injected [^{3}H]TO-labeled TG-rich VLDL-like emulsion particles, which have been previously shown to mimic the metabolic behavior of TG-rich lipoproteins (30), and studied the plasma clearance and organ distribution of [^{3}H]TO-derived fatty acids (FA) in mice treated with rimonabant or vehicle for 4 weeks. Rimonabant accelerated clearance of [^{3}H]TO from plasma ($t_{½}$ =3.9 ± 0.6 *vs.* 6.4 ± 0.4 min, P<0.05) **(FIGURE 2D)**, as explained by increased uptake of [^{3}H]TO-derived activity by energy-dissipating BAT (+53%, P<0.05; **FIGURE 2E)**. Of note, rimonabant decreased the uptake of [^{3}H]TO by the energy-storing sWAT depot (-42%, P<0.05).

To further investigate the molecular mechanism by which systemic CB1R blockade increased FA uptake by BAT, the mRNA expression of genes involved in both BAT differentiation, BAT activity, TG lipolysis and FA uptake were determined. Rimonabant did not affect expression of genes involved in BAT differentiation *(Pgc1α*, *Prdm16)* and intracellular lipolysis *(Hsl, Atgl)* (data not shown). However, as shown in **FIGURE 2F,** rimonabant increased expression of *Lpl* (+30%, P<0.05) and *Cd36* (+24%, P<0.05) that drive extracellular VLDL-TG lipolysis and subsequent uptake of FA by BAT (18). In addition, rimonabant increased expression of *Ucp1,* which encodes the uncoupling protein that mediates thermogenesis (+49%, P<0.05). Furthermore, histology showed a more intense immunohistochemical staining of UCP-1 in BAT **(FIGURE 2G)** as well as a decrease in intracellular lipid droplet size, reflected by a decrease in relative lipid area (-39%, P<0.001; **FIGURE 2H)**, both pointing to more active BAT (37). Thus, these data provide strong evidence that systemic CB1R antagonism diminishes dyslipidemia and increases energy expenditure, by promoting VLDL-TG uptake and subsequent combustion by BAT.

Systemic CB1R blockade by rimonabant diminishes TG storage in WAT and liver. To investigate whether the increased flux of TG towards BAT reduces (ectopic) TG accumulation, we analyzed WAT and the liver in more detail. Indeed, from the VLDL-TG clearance experiment it appeared that retention of [^{3}H]TO-derived activity by the energy storing sWAT depot was diminished after rimonabant treatment (-42%, P<0.05; **FIGURE 2E)**. In line with this, the cell size of white adipocytes was decreased in this depot as evident after H&E staining **(SUPPL. FIGURE 1A)**. In addition, rimonabant diminished expression of the lipogenic genes *Fasn* (-58%, P<0.05) and *Scd1* (-54%, P<0.05), while it increased expression of the lipolytic enzyme hormone sensitive lipase *(Hsl)* (+126%, P<0.05) in WAT **(SUPPL. FIGURE 1B)**, suggesting net FA efflux from WAT. In liver, rimonabant markedly decreased liver weight **(SUPPL. FIGURE 2A)**, which was

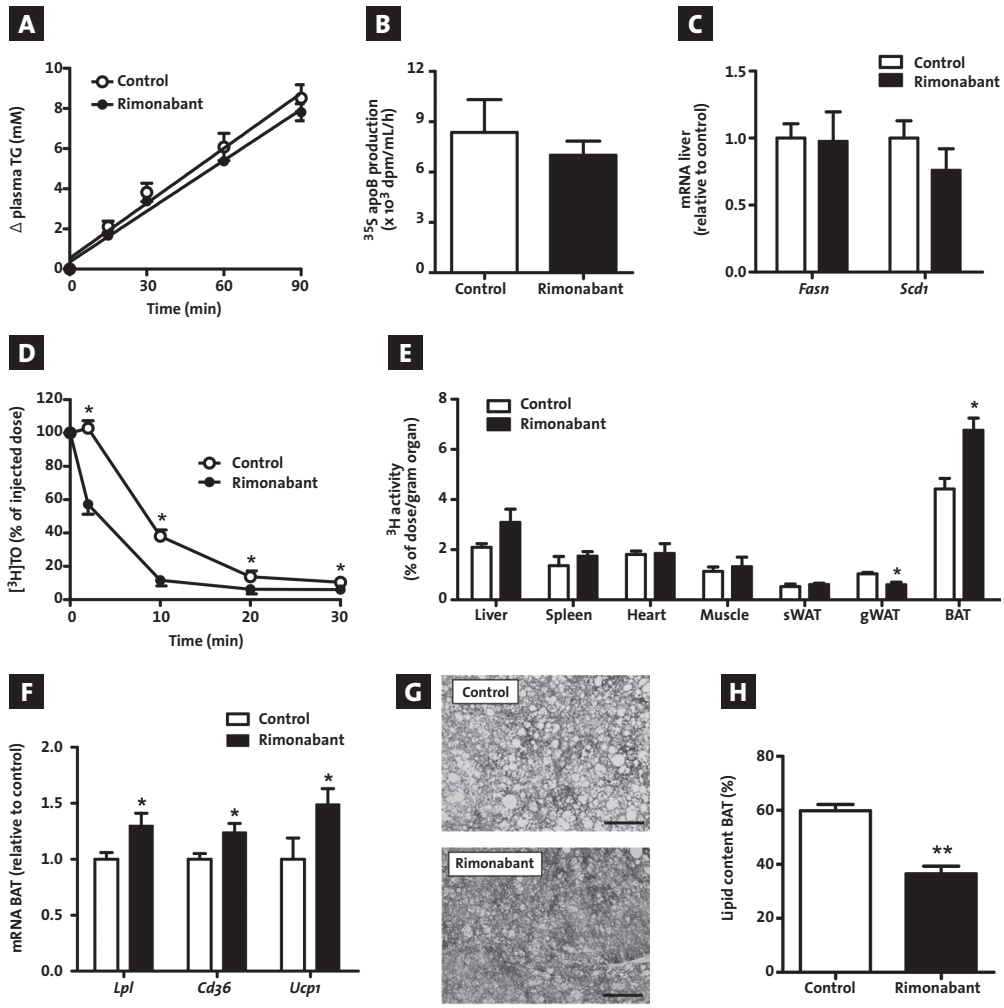

FIGURE 2 – Systemic CB1R blockade by rimonabant in DIO mice attenuates dyslipidemia by activating brown adipose tissue. Male E3L.CETP mice were fed a HFD for 12 weeks to induce DIO and were then treated with rimonabant or vehicle for 4 weeks while housed at 21°C **A** After 4 weeks of treatment, 4-hour fasted mice were injected intravenously with Tran[^{35}S] and TritonWR1339 and blood samples were drawn at the indicated time points. TG concentrations were determined and plotted as the increase in plasma TG relative to t=0. **B** ApoB production rate, as measured by counting ^{35}S-activity in the VLDL fraction isolated after 90 min. **C** Expression of *Fasn* and *Scd1* in liver as measured by qRT-PCR. **D** After 4 weeks of treatment, 4-hour fasted mice were injected intravenously with [^{3}H]TO-labeled VLDL-like emulsion particles, blood was collected at the indicated time points and radioactivity was measured in plasma. **E** Uptake of [^{3}H]TO-derived radioactivity by various organs was determined, and expressed as percentage of the injected dose per gram wet tissue weight. **F** Expression of *Lpl, Cd36,* and *Ucp1* in BAT as measured by qRT-PCR. **G** Representative pictures of immunohistochemical UCP-1 stainings of BAT in vehicle (top) and rimonabant (bottom) treated mice. Pictures were taken at 100x magnification (scale bar 100 µm). **H** Percentual lipid content in BAT tissue sections as quantified by use of ImageJ.

Values are means ± SEM (n=9) and expression of genes was corrected for the housekeeping genes ß2-microglobulin and 36b4. *P<0.05, ***P<0.001 compared to the control group.

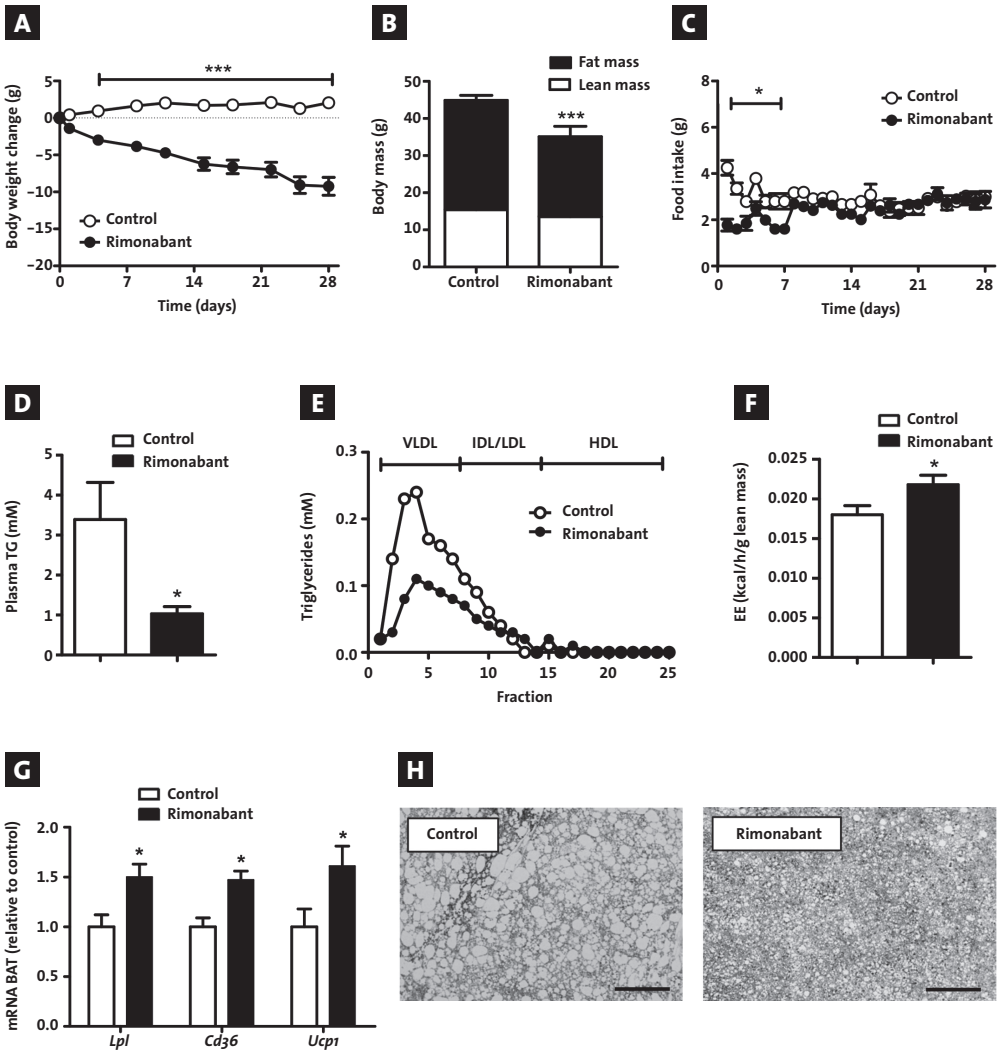

FIGURE 3 – The anti-obesity and lipid-lowering effects of systemic CB1R blockade by rimonabant in DIO mice are not abrogated at thermoneutrality. Male E3L.CETP mice were fed a HFD for 12 weeks to induce DIO and were then treated with rimonabant or vehicle for 4 weeks while housed at 28°C **A**. Body weight change (g) during the treatment period. **B** Lean and fat mass (g) as measured via DEXA-scan after 4 weeks of treatment. **C** Mean daily food intake (g) during the treatment period. **D** Plasma triglyceride (TG) levels in 4-hour fasted mice after 4 weeks of treatment. **E** TG distribution over lipoproteins after separation from pooled plasma (n=9 per group) by FPLC. **F** Energy expenditure (EE) as measured during 5 consecutive days in the fourth week of treatment via fully automatic metabolic cages, corrected for lean mass. **G** Expression of *Lpl*, *Cd36*, and *Ucp1* in BAT as measured by qRT-PCR **H** Representative pictures of immunohistochemical UCP-1 stainings of BAT in vehicle (left) and rimonabant (right) treated animals. Pictures were taken at 100x magnification (scale bar 100 µm).

Values are means ± SEM (n=9) *P<0.05, ** P<0.01, ***P<0.001 compared to the control group.

accompanied by a reduction in liver TG content (-45%, P<0.01) **(SUPPL. FIGURE 2B)** and smaller intracellular lipid vacuoles **(SUPPL. FIGURE 2C)**. Furthermore, rimonabant caused a (likely compensatory) downregulation of hepatic expression of genes involved in lipid oxidation, such as acyl-CoA synthetase long-chain family member 1 *(Acsl1)* and acetyl-CoA carboxylase 2 *(Acc2)* **(SUPPL. FIGURE 2D)**, while genes involved in lipogenesis were not affected **(FIGURE 2C)**. Thus, these data suggest that systemic CB1R blockade reduces storage of TG in WAT and liver, which may, at least in part, be a consequence of increased FA demand and flux towards BAT.

The anti-obesity and lipid-lowering effects of systemic CB1R blockade by rimonabant are not abrogated at thermoneutrality. BAT is densely innervated by the sympathetic nervous system (SNS) (19). Therefore, one of the mechanisms by which systemic CB1R blockade may lead to BAT activation could involve central CB1R blockade resulting in increased sympathetic outflow towards BAT. To investigate whether rimonabant acts centrally by increasing sympathetic nervous system (SNS) activation towards BAT, we next evaluated the effects of rimonabant in DIO mice that were housed at thermoneutral temperature (28°C). At thermoneutrality, rimonabant still markedly reduced obesity **(FIGURE 3A-B)** without affecting lean mass. This was accompanied by a transient decrease in food intake (i.e. until day 6) **(FIGURE 3C)**. Importantly, at thermoneutrality rimonabant still lowered plasma TG (-70%, P<0.05; **FIGURE 3D)**, which was mainly due to a reduction in VLDL-TG (AUC -52%; **FIGURE 3E)**. Furthermore, rimonabant still increased whole-body fat and carbohydrate oxidation **(SUPPL. FIGURE 3A-B)**, resulting in increased total energy expenditure (+21%, P<0.05; **FIGURE 3F)**, accompanied by increased markers of BAT activation both on mRNA **(FIGURE 3G)** and histological levels **(FIGURE 3H)**. Thus, these data suggest that the reduction in dyslipidemia, increase in energy expenditure and activation of BAT by systemic CB1R blockade occurs at least in part independent of SNS activation of BAT.

In vitro CB1R blockade by rimonabant induces activation of brown adipocytes and stimulation of AMPK phosphorylation. To explore the possibility that direct blockade of a CB1R in BAT may be responsible for the anti-obesity and lipid-lowering effect induced by systemic CB1R blockade, we first investigated whether the CB1R is expressed on BAT. Indeed, western blots on protein from tissues derived from untreated mice showed that the CB1R is highly expressed in BAT **(FIGURE 4A)**, even when compared to the expression in hypothalamus and liver. Furthermore, *in vitro* treatment of T37i brown adipocytes with rimonabant dose-dependently increased glycerol release **(FIGURE 4B)**, pointing to increased intracellular lipolysis, and upregulated UCP-1 protein **(FIGURE 4C)**. AMP-activated protein kinase (AMPK) serves as an intracellular energy sensor and activation of AMPK by means of phosphorylation results in enhanced fatty acid and glucose oxidation in a variety of tissues (38). Of note, CB1R blockade has been shown to increase AMPK phosphorylation in both liver cells (39) and white adipocytes (40). In line with this, we found that *in vitro* treatment of cultured T37i brown adipocytes with rimonabant induced AMPK phosphorylation **(FIGURE 4D)** as well as phosphorylation of ACC **(FIGURE 4E)**, the downstream effector of AMPK.

Altogether, these data indicate that direct blockade of the CB1R on brown adipocytes directly stimulates their activity with respect to intracellular lipolysis and UCP-1 protein content, accompanied by enhanced phosphorylation of AMPK and ACC.

Strictly peripheral CB1R blockade by AM6545 reduces obesity and dyslipidemia and increases energy expenditure in DIO mice. To investigate whether peripheral CB1R blockade is sufficient to induce weight loss and reverse dyslipidemia *in vivo,* we treated DIO mice for four weeks with vehicle or AM6545, a peripherally restricted CB1R antagonist that has been previously shown not to elicit central side effects (17). AM6545 markedly reduced body weight (-19%, P<0.001; **FIGURE 5A)** and fat mass (-23%, P<0.01; **FIGURE 5B)**, without altering lean

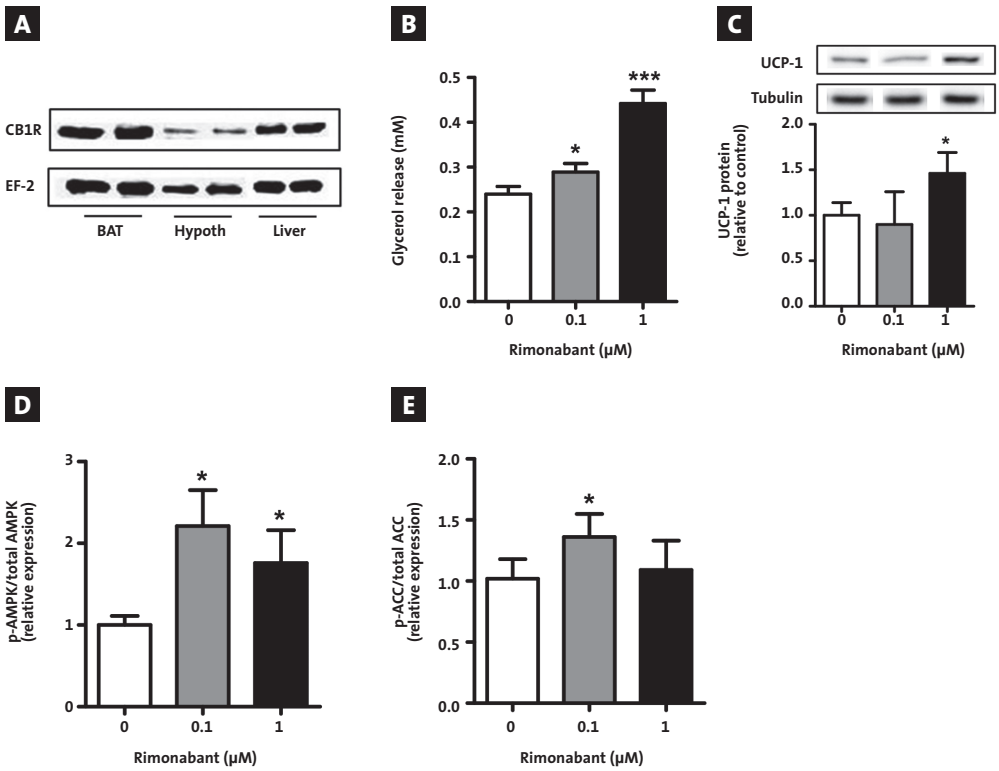

FIGURE 4 – Rimonabant directly stimulates BAT activity in T37i brown adipocytes in vitro. **A** CB1R protein expression was measured via western blot in BAT, hypothalamus and liver derived from diet-induced obese E3L.CETP transgenic mice with elongation factor 2 (EF-2) as housekeeping protein. **B-F** T37i brown adipocytes were treated with rimonabant (0, 0.1 or 1 μM) for 8 hours and **B** glycerol release was measured in the supernatant, and protein content of (C) UCP-1, (D) p-AMPK/AMPK **E** p-ACC/ACC and **F** Pgc1α was measured via western blot. Tubulin was used as housekeeping protein.

Values are means ± SD (n=3) *P<0.05, ***P<0.001 compared to the control group.

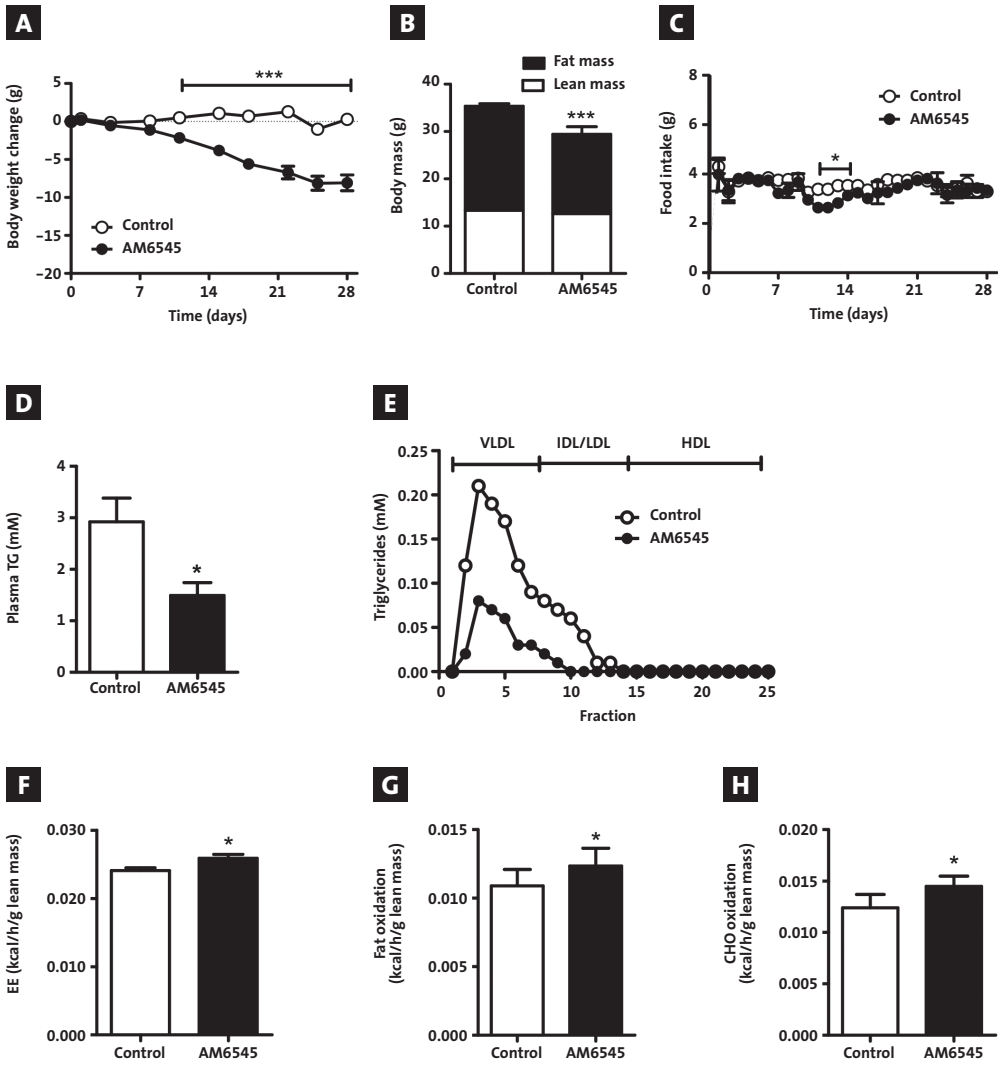

FIGURE 5 – Strictly peripheral CB1R blockade by AM6545 reduces obesity and dyslipidemia and increases energy expenditure in DIO mice. Male E3L.CETP mice were fed a HFD for 12 weeks to induce DIO and were then treated with AM6545 or vehicle for 4 weeks while housed at 21°C. **A** Body weight change (g) during the treatment period. **B** Lean and fat mass (g) as measured via DEXA-scan after 4 weeks of treatment. **C** Mean daily food intake (g) during the treatment period. **D** Plasma triglyceride (TG) levels in 4-hour fasted mice after 4 weeks of treatment. **E** TG distribution over lipoproteins after separation from pooled plasma (n=9 per group) by FPLC. **F-H** energy expenditure, fat oxidation and carbohydrate (CHO) oxidation as measured during 5 consecutive days in the fourth week of treatment via fully automatic metabolic cages, corrected for lean mass.
Values are means ± SD (n=9) *P<0.05, ***P<0.001 compared to the control group.

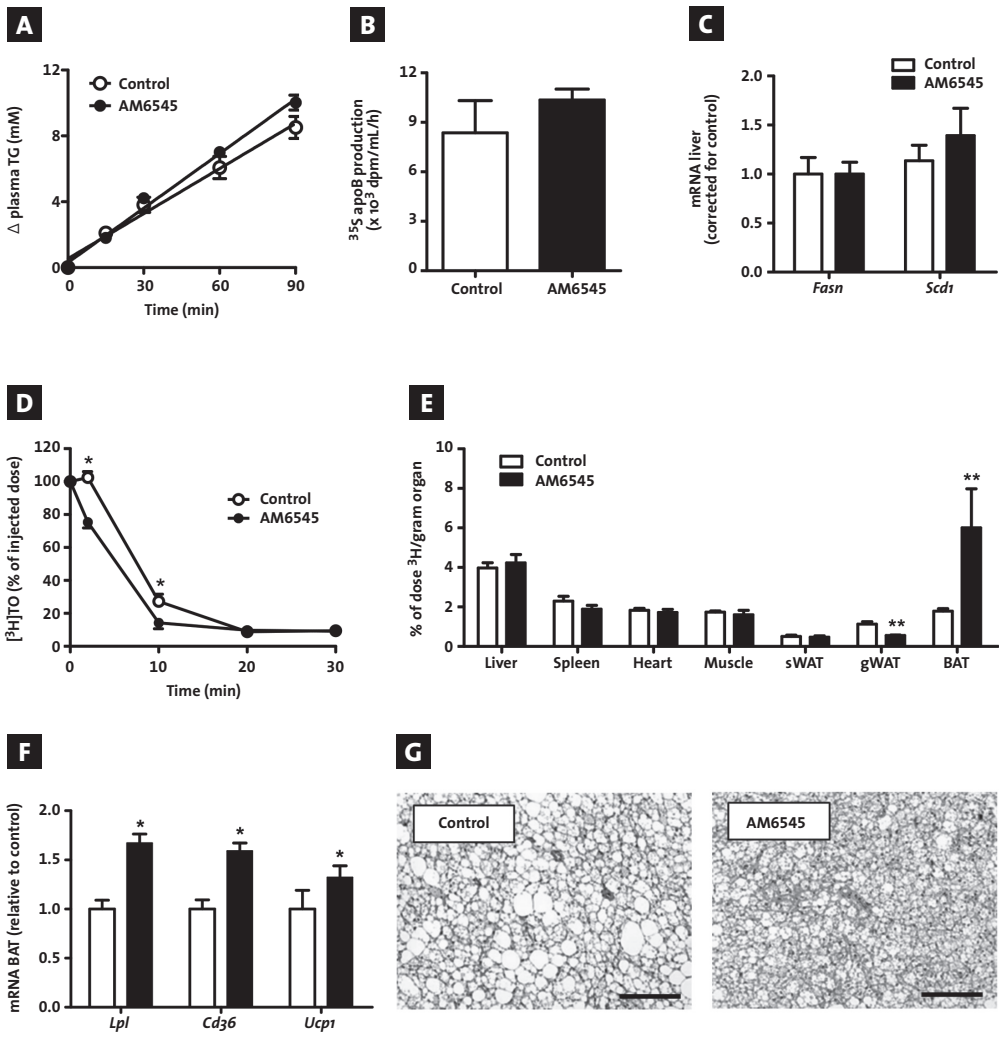

FIGURE 6 – Strictly peripheral CB1R blockade by AM6545 attenuates dyslipidemia in DIO mice by activating brown adipose tissue. Male E3L.CETP mice were fed a HFD for 12 weeks to induce DIO and were then treated with AM6545 or vehicle for 4 weeks while housed at 21°C. **A** After 4 weeks of treatment, 4-hour fasted mice were injected intravenously with Tran[^{35}S] and TritonWR1339 and blood samples were drawn at the indicated time points. TG concentrations were determined and plotted as the increase in plasma TG relative to t=0. **B** ApoB production rate, as measured by counting [^{35}S]-activity in the VLDL fraction after 90 min. **C** Expression of *Fasn* and *Scd1* in liver as measured by qRT-PCR. **D** After 4 weeks of treatment, 4-hour fasted mice were injected intravenously with [^{3}H]TO-labeled VLDL-like emulsion particles. Blood was collected at the indicated time points and radioactivity was measured in plasma. **E** Uptake of [^{3}H]TO-derived radioactivity by various organs, and expression per gram wet tissue weight. **F** Expression of *Lpl, Cd36,* and *Ucp1* in BAT as measured by qRT-PCR. (G) Representative pictures of immunohistochemical UCP-1 stainings of BAT in vehicle (left) and rimonabant (right) treated animals. Pictures were taken at 100x magnification (scale bar 100 µm).

Values are means ± SEM (n=9) and expression of genes was corrected for the housekeeping genes ß2-microglobulin and 36b4. *P<0.05, **P<0.01, ***P<0.001 compared to the control group.

mass. AM6545 did not induce the initial transient decrease in food intake as seen with rimonabant, although a slight decrease was evident later during the treatment period **(FIGURE 5C)**. However, total caloric intake was not affected. Furthermore, AM6545 substantially decreased plasma TG levels (-49%, P<0.05; **FIGURE 5D)**, which mostly resulted from a reduction in VLDL-TG (AUC -73%; **FIGURE 5E)**. In addition, AM6545 increased total energy expenditure **(FIGURE 5F)**, which was due to an increase in both fat and carbohydrate oxidation **(FIGURE 5G-H)**. Thus, these data demonstrate that peripheral CB1R blockade is sufficient to diminish obesity and dyslipidemia in DIO.

Strictly peripheral CB1R blockade by AM6545 attenuates dyslipidemia by activating brown adipose tissue. To investigate whether peripheral CB1R blockade also diminished dyslipidemia by increasing FA uptake by BAT, we again assessed VLDL-TG production and clearance. Just like rimonabant, AM6545 did not affect the production rates of VLDL-TG and VLDL-apoB **(FIGURE 6A-B)** or hepatic expression of lipogenic genes **(FIGURE 6C)**. Instead, AM6545 also accelerated clearance of [^{3}H]TO-labeled VLDL-like emulsion particles from plasma **(FIGURE 6D)**, accompanied by a marked increase of 3H retention by BAT (+235%, P<0.01; **FIGURE 6E)**, and a decrease in ^{3}H uptake by sWAT (-51%, P<0.01). In BAT, AM6545 increased expression of *Lpl* (+67%,P<0.05), *Cd36* (+59%, P<0.05) and *Ucp1* (+32%, P<0.05; **FIGURE 6F)** and decreased lipid content **(FIGURE 6G)**, all pointing to increased BAT activity. AM6545 also decreased white adipocyte size **(SUPPL. FIGURE 4A)** and liver weight (-24%, P<0.001; **SUPPL. FIGURE 4B)** accompanied by a reduction in liver TG content (-17%, P<0.05) **(SUPPL. FIGURE 4C)** and lipid vacuole size **(SUPPL. FIGURE 4D)**. Thus, peripheral CB1R blockade is sufficient to diminish dyslipidemia, and probably also obesity, by promoting VLDL-TG uptake and subsequent combustion of engulfed FA by BAT.

DISCUSSION

Systemic CB1R blockade by the inverse CB1R agonist rimonabant alleviates the excess body weight and dyslipidemia that are associated with obesity, both in mice and in humans (8-12). In this study, we demonstrate that systemic CB1R blockade reverses DIO and reduces plasma VLDL-TG by selectively increasing VLDL-TG clearance by metabolically active BAT followed by combustion. Of note, the mechanism involves peripheral activation of BAT since the effects were still present at thermoneutrality and could be recapitulated by using the strictly peripheral (17) CB1R antagonist AM6545. Accordingly, cultured brown adipocytes could be activated by blockade of the CB1R with rimonabant.

Systemic CB1R blockade by rimonabant resulted in massive activation of BAT, as evidenced by reduced lipid content and increased UCP-1 expression, accompanied by increased energy expenditure, which is in accordance with previous studies (36,41). Of note, by performing kinetic studies with radioactively labeled VLDL-TG we provided clear evidence that the TG-lowering effect of rimonabant is due to increased uptake of TG-derived FAs by BAT.

Since metabolically active BAT has been shown to be present and active in human adults (20-23), it is tempting to speculate that the body weight-reducing and TG-lowering effects of rimonabant previously found in obese subjects might be due to activation of BAT, although the precise role of BAT in TG metabolism in humans remains to be established.

Previous studies suggested central CB1R blockade as the main mechanism by which rimonabant induces BAT activation, resulting in increased sympathetic outflow towards BAT and increased energy expenditure (36,41). For instance, Bajzer and colleagues (36) reported that denervation of BAT in mice blunted the effect of rimonabant on insulin-mediated glucose uptake. However, in their study, the increase in energy expenditure and the reduction in body weight and fat mass were not blunted by BAT denervation, suggesting that a peripheral mechanism is at least in part involved in these beneficial effects. Indeed, we found that treatment of DIO mice with the strictly peripheral CB1R antagonist AM6545 still resulted in increased energy expenditure accompanied by increased uptake of TG-derived FAs by BAT as well as significant weight loss and reduction in dyslipidemia. Furthermore, we showed that the CB1R is highly expressed in BAT, and rimonabant increased the activity of brown adipocytes, further supporting the possibility of a peripheral mode of action of CB1R blockade in BAT.

We found that systemic blockade of the CB1R by rimonabant did not affect VLDL-TG production following either systemic or selective peripheral CB1R blockade. In contrast, a study by Tam and colleagues (17) reported that blocking the peripheral CB1R by AM6545 treatment resulted in a marked increase in the production of VLDL-TG in both DIO C57Bl/6 and leptin-deficient ob/ob mice. This might be explained by differences in study set-up, since Tam and colleagues measured VLDL-TG production after 1 week of treatment while in the present study VLDL-TG production was measured after 4 weeks. Likely, CB1R blockade transiently increases VLDL-TG production, leading to a fast initial reduction in hepatic steatosis as was also observed in their study. The subsequent normalization in VLDL production that we found in our study after 4 weeks of treatment may then be the consequence of a lower supply of FFAs towards the liver for incorporation into VLDL-TG, since these are efficiently cleared by BAT.

While we provide clear evidence that the TG-lowering effect of CB1R blockade is due to peripheral activation of BAT, the mechanism by which CB1R blockade lowers body weight and fat mass is less clear and no consistent mechanism has been reported up to date. Although BAT activation has been repeatedly shown to decrease body weight and fat mass (18,42,43), we cannot exclude that CB1R blockade on peripheral tissues other than BAT may contribute to the weight-reducing effect. For instance, the CB1R has been shown to be present on white adipocytes (16) and treatment of mice with rimonabant and AM6545 increased lipolysis (17,44,45). Accordingly, we also found that rimonabant increased mRNA expression of *Hsl* in subcutaneous WAT. Furthermore, the weight-reducing effect of global CB1R blockade is also at least in part due to an initial transient decrease in food intake induced by rimonabant. The greater efficacy of rimonabant over AM6545 in reducing body weight is then likely explained by the fact that AM6545 did not affect total caloric intake over the treatment period, as has been shown before (17). Thus, future studies are needed to

elucidate the specific contribution of BAT in the weight-reducing effect of (peripheral) CB1R blockade.

The intracellular mechanism by which CB1R blockade is linked to BAT thermogenesis likely involves phosphorylation of AMP-activated kinase (AMPK), a key evolutionary conserved cellular energy sensor that regulates metabolism (37). We show that CB1R blockade resulted in increased AMPK phosphorylation in brown adipocytes, which is in accordance with previous studies performed in hepatocytes (39) and white adipocytes (40). Thus, AMPK might be a central player by which CB1R blockade results in BAT activation. Future studies should be directed at investigating these pathways in more detail.

Together, our study shows that CB1R blockade diminishes dyslipidemia by inducing BAT-mediated VLDL-TG uptake and BAT thermogenesis via a peripheral mode of action. Our data suggest that blockade of the peripheral CB1R in BAT may be a promising therapy to combat obesity and to lower cardiovascular risk without inducing centrally mediated side effects.

ACKNOWLEDGEMENTS

MR Boon is supported by a grant from the Board of Directors of LUMC. PCN Rensen is Established Investigator of the Netherlands Heart Foundation (grant 2009T087). Furthermore, we acknowledge the support from the "Netherlands CardioVascular Research Initiative: the Dutch Heart Foundation, Dutch Federation of University Medical Centers, the Netherlands Organisation for Health Research and Development and the Royal Netherlands Academy of Sciences" for the GENIUS project "Generating the best evidence-based pharmaceutical targets for atherosclerosis" (CVON2011-19).

The authors also thank Lianne van der Wee and Trea Streefland (LUMC, dept. of Endocrinology) for their excellent technical assistance.

REFERENCES

1 Pagotto, U., Marsicano, G., Cota, D., Lutz, B., and Pasquali, R. (2006) The emerging role of the endocannabinoid system in endocrine regulation and energy balance. *Endocr Rev.* **27,** 73-100.

2 Piomelli, D. (2003) The molecular logic of endocannabinoid signalling. *Nat Rev Neurosci.* **4,** 873-884.

3 De Petrocellis, L., Cascio, M.G., and Di Marzo, V. (2004) The endocannabinoid system: a general view and latest additions. *Br J Pharmacol.* **141,** 765–774.

4 Howlett, A.C., Barth, F., Bonner, T.I., Cabral, G., Casellas, P., Devane, W.A., Felder, C.C., Herkenham, M., Mackie, K., Martin, B.R., Mechoulam, R., and Pertwee, R.G. (2002) International Union of Pharmacology. XXVII. Classification of cannabinoid receptors. *Pharmacol Rev.* **54,** 161–202.

5 Ravinet-Trillou, C., Delgorge, C., Menet, C., Arnone, M., and Soubrié, P. (2004) CB1 cannabinoid receptor knockout in mice leads to leanness, resistance to diet-induced obesity and enhanced leptin sensitivity. *Int J Obes Relat Metab Disord.* **28,** 640–648.

6 Engeli, S., Böhnke, J., Feldpausch, M., Gorzelniak, K. Janke, J., Bátkai, S., Pacher, P., Harvey-White, J., Luft, F.C., Sharma, A.M., and Jordan, J. (2005) Activation of the peripheral endocannabinoid system in human obesity. *Diabetes* **54,** 2838–2843.

7 Blüher, M., Engeli, S., Klöting, N., Berndt, J., Fasshauer, M., Bátkai, S., Pacher, P., Schön, M.R., Jordan, J., and Stumvoll, M. (2006) Dysregulation of the peripheral and adipose tissue endocannabinoid system in human abdominal obesity. *Diabetes.* **55,** 3053–3060.

8 Ravinet Trillou, C., Arnone, M., Delgorge, C., Gonalons, N., Keane, P., Maffrand, J.P., and Soubrie, P. (2003) Anti-obesity effect of SR141716, a CB1 receptor antagonist, in diet-induced obese mice. *Am J Physiol Regul Integr Comp Physiol.* **284,** R345–R353.

9 Gary-Bobo, M., Elachouri, G., Gallas, J.F., Janiak, P., Marini, P., Ravinet-Trillou, C., Chabbert, M., Cruccioli, N., Pfersdorff, C., Roque, C., Arnone, M., Croci, T., Soubrié, P., Oury-Donat, F., Maffrand, J.P., Scatton, B., Lacheretz, F., Le Fur, G., Herbert, J.M., and Bensaid, M. (2007) Rimonabant reduces obesity-associated hepatic steatosis and features of metabolic syndrome in obese Zucker fa/fa rats. *Hepatology* **46,** 122–129.

10 Van Gaal, L.F., Rissanen, A.M., Scheen, A.J., Ziegler, O., and Rossner, S. (2005) Effects of the cannabinoid-1 receptor blocker rimonabant on weight reduction and cardiovascular risk factors in overweight patients: 1-year experience from the RIO-Europe study. *Lancet* **365,** 1389–1397.

11 Despres, J.P., Golay, A., and Sjostrom, L. (2005) Effects of rimonabant on metabolic risk factors in overweight patients with dyslipidemia. *N Engl J Med.* **353,** 121–2134.

12 Pi-Sunyer, F.X., Aronne, L.J., Heshmati, H.M., Devin, J., and Rosenstock, J. (2006) Effect of rimonabant, a cannabinoid-1 receptor blocker, on weight and cardiometabolic risk factors in overweight or obese patients: RIONorth America: a randomized controlled trial. *JAMA* **295,** 761–775.

13 Addy, C., Wright, H., Van Laere, K., Gantz, I., Erondu, N., Musser, B.J., Lu, K., Yuan, J., Sanabria-Bohórquez, S.M., Stoch, A., Stevens, C., Fong, T.M., De Lepeleire, I., Cilissen, C., Cote, J., Rosko, K., Gendrano, I.N. 3rd, Nguyen, A.M., Gumbiner, B., Rothenberg, P., de Hoon, J., Bormans, G., Depré, M., Eng, W.S., Ravussin, E., Klein, S., Blundell, J., Herman, G.A., Burns, H.D., Hargreaves, R.J., Wagner, J., Gottesdiener, K., Amatruda, J.M., and Heymsfield, S.B. (2008) The acyclic cb1r inverse agonist taranabant mediates weight loss by increasing energy expenditure and decreasing caloric intake. *Cell Metab.* **7,** 68–78.

14 Osei-Hyiaman, D., DePetrillo, M., Pacher, P., Liu, J., Radaeva, S., Bátkai, S., Harvey-White, J., Mackie, K., Offertáler, L., Wang, L., and Kunos, G. (2005) Endocannabinoid activation at hepatic CB1 receptors stimulates fatty acid synthesis and contributes to diet-induced obesity. *J Clin Invest.* **115,** 1298–1305.

15 Eckardt, K., Sell, H., Taube, A., Koenen, M., Platzbecker, B., Cramer, A., Horrighs, A., Lehtonen, M., Tennagels, N., and Eckel, J. (2009) Cannabinoid type 1 receptors in human skeletal muscle cells participate in the negative crosstalk between fat and muscle. *Diabetologia* **52,** 664–674.
16 Cota, D., Marsicano, G., Tschöp, M., Grübler, Y., Flachskamm, C., Schubert, M., Auer, D., Yassouridis, A., Thöne-Reineke, C., Ortmann, S., Tomassoni, F., Cervino, C., Nisoli, E., Linthorst, AC., Pasquali, R., Lutz, B., Stalla, G.K., and Pagotto, U. (2003) The endogenous cannabinoid system affects energy balance via central orexigenic drive and peripheral lipogenesis. *J Clin Invest*. **112,** 423–431.
17 Tam, J., Vemuri, V.K., Liu, J., Bátkai, S., Mukhopadhyay, B., Godlewski, G., Osei-Hyiaman, D., Ohnuma, S., Ambudkar, S.V., Pickel, J., Makriyannis, A., and Kunos, G. (2010) Peripheral CB1 cannabinoid receptor blockade improves cardiometabolic risk in mouse models of obesity. *J Clin Invest*. **120,** 2953-2966.
18 Bartelt, A., Bruns, O.T., Reimer, R., Hohenberg, H., Ittrich, H., Peldschus, K., Kaul, M.G., Tromsdorf, U.I., Weller, H., Waurisch, C., Eychmüller, A., Gordts, P.L., Rinninger, F., Bruegelmann, K., Freund, B., Nielsen, P., Merkel, M., and Heeren, J. (2011) Brown adipose tissue activity controls triglyceride clearance. *Nat Med*. **17,** 200-205.
19 Cannon, B., and Nedergaard, J. (2004) Brown adipose tissue: function and physiological significance. *Physiol Rev*. **84,** 277-359.
20 Cypess, A.M., Lehman, S., Williams, G., Tal, I., Rodman, D., Goldfine, A.B., Kuo, F.C., Palmer, E.L., Tseng, Y.H., Doria, A., Kolodny, G.M., and Kahn, C.R. (2009) Identification and importance of brown adipose tissue in adult humans. *N Engl J Med*. **360,** 1509-1517.
21 Virtanen, K.A., Lidell, M.E., Orava, J., Heglind, M., Westergren, R., Niemi, T., Taittonen, M., Laine, J., Savisto, N.J., Enerbäck, S., and Nuutila, P. (2009) Functional brown adipose tissue in healthy adults. *N Engl J Med*. **360,** 1518-1525.
22 van Marken Lichtenbelt, W.D., Vanhommerig, J.W., Smulders, N.M., Drossaerts, J.M., Kemerink, G.J., Bouvy, N.D., Schrauwen, P., and Teule, G.J. (2009) Cold-activated brown adipose tissue in healthy men. *N Engl J Med*. **360,** 1500-1508.
23 Bakker, L.E.H., Boon, M.R., Van der Linden, R.A.D., Pereira Aris-Bouda, L., Van Klinken, J.B., Smit, F., Verberne, H.J., Jukema, J.W., Tamsma, J.T., Havekes, L.M., Van Marken Lichtenbelt, W.D., Jazet, I.M., and Rensen, P.C.N. (2013) Brown adipose tissue volume in healthy lean south Asian adults compared with white Caucasians: a prospective, case-controlled observational study. *The Lancet Diabetes and Endocrinology,* in press.
24 Westerterp, M., van der Hoogt, C.C., de Haan, W., Offerman, E.H., Dallinga-Thie, G.M., Jukema, J.W., Havekes, L.M., and Rensen, P.C. (2006) Cholesteryl ester transfer protein decreases high-density lipoprotein and severely aggravates atherosclerosis in APOE*3-Leiden mice. *Arterioscler Thromb Vasc Biol* **26,** 2552-2559.
25 de Haan, W., van der Hoogt, C.C., Westerterp, M., Hoekstra, M., Dallinga-Thie, G.M., Princen, H.M., Romijn, J.A., Jukema, J.W., Havekes, L.M., and Rensen, P.C. (2008) Atorvastatin increases HDL cholesterol by reducing CETP expression in cholesterol-fed APOE*3-Leiden.CETP mice. *Atherosclerosis*. **197,** 57-63.
26 van der Hoogt, C.C., de Haan, W., Westerterp, M., Hoekstra, M., Dallinga-Thie, G.M., Romijn, J.A., Princen, H.M., Jukema, J.W., Havekes, L.M., and Rensen, P.C. (2007) Fenofibrate increases HDL cholesterol by reducing the expression of the cholesteryl ester transfer protein. *J Lipid Res*. **48**, 1763-1771.
27 Van Klinken, J.B., Van den Berg, S.A.A., Havekes, L.M., and Willems van Dijk, K. (2012) Estimation of activity related energy expenditure and resting metabolic rate in freely moving mice from indirect calorimetry data. *PLoS One* **7,** e36162.
28 Feurer, I., and Mullen, J.L. (1986) Beside measurement of resting energy expenditure and respiratory quotient via indirect calorimetry. *Nutr Clin Prac*. **1,** 43-49.

29 Zambon, A., Hashimoto, S.I., and Brunzell, J.D. (1993) Analysis of techniques to obtain plasma for measurement of levels of free fatty acids. *J Lipid Res.* **34,** 1021-1028.
30 Rensen, P.C., van Dijk, M.C., Havenaar, E.C., Bijsterbosch, M.K., Kruijt, J.K., and van Berkel, T.J. (1995) Selective liver targeting of antivirals by recombinant chylomicrons--a new therapeutic approach to hepatitis B. *Nat Med.* **1,** 221-225.
31 Jong, M.C., Rensen, P.C., Dahlmans, V.E., van der Boom, H., van Berkel, T.J., and Havekes, L.M. (2001) Apolipoprotein C-III deficiency accelerates triglyceride hydrolysis by lipoprotein lipase in wild-type and apoE knockout mice. *J Lipid Res.* **42,** 1578-1585.
32 Redgrave, T.G., Roberts, D.C., and West, C.E. (1975) Separation of plasma lipoproteins by density-gradient ultracentrifugation. *Anal Biochem.* **65,** 42-49.
33 Bligh, E.G., and Dyer, W.J. (1959) A rapid method of total lipid extraction and purification. *Can J Biochem Physiol.* **37,** 911-917.
34 Zennaro, M.C., Le Menuet, D., Viengchareun, S., Walker, F., Ricquier, D., and Lombes, M. (1998) Hibernoma development in transgenic mice identifies brown adipose tissue as a novel target of aldosterone action. *J Clin Invest.* **101,** 1254–1260.
35 Hu, C., Wei, H., van den Hoek, A.M., Wang, M., van der Heijden, R., Spijksma, G., Reijmers, T.H., Bouwman, J., Wopereis, S., Havekes, L.M., Verheij, E., Hankemeier, T., Xu, G., and van der Greef, J. (2011) Plasma and liver lipidomics response to an intervention of rimonabant in ApoE*3Leiden. CETP transgenic mice. *PLoS One* **6,** e19423.
36 Bajzer, M., Olivieri, M., Haas, M.K., Pfluger, P.T., Magrisso, I.J., Foster, M.T., Tschöp, M.H., Krawczewski-Carhuatanta, K.A., Cota, D., and Obici, S. (2011) Cannabinoid receptor (CB1) antagonism enhances glucose utilisation and activates brown adipose tissue in diet-induced obese mice. *Diabetologia.* **54,** 3121-3131.
37 Hardie, D.G., Ross, F.A., and Hawley, S.A. (2012) AMPK: a nutrient and energy sensor that maintains energy homeostasis. *Nat Rev Mol Cell Biol.* **13,** 251-262.
38 Wu, H.M., Yang, Y.M., and Kim, S.G. (2011) Rimonabant, a cannabinoid receptor type 1 inverse agonist, inhibits hepatocyte lipogenesis by activating liver kinase B1 and AMP-activated protein kinase axis downstream of Gα i/o inhibition. *Mol Pharmacol.* **80,** 859-869.
39 Tedesco, L. (2008) Cannabinoid type 1 receptor blockade promotes mitochondrial biogenesis through endothelial nitric oxide synthase expression in white adipocytes. *Diabetes.* 57, 2028-2036.
40 Ortega-Molina, A., Efeyan, A., Lopez-Guadamillas, E., Muñoz-Martin, M., Gómez-López, G., Cañamero, M., Mulero, F., Pastor, J., Martinez, S., Romanos, E., Mar Gonzalez-Barroso, M., Rial, E., Valverde, A.M., Bischoff, J.R., and Serrano, M. (2012) Pten positively regulates brown adipose tissue function, energy expenditure and longevity. *Cell Metab.* **7,** 382-394.
41 Verty, A.N., Allen, A.M., and Oldfield, B.J. (2009) The effects of rimonabant on brown adipose tissue in rat: implications for energy expenditure. *Obesity (Silver Spring).* **17,** 254–261.
42 Tseng, Y.H., Kokkotou, E., Schulz, T.J., Huang, T.L., Winnay, J.N., Taniguchi, C.M., Tran, T.T., Suzuki, R., Espinoza, D.O., Yamamoto, Y., Ahrens, M.J., Dudley, A.T., Norris, A.W., Kulkarni, R.N., and Kahn, C.R. (2008) New role of bone morphogenetic protein 7 in brown adipogenesis and energy expenditure. *Nature.* **454,** 1000-1004.
43 Whittle, A.J., Carobbio, S., Martins, L., Slawik, M., Hondares, E., Vázquez, M.J., Morgan, D., Csikasz, R.I., Gallego, R., Rodriguez-Cuenca, S., Dale, M., Virtue, S., Villarroya, F., Cannon, B., Rahmouni, K., López, M., and Vidal-Puig, A. (2012) BMP8B increases brown adipose tissue thermogenesis through both central and peripheral actions. *Cell.* **149,** 871-885.
44 Jbilo, O., Ravinet-Trillou, C., Arnone, M., Buisson, I., Bribes, E., Péleraux, A., Pénarier, G., Soubrié, P., Le Fur, G., Galiègue, S., and Casellas, P. (2005) The CB1 receptor antagonist rimonabant reverses the diet-induced obesity phenotype through regulation of lipolysis and energy balance. *FASEB J.* **19,** 1567-1569.

45 Mølhøj, S., Hansen, H.S., Schweiger, M., Zimmermann, R., Johansen, T., and Malmlöf, K. (2010) Effect of the cannabinoid receptor-1 antagonist rimonabant on lipolysis in rats. *Eur J Pharmacol.* **646,** 38-45.

SUPPLEMENTARY APPENDIX

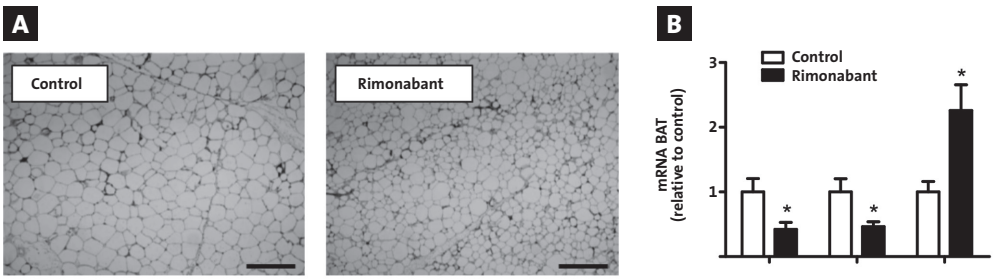

SUPPLEMENTARY FIGURE 1 – Effect of systemic CB1R blockade by rimonabant on subcutaneous WAT. Male E3L. CETP mice were fed a HFD for 12 weeks to induce diet-induced obesity and were then treated with rimonabant or vehicle for 4 weeks while being housed at an environmental temperature of 21°C. **A** Representative pictures of H&E stainings of sWAT in vehicle (left) and rimonabant (right) treated animals. Sections were enlarged 100x (scale bar 100 µm). **B** Expression of *Fasn*, *Scd1*, and *Hsl* in sWAT as measured by qRT-PCR.

Values are means ± SEM (n=9) and expression of genes was corrected for the housekeeping genes ß2-microglobulin and 36b4. *P<0.05 compared to the control group.

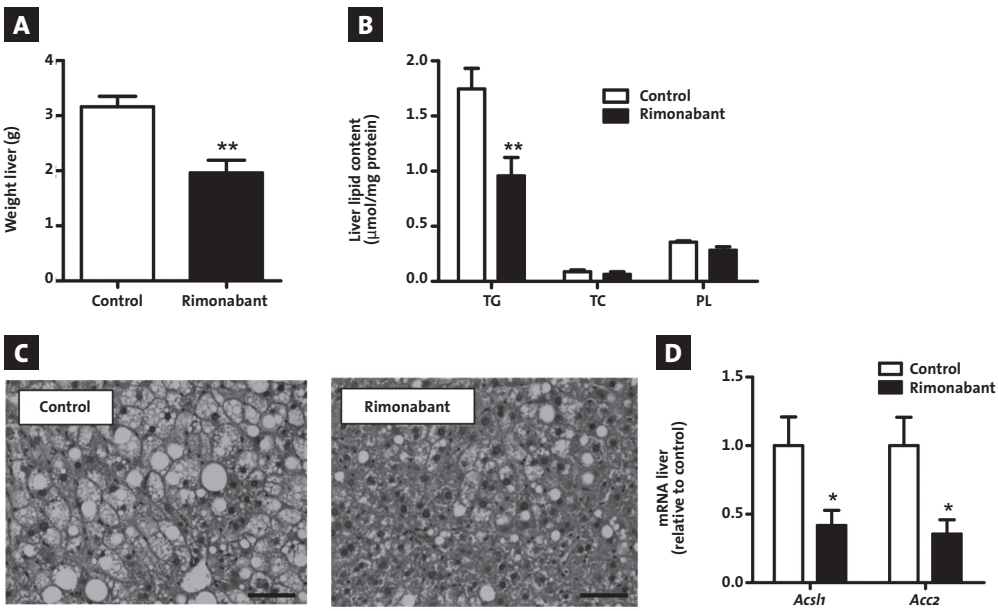

SUPPLEMENTARY FIGURE 2 – Effect of systemic CB1R blockade by rimonabant on hepatic steatosis. Male E3L. CETP mice were fed a HFD for 12 weeks to induce diet-induced obesity and were then treated with rimonabant or vehicle for 4 weeks while being housed at an environmental temperature of 21°C. **A** Liver weight (g). **B** Liver content of triglycerides (TG), total cholesterol (TC) and phospholipids (PL). **C** Representative pictures of H&E stainings of livers from vehicle (left) and rimonabant (right) treated animals. Pictures were taken at 100x magnification (scale bar 100 µm). **D** Expression of *Acsl1* and *Acc2* in liver as measured by qRT-PCR.

Values are means ± SEM (n=9) and expression of genes was corrected for the housekeeping genes ß2-microglobulin and 36b4. *P<0.05 , **P<0.01 compared to the control group.

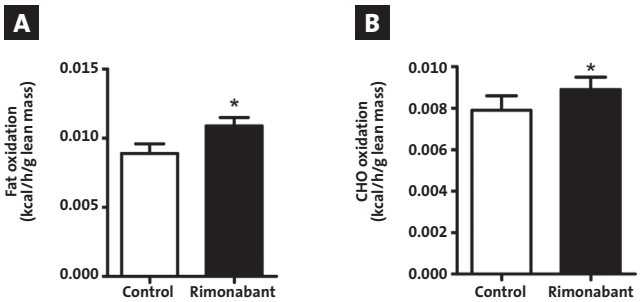

SUPPLEMENTARY FIGURE 3 – Systemic CB1R blockade increases fat and carbohydrate oxidation at thermoneutrality. Male E3L.CETP mice were fed a HFD for 12 weeks to induce diet-induced obesity and were then treated with rimonabant or vehicle for 4 weeks while being housed at an environmental temperature of 28°C. **A-B** Fat and carbohydrate (CH) oxidation as measured during 5 consecutive days in the fourth week of treatment via fully automatic metabolic cages, corrected for lean body mass.

Values are means ± SEM (n=9). *P<0.05 compared to the control group.

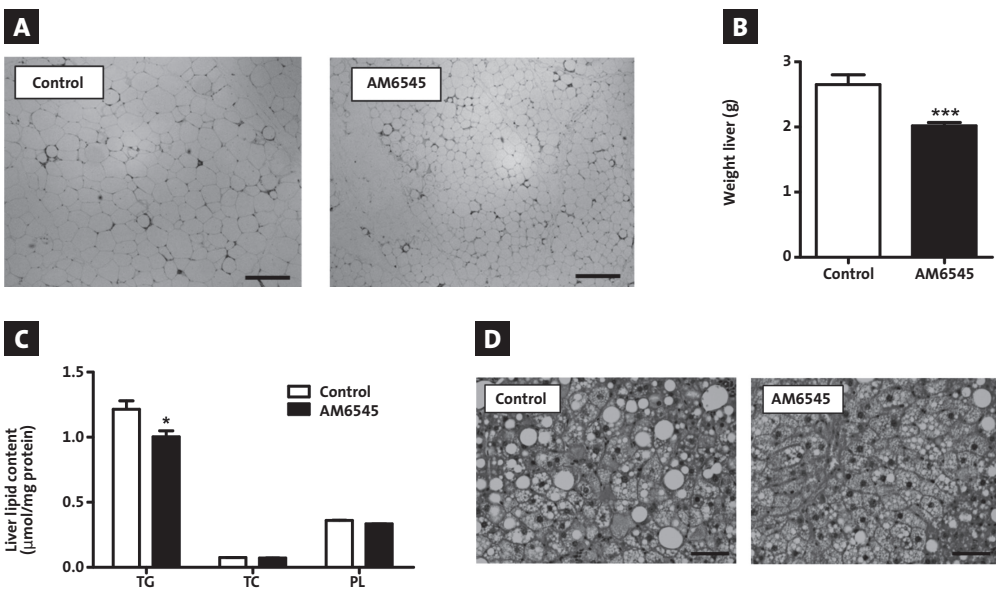

SUPPLEMENTARY FIGURE 4 – Effect of strictly peripheral CB1R blockade by AM6545 on lipid storage in sWAT and liver. Male E3L.CETP mice were fed a HFD for 12 weeks to induce diet-induced obesity and were then treated with AM6545 or vehicle for 4 weeks while being housed at an environmental temperature of 21°C. **A** Representative pictures of H&E stainings of sWAT in vehicle (left) and AM6545 (right) treated animals. Pictures were taken at 100x magnification (scale bar 100 µm). **B** Liver weight (g). **C** Liver content of triglycerides (TG), total cholesterol (TC) and phospholipids (PL). **D** Representative pictures of H&E stainings of liver in vehicle (left) and AM6545 (right) treated animals. Pictures were taken at 100x magnification (scale bar 100 µm). Sections were enlarged 100x (scale bar 100 µm).

Values are means ± SEM (n=9). *P<0.05 , ***P<0.001 compared to the control group.

INHIBITION OF THE CENTRAL MELANOCORTIN SYSTEM DECREASES BROWN ADIPOSE TISSUE ACTIVITY

SANDER KOOIJMAN
MARIËTTE R. BOON
EDWIN T. PARLEVLIET
JANINE J. GEERLING
VERA VAN DE POL
JOHANNES A. ROMIJN
LOUIS M. HAVEKES
ILLIANA MEURS
PATRICK C.N. RENSEN

J Lipid Res 2014, conditionally accepted.

ABBREVATIONS

[^{14}C]CO	[^{14}C]cholesteryl oleate;
[^{3}H]TO	glycerol tri[^{3}H]oleate
AgRP	agouti-related protein
BAT	brown adipose tissue
EE	energy expenditure
FFM	fat-free mass
GLP-1	glucagon-like peptide-1
i.c.v.	intracerebroventricular
i.v.	intravenous
LPL	lipoprotein lipase
MC3/4R	melanocortin 3/4 receptor
NPY	neuropeptide Y
PL	phospholipids
RER	respiratory exchange ratio
SNS	sympathetic nervous system
TC	total cholesterol
TG	triglycerides
UCP-1	uncoupling protein-1
WAT	white adipose tissue

ABSTRACT

The melanocortin system is an important regulator of energy balance and MC4R deficiency is the most common monogenic cause of obesity. We investigated whether the relationship between melanocortin system activity and energy expenditure is mediated by brown adipose tissue (BAT) activity. Therefore, female APOE*3-Leiden. CETP transgenic mice were fed a Western-type diet for 4 weeks and infused intracerebroventricularly with the MC3/4R antagonist SHU9119 or vehicle for 2 weeks. SHU9119 increased food intake (+30%), body fat (+50%) and decreased energy expenditure by reduction in fat oxidation (-42%). In addition, SHU9119 impaired plasma clearance of VLDL-TG, which was solely explained by reduced TG uptake by BAT. In line with this, SHU9119 decreased uncoupling protein-1 protein levels in BAT (-60%) and induced large intracellular lipid droplets, indicative of severely disturbed BAT activity. Finally, SHU9119-treated mice pair-fed to the vehicle-treated group still exhibited these effects, indicating that MC4R inhibition impairs BAT activity independent of food intake. We conclude that inhibition of central MC3/4R signaling impairs BAT function, which is accompanied by reduced energy expenditure thereby promoting adiposity. We anticipate that activation of MC4R is a promising strategy to combat obesity by increasing BAT activity.

INTRODUCTION

The hypothalamus is important in the regulation of energy balance. Activation of pro-opiomelanocortin neurons, *e.g.* by insulin or leptin, induces secretion of α-melanocyte-stimulating hormone, which in turn stimulates melanocortin -3 and -4 receptors (MC3R/MC4R) within the paraventricular nucleus to cause a negative energy balance (1). Accordingly, activation of central MC4R in rodent models results in anorexia and weight loss (2), whereas blockade or targeted gene disruption induces hyperphagia and obesity, even on regular chow diet (3,4). Loss-of-function mutations in MC4R are the most common monogenic form of obesity in humans and are associated with severe obesity in childhood (5). In addition, recent meta-analyses of genome-wide association studies identified common variants near MC4R to influence fat mass, obesity and obesity risk (6,7). These observations support an essential role for the melanocortin system in the regulation of energy homeostasis across mammalian species.

In addition to the effects of the melanocortin system on food intake, this system also affects energy balance via other pathways. This notion is supported by the observation that pharmacological inhibition of central MC4R by intracerebroventricular (i.c.v.) administration of the synthetic MC3/4R antagonist SHU9119 still increases body fat in pair-fed rats (8). Moreover, the peripheral effects of the central melanocortin system involves alterations in the activity of the sympathetic nervous system (SNS), as i.c.v. administration of the MC3/4R agonist MTII dose-dependently increases renal sympathetic activity in mice (9). Furthermore, ablation of neurons that produce agouti-related protein (AgRP), the endogenous antagonist for MC4R, in mice changes autonomic output into metabolic organs, accompanied by a changed respiratory exchange ratio (RER) indicating altered nutrient combustion (10). Additionally, chronic i.c.v. SHU9119 treatment in rats increases the RER (8), indicative of reduced lipid utilization. Interestingly, variants near and in the MC4R gene in humans are not only associated with an increased RER (8), but also with reduced total energy expenditure (EE) (11,12), underscoring the importance of the melanocortin system in the regulation of EE.

A recently discovered and highly important contributor to EE is brown adipose tissue (BAT). BAT contributes to EE by combusting high amounts of TG into heat, a process mediated by uncoupling protein-1 (UCP-1) (13). Interestingly, MC4R expressing neurons project onto BAT (14), indicating that BAT may mediate the association between MC4R signaling and EE. Therefore, the aim of this study was to evaluate the role of the melanocortin system in BAT activity. For this purpose, we inhibited melanocortin receptor signaling using the MC3/4R antagonist SHU9119 in APOE*3-Leiden.CETP transgenic mice.

MATERIALS & METHODS

Animals and diet

Female APOE*3-Leiden.CETP mice on a C57Bl/6J background (15) were bred at our institutional animal facility and housed under standard conditions with a 12-12 h light-dark cycle with *ad libitum* access to food and water unless stated otherwise. From 12-22 weeks after birth, they were fed a Western-type diet containing 15% (w/w) cacao butter and 0.1% cholesterol (AB Diets, Woerden, The Netherlands) for the duration of the study. After 4 weeks of run-in diet, mice were randomized into groups that received i.c.v. administration of artificial cerebrospinal fluid (vehicle) or SHU9119 (5 nmol/day; Bachem, Bubendorf, Germany) in vehicle during 14-17 days. Since SHU9119 induces hyperphagia (3), the effect of SHU9119 on BAT activity independent of food intake was also investigated by using an extra treated group that was pair-fed to the vehicle-treated group. All animal experiments were approved by the institutional ethics committee on animal care and experimentation at Leiden University Medical Center.

Surgical procedure

For continuous i.c.v. administration of SHU9119 *vs.* vehicle, mice were sedated using a mixture of dexmedetomidine (0.5 mg/kg), midazolam (5 mg/kg) and fentanyl (0.05 mg/kg), and cannulas (Brain Infusion Kit 3, ALZET Cupertino, CA, USA) were stereotactically placed in the left lateral ventricle of the brain (coordinates: -0.45 mm anteroposterior, -1.00 mm lateral and 2.50 mm dorsoventral from bregma). Osmotic mini-pumps (Model 1004, Alzet, CA) attached to the cannula via a catheter were implanted subcutaneously on the back slightly posterior to the scapulae. The skin was sutured and the sedation was antagonized with a mixture of antiparnezol (2.5 mg/kg), flumanezil (0.5 mg/kg) and naloxon (1.2 mg/kg). Buprenorphine (0.9 µg) was used as pain killer. After the surgery, mice were housed individually and food intake and body weight were monitored on a daily basis. By filling the catheters with vehicle, mice were allowed to recover for four days before actually receiving the assigned treatment for 17 days (collection of organs or VLDL production) or 14 days (indirect calorimetry and VLDL clearance).

Body composition

After 17 days of treatment, body composition (lean mass and fat mass) was determined in conscious mice using an EchoMRI-100 (EchoMRI, Houston, Texas).

Indirect calorimetry

During the first 5 days of treatment, oxygen uptake ($V\dot{}O_2$), carbon dioxide production ($V\dot{}CO_2$) and physical activity were measured in fully automatic metabolic cages (LabMaster System, TSE Systems, Bad Homburg, Germany). The average RER, EE, carbohydrate and fat oxidation rates were calculated as described previously (16).

Liver lipid staining and content

Liver samples were perfused with PBS, collected, snap frozen and stored at -80°C. Sections of 10 µm were cut, fixed in 4% paraformaldehyde and stained with Oil-red-O and Mayer's hematoxylin. Lipids were extracted according to a modified protocol from Bligh and Dyer (17). In short, small liver pieces were homogenized in ice-cold methanol (10 µL/mg tissue). 1.8 mL of CH_3OH: $CHCl_3$ (3:1, vol/vol) was added to 45 µL of homogenate. After vigorous mixing and centrifugation, the supernatant was dried and suspended in 2% Triton X-100. Concentrations of hepatic TG, total cholesterol (TC) and phospholipids (PL) were measured using commercially available enzymatic kits for TG (11488872, Roche Diagnostics, Germany), TC (11489232, Roche Diagnostics, Mannheim, Germany) and PL (3009, Instruchemie, Delfzijl, the Netherlands). Liver lipids were expressed per milligram of protein, which was determined using the BCA protein assay kit (Thermo Scientific, Rockford, IL, USA).

VLDL production

After 17 days of treatment, after 4 h of fasting (from 8.00 h to 12.00 h), the VLDL production rate was assessed. Mice were sedated using a mixture of ventranquil (6.25 mg/kg), dormicum (6.25 mg/kg), and fentanyl (0.31 mg/kg). Subsequently, mice were injected intravenously (i.v.) with 100 µL PBS containing 150 µCi Tran^{35}S label to measure *de novo* apoB synthesis and blood samples were taken via tail bleeding (t=0). 30 min after injection of the Tran^{35}S label, the mice received an i.v. injection of 500 mg of tyloxapol (Triton WR-1339, Sigma Aldrich, Germany) per kg body weight as 10% (w/w) solution in PBS, to block VLDL-TG clearance by lipoprotein lipase (LPL)-mediated TG hydrolysis. Additional blood samples were taken at t=15, 30, 60 and 90 min after tyloxapol injection and used for determination of plasma TG concentration. After 120 min, the mice were exsanguinated via the retro-orbital plexus. VLDL was isolated from serum after density gradient ultracentrifugation and counted for incorporated ^{35}S-activity. VLDL particle size was determined using a Zetasizer (Malvern Instruments, Malvern, UK) and VLDL lipid composition was determined as described above.

BAT histology and UCP-1 analysis

After 17 days of SHU9119 treatment, a part of interscapular BAT was fixed in 4% paraformaldehyde in PBS (pH 7.4) for 24 h, dehydrated and embedded in paraffin. 10 µm sections were cut, rehydrated and stained with Mayer's hematoxylin and eosin. Another part of BAT was snap frozen and stored at -80°C. These BAT samples were homogenized in RIPA buffer, centrifuged and protein concentration was determined using the BCA protein assay kit (Thermo Scientific, Rockford, IL, USA). Samples were diluted and denatured for 5 min at 95°C after adding Laemmli Sample Buffer (1:1, vol/vol; Serva, Heidelberg, Germany). Proteins within homogenates (1 µg protein) were separated on a 10% SDS-page gel and subsequently transferred onto blotting membrane. The blotting membranes were then washed with PBS+0.1% Tween (PBS+T), blocked with 5% milk powder in PBS+T and incubated O/N at 4°C with the first antibody (anti-UCP-1 rabbit polyclonal; 1:5,000; Ab U6382, Sigma Aldrich, Germany). After washing (PBS-T) the second antibody (anti-rabbit IgG HRP conjugate; 1:5,000; Promega, Madison, WI, USA) was added. After another wash with PBS-T and PBS,

SuperSignal Western Blot Enhancer (Thermo Scientific, Rockford, IL, USA) was added to the blotting membranes after which they were analyzed with Bio-Rad Quantity One.

VLDL clearance experiment

Glycerol tri[^{3}H]oleate ([^{3}H]TO) and [^{14}C]cholesteryl oleate ([^{14}C]CO) double-labeled VLDL-like emulsion particles (80 nm) were prepared as previously described (18). After 14 days of i.c.v. SHU9119 or vehicle treatment, mice were fasted for 4 h (from 8.00 h to 12.00 h) and injected i.v. with the radiolabeled emulsion particles (1.0 mg TG in 200 µL PBS) via the tail vein. At time points t=2, 5, 10 and 15 min after injection, blood was taken from the tail vein to determine the serum decay of both radiolabels. Immediately after the last blood withdrawal, mice were euthanized by cervical dislocation and perfused with ice-cold PBS for 5 min. Organs were harvested, weighed, and the uptake of ^{3}H and ^{14}C radioactivity was determined.

Statistical analysis

Differences between groups were determined using independent sample T-tests for normally distributed data and Mann-Whitney U tests for non-normal distributed data. Serum decay in the VLDL clearance experiment was analyzed using repeated measurements ANOVA with a Tukey's Post-Hoc test. Probability values less than 0.05 were considered statistically significant. Data are presented as means ± SEM.

RESULTS

SHU9119 increases body weight and fat mass independent of food intake

APOE*3-Leiden.CETP mice were treated i.c.v. with SHU9119 or vehicle for 17 days. In *ad libitum* fed mice, throughout the treatment period, SHU9119 consistently increased food intake (on average 4.04±0.21 *vs.* 3.18±0.13 g/day, $p<0.01$) **(FIGURE 1A)**, concomitantly with an increased body weight gain (after 17 days: 6.68±0.58 *vs.* 0.70±0.14 g, $p<0.001$). Obviously, SHU9119 also increased body weight in pair-fed mice when compared to vehicle-treated mice (4.14±0.45 *vs.* 0.70±0.14 g, $p<0.01$) **(FIGURE 1B)** indicating that the SHU9119-induced weight gain is independent of food intake. Determination of body composition using EchoMRI revealed that SHU9119 increased body weight under both *ad libitum* feeding and pair-fed conditions due to a selective increase in fat mass (10.6±1.2 and 9.6±1.0 *vs.* 4.9±1.1 g, $p<0.05$) **(FIGURE 1C)**. The SHU9119-induced increase in body weight and fat mass was accompanied by an increase in gonadal white adipose tissue (gWAT) weight, both in *ad libitum* feeding conditions (+124%; 1.32±0.13 *vs.* 0.59±0.12 g, $p<0.001$) and pair-fed conditions (+124%; 1.32±0.16 *vs.* 0.59±0.12 g, $p<0.01$) **(FIGURE 1D)**.

SHU9119 reduces whole body fat oxidation independent of food intake

Since SHU9119 induced fat accumulation independent of food intake, we reasoned that SHU9119 likely affected EE. Therefore, we next assessed the effect of SHU9119 on energy

metabolism. Fully automated metabolic cages were used during the first 5 days of treatment in order to prevent a potential confounding effect of differences in body weight. Indeed, in *ad libitum* fed mice, SHU9119 decreased EE (-10%; 23.7±0.3 *vs.* 26.4±0.2 cal/h/g fat-free mass [FFM], p<0.05) **(FIGURE 2A)** and increased RER (0.92±0.01 *vs.* 0.88±0.00 p<0.01) **(FIGURE 2B)**. These effects were not caused by an effect on carbohydrate oxidation **(FIGURE 2C)** but rather by a large reduction in fat oxidation (-43%; 5.1±1.0 *vs.* 8.9±0.3 cal/h/g FFM, p<0.001) **(FIGURE 2D)**. SHU9119 also reduced activity of the animals (-46%; 67±6 *vs.* 123±5 A.U., p<0.05; not shown). Strikingly, the effects of SHU9119 in pair-fed mice, as compared to the control group, were essentially similar as in *ad libitum* fed mice with respect to EE (23.9±0.1 cal/h/g FFM; p<0.01), RER (0.91±0.01; p<0.01), fatty acid oxidation (5.3±0.5 cal/h/g FFM; p<0.001) and activity (75±3 A.U.; p<0.05). Apparently, SHU9119 reduced EE, mainly because of reduced fat oxidation and independent of food intake.

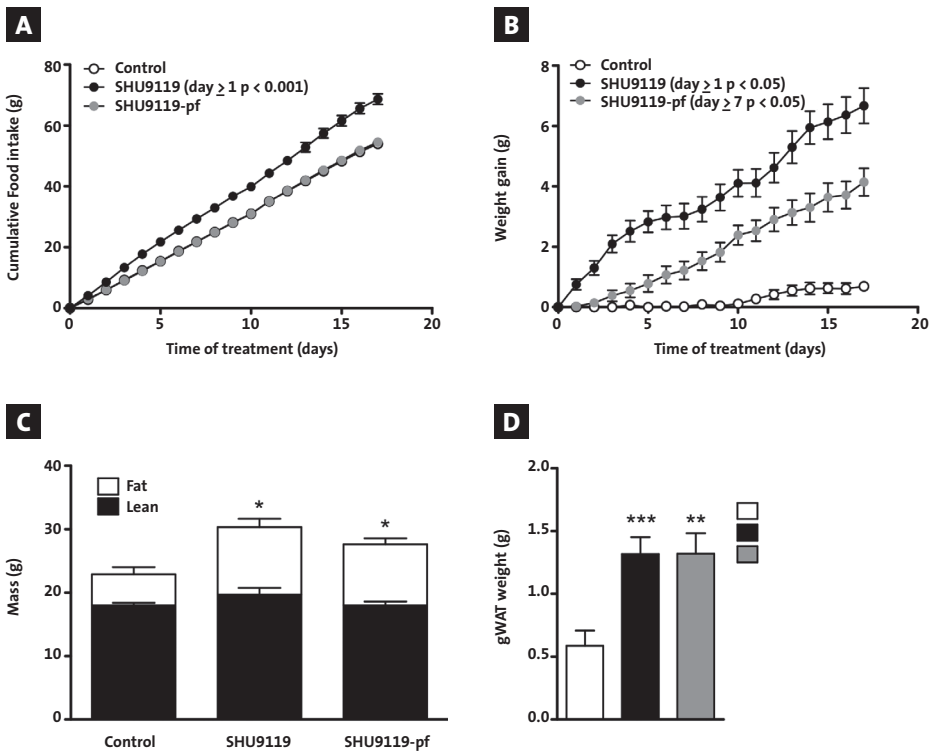

FIGURE 1 – SHU9119 increases body weight and fat mass independent of food intake. APOE*3-Leiden.CETP mice were treated intracerebroventricularly with vehicle (n=21) or SHU9119 (5 nmol/day) while being fed *ad libitum* (n=21) or being pair-fed (pf) to the vehicle-treated group (n=22). Food intake **A** and body weight gain **B** were monitored on a daily basis. After 17 days of treatment, lean and fat mass were measured in a random selection of the mice (n=3-4 per group) using EchoMRI **C**. Part of the mice were used for the collection of organs, and weight of gonadal white adipose tissue was determined (n=10-11 per group) **D**.
Values are means ± SEM. *p<0.05, **p<0.01, ***p<0.001 compared to control.

SHU9119 induces hepatic steatosis, and this is due to increased food intake

Since the liver is an important player in TG storage and secretion, we evaluated the effect of SHU9119 on liver weight and TG content as well as on hepatic VLDL-TG secretion. SHU9119 induced hepatomegaly as evidenced by increased liver weight (+85%; 2.17±0.11 *vs.* 1.17±0.06 g, p<0.001) **(FIGURE 3A)** and aggravated hepatic steatosis, as shown by a selective increase in liver TG (+57%; 689±33 *vs.* 439±37 nmol/mg protein, p<0.001) **(FIGURE 3B)** and neutral lipid staining **(FIGURE 3C)**. However, the effects of SHU9119 on the liver were fully attributed to the induction of hyperphagia, as hepatomegaly and hepatic steatosis were not induced under pair-fed conditions **(FIGURES 3A-C)**. SHU9119 did not affect the VLDL-TG production rate in mice that were either fed *ad libitum* (3.39±0.14 mmol/L/h) or pair-fed (3.61±0.37 mmol/L/h) as compared to control mice (3.59±0.29 mmol/L/h) **(FIGURES 3D, E)**. The VLDL-apoB production rate was slightly decreased in SHU9119-treated mice, but not in pair-fed SHU9119-treated

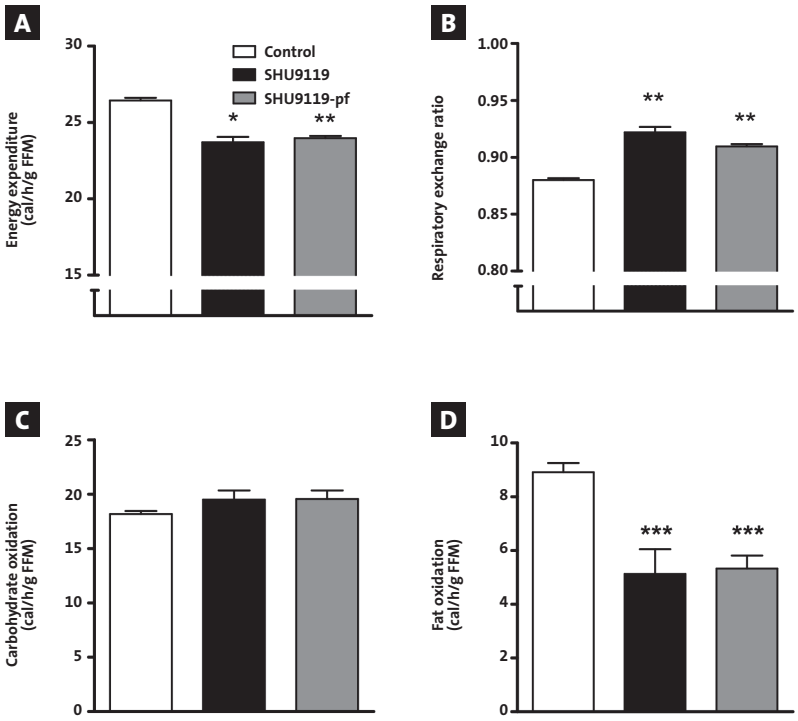

FIGURE 2 – SHU9119 lowers energy expenditure by reducing fat oxidation independent of food intake. APOE*3-Leiden.CETP mice were treated intracerebroventricularly with vehicle (n=9) or SHU9119 (5 nmol/day) while being fed *ad libitum* (n=6) or being pair-fed (pf) to the vehicle-treated group (n=9). During the first 5 days of treatment, mice were housed in fully automated metabolic cages. Energy expenditure **A**, respiratory exchange ratio **B**, carbohydrate oxidation **C** and fat oxidation **D** were calculated from O_2 uptake and CO_2 excretion.

Values are means ± SEM. *p<0.05, **p<0.01, ***p<0.001 compared to control.

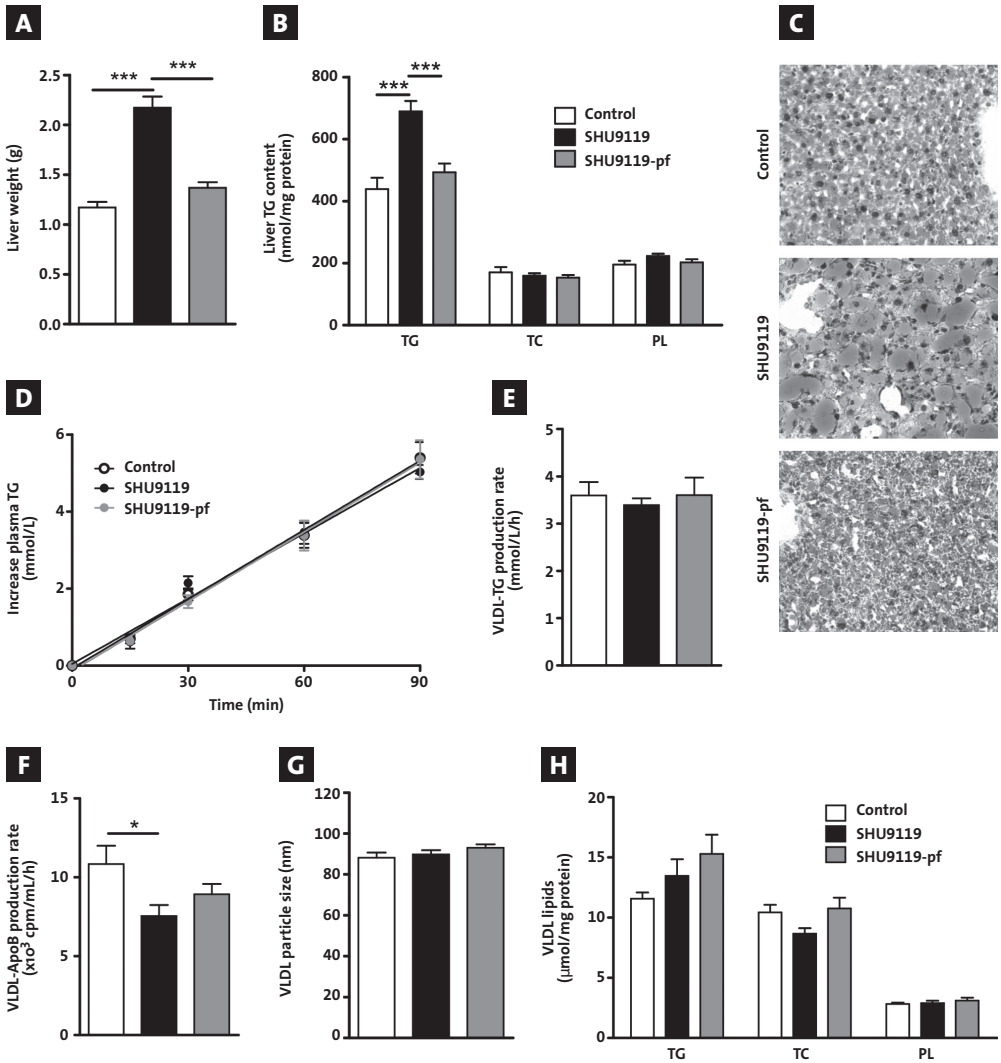

FIGURE 3 – SHU9119 induces hepatomegaly and steatosis only in *ad libitum* fed mice. APOE*3-Leiden.CETP mice were treated intracerebroventricularly with vehicle (n=21) or SHU9119 (5 nmol/day) while being fed *ad libitum* (n=21) or being pair-fed (pf) to the vehicle-treated group (n=20). After 17 days of treatment, part of the mice were sacrificed (n=10-11 per group) to collect organs and determine liver weight **A**, and to determine liver content of triglycerides (TG), total cholesterol (TC) and phospholipids (PL) **B**. Frozen liver samples were sectioned and stained with a neutral lipid staining (Oil-red-O) and hematoxylin, and representative pictures are shown **C**. The remaining mice (n=8-10 per group) were 4 h fasted, consecutively injected with Trans^{35}S label and tyloxapol, and blood samples were drawn up to 90 min after tyloxapol injection. Plasma TG concentration was determined and plotted as the increase in plasma TG relative to t=0 **D**. The rate of TG production was calculated from the slopes of the curves from the individual mice **E**. After 120 min, the total VLDL fraction was isolated by ultracentrifugation and the rate of newly synthesized VLDL-ApoB was determined **F**. The VLDL fractions were assayed for particle size **G** and lipid content **H**.

Values are means ± SEM. *p<0.05, ***p<0.001 compared to control.

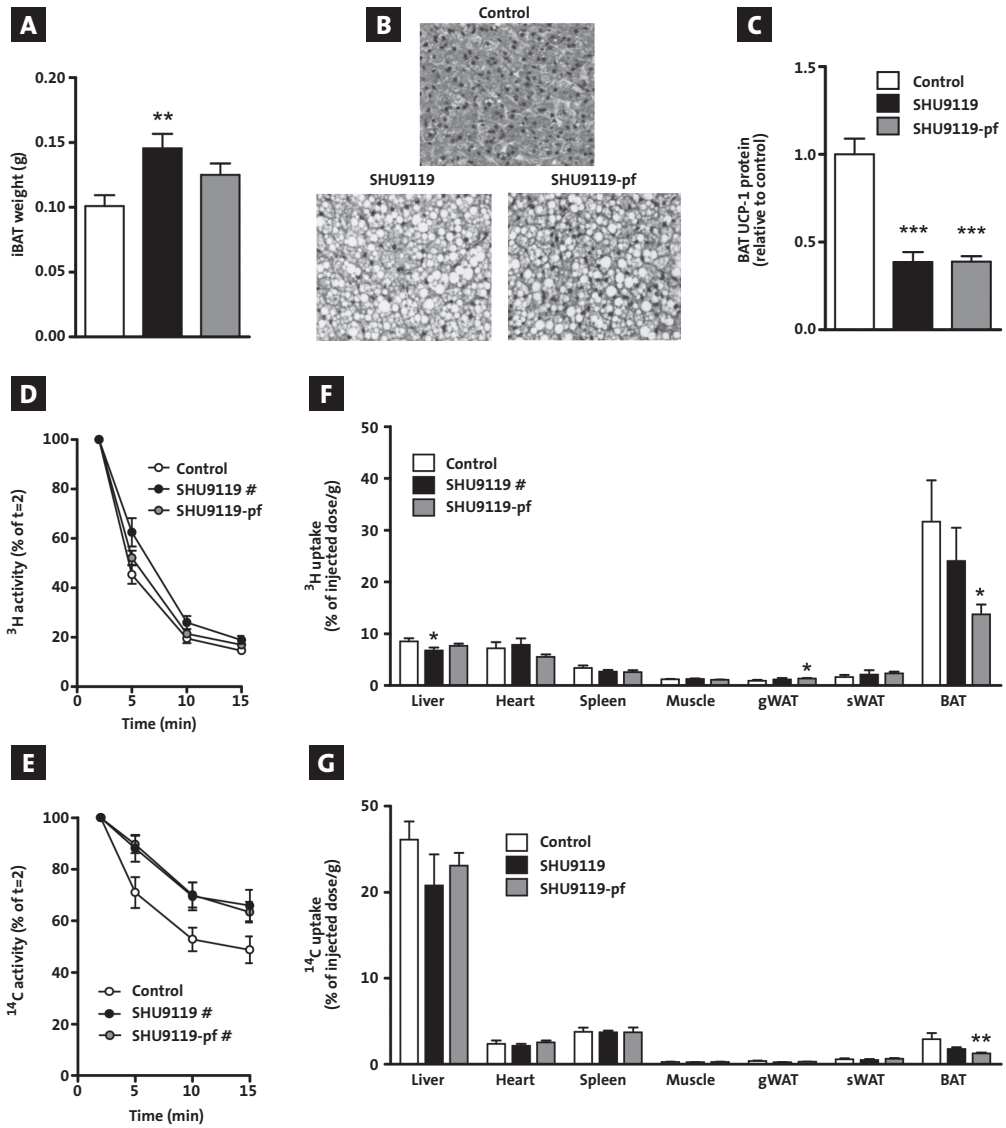

FIGURE 4 – SHU9119 causes malfunction of brown adipose tissue. APOE*3-Leiden.CETP mice were treated intracerebroventricularly with vehicle (n=21) or SHU9119 (5 nmol/day) while being fed *ad libitum* (n=21) or being pair-fed (pf) to the vehicle-treated group (n=22). After 17 days of treatment, part of the mice were sacrificed (n=10-11 per group) to collect organs and determine interscapular brown adipose tissue weight (iBAT) **A** and morphology **B**, and to determine UCP-1 protein content **C**. In a second experiment, after 14 days of i.c.v. treatment with vehicle (n=8) or SHU9119 (5 nmol/day) while being fed *ad libitum* (n=5) or being pf to the vehicle-treated group (n=9), mice were 4h fasted and consecutively injected with ^{3}H]TO and [^{14}C]CO-labeled VLDL-like emulsion particles. Plasma [^{3}H]TO **D** and [^{14}C]CO **E** were determined at the indicated time points and plotted relative to the dosage at t=2 min. At 15 min after injection, organs were isolated and uptake of the ^{3}H-activity **F** and ^{14}C-activity **G** was determined.

Values are means ± SEM. #p<0.05, *p<0.05. **p<0.01, ***p<0.001 compared to control.

mice **(FIGURE 3F)**. In line with these observations, SHU9119 did not affect VLDL particle size **(FIGURE 3G)**, VLDL composition **(FIGURE 3H)**, or hepatic expression of the genes *Apob, Mttp, Dgat2* involved in VLDL synthesis (not shown). Taken together, SHU9119 induced hepatic steatosis secondary to its induction of hyperphagia and without affecting VLDL-TG secretion.

SHU9119 induces brown adipose tissue dysfunction independent of food intake

Since BAT strongly contributes to fat oxidation and total energy expenditure, we subsequently determined the effect of SHU9119 treatment on BAT function. SHU9119 treatment increased BAT weight in *ad libitum* fed mice (+50%; 0.15±0.01 *vs.* 0.10±0.01 g, p<0.01) and tended to increase BAT weight in pair-fed animals (+24%; 0.13±0.01 g, p=0.06) **(FIGURE 4A)**. Surprisingly, SHU9119 dramatically increased intracellular lipid droplet size in BAT in both *ad libitum* fed and pair-fed mice **(FIGURE 4B)**, along with largely reduced UCP-1 protein levels in BAT (-61%; p<0.001 and -61%, p<0.001) **(FIGURE 4C)**. These data imply that SHU9119 decreases BAT activity independent of food intake, which may result in a decreased capacity of BAT to take up VLDL-TG for subsequent combustion as well as decreased burning of intracellulary stored TG.

Therefore, we next determined the effect of SHU9119 on the kinetics of i.v. injected [^{3}H]TO and [^{14}C]CO double-labeled VLDL-like emulsion particles after 14 days of treatment. SHU9119 impaired the plasma decay of [^{3}H]TO **(FIGURE 4D)** and [^{14}C]CO **(FIGURE 4E)** under *ad libitum* fed conditions, and that of [^{14}C]CO under pair-fed conditions **(FIGURE 4E)**. At 15 min after injection, the distribution of radiolabels over the organs was assessed. In control mice, [^{3}H]TO uptake by BAT (31.6±8.0%/g) was much higher than the uptake by liver (~4-fold), muscle (~25-fold) and WAT (~25-fold). Interestingly, SHU9119 tended to selectively decrease the uptake of [^{3}H]TO by BAT in the *ad libitum* fed group, and significantly did so in mice pair-fed to the control group (-57%; 13.7±1.9% of injected dose/g; p<0.05) **(FIGURE 4F).** In the control group, as compared to the ^{3}H-label, the uptake of the ^{14}C-label was much lower in BAT (~10-fold), muscle (~4-fold), heart (~3-fold) and WAT (~3-fold), while the uptake of ^{14}C-label was higher in liver (~3-fold). This pattern is compatible with selective delipidation of the VLDL-like emulsion particles in plasma by the LPL-expressing tissues *(i.e.* uptake of ^{3}H activity), with subsequent uptake of the core remnant by the liver *(i.e.* uptake of ^{14}C activity). SHU9119 treatment tended to reduce the uptake of [^{14}C]CO in the liver of both *ad libitum* fed mice(-20%; 20.8±3.6 %/g; p=0.11) and pair-fed mice (-11%; 23.1±1.5 %/g; p=0.25) as compared to the control group (26.1±2.1 %/g), whereas it decreased the uptake of [^{14}C]CO by BAT (ad libitum fed: -39%; p=0.24 ; pair-fed: -57%; p<0.01) **(FIGURE 4G)**.

DISCUSSION

The melanocortin system is an important regulator of energy balance and MC4R deficiency is the most common monogenic cause of obesity. BAT recently emerged as an important player in energy expenditure by combusting high amounts of TG towards heat. In addition,

MC4R expressing neurons project onto BAT (14). Hence, the association between MC4R and energy expenditure may be mediated by BAT. In the current study we aimed to evaluate the direct effect of the melanocortin system on BAT activity. For this purpose, we inhibited the central melanocortin system using the MC3/4R synthetic antagonist SHU9119 in APOE*3-Leiden,CETP mice. We found that i.c.v. administration of SHU9119 decreased EE and BAT activity, concomitant with selectively impaired uptake of TG from plasma by BAT, independent of food intake.

Both in *ad libitum* as well in pair-fed conditions, SHU9119 treatment increased body weight and WAT mass. These data are in line with those of Nogueiras *et al.* (8), who attributed weight gain and adiposity upon SHU9119 treatment to an increase in both lipid uptake as well as TG synthesis for storage in WAT. We also showed that in *ad libitum* fed conditions, SHU9119 induced ectopic lipid deposition in the liver, manifested by hepatomegaly and hepatic steatosis. Hepatic steatosis did not develop in pair-fed mice, indicating that this effect is a direct consequence of SHU9119-induced hyperphagia. Similar effects on the liver are observed after 4 days of i.c.v. SHU9119 treatment in rats (19) and in MC4R deficient mice, which in addition develop steatohepatitis when fed a high-fat diet and have therefore been proposed as a novel mouse model for non-alcoholic steatohepatitis (NASH) (20). Although hepatic steatosis could promote the secretion of hepatic lipid as VLDL (21), SHU9119 did not increase the production, size or composition of newly synthesized VLDL. Our data corroborate those of Stafford *et al.*(22) who showed that a single i.c.v. injection of 15 µg SHU9119 does not affect VLDL-TG production in rats.

Because SHU9119 was able to increase body adiposity independent of a change in food intake, we reasoned that SHU9119 reduces EE. Indeed, studies with metabolic cages confirmed that inhibition of the central melanocortin system reduced EE. SHU9119 treatment attenuated locomotor activity to some extent, which may have contributed to this decreased EE. More specifically, SHU9119 selectively reduced fat oxidation, whereas carbohydrate oxidation remained unaffected. This reduction in fat oxidation and total EE occurred independently of food intake and before changes in body weight were observed, indicative of a causal relation between reduced energy expenditure and the induction of obesity. Likewise, a previous study has shown that 7 days of i.c.v. injections with SHU9119 in rats increased the RER and thereby decreased fat utilization independent of food intake (8). As locomotor activity was not affected in that study, reduced fat oxidation may be dominant over the effect of decreased locomotor activity in the decrease in EE. In addition, MC4R-deficient humans also display an increase in RER (8). Taken together, we suggest that, in general, inhibition of the melanocortin system results in a shift towards decreased metabolic use of lipids leading to elevated fat deposition in WAT.

Since BAT is a highly active metabolic tissue involved in EE and regulation of weight gain, we next proposed that the reduction in fat oxidation could be largely attributed to decreased activity of BAT. Indeed, in both *ad libitum* and pair-fed conditions, analysis of BAT revealed that SHU9119 largely increased intracellular lipid stores and decreased the protein level of the UCP-1, both indicative of reduced BAT activity (23). These data corroborate previous findings showing that chronic i.c.v. treatment of *ad libitum* fed rats with SHU9119 lowered

BAT temperature during the night (24). Moreover, 7 daily i.c.v. injections of AgRP, the endogenous antagonist for MC4R, decreased UCP-1 gene expression in pair-fed rats (25), while acute i.c.v. injections of GLP-1, which indirectly stimulates MC4R, increased BAT thermogenesis by increasing activity of the sympathetic fibers towards BAT (26). These data can explain previous observations that MC4R deficient mice are unable to increase UCP-1 levels in BAT upon a high fat diet or cold stimulus (14). Since the activity of BAT is dependent on output from the SNS from the hypothalamus (27,28), it is likely that inhibition of the melanocortin system reduces sympathetic output to BAT.

Recently, Bartelt *et al.* (13) identified BAT as a major organ involved in plasma VLDL-TG clearance, with 24 hours of cold induction resulting in normalisation of plasma TG levels in hypertriglyceridemic mice. In a first experiment, we did observe a large increase in plasma TG levels upon 17 days of SHU9119 treatment under *ad libitum* conditions **(SUPPLEMENTAL FIGURE 1A)**, which would be consistent with reduced uptake of TG by BAT. However, in a subsequent study the SHU9119-induced increase in plasma TG only reached significance under pair-fed conditions **(SUPPLEMENTAL FIGURE 1B)**. Likewise, i.c.v. infusion of the MC4R synthetic antagonist HS104 also failed to increase plasma TG levels in pair-fed rats (29). It should be noted that MC4R deficient mice have only modestly increased plasma TG levels compared to control mice (+30%) (30), implying that partial inhibition of MC4R by SHU9119 may be insufficient to significantly increase plasma TG levels. In heterozygous MC4R-deficient subjects, plasma TG levels are increased (1.7 *vs.* 1.3 mmol/L) (31), indicating that the melanocortin system does play a role in the regulation of plasma VLDL-TG levels in humans.

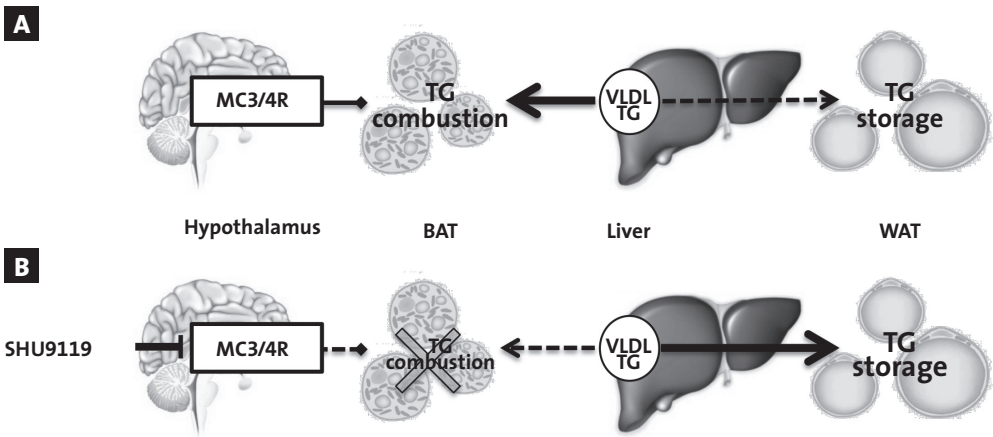

FIGURE 5 – Proposed model of the effect of SHU9119 on peripheral triglyceride metabolism. Under physiological conditions MC3/4R signalling is required for basal combustion of VLDL-derived triglycerides (TG) in brown adipose tissue (BAT), preventing storage of excess TG in WAT **A**. Inhibition of central MC3/4R signaling by SHU9119 reduces BAT activity, thereby reducing the uptake and combustion of VLDL-TG by BAT. As a consequence, excess TG is stored in WAT, independent of SHU9119-induced hyperphagia **B**.

Recently, Perez-Tilve *et al.* (32) demonstrated that inhibition of the central melanocortin neurons by either ghrelin or SHU9119 in wild-type mice increased circulating cholesterol, related to a decreased hepatic expression of SR-BI involved in the selective hepatic uptake of HDL-cholesteryl esters. In our study in APOE*3-Leiden.CETP mice with a human-like lipoprotein metabolism, SHU9119 did not increase total cholesterol **(SUPPLEMENTAL FIGURE 1)** despite decreased hepatic SR-BI expression **(SUPPLEMENTAL FIGURE 2)**. This is likely due to the expression of human CETP that provides an alternative route for the clearance of HDL-cholesterol, as CETP expression in SR-BI-deficient mice also precludes an increase in HDL-cholesterol (33). Likewise, humans with heterozygous MC4R deficiency also do not have increased HDL-cholesterol levels (31), pointing to a species-dependent effect of MC4R function on HDL-cholesterol levels.

In conclusion, inhibition of central MC3/4R signaling by SHU9119 reduces BAT activity thereby reducing the uptake and combustion of VLDL-TG by BAT. As a consequence, excess lipids are stored in WAT **(FIGURE 5)**. We anticipate that MC4R agonists that are currently in development to combat obesity, increase energy expenditure through activation of BAT.

ACKNOWLEDGEMENTS

We acknowledge the support from the Netherlands CardioVascular Research Initiative: 'the Dutch Heart Foundation, Dutch Federation of University Medical Centers, the Netherlands Organisation for Health Research and Development and the Royal Netherlands Academy of Sciences' for the GENIUS project 'Generating the best evidence-based pharmaceutical targets for atherosclerosis' (CVON2011-19). PCN Rensen is an Established Investigator of the Netherlands Heart Foundation (grant 2009T038).

REFERENCES

1 Garfield AS, Lam DD, Marston OJ, Przydzial MJ, Heisler LK: Role of central melanocortin pathways in energy homeostasis. *Trends Endocrinol Metab* 20:203-215, 2009.

2 Nargund RP, Strack AM, Fong TM: Melanocortin-4 receptor (MC4R) agonists for the treatment of obesity. *J Med Chem* 49:4035-4043, 2006.

3 Fan W, Boston BA, Kesterson RA, Hruby VJ, Cone RD: Role of melanocortinergic neurons in feeding and the agouti obesity syndrome. *Nature* 385:165-168, 1997.

4 Huszar D, Lynch CA, Fairchild-Huntress V, Dunmore JH, Fang Q, Berkemeier LR, et al. Targeted disruption of the melanocortin-4 receptor results in obesity in mice. *Cell* 88:131-141, 1997.

5 Farooqi IS, Keogh JM, Yeo GS, Lank EJ, Cheetham T, O'Rahilly S: Clinical spectrum of obesity and mutations in the melanocortin 4 receptor gene. *N Engl J Med* 348:1085-1095, 2003.

6 Loos RJ, Lindgren CM, Li S, Wheeler E, Zhao JH, Prokopenko I, et al. Common variants near MC4R are associated with fat mass, weight and risk of obesity. *Nat Genet* 40:768-775, 2008.

7 Xi B, Chandak GR, Shen Y, Wang Q, Zhou D: Association between common polymorphism near the MC4R gene and obesity risk: a systematic review and meta-analysis. *PLoS One* 7:e45731, 2012.

8 Nogueiras R, Wiedmer P, Perez-Tilve D, Veyrat-Durebex C, Keogh JM, Sutton GM, et al. The central melanocortin system directly controls peripheral lipid metabolism. *J Clin Invest* 117:3475-3488, 2007.

9 Rahmouni K, Haynes WG, Morgan DA, Mark AL: Role of melanocortin-4 receptors in mediating renal sympathoactivation to leptin and insulin. *J Neurosci* 23:5998-6004, 2003.

10 Joly-Amado A, Denis RG, Castel J, Lacombe A, Cansell C, Rouch C, et al. Hypothalamic AgRP-neurons control peripheral substrate utilization and nutrient partitioning. *EMBO J* 31:4276-4288, 2012.

11 Cole SA, Butte NF, Voruganti VS, Cai G, Haack K, Kent JW, et al. Evidence that multiple genetic variants of MC4R play a functional role in the regulation of energy expenditure and appetite in Hispanic children. *Am J Clin Nutr* 91:191-199, 2010.

12 Krakoff J, Ma L, Kobes S, Knowler WC, Hanson RL, Bogardus C, et al. Lower metabolic rate in individuals heterozygous for either a frameshift or a functional missense MC4R variant. *Diabetes* 57:3267-3272, 2008.

13 Bartelt A, Bruns OT, Reimer R, Hohenberg H, Ittrich H, Peldschus K, et al. Brown adipose tissue activity controls triglyceride clearance. *Nat Med* 17:200-205, 2011.

14 Voss-Andreae A, Murphy JG, Ellacott KL, Stuart RC, Nillni EA, Cone RD, et al. Role of the central melanocortin circuitry in adaptive thermogenesis of brown adipose tissue. *Endocrinology* 148:1550-1560, 2007.

15 Westerterp M, van der Hoogt CC, de HW, Offerman EH, Dallinga-Thie GM, Jukema JW, et al. Cholesteryl ester transfer protein decreases high-density lipoprotein and severely aggravates atherosclerosis in APOE*3-Leiden mice. *Arterioscler Thromb Vasc Biol* 26:2552-2559, 2006.

16 Van Klinken JB, van den Berg SA, Havekes LM, Willems Van DK: Estimation of activity related energy expenditure and resting metabolic rate in freely moving mice from indirect calorimetry data. *PLoS One* 7:e36162, 2012.

17 Bligh EG, Dyer WJ: A rapid method of total lipid extraction and purification. *Can J Biochem Physiol* 37:911-917, 1959.

18 Rensen PC, Herijgers N, Netscher MH, Meskers SC, Van EM, Van Berkel TJ: Particle size determines the specificity of apolipoprotein E-containing triglyceride-rich emulsions for the LDL receptor versus hepatic remnant receptor in vivo. *J Lipid Res* 38:1070-1084, 1997.

19 Wiedmer P, Chaudhary N, Rath M, Yi CX, Ananthakrishnan G, Nogueiras R, et al. The HPA axis modulates the CNS melanocortin control of liver triacylglyceride metabolism. *Physiol Behav* 105:791-799, 2012.

20 Itoh M, Suganami T, Nakagawa N, Tanaka M, Yamamoto Y, Kamei Y, et al. Melanocortin 4 receptor-deficient mice as a novel mouse model of nonalcoholic steatohepatitis. *Am J Pathol* 179:2454-2463, 2011.
21 Adiels M, Taskinen MR, Packard C, Caslake MJ, Soro-Paavonen A, Westerbacka J, et al. Overproduction of large VLDL particles is driven by increased liver fat content in man. *Diabetologia* 49:755-765, 2006.
22 Stafford JM, Yu F, Printz R, Hasty AH, Swift LL, Niswender KD: Central nervous system neuropeptide Y signaling modulates VLDL triglyceride secretion. *Diabetes* 57:1482-1490, 2008.
23 Carobbio S, Rosen B, Vidal-Puig A: Adipogenesis: new insights into brown adipose tissue differentiation. *J Mol Endocrinol* 2013.
24 Verty AN, Allen AM, Oldfield BJ: The endogenous actions of hypothalamic peptides on brown adipose tissue thermogenesis in the rat. *Endocrinology* 151:4236-4246, 2010.
25 Small CJ, Kim MS, Stanley SA, Mitchell JR, Murphy K, Morgan DG, et al. Effects of chronic central nervous system administration of agouti-related protein in pair-fed animals. *Diabetes* 50:248-254, 2001.
26 Lockie SH, Heppner KM, Chaudhary N, Chabenne JR, Morgan DA, Veyrat-Durebex C, et al. Direct control of brown adipose tissue thermogenesis by central nervous system glucagon-like peptide-1 receptor signaling. *Diabetes* 61:2753-2762, 2012.
27 Bartness TJ, Vaughan CH, Song CK: Sympathetic and sensory innervation of brown adipose tissue. *Int J Obes (Lond)* 34 Suppl 1:S36-S42, 2010.
28 Morrison SF, Madden CJ, Tupone D: Central control of brown adipose tissue thermogenesis. *Front Endocrinol (Lausanne)* 3: 2012.
29 Baran K, Preston E, Wilks D, Cooney GJ, Kraegen EW, Sainsbury A: Chronic central melanocortin-4 receptor antagonism and central neuropeptide-Y infusion in rats produce increased adiposity by divergent pathways. *Diabetes* 51:152-158, 2002.
30 Iqbal J, Li X, Chang BH, Chan L, Schwartz GJ, Chua SC, et al. An intrinsic gut leptin-melanocortin pathway modulates intestinal microsomal triglyceride transfer protein and lipid absorption. *J Lipid Res* 51:1929-1942, 2010.
31 Greenfield JR, Miller JW, Keogh JM, Henning E, Satterwhite JH, Cameron GS, et al. Modulation of blood pressure by central melanocortinergic pathways. *N Engl J Med* 360:44-52, 2009.
32 Perez-Tilve D, Hofmann SM, Basford J, Nogueiras R, Pfluger PT, Patterson JT, et al. Melanocortin signaling in the CNS directly regulates circulating cholesterol. *Nat Neurosci* 13:877-882, 2010.
33 Hildebrand RB, Lammers B, Meurs I, Korporaal SJ, de HW, Zhao Y,et al. Restoration of high-density lipoprotein levels by cholesteryl ester transfer protein expression in scavenger receptor class B type I (SR-BI) knockout mice does not normalize pathologies associated with SR-BI deficiency. *Arterioscler Thromb Vasc Biol* 30:1439-1445, 2010.

SUPPLEMENTARY APPENDIX

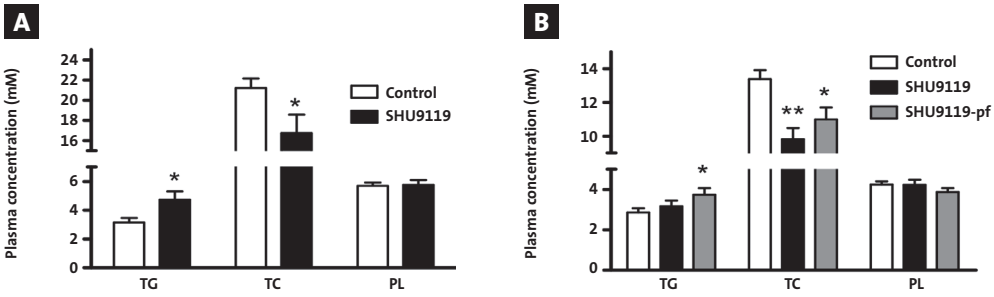

SUPPLEMENTARY FIGURE 1 – Effect of SHU9119 on plasma lipid levels. **A** In a first experiment, APOE*3-Leiden.CETP mice were treated intracerebroventricularly with vehicle (n=10) or SHU9119 (5 nmol/day) (n=7). After 17 days of treatment, blood was drawn after a 4 h fast (from 8.00 h to 12.00 h) via tail vein bleeding in paraoxon-coated capillary tubes to prevent *ex vivo* lipolysis and assayed for triglycerides (TG), total cholesterol (TC) and phospholipids (PL) using commercially available enzymatic kits for TG (11488872, Roche Diagnostics, Germany), TC (11489232, Roche Diagnostics, Mannheim, Germany) and PL (3009, Instruchemie, Delfzijl, the Netherlands). **B** In a second experiment, mice were treated i.c.v. with vehicle (n=21) or SHU9119 (5 nmol/day) while being fed *ad libitum* (n=21) or being pair-fed (pf) to the vehicle-treated group (n=22). Plasma lipids were determined after 4 h of fasting.

Values are means ± SEM. *p<0.05, **p<0.01 compared to control.

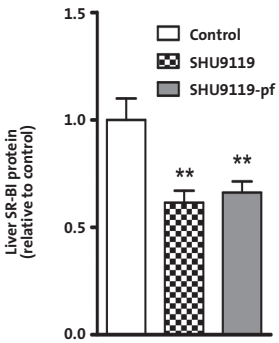

SUPPLEMENTARY FIGURE 2 – Effect of SHU9119 on hepatic SR-BI protein levels. APOE*3-Leiden.CETP mice were treated intracerebroventricularly with vehicle (n=21) or SHU9119 (5 nmol/day) while being fed *ad libitum* (n=21) or being pair-fed (pf) to the vehicle-treated group (n=20). After 17 days of treatment, part of the mouse groups were sacrificed (n=10-11 per group) to collect organs and determine hepatic SR-BI protein levels.

Values are means ± SEM. **p<0.01 compared to control.

CENTRAL ROLE FOR BROWN ADIPOSE TISSUE IN DYSLIPIDEMIA AND ATHEROSCLEROSIS DEVELOPMENT

MARIËTTE R. BOON
JIMMY F.P. BERBÉE*
P. PADMINI S.J. KHEDOE*
ALEXANDER BARTELT*
CHRISTIAN SCHLEIN
ANNA WORTHMANN
CLARA WEIGELT
CAROLINE JUNG
SANDER KOOIJMAN
NADIA VAZIRPANAH
LINDA P.J. BROUWERS
PHILIP L.S.M. GORDTS
JEFFREY D. ESKO
PIETER S. HIEMSTRA
LOUIS M. HAVEKES
LUDGER SCHEJA
JOERG HEEREN
PATRICK C.N. RENSEN

* These authors contributed equally to this work

Submitted.

ABBREVATIONS

ApoE	Apolipoprotein E
ß3-AR	ß3-adrenergic receptor
BAT	Brown adipose tissue
CB1R	Cannabinoid 1 receptor
CVD	Cardiovascular diseases
E3L.CETP	APOE*3-Leiden.cholesteryl ester transfer protein
EE	Energy expenditure
FA	Fatty acids
FGF21	Fibroblast growth factor 21
FPLC	Fast performance liquid chromatography
PEG	Polyethylene glycol
HE	Hematoxylin-eosin
iBAT	interscapular BAT
LDLR	Low-density lipoprotein receptor
PCSK9	Proprotein convertase subtilisin/kexin type 9
SQRT	Square root
TC	Total cholesterol
TG	Triglycerides
TO	Triolein
(V)LDL-C	(Very-)low-density lipoprotein-cholesterol
WAT	White adipose tissue
WTD	Western-type diet
UCP1	Uncoupling protein-1

ABSTRACT

Brown adipose tissue (BAT) combusts high amounts of fatty acids into heat, thereby lowering plasma triglyceride levels and reducing obesity. However, the precise role of BAT in plasma cholesterol metabolism and atherosclerosis development remains unclear. Here we show that BAT activation by the ß3-adrenergic receptor agonist CL316243 in dyslipidemic *APOE*3-Leiden.CETP* mice, a well-established model for human-like lipoprotein metabolism, increases energy expenditure, lowers body fat and plasma triglyceride levels, and attenuates plasma cholesterol levels and the development of atherosclerosis. Mechanistically, we show that BAT activation enhanced the selective uptake of fatty acids from glycerol tri[^{3}H]oleate-labeled VLDL-like emulsion particles into BAT. Importantly, the cholesterol and atherosclerosis lowering effects of BAT activation were dependent on a functional hepatic apoE-LDLR clearance pathway, as BAT activation in *Apoe*$^{-/-}$ and *Ldlr*$^{-/-}$ mice, while lowering triglyceride levels, did not attenuate hypercholesterolemia and atherosclerosis. We demonstrate that activation of BAT is a powerful therapeutic tool to improve dyslipidemia and protect from atherosclerosis.

INTRODUCTION

Cardiovascular diseases (CVD) are the leading cause of morbidity and mortality in the Western world, and are mainly caused by atherosclerosis for which dyslipidemia is a main risk factor. As current treatment strategies of atherogenic dyslipidemia prevent only 30% of all cardiovascular events (1), novel treatment strategies are highly warranted.

Brown adipose tissue (BAT) is a highly active metabolic tissue being present and active in adults (2,3). Brown adipocytes are mainly present in fat pads, but also lie scattered in certain white adipose tissue (WAT) depots. The development of these so-called peripheral, inducible brown adipocytes or 'beige cells' can be stimulated by prolonged cold exposure or pharmacological adrenergic stimulation, a process called 'browning' (4,5). Both brown and beige adipocytes are characterized by a large number of mitochondria and numerous small lipid droplets and both cell types are functionally thermogenic (6). Physiologically, BAT is activated by cold exposure via sympathetic neurons that release noradrenalin (7). The noradrenalin-stimulated activation of brown adipocytes can be pharmacologically mimicked by selective ß3-adrenergic receptor (ß3-AR) treatment (8,9). Activation of the ß3-AR rapidly induces intracellular lipolysis of TG from lipid droplets, releasing fatty acids (FA). FA are directed towards mitochondria where they either allosterically activate the uncoupling protein-1 (UCP1) in the inner membrane of the mitochondrion (10), or undergo oxidation. The intracellular TG stores of the brown adipocyte are replenished mainly by uptake of FA derived from TG-rich lipoproteins in the plasma (11).

The magnitude of the plasma TG clearance capacity of BAT became clear only recently. We showed that activation of BAT in mice via cold or metformin potently reduces plasma TG levels and obesity (12,13). Therefore, activation of BAT is now considered a promising new therapeutic avenue to combat hypertriglyceridemia and obesity (14,15). However, increased turnover of plasma lipoproteins may also lead to adverse side effects when pro-atherogenic cholesterol-rich remnants that arise from TG turnover accumulate in plasma. In that vein, BAT activation by cold exposure has been described to aggravate hypercholesterolemia and atherosclerosis development in *Apoe*$^{-/-}$ and *Ldlr*$^{-/-}$ mice (16). We reasoned that the enhanced clearance of plasma TG upon BAT activation requires efficient clearance of cholesterol-enriched lipoprotein remnants by the liver, a pathway that is considered to be crucially dependent on a functional apoE-LDLR axis. Here, we investigate the effects of ß3-AR-mediated BAT activation on cholesterol metabolism and atherosclerosis development in *APOE*3-Leiden.CETP* (E3L.CETP), a well-established model for human-like lipoprotein metabolism that unlike *Apoe*$^{-/-}$ and *Ldlr*$^{-/-}$ mice responds well to the lipid-lowering and anti-atherogenic effects of statins, fibrates and niacin (17-19).

We show that pharmacological activation of BAT in *E3L.CETP* mice enhances lipolytic conversion of TG-rich lipoproteins in BAT, resulting in a pronounced reduction in plasma cholesterol and TG levels and ultimately marked attenuation of atherosclerosis development. In addition, we show that *Apoe*$^{-/-}$ and *Ldlr*$^{-/-}$ mice do not respond to the plasma cholesterol-lowering activity of BAT and are not protected from atherosclerosis development, underlining the importance of the apoE-LDLR axis for the anti-atherogenic potential of BAT.

RESULTS

Activation of BAT augments fatty acid combustion and uptake under atherogenic conditions

We first assessed the effect of BAT activation on energy expenditure and lipid storage in *E3L.CETP* mice fed an atherogenic Western-type diet (WTD) for 10 weeks while treated with the selective ß3-AR agonist CL316243 (3x 20 µg/mouse/week; subcutaneous) or vehicle (PBS). ß3-AR agonism tended to reduce body mass (up to -8%; P=0.05; **FIGURE 1A)** and markedly reduced total fat mass gain (up to -81%; P<0.001; **FIGURE 1B)**, without affecting lean mass **(FIGURE 1C)**. Accordingly, in the ß3-AR agonist-treated mice the weight of the individual WAT pads was lower (ranging from -25 to -52%; P<0.05; **FIGURE S1A)**, and the lipid droplets within white adipocytes were smaller (-48%; P<0.001; **FIGURES S1B-C)**.

The ß3-AR-mediated reduction in body fat gain was likely the consequence of increased adaptive thermogenesis as energy expenditure was markedly increased on the day of treatment (+17%; P<0.001; **FIGURE 1D)** without differences in activity levels **(FIGURE 1E)** or food intake (not shown). The increase in energy expenditure was confined to an increased fat oxidation (+67%; P<0.001; **FIGURE 1F)** rather than carbohydrate oxidation **(FIGURE 1G)**, and consequently, ß3-AR agonism reduced the respiratory exchange ratio (-3.5%; P<0.001; **FIGURE 1H)**. The enhanced energy expenditure was accompanied by a marked activation of interscapular BAT (iBAT) as evidenced by reduced intracellular lipid vacuole size in iBAT (-87%; P<0.05; **FIGURES S2A-B)**, reduced BAT pads weight (approx. -25%; **FIGURE S1A)**, and increased expression of UCP1 (+43%; P<0.01; **FIGURES S2C-D)**. In addition, ß3-AR agonism increased browning of WAT **(FIGURES S3A-B)**.

BAT activation markedly reduced plasma TG levels throughout the treatment period (-54%; P<0.001; **FIGURE 2A)**, caused by a reduction in VLDL-TG **(FIGURE 2B)**. To confirm that this reduction was caused by enhanced uptake of TG-derived FA by BAT, we determined the effect of BAT activation on the serum decay and organ uptake of glycerol tri[^{3}H]oleate (triolein, TO)-labeled VLDL-mimicking emulsion particles (20). Indeed, ß3-AR agonism markedly accelerated the serum clearance of [^{3}H]TO **(FIGURE 2C;** $t_{½}$= 1.7±0.2 *vs.* 3.6±0.8 min; P<0.05) by selectively increasing the uptake of [^{3}H]TO-derived activity by the various BAT depots (approx. +120%; P<0.05; **FIGURE 2D)**. Interestingly, the uptake of [^{3}H]oleate by WAT fat depots was also increased (approx. +120%; P<0.01), indicating enhanced uptake by beige adipocytes within WAT. Taken together, these data show that also under atherogenic conditions ß3-AR agonism activates BAT *E3L.CETP* mice, resulting in increased uptake and combustion of VLDL-TG-derived FA and a consequent decrease in plasma TG levels.

Activation of BAT reduces cholesterol-rich remnant lipoproteins levels

Since disturbed cholesterol metabolism rather than disturbed triglyceride metabolism is the main determinant for atherosclerosis development (21), we next investigated the effect of BAT activation on cholesterol metabolism in *E3L.CETP* mice. BAT activation consistently reduced plasma total cholesterol (TC) levels throughout the treatment period (approx. -23%; P<0.05; **FIGURE 2E)** which was due to a reduction of plasma (V)LDL-cholesterol ((V)LDL-C) levels (approx. -27%; P<0.05; **FIGURE 2F)**. Lipoprotein fractionation using fast performance liquid chromatography (FPLC) confirmed the improved cholesterol profile **(FIGURE 2G)**.

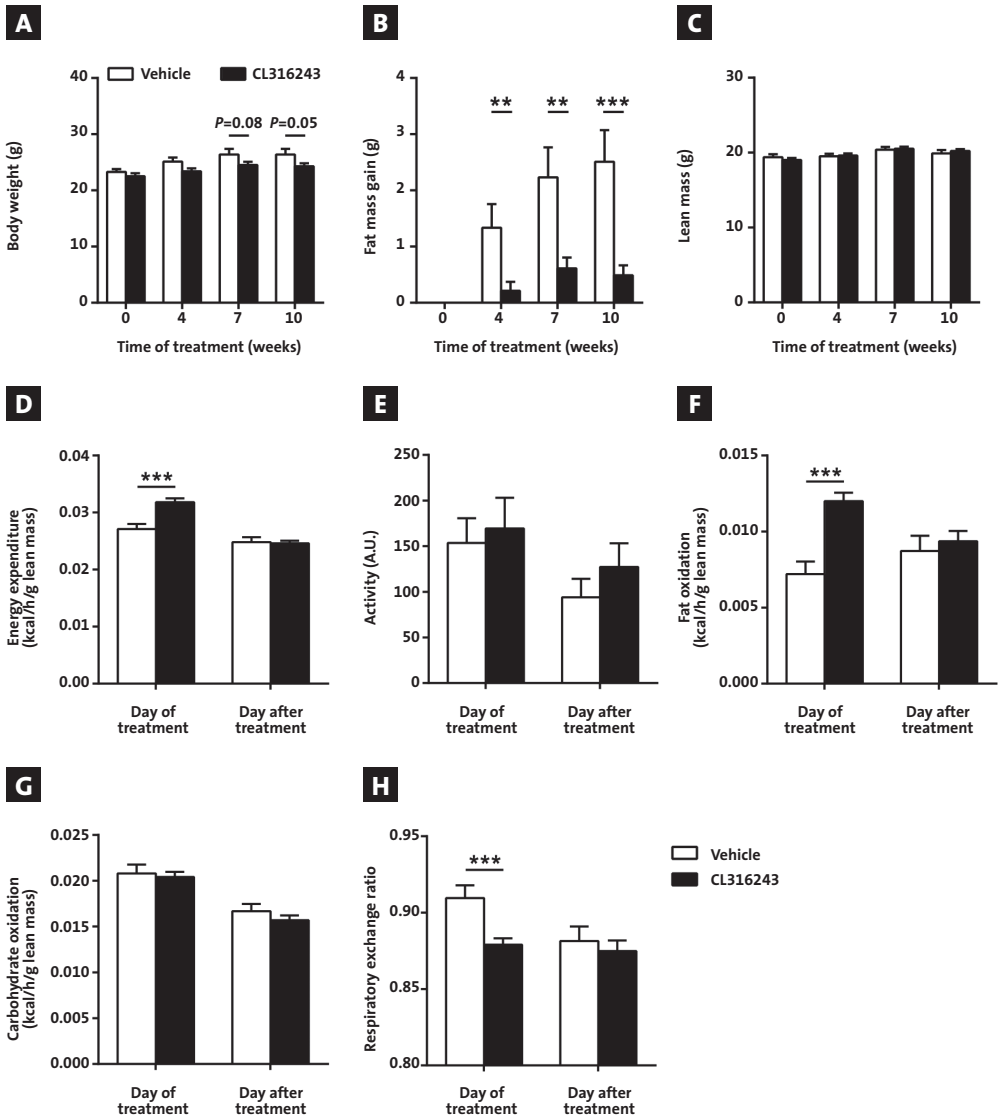

FIGURE 1 – 3-AR agonism reduces body fat mass and increases energy expenditure. Western-type diet-fed *E3L.CETP* mice were treated with the ß3-AR agonist CL316243 or vehicle and body weight **A**, gain of total body fat mass **B** and lean mass **C** were determined at the indicated time points. During the ninth week of treatment, mice were housed in fully automated metabolic cages and energy expenditure **D**, physical activity **E**, fat oxidation **F** and carbohydrate oxidation **G** were determined. In addition, respiratory exchange ratio was determined **H**. Data are shown as the first 12 hours directly after the injection with CL316243 or vehicle ('Day of treatment') and the same 12-hours period 24 hours later ('Day after treatment').

Values are means ± S.E.M. (n=13-19 per group). ***P*<0.01, ****P*<0.001

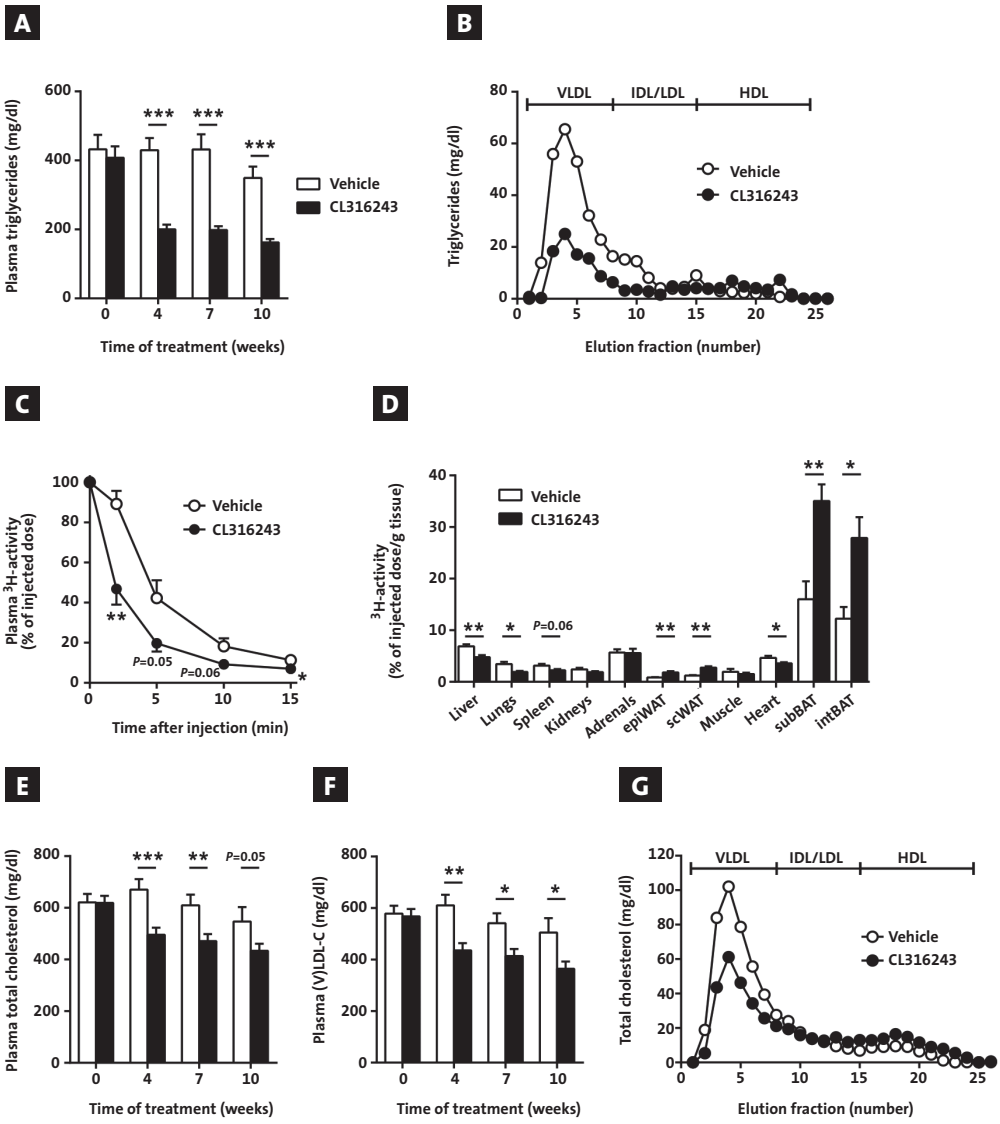

FIGURE 2 – Activation of BAT improves both TG and cholesterol metabolism. Western-type diet-fed *E3L.CETP* mice were treated with the ß3-AR agonist CL316243 or vehicle and fasting plasma TG levels **A** were measured at the indicated time points. The distribution of TG over lipoproteins was determined after 10 weeks of treatment on pooled plasma samples per group **B**. CL316243- and vehicle-treated mice were injected with [3H]TO-labeled VLDL-like emulsion particles and clearance from plasma **C** and organ and tissue uptake 15 min after injection **D** were determined. Fasting plasma total cholesterol **E** and (V)LDL-cholesterol ((V)LDL-C; **F**) were assessed at the indicated times during the study. The distribution of total cholesterol over lipoproteins was determined after 10 weeks of treatment on pooled plasma samples per group **G**.

Values are means ± S.E.M. (n=13-19 per group). **P*<0.05, ***P*<0.01, ****P*<0.001

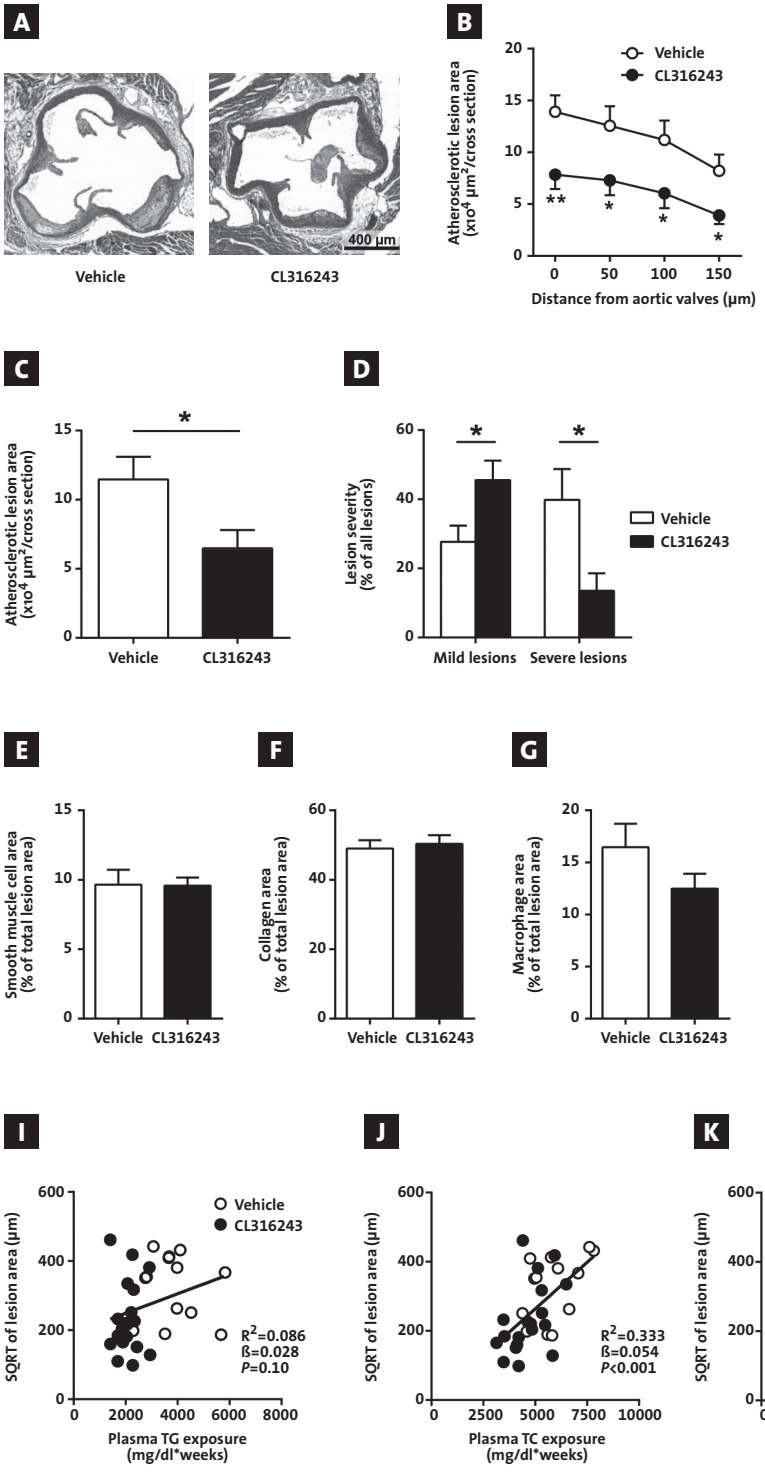
A
400 µm
Vehicle
CL316243
B
Vehicle
CL316243
Atherosclerotic lesion area (x10⁴ µm²/cross section)
Distance from aortic valves (µm)
C
Atherosclerotic lesion area (x10⁴ µm²/cross section)
Vehicle
CL316243
D
Lesion severity (% of all lesions)
Mild lesions
Severe lesions
Vehicle
CL316243
E
Smooth muscle cell area (% of total lesion area)
F
Collagen area (% of total lesion area)
G
Macrophage area (% of total lesion area)
H
Stability index (collagen/macrophage area)
P=0.12
I
SQRT of lesion area (µm)
Plasma TG exposure (mg/dl*weeks)
R²=0.086
ß=0.028
P=0.10
J
SQRT of lesion area (µm)
Plasma TC exposure (mg/dl*weeks)
R²=0.333
ß=0.054
P<0.001
K
SQRT of lesion area (µm)
Plasma (V)LDL-C exposure (mg/dl*weeks)
R²=0.358
ß=0.055
P<0.001

FIGURE 3 – Activation of BAT reduces atherosclerotic lesion development and severity via improving the plasma cholesterol profile. Slides of the valve area of the aortic root of ß3-AR agonist CL316243- and vehicle-treated *E3L.CETP* mice were stained with hematoxylin-phloxine-saffron and representative pictures are shown **A**. Lesion area as a function of distance was determined in four consecutive sections per mouse starting from the appearance of open aortic valve leaflets **B**. The mean atherosclerotic lesion area was determined from the four cross sections from B **C** and lesions were categorized according to lesion severity **D**. The smooth muscle cell **E**, collagen **F** and macrophage **G** content of the lesions were determined and the stability index (collagen/macrophage content of the lesions; **H**) was calculated. The square root (SQRT) of the atherosclerotic lesion area from B was plotted against the plasma total TG **I**, total cholesterol **J** and (V)LDL-cholesterol ((V)LDL-C; K) exposure during the 10 week treatment period. Linear regression analyses were performed.
Values are means ± S.E.M. (n=13-19 per group). **P*<0.05, ***P*<0.01

Activation of BAT reduces atherosclerosis development by improving the plasma cholesterol profile

Next, we studied whether the decreased (V)LDL levels were accompanied by reduced atherosclerosis development. To this end, we determined atherosclerotic lesion area as well as severity and composition of the lesions in the root of the aortic arch after 10 weeks of BAT activation. Indeed, sustained BAT activation by ß3-AR agonism markedly reduced atherosclerotic lesion area throughout the aortic root **(FIGURES 3A-B)**, resulting in 43% lower mean atherosclerotic lesion area **(FIGURE 3C)**. BAT activation clearly reduced the severity of the lesions, as indicated by more mild lesions *(i.e.* type I-III; +64%; *P*<0.05) and less severe lesions *(i.e.* type IV-V; -66%; *P*<0.05) **(FIGURE 3D)** without significantly affecting atherosclerotic lesion composition *(i.e.* collagen, vascular smooth muscle cell and macrophage content of the lesions; **FIGURES 3E-G)** or the lesion stability index *(i.e.* ratio collagen/macrophage area; **FIGURE 3H)**.
To evaluate the contribution of TG versus TC lowering to the reduction in atherosclerosis, univariate regression analyses were performed. To linearize data for analysis, the atherosclerotic lesion area was square root (SQRT)-transformed (19) and plotted against the exposure *(i.e.* AUC of plasma lipid for the complete treatment period) of TG, and TC. The SQRT of the lesion area did not correlate with plasma TG exposure (ß=0.028; R^2=0.086; *P*=0.10; **FIGURE 3I)**, but did correlate with plasma TC exposure (ß=0.054; R^2=0.333; P<0.001; **FIGURE 3J)**. Additional univariate regression analyses showed that the (V)LDL-C exposure specifically predicts the SQRT of the lesion area (ß=0.055; R^2=0.358; P<0.001; **FIGURE 3K)**. These analyses thus strongly indicate that a reduction in plasma (V)LDL-C is the main contributor to the anti-atherogenic effect of ß3-AR-mediated activation of BAT.

The anti-atherogenic potential of BAT activation crucially depends on functional hepatic lipoprotein clearance

As BAT activation by cold in *Apoe*$^{-/-}$ and *Ldlr*$^{-/-}$ mice has been described to aggravate atherosclerosis development (16), we evaluated the role of apoE, the main clearance ligand for TG-rich lipoprotein remnants, in the (V)LDL-C-reducing effect of BAT activation. In order to control for increases in food intake as described in these mouse models during cold adaption (16), as well as to match dietary cholesterol intake we studied the effect of ß3-AR-mediated BAT activation in WTD-pair-fed *Apoe*$^{-/-}$ mice. Similar as in *E3L.CETP* mice, activation of BAT

reduced body weight, WAT pad size and plasma TG levels **(FIGURES 4A** and **S4A-C)**. However, activation of BAT did neither reduce plasma TC and (V)LDL-C levels **(FIGURES 4B** and **S4D)** nor did it reduce atherosclerosis development **(FIGURES 4C-D)** or alter plaque composition (data not shown) in *Apoe*$^{-/-}$ mice. Accordingly, the SQRT of the lesion area did not correlate with either total plasma TG exposure or plasma TC exposure during the study **(FIGURES 4E-F)**.

As the (V)LDL-C-reducing effect of BAT activation thus crucially depends on apoE-mediated clearance, we next investigated the role of the LDLR, the main hepatic clearance receptor for apoE-containing lipoprotein remnants. Similar as in *E3L.CETP* mice, activation of BAT

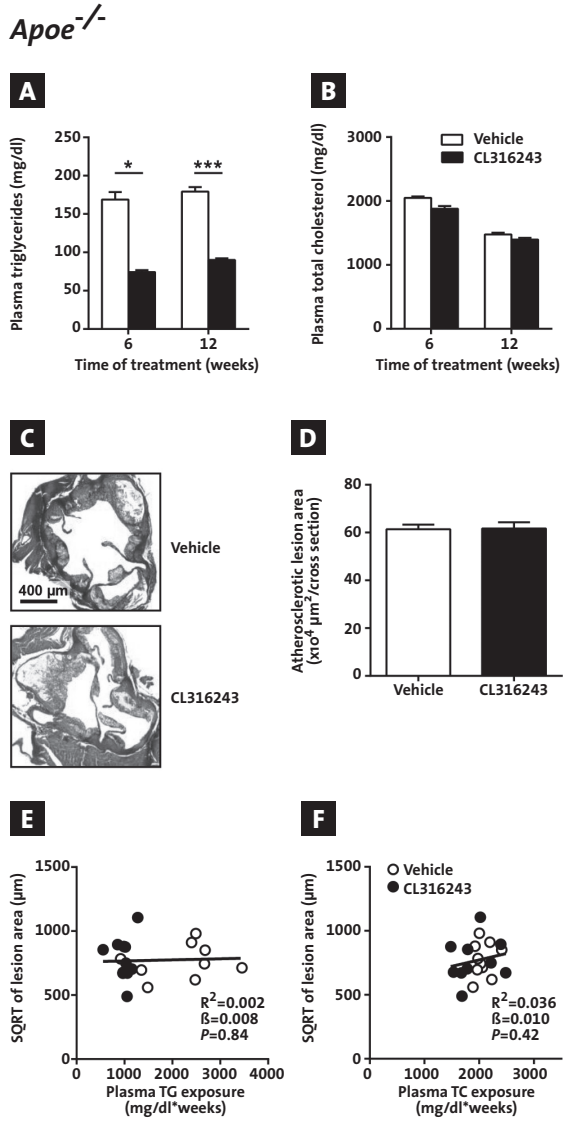

FIGURE 4 – Activation of BAT in *Apoe*$^{-/-}$ and *Ldlr*$^{-/-}$ mice reduces plasma TG, but not TC and atherosclerosis. Western-type diet-fed *Apoe*$^{-/-}$ mice were treated with the ß3-AR agonist CL316243 or vehicle and fasting plasma TG **A** and total cholesterol **B** levels were measured at the indicated time points. Slides of the valve area of the aortic root of CL316243- or vehicle-treated *Apoe*$^{-/-}$ mice were stained with hematoxylin-phloxine-saffron (HPS) and representative pictures are shown **C**. Mean atherosclerotic lesion area was determined from four consecutive cross sections per mouse starting from the appearance of open aortic valve leaflets **D**. The square root (SQRT) of the atherosclerotic lesion area from D in *Apoe*$^{-/-}$ mice was plotted against the plasma total TG **E** and total cholesterol **F** exposure during the 12-week treatment period. Linear regression analyses were performed.

reduced body weight, WAT pad size and plasma TG levels in WTD-pair-fed *Ldlr*$^{-/-}$ mice **(FIGURES 4G** and **S5A-C)**. However, activation of BAT in *Ldlr*$^{-/-}$ mice did neither reduce plasma TC and (V) LDL-C levels **(FIGURES 4H** and **S5D)**, nor reduce atherosclerosis development **(FIGURES 4I-J)** or alter plaque composition (data not shown), nor did the SQRT of the lesion area correlate with the total plasma TG and TC exposure during the study **(FIGURES 4K-L)**. Taken together, these findings indicate that activation of BAT reduces plasma (V)LDL-C and subsequently reduces atherosclerosis development through enhanced LDLR-mediated hepatic clearance of apoE-containing lipoprotein remnants.

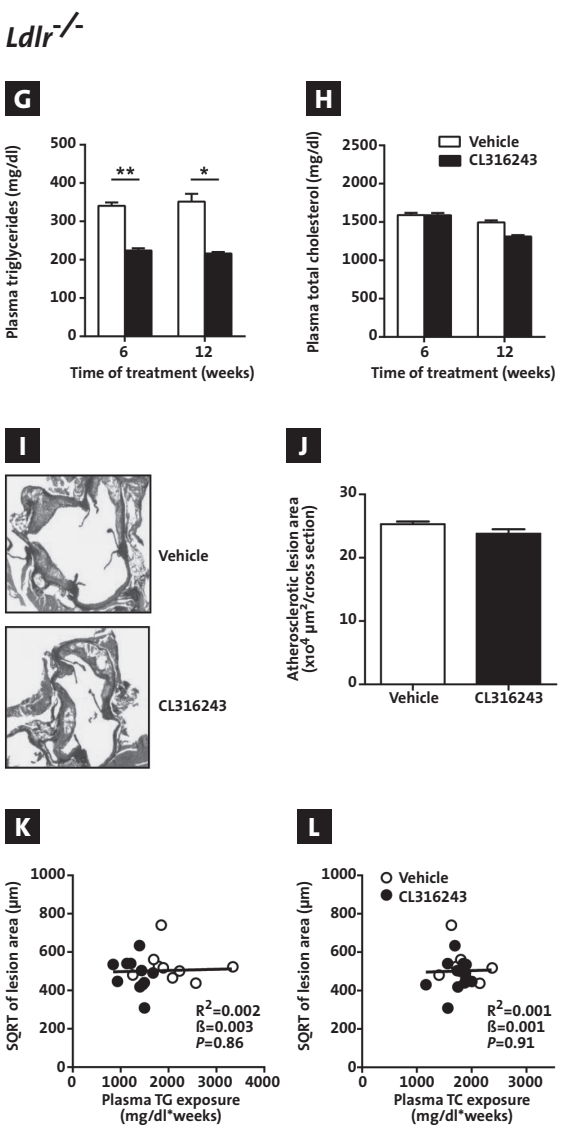

Western-type diet-fed *Ldlr*$^{-/-}$ mice were treated with the ß3-AR agonist CL316243 or vehicle and fasting plasma TG **G** and total cholesterol **H** levels were measured at the indicated time points. Slides of the valve area of the aortic root of CL316243- or vehicle-treated *Ldlr*$^{-/-}$ mice were stained with HPS and representative pictures are shown **I**. Mean atherosclerotic lesion area was determined from four consecutive cross sections per mouse starting from the appearance of open aortic valve leaflets **J**. The square root (SQRT) of the atherosclerotic lesion area from J in *Ldlr*$^{-/-}$ mice was plotted against the plasma total TG **K** and total cholesterol **L** exposure during the 12-week treatment period. Linear regression analyses were performed.

Values are means ± S.E.M. (n=8-11 per group or pool). **P*<0.05, ***P*<0.01, ****P*<0.001

DISCUSSION

Since its rediscovery in human adults in 2009 (2,3,22), BAT has been considered a promising therapeutic target for obesity and associated metabolic disorders. The anti-obesity potential of BAT has been irrefutably proven in murine studies (23,24) and shown in human studies (2,25,26). However, the effect of BAT activation on cholesterol metabolism and atherosclerosis development remained controversial if not elusive. The present study demonstrates that activation of BAT potently improves plasma cholesterol metabolism via a mechanism involving local lipolysis of TG-rich lipoproteins in BAT followed by increased clearance of apoE-containing lipoprotein remnants via the LDLR pathway. As a result, BAT activation reduces atherosclerotic lesion size and severity.

We observed that BAT activation decreased atherosclerosis development in *E3L.CETP* mice that possess a functional apoE-LDLR clearance pathway, but not in *Apoe*$^{-/-}$ and *Ldlr*$^{-/-}$ mice, both of which have an abrogated apoE-LDLR clearance pathway. This indicates that a crucial event in the anti-atherogenic property of BAT is the concomitant ability of the liver to clear apoE-enriched lipoprotein remnants, generated by BAT-mediated lipolysis of TG-rich lipoproteins, via the LDLR. *E3L.CETP* mice express a naturally occurring mutant form of human apoE3 that slows down remnant clearance, but does not abrogate the interaction with the LDLR (27). This results in an attenuated hepatic remnant clearance that is sufficient to induce dyslipidemia and atherosclerosis when feeding a WTD, but, importantly, the hepatic remnant clearance route is still functional and can be modulated. Accordingly, *E3L.CETP* mice respond to cholesterol-lowering drugs such as statins (18), fibrates (17) and niacin (19) in a similar manner as humans, whereas *Apoe*$^{-/-}$ and *Ldlr*$^{-/-}$ mice do not. According to this view, it is not surprising that Dong *et al.* (16) recently observed that BAT activation by cold in *Apoe*$^{-/-}$ and *Ldlr*$^{-/-}$ mice actually increased plasma (V)LDL-C levels and atherosclerosis. Likely, in these hyperlipidemic mouse models prolonged BAT activation results in lipoprotein remnant levels in plasma exceeding the hepatic clearance capacity.

Our work sets the foundation for future studies that may investigate the anti-atherogenic potential of BAT in humans. As the discovery that functional BAT is present and active in human adults was made only in the last decade (2,3), recent studies have focused on the physiological relevance of BAT for humans. That BAT is likely involved in energy metabolism and obesity development in humans appeared from studies that showed that BAT activity is inversely correlated to obesity (28) and that cold acclimation recruits BAT (29) and lowers fat mass (26). In addition, South Asians, who have a high susceptibility to metabolic disorders, have decreased energy expenditure associated with decreased BAT volume and activity (30). Importantly, BAT activation by means of cold acclimation also improved cholesterol metabolism in human patients with hypercholesterolemia (31), underscoring the potential of BAT activation as an anti-atherogenic treatment in humans. Future prospective studies are evidently needed to verify the anti-atherogenic properties of BAT activation in human subjects.

Though the ß3-AR is abundantly present on rodent BAT, it is still uncertain whether this isoform also controls BAT activity in humans. Although differentiated brown adipocytes from human multipotent adipose-derived stem cells could be activated by the ß3-AR agonist

CL316243 (32), treatment of humans with ß3-AR agonists showed no or only minor improvement of metabolic parameters (33,34). This may be due to low bioavailability of the agonist or low ß3-AR expression in human BAT, as plasma concentration of the agonist and reduction in fat mass and resting metabolic rate were in fact positively correlated. Alternatively, the ß1-AR and/or ß2-AR may be involved in human BAT function, as blockade of these receptors by propranolol decreased ^{18}F-fluorodeoxyglucose uptake by BAT as visualized by PET-CT scans (35), though the thermogenic responses remain unaffected (36). Collectively, this may suggest that ^{18}F-fluorodeoxyglucose uptake is regulated by ß1- or ß2-ARs, whereas mitochondrial uncoupling itself is regulated by ß3-ARs. Future studies should thus be directed at investigating the precise role of ß-ARs in human BAT function.

The long-term objective of this work is to set out novel therapeutic targets to activate BAT beyond ß-AR stimulation. Promising targets include the cannabinoid 1 receptor (CB1R) on BAT (Boon and Rensen, unpublished), irisin (37) and the fibroblast growth factor FGF21 (37), which massively activate BAT and induce browning in mice, and lowers plasma cholesterol in both mice and humans (37-39).

In conclusion, our data demonstrate that activation of BAT lowers plasma cholesterol levels and protects against atherosclerosis development, a scenario that is dependent on the apoE-LDLR clearance pathway for lipoprotein remnants. Future research should focus on elucidating whether BAT activation is a valuable strategy to combat obesity and atherosclerosis in humans. We expect that BAT activation, resulting in accelerated generation of lipoprotein remnants, should preferentially be combined with strategies that increase hepatic LDLR expression, including statins and/or PCSK9 blockers, fully unraveling the therapeutic potential of BAT for atherosclerosis prevention and treatment.

EXPERIMENTAL PROCEDURES

Animals, diet and ß3-AR agonist treatment

Female *E3L* were crossbred with mice expressing human cholesteryl ester transfer protein (CETP) under control of its natural flanking regions to generate heterozygous *E3L.CETP* mice (18). Female *E3L.CETP* mice were 10-12 weeks of age and housed under standard conditions with a 12-hours light/dark cycle, free access to food and water and 22°C room temperature. Mice were fed a Western-type diet (WTD) supplemented with 0.1% cholesterol and treated with the ß3-AR agonist CL316243 (Tocris Bioscience Bristol, United Kingdom; 3x 20 µg/mouse/week; subcutaneous) or vehicle (PBS). Food intake and body weight as well as total body fat and lean mass by Echo-MRI were monitored during the studies. Male *Apoe*$^{-/-}$ and *Ldlr*$^{-/-}$ mice (Jackson Laboratory, Bar Harbor, ME) were fed a WTD supplemented with 0.2% cholesterol with or without CL316243 (0.001% w/w). As CL316243 treatment of *Apoe*$^{-/-}$ and *Ldlr*$^{-/-}$ mice increased food intake, these mice were pair-fed to their respective controls after onset of effect. All animal experiments were approved by the Institutional Ethics Committees on Animal Care and Experimentation.

Indirect calorimetry

Indirect calorimetry was performed in fully automatic metabolic cages (LabMaster System, TSE Systems, Bad Homburg, Germany) during the ninth week of treatment. After 1 day of acclimatization, O_2 consumption, CO_2 production and caloric intake were measured for 3 consecutive days. Carbohydrate and fat oxidation rates were calculated from O_2 consumption and CO_2 production as described previously (40). Total energy expenditure (EE) was calculated from the sum of carbohydrate and fat oxidation. Physical activity was monitored using infrared sensor frames. The first 12 h directly after injection with CL316243 or vehicle ('Day of treatment') were analysed and compared to the same 12-h period 24 h later ('Day after treatment').

***In vivo* serum decay and organ uptake of VLDL-like emulsion particles**

VLDL-like TG-rich emulsion particles (80 nm) labeled with glycerol tri[^{3}H]-oleate (triolein, TO) were prepared and characterized as described previously (20). After 4 weeks of treatment with the ß3-AR agonist CL316243 mice were fasted for 4 h, and injected (t=0) via the tail vein with the emulsion particles (1.0 mg TG/mouse in 200 µl PBS). Blood samples were taken from the tail vein at 2, 5, 10 and 15 min after injection to determine the serum decay of [^{3}H] TO. Plasma volumes were calculated as 0.04706 x body weight (g) as described (41). After 15 min, mice were sacrificed by cervical dislocation and perfused with ice-cold heparin solution (0.1% v/v in PBS) via the heart to remove blood from the organs and tissues. Subsequently, organs and tissues were isolated, dissolved overnight at 56°C in Tissue Solubilizer (Amersham Biosciences, Rosendaal, The Netherlands), and quantified for ^{3}H-activity. Uptake of [^{3}H] TO-derived radioactivity by the organs and tissues was expressed per gram wet tissue weight.

Plasma parameters and lipoprotein profiles

Blood was collected from the tail vein of 4-h fasted mice into EDTA- *(E3L.CETP)* or lithium-heparin-coated tubes (*Apoe*$^{-/-}$ and *Ldlr*$^{-/-}$ mice). Tubes were placed on ice, centrifuged, and plasma was isolated and assayed for TG and TC using commercially available enzymatic kits from Roche Diagnostics (Mannheim, Germany). Plasma HDL-C levels were determined by precipitating apoB-containing lipoproteins from plasma by addition of 20% polyethylene glycol (PEG) in 200 mM glycine buffer with pH 10, and TC was measured in the supernatant as described above. Plasma (V)LDL-C levels were calculated by extraction of HDL-C from TC levels. The distribution of triglycerides and cholesterol over lipoproteins was determined in pooled plasma by fast performance liquid chromatography on a Superose 6 column (GE Healthcare, Piscataway, NJ).

Sacrification and Histology of BAT and WAT

At the end of the study mice were anesthetized by intraperitoneal injection of acepromazine (6.25 mg/kg; Alfasan, Woerden, The Netherlands), midazolam (0.25 mg/kg; Roche, Mijdrecht, The Netherlands) and fentanyl (0.31 mg/kg; Janssen-Cilag, Tilburg, The Netherlands), bled and killed by cervical dislocation or transcardial blood withdrawal. The blood circulation was

perfused with ice-cold heparin solution (0.1% v/v in PBS) and organs and tissues were weighed and collected for further analyses. Epididymal WAT and interscapular BAT were removed and fixated in phosphate-buffered 4% formaldehyde and embedded in paraffin. Hematoxylin-eosin (HE) staining was performed using standard protocols. Intracellular lipid droplet size in WAT and percentage of lipid-droplet-positive area in BAT were quantified using Image J software (version 1.47).

For UCP1 staining, 5 µm sections were deparafinnated in xylene, rehydrated in ethanol and treated with 3% H_2O_2 (Sigma-Aldrich, Zwijndrecht, The Netherlands) in absolute methanol for 30 min to block endogenous peroxidase activity. Sections were immersed in citrate buffer (10 mM, pH 6) and boiled for 10 min. Slides were blocked with 1.3% normal goat serum (in PBS) and incubated overnight at 4°C with rabbit monoclonal anti-UCP1 antibody (Abcam, Cambridge, United Kingdom; 1:400 in 1.3% normal goat serum). Subsequently, sections were incubated for 60 min with biotinylated goat α-rabbit secondary antibody (Vector Labs, Burlingame, CA) diluted in 1.3% normal goat serum. Immunostaining was amplified using Vector Laboratories Elite ABC kit (Vector Labs) and the immunoperoxidase complex was visulalized with Nova Red (Vector Labs). Counterstaining was performed with Mayer's hematoxylin (1:4). Expression of UCP1 was quantified using Image J software (version 1.47).

Atherosclerosis quantification

Hearts were collected and fixated in phosphate-buffered 4% formaldehyde, embedded in paraffin and perpendicular to the axis of the aorta cross-sectioned (5 µm) throughout the aortic root area starting from the appearance of open aortic valve leaflets. Per mouse 4 sections with 50 µm intervals were used for atherosclerosis measurements. Sections were stained with hematoxylin-phloxine-saffron for histological analysis. Lesions were categorized for lesion severity according to the guidelines of the American Heart Association adapted for mice (42). Various types of lesions were discerned: mild lesions (types 1-3) and severe lesions (types 4-5). Lesion area was determined using Image J Software (version 1.47). Lesion composition with respect to smooth muscle cell and collagen content was determined as described previously (42). Rat monoclonal anti-MAC-3 antibody (BD Pharmingen, San Diego, CA) was used to quantify macrophage area. The stability index was calculated by dividing the collagen by the macrophage area.

Statistical analyses

Statistical analyses were assessed using the unpaired two-tailed Student's t-test. Univariate regression analyses were performed to test for significant correlations between atherosclerotic lesion area and plasma lipid exposures during the study. Multiple regression analysis was performed to predict the contribution of plasma TG and TC exposures during the study to the atherosclerotic lesion area. The square root (SQRT) of the lesion area was taken to linearize the relationship with the plasma lipid exposures. Data are presented as mean ± S.E.M., unless indicated otherwise. A probability level *(P)* of 0.05 was considered significant. SPSS 20.0 for Windows (SPSS, Chicago, IL) was used for statistical analyses.

ACKNOWLEDGMENTS

This study is supported by 'the Netherlands CardioVascular Research Initiative: the Dutch Heart Foundation, Dutch Federation of University Medical Centers, the Netherlands Organisation for Health Research and Development and the Royal Netherlands Academy of Sciences' for the GENIUS project 'Generating the best evidence-based pharmaceutical targets for atherosclerosis' (CVON2011-19). M.R. Boon is supported by a personal grant from the Board of Directors of LUMC, P.P.S.J. Khedoe by a grant of the Lung Foundation Netherlands (grant 3.2.10.048), and P.C.N. Rensen is an Established Investigator of the Netherlands Heart Foundation (grant 2009T038). A. Bartelt was supported by a Postdoctoral Fellowship Award from the European Atherosclerosis Society (EAS) and a Research Fellowship from the German Research Foundation (DFG; BA 4925/1-1). J. Heeren is supported by a grant from the Fondation Leducq – Triglyceride Metabolism in Obesity and Cardiovascular Disease. Furthermore, the authors thank Isabel M. Mol, Lianne C.J.A. van der Wee-Pals, Trea Streefland and Chris van der Bent (Dept. of Endocrinology and Metabolic Diseases, LUMC, Leiden, The Netherlands) as well as Sandra Ehret (Dept. of Biochemistry and Molecular Cell Biology, Hamburg, Germany) for their excellent technical assistance and Dr. Jan B. van Klinken (Dept. of Human Genetics, LUMC, Leiden, The Netherlands) for help with statistical analysis. The authors would like to thank A.J. Whittle and A. Vidal-Puig for critical discussions.

REFERENCES

1 Jukema JW, Cannon CP, de Craen AJ, et al. The controversies of statin therapy: weighing the evidence. *J Am Coll Cardiol* 60:875-881, 2012.

2 van Marken Lichtenbelt WD, Vanhommerig JW, Smulders NM, et al. Cold-activated brown adipose tissue in healthy men. *N Engl J Med* 360:1500-1508, 2009.

3 Virtanen KA, Lidell ME, Orava J, et al. Functional brown adipose tissue in healthy adults. *N Engl J Med* 360:1518-1525, 2009.

4 Bartelt A, Heeren J: Adipose tissue browning and metabolic health. *Nat Rev Endocrinol* 2013.

5 Wu J, Bostrom P, Sparks LM, et al. Beige adipocytes are a distinct type of thermogenic fat cell in mouse and human. *Cell* 150:366-376, 2012.

6 Shabalina IG, Petrovic N, de Jong JM, et al. UCP1 in brite/beige adipose tissue mitochondria is functionally thermogenic. *Cell Rep* 5:1196-1203, 2013.

7 Cannon B, Nedergaard J: Brown adipose tissue: function and physiological significance. *Physiol Rev* 84:277-359, 2004.

8 Lowell BB, Spiegelman BM: Towards a molecular understanding of adaptive thermogenesis. *Nature* 404:652-660, 2000.

9 Zhao J, Cannon B, Nedergaard J: Thermogenesis is beta3- but not beta1-adrenergically mediated in rat brown fat cells, even after cold acclimation. *Am J Physiol* 275:R2002-R2011, 1998.

10 Fedorenko A, Lishko PV, Kirichok Y: Mechanism of fatty-acid-dependent UCP1 uncoupling in brown fat mitochondria. *Cell* 151:400-413, 2012.

11 Bartelt A, Merkel M, Heeren J: A new, powerful player in lipoprotein metabolism: brown adipose tissue. *J Mol Med (Berl)* 90:887-893, 2012.

12 Bartelt A, Bruns OT, Reimer R, et al. Brown adipose tissue activity controls triglyceride clearance. *Nat Med* 17:200-205, 2011.

13 Geerling JJ, Boon MR, van der Zon GC, et al. Metformin lowers plasma triglycerides by promoting VLDL-triglyceride clearance by brown adipose tissue in mice. *Diabetes* 2013.

14 Bartelt A, Heeren J: The holy grail of metabolic disease: brown adipose tissue. *Curr Opin Lipidol* 23:190-195, 2012.

15 Harms M, Seale P: Brown and beige fat: development, function and therapeutic potential. *Nat Med* 19:1252-1263, 2013.

16 Dong M, Yang X, Lim S, et al. Cold exposure promotes atherosclerotic plaque growth and instability via UCP1-dependent lipolysis. *Cell Metab* 18:118-129, 2013.

17 Bijland S, Pieterman EJ, Maas AC, et al. Fenofibrate increases very low density lipoprotein triglyceride production despite reducing plasma triglyceride levels in APOE*3-Leiden.CETP mice. *J Biol Chem* 285:25168-25175, 2010.

18 De Haan W, de Vries-van der Weij, van der Hoorn JW, et al. Torcetrapib does not reduce atherosclerosis beyond atorvastatin and induces more proinflammatory lesions than atorvastatin. *Circulation* 117:2515-2522, 2008.

19 Kuhnast S, Louwe MC, Heemskerk MM, et al. Niacin Reduces Atherosclerosis Development in APOE*3Leiden.CETP Mice Mainly by Reducing NonHDL-Cholesterol. *PLoS One* 8:e66467, 2013.

20 Rensen PC, van Dijk MC, Havenaar EC, et al. Selective liver targeting of antivirals by recombinant chylomicrons--a new therapeutic approach to hepatitis B. *Nat Med* 1:221-225, 1995.

21 Libby P, Ridker PM, Hansson GK: Progress and challenges in translating the biology of atherosclerosis. *Nature* 473:317-325, 2011.

22 Cypess AM, Lehman S, Williams G, et al. Identification and importance of brown adipose tissue in adult humans. *N Engl J Med* 360:1509-1517, 2009.

23 Dulloo AG, Miller DS: Energy balance following sympathetic denervation of brown adipose tissue. *Can J Physiol Pharmacol* 62:235-240, 1984.

24 Kozak LP, Koza RA, Anunciado-Koza R: Brown fat thermogenesis and body weight regulation in mice: relevance to humans. *Int J Obes (Lond)* 34 Suppl 1:S23-S27, 2010.

25 Wang Q, Zhang M, Ning G, et al. Brown adipose tissue in humans is activated by elevated plasma catecholamines levels and is inversely related to central obesity. *PLoS One* 6:e21006, 2011.

26 Yoneshiro T, Aita S, Matsushita M, et al. Recruited brown adipose tissue as an antiobesity agent in humans. *J Clin Invest* 123:3404-3408, 2013.
27 van Vlijmen BJ, van den Maagdenberg AM, Gijbels MJ, et al. Diet-induced hyperlipoproteinemia and atherosclerosis in apolipoprotein E3-Leiden transgenic mice. *J Clin Invest* 93:1403-1410, 1994.
28 Vijgen GH, Bouvy ND, Teule GJ, et al. Brown adipose tissue in morbidly obese subjects. *PLoS One* 6:e17247, 2011.
29 van der Lans AA, Hoeks J, Brans B, et al. Cold acclimation recruits human brown fat and increases nonshivering thermogenesis. *J Clin Invest* 123:3395-3403, 2013.
30 Bakker LE, Boon MR, van der Linden RA, et al. Brown adipose tissue volume in healthy lean south Asian adults compared with white Caucasians: a prospective, case-controlled observational study. *Lancet Diabetes Endocrinol* in press: 2014.
31 De Lorenzo F, Mukherjee M, Kadziola Z, et al. Central cooling effects in patients with hypercholesterolaemia. *Clin Sci (Lond)* 95:213-217, 1998.
32 Mattsson CL, Csikasz RI, Chernogubova E, et al. beta(1)-Adrenergic receptors increase UCP1 in human MADS brown adipocytes and rescue cold-acclimated beta(3)-adrenergic receptor-knockout mice via nonshivering thermogenesis. *Am J Physiol Endocrinol Metab* 301:E1108-E1118, 2011.
33 Larsen TM, Toubro S, van Baak MA, et al. Effect of a 28-d treatment with L-796568, a novel beta(3)-adrenergic receptor agonist, on energy expenditure and body composition in obese men. *Am J Clin Nutr* 76:780-788, 2002.
34 Redman LM, de JL, Fang X, et al. Lack of an effect of a novel beta3-adrenoceptor agonist, TAK-677, on energy metabolism in obese individuals: a double-blind, placebo-controlled randomized study. *J Clin Endocrinol Metab* 92:527-531, 2007.
35 Parysow O, Mollerach AM, Jager V, et al. Low-dose oral propranolol could reduce brown adipose tissue F-18 FDG uptake in patients undergoing PET scans. *Clin Nucl Med* 32:351-357, 2007.
36 Wijers SL, Saris WH, van Marken Lichtenbelt WD: Cold-induced adaptive thermogenesis in lean and obese. *Obesity (Silver Spring)* 18:1092-1099, 2010.
37 Lee P, Linderman JD, Smith S, et al. Irisin and FGF21 Are Cold-Induced Endocrine Activators of Brown Fat Function in Humans. *Cell Metab* 19:302-309, 2014.
38 Emanuelli B, Vienberg SG, Smyth G, et al. Interplay between FGF21 and insulin action in the liver regulates metabolism. *J Clin Invest* 2014.
39 Gaich G, Chien JY, Fu H, et al. The effects of LY2405319, an FGF21 analog, in obese human subjects with type 2 diabetes. *Cell Metab* 18:333-340, 2013.
40 van Klinken JB, van den Berg SA, Havekes LM, et al. Estimation of activity related energy expenditure and resting metabolic rate in freely moving mice from indirect calorimetry data. *PLoS One* 7:e36162, 2012.
41 Jong MC, Rensen PC, Dahlmans VE, et al. Apolipoprotein C-III deficiency accelerates triglyceride hydrolysis by lipoprotein lipase in wild-type and apoE knockout mice. *J Lipid Res* 42:1578-1585, 2001.
42 Wong MC, van Diepen JA, Hu L, et al. Hepatocyte-specific IKKbeta expression aggravates atherosclerosis development in APOE*3-Leiden mice. *Atherosclerosis* 220:362-368, 2012.

SUPPLEMENTARY APPENDIX

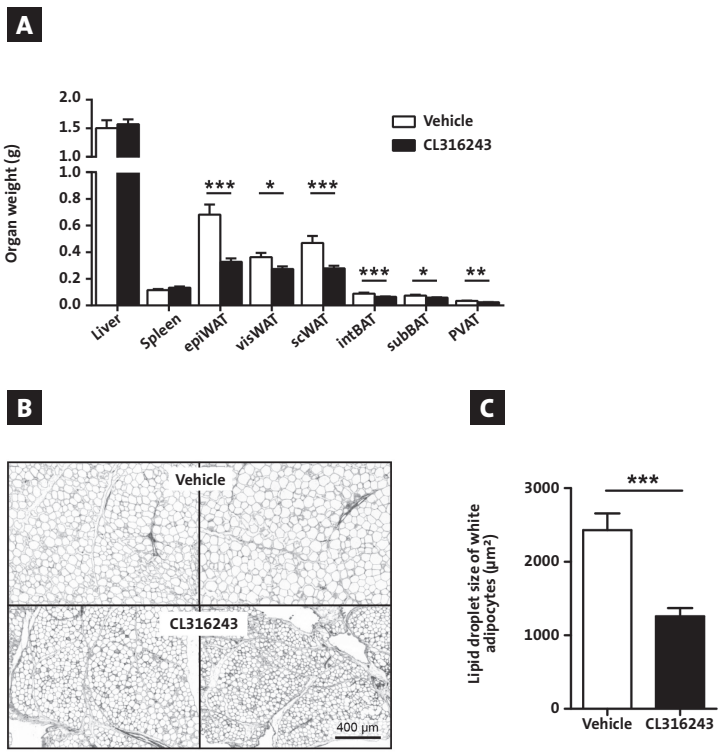

FIGURE S1 – ß3-AR agonism reduces adiposity and lipid droplet size in white adipose tissue. *E3L.CETP* mice were fed a Western-type diet and treated with the ß3-AR agonist CL316243 or vehicle for 10 weeks. After sacrification at week 10, the weight of various organs was determined **A**. Epididymal white adipose tissue (epiWAT) was stained with hematoxylin-eosin (HE) and representative pictures are shown **B**. Lipid droplet size of white adipocytes was determined using Image J software **C**. visWAT, visceral WAT; scWAT, subcutaneous WAT; intBAT, interscapular brown adipose tissue; subBAT, subscapular BAT; PVAT, perivascular adipose tissue.
Values are means ± S.E.M. (panel A-B: n=13-19 per group; panel D: n=8 per group). *P<0.05, **P<0.01, ***P<0.001.

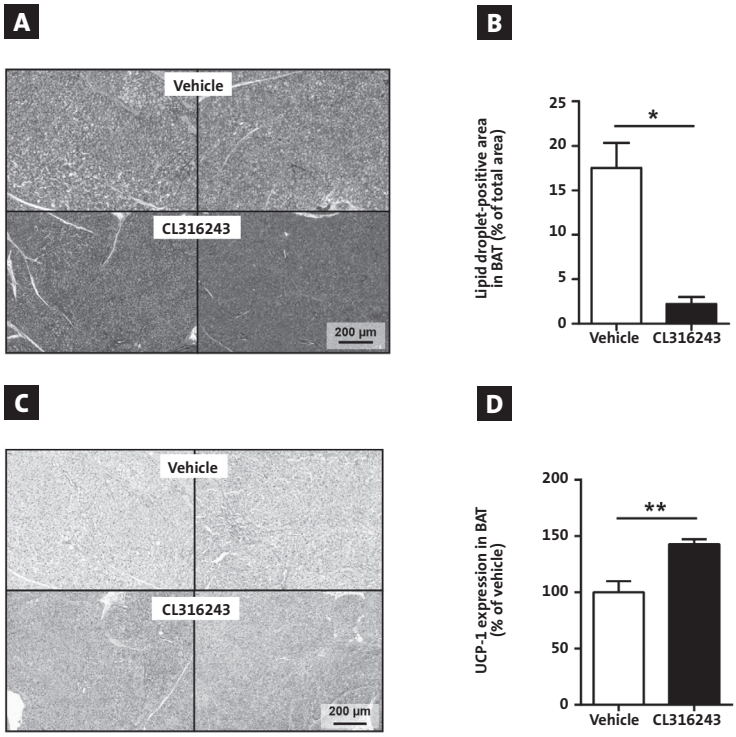

FIGURE S2 – ß3-AR agonism markedly increases brown adipose tissue activity. *E3L.CETP* mice were fed a Western-type diet and treated with vehicle or the ß3-AR agonist CL316243 during 10 weeks. Interscapular BAT was stained with HE and representative pictures are shown **A**. Lipid droplet-positive area was quantified using Image J software **B**. In addition, representative pictures are shown of UCP1-stained interscapular BAT **C**. The UCP1 expression was quantified using Image J software **D**.

Values are means ± S.E.M. (panel B: n=3 per group; panel D: n=7-8 per group). *P<0.05, **P<0.01.

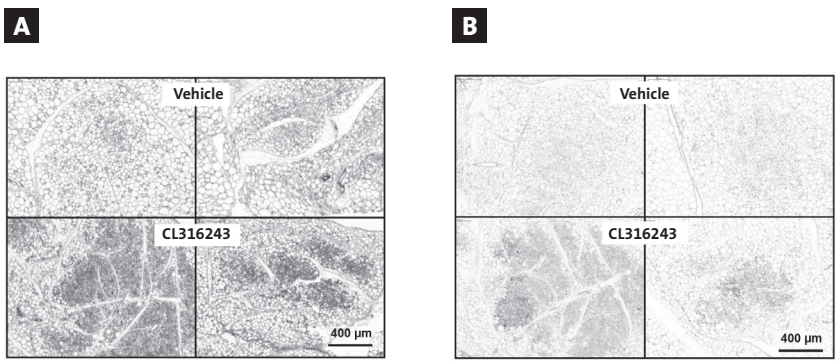

FIGURE S3 – ß3-AR agonism increases browning of white adipose tissue. *E3L.CETP* mice were fed a Western-type diet and treated with vehicle or the ß3-AR agonist CL316243 for 10 weeks. Epididymal WAT was stained with HE **A** and for UCP1 **B**, and representative pictures are shown.

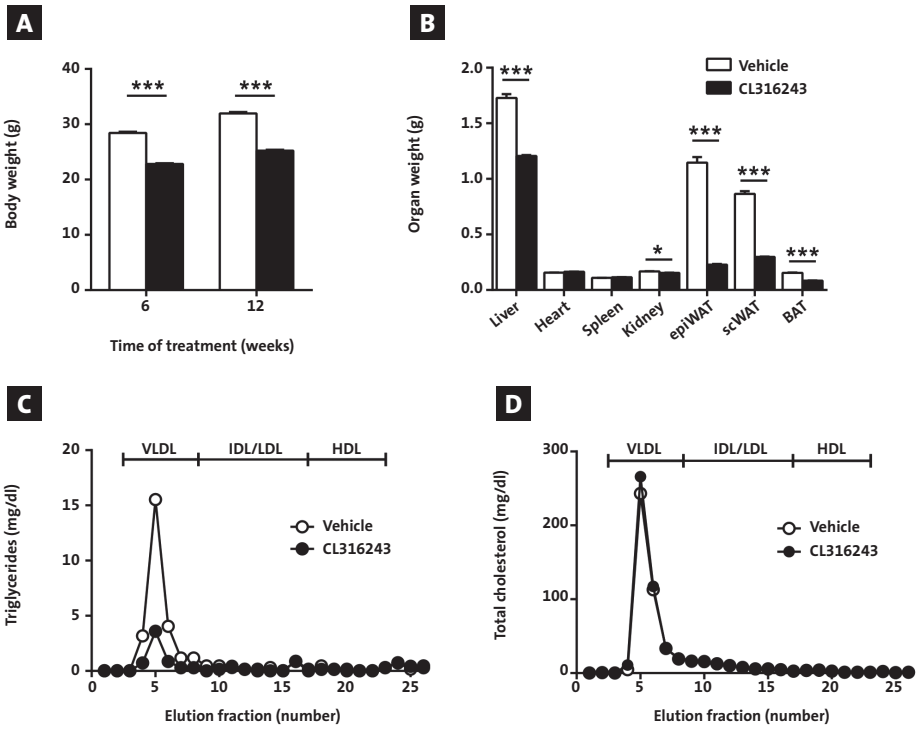

FIGURE S4 – BAT activation in *Apoe*$^{-/-}$ mice reduces fat mass and plasma triglycerides, but not total cholesterol.
Apoe$^{-/-}$ mice were fed a Western-type diet and treated with vehicle or the ß3-AR agonist CL316243, pair-fed to the vehicle-treated group, during 12 weeks. Body weight was determined after 6 and 12 weeks of treatment **A**. Organ weight was determined after sacrification at week 12 **B**. The distribution of triglycerides **C** and cholesterol **D** over lipoproteins was determined at week 12 in fasted plasma samples that were pooled per group.
Values are means ± S.E.M. (n=9-10 per group). *P<0.05, ***P<0.001.

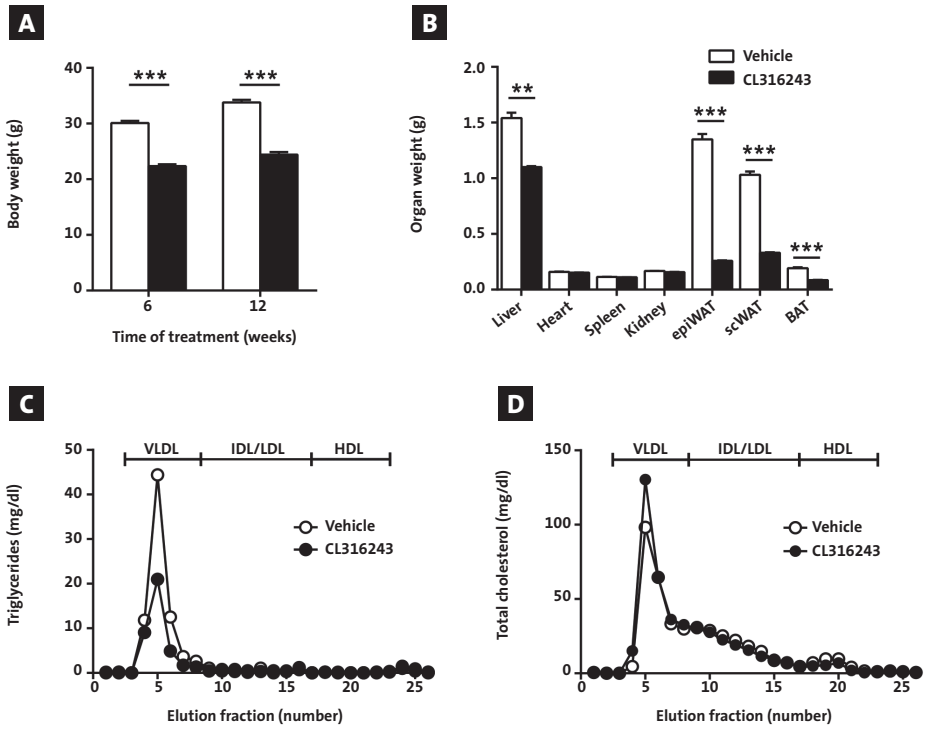

FIGURE S5 – BAT activation in *Ldlr*$^{-/-}$ mice reduces fat mass and plasma triglycerides, but not total cholesterol. *Ldlr*$^{-/-}$ mice were fed a Western-type diet and treated with vehicle or the ß3-AR agonist CL316243, pair-fed to the vehicle-treated group, during 12 weeks. Body weight was determined after 6 and 12 weeks of treatment **A**. Organ weight was determined after sacrification at week 12 **B**. The distribution of triglycerides **C** and cholesterol **D** over lipoproteins was determined at week 12 in fasted plasma samples that were pooled per group. Values are means ± S.E.M. (n=8-11 per group). **P<0.01, ***P<0.001.

PART 3

HUMAN STUDIES ON ROLE OF BROWN ADIPOSE TISSUE IN METABOLISM AND OBESITY

SHORT-TERM HIGH-FAT DIET INCREASES MACROPHAGE MARKERS IN SKELETAL MUSCLE ACCOMPANIED BY IMPAIRED INSULIN SIGNALING IN HEALTHY MALE SUBJECTS

MARIËTTE R. BOON
LEONTINE E.H. BAKKER
MARIËLLE C. HAKS
EDWIN QUINTEN
LIANNE VAN BEEK
YANAN WANG
LINDA VAN SCHINKEL
VANESSA VAN HARMELEN
A. EDO MEINDERS
LAMB H.J.
TOM H.M. OTTENHOFF
KO WILLEMS VAN DIJK
BRUNO GUIGAS
INGRID M. JAZET
PATRICK C.N. RENSEN

Clin Sci 2014, conditionally accepted.

ABBREVATIONS

CETP	cholesteryl ester transfer protein
hsCRP	high sensitive C-reactive protein
(F)FA	(free) fatty acid
GLUT-4	glucose transporter 4
GYS1	glycogen synthase 1
HFD	high-fat diet
HFHC	high-fat high calorie
INSR	insulin receptor
IR	insulin resistance
RT-MLPA	dual color reverse transcriptase multiplex ligation-dependent probe amplification
SLC2A4	solute carrier family 2
TBC1D1	TBC1 domain family member 1
TBC1D4	TBC1 domain family member 4
TG	triglyceride
(s)WAT	(subcutaneous) white adipose tissue

ABSTRACT

Recent studies have demonstrated elevated macrophage markers in skeletal muscle of obese subjects, that inversely related to insulin sensitivity. The aim of the present study was to investigate whether short-term high-fat high calorie (HFHC) diet already increases macrophage markers and affects glucose metabolism in skeletal muscle of healthy lean subjects. To this end, 24 healthy lean young male subjects received a 5-day HFHC diet. Before and after the diet, muscle and subcutaneous white adipose tissue (sWAT) biopsies were taken and mRNA expression levels of relevant genes, plasma glucose, insulin, C-peptide and cholesteryl ester transfer protein (CETP) levels were measured. 5 days of HFHC diet markedly increased mRNA expression of the general macrophage markers *CD68* (3.7-fold, $P<0.01$) and *CD14* (3.2-fold, $P<0.01$), as well as the M1 macrophage marker *MARCO* (11.2-fold, $P<0.05$) in muscle. This was accompanied by downregulation of *TBC1D1, SLC2A4* and *GYS1* mRNA expression, all involved in uptake and storage of glucose, and elevation of plasma glucose (+4%, $P<0.001$) and insulin (+55%, $P<0.001$) levels together with HOMA-IR (+48%, $P<0.001$), suggesting development of insulin resistance. Furthermore, plasma CETP levels, a marker of liver macrophage content, were increased (+21%, $P<0.001$) while macrophage content in sWAT remained unchanged. Short-term HFHC diet increases expression of macrophage markers in skeletal muscle, but not sWAT, of healthy male subjects accompanied by reduced markers of insulin signalling and development of insulin resistance. Therefore, recruitment of macrophages into muscle may be an early event in development of insulin resistance in the course of obesity.

INTRODUCTION

Skeletal muscle is the primary site of dietary glucose disposal *in vivo*. Insulin stimulates glucose uptake into muscle through an elaborate signaling cascade eventually resulting in mobilization of glucose transporter 4 (GLUT-4) channels to the plasma membrane that mediate glucose uptake (1). High-fat diet (HFD) feeding impairs whole-body insulin sensitivity and substrate homeostasis in both mice and humans (2,3). Skeletal muscle insulin resistance (IR) is the major contributor to development of whole-body IR (4) but the exact underlying molecular mechanism remains to be elucidated, although various hypotheses have been proposed.

First, lipid accumulation inside muscle cells and the formation of subsequent lipid metabolites *(e.g.* diacylglycerols, ceramides and acylcarnitines) contribute to muscle IR by interfering with the insulin signaling cascade (5).

Second, fatty acids (FAs) trigger activation of inflammatory signals in myocytes, and also in innate immune cells such as macrophages, leading to the release of pro-inflammatory cytokines that result in low-grade systemic inflammation (6,7). *In vitro* studies support this concept, showing that FAs promote release of pro-inflammatory cytokines by macrophages that, in turn, induce IR in skeletal muscle cells (8). Of note, cytokines can directly influence insulin actions on muscle. For example, the pro-inflammatory cytokine TNFα caused IR and impaired glucose uptake in primary human myocytes (9).

A third mechanism underlying the development of muscle IR in response to HFD may involve recruitment of macrophages into the muscle tissue itself. Hong et al (10) showed that HFD increased the number of M1-activated (CD11c+) macrophages in skeletal muscle in mice. Of note, this was corrected by transgenic overexpression of the anti-inflammatory cytokine IL-10 in skeletal muscle, which also improved whole-body insulin sensitivity. In humans, Varma et al (8) showed that the skeletal muscle from obese subjects contained 2.5-fold higher CD68+ macrophage numbers in skeletal muscle compared to lean subjects. Strikingly, their study showed that macrophage content in muscle was strongly associated with BMI and inversely related to insulin sensitivity.

Taken together, these data suggest that HFD results in recruitment of pro-inflammatory macrophages in muscle which contribute to the development of muscle IR by releasing pro-inflammatory cytokines. However, the timing at which macrophages are recruited into skeletal muscle in the time course of HFD-induced obesity and the possible involvement of other, adaptive, immune cell types is currently unknown and may either be an early event or a late consequence when chronic low-grade inflammation has already developed. To investigate this issue, we subjected healthy, male lean subjects for 5 days to a high-fat high calorie (HFHC) diet and studied expression of markers for macrophages, T cells, pattern recognition receptors, as well as markers for glucose metabolism, in skeletal muscle biopsies before and after the diet. Furthermore, to investigate whether short-term HFD results in influx of macrophages in other tissues besides muscle, we investigated expression of macrophage markers in subcutaneous white adipose tissue (sWAT) biopsies as well as plasma cholesteryl ester transfer protein (CETP) levels as a marker of the liver macrophage content (11).

METHODS AND MATERIALS

Study participants

24 Dutch, lean (BMI < 25 kg/m^2) and healthy males of Caucasian (n=12) and South Asian (n=12) ethnicity between 19 and 25 years of age and with a positive family history of type 2 diabetes were enrolled via local advertisements. All subjects underwent a medical screening including their medical history, a physical examination, blood chemistry tests and an oral glucose tolerance test to exclude individuals with type 2 diabetes according to the American Diabetes Association (ADA) 2010 criteria. Other exclusion criteria were rigorous exercise, smoking and recent body weight change. The present study was approved by the Medical Ethical Committee of the Leiden University Medical Centre and performed in accordance with the principles of the revised Declaration of Helsinki. All volunteers gave written informed consent before participation.

Study design

Subjects were studied before and after a 5-day HFHC diet, consisting of the subject's regular diet, supplemented with 375 ml of cream per day (=1275 kcal/day extra containing 94% fat). They were instructed not to alter life style habits, and not to perform physical activity in the last 48 hours prior to the study days. Furthermore, subjects were asked to keep a food diary before and during the HFHC diet to estimate normal dietary intake, and to check for compliance and compensation behavior respectively. Diaries were entered and analyzed using a specialized internet application (http://www.dieetinzicht.nl, Dutch). Magnetic resonance (MR) studies were performed shortly before and on the fifth day of the HFHC diet. In addition, one day before and one day after the diet anthropometric measurements were performed and muscle and subcutaneous white adipose tissue biopsies were obtained from all subjects in fasted condition.

MR studies

Hepatic triglyceride content was assessed by proton MR-spectroscopy (^{1}H-MRS; Gyroscan ACS-NT15; Philips, The Netherlands) in postprandial state (five hours after the last meal), as previously described (12). Vertebra Th12 was used as a marker to ascertain the same position of the 8-ml-voxel at both study days. A spectrum with water suppression as internal standard was obtained, and 64 averages were collected without water suppression. The spectra were fitted using Java-base MR user interface software (jMRUI version 2.2) (12). The percentage of hepatic triglyceride (TG) signals was calculated as: (signal amplitude hepatic TG/ signal amplitude water) x 100.

Anthropometric measurements

Anthropometric measurements were performed after an overnight fast. Body composition (fat and lean body mass) was assessed by bioelectrical impedance analysis (BIA; Bodystat® 1500, Bodystat Ltd., Douglas, UK).

Skeletal muscle biopsies
Muscle biopsies from the *m. vastus lateralis* (approx. 75-100 mg) were collected one day before and one day after the diet intervention in fasted condition under localized anesthesia, using a modified Bergström needle, as previously described (13). Muscle samples were snap-frozen in liquid nitrogen and stored at -80°C until further analysis.

White adipose tissue biopsies
Subcutaneous fat biopsies were obtained from the umbilical region in fasted condition under localized anesthesia, using a syringe with needle while applying suction. Fat samples were immediately submersed into a medium (DMEM/F12 + Glutamax) until further analysis. Of note, analysis was done in a subset of subjects (n=8) due to limited availability of tissue in lean subjects.

Laboratory analysis
Fasting serum glucose, total cholesterol, HDL-cholesterol and triglycerides (TG) were measured on a Modular P800 analyzer (Roche, Almere, The Netherlands). LDL-cholesterol was calculated according to Friedewald's formula (14). Serum insulin and C-peptide levels were analyzed on an Immulite 2500 (Siemens, The Netherlands). The HOMA-IR index was calculated using the formula: fasting insulin (pmol/L) x fasting glucose (mmol/L)/22.5. Plasma free fatty acid (FFA) concentrations were determined by a colorimetric method (Wako Chemicals, Germany). ELISA kits were used to measure serum levels of high-sensitive C-reactive protein (hsCRP) (Meso Scale Discovery, Gaithersburg, USA), adiponectin (Cayman Chemical, Ann Arbor, USA) and CETP concentration (ALPCO Diagnostics, Salem, USA) according to the manufacturers' instructions.

RNA isolation
Total RNA was isolated from skeletal muscle biopsies (approx. 25-30 mg) using the phenol-chloroform extraction method (Tripure RNA Isolation reagent, Roche, Germany) and treated with a DNAse kit (TURBO DNAse, Life Technologies, The Netherlands) according to the manufacturer's instruction. Amount of RNA was determined by NanoDrop.

cDNA synthesis and real-time PCR
For RT-PCR, first-strand cDNA was synthesized from 1 µg total RNA using a Superscript first strand synthesis kit (Invitrogen, The Netherlands). Real-time PCR was carried out on the IQ5 PCR machine (Bio-Rad) using the Sensimix SYBRGreen RT-PCR mix (Quantace). Melt curve analysis was included to assure a single PCR product was formed. Expression levels were normalized to ribosomal protein S18 (RPS18). Primer sequences are listed in **SUPPLEMENTARY TABLE 1.**

dcRT-MLPA assay
A dual-color reverse transcriptase multiplex ligation-dependent probe amplification (dcRT-MLPA) assay was performed as described previously (15). Briefly, for each target-specific

sequence, a specific RT primer was designed located immediately downstream of the left and right hand half-probe target sequence. Following reverse transcription, left and right hand half-probes were hybridized to the cDNA at 60°C overnight. Annealed half-probes were ligated and subsequently amplified by PCR (33 cycles of 30 s at 95°C, 30 s at 58°C and 60 s at 72°C, followed by 1 cycle of 20 min at 72°C). PCR amplification products were 1:10 diluted in HiDi formamide-containing 400HD ROX size standard and analyzed on an Applied Biosystems 3730 capillary sequencer in GeneScan mode (Applied Biosystems).

Trace data were analyzed using the GeneMapper software package (Applied Biosystems). The areas of each assigned peak (in arbitrary units) were exported for further analysis in Microsoft Excel spreadsheet software. Data were normalized to beta-2-microglobulin (B2M) and signals below the threshold value for noise cutoff in GeneMapper (log2 transformed peak area 7.64) were assigned the threshold value for noise cutoff

Immunohistochemical stainings

Formalin-fixed-paraffin-embedded subcutaneous adipose tissue sections were used for immunohistochemistry of CD68. Antigens were retrieved using citrate buffer. The primary antibody was mouse-anti-human CD68 (1:800 dilution, clone KP1, from Dako, Glostrup, Denmark). Staining and counterstaining was done with Nova Red (Vector labs, Brunschwig Chemie, Amsterdam, The Netherlands) and haematoxylin, respectively. Crown-like structures (CLS) were counted according to the criterion that a CLS consisted of three or more CD68 positive cells surrounding an adipocyte.

Statistical analysis

The data of South Asian and Caucasian subjects were pooled for all analyses since no significant differences were observed between ethnicities for baseline values or diet effects. Data are presented as mean ± SEM. Paired T-tests were applied to assess mean differences before and after the diet intervention. Significance level was set at $P<0.05$. Statistical analyses were performed using SPSS for Windows version 20.0 (IBM, USA).

RESULTS

Clinical characteristics

Clinical characteristics are shown in **TABLE 1**. Mean age was 22.1±0.4 years and mean BMI was 21.5±0.4 kg/cm^2. Five days of HFHC diet resulted in a small but significant increase in body weight (+0.7%, $P<0.01$) and BMI (+0.9%, $P<0.01$), while waist circumference and percentage of fat mass remained unchanged. Although plasma FFA, serum TG and total cholesterol levels did not change significantly upon the HFHC diet, HDL-C and LDL-C did increase (both +9%, $P<0.01$). Furthermore, the HFHC diet significantly increased fasting glucose (+4%), insulin (+55%) and C-peptide (+29%) levels, as well as the HOMA-IR index (+ 48%) (all $P<0.001$).

HFHC diet and markers of glucose uptake/metabolism and muscle inflammation

The HFHC diet did not affect mRNA expression of the insulin receptor *(INSR)* and its downstream signaling target *TBC1D4* (encoding AS160) in muscle biopsies **(FIG 1A)**. However, a diminished expression of TBC1D1 (-23%, P<0.05), *SLC2A4* encoding GLUT-4 (-34%, P<0.001) and GYS-1 (-35%, P<0.001), all involved in uptake and storage of glucose, was evident.

Using the dcRT-MLPA assay, we measured mRNA expression of a large panel of inflammatory genes, including markers for innate and adaptive immune cells, pattern recognition receptors and cytokines in muscle biopsies before and after the HFHC diet **(TABLE 2)**. Of note, the HFHC diet significantly upregulated the expression of *CD14* (+118%, P<0.05), a general macrophage marker, and the expression of *MARCO* (+415%, P<0.05), a scavenger receptor that is mainly present on pro-inflammatory M1 macrophages (16). In line with this, expression of the anti-inflammatory cytokine *IL10* tended to be downregulated (-27%, P=0.10).

Furthermore, expression of the general T-cell marker *CD3* was undetectable in the muscle biopsies, pointing to absence or very low presence of T-cells. Expression of *CD4,* a T-helper cell marker that is also expressed by innate immune cells such as monocytes and macro-

TABLE 1 - **Anthropometrics and metabolic characteristics before and after a 5-day HFHC diet in healthy, young male subjects**

	Before HFHC diet (n= 24)	After HFHC diet (n=24)
Age (years)	22.1 ± 0.4	
Length (m)	1.79 ± 0.01	
Weight (kg)	69.1 ± 1.9	**69.6 ± 1.9****
BMI (kg/cm2)	21.5 ± 0.4	**21.7 ± 0.4****
Waist (cm)	80.1 ± 1.5	80.8 ± 1.7
Fat mass (%)	13.2 ± 0.7	13.0 ± 0.7
Total cholesterol (mmol/L)	4.16 ± 0.19	4.51 ± 0.17
HDL-C (mmol/L)	1.22 ± 0.05	**1.33 ± 0.04****
LDL-C (mmol/L)	2.51 ± 0.17	**2.74 ± 0.15****
Triglycerides (mmol/L)	0.96 ± 0.08	0.97 ± 0.08
FFA (mmol/L)	0.49 ± 0.03	0.48 ± 0.03
Glucose (mmol/L)	5.17 ± 0.06	**5.37 ± 0.06*****
Insulin (pmol/L)	4.53 ± 1.00	**7.02 ± 1.16*****
C-peptide (nmol/L)	0.49 ± 0.03	**0.63 ± 0.04*****
HOMA-IR	1.62 ± 0.26	**2.39 ± 0.32*****
hsCRP (µg/mL)	0.94 ± 0.23	1.16 ± 0.24
Adiponectin (µg/mL)	6.27 ± 0.63	6.58 ± 0.50
Hepatic TG content (%)	1.57 ± 0.27	**3.43 ± 0.49*****
CETP mass (µg/mL)	1.69 ± 0.09	**2.02 ± 0.10*****

Data are presented as mean ± SEM. ** P<0.01, *** P<0.001 vs. before diet. HDL-C, high-density lipoprotein cholesterol; LDL, low-density lipoprotein cholesterol; FFA, free fatty acid; hsCRP, high-sensitive C-reactive protein; TG, triglyceride; CETP, cholesteryl ester transfer protein.

TABLE 2 - Expression of adaptive and innate immune markers in muscle biopsies before and after a 5-day HFHC diet in healthy male subjects

Gene	Baseline	HFHC (fold change vs baseline)	P-value
Immune cell subset markers			
CD14	**1.00 ± 0.16**	**2.18 ± 0.23**	**0.04***
CD163	1.00 ± 0.10	0.84 ± 0.15	0.31
NCAM1	1.00 ± 0.14	1.15 ± 0.13	0.37
CD19	1.00 ± 0.12	1.09 ± 0.16	0.61
BLR1	1.00 ± 0.15	0.84 ± 0.14	0.42
FCGR1A#	1.00 ± 0.00	1.68 ± 0.26	0.13
T cell subsets			
CD3E#	1.00 ± 0.00	1.01 ± 0.01	0.33
CD4	**1.00 ± 0.09**	**1.48 ± 0.15**	**0.04***
CD8A	1.00 ± 0.14	0.89 ± 0.15	0.61
IL7-R	1.00 ± 0.06	0.93 ± 0.10	0.53
CCR7	1.00 ± 0.08	0.87 ± 0.11	0.26
Th1 response			
CXCL10	1.00 ± 0.10	0.98 ± 0.11	0.88
IFNG	1.00 ± 0.27	1.62 ± 0.28	0.28
IL-2	1.00 ± 0.17	1.06 ± 0.17	0.84
IL-1B	1.00 ± 0.13	0.93 ± 0.15	0.78
TNF	1.00 ± 0.08	1.09 ± 0.10	0.52
Th2 response			
IL-4#	1.00 ± 0.29	0.79 ± 0.24	0.56
IL-4d2	1.00 ± 0.35	0.79 ± 0.35	0.65
IL-5	1.00 ± 0.24	1.04 ± 0.24	1.00
IL-6	1.00 ± 0.11	1.08 ± 0.14	0.70
IL-9#	1.00 ± 0.00	1.17 ± 0.10	0.16
IL-10	1.00 ± 0.17	0.73 ± 0.19	0.13
IL-13	1.00 ± 0.45	1.94 ± 0.28	0.26
Treg markers			
CCL4	1.00 ± 0.16	1.11 ± 0.15	0.80
CTLA4	1.00 ± 0.13	0.88 ± 0.13	0.38
LAG3	1.00 ± 0.29	0.43 ± 0.42	0.08
TGF-B1	1.00 ± 0.13	1.12 ± 0.11	0.42
Key MF1 and MF2 cytokines			
IL-12A	1.00 ± 0.32	0.89 ± 0.46	0.82
IL-12B	1.00 ± 0.39	1.10 ± 0.36	0.85
IL-23A	1.00 ± 0.08	0.81 ± 0.13	0.22
CCL2#	1.00 ± 0.44	1.78 ± 0.40	0.37
CCL5	1.00 ± 0.09	0.90 ± 0.10	0.51

Gene	Baseline	HFHC (fold change vs baseline)	P-value
CCL19	1.00 ± 0.11	1.07 ± 0.13	0.66
CCL22	1.00 ± 0.08	0.85 ± 0.06	0.16
CXCL13#	1.00 ± 0.40	0.97 ± 0.38	0.96
Scavenger receptors			
MARCO	**1.00 ± 0.23**	**5.15 ± 0.37**	**0.04***
Pattern recognition receptors			
TLR1#	1.00 ± 0.00	1.55 ± 0.36	0.33
TLR2#	1.00 ± 0.51	0.17 ± 0.00	0.11
TLR3	1.00 ± 0.11	1.07 ± 0.14	0.68
TLR4	1.00 ± 0.29	1.20 ± 0.33	0.67
TLR5	1.00 ± 0.57	0.46 ± 0.65	0.33
TLR6	1.00 ± 0.37	1.28 ± 0.32	0.64
TLR7	1.00 ± 0.12	0.96 ± 0.15	0.83
TLR8	1.00 ± 0.10	0.96 ± 0.17	0.85
TLR9	1.00 ± 0.11	0.79 ± 0.14	0.21
TLR10##	1.00 ± 0.00	2.36 ± 0.59	0.33
NOD1	1.00 ± 0.24	1.06 ± 0.15	0.83
NOD2#	1.00 ± 0.00	1.33 ± 0.26	0.33
MRC1	1.00 ± 0.23	1.63 ± 0.18	0.06
MRC2	1.00 ± 0.05	0.91 ± 0.11	0.48
CD209	1.00 ± 0.14	1.02 ± 0.16	0.94
CLEC7A	1.00 ± 0.17	1.23 ± 0.19	0.38
Inflammasome components			
NLRP1#	1.00 ± 0.51	0.21 ± 0.00	0.13
NLRP2	1.00 ± 0.10	1.00 ± 0.15	0.99
NLRP3#	1.00 ± 0.42	0.85 ± 0.32	0.77
NLRP4	1.00 ± 0.16	0.86 ± 0.22	0.56
NLRP7	1.00 ± 0.37	0.88 ± 0.35	0.78
NLRC4	1.00 ± 0.05	0.89 ± 0.10	0.37

Data are presented as mean ± SEM and expressed relative to baseline. *P<0.05 vs. before diet. # Low expression of gene.

phages (17), was detectable and increased upon the HFHC diet (+48%, P<0.05). Given the absence of CD3 in the muscle biopsies, the increase in CD4 expression probably reflects increased expression by innate immune cells. Other inflammatory markers remained unaffected.

Thus, these data suggested that upon a short-term HFHC diet, especially markers of innate immunity were upregulated in muscle. We confirmed these findings by performing RT-PCR analyses on several macrophage markers in the muscle biopsies **(FIG 1B)**. More specifically, the HFHC diet upregulated the general macrophage markers *CD68* (3.7-fold, P<0.01) and *CD14* (3.2-fold, P<0.01), as well as the M1 marker *MARCO* (11.2-fold, P<0.05). Hence, short-term HFHC diet resulted in increased expression of pro-inflammatory M1 macrophages in muscle.

HFHC diet and markers of inflammation in other tissues

Since HFD-induced obesity is often associated with influx of pro-inflammatory macrophages and appearance of crown-like structures (CLS) in WAT (18), we next investigated whether markers of macrophage infiltration were also evident in WAT after 5 days of HFHC diet in healthy lean subjects. Due to the very small amount of tissue, we could only perform immunohistological staining of CD68 in subcutaneous WAT taken before and after the diet intervention in a subset of subjects. At baseline, solitary macrophages were identified sporadically in the WAT biopsies, while no CLS were observed. After the HFHC diet, influx of solitary macrophages increased in only a few subjects as did the appearance of CLS in WAT **(SUPPLEMENTARY FIGURE 1A-B)**, however, these effects were not statistically significant. Further-

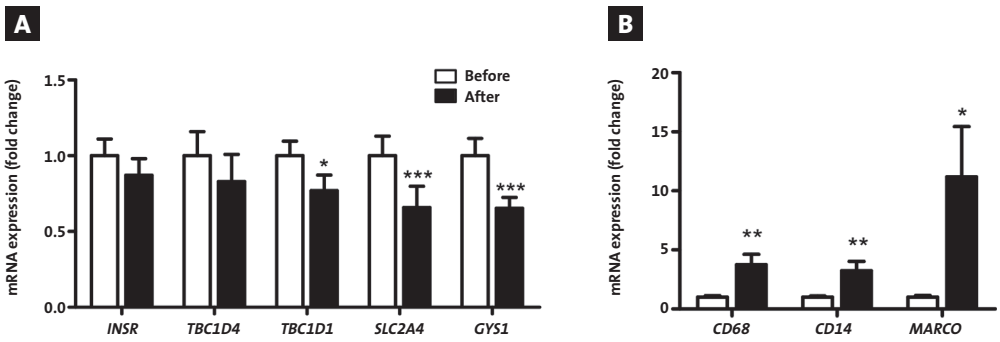

FIGURE 1 - Effect of short-term HFHC diet on expression of insulin signaling and macrophage markers in muscle in healthy male subjects. mRNA expression levels of genes related to glucose uptake/metabolism **A** and macrophage markers **B** were measured in skeletal muscle biopsies of healthy male subjects (n=24) obtained before (white bars) and after (black bars) a 5-day HFHC diet. Expression levels are normalized to the housekeeping gene *S18* and expressed as fold change compared to baseline as mean ± SEM. *P<0.05, **P<0.01 and ***P<0.001 vs. before diet.

HFHC, high-fat high calorie. INSR, insulin receptor. TBC1D4, TBC1 domain family member 4. TBC1D1, TBC1 domain family member 1. SLC2A4 solute carrier family 2. GYS1, glycogen synthase 1.

more, plasma adiponectin, an adipocyte-derived hormone that is suggested to play a role in suppression of the development of obesity and IR (19), did not change upon the dietary intervention **(TABLE 1)**.

The HFHC diet increased the liver triglyceride (TG) content (+118%, P<0.001; **TABLE 1**). For obvious reasons we could not obtain liver biopsies from our healthy subjects to measure macrophage content. However, we have recently shown that plasma CETP levels highly correlate with levels of general macrophage markers in liver biopsies (Wang and Rensen et al, *unpublished)* and therefore, we measured plasma CETP levels as a marker of liver macrophage content. Intriguingly, plasma CETP levels increased upon the HFHC diet (+21%, P<0.001; **TABLE 1)**, suggesting influx of macrophages into the liver. Furthermore, after the HFHC diet plasma CRP levels tended to increase (+24%, P=0.06; **TABLE 1)**, pointing to low-grade systemic inflammation.

DISCUSSION

Recent studies have detected elevated numbers of macrophage markers in skeletal muscle during chronic HFD feeding and obesity, but the timing at which these macrophages are recruited and their role in the development of muscle and whole-body IR is unknown. The present study demonstrates that only 5 days of HFHC diet resulted in a marked increase in expression of macrophage markers in muscle of healthy lean male subjects. Moreover, this was accompanied by downregulation of genes involved in glucose metabolism and elevation of fasting plasma glucose and insulin levels and HOMA-IR index. Of note, plasma CETP levels, which were previously shown by our group to correlate with liver macrophage content, increased while macrophage content in the subcutaneous WAT depot remained unchanged.

As in other organs, resident macrophages are present in human skeletal muscle (8) where they contribute to regeneration and revascularization in case of damage (20). In accordance with these data, we found that the general macrophage markers CD14 and CD68 were significantly expressed in skeletal muscle of healthy lean men. Of note, the homeostatic functions of muscle macrophages are exerted only when the macrophages are in their M2 (anti-inflammatory) phenotypic polarization stage (21,22). In response to different stimuli, such as circulating FA, macrophages are polarized towards an M1-like (inflammatory) phenotype, leading to release of pro-inflammatory cytokines which can induce IR in myocytes (8). Indeed, previous mouse and human studies have repeatedly observed increased numbers of activated M1 (CD11c+) macrophages in skeletal muscle tissue in the context of obesity and IR (23-26). Intriguingly, our data demonstrate that the increased expression of M1 macrophages in skeletal muscle occurs already after short-term HFD and even in healthy young subjects, supporting the concept that recruitment of M1 macrophages into skeletal muscle is an early event in the time course of HFD-induced obesity.

What would be the trigger of the extensive increase in macrophage markers in muscle

and does this mainly reflect activation of resident macrophages or increased influx from blood-derived monocytes? We speculate that both mechanisms are involved. The fact that the expression of general macrophage markers (CD68 and CD14) was increased, is most easily explained by an increased influx of these cells into muscle, rather than by upregulation of the expression of these genes in resident macrophages. The trigger that stimulated this influx is likely the high load of saturated FAs ingested with the HFHC diet. Saturated FAs can signal via Toll-like receptors (TLRs), particularly TLR-4 that is present on both macrophages and myocytes (27). Activation of TLR-4 stimulates the transcription and release of various chemokines and pro-inflammatory cytokines, such as MCP-1 or tumor necrosis factor-α (TNF-α), which attract other macrophages and may also directly impair insulin signaling in skeletal muscle (5; 28,29). In the present study, we did not find effects of the HFHC diet on gene expression of Toll-like receptors or pro-inflammatory cytokines such as TNF-α in skeletal muscle. However, we cannot exclude that either local release of pro-inflammatory cytokines or activation of TLR-4-driven signaling pathways might have occurred in this tissue.

Intriguingly, while we found that expression of macrophage markers was markedly increased in skeletal muscle upon the HFHC diet, no significant increase could be identified in the subcutaneous WAT depot. This might be in part due to the fact that visceral adipose tissue (VAT) seems to be more closely associated with the inflammatory state than subcutaneous adipose tissue (30). Furthermore, muscle cells might be more prone to release macrophage attractant factors in the presence of pro-inflammatory stimuli compared to adipocytes. Indeed, a recent study demonstrated that the presence of both macrophages and the saturated FA palmitate exerted a synergistic effect on MCP-1 release by muscle cells, resulting in greater attraction of macrophages (8). To our knowledge, such a positive feedback-loop has not been demonstrated for adipocytes.

Besides a large increase in macrophage markers in muscle upon the HFHC diet, the increased plasma CETP levels suggests increased hepatic macrophage content as well. Our group has recently shown that the hepatic macrophage is the main producer of plasma CETP (Wang et al., *unpublished),* meaning that an increase in plasma CETP levels reflects an increase in hepatic macrophages. Interestingly, various studies have shown that pro-inflammatory cytokines also impaired insulin signaling in hepatocytes (31). Thus, it is tempting to speculate that dietary saturated FAs may have resulted in influx of pro-inflammatory M1 macrophages in the liver, leading to release of pro-inflammatory cytokines and subsequent impairment of hepatic insulin signaling. This mechanism may also explain the previously found reduced suppression of endogenous glucose production in response to 5 days of HFHC diet (32).

A potential limitation of the current study could be that we determined immune cell markers via MLPA-assay and RT-PCR instead of performing fluorescence-activated cell sorting (FACS) analyses, a method by which true cell counts are determined. However, performing FACS analyses would require relatively large amounts of muscle tissues, the collection of which was not feasible in the current study.

In conclusion, we show that 5 days of HFHC diet resulted in a marked increase in gene expression of M1 macrophage markers in skeletal muscle of healthy lean male subjects, a

feature associated with apparent impairment in whole-body insulin sensitivity and glucose homeostasis. Future studies should be directed at unraveling the precise contribution of muscle macrophages in the development of peripheral IR, with the ultimate goal to develop novel therapeutic targets that decrease inflammation-induced IR without interfering with all innate immune functions.

ACKNOWLEDGEMENTS

This study was financed by the Dutch Diabetes Research Foundation (grant 2012.11.1500 to P.C.N. Rensen and M.R. Boon). M.R. Boon is also supported by the Board of Directors of the Leiden University Medical Center (LUMC). P.C.N. Rensen is Established Investigator of the Netherlands Heart Foundation (grant 2009T038). We also thank Roba Metals B. V. IJsselstein (Utrecht, The Netherlands) for financial support. The work received additional support from European Union's Seventh Framework Programme projects TANDEM (grant 305279), ADITEC (grant 280873) and a project sponsored by the Netherlands Relief Foundation. The funders did not have any role in the design or interpretation of the study. The authors thank Annemieke Visser (LUMC, dept. of Immunohaematobiology) and Lianne van der Wee-Pals (LUMC, dept. of Endocrinology) for their help with performing WAT staining, and to Gerard van der Zon (LUMC, dept. of Molecular Cell Biology) for his help with performing the RT-PCR analyses on muscle biopsies. Furthermore, we thank Bep Ladan-Eygenraam (LUMC) for her excellent technical assistance during conductance of the study.

The authors have no potential conflicts of interest relevant to this article.

MRB, LEHB, AEM, IMJ and PCNR designed research; MRB, LEHB, MCH, EQ, LvB, YW, VvH and BG conducted research; MRB, LEHB, and MCH analyzed data; MRB, LEHB, BG, IMJ, and PCNR wrote the paper; MCH, EQ, LvB, YW, VvH, AEM, THMO, KWvD, BG, IMJ and PCNR contributed to the discussion, and reviewed and edited the manuscript; MRB and LEHB had primary responsibility for final content. All authors read and approved the final manuscript.

L.E.H.B, M.R.B, I.M.J and P.C.N.R. are the guarantors of this work and, as such, have full access to all the data generated in the framework of the study and take responsibility for their integrity and the accuracy of their analysis.

REFERENCES

1 Zaid H, Antonescu CN, Randhawa VK, Klip A. Insulin action on glucose transporters through molecular switches, tracks and tethers. Biochem J 2008;13:201-215.

2 Kim JK, Gimeno RE, Higashimori T, Kim HJ, Choi H, Punreddy S, Mozell RL, Tan G, Stricker-Krongrad A, Hirsch DJ, Fillmore JJ, Liu ZX, Dong J, Cline G, Stahl A, Lodish HF, Shulman GI. Inactivation of fatty acid transport protein 1 prevents fat-induced insulin resistance in skeletal muscle. J Clin Invest 2004;113:756-763.

3 Shulman GI. Unraveling the cellular mechanism of insulin resistance in humans: new insights from magnetic resonance spectroscopy. Physiology 2004;19:183-190.

4 DeFronzo RA. Bantin Lecture. From the triumvirate to the ominous octet: a new paradigm for the treatment of type 2 diabetes mellitus. Diabetes 2009;58:773-795.

5 Kewalramani G, Bilan PJ, Klip A. Muscle insulin resistance: assault by lipids, cytokines and local macrophages. Curr Opin Clin Nutr Metab Care 2010;13:382-390.

6 Bilan PJ, Samokhvalov V, Koshkina A, Schertzer JD, Samaan MC, Klip A. Direct and macrophage-mediated actions of fatty acids causing insulin resistance in muscle cells. Arch Physiol Biochem 2009;115:176-190.

7 Shi H, Kokoeva MV, Inouye K, Tzameli I, Yin H, Flier JS. TLR4 links innate immunity and fatty acid-induced insulin resistance. J Clin Invest 2006;116:3015-3025.

8 Varma V, Yao-Borengasser A, Rasouli N, Nolen GT, Phanavanh B, Starks T, Gurley C, Simpson P, McGehee RE Jr, Kern PA, Peterson CA. Muscle inflammatory response and insulin resistance: synergistic interaction between macrophages and fatty acids leads to impaired insulin action. Am J Physiol Endocrinol Metab 2009; 296: E1300-10.

9 Austin RL, Rune A, Bouzakri K, Zierath JR, Krook A. siRNA-mediated reduction of inhibitor of nuclear factor-kappaB kinase prevents tumor necrosis factor-alpha-induced insulin resistance in human skeletal muscle. Diabetes 2008;57:2066-2073.

10 Hong EG, Ko HJ, Cho YR, Kim HJ, Ma Z, Yu TY, Friedline RH, Kurt-Jones E, Finberg R, Fischer MA, Granger EL, Norbury CC, Hauschka SD, Philbrick WM, Lee CG, Elias JA, Kim JK. Interleukin-10 prevents diet-induced insulin resistance by attenuating macrophage and cytokine response in skeletal muscle. Diabetes 2009;58:2525-2535.

11 Widya RL, Hammer S, Boon MR, Van der Meer RW, Smit JWA, De Roos A, Rensen PC, Lamb HJ. Effects of Short-Term Nutritional Interventions on Right Ventricular Function in Healthy Men. PLoS One 2013;8:e76406.

12 van der Meer RW, Hammer S, Lamb HJ, Frolich M, Diamant M, Rijzewijk LJ, de Roos A, Romijn JA, Smit JW. Effects of short-term high-fat, high-energy diet on hepatic and myocardial triglyceride content in healthy men. J Clin Endocrinol Metab 2008;93:2702-2708.

13 Bergstrom J. Percutaneous needle biopsy of skeletal muscle in physiological and clinical research. Scand J Clin Lab Invest 1975; 35:609-616.

14 Friedewald WT, Levy RI, Fredrickson DS. Estimation of the concentration of low-density lipoprotein cholesterol in plasma, without use of the preparative ultracentrifuge. Clin Chem 1972;18:499-502.

15 Joosten SA, Goeman JJ, Sutherland JS, Opmeer L, de Boer KG, Jacobsen M, Kaufmann SH, Finos L, Magis-Escurra C, Ota MO, Ottenhoff TH, Haks MC. Identification of biomarkers for tuberculosis disease using a novel dual-color RT-MLPA assay. Genes Immun 2012;13:71-82.

16 Murray PJ, Wynn TA. Protective and pathogenic functions of macrophage subsets. Nature Rev Immunol 2011;11:723-737.

17 Gibbings D, Befus AD. CD4 and CD8: an inside-out coreceptor model for innate immune cells. J Leukoc Biol 2009;86:251-259.

18 Weisberg SP, McCann D, Desai M, Rosenbaum M, Leibel RL, Ferrante AW. Obesity is associated with macrophage accumulation in adipose tissue. J Clin Invest 2003;11:1796-1808.

19 Ukkola O, Santaniemi M. Adiponectin: a link between excess adiposity and associated comorbidities? J Mol Med 2002;80:696-702.
20 Olefsky JM, Glass CK. Macrophages, inflammation, and insulin resistance. Annu Rev Physiol 2010;72:219–246.
21 Verreck FA, de Boer T, Langenberg DM, Hoeve MA, Kramer M, Vaisberg E, Kastelein R, Kolk A, de Waal-Malefyt R, Ottenhoff TH. Human IL-23-producing type 1 macrophages promote but IL-10-producting type 2 macrophages subvert immunity to (myco)bacteria. Proc Natl Acad Sci U S A 2004;30:4560-4565.
22 Verreck FA, de Boer T, Langenberg DM, van der Zanden L, Ottenhoff TH. Phenotypic and functional profiling of human proinflammatory type-1 and anti-inflammatory type-2 macrophages in response to microbial antigens and IFN-gamma- and CD40L-mediated costrimulation. J Leukoc Biol 2006;79:285-293.
23 Nguyen MT, Favelyukis S, Nguyen AK, Reichart D, Scott PA, Jenn A, Liu-Bryan R, Glass CK, Neels JG, Olefsky JM. A Subpopulation of macrophages infiltrates hypertrophic adipose tissue and is activated by free fatty acids via toll-like receptors 2 and 4 and JNK-dependent pathways. J Biol Chem 2007;282:35279–35292.
24 Patsouris D, Li PP, Thapar D, Chapman J, Olefsky JM, Neels JG. Ablation of CD11c-positive cells normalizes insulin sensitivity in obese insulin resistant animals. Cell Metab 2008;8:301–309.
25 Hevener AL, Olefsky JM, Reichart D, Nguyen MT, Bandyopadyhay G, Leung HY, Watt MJ, Benner C, Febbraio MA, Nguyen AK, Folian B, Subramaniam S, Gonzalez FJ, Glass CK, Ricote M. Macrophage PPAR gamma is required for normal skeletal muscle and hepatic insulin sensitivity and full antidiabetic effects of thiazolidinediones. J Clin Invest 2007; 117:1658-1669.
26 Fink LN, Oberbach A, Jensen TE, Sams A, Blüher M, Klip A. Muscle-infiltrating macrophages in type 2 diabetes. Diabetes 2012;61:106-OR.
27 Kraegen EW. Development of muscle insulin resistance after liver insulin resistance in high-fat-fed rats. Diabetes 1991;40:1397–1403.
28 Sell H, Eckel J. Monocyte chemotactic protein-1 and its role in insulin resistance. Curr Opin Lipidol 2007;18:258–262.
29 Yang H, Youm Y-H, Vandanmagsar B, Ravussin A, Gimble JM, Greenway F, Stephens JM, Mynatt RL, Dixit VD. Obesity increases the production of proinflammatory mediators from adipose tissue T cells and compromises TCR repertoire diversity: implications for systemic inflammation and insulin resistance. J Immunol 2010;185:1836-1845.
30 Bruun JM, Helge JW, Richelsen B, Stallknecht B. Diet and exercise reduce low-grade inflammation and macrophage infiltration in adipose tissue but not in skeletal muscle in severely obese subjects. Am J Physiol Endocrinol Metab 2006;290:E961-967.
31 de Luca C, Olefsky JM. Inflammation and insulin resistance. FEBS Lett 2008;582:97–105.
32 Brøns C, Jensen CB, Storgaard H, Hiscock NJ, White A, Appel JS, Jacobsen S, Nilsson E, Larsen CM, Astrup A, Quistorff B, Vaag A. Impact of short-term high-fat feeding on glucose and insulin metabolism in young healthy men. J Physiol 2009;587:2387-2397.

SUPPLEMENTARY DATA

SUPPLEMENTARY TABLE 1 - **Primer sequences**

Gene	Forward primer	Reverse primer
CD14	CGCTCCGAGATGCATGTG	AGCCCAGCGAACGACAGA
CD68	AGCCCAGATTCAGATTCGAG	GGGAATGAGAGAAGCAGGTG
GYS1	TGGGGCTACACACCGGCTGA	GCGGAACCGCCGGTCAAGAA
INSR	GGGCAACGGCTCTTGGACGG	CGGCCCATCTGGCTGCCTCTT
MARCO	CTGGAGAACACCTGGCTCA	CCCTTGTGACCTTGAAGAC
RPS18	GGACCTGGCTGTATTTTCCA	GAGGATGAGGTGGAACGTGT
SLC2A4 (GLUT-4)	GCTACCTCTACATCATCCAGAATCTC	CCAGAAACATCGGCCCA
TBC1D1	GGGCAAGGTGTGCCACGTCA	TCGCATGCTGCTGGGAAGTCA
TBC1D4 (AS160)	GGCTGGAGTCCTGCTTCTGCAC	GCTGGTACATTTGAATCTGCAGCGA

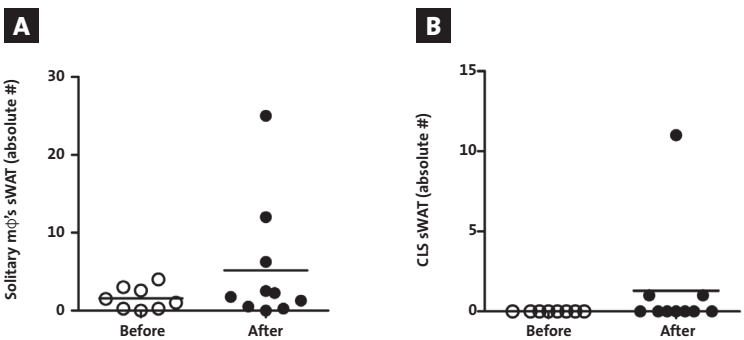

SUPPLEMENTARY FIGURE 1 - Effect of short-term HFHC diet on macrophage content in subcutaneous white adipose tissue in healthy male subjects. The number of solitary macrophages and CLS were counted following a CD68 (macrophage) staining in sWAT biopsies of healthy male subjects (n=8) obtained before (open dots) and after (closed dots) a 5-day HFHC diet. Counts represent absolute numbers.

HFHC, high-fat high calorie. CLS, crown-like structure. sWAT, subcutaneous white adipose tissue.

10

E-SELECTIN IS ELEVATED IN CORD BLOOD OF SOUTH ASIAN NEONATES COMPARED WITH CAUCASIAN NEONATES

MARIËTTE R. BOON
NASRA S. KARAMALI
CHRISTIANNE J.M. DE GROOT
LOTTE VAN STEIJN
HUMPHREY H. KANHAI
CHRIS VAN DER BENT
JIMMY F.P. BERBÉE
BAREND MIDDELKOOP
PATRICK C.N. RENSEN
JOUKE T. TAMSMA

Journal of Pediatrics 2012; 160: 844-8.

ABBREVATIONS

BMI	Body mass index
CAD	Coronary artery disease
CRP	C-reactive protein
ICAM-1	Intercellular adhesion molecule 1
VCAM-1	Vascular cell adhesion molecule 1

ABSTRACT

To test the hypothesis that the increased risk of type 2 diabetes mellitus and coronary artery disease in South Asian subjects could be caused by the presence of endothelial dysfunction in early life. Westudied markers of endothelial dysfunction in umbilical cord blood of South Asian neonates and compared these with that of Caucasian control subjects. FromSouth Asian (n=57) and Caucasian (n=21) neonates, cord blood was collected and levels of glucose, insulin, lipids, and markers of endothelial dysfunction (E-selectin, intercellular adhesion molecule 1, vascular cell adhesion molecule 1) and inflammation (C-reactive protein) were measured. Plasma E-selectin levels were significantly higher in South Asian neonates (46.7 versus 33.5 ng/mL, *P*<.001), and levels of intercellular adhesion molecule 1 and vascular cell adhesion molecule 1 did not differ. Furthermore, South Asian neonates had hyperinsulinemia (*P*=.043), dyslipidemia (with significantly higher triglyceride and lower high-density lipoprotein cholesterol levels), and higher C-reactive protein levels (75.7 versus 43.8 ng/mL, *P*=.009). In conclusion, South Asian newborns are characterized by elevated E-selectin levels in line with the hypothesis that endothelial dysfunction is present early in life. In addition, hyperinsulinemia, dyslipidemia, and inflammation are present. Because many pathogenic variables for coronary artery disease and type 2 diabetes are already present at birth in South Asian patients, the question arises whether rigorous childhood lifestyle intervention could be beneficial. *(J Pediatr 2012;160:844-8)*.

INTRODUCTION

South Asian people originate from the Indian subcontinent (India, Pakistan, Bangladesh, Sri Lanka, and Nepal) and represent one-fifth of the world's population.[1] They are at higher risk of coronary artery disease (CAD) and its subsequent morbidity and mortality than Caucasian individuals.[2,3] Several studies show that CAD in South Asian patients is not only much more prevalent compared with white European patients, but also starts at an earlier age.[4-6] Conventional coronary risk factors, including smoking, hypercholesterolemia, and hypertension, do not explain their increased CAD risk compared with Caucasian subjects.[2] Although type 2 diabetes mellitus and insulin resistance are significantly more prevalent in South Asian patients, this appears to contribute only to some of the excess risk.[7] Thus, residual risk is present, suggesting that additional factors may play a role. An ethnic susceptibility for endothelial dysfunction in the South Asian population has been hypothesized, because endothelial dysfunction plays a key role in the initiation of atherosclerosis.[8,9]

Although endothelial dysfunction contributes to atherosclerosis in large arteries, it has been suggested that in the capillary and arteriolar endothelium, it may contribute to the development of type 2 diabetes mellitus.[10-12] Indeed, Meigs and coworkers[10] found that endothelial dysfunction, as measured with elevated levels of the biomarker E-selectin in blood, predicted the occurrence of type 2 diabetes mellitus in adult women, and intercellular adhesion molecule 1 (ICAM-1) and vascular cell adhesion molecule 1 (VCAM-1), which are other and less sensitive markers of endothelial dysfunction, did not. These results were still found after correction for several known risk factors, such as body mass index (BMI), family history of diabetes mellitus, smoking, and subclinical inflammation.

We hypothesized that in South Asian subjects, both the residual risk for CAD and the high prevalence of type 2 diabetes mellitus could be caused by the presence of a susceptibility to endothelial dysfunction. We examined the presence of E-selectin, ICAM-1, and VCAM-1 in umbilical cord plasma of South Asian neonates and Caucasian control subjects.

METHODS

Umbilical venous cord blood was collected from South Asian neonates living in the Netherlands (n=21), from South Asian neonates living in Surinam (n=36), and from Caucasian neonates living in the Netherlands (n=21). In total, 78 neonates, all born between Jan 1, 2006, and Jan 1, 2009, were examined in two hospitals in Paramaribo, Surinam,[13] and in one hospital in The Hague, the Netherlands, after their mothers had given informed consent and approval had been obtained by the local ethics committee. Live-born singleton babies with 4 South Asian grandparents or 4 Caucasian grandparents were included. Pregnancies complicated by pre-eclampsia were excluded. Gestational age was based on last menstrual period or ultrasound scanning (before 12 weeks). Birth weights were taken from the medical records and information about the mother of the neonate (maternal

disease including diabetes mellitus, hypertension, hyperthyroidism, and hypothyroidism; gestational age; parity; usage of medication; and age). For both the mother and father of the baby, a questionnaire was used to gather information on family history of diabetes mellitus, hypertension, and coronary events. Family history was marked as "positive" when one of the family members (grandparents, parents, brothers/sisters) had been diagnosed with the disease. Furthermore, the health status of the father was assessed.

Immediately after delivery, 20 mL of cord blood was collected from the umbilical vein with standard protocols. Within 1 hour, the cord blood was centrifuged. Plasma insulin and glucose levels were measured immediately, and a portion of the plasma was frozen and stored at 80C. The stored samples from Surinam and the Netherlands were transported in special media to the Leiden University Medical Center (Leiden, The Netherlands), where markers of endothelial dysfunction (E-selectin, ICAM-1, and VCAM-1) and C-reactive protein (CRP) were measured (Meso Scale Discovery, Gaithersburg, Maryland). Furthermore, cholesterol and triglyceride levels were determined by using commercially available kits (Roche Diagnostics Cholesterol reagent and Triglyceride reagent, respectively; Roche Diagnostics, Almere, The Netherlands). High-density lipoprotein cholesterol levels were determined by precipitating the apoB-containing lipoproteins as described previously.[14] Non-high-density lipoprotein cholesterol levels were calculated by subtracting the high-density lipoprotein cholesterol levels from the total cholesterol levels.

Statistical Analysis

All data were analyzed with SPSS software version 17.0 (SPSS, Chicago, Illinois). Mean differences in gestational age, birth weight, APGAR scores, and levels of E-selectin, ICAM-1, VCAM-1, CRP, and glucose were compared between South Asian neonates and Caucasian neonates by using independent *t* tests. Birth weight and levels of E-selectin, CRP, and glucose were skewed and required log transformation to satisfy assumptions of normality. Maternal age and insulin levels were not normally distributed, even after log transformation. Differences in maternal age and insulin measures therefore were compared with the non-parametric Mann- Whitney test. Differences in the prevalence of chronic diseases in the mothers, smoking, alcohol and drug use, and sex of the neonates were tested with the χ^2 test. Outliers were detected with the Grubb's test. In the case of CRP, two significant outliers (one in each group) were detected, which were subsequently excluded.

RESULTS

The South Asian neonates living in Surinam and the Netherlands were clustered in one group ("South Asians," n=57) because no significant differences were observed for sex, birth weight, maternal age, and plasma E-selectin levels. The characteristics of the South Asian and Caucasian groups are given in **(TABLE 1)**. South Asian mothers were significantly younger than Caucasian mothers. Pre-pregnancy BMI did not differ between South Asian mothers

and Caucasian mothers, with mean values of 23.6 and 23.7, respectively (*P*=.93). Infants were equally exposed to maternal chronic disease, such as asthma, diabetes mellitus, hypothyroidism, hyperthyroidism, and hypertension. More specifically, 6 of the South Asian women (10.7%) had some form of diabetes mellitus (type 1, type 2, or gestational diabetes) during pregnancy, compared with two women in the Caucasian group (9.5%), which was not significantly different (data not shown). Furthermore, 6 of the South Asian women had pre-existent or pregnancyinduced hypertension, compared with 3 women in the Caucasian group (*P*=.116). Although maternal smoking and drug use did not differ between the groups, Caucasian mothers drank alcohol more often during pregnancy. Birth weight was approximately 400 g lower for South Asian babies (*P*=.002), and gestational age was 2 days longer for South Asian neonates, which was not significantly different (*P*=.437). Apgar scores after 5 minutes did not differ. Furthermore, there was no difference in sex of the neonate in the groups: 48% of South Asian babies were female, compared with 49% of Caucasian babies (*P*=.947).

TABLE 1 - **Characteristics of mothers and neonates**

	Caucasian (n=21)	South Asian (n=57)	*P* value
Mothers			
Age, years†	33.9 (3.6)	31.1 (4.7)	.012
Pre-pregnancy BMI	23.7 (5.0)	23.6 (4.7)	.93
Chronic disease‡	24% (5)	24% (5)	.811
Smoking‡	5% (1)	7% (4)	.800
Alcohol use‡	30% (6)	2% (1)	.000
Drug use‡	0% (0)	2% (1)	.555
Neonates			
Gestational age, days	273.8 (9.7)	275.9 (10.8)	.437
Birth weight, g*	3516 (525)	3113 (489)	.002
Apgar score 5 min†	9.8	9.6	.485

Data represent mean (SD) or percentage (absolute number).
*After log transformation.
†Non-parametric tests.
‡χ^2 test.

TABLE 2 - **Mode of delivery**

	Caucasian (n=21)	South Asian (n=57)
Vaginal delivery	52% (11)	45% (28)
Cesarean delivery	14% (3)	44% (27)
Vacuum extraction	19% (4)	8% (5)
Assisted delivery (forceps)	0% (0)	3% (2)
Induced labor	14% (3)	0% (0)

Data represent percentage (absolute number).

Mode of delivery is summarized in **(TABLE 2)**. Cesarean delivery was more common in South Asian women, and vacuum extraction was more common in Caucasian women.

In **(TABLE 3)**, the health status of the father and the family history of both the mother and father of the neonates is shown. Although most measurements did not differ, South Asian fathers had a positive family history for diabetes mellitus more often (*P*=.04).

As shown in **(TABLE 4)**, CRP levels were significantly higher in South Asian neonates compared with Caucasian neonates (75.7 versus 43.8 ng/mL; *P*=.009). Glucose levels did not significantly differ between South Asian babies and Caucasian babies (not significant, *P* = .116). Mean insulin levels, however, were found to be 16.6 mmol/L in South Asian babies and 6.9 mmol/L in Caucasian neonates (*P*=.043). Furthermore, South Asian neonates had significantly higher triglyceride levels (0.38 versus 0.27 mmol/L; *P*=.009). Total cholesterol levels did not differ in the groups (1.57 versus 1.60 mmol/L; *P*=.717). South Asian babies had significantly higher non high-density lipoprotein cholesterol levels (0.66 versus 0.53 mmol/L;

TABLE 3 - **Family history**

	Caucasian	South Asian	*P* value
Fathers			
Chronic disease (n=21 & n=57)	14% (3)	13% (8)	.872
Positive family history diabetes (n=19 & n=54)	32% (6)	59% (32)	.038
Positive family history hypertension (n=18 & n=52)	50% (9)	60% (31)	.477
Positive family history coronary event (n=19 & n=49)	16% (3)	35% (17)	.125
Mothers			
Positive family history diabetes (n=20 & n=57)	45% (9)	67% (38)	.087
Positive family history hypertension (n=20 & n=58)	50% (10)	60% (35)	.419
Positive family history coronary event (n= 8 & n=56)	22% (4)	32% (18)	.423

Data represent percentage (absolute number).

TABLE 4 - **Metabolic parameters**

	Caucasian (n=21)	South Asian (n=57)	Delta	*P* value
CRP, ng/mL*	43.8 (26.1)	75.7 (48.3)	+73%	.009
Glucose, mM*	4.7 (1.15)	5.7 (2.40)		.120
Insulin, mM†	6.9 (10.2)	16.6 (29.6)	+141%	.043
Triglycerides, mM*	0.27 (0.09)	0.38 (0.19)	+41%	.009
Total cholesterol, mM	1.60 (0.38)	1.57 (0.37)		.717
Non-HDL-cholesterol, mM	0.53 (0.22)	0.66 (0.27)	+25%	.040
HDL-cholesterol, mM	1.08 (0.24)	0.91 (0.17)	–16%	.001

Data represent mean (SD).
HDL, high-density lipoprotein.
* After log transformation.
† Non-parametric test.

P=.040) and lower high-density lipoprotein cholesterol levels (0.91 versus 1.08; *P*=.001) compared with Caucasian neonates.

E-selectin levels were significantly higher in cord blood of South Asian neonates compared with that of Caucasian newborns (46.7 versus 33.5 ng/mL, *P*<.001). Levels of ICAM-1 and VCAM-1 did not differ significantly in the groups **(FIGURE)**. A multivariate analysis was performed with E-selectin levels as dependent variable and ethnicity, maternal age, birth weight, insulin levels, and CRP levels as co-variates. In this analysis, ethnicity significantly contributed to explain the variety of E-selectin. After correction for the aforementioned co-variates, the estimated E-selectin levels were found to be 42.5 and 34.5 ng/mL for South Asian and Caucasian neonates, respectively (*P*=.047).

Although the mode of delivery differed in the ethnic groups, stratification of the data showed that they did not influence E-selectin and other cord blood measures. Furthermore, no correlation was found between maternal pre-pregnancy BMI and cord plasma E-selectin levels (r^2=0.00093, *P*=.81), cord plasma triglyceride levels (r^2=0.015, *P*=.33), and cord plasma CRP levels (r^2=0.0044, *P*=.60).

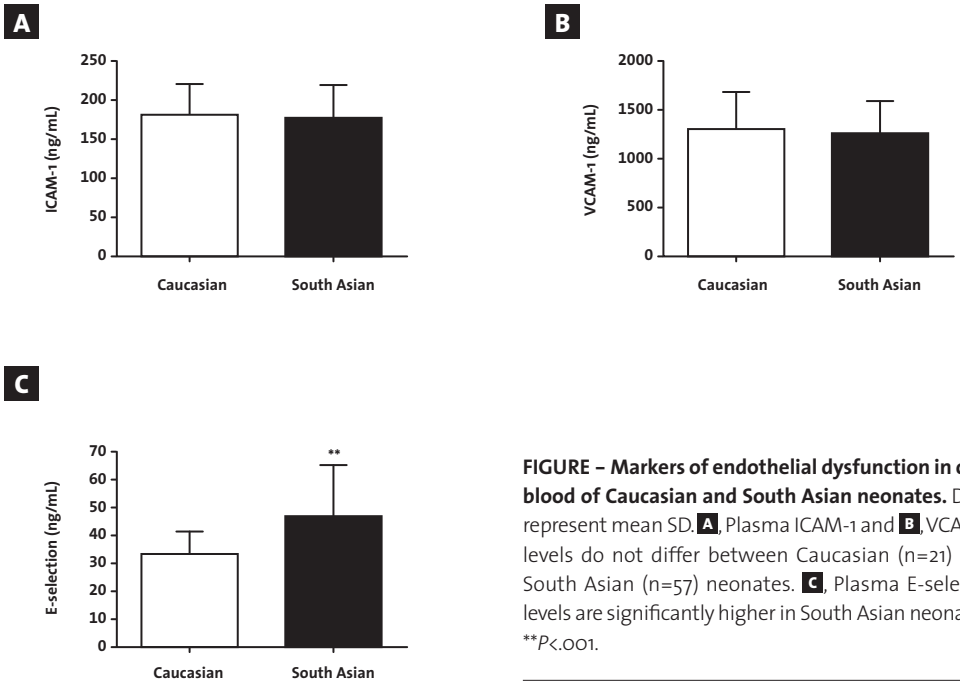

FIGURE – Markers of endothelial dysfunction in cord blood of Caucasian and South Asian neonates. Data represent mean SD. **A**, Plasma ICAM-1 and **B**, VCAM-1 levels do not differ between Caucasian (n=21) and South Asian (n=57) neonates. **C**, Plasma E-selectin levels are significantly higher in South Asian neonates. ***P*<.001.

DISCUSSION

The link between endothelial dysfunction and type 2 diabetes mellitus has been described by Meigs and co-workers,[10] who found that elevated levels of the biomarker E-selectin (but not ICAM-1 and VCAM-1) in serum predicts the occurrence of type 2 diabetes mellitus in adult women. We found a very similar pattern in South Asian newborns immediately after birth; E-selectin levels were elevated, but ICAM-1 and VCAM-1 levels were not.

Earlier research supports our finding of the presence of susceptibility for endothelial dysfunction in the South Asian population. In healthy South Asian men, impaired brachial artery response to reactive hyperemia has been demonstrated. This was independent of both conventional risk factors and markers of insulin resistance, supporting the presence of endothelial dysfunction.[15] Our study, however, supports the hypothesis that endothelial dysfunction in South Asians is present as early as at birth.

A recent study performed by Whincup et al[16] showed that type 2 diabetes mellitus precursors are already present in apparently healthy South Asian children 9 to 10 years of age. These children were found to have higher levels of hemoglobin A1c, insulin, triglycerides, and CRP and lower levels of high-density lipoprotein cholesterol compared with Caucasian children. In our study, we showed that South Asian newborns are not only characterized by elevated E-selectin levels, but also by hyperinsulinemia, inflammation, and dyslipidemia (elevated triglyceride levels, elevated non-high-density lipoprotein cholesterol levels, and decreased high-density lipoprotein cholesterol levels).

Thus, in South Asian patients, many potential pathogenic variables for CAD and type 2 diabetes mellitus are already present as early as at birth. Apparently, at least some of the risk factors responsible for the ethnic differences in CAD and type 2 diabetes mellitus are operating well before adult life, potentially offering opportunities for early prevention.

There are some potential limitations to our study. First, cord blood E-selectin levels were used as a marker of endothelial dysfunction. It is not known whether E-selectin levels in the cord blood purely reflect neonatal E-selectin levels or whether they could also be partly derived from maternal origin. Unfortunately, in our study, levels of maternal E-selectin were not measured. However, an earlier study by Krauss et al[17] showed that, in both normal and pre-eclamptic pregnancies, cord blood levels of E-selectin, ICAM-1, and VCAM-1 did not correlate with maternal levels, despite mothers with pre-eclampsia having significantly elevated levels of these factors. This suggests that these endothelial adhesion molecules are differently regulated in the fetus and, very likely, originate from the fetus. Second, the sample size of both groups was relatively small. However, the elevation of metabolic variables and E-selectin levels in South Asian newborns were found to be significantly different compared with that in the control group. The South Asian neonates included in our study were from both Surinam and the Netherlands. Place of birth was not associated with sex, birth weight, maternal age, or plasma E-selectin levels. Moreover, the South Asian neonates living in the Netherlands all had grandparents who originally descended from Surinam. Lastly, this study is a cross-sectional study and is thus not able to show whether the presence of endothelial dysfunction in South Asian neonates indeed leads to the generation of CAD and

type 2 diabetes mellitus later in life. However, because endothelial dysfunction is considered a risk factor for the development of atherosclerosis,[8] its contribution to the development of CAD is highly plausible. Moreover, in light of the fastemerging field of non-traditional risk factors and biomarkers for cardiovascular disease[18] in South Asian children, E-selectin might be a biomarker for future cardiovascular disease. Furthermore, because of the cross-sectional design of our study, it is not possible to draw conclusions about whether the endothelial dysfunction found in the South Asian neonates has an ethnic or genetic origin. Future studies, for example studies in which the effect of intrauterine conditions on endothelial function in South Asians is studied, could clarify this.

Potentially, many pathogenic variables for CAD and type 2 diabetes mellitus are already present right after birth in South Asians, so the question arises whether rigorous childhood lifestyle intervention could be beneficial in these vulnerable children.

REFERENCES

1 Gupta M, Singh N, Verma S. South Asians and cardiovascular risk: what clinicians should know. Circulation 2006;113:e924-9.
2 Balarajan R. Ethnicity and variations in the nation's health. Health Trends 1995;27:114-9.
3 McKeigue PM, Miller GJ, Marmot MG. Coronary heart disease in south Asians overseas: a review. J Clin Epidemiol 1989;42:597-609.
4 Anand SS, Yusuf S. Risk factors for cardiovascular disease in Canadians of South Asian and European origin: a pilot study of the Study of Heart Assessment and Risk in Ethnic Groups (SHARE). Clin Invest Med 1997; 20:204-10.
5 Balarajan R. Ethnic differences in mortality from ischaemic heart disease and cerebrovascular disease in England and Wales. BMJ 1991;302: 560-4.
6 Joshi P, Islam S, Pais P, Reddy S, Dorairaj P, Kazmi K, et al. Risk factors for early myocardial infarction in South Asians compared with individuals in other countries. JAMA 2007;297:286-94.
7 McKeigue PM, Shah B, Marmot MG. Relation of central obesity and insulin resistance with high diabetes prevalence and cardiovascular risk in South Asians. Lancet 1991;337:382-6.
8 Harrison DG. Cellular and molecular mechanisms of endothelial cell dysfunction. J Clin Invest 1997;100:2153-7.
9 Verma S, Anderson TJ. Fundamentals of endothelial function for the clinical cardiologist. Circulation 2002;105:546-9.
10 Meigs JB, Hu FB, Rifai N, Manson JE. Biomarkers of endothelial dysfunction and risk of type 2 diabetes mellitus. JAMA 2004;291: 1978-86.
11 Pinkney JH, Stehouwer CD, Coppack SW, Yudkin JS. Endothelial dysfunction: cause of the insulin resistance syndrome. Diabetes 1997; 46(Suppl. 2):S9-13.
12 Thorand B, Baumert J, Chambless L, Meisinger C, Kolb H, Doring A, et al. Elevated markers of endothelial dysfunction predict type 2 diabetes mellitus in middle-aged men and women from the general population. Arterioscler Thromb Vasc Biol 2006;26:398-405.
13 van Steijn L, Karamali NS, Kanhai HH, Ariens GA, Fall CH, Yajnik CS, et al. Neonatal anthropometry: thin-fat phenotype in fourth to fifth generation South Asian neonates in Surinam. Int J Obes (Lond) 2009;33: 1326-9.
14 van der Hoorn JW, de Haan W, Berbee JF, Havekes LM, Jukema JW, Rensen PC, et al. Niacin increases HDL by reducing hepatic expression and plasma levels of cholesteryl ester transfer protein in APOE3Leiden.CETP mice. Arterioscler Thromb Vasc Biol 2008;28:2016-22.
15 Murphy C, Kanaganayagam GS, Jiang B, Chowienczyk PJ, Zbinden R, Saha M, et al. Vascular dysfunction and reduced circulating endothelial progenitor cells in young healthy UK South Asian men. Arterioscler Thromb Vasc Biol 2007;27:936-42.
16 Whincup PH, Nightingale CM, Owen CG, Rudnicka AR, Gibb I, McKay CM, et al. Early emergence of ethnic differences in type 2 diabetes precursors in the UK: the Child Heart and Health Study in England (CHASE Study). PLoS Med 2010;7:e1000263.
17 Krauss T, Azab H, Dietrich M, Augustin HG. Fetal plasma levels of circulating endothelial cell adhesion molecules in normal and preeclamptic pregnancies. Eur J Obstet Gynecol Reprod Biol 1998;78:41-5.
18 Balagopal PB, de Ferranti SD, Cook S, Daniels SR, Gidding SS, Hayman LL, et al. Nontraditional risk factors and biomarkers for cardiovascular disease: mechanistic, research, and clinical considerations for youth: a scientific statement from the American Heart Association. Circulation 2011;123:2749-69.

11

SOUTH ASIANS EXHIBIT DISTURBED HDL FUNCTIONALITY AS COMPARED TO WHITE CAUCASIANS

MARIËTTE R. BOON*
LEONTINE E.H. BAKKER*
WIJTSKE ANNEMA
ARNE DIKKERS
J. WOUTER JUKEMA
LOUIS M. HAVEKES
A. EDO MEINDERS
UWE J.F. TIETGE
INGRID M. JAZET
PATRICK C.N. RENSEN

* Both authors contributed equally

In preparation.

12

ABSTRACT

South Asians have an exceptionally high risk of developing cardiovascular disease (CVD) compared to white Caucasians. A possible contributing factor might be dysfunction of high density lipoprotein (HDL). This study aimed to compare HDL function in neonates, adolescents and adults of both ethnicities. HDL functionality with respect to cholesterol efflux, anti-oxidation and anti-inflammation was determined using fasting plasma samples from South Asian and white Caucasian neonates (n=14 each), adolescent, healthy men (n=12 each, 18-25y), and adult, overweight men (n=12 each, 40-50y). Adolescents were subjected to a 5-day high fat high calorie diet (HCD) and adults to an 8-day very low calorie diet (LCD). In neonates, anti-inflammatory capacity was reduced in South Asian neonates (22.9±0.7 *vs.* 35.9±1.9%, $p<0.00001$) while cholesterol efflux and anti-oxidative capacity of HDL were comparable between groups. In adolescents, all three measures of HDL functionality were comparable between groups. Cholesterol efflux capacity increased in response to the HCD in South Asians (+6.3±2.9%, $p=0.073$) and Caucasians (+11.8±3.4%, $p=0.002$). In adults, anti-oxidative capacity was lower in South Asians before LCD (18.1±2.6 *vs.* 24.2±2.2%, $p=0.077$) and after LCD (16.4±2.4 *vs.* 27.6±2.7%, $p=0.003$). Anti-inflammatory capacity was negatively affected by the diet only in South Asians (-12.2±4.3%, $p=0.005$). Cholesterol efflux capacity was significantly reduced after the LCD in both South Asians (-10.3±2.4%, $p<0.001$) and Caucasians (-13.7±1.9%, $p<0.0001$). In conclusion, South Asians exhibit disturbed function of HDL compared to Caucasians, which may contribute to their excess risk of CVD.

INTRODUCTION

The burden and mortality of cardiovascular disease (CVD) are significantly increased among both native and migrant South Asians compared to people of white Caucasian descent. The age-standardized mortality rate from CVD is around 50% higher for South Asians (1-4). In addition, CVD is more aggressive and has higher mortality rates at younger ages in South Asians (1,2,5-7). The underlying mechanism of this excess risk is still poorly understood. Traditional risk factors such as smoking, hypertension, and type 2 diabetes (T2D) seem to account for only part of the excess risk in South Asians (3,8-11). Thus, additional factors must be involved. One of these factors may be dysfunction of high density lipoprotein (HDL).

Numerous clinical and epidemiological studies have consistently shown a strong inverse association between the level of HDL-cholesterol and cardiovascular risk (12-17). The cardiovascular protective effects of HDL have been attributed to several anti-atherogenic functional properties, including: HDL (i) prevents LDL oxidation, (ii) is anti-inflammatory, and (iii) stimulates cholesterol efflux from foam cells (18-22). Of note, recent evidence suggests that HDL functionality might be affected independent of changes in plasma HDL-cholesterol level (23,24). In trials that aimed at raising HDL-cholesterol levels with niacin or dalcetrapib on top of LDL lowering, no decrease in the occurrence of cardiovascular endpoints was observed compared to treatment with LDL lowering only (25,26). This suggests that simply raising HDL-cholesterol levels is not sufficient to lower CVD risk and that HDL functionality may thus be more importantly linked to CVD than plasma HDL-cholesterol concentrations. Indeed, previous studies showed that HDL is dysfunctional in patients with coronary atherosclerosis, in men with cardiovascular risk factors, and in patients with an acute phase response after surgery (27-30).

HDL functionality can not only be influenced by the cardiovascular health status, but also by dietary intervention. A 3-week high-fiber-low-fat diet and exercise intervention converted HDL from pro- to anti-inflammatory (29). Furthermore, data from our study group demonstrated a decrease in cholesterol efflux capacity of HDL after very low calorie diet (LCD)-induced weight loss (31).

Interestingly, multiple studies have repeatedly found lower HDL-cholesterol levels in South Asians compared to white Caucasians, even in South Asian neonates (32-39). In addition, South Asians seem to have relatively more small HDL particles, which are associated with decreased cardiac protection compared to normal sized HDL particles (40-42). Remarkably, though, little is known about HDL functionality in South Asians. Therefore, this study aimed to compare HDL function in South Asian and white Caucasian subjects. In particular, we were interested in the following questions: (i) is HDL function impaired in middle-aged overweight South Asians compared to matched Caucasians?, (ii) if so, is this dysfunction already present in young healthy subjects and/or even at birth?, and (iii) is the effect of short-term dietary intervention on HDL function different between South Asians and Caucasians? To answer these questions, we determined three functions of HDL, namely its ability to induce cholesterol efflux and its anti-oxidative and anti-inflammatory properties, in neonates, in young healthy men (adolescents) and in middle-aged overweight men

(adults). The adolescents and adults were subjected to a 5-day high-fat-high-calorie diet (HCD) and an 8-day LCD respectively.

METHODS

Subjects

Neonates. Umbilical venous cord blood was collected from 28 neonates (14 South Asian and 14 Caucasian neonates) as described previously (32). All neonates were born between Jan 1, 2006, and Jan 1, 2009, and were examined after their mothers had given informed consent and approval had been obtained by the local ethics committee. Live-born singleton babies with 4 South Asian grandparents or 4 Caucasian grandparents were included. Pregnancies complicated by pre-eclampsia were excluded. Gestational age was based on last menstrual period or ultrasound scanning (before 12 weeks). Birth weights were taken from the medical records. Immediately after delivery, 20 mL of cord blood was collected from the umbilical vein according to standard protocols. South Asian and Caucasian neonates were matched for HDL-cholesterol level.

Adolescents and adults. 24 young healthy Dutch males (adolescents; age 18-25y, BMI <25 kg/m^2) and 24 middle-aged overweight Dutch males (adults; age 40-50y, BMI 25-30 kg/m^2) were enrolled via local advertisements. Subjects were of South Asian (n=12 for each group) or Caucasian (n=12 for each group) origin. They underwent a medical screening including their medical history, a physical examination, blood chemistry tests and an oral glucose tolerance test (OGTT) to exclude individuals with T2D. Other exclusion criteria were CVD, any significant chronic disease, use of medication known to influence lipid metabolism, rigorous exercise, smoking and recent body weight change. The study was approved by the Medical Ethical Committee of the Leiden University Medical Centre and performed in accordance with the principles of the revised Declaration of Helsinki. Written informed consent was obtained from all subjects prior to participation.

Dietary interventions adolescents and adults

The adolescents were subjected to a 5-day HCD, consisting of the subject's regular diet, supplemented with 375 mL of cream per day (1275 kcal/day, 94% fat), yielding to approx. 3775 kcal/day and 54% of fat. The adults received an 8-day LCD, consisting of three sachets of Modifast per day (approx. 450 kcal/day, 50 g protein, 50-60 g carbohydrates, 7 g lipids and 15 g dietary fibers). Subjects were instructed not to alter life style habits, and not to perform physical activity in the last 48 h before the study days. One day before and one day after the dietary interventions blood samples were obtained from all subjects after a 10h overnight fast.

Laboratory analyses

Fasting plasma total cholesterol, triglycerides and glucose were measured on a Modular P800 analyzer (Roche, Almere, The Netherlands) using commercially available enzymatic

kits from Roche Molecular Biochemicals (total cholesterol, triglycerides) and Instruchemie, Delfzijl, The Netherlands (glucose). HDL-cholesterol levels were determined after precipitating the apoB-containing lipoproteins as described previously (43). LDL-cholesterol was calculated according to Friedewald's formula (44). Serum insulin levels were analyzed using a commercially available chemiluminescence immunometric assay on an Immulite 2500 analyzer (Siemens Healthcare Medical Diagnostics, Germany).

HDL function measurements

ApoB-containing lipoproteins were precipitated by adding 100 µL 36% polyethylene glycol (PEG 6000, Sigma, St. Louis, MO, USA) in 10 mM HEPES (pH = 8.0) to 200 µL plasma. Subsequently, samples were incubated for 30 min on ice and centrifuged for 30 min at 2200 g (45). The HDL-containing supernatant was collected, kept on ice, and used within the same week for HDL function assays.

Cholesterol efflux capacity. To determine HDL-mediated cholesterol efflux, THP-1 human monocytes (ATCC via LGC Promochem, Teddington, UK) were differentiated into macrophages in the presence of 100 nM phorbol myristate acetate (46). Differentiated THP-1 macrophages were then loaded with 50 µg/mL acetylated LDL and 1 µCi/mL [^{3}H]cholesterol (Perkin Elmer, Boston, MA, USA) for 24 h. Next, macrophages were equilibrated for 18 h in RPMI 1640 medium containing 2% bovine serum albumin (46). Thereafter, 2% apoB-depleted plasma was added to the macrophages. After 5 h, effluxed radioactivity was determined by liquid scintillation counting (Packard 1600CA Tri-Carb, Packard, Meriden, CT, USA). Then the plates were washed two times with PBS and cells were lysed with 0.1 M NaOH (30 min incubation at room temperature). Subsequently, the radioactivity within the cells was counted. Efflux per well is expressed as the percentage of radioactivity released into the medium related to the total initial dose of radioactivity. To correct for nonspecific efflux, we subtracted values obtained from control cells without added apoB-depleted plasma.

Anti-oxidative capacity. The anti-oxidative properties of HDL were assessed by measuring the capacity of HDL from the respective groups to inhibit the oxidation of native LDL using a previously published method (45). LDL was isolated from plasma of a fasted healthy male donor by density gradient ultracentrifugation (1.019 < d < 1.063 g/mL) (47). LDL (100 mg/dL cholesterol) was then oxidized with 5 mM 2,2′-azobis(2-methylpropionamidine) dihydrochloride (AAPH) for 24 h at 37°C either in the presence of 10% apoB-depleted plasma or an equal volume of precipitation reagent in PBS as a control. Protein was precipitated with 10% trichloroacetic acid. Then, the accumulation of thiobarbituric acid reactive substances (TBARS) as a measure of oxidative modification was determined by incubating the samples for 10 min at 99°C and measuring the fluorescence at 485 nm excitation and 545 nm emission using 1,1,3,3-tetramethoxypropane as a standard as published previously (47). The anti-oxidative capacity of HDL was expressed as the amount of TBARS accumulating in the samples relative to control LDL oxidized in the absence of HDL.

Anti-inflammatory capacity. Anti-inflammatory properties of HDL were assessed using human umbilical vein endothelial cells (HUVECs, provided by the Endothelial Cell Core Facility of the UMCG) isolated and cultured as described previously (48). HUVECs were

pre-incubated with 2% apoB-depleted plasma or an equal volume of precipitation reagent in PBS as a control for 1 h. Then, 10 ng/mL tumor necrosis factor α (TNF-α; R&D systems, Abingdon, UK) was added. After an additional incubation for 8 h, total RNA was isolated using Trizol (Invitrogen, Carlsbad, CA, USA) and quantified with a NanoDrop ND-100 UV-Vis spectrophotometer (NanoDrop Technologies, Wilmington, DE, USA). One μg of total RNA was reversed transcriped into cDNA (Invitrogen). Real-time quantitative PCR was performed on an ABI-Prism 7700 (Applied Biosystems) sequence detector (49). Vascular cell adhesion molecule-1 (VCAM-1) mRNA expression was calculated relative to the expression of the housekeeping gene cyclophilin.

Statistical analysis

Data are presented as mean ± SEM when normally distributed or as median (IQR) when not normally distributed. A mixed effects model was applied to assess mean differences before and after the intervention within and between groups, and to determine differences in diet effect. Groups and intervention were modeled as fixed effects and the subject specific deviances from the group mean were modeled as random effects. Nonparametric tests (Wilcoxon signed-rank test within group, Mann-Whitney between groups) were performed when appropriate. Significance level was set at $p<0.05$. Statistical analyses were performed using SPSS for Windows version 20.0 (IBM, USA).

RESULTS

Clinical characteristics

Clinical characteristics are shown in **TABLE 1**.

Neonates. Mean gestational age was 278 ± 2 days. Birth weight tended to be lower in South Asian neonates (p=0.078). Glucose levels were comparable between groups, but insulin levels were significantly higher in South Asian neonates (p=0.044). No significant differences were observed in lipid levels.

Adolescents. Mean age was 22.1 ± 0.4 years. BMI did not differ between groups (at baseline 20.9 ± 0.6 (South Asians) *vs.* 22.2 ± 0.6 kg/m² (Caucasians), p=0.11). Fasting glucose, insulin, triglyceride, HDL-cholesterol and phospholipid levels were comparable at baseline, while total cholesterol levels were significantly higher and LDL-cholesterol tended (p=0.055) to be higher in South Asians. After the HCD, anthropometric parameters were unchanged. Fasting glucose and insulin levels were significantly increased only in South Asians. The HCD induced a significant increase in total cholesterol, HDL-cholesterol and LDL-cholesterol levels in Caucasians. In South Asians only HDL-cholesterol showed a tendency to increase (p=0.060). Phospholipids increased significantly to a similar degree in both groups.

Adults. Mean age was 44.6 ± 0.8 years. BMI did not differ between groups (at baseline 28.4 ± 0.4 (South Asians) *vs.* 28.1 ± 0.5 kg/m² (Caucasians), p=0.65). Fasting glucose and lipid levels were comparable between groups, whereas insulin levels were significantly higher in

South Asians (p=0.002). After the LCD, anthropometric parameters were significantly reduced in both groups. The mean reduction in body weight was 4.0±0.2 kg, of which approximately 50% was fat mass. Furthermore, caloric restriction induced a comparable, significant decrease in fasting plasma glucose, insulin, triglyceride, total cholesterol and phospholipid levels. HDL-cholesterol and LDL-cholesterol levels were not affected by the diet.

Of note, HDL-cholesterol levels were significantly lower in adult South Asians *vs.* adolescent South Asians (p=0.027). Furthermore, HDL-cholesterol was significantly lower at neonatal age compared to adolescent age for both South Asian (p=0.001 and p=0.040) and Caucasian (p=0.005 and p=0.017) subjects.

HDL functionality

The functionalities of HDL in Caucasians and South Asians with respect to inducing cholesterol efflux and anti-oxidative and anti-inflammatory action are depicted in **FIGURE 1.**

Cholesterol efflux capacity is affected by dietary intervention. The ability of HDL to elicit cholesterol efflux from macrophages did not differ between groups for all ages, both at baseline and after the dietary interventions. However, the HCD led to a significant increase in

TABLE 1 – Clinical and metabolic characteristics in South Asian and Caucasian neonates, and in adolescent healthy and adult overweight South Asian and Caucasian men before and after a 5-day HCD and 8-day LCD, respectively.

	Neonates	
	Caucasians	**South Asians**
Clinical characteristics		
(Gestational) age (days or years)	277 ± 3	279 ± 2
length (m)		
weight (g or kg)	3474 ± 133	3148 ± 118
body mass index (kg/m^2)		
waist (cm)		
Fasting plasma and serum levels		
glucose (mmol/L)	4.7 ± 0.4	4.7 ± 0.3
insulin (mU/L)	4.4 (3.9)	7.9 (6.7)*
triglycerides (mmol/L)	0.29 (0.13)	0.29 (0.33)
total cholesterol (mmol/L)	1.48 ± 0.09	1.55 ± 0.09
HDL-cholesterol (mmol/L)	0.98 ± 0.04	0.94 ± 0.04
LDL-cholesterol (mmol/L)	0.37 ± 0.07	0.43 ± 0.07

Data are presented as mean ± SEM or median (IQR). HCD, 5-day high fat high calorie diet. LCD, 8-day very low calorie diet. † p<0.05, †† p<0.005 within group *vs.* before diet.
* p<0.05, ** p<0.005 *vs.* Caucasians. ‡ p<0.05, ‡‡ p<0.005 diet effect *vs.* Caucasians.

cholesterol efflux ability in Caucasian adolescents (+11.8 ± 3.4%, p=0.002), while in South Asian adolescents there was a tendency towards an increase (+6.3 ± 2.9%, p=0.073). On the other hand, the LCD in the adult group resulted in a significantly lower cholesterol efflux capacity for both ethnicities (South Asians: -10.3 ± 2.4% (p<0.001) *vs.* Caucasians: -13.7 ± 1.9% (p<0.0001)). Cholesterol efflux capacity was comparable throughout different ages for both ethnic groups.

Anti-oxidative capacity is impaired in adult South Asians. The ability of HDL to prevent oxidation of LDL was comparable between groups at neonatal and adolescent age. However, this ability was markedly impaired in adult South-Asian subjects compared to Caucasians (before LCD: 18.1 ± 2.6 *vs.* 24.2 ± 2.2%, p=0.077; after LCD: 16.4 ± 2.4 *vs.* 27.6 ± 2.7%, p=0.003). Anti-oxidative capacity was not affected by dietary intervention. Of note, anti-oxidative capacity was significantly lower in adult South Asians compared to adolescent South Asians (p<0.005), while for Caucasian subjects anti-oxidative capacity was comparable between both age groups (p=0.160). Furthermore, anti-oxidative capacity was markedly lower at neonatal age compared to adolescent and adult age for both South Asian (*vs.* adolescents: p=0.00004, *vs.* adults: p=0.048) and Caucasian (*vs.* adolescents: p=0.000008; *vs.* adults: p=0.00007) subjects.

Group 18 – 25 years				**Group 40 – 50 years**			
Caucasians		**South Asians**		**Caucasians**		**South Asians**	
before HCD	**after HCD**	**before HCD**	**after HCD**	**before LCD**	**after LCD**	**before LCD**	**after LCD**
22.1 ± 0.6		22.2 ± 0.7		44.3 ± 1.1		44.9 ± 0.9	
1.84 ± 0.01		1.74 ± 0.02**		1.81 ± 0.02		1.75 ± 0.01**	
75.1 ± 1.8	75.6 ± 1.8	63.2 ± 2.3**	63.7 ± 2.3† **	92.6 ± 2.5	88.2 ± 2.5††	86.7 ± 1.4	83.2 ± 1.6†† ‡
22.2 ± 0.6	22.4 ± 0.6	20.9 ± 0.6	21.0 ± 0.6†	28.1 ± 0.5	26.8 ± 0.5††	28.4 ± 0.4	27.3 ± 0.4††
81.3 ± 2.2	82.0 ± 2.3	78.9 ± 2.2	79.5 ± 2.6	103 ± 1.8	100 ± 1.6††	101 ± 1.6	98 ± 1.5††
5.1 ± 0.1	5.2 ± 0.1	5.3 ± 0.1	5.5 ± 0.1†† *	5.3 ± 0.2	4.5 ± 0.2††	5.3 ± 0.1	4.5 ± 0.1††
4.8 (4.5)	7.0 (6.6)	7.1 (4.2)	10.6 (4.9)†† ** ‡‡	8.9 (3.3)	3.7 (4.9)††	11.7 (2.8)**	4.8 (5.8)††
0.79 (0.26)	0.75 (0.67)	0.98 (0.75)	1.08 (0.70)	1.29 (2.48)	0.89 (0.18)††	1.78 (2.91)	0.91 (0.25)††
3.75 ± 0.19	4.25 ± 0.22††	4.60 ± 0.30*	4.79 ± 0.24	5.56 ± 0.24	4.72 ± 0.33††	5.74 ± 0.28	5.13 ± 0.26††
1.18 ± 0.05	1.31 ± 0.06†	1.26 ± 0.08	1.36 ± 0.07	1.09 ± 0.08	0.99 ± 0.06	1.00 ± 0.07	0.95 ± 0.05
2.21 ± 0.21	2.55 ± 0.22††	2.83 ± 0.24	2.95 ± 0.20	3.54 ± 0.28	3.42 ± 0.37	3.58 ± 0.25	3.77 ± 0.24

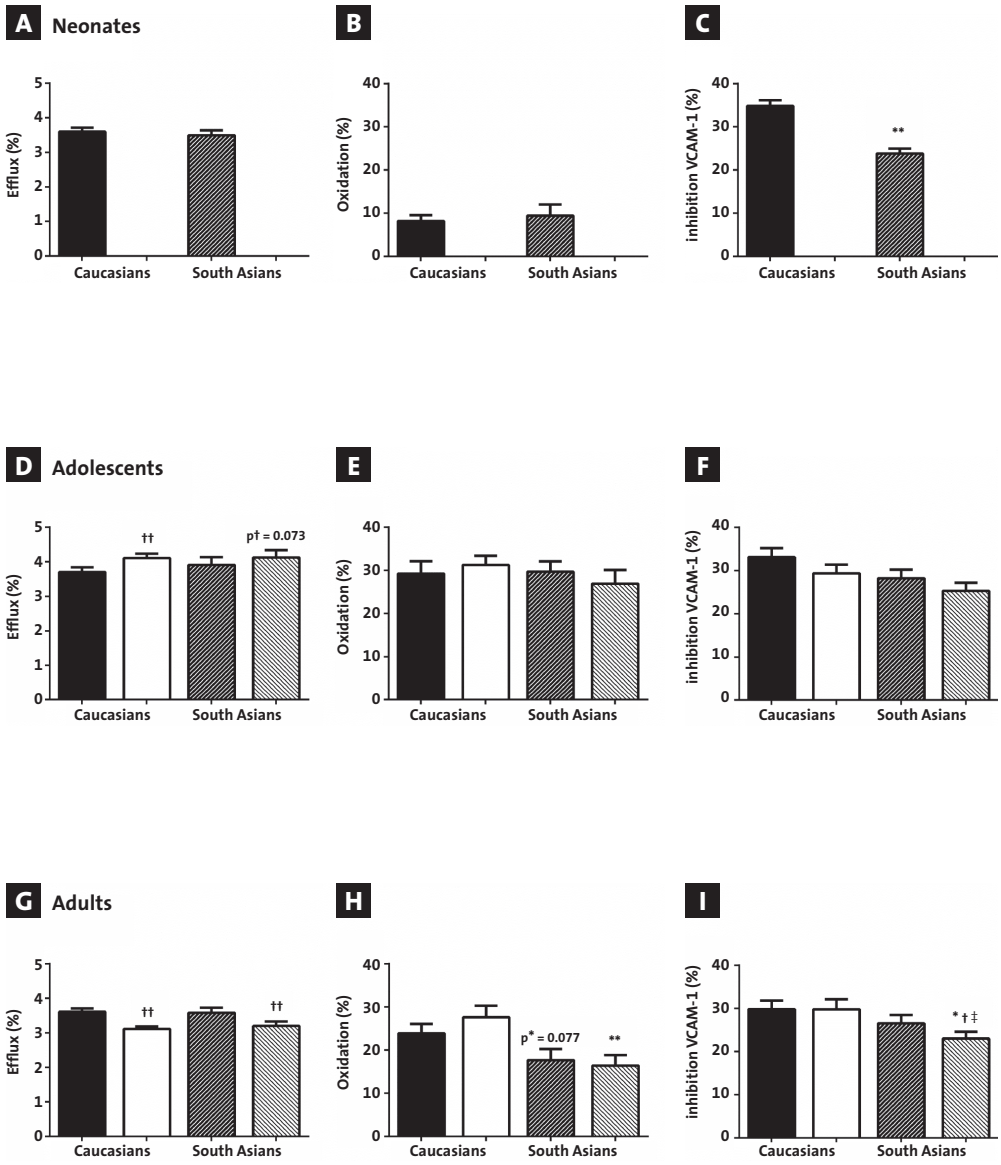

FIGURE 1 – HDL functionality in Caucasian (solid black) and South Asian (striped black) neonates, and in adolescent healthy and adult overweight Caucasian and South Asian men before (solid black and striped black, respectively) and after (solid white and striped white, respectively) a 5-day HCD and 8-day LCD, respectively. HDL function was determined as **A** **D** **G**) induction of cholesterol efflux from cholesterol-laden THP-1 cells, **B** **E** **H**) protection against oxidation of LDL, and **C** **F** **I**) protection of HUVECs against TNFα-induced inflammation as determined by VCAM-1 expression. Assays were performed as detailed in methods.

Data are presented as mean ± SEM. † p<0.05, †† p<0.005 within group *vs.* before diet. * p<0.05, ** p<0.005 *vs.* Caucasians. ‡ p<0.05 diet effect *vs.* Caucasians.

Anti-inflammatory capacity is impaired in South Asian neonates and is negatively affected by an 8-day LCD in South Asian adults only. The anti-inflammatory capacity of HDL was significantly lower in South Asian neonates (22.9 ± 0.7 *vs.* 35.9 ± 1.9%, p<0.00001), a difference that disappeared at adolescent and adult age, at least at baseline. A 5-day HCD had no impact on anti-inflammatory capacity. Remarkably, though, anti-inflammatory capacity was negatively affected by an 8-day LCD in adult South Asians only (-12.2 ± 4.3% (p=0.005) *vs.* +0.2 ± 4.2% (p=0.984)), resulting in a significantly lower anti-inflammatory capacity compared to adult Caucasians after the diet (23.0 ± 1.6% *vs.* 29.8 ± 2.3%, p=0.024). Anti-inflammatory capacity was significantly higher in Caucasian neonates compared to Caucasian adults (p=0.044). No other significant differences were observed for anti-inflammatory capacity at different ages.

Cholesterol efflux capacity positively correlates with HDL-cholesterol and phospholipid levels
Linear regression analysis showed a clear positive correlation between cholesterol efflux capacity and HDL-cholesterol levels for all ages at baseline (neonates: R^2=0.451, β=0.672, p<0.0001; adolescents: R^2=0.286, β=0.534, p=0.009; adults: R^2=0.201, β=0.448, p=0.032; **FIGURE 2)**. The same was true for cholesterol efflux capacity and HDL-phospholipid levels (neonates: R^2=0.277, β=0.527, p=0.004; adolescents: R^2=0.293, β=0.541, p=0.008; adults: R^2=0.176, β=0.419, p=0.047). In addition, cholesterol efflux capacity was positively correlated with HDL-cholesterol after the diet (adolescents: R^2=0.456, β=0.676, p=0.0004; adults: R^2=0.307, β=0.554, p=0.006) and for diet effect (delta HDL-cholesterol; adolescents: R^2=0.395, β=0.629, p=0.001; adults: R^2=0.240, β=0.489, p=0.018). Of note, correlations were pooled for South Asians and Caucasians. Similar correlations were observed per group, although these did not always reach statistical significance, probably due to a limited number of subjects.

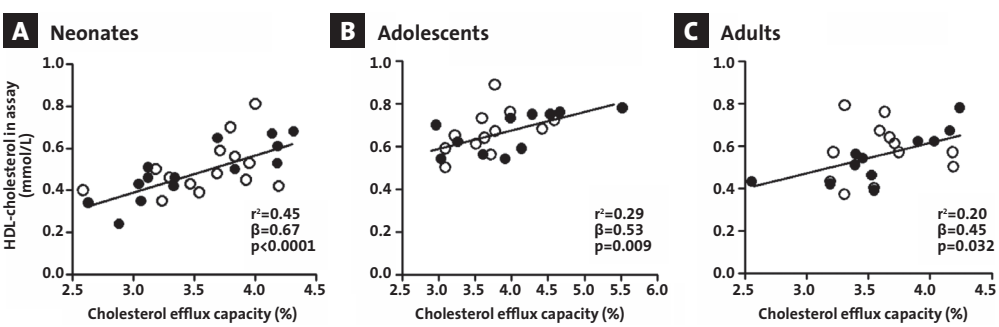

FIGURE 2 – Correlations of cholesterol efflux capacity with HDL-cholesterol. Cholesterol efflux capacity in relation to HDL-cholesterol levels in South Asian and Caucasian neonates **A**, and in adolescent healthy **B** and adult overweight **C** South Asian and Caucasian men, respectively. Correlations were determined by linear regression analysis. Caucasian subjects are depicted in open circles and South Asian subjects in closed circles. HDL-cholesterol values in this figure are after precipitation.

Anti-oxidative and anti-inflammatory capacity did not correlate with HDL-cholesterol levels nor with phospholipid levels for all ages (data not shown). As expected, HDL-cholesterol and HDL-phospholipid levels were positively correlated for all ages and all conditions (data not shown).

DISCUSSION

South Asians have an exceptionally high risk to develop CVD compared to Caucasians. A possible contributing factor might be dysfunctionality of HDL, which has been shown to be associated with cardiovascular disease in human studies. Interestingly, the current study showed that the ability of HDL to prevent oxidation of LDL was impaired in adult overweight South Asian males compared to matched Caucasians. At younger ages, the anti-oxidative function of HDL was still comparable between both ethnicities. In contrast, the anti-inflammatory capacity of HDL was markedly lower in South Asian neonates, a difference that was not present at adolescent and adult age. However, short-term caloric restriction at adult age significantly impaired anti-inflammatory capacity in South Asians only. Finally, the ability of HDL to induce cholesterol efflux was similar between South Asians and Caucasians, albeit that in both ethnic groups cholesterol efflux was increased after a 5-day HCD and reduced after an 8-day LCD.

HDL functionality between ethnic groups

Several recent studies have reported lower HDL-cholesterol levels in South Asians as compared to Caucasians (33-39), even already at birth (32). Surprisingly, little is known about HDL functionality in South Asians. To date only one cross-sectional, uncontrolled pilot study assessed the anti-oxidative capacity of HDL in 28 South Asian immigrants in the USA (50). They found dysfunctional HDL, as measured by a cell-free assay, in 50% of the participants, which was significantly correlated with carotid intima media thickness, a surrogate marker of atherosclerosis. However, no Caucasian control group was included, so no statements could be made on the ethnic implication of this percentage. In the present study, HDL-cholesterol levels were comparable between South Asians and Caucasians for all ages. For the neonates this was due to the fact that we matched the groups on HDL-C levels. For the adolescents and adults, this is probably due to lack of power to detect differences on HDL levels. However, despite equal HDL-cholesterol levels, we still observed several differences in HDL functionality between both ethnicities, suggesting that the HDL-cholesterol level was not a confounder in the current set-up. Recent evidence indeed suggests that HDL functionality might be affected independent of changes in plasma HDL-cholesterol levels and may be more important than plasma HDL-cholesterol concentrations with respect to prediction of the cardioprotective effect of HDL (23,24).

The oxidative modification of LDL is an important step in the initiation and progression of atherosclerosis as it results in enhanced uptake of LDL by macrophages and subsequent

foam cell formation. HDL is able to prevent the oxidation of LDL and hence its subsequent atherogenic actions by various mechanisms (22,51). In the present study, we observed that the ability of HDL to prevent oxidation of LDL was markedly lower in adult South Asian adult men compared to matched Caucasian men. Therefore, the reduced anti-oxidative capacity of HDL in South Asians may be involved in the increased risk of CVD in this ethnic group. Interestingly, the anti-oxidative capacity of HDL was only impaired in adult overweight South Asians and not at adolescent and neonatal age, suggesting that the ability of HDL to protect against LDL oxidation deteriorates with age. Indeed, for South Asians anti-oxidative capacity was significantly lower in adult compared to adolescent subjects (p=0.002), while for Caucasians this capacity was comparable between both age groups (p=0.160). On the underlying mechanism behind this deterioration we can only speculate, but this might be due to exogenous factors such as insulin resistance (IR) and T2D, which are also known to be considerably more prevalent in people of South Asian origin, especially at higher age. Indeed, it has been shown that IR and T2D are associated with a decrease in HDL-cholesterol levels, altered HDL composition and impaired HDL function (20). Elevated levels of free fatty acids and disturbed insulin action may contribute to low HDL-cholesterol in T2D by modifying lipolysis, apolipoprotein A-I production, as well as the activities of ATP-binding cassette transporter A1 (ABCA1) and lipid transfer (20). In the current study plasma insulin levels were significantly higher in the South Asian adults, pointing to IR. Interestingly, Mulder et al (45) showed that the anti-oxidative capacity of HDL from T2D patients is inversely related to skin autofluorescence, a non-invasive marker of tissue advanced glycation end products (AGEs), suggesting that impaired anti-oxidative capacity of HDL may contribute to tissue accumulation of AGEs and thereby to the development of long term diabetic complications. Thus, IR may affect the ability of HDL to prevent oxidation of LDL or, *vice versa,* HDL dysfunction may also be involved in the increased risk of T2D and diabetes-related complication in South Asians.

Another interesting finding is that anti-oxidative capacity of HDL was significantly impaired at neonatal age compared to adolescent and adult age for both South Asian and Caucasian subjects. This is in line with a study of Sreckovic et al (52) who compared fetal to maternal HDL functionality and found lower anti-oxidative capacity of fetal HDL, as measured by Cu^{2+}-induced oxidation. This was likely the consequence of a 7-fold lower HDL-associated PON1 protein content and activity in the fetal than in the maternal circulation, as PON1 is an HDL-associated enzyme that inhibits LDL and HDL oxidation. The underlying reason for the lower anti-oxidative function of HDL is unknown, but it is one of the reasons why neonates are more prone to oxidative stress than are young children and adults (53).

HDL has several anti-inflammatory effects, such as the ability to inhibit cytokine-induced expression of adhesion molecules on endothelial cells, and to control the adaptive immune system (51,54). Since suppression of immunity in neonates is important during pregnancy to prevent miscarriage, this may explain why we found higher anti-inflammatory capacity of HDL in neonates as compared to adults. Furthermore, the anti-inflammatory capacity of HDL was significantly lower in South Asian neonates (-36%). Interestingly, we previously found higher levels of the adhesion molecule E-selectin in cord blood of the same

cohort of South Asian neonates as compared to Caucasians (32). This is a marker of endothelial activation which may thus be the consequence of the lower anti-inflammatory capacity of HDL. We did not find a difference in anti-inflammatory capacity of HDL at adolescent and adult age, thus the opposite direction of effect as compared to anti-oxidative function. This could suggest that during development the lower anti-inflammatory functions in South Asians recovers. However, a basis for atherosclerosis and the concomitant risk of CVD is then probably already formed.

Finally, cholesterol efflux capacity did not differ between groups for all ages. The ability of HDL to stimulate cholesterol efflux involves transport of cholesterol from peripheral cells, particularly foam cells within atherosclerotic plaques, to the liver for final excretion into bile and faeces, i.e. the reverse cholesterol transport pathway (51,54). This ability of HDL therefore might reverse or prevent the formation of macrophage foam cells and is thus an important atheroprotective property, however, deterioration of this function is likely not involved in the high CVD risk of the South Asian population.

Response of HDL functionality to short-term dietary intervention

HDL functionality was also assessed in response to short-term dietary intervention in order to investigate ethnic differences upon dietary stimuli. Previous studies have demonstrated that HDL-cholesterol levels can be influenced by dietary intervention, with an increase in response to short-term high fat diets (55-57), and a reduction after low fat diets (29). Moreover, a 3-week high-fiber-low-fat diet and exercise intervention converted HDL from pro- to anti-inflammatory (29). Furthermore, data from our study group demonstrated a decrease in cholesterol efflux capacity of HDL after weight loss (31).

In the present study, a 5-day HCD increased HDL-cholesterol, whereas an 8-day LCD did not affect HDL-cholesterol levels and decreased HDL-phospholipids. Cholesterol efflux ability was enhanced in response to a 5-day HCD, and reduced after an 8-day LCD, which might be explained by the increase in HDL-cholesterol and phospholipid levels and decrease in phospholipids, respectively. Indeed, in both the adolescent group and adult group cholesterol efflux capacity was positively correlated with HDL-cholesterol and phospholipid levels **(FIGURE 2)**.

Interestingly, anti-inflammatory capacity was significantly impaired after an 8-day LCD only in South Asians. Hence, instead of being beneficial, caloric restriction appears to be detrimental to South Asians with respect to anti-inflammatory function of HDL. Possibly, this worsening of HDL anti-inflammatory capacity may only be present in the calorie-restricted state, returning to normal or even improving after weight loss and re-introduction of a normal diet. Indeed, our group previously assessed the short- and long-term effects of a 4-month LCD on low-grade inflammation in obese patients with T2D, and demonstrated that the beneficial effects on chronic inflammation became apparent only when patients were on a eucaloric diet, suggesting that severe caloric restriction at first increased cytokine production by adipose tissue macrophages and that the beneficial effects of weight loss became apparent only in the eucaloric state (58). Hence, perhaps the initial response to caloric restriction is worse in South Asians compared to Caucasians, but may normalize later

on. This may, at least in part, be due to the fact that South Asians have higher release of pro-inflammatory cytokines, such as interleukin-6 and tumor necrosis factor-α (TNF-α), by adipocytes, which may aggravate in case of caloric restriction (59,60). As mentioned above, one of the anti-inflammatory properties of HDL includes the ability to inhibit cytokine-induced adhesion molecule expression by the endothelium (61). Although the exact mechanism remains elusive, it has been postulated that HDL inhibits TNF-α-induced activation of the sphingosine kinase signal transduction pathway in endothelial cells, resulting in a decrease in sphingosine 1-phosphate production and adhesion protein expression. This also leads to reduced TNF-α-mediated activation of extracellular signal-regulated kinases and nuclear factor κβ (NF- κβ) cascade activity and ultimately to inhibition of endothelial inflammation (61). All and all, further research is needed to elucidate why South Asians respond differently compared to Caucasians to caloric restriction concerning HDL anti-inflammatory functionality

This study is not without limitations. The sample sizes are relatively small, which might limit generalization potential. On the other hand, subjects were their own controls (with respect to diet intervention), which increases power to detect relevant differences. Strengths of this study are the assessment of several HDL functions, in comparison to Caucasians, at three different age categories, and in response to dietary intervention.

In conclusion, we showed that adult, overweight South Asians have impaired anti-oxidative capacity of HDL, which is not yet present at a young age and, therefore, likely the consequence of environmental factors. Furthermore, anti-inflammatory capacity was reduced in South Asian neonates, and was significantly impaired in response to short-term caloric restriction in South Asian adults. These impairments in HDL functionality may contribute to the excess risk of CVD, and possibly of T2D, in people of South Asian origin. Therefore, future studies should be directed at developing treatment strategies that improve HDL functionality, and at investigating whether these strategies will lower cardiovascular risk in South Asian subjects.

REFERENCES

1 Balarajan R: Ethnic differences in mortality from ischaemic heart disease and cerebrovascular disease in England and Wales. *BMJ* 302:560-564, 1991.

2 Chaturvedi N, Fuller JH: Ethnic differences in mortality from cardiovascular disease in the UK: do they persist in people with diabetes? *J Epidemiol Community Health* 50:137-139, 1996.

3 Forouhi NG, Sattar N, Tillin T, et al. Do known risk factors explain the higher coronary heart disease mortality in South Asian compared with European men? Prospective follow-up of the Southall and Brent studies, UK. *Diabetologia* 49:2580-2588, 2006.

4 Wild SH, Fischbacher C, Brock A, et al. Mortality from all causes and circulatory disease by country of birth in England and Wales 2001-2003. *J Public Health (Oxf)* 29:191-198, 2007.

5 Anand SS, Yusuf S, Vuksan V, et al. Differences in risk factors, atherosclerosis, and cardiovascular disease between ethnic groups in Canada: the Study of Health Assessment and Risk in Ethnic groups (SHARE). *Lancet* 356:279-284, 2000.

6 Enas EA, Yusuf S, Mehta JL: Prevalence of coronary artery disease in Asian Indians. *Am J Cardiol* 70:945-949, 1992.

7 Joshi P, Islam S, Pais P, et al. Risk factors for early myocardial infarction in South Asians compared with individuals in other countries. *JAMA* 297:286-294, 2007.

8 Becker E, Boreham R, Chaudhury M, et al. *Health Survey for England 2004 Volume 1 The health of minority ethnic groups*. The Information Centre, 2006.

9 Bindraban NR, van Valkengoed IG, Mairuhu G, et al. Prevalence of diabetes mellitus and the performance of a risk score among Hindustani Surinamese, African Surinamese and ethnic Dutch: a cross-sectional population-based study. *BMC Public Health* 8:271, 2008.

10 McKeigue PM, Ferrie JE, Pierpoint T, et al. Association of early-onset coronary heart disease in South Asian men with glucose intolerance and hyperinsulinemia. *Circulation* 87:152-161, 1993.

11 Whiting DR, Guariguata L, Weil C, et al. IDF diabetes atlas: global estimates of the prevalence of diabetes for 2011 and 2030. *Diabetes Res Clin Pract* 94:311-321, 2011.

12 Assmann G, Schulte H, von EA, et al. High-density lipoprotein cholesterol as a predictor of coronary heart disease risk. The PROCAM experience and pathophysiological implications for reverse cholesterol transport. *Atherosclerosis* 124 Suppl:S11-S20, 1996.

13 Barter P, Gotto AM, LaRosa JC, et al. HDL cholesterol, very low levels of LDL cholesterol, and cardiovascular events. *N Engl J Med* 357:1301-1310, 2007.

14 Di AE, Sarwar N, Perry P, et al. Major lipids, apolipoproteins, and risk of vascular disease. *JAMA* 302:1993-2000, 2009.

15 Gordon DJ, Rifkind BM: High-density lipoprotein--the clinical implications of recent studies. *N Engl J Med* 321:1311-1316, 1989.

16 Sharrett AR, Ballantyne CM, Coady SA, et al. Coronary heart disease prediction from lipoprotein cholesterol levels, triglycerides, lipoprotein(a), apolipoproteins A-I and B, and HDL density subfractions: The Atherosclerosis Risk in Communities (ARIC) Study. *Circulation* 104:1108-1113, 2001.

17 Wilson PW, Abbott RD, Castelli WP: High density lipoprotein cholesterol and mortality. The Framingham Heart Study. *Arteriosclerosis* 8:737-741, 1988.

18 Movva R, Rader DJ: Laboratory assessment of HDL heterogeneity and function. *Clin Chem* 54:788-800, 2008.

19 Nofer JR, Kehrel B, Fobker M, et al. HDL and arteriosclerosis: beyond reverse cholesterol transport. *Atherosclerosis* 161:1-16, 2002.

20 Rohrer L, Hersberger M, von EA: High density lipoproteins in the intersection of diabetes mellitus, inflammation and cardiovascular disease. *Curr Opin Lipidol* 15:269-278, 2004.

21 von EA, Nofer JR, Assmann G: High density lipoproteins and arteriosclerosis. Role of cholesterol efflux and reverse cholesterol transport. *Arterioscler Thromb Vasc Biol* 21:13-27, 2001.

22 von EA, Hersberger M, Rohrer L: Current understanding of the metabolism and biological actions of HDL. *Curr Opin Clin Nutr Metab Care* 8:147-152, 2005.
23 Corsetti JP, Gansevoort RT, Sparks CE, et al. Inflammation reduces HDL protection against primary cardiac risk. *Eur J Clin Invest* 40:483-489, 2010.
24 deGoma EM, deGoma RL, Rader DJ: Beyond high-density lipoprotein cholesterol levels evaluating high-density lipoprotein function as influenced by novel therapeutic approaches. *J Am Coll Cardiol* 51:2199-2211, 2008.
25 Sharma M: Combination therapy for dyslipidemia. *Curr Opin Cardiol* 26:420-423, 2011.
26 Schwartz GG, Olsson AG, Abt M, et al. Effects of dalcetrapib in patients with a recent acute coronary syndrome. *N Engl J Med* 367:2089-2099, 2012.
27 Ansell BJ, Navab M, Hama S, et al. Inflammatory/antiinflammatory properties of high-density lipoprotein distinguish patients from control subjects better than high-density lipoprotein cholesterol levels and are favorably affected by simvastatin treatment. *Circulation* 108:2751-2756, 2003.
28 Navab M, Hama SY, Hough GP, et al. A cell-free assay for detecting HDL that is dysfunctional in preventing the formation of or inactivating oxidized phospholipids. *J Lipid Res* 42:1308-1317, 2001.
29 Roberts CK, Ng C, Hama S, et al. Effect of a short-term diet and exercise intervention on inflammatory/anti-inflammatory properties of HDL in overweight/obese men with cardiovascular risk factors. *J Appl Physiol* 101:1727-1732, 2006.
30 Van Lenten BJ, Hama SY, de Beer FC, et al. Anti-inflammatory HDL becomes pro-inflammatory during the acute phase response. Loss of protective effect of HDL against LDL oxidation in aortic wall cell cocultures. *J Clin Invest* 96:2758-2767, 1995.
31 Wang Y, Snel M, Jonker JT, et al. Prolonged caloric restriction in obese patients with type 2 diabetes mellitus decreases plasma CETP and increases apolipoprotein AI levels without improving the cholesterol efflux properties of HDL. *Diabetes Care* 34:2576-2580, 2011.
32 Boon MR, Karamali NS, de Groot CJ, et al. E-Selectin is Elevated in Cord Blood of South Asian Neonates Compared with Caucasian Neonates. *J Pediatr* 2011.
33 Ajjan R, Carter AM, Somani R, et al. Ethnic differences in cardiovascular risk factors in healthy Caucasian and South Asian individuals with the metabolic syndrome. *J Thromb Haemost* 5:754-760, 2007.
34 Chambers JC, Eda S, Bassett P, et al. C-reactive protein, insulin resistance, central obesity, and coronary heart disease risk in Indian Asians from the United Kingdom compared with European whites. *Circulation* 104:145-150, 2001.
35 Chandalia M, Abate N, Garg A, et al. Relationship between generalized and upper body obesity to insulin resistance in Asian Indian men. *J Clin Endocrinol Metab* 84:2329-2335, 1999.
36 Ehtisham S, Crabtree N, Clark P, et al. Ethnic differences in insulin resistance and body composition in United Kingdom adolescents. *J Clin Endocrinol Metab* 90:3963-3969, 2005.
37 McKeigue PM, Marmot MG, Syndercombe Court YD, et al. Diabetes, hyperinsulinaemia, and coronary risk factors in Bangladeshis in east London. *Br Heart J* 60:390-396, 1988.
38 McKeigue PM, Shah B, Marmot MG: Relation of central obesity and insulin resistance with high diabetes prevalence and cardiovascular risk in South Asians. *Lancet* 337:382-386, 1991.
39 Raji A, Gerhard-Herman MD, Warren M, et al. Insulin resistance and vascular dysfunction in nondiabetic Asian Indians. *J Clin Endocrinol Metab* 89:3965-3972, 2004.
40 Superko HR, Enas EA, Kotha P, et al. High-density lipoprotein subclass distribution in individuals of Asian Indian descent: the National Asian Indian Heart Disease Project. *Prev Cardiol* 8:81-86, 2005.

41 Bhalodkar NC, Blum S, Rana T, et al. Comparison of levels of large and small high-density lipoprotein cholesterol in Asian Indian men compared with Caucasian men in the Framingham Offspring Study. *Am J Cardiol* 94:1561-1563, 2004.
42 Johansson J, Carlson LA, Landou C, et al. High density lipoproteins and coronary atherosclerosis. A strong inverse relation with the largest particles is confined to normotriglyceridemic patients. *Arterioscler Thromb* 11:174-182, 1991.
43 van der Hoorn JW, de HW, Berbee JF, et al. Niacin increases HDL by reducing hepatic expression and plasma levels of cholesteryl ester transfer protein in APOE*3Leiden.CETP mice. *Arterioscler Thromb Vasc Biol* 28:2016-2022, 2008.
44 Friedewald WT, Levy RI, Fredrickson DS: Estimation of the concentration of low-density lipoprotein cholesterol in plasma, without use of the preparative ultracentrifuge. *Clin Chem* 18:499-502, 1972.
45 Mulder DJ, de Boer JF, Graaff R, et al. Skin autofluorescence is inversely related to HDL anti-oxidative capacity in type 2 diabetes mellitus. *Atherosclerosis* 218:102-106, 2011.
46 Annema W, Nijstad N, Tolle M, et al. Myeloperoxidase and serum amyloid A contribute to impaired in vivo reverse cholesterol transport during the acute phase response but not group IIA secretory phospholipase A(2). *J Lipid Res* 51:743-754, 2010.
47 Tietge UJ, Pratico D, Ding T, et al. Macrophage-specific expression of group IIA sPLA2 results in accelerated atherogenesis by increasing oxidative stress. *J Lipid Res* 46:1604-1614, 2005.
48 Nijstad N, de Boer JF, Lagor WR, et al. Overexpression of apolipoprotein O does not impact on plasma HDL levels or functionality in human apolipoprotein A-I transgenic mice. *Biochim Biophys Acta* 1811:294-299, 2011.
49 Tietge UJ, Nijstad N, Havinga R, et al. Secretory phospholipase A2 increases SR-BI-mediated selective uptake from HDL but not biliary cholesterol secretion. *J Lipid Res* 49:563-571, 2008.
50 Dodani S, Kaur R, Reddy S, et al. Can dysfunctional HDL explain high coronary artery disease risk in South Asians? *Int J Cardiol* 129:125-132, 2008.
51 HB G, Rao VS, Kakkar VV: Friend Turns Foe: Transformation of Anti-Inflammatory HDL to Proinflammatory HDL during Acute-Phase Response. *Cholesterol* 2011:274629, 2011.
52 Sreckovic I, Birner-Gruenberger R, Obrist B, et al. Distinct composition of human fetal HDL attenuates its anti-oxidative capacity. *Biochim Biophys Acta* 1831:737-746, 2013.
53 Gitto E, Pellegrino S, D'Arrigo S, et al. Oxidative stress in resuscitation and in ventilation of newborns. *Eur Respir J* 34:1461-1469, 2009.
54 Annema W, von EA: High-density lipoproteins. Multifunctional but vulnerable protections from atherosclerosis. *Circ J* 77:2432-2448, 2013.
55 Guay V, Lamarche B, Charest A, et al. Effect of short-term low- and high-fat diets on low-density lipoprotein particle size in normolipidemic subjects. *Metabolism* 61:76-83, 2012.
56 Tremblay AJ, Lamarche B, Guay V, et al. Short-term, high-fat diet increases the expression of key intestinal genes involved in lipoprotein metabolism in healthy men. *Am J Clin Nutr* 98:32-41, 2013.
57 Wadden D, Cahill F, Amini P, et al. Serum acylated ghrelin concentrations in response to short-term overfeeding in normal weight, overweight, and obese men. *PLoS One* 7:e45748, 2012.
58 Snel M, van Diepen JA, Stijnen T, et al. Immediate and long-term effects of addition of exercise to a 16-week very low calorie diet on low-grade inflammation in obese, insulin-dependent type 2 diabetic patients. *Food Chem Toxicol* 49:3104-3111, 2011.
59 Peters MJ, Ghouri N, McKeigue P, et al. Circulating IL-6 concentrations and associated anthropometric and metabolic parameters in South Asian men and women in comparison to European whites. *Cytokine* 61:29-32, 2013.
60 Petersen KF, Dufour S, Feng J, et al. Increased prevalence of insulin resistance and non-alcoholic fatty liver disease in Asian-Indian men. *Proc Natl Acad Sci U S A* 103:18273-18277, 2006.
61 Xia P, Vadas MA, Rye KA, et al. High density lipoproteins (HDL) interrupt the sphingosine kinase signaling pathway. A possible mechanism for protection against atherosclerosis by HDL. *J Biol Chem* 274:33143-33147, 1999.

BROWN ADIPOSE TISSUE VOLUME IS MARKEDLY LOWER IN HEALTHY LEAN ADOLESCENTS FROM SOUTH ASIAN COMPARED TO WHITE CAUCASIAN ORIGIN

MARIËTTE R. BOON*
LEONTINE E.H. BAKKER*
RIANNE A.D. VAN DER LINDEN
LENKA PEREIRA ARIAS-BOUDA
JAN B. VAN KLINKEN
FRITS SMIT
HEIN J. VERBERNE
J. WOUTER JUKEMA
JOUKE T. TAMSMA
LOUIS M. HAVEKES
WOUTER D. VAN MARKEN LICHTENBELT
INGRID M. JAZET
PATRICK C.N. RENSEN

* Both authors contributed equally

The Lancet Diabetes & Endocrinology 2014; 2: 210-217.

13

ABSTRACT

South Asians have an exceptionally high risk of developing type 2 diabetes mellitus (T2DM) compared to white Caucasians. Though the underlying cause is still poorly understood, it is assumed that an ethnic susceptibility towards a disturbed energy metabolism might be present. Brown adipose tissue (BAT) has emerged as an important player in energy metabolism by combusting fatty acids and glucose towards heat. We, therefore, hypothesized that a low total BAT activity might underlie the susceptibility for T2DM in South Asians. BAT volume and activity were measured in healthy lean adolescents (mean age 24•1±0•8 years) from South Asian (n=12) and white Caucasian (n=12) origin, matched for BMI, using cold-induced 18F-FDG-PET-CT-scans. Furthermore, resting energy expenditure (REE), non-shivering thermogenesis (NST) and serum parameters were assessed. Thermoneutral REE was lower in South Asian compared to white Caucasian adolescents (-32%, P=0•001). Upon cold exposure, the shiver temperature of South Asians was higher (+2•0°C, P=0•007). Furthermore, cold exposure significantly increased NST in white Caucasians (+20%, P<0•0001), but not in South Asians. Though the SUVmax and SUVmean of 18F-FDG in BAT did not differ, total BAT volume was markedly lower in South Asians (-34%, P=0•04). Taken the subjects together, BAT volume correlated positively with basal REE (ß=0.44; P=0•04). In conclusion, healthy South Asian adolescents have lower REE, NST, as well as lower BAT volume compared to matched white Caucasians. This might underlie their high susceptibility to develop metabolic disturbances, such as obesity and T2DM. Future studies should focus on developing novel strategies to increase BAT volume and activity.

INTRODUCTION

South Asian individuals originate from the Indian subcontinent and constitute a fifth of the world's population. The risk of development of type 2 diabetes and its related complications is very high in native and migrant south Asians compared with people of white Caucasian descent, and prevalence is increasing.[1] Moreover, type 2 diabetes occurs at a younger age and lower BMI in south Asians than Caucasians,[2,3] and the risk of complications related to diabetes is increased in this group.[4,5] The underlying cause of this excess risk is incompletely understood, but might involve a common disadvantageous metabolic phenotype, consisting of central obesity, insulin resistance, and dyslipidaemia.[6,7] A common assumption is that ethnic susceptibility towards a disturbed energy homoeostasis (eg, reduced oxidation of glucose and fatty acids by mitochondria) underlies this phenotype.[8]

Recently, brown adipose tissue (BAT) has been identified to have a role in energy homoeostasis in humans.[9–12] In contrast to white adipose tissue, BAT burns triglycerides and glucose to generate heat through a process called mitochondrial uncoupling.[13] A main stimulator for BAT activation is cold and repeated cold exposure leads to recruitment of BAT in healthy humans.[14] BAT volume and activity—as assessed after exposure to cold by use of ^{18}F-fluorodeoxyglucose (^{18}F-FDG) PET CT scans—are inversely related to BMI and percentage of body fat in adult humans, suggesting an inverse association between BAT and obesity.[11,15,16] Besides a clear role for BAT in triglyceride metabolism,[17] this tissue is also thought to contribute to glucose homoeostasis, especially in resting conditions when glucose use by skeletal muscle is minimal.[18] Notably, BAT seems to contribute to non-shivering thermogenesis[12,16] and fully activated BAT in humans has been estimated to contribute up to 15–20% of total energy expenditure.[13]

Because BAT is involved in total energy expenditure and clearance of serum triglycerides and glucose, thereby protecting against metabolic disturbances, we postulated that a low BAT volume or activity might underlie the disadvantageous metabolic phenotype and susceptibility to type 2 diabetes in south Asians. Therefore, we investigated resting energy expenditure and BAT volume and activity in young healthy lean south Asian men and matched white Caucasians (hereafter referred to as Caucasians), by use of a ventilated hood technique and cold-induced ^{18}F-FDG PET CT scans. In addition, we examined the effect of cold exposure on non-shivering thermogenesis, thermoregulation, and plasma lipid levels.

METHODS

Study design and participants

We enrolled Dutch south Asian participants (ie, individuals with two south Asian parents born in the Netherlands) and matched Dutch Caucasian participants at The Rijnland Hospital in Leiderdorp in the Netherlands. We recruited eligible healthy men aged 18–28 years with a lean body type (BMI <25 kg/m^2) via local advertisements. Participants under-

TABLE 1 - **Characteristics of study participants**

	Caucasians (n=12)	South Asians (n=12)	*P* value*
Age, years	24·6 (2·8)	23·6 (2·8)	0·39
Height, m	1·85 (0·04)	1·74 (0·06)	<0·0001
Weight, kg	75·1 (7·2)	65·0 (8·5)	0·0051
BMI, kg/m^2	22·0 (1·6)	21·5 (2·0)	0·50
Waist circumference, cm	84 (5·1)	83 (7·7)	0·80
Hip circumference, cm	96 (3·5)	89 (5·7)	0·0041
Waist-to-hip ratio	0·88 (0·04)	0·93 (0·04)	0·0047
Fat mass, %	18·3% (5·0)	23·9% (5·0)	0·0123
Fat mass, kg	13·9 (4·3)	15·8 (4·6)	0·31
Lean body mass, %	77·6% (4·8)	72·1% (4·7)	0·0107
Lean body mass, kg	58·5 (6·0)	46·8 (5·1)	<0·0001
Bone mineral content, %	4·1% (0·2)	4·0% (0·4)	0·49
Bone mineral mass, kg	3·1 (0·3)	2·6 (0·3)	0·0008

Data are mean (SD). *Unpaired *t* test.

went medical screening to obtain their medical history and a physical examination, blood chemistry tests, and an oral glucose tolerance test to exclude individuals with type 2 diabetes according to the American Diabetes Association 2010 criteria. Other exclusion criteria were rigorous exercise (>10 h of exercise per week), smoking, and recent bodyweight change (>3 kg weight gain or loss within 3 months before enrolment). Participants were matched for BMI with a pairwise approach. The study was approved by the Medical Ethical Committee of the Leiden University Medical Center and undertaken in accordance with the principles of the revised Declaration of Helsinki. All volunteers provided written informed consent.

Procedures

We assessed participants in the morning after a 10 h overnight fast and after 24 h without exercise. Participants wore standardised clothing, consisting of a T shirt and boxer shorts. We determined body composition by means of dual-energy x-ray absorptiometry (iDXA, GE Healthcare, UK). We inserted a cannula in the left antecubital vein for blood sampling and injection of ^{18}F-FDG. The appendix contains further details on study techniques.

To activate BAT, we applied two water perfused cooling mattresses (Blanketrol III, Cincinnati Sub-Zero Products, Cincinnati, OH, USA).[16] During the procedure participants stayed in a clinical examination room. The protocol started with a baseline period of 1 h in thermoneutral condition, after which participants were exposed to mild cold. Because the onset temperature of shivering is very variable and dependent on the individual (eg, because of differences in body composition),[13] we used an individualised cooling protocol to ensure maximum non-shivering thermogenesis, and thus a maximum level of BAT activity, for each participant. Cooling started at 32°C and temperature was gradually decreased until shivering occurred. Temperature was then raised by 3–4°C and the cooling

TABLE 2 - **Cardiovascular parameters and fasting serum levels in thermoneutral and cold-induced conditions**

	Caucasians (n=12)		
	Thermoneutral	**Cold-induced**	**Within-group change (95% CI); *P* value**
Systolic blood pressure, mm Hg	135 (11)	143 (13)	6% (–1 to 13); *P*=0·082
Diastolic blood pressure, mm Hg	77 (6)	84 (6)	10% (3 to 16); *P*=0·0051
Heart rate, beats per min	64 (10)	57 (10)	–9% (–16 to –2); *P*=0·0172
Glucose, mmol/L	4·17 (0·26)	4·32 (0·29)	4% (–1 to 9); *P*=0·213
Triglyceride concentration, mmol/L	0·78 (0·58-0·96)	0·92 (0·69-1·32)	27% (6 to 48); *P*=0·0142
Free fatty acid concentration, mmol/L	0·66 (0·30)	0·99 (0·29)	50% (34 to 66); *P*<0·0001
Free fatty acid concentration, mmol/L per $kg_{fatmass}$	0·052 (0·035)	0·078 (0·034)	50% (34 to 66); *P*<0·0001

Data are mean (SD) or median (IQR), unless otherwise stated. All *P* values are based on a mixed model.
**P* value for cooling effect in the south Asian group vs Caucasian group.
‡P=0·0046 for cold-induced value in the south Asian group vs the Caucasian group.

TABLE 3- **Indirect calorimetry in thermoneutral and cold-induced conditions**

	Caucasians (n=12)		
	Thermoneutral	**Cold-induced**	**Within-group change (95% CI); *P* value**
Resting energy expenditure, kcal per day	1689 (193)	2027 (471)	20% (9 to 31); *P*=0·0011
Lipid oxidation, g/min	0·063 (0·024)	0·092 (0·040)	46% (24 to 70); *P*<0·0001
Glucose oxidation, g/min	0·151 (0·057)	0·141 (0·037)	–6% (–23 to 12); *P*=0·277
Respiratory quotient	0·85 (0·06)	0·82 (0·04)	–4% (–6 to –1); *P*=0·0303

Data are mean (SD), unless otherwise stated. All *P* values are based on a mixed model.
**P* value for cooling effects in the south Asian group vs Caucasians.
†*P*=0·0008 for thermoneutral value in the South Asian group vs Caucasian group.
‡*P*<0·0001 for cold-induced value in the South Asian group vs Caucasian group.
§*P*=0·0058 for cold-induced value in the South Asian group vs Caucasian group.
¶*P*=0·0285 for thermoneutral value in the South Asian group vs Caucasian group.

South Asians (n=12)			Between-group difference in cooling effect	
Thermoneutral	**Cold-induced**	**Within-group change (95% CI); *P* value**	**Difference (95% CI)**	***P* value***
126 (18)	125 (13)‡	0% (–6 to 6); *P*=0·759	8 (–3 to – 20)	0·141
73 (9)	79 (8)	9% (3 to 16); *P*=0·0093	1 (–6 to –8)	0·810
62 (8)	54 (8)	–12% (–19 to –5); *P*=0·0027	2 (–5 to –8)	0·620
4·30 (0·42)	4·26 (0·58)	–1% (–7 to 5); *P*=0·698	0·20 (–0·15 to –0·54)	0·244
0·77 (0·57–0·82)	0·90 (0·76-0·96)	34% (13 to 56); *P*=0·0029	–0·05 (–0·29 to –0·18)	0·624
0·88 (0·39)	0·97 (0·37)	10% (–2 to 23); *P*=0·099	0·24 (0·08 to –0·39)	0·0046
0·069 (0·037)	0·075 (0·035)	10% (–2 to 23); *P*=0·099	0·020 (0·010 to –0·030)	0·0046

South Asians (n=12)			Between-group difference in cooling effect	
Thermoneutral	**Cold-induced**	**Within-group change (95% CI); *P* value**	**Difference (95% CI)**	***P* value***
1297 (123)†	1462 (127)‡	13% (–1% to 27%); *P*=0·072	171 (–89 to –430)	0·186
0·049 (0·009)	0·062 (0·014)§	26% (–7% to 46%); *P*=0·072	0·016 (–0·004 to –0·036)	0·119
0·114 (0·014)¶	0·111 (0·036)	–0·3% (–25% to 24%); *P*=0·804	–0·011 (–0·046 to –0·025)	0·538
0·84 (0·02)	0·82 (0·04)	–2% (–6% to 1%); *P*=0·128	–0·01 (–0·05 to –0·03)	0·577

TABLE 4 - **Thermoregulation in thermoneutral and cold-induced conditions**

	Caucasians (n=12)		
	Thermoneutral	**Cold-induced**	***P* value†**
Shiver temperature	...	8·9 (1·5)	...
Cooling temperature	...	19·8 (2·5)	...
Core temperature	36·8 (0·2)	36·6 (0·3)	0·130
Skin temperature	33·1 (0·5)	28·6 (1·0)	<0·0001
Proximal skin temperature	34·4 (0·4)	30·8 (1·0)	<0·0001
Distal skin temperature	31·8 (0·9)	26·3 (1·4)	<0·0001
Core mean skin temperature gradient	3·6 (0·4)	7·9 (0·9)	<0·0001
Core distal skin temperature gradient	4·8 (0·7)	10·0 (1·4)	<0·0001

Data are mean (SD) in degrees centigrade.
**P* value for between-group difference in cooling effects, or difference in shiver temperature and cooling temperature based on an unpaired *t* test.
†*P* value for withingroup change from thermoneutral to cold-induced condition.
All *P* values are based on a mixed model, except for shiver temperature and cooling temperature (unpaired *t* test).

period of 2 h was started (defined as t_{cold}=0 min). If shivering occurred, the temperature was raised by 1°C until shivering stopped. We detected shivering visually or it was reported by participants. After 1 h of cooling (t_{cold}=60 min), we injected 2 MBq/kg ^{18}F-FDG intravenously. To exclude artefacts of muscle activity, participants were instructed to lie still. We collected venous blood when participants were thermoneutral and when they were in a cold-induced condition (t_{cold}=110 min) and did indirect calorimetry with a ventilated hood (Oxycon Pro, CareFusion, Germany) in thermoneutral condition and t_{cold} of 80–110 min. After 2 h of cooling (tcold=120 min) we did ^{18}F-FDG PET CT imaging to quantify BAT volume an activity.

Imaging was done with a PET CT scanner (Gemini TF PET CT, Philips, Netherlands) as described previously (appendix).[11] Imaging started with a low-dose CT scan (effective dose 2 mSv), immediately followed by a PET scan. We used the CT scan for attenuation correction and localisation of the ^{18}F-FDG uptake sites. Both image sets were reconstructed in transaxial, coronal, and sagittal images with a slice thickness of 4 mm. PET CT images were interpreted by a nuclear medicine physician (LPAB) and a researcher (MRB or RADL), who were masked to patient group, with dedicated software (Hermes Hybrid Viewer, Hermes Medical Solutions, Sweden). We quantified BAT activity and detectable volume in the region of interest by auto-contouring the BAT areas with a set threshold (standardised uptake value [SUV] of 2·0 g/mL).

To register temperature changes, we measured core body temperature in the small intestine at 1 min intervals with an ingestible telemetric capsule (Jonah, BMedical, Australia). Measurement of core temperature did not work in two participants (one in each group). We also measured skin temperature at 1 min intervals by wireless iButtons (Maxim, USA) placed at different positions on the skin.[19]

We report total detectable BAT volume in mL and BAT activity in terms of SUV (the ratio

South Asians (n=12)			Between-group difference in cooling effect	
Thermoneutral	**Cold-induced**	***P* value†**	**Difference (95% CI)**	***P* value***
...	10·9 (1·8)	...	...	0·0067
...	18·7 (2·2)	...	...	0·271
36·6 (0·3)	36·8 (0·2)	0·128	–0·4 (–0·7 to –0·0)	0·0339
33·4 (0·7)	28·8 (1·0)	<0·0001	0·1 (-0·7 to -0·8)	0·836
34·4 (0·4)	31·0 (1·1)	<0·0001	–0·2 (–1·0 to –0·5)	0·535
32·5 (1·3)	26·6 (1·5)	<0·0001	0·4 (–0·7 to –1·5)	0·482
3·2 (1·0)	8·1 (1·1)	<0·0001	–0·5 (–1·4 to –0·6)	0·643
4·1 (1·5)	10·2 (1·5)	<0·0001	–0·8 (–2·2 to –0·6)	0·236

of activity in kBq/mL within the region of interest and the injected activity [kBq] per body-weight [g]). We established maximum SUV (SUV_{max}) in g/mL and the average SUV (SUV_{mean}) in g/mL within the volume of interest. We assessed energy expenditure, respiratory quotient, and rates of substrate oxidation every 1 min as described previously.[20,21] We measured skin temperatures according to the 14 point International Organization for Standardization method (appendix).[19]

We used enzymatic kits to measure serum triglyceride concentrations (Roche Diagnostics, Netherlands), serum glucose concentrations (Instruchemie, Delfzijl, Netherlands) and free fatty acid concentrations (Wako Chemicals, Germany).

Statistical analysis

Normally distributed data are shown as mean (SD) and non-normally distributed data are shown as median (IQR). We applied a mixed-effects model to assess mean differences before and after cold exposure within and between groups, and to determine differences in the effect of cold exposure. We modelled groups and interventions as fixed effects and modelled participant-specific deviances from the group mean as random effects. We used unpaired *t* tests to compare baseline characteristics and BAT parameters between groups. We used non-parametric tests (Wilcoxon signed-rank test for within-group analyses and Mann-Whitney tests for between-group analyses) when appropriate. We used ANCOVA to correct parameters for lean body mass. Linear regression analyses were done to identify correlations between variables. The significance level was set at $p<0·05$. We did not adjust for multiple testing. All statistical analyses were done with SPSS for Windows version 20.0.

This study is registered with the Netherlands Trial Register, number 2473.

RESULTS

Between March 1, 2013, and June 1, 2013, we enrolled 12 South Asian participants and 12 Caucasian participants. Mean age and BMI values did not differ between groups, but south Asian participants were shorter and lighter than were Caucasian participants **(TABLE 1).** The percentage of fat mass was higher in south Asians than Caucasians and, consequently, the percentage of lean body mass was lower. Additionally, the waist-to-hip ratio was higher in south Asians than Caucasians. One Caucasian participant developed hyperventilation after ^{18}F-FDG administration, and was excluded from all cold-induced and BAT comparisons.

Cold exposure increased diastolic blood pressure and decreased heart rate in both groups **(TABLE 2)**. Cold exposure did not seem to affect systolic blood pressure, but systolic

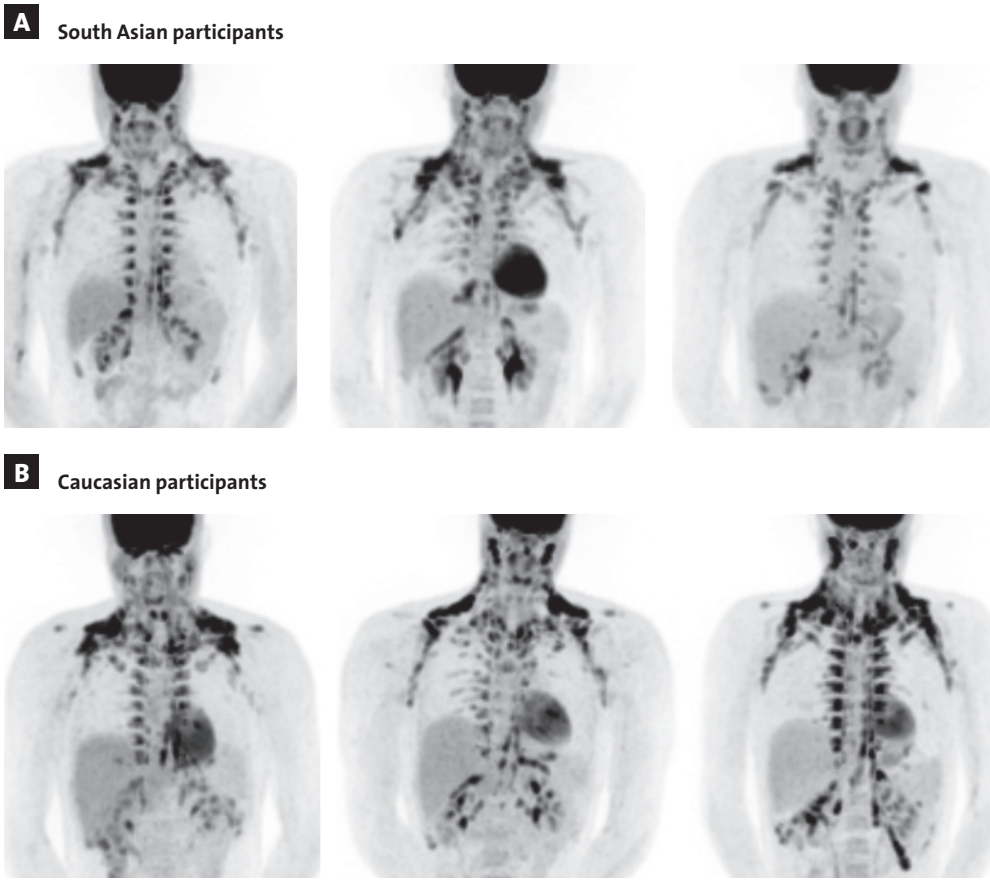

FIGURE 1 - **Brown adipose tissue activity as assessed by ^{18}F-fluorodeoxyglucose PET CT scans in three representative healthy young south Asian men A and matched Caucasians B.** Black areas show uptake of ^{18}F-fluorodeoxyglucose in brown adipose tissue, and other glucose-consuming tissues such as brain and heart, and to a lesser degree liver. Kidney calyces and ureters are visible due to clearance of the tracer.

blood pressure during cold exposure was significantly lower in south Asian participants than in Caucasian participants **(TABLE 2)**.

Fasting thermoneutral glucose and lipid concentrations did not differ between groups **(TABLE 2)**. Cooling did not affect serum glucose concentrations, but increased serum triglyceride concentrations in both groups. Of note, a significant cold-induced increase in serum free fatty acid concentrations was present in Caucasian participants, but not in south Asian participants. The ethnic difference in cold-induced free fatty acid release was even more pronounced after dividing serum free fatty acid levels by total fat mass, which is the main source of serum free fatty acid **(TABLE 2)**.

Before cooling, resting energy expenditure was 32% lower in south Asians than it was in Caucasians **(TABLE 3)**. This difference persisted after correction for lean body mass with ANCOVA (intercept 177 kcal per day [SD 173] vs 290 kcal per day [215]; P=0·0316; appendix). During cold exposure, non-shivering thermogenesis increased significantly in Caucasians (by 20%; 1689 kcal per day [SD 193] vs 2027 kcal per day [471]; p<0·0001), but not in south Asians (by 13%; 1297 kcal per day [123] kcal per day vs 1462 [127]; P=0·09) (appendix). Furthermore, cold exposure significantly increased lipid oxidation only in Caucasians,

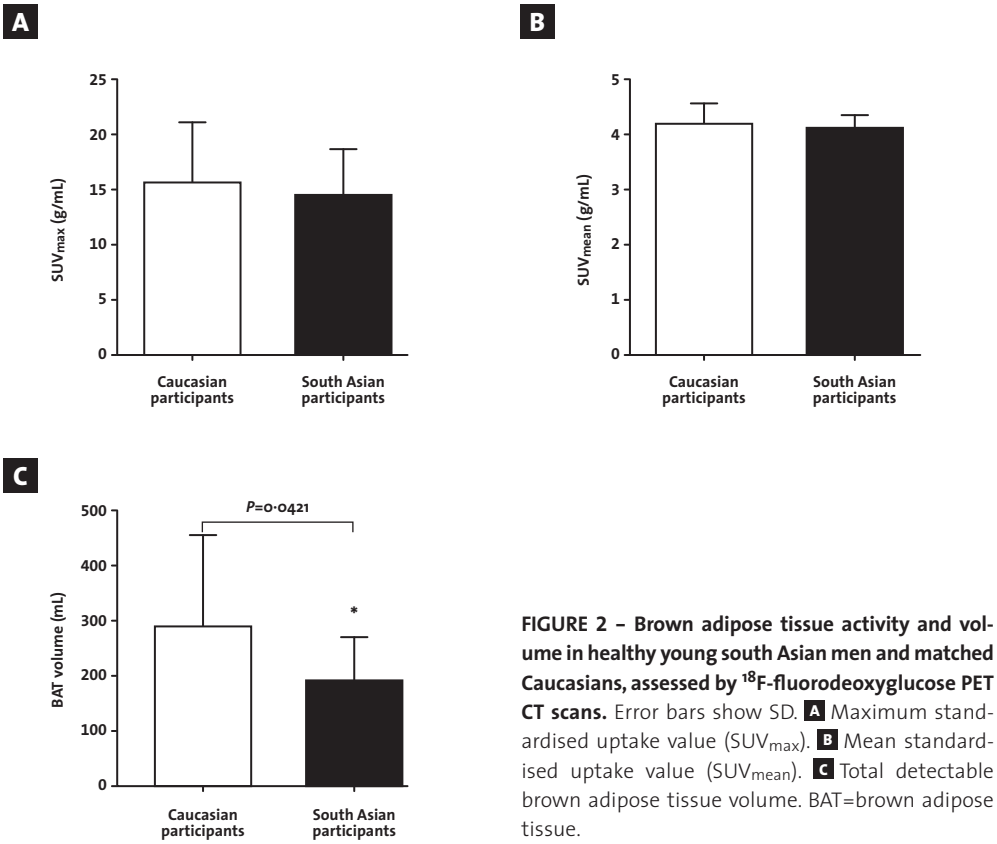

FIGURE 2 – Brown adipose tissue activity and volume in healthy young south Asian men and matched Caucasians, assessed by ^{18}F-fluorodeoxyglucose PET CT scans. Error bars show SD. **A** Maximum standardised uptake value (SUV_{max}). **B** Mean standardised uptake value (SUV_{mean}). **C** Total detectable brown adipose tissue volume. BAT=brown adipose tissue.

whereas glucose oxidation was not affected in either group **(TABLE 3)**. In line with this finding, cold exposure significantly decreased respiratory quotient in Caucasians only **(TABLE 3)**. Despite an increased fat mass percentage, the temperature at which shivering started was higher in south Asians than it was in Caucasians **(TABLE 4)**. Due to individual fine-tuning of the environmental temperature during non-shivering thermogenesis, mean environmental cooling temperature did not differ between groups during the second half of cooling **(TABLE 4)**. Core temperature was not affected by cold exposure. Mean overall, proximal, and distal skin temperatures decreased substantially to much the same extent in both groups **(TABLE 4)**. Consequently, core distal and core mean skin temperature gradients were significantly higher during cooling, suggesting an insulative response in south Asian and Caucasian participants.

In 22 (96%) of 23 assessable participants, active BAT was detected by ^{18}F-FDG uptake in the classic regions for this tissue **(FIGURE 1)**.[15] The only participant who did not have cold-induced BAT activity was Caucasian and also had the lowest resting energy expenditure in that group. SUV_{max} and SUV_{mean} in the volume of interest with metabolically active BAT did not differ between south Asian and Caucasian participants **(FIGURE 2)**. Notably, detectable BAT volume was substantially lower in south Asians (188 mL [SD 81]) than it was in Caucasians (287 mL [169]; difference –34%, P=0·04), as shown in a representative sample of patients in **FIGURE 1**. Linear regression analysis showed a clear positive correlation between SUVmax and BAT volume **(FIGURE 3)**. Furthermore, thermoneutral serum free fatty acid concentration correlated with BAT volume in Caucasian participants (R^2=0·49, ß=0·70, P=0·02), but not in south Asian participants (R^2=0·0009, ß=0·03, P=0·97). Thermoneutral resting energy expenditure did not correlate with BAT volume in individual groups. However,

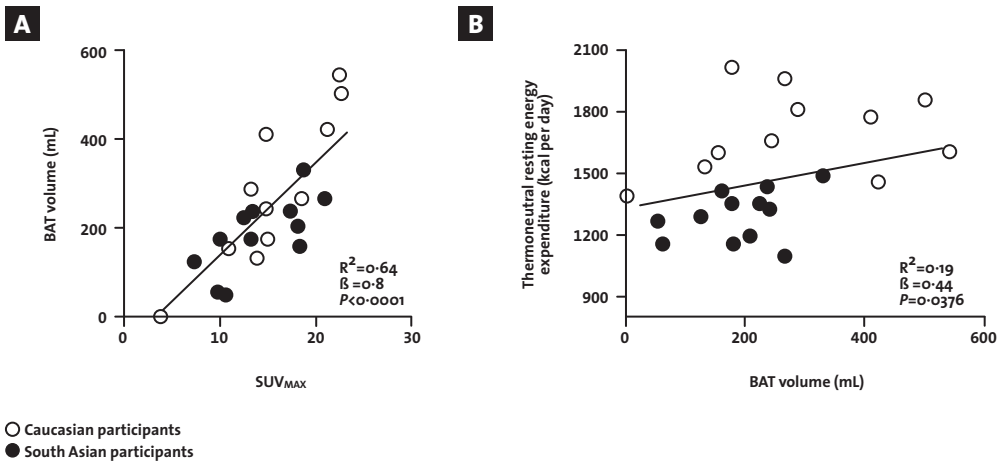

FIGURE 3 – Correlations with brown adipose tissue. BAT volume in relation to SUV_{max} **A** and thermoneutral resting energy expenditure **B**. Correlations were determined with linear regression analysis. BAT=brown adipose tissue. SUV_{max}=maximum standardised update of ^{18}F-fluorodeoxyglucose.

with pooling of all participants, there was a weak but significant positive association between thermoneutral resting energy expenditure and BAT volume (R^2=0·19, ß=0·44, P=0·038; **FIGURE 3)**, strongly suggesting that BAT is involved in total energy metabolism.

DISCUSSION

In our study, healthy, young, lean south Asian participants had lower resting energy expenditures than did equivalent Caucasians. Notably, the detectable volume of metabolically active BAT, which has previously been shown to significantly contribute to energy metabolism,[11,15] was substantially lower in south Asian participants than Caucasians. These findings were corroborated by an increased shiver temperature and lower cold-induced non-shivering thermogenesis in south Asians compared with Caucasians.

We detected BAT in 96% of assessable participants, which corresponds to the proportions noted in previous studies (Panel).[11,23] Moreover, as reported previously,[13,23] cold exposure in Caucasian participants resulted in increased serum free fatty acid concentrations, lipid oxidation, systolic blood pressure, and non-shivering thermogenesis (which aims to prevent a drop in core body temperature). In south Asians, all of these responses were less pronounced. Our previous study[14] suggested that BAT, and not muscle, is responsible for nonshivering thermogenesis via mitochondrial uncoupling. Lean participants with detectable BAT activity have significantly higher non-shivering thermogenesis than those without detectable activity.[12] Therefore, less BAT volume might underlie the smaller increase in nonshivering thermogenesis in south Asians; however, we did not identify a correlation between BAT volume and non-shivering thermogenesis, which has been shown previously,[12,16,24] albeit not consistently.[11,25]

Because cold-induced increases in lipolysis and systolic blood pressure are mediated by sympathetic activation, the lower response in south Asians might be attributable to a lower cold-induced sympathetic activation. We cannot rule out the possibility that this change was attributable to the fact that south Asians were initially cooled from a somewhat higher initial shiver temperature, resulting in less sympathetic outflow. However, SUV_{max} and SUV_{mean} did not differ between groups, suggesting that BAT could be equally stimulated in all individuals by cold exposure. Thus, signs of lower sympathetic activation were only present in the white adipose tissue depot and the vasculature, and not in BAT. This finding can be explained because sympathetic outflow neurons towards various organs derive from different brain regions.[26] A lower sympathetic response in south Asians might, at least in part, underlie their lower resting energy expenditure, because the reduced liberation of free fatty acids from white adipose tissue in plasma could have lowered the availability of free fatty acids for combustion by BAT, resulting in lower fat oxidation. Future studies would be needed to investigate a potentially different (organspecific) sympathetic response in south Asians and the potential link with resting energy expenditure.

South Asians had a significantly increased shivering temperature on cold exposure,

despite their overall increased total percentage of fat mass compared with Caucasians. Conversely, obese participants have lower shivering temperatures than do lean participants because of increased insulation.[16] An impaired capacity of BAT to contribute to total heat production might underlie the accelerated action of the muscles to produce heat by shivering in south Asians. This assumption is supported by a study of Ouellet and colleagues[10] in which participants with high BAT volumes had reduced rates of shivering during cooling. However, we cannot exclude the possibility that the increased shivering temperature in south Asians could, at least in part, be influenced by their small body size and lower lean body mass.

It could be argued that low energy metabolism in south Asians is not be solely attributable to decreased BAT volume but also because of diminished oxidative metabolism in muscle. We obtained muscle biopsies from the same participants as in this study before and after a short-term high-fat diet challenge, and did not observe differences in skeletal muscle insulin signalling or expression of genes involved in oxidative phosphorylation and mitochondrial biogenesis.[27] Furthermore, food intake and levels of physical activity did not differ between south Asians and Caucasians. Thus, the lower resting energy expenditure which we found in south Asians is probably not a consequence of a lower food intake or lower levels of physical activity.

The question remains as to what mechanisms underlie the decreased BAT volume in south Asians. Because this decrease is noted in healthy young adults without differences in the degree of ^{18}F-FDG uptake, as shown by equivalent SUV_{max} and SUV_{mean} values, a defect could have arisen in BAT differentiation. However, ^{18}F-FDG uptake only represents glucose uptake by the tissue and not metabolism itself. Therefore, a potential dysfunction in oxidative metabolism in the tissue cannot be excluded and should be investigated further, for example with an ^{11}C-acetate tracer as described previously[10] or by study of BAT biopsies. The underlying cause of lower BAT volume in south Asians might be genetic (ie, blunted expression of signalling molecules involved in BAT differentiation), environmental (ie, clothing or heating), or a combination of the two.

Our study had limitations. Although our group size was in line with several landmark BAT studies[9,11] and provided sufficient power to identify differences in detectable BAT volume between south Asians and Caucasians, the study may have been underpowered for some correlations. Strengths of our study included large number of measurements we did alongside ^{18}F-FDG PET CT scans, such as indirect calorimetry and temperature records, and the use of a personalised cooling protocol with water-perfused cooling mattresses, which results in maximal BAT activity and detectable BAT volume in non-shivering conditions.[13] This personalised cooling protocol might explain why in a recent study by Admiraal and colleagues,[22] in which all participants were cooled in an air-cooled chamber with a stable temperature of 17°C, no difference in BAT volume could be identified in south Asian compared with Caucasian participants. Because water has a higher heat transfer coefficient than air, water cooling results in more rapid cooling of participants and, possibly, an increased ability to detect BAT. Median BAT volume in Caucasian patients in the Admiraal study[22] was only 16 mL compared with 287 mL in our study. Thus, the less-intense cooling protocol in that study might have underestimated BAT volumes in their study participants.

Moreover, exposure of all participants to a stable room temperature of 17°C might have led to underestimation of BAT volume in Caucasian participants compared with south Asian participants, because Caucasians begin (according to our study) to shiver at lower temperatures. A possible drawback of the use of a personalised cooling protocol is that differences in environmental temperature could induce differences in BAT activity, because a strong positive association exists between environmental temperature and thermogenesis.[28] However, we do not believe such differences arose in our study because SUV_{max} and SUV_{mean} did not differ between the groups, suggesting equal BAT activation.

This study has important clinical implications. Until now, little was known about the underlying mechanisms of the disadvantageous metabolic phenotype and the consequently high risk of type 2 diabetes in south Asians. Therefore, treatment options and, more importantly, preventive strategies are unfocused and of limited efficacy in south Asians. Increasing the volume or activity of BAT, resulting in increased clearance of glucose and fatty acids and increased total energy expenditure, might be of great therapeutic potential in this group. We recently showed that BAT can be recruited in humans following 10 days of cold intervention.[14] Future studies should be directed towards the efficacy of this strategy, as well as other options, such as medication, to increase BAT volume or activity. These strategies might ultimately be useful for improving the metabolic phenotype in south Asians with type 2 diabetes or at high risk of developing the disease.

ACKNOWLEDGEMENTS

This work is financed by the Dutch Diabetes Research Foundation (grant 2012.11.1500 to PCNR and MRB). MRB is supported by the Board of Directors of the Leiden University Medical Center (LUMC) and PCNR is Established Investigator of the Netherlands Heart Foundation (grant 2009T038). We thank Roba Metals B V IJsselstein (Utrecht, Netherlands) for financial support. The Blanketrol III cooling device was kindly provided by FMH Medical (Veenendaal, Netherlands). We thank Bram Sinon and Tjerk Lugthart (Rijnland Hospital, Leiderdorp, Netherlands) for their excellent technical assistance.

REFERENCES

1 Whiting DR, Guariguata L, Weil C, Shaw J. IDF diabetes atlas: global estimates of the prevalence of diabetes for 2011 and 2030. *Diabetes Res Clin Pract* 2011; **94:** 311–21.

2 Bindraban NR, van Valkengoed IG, Mairuhu G, et al. Prevalence of diabetes mellitus and the performance of a risk score among Hindustani Surinamese, African Surinamese and ethnic Dutch: a cross-sectional population-based study. *BMC Public Health 2008;* **8:** 271.

3 Chiu M, Austin PC, Manuel DG, Shah BR, Tu JV. Deriving ethnic-specific BMI cutoff points for assessing diabetes risk. *Diabetes Care* 2011; **34:** 1741–48.

4 Chandie Shaw PK, Baboe F, van Es LA, van der Vijver JC, van de Ree MA, Rabelink TJ. South-Asian type 2 diabetic patients have higher incidence and faster progression of renal disease compared with Dutch-European diabetic patients. *Diabetes Care* 2006; **29:** 1383–85.

5 Chaturvedi N, Fuller JH. Ethnic differences in mortality from cardiovascular disease in the UK: do they persist in people with diabetes? *J Epidemiol Community Health* 1996; **50:** 137–39.

6 McKeigue PM, Shah B, Marmot MG. Relation of central obesity and insulin resistance with high diabetes prevalence and cardiovascular risk in south Asians. *Lancet* 1991; **337:** 382–86.

7 Boon MR, Karamali NS, de Groot CJ, et al. E-Selectin is elevated in cord blood of south Asian neonates compared with Caucasian neonates. *J Pediatr* 2011; **160:** 844–48.

8 Hall LML, Moran CN, Milne GR, et al. Fat oxidation, fitness and skeletal muscle expression of oxidative/lipid metabolism genes in south Asians: implications for insulin resistance? *PLoS One* 2010; **5:** e14197.

9 Cypess AM, Chen YC, Sze C, et al. Cold but not sympathomimetics activates human brown adipose tissue in vivo. *Proc Natl Acad Sci* USA 2012; **109:** 10001–05.

10 Ouellet V, Labbe SM, Blondin DP, et al. Brown adipose tissue oxidative metabolism contributes to energy expenditure during acute cold exposure in humans. J Clin Invest 2012; 122: 545–52.

11 Van Marken Lichtenbelt WD, Vanhommerig JW, Smulders NM, et al. Cold-activated brown adipose tissue in healthy men. *N Engl J Med* 2009; **360:** 1500–08.

12 Yoneshiro T, Aita S, Matsushita M, et al. Brown adipose tissue, whole-body energy expenditure, and thermogenesis in healthy adult men. *Obesity* 2012; **19:** 13–16.

13 Van Marken Lichtenbelt WD, Schrauwen P. Implications of nonshivering thermogenesis for energy balance regulation in humans. *Am J Physiol Regul Integr Comp Physiol* 2011; **301:** R285–96.

14 Van der Lans AA, Hoeks J, Brans B, et al. Cold acclimation recruits brown fat and increases nonshivering thermogenesis. *J Clin Invest* 2013; **123:** 3395–403.

15 Cypess AM, Lehman S, Williams G, et al. Identification and importance of brown adipose tissue in adult humans. *N Engl J Med* 2009; **360:** 1509–17.

16 Vijgen GH, Bouvy ND, Teule GJ, Brans B, Schrauwen P, van Marken Lichtenbelt WD. Brown adipose tissue in morbidly obese subjects. *PLoS One* 2011; **6:** e17247.

17 Bartelt A, Bruns OT, Reimer R, et al. Brown adipose tissue controls triglyceride clearance. Nat Med 2011; **17:** 200–05.

18 Stanford KI, Middelbeek RJ, Townsend KL, et al. Brown adipose tissue regulates glucose homeostasis and insulin sensitivity. *J Clin Invest* 2013; **123:** 215–23.

19 van Marken Lichtenbelt WD, Daanen HA, Wouters L, et al. Evaluation of wireless determination of skin temperature using iButtons. *Physiol Behav* 2006; **88:** 489–97.

20 Simonson DC, DeFronzo RA. Indirect calorimetry: methodological and interpretative problems. *Am J Physiol* 1990; 258: E399–412.

21 Feurer I, Mullen JL. Beside measurement of resting energy expenditure and respiratory quotient via indirect calorimetry. *Nutr Clin Prac* 1986; **1:** 43–49.

22 Admiraal WM, Verberne HJ, Karamat FA, Soeters MR, Hoekstra JB, Holleman F. Cold-induced activity of brown adipose tissue in young lean men of South-Asian and European origin. *Diabetologia* 2013; **56:** 2231–37.
23 Vosselman MJ, Brans B, Van der Lans AA, et al. Brown adipose tissue activity after a high-calorie meal in humans. *Am J Clin Nutr* 2013; **98:** 57–64.
24 Orava J, Nuutila P, Lidell M, et al. Different metabolic responses of human brown adipose tissue to activation by cold and insulin. *Cell Metab* 2011; **14:** 272–79.
25 Vosselman MJ, van der Lans AA, Brans B, et al. Systemic beta-adrenergic stimulation of thermogenesis is not accompanied by brown adipose tissue activity in humans. *Diabetes* 2012; **6:** 3106–13.
26 Llewellyn-Smith IJ. Anatomy of synaptic circuits controlling the activity of sympathetic preganglionic neurons. *J Chem Neuroanat* 2009; **38:** 231–39.
27 Bakker LEH, van Schinkel LD, Guigas B, et al. A 5-day high fat high calorie diet impairs insulin sensitivity in healthy, young south Asian men but not in Caucasian men. *Diabetes* (in press).
28 Cannon B, Nedergaard J. Nonshivering thermogenesis and its adequate measurement in metabolic studies. *J Exp Biol* 2011; **214:** 242–53.

SUPPLEMENTARY APPENDIX

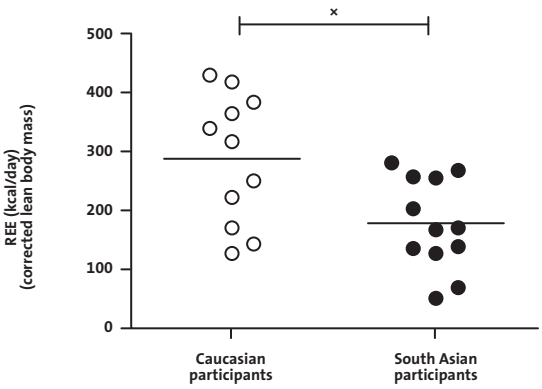

SUPPLEMENTARY FIGURE 1

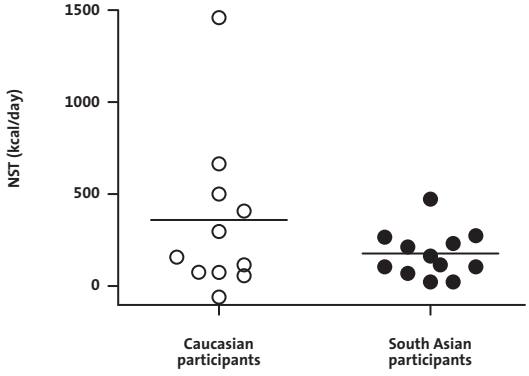

SUPPLEMENTARY FIGURE 2

SUPRACLAVICULAR SKIN TEMPERATURE AS A MEASURE OF ^{18}F-FDG UPTAKE BY BAT IN HUMAN SUBJECTS

MARIËTTE R. BOON
LEONTINE E.H. BAKKER
RIANNE A.D. VAN DER LINDEN
LENKA PEREIRA ARIAS-BOUDA
FRITS SMIT
HEIN J. VERBERNE
WOUTER D. VAN MARKEN LICHTENBELT
INGRID M. JAZET
PATRICK C.N. RENSEN

PLoS One 2014, revision invited.

14

ABSTRACT

Brown adipose tissue (BAT) has emerged as a novel player in energy homeostasis in humans and is considered a potential new target for combating obesity and related diseases. The current 'gold standard' for quantification of BAT volume and activity is cold-induced ^{18}F-FDG uptake in BAT. However, use of this technique is limited by cost and radiation exposure. Given the fact that BAT is a thermogenic tissue, mainly located in the supraclavicular region, the aim of the current study was to investigate whether cold-induced supraclavicular skin temperature and core body temperature may be alternative markers of BAT activation in humans. BAT volume and activity were measured in 24 healthy lean adolescent males (mean age 24.1 ± 0.8 years), using cold-induced ^{18}F-FDG uptake with PET-CT. Core body temperature was measured continuously in the small intestine with use of an ingestible telemetric capsule and skin temperature was measured by eighteen wireless iButtons attached to the skin following ISO-defined locations. Proximal and distal (hand/feet) skin temperatures markedly decreased upon cold exposure, while supraclavicular skin temperature significantly increased (35.2±0.1 *vs.* 35.5±0.1°C, p=0.001). Furthermore, cold-induced supraclavicular skin temperature positively correlated with both total (R^2=0.28, P=0.010) and clavicular BAT volume (R2=0.20, P=0.030) and clavicular SUV_{max} (R^2=0.27, P=0.010), while core body temperature did not. In conclusion, supraclavicular skin temperature as measured by iButtonsmay have predicitive value for BAT detection in adult humans. This is highly desirable considering the increasing interest in pharmacological interventions to stimulate BAT in human subjects.

INTRODUCTION

Brown adipose tissue (BAT) is a highly metabolically active tissue involved in facultative thermogenesis in mice (reviewed in [1]) and humans [2–5]. Cold-induced ^{18}F-fluorodeoxyglucose (FDG) positron emission tomography-computed tomography (PET-CT) studies in humans have shown that BAT is mainly present in the neck area and along the great vessels [6]. At these strategic locations, the produced heat can immediately be dispersed throughout the body. In addition, brown-like adipocytes, so-called 'beige' adipocytes, are present within white adipose tissue and these may contribute to total energy expenditure and thermogenesis as well, albeit to a lesser extent as the 'classical' brown adipocytes [7]. In order to execute their function, brown adipocytes contain a wealth of mitochondria that express uncoupling protein 1 (UCP-1), which uncouples respiration from adenosine triphosphate (ATP) synthesis, leading to heat production [1]. As a substrate, brown adipocytes oxidize triglyceride-derived fatty acids and glucose. In line with this, in mice, BAT is importantly involved in plasma triglyceride clearance [8] and contributes to glucose homeostasis [9]. Furthermore, in humans, BAT activation by means of cold induction results in elevation of plasma free fatty acids (FFA) levels and a steep increase in fat oxidation [10].

It has been estimated that fully activated BAT in humans can contribute to up to 15-20% of total energy expenditure [11]. The fact that obese individuals have lower BAT volume and activity supports the metabolic importance of BAT [6,12,13]. Of note, we recently showed that the South Asian population, which is highly susceptible of developing a disadvantageous metabolic phenotype along with type 2 diabetes, has markedly lower BAT volume along with lower resting energy expenditure and non-shivering thermogenesis, further supporting a role of BAT in whole-body metabolism [14]. Therefore, stimulation of BAT is currently considered a potential preventive and therapeutic target in the combat against obesity and related diseases, such as dyslipidemia and type 2 diabetes. In fact, the modest decrease in body weight as evoked by the anti-diabetic drug metformin may be due to activation of BAT [15].

The current 'gold standard' for determination of BAT volume and BAT activity in human subjects is cold-induced ^{18}F-FDG uptake as assessed with PET-CT, for which subjects are cooled for approximately 2 hours at a temperature just above their shivering temperature [4,12,13,16], followed by infusion of ^{18}F-FDG and performance of a PET-CT scan. ^{18}F-FDG is an analogue of glucose that is taken up by glucose transporters. Once taken up, ^{18}F-FDG is phosphorylated but is no substrate for further metabolism and becomes trapped in metabolically active, glucose-using tissues, amongst which BAT, allowing the assessment of glucose uptake by tissues by PET-CT. ^{18}F-FDG uptake by activated BAT regions on the PET-CT scan can be quantified, resulting in measures for BAT volume as well as for maximal ^{18}F-FDG uptake (maximal standardized uptake value, 'SUV_{max}') and mean ^{18}F-FDG uptake (mean standardized uptake value, 'SUV_{mean}'), which may be considered measures for the level of BAT activation.

Interestingly, in mice, in which most BAT is present in the interscapular region, 'interscapular temperature' is commonly used as a measure for BAT activity [17], as well as core body temperature [18]. For instance, activation of BAT by the cannabinoid 1 receptor inverse

agonist rimonabant resulted in a transient but steep increase in interscapular temperature as recorded by implantable temperature probes [17]. Since in humans a large part of BAT is located in the supraclavicular region, recording cold-induced skin temperature in this specific area may be an attractive alternative for measuring BAT activity instead of the ^{18}F-FDG scans which are relatively expensive and pose a radiation burden on study subjects. Therefore, the aim of the current study was to investigate whether cold-induced supraclavicular skin temperature as measured with wireless temperature sensors and core body temperature as measured in the small intestine with an ingestible telemetric temperature sensor correlate with ^{18}F-FDG uptake by BAT as measured with PET-CT imaging in lean, healthy males.

METHODS

Subjects

24 Dutch healthy, lean (BMI < 25 kg/m^2) males of white Caucasian (n=12) and South Asian (n=12) origin between 18 and 28 years of age were enrolled via local advertisements as described previously [14]. Subjects underwent a medical screening including their medical history, a physical examination, blood chemistry tests and an oral glucose tolerance test to exclude individuals with type 2 diabetes according to the American Diabetes Association 2010 criteria. Other exclusion criteria were rigorous exercise, smoking and recent body weight change. The present study was approved by the Medical Ethical Committee of the Leiden University Medical Center and performed in accordance with the principles of the revised Declaration of Helsinki. All volunteers gave written informed consent before participation.

Study design

The study was conducted in The Rijnland Hospital, Leiderdorp (The Netherlands). Subjects were studied in the morning after a 10-hour overnight fast and subjects were not allowed to exercise 24 hours prior to the study. Subjects wore standardized clothing, consisting of a T-shirt and boxer short. Upon arrival, subjects ingested a telemetric capsule to measure core body temperature, and eighteen wireless iButtons were attached to the skin to measure skin temperature (see below). A cannula was inserted in the left antecubital vein for ^{18}F-FDG injection.

Cooling protocol. To activate BAT an individualized cooling protocol was applied, using two water perfused cooling mattresses (Blanketrol® III, Cincinatti Sub-Zero (CSZ) Products, Inc), as described previously [14]. Importantly, the cooling mattresses covered the anterior and posterior sides of the body of the subject, from the caudal part of the chin and upper side of the neck, respectively, until the ankles or lower legs, depending on the height of the subject. Thus, the clavicular region of the subject was fully covered in each subject. The protocol started with a baseline period of one hour in thermoneutral condition, after which

subjects were exposed to mild cold. Cooling started at 32°C and temperature was gradually decreased until shivering occurred. Temperature was then raised with 3-4°C and the cooling period of two hours was started (t_{cold}=0min). At the end of the first hour (t_{cold}=60min) of cooling ^{18}F-FDG was injected intravenously (2 MBq/kg). Both in thermoneutral and cold-induced condition (t_{cold}=110min) indirect calorimetry was performed with a ventilated hood (Oxycon Pro™, CareFusion, Germany) (t_{cold}=80-110min). After the second hour (t_{cold}=120min) of cooling ^{18}F-FDG-PET-CT imaging was performed to quantify BAT.

^{18}F-FDG-PET-CT-scan. Imaging was performed on a PET-CT-scanner (Gemini TF PET-CT, Philips, The Netherlands) as described previously [14]. Blind to subject characteristics, both a nuclear medicine physician and two researchers analyzed the PET-CT images using dedicated software (Hermes Hybrid Viewer™, Hermes Medical Solutions AB, Sweden). BAT activity and detectable BAT volume were quantified in the region of interest (as assessed by CT) by auto-contouring the BAT areas with a set threshold (SUV of 2.0 g/mL).

Temperature registration. Core body temperature was measured continuously in the small intestine with the use of an ingestible telemetric capsule (Jonah™, BMedical, Australia) that recorded core body temperature at 1-minute intervals. Skin temperature was measured at 1-minute intervals by wireless iButtons (iButton®, Maxim, USA) [19]. An iButton contains a semiconductor temperature sensor, a computer chip with a real time clock and memory, and a battery. In total eighteen iButtons were attached to the skin with adhesive tape at the following ISO-defined locations: forehead, supraclavicular (left and right), clavicular (left and right), subclavicular (left and right), sternal (left and right) (see **FIGURE 1A)**, supra umbilicular, anterior thigh (left and right), lateral thigh (left and right), flat of the hand (left and right) and bow of the foot (left and right).

Calculations

Total detectable BAT volume: In every slice, BAT size (measured in square centimetres) was quantified in the anatomical regions of interest (ROIs) using the auto contouring and region growing tool of the Hybrid Viewer. Detectable BAT volume (measured in millilitres) was calculated by summing up the ROIs from the individual slices, establishing a volume of interest (VOI). Since the localization of BAT differs between individuals (e.g. some have more BAT in the clavicular region, some more in the paravertebral region), both total detectable BAT volume and BAT volume in the clavicular region were quantified **(FIGURE 1B)**.

BAT activity: Within every region of interest, the Hybrid Viewer provided two measures of ^{18}F-FDG uptake, the maximal and mean standardized uptake value (SUV_{max} and SUV_{mean}, respectively). The standardized uptake value (SUV) is defined as the ratio of activity [kBq per mL] within the region of interest (ROI) and the injected activity [kBq] per bodyweight [g] and is expressed in g/mL. For SUV_{max}, the highest value in the VOI was taken. For SUV_{mean} the mean value within the VOI was determined.

Skin temperature measurements: Distal skin temperature was calculated as the average temperature of hands and feet and proximal skin temperature as the weighted average temperature of claviculae, anterior thigh and umbilicus (Tprox=0·383*Tavg_thighs + 0·293*Tavg_clav + 0·324*Tavg_umbilicus) according to the equation of Van Marken Lichten-

belt et al [19], based on the formulas by Kräuchi et al [20] and Hardy et al [21]. Mean skin temperature was calculated as the average of distal and proximal skin temperature. Core mean skin temperature gradient was calculated as the difference between core and mean skin temperature, and core distal skin temperature gradient as the difference between core and distal skin temperature. For thermoneutral skin temperature, the mean temperature of the second half of the thermoneutral period was calculated for each iButton. Cold-induced skin temperature was calculated as the mean skin temperature during the twenty minutes following ^{18}F-FDG administration, i.e., at the beginning of the second hour of cooling.

Statistical analysis

Data are presented as mean ± SEM. Paired t-tests were used to assess mean differences before and after cold exposure. To identify correlations between variables, linear regression analyses were performed. Significance level was set at $P<0.05$. Statistical analyses were performed using SPSS for Windows version 20.0 (IBM, USA).

RESULTS

Clinical characteristics

Clinical characteristics are shown in **TABLE 1**. Part of these data have recently been published for white Caucasians and South Asians separately [14]. However, analysis of covariance showed that there was no interaction between ethnicity and BAT volume with supraclavicular temperature as dependent factor ($p=0.36$) and that there was no difference in the intercept between South Asian and white Caucasian subjects ($p=0.33$). We, therefore, pooled the data for both ethnicities. One subject developed hyperventilation following ^{18}F-FDG administration,

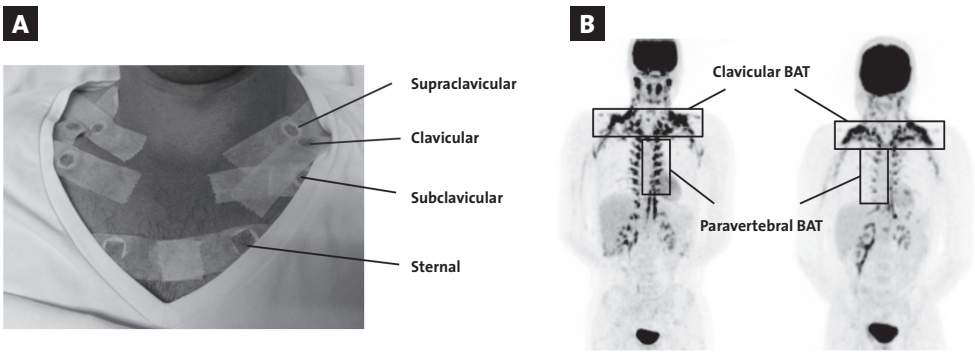

FIGURE 1 – Location of iButtons and clavicular and paravertebral brown adipose tissue. In the clavicular and sternal region, iButtons were symmetrically attached at the supraclavicular, clavicular, subclavicular and sternal region **A**. Clavicular and paravertebral brown adipose tissue regions in young, healthy male subjects as assessed by PET-CT scan with ^{18}F-FDG **B**.

TABLE 1 - **Clinical characteristics in young, healthy, male subjects**

	Healthy male subjects (n=24)	
	Thermoneutral	**Cold-induced**
age (years)	24.1 ± 0.6	
body mass index (kg/m^2)	21.7 ± 0.4	
systolic blood pressure (mmHg)	119 ± 2	134 ± 4**
diastolic blood pressure (mmHg)	66 ± 1	82 ± 2**
heart rate (bpm)	60 ± 2	57 ± 2
SUV_{max} (g/mL)		15 ± 1.0
SUV_{mean} (g/mL)		4.1 ± 0.1
Total BAT volume (mL)		235 ± 29
Clavicular SUV_{max} (g/mL)		14 ± 1
Clavicular SUV_{mean} (g/mL)		4.6 ± 1
Clavicular BAT volume (mL)		84 ± 1
Resting energy expenditure (kcal/day)	1493 ± 52	1732 ± 91**

Data are presented as mean ± SEM. ** p<0.005 vs. thermoneutral condition.

TABLE 2 - **Thermoregulation in thermoneutral and cold-induced condition in young, healthy, male subjects**

	Healthy male subjects (n=24)	
	Thermoneutral	**Cold-induced**
shiver temp		9.9 ± 0.4
core body temp	36.7 ± 0.1	36.7 ± 0.1
mean skin temp	33.3 ± 0.1	28.7 ± 0.2**
mean proximal skin temp	34.4 ± 0.1	30.9 ± 0.2**
supraclavicular skin temp	35.2 ± 0.1	35.5 ± 0.1**
clavicular skin temp	34.4 ± 0.1	34.2 ± 0.2
subclavicular skin temp	34.4 ± 0.1	33.6 ± 0.2**
mean distal skin temp	32.3 ± 0.2	26.5 ± 0.3**
forehead skin temp	33.7 ± 0.1	33.2 ± 0.1**
distal proximal skin temp gradient	−2.2 ± 0.2	−4.4 ± 0.3**
core mean skin temp gradient	3.3 ± 0.1	8.0 ± 0.2**
core distal skin temp gradient	4.4 ± 0.3	10.1 ±0.3**
core proximal skin temp gradient	2.3 ± 0.1	5.9 ± 0.2**

Data are presented as mean ± SEM. Units are in degrees Celsius. **p<0.005 vs. thermoneutral condition. Temp, temperature.

and was therefore excluded from all cold-induced and BAT measurements. Mean age was 24.1 ± 0.6 years and mean BMI was 21.7 ± 0.4 kg/cm^2. Systolic and diastolic blood pressure were significantly increased in response to cold (119 ± 2 vs. 134 ± 4 mmHg, p=0.00002; 66 ± 1 *vs.* 82 ± 2 mmHg, p=0.000000), while heart rate was not affected.

In all subjects active BAT was detected, as evidenced by ^{18}F-FDG uptake in the classical BAT regions, though one subject exhibited only 1.5 mL of detectable BAT. Mean total BAT volume was 235 ± 29 mL. Mean SUV_{max} was 15 ± 1 g/mL, and mean SUV_{mean} was 4.1 ± 0.1 g/mL for total BAT volume. In the clavicular region, mean BAT volume was 84 ± 11 mL. Mean SUV_{max} in this region was 14 ± 1 g/mL, while mean SUV_{mean} was 4.6 ± 0.1 g/mL. Cold stimulation resulted in an increase in energy expenditure, i.e. nonshivering thermogenesis, by 16% (16 ± 4%, p=0.001).

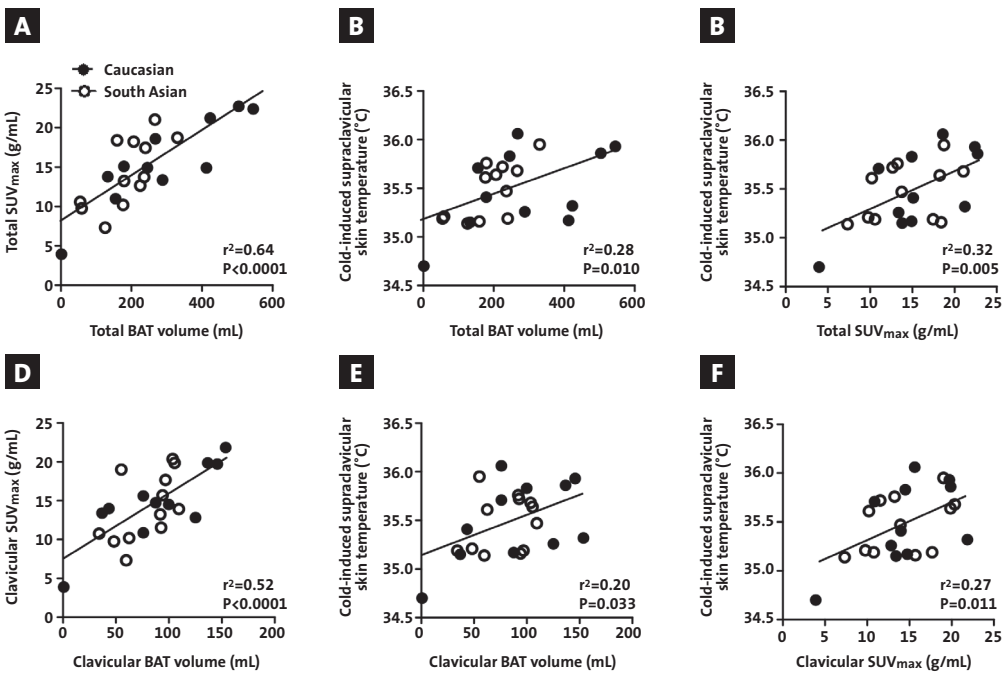

FIGURE 2 – Correlations between cold-induced supraclavicular skin temperature and ^{18}F-FDG uptake by brown adipose tissue in young, healthy male subjects. Total SUVmax in relation to total BAT volume **A**. Cold-induced supraclavicular skin temperature in relation to total BAT volume **B** and total SUV_{max} **C**). Clavicular SUV_{max} in relation to clavicular BAT volume **D**. Cold-induced supraclavicular skin temperature in relation to clavicular BAT volume **E** and clavicular SUV_{max} **F**. Correlations were determined by linear regression analysis. Open circles represent South Asian subjects, black circles white Caucasian subjects. BAT, brown adipose tissue. SUV, standard uptake value.

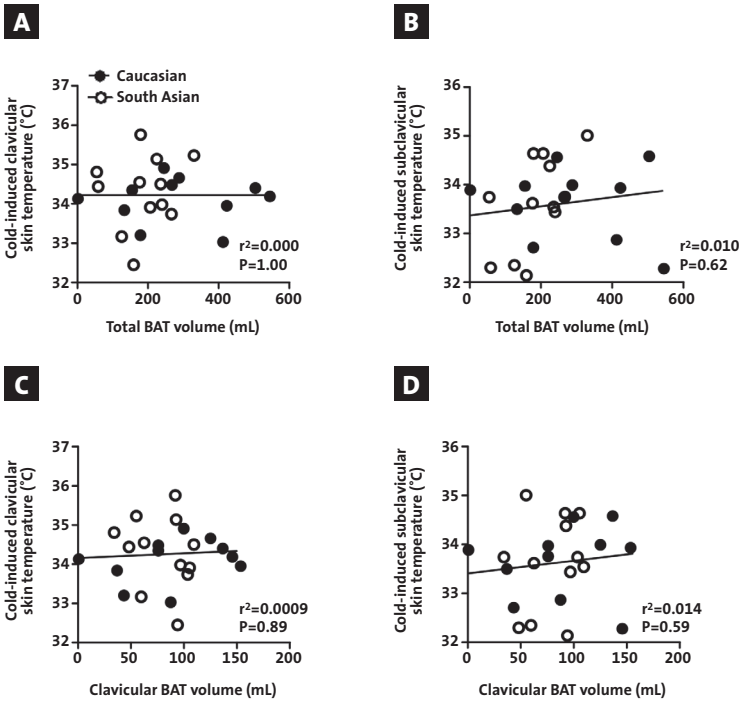

FIGURE 3 – Correlations between cold-induced clavicular and subclavicular skin temperature and ^{18}F-FDG uptake by brown adipose tissue in young, healthy male subjects. Cold-induced clavicular and subclavicular skin temperature in relation to total BAT volume (**A** and **B**, respectively) and clavicular BAT volume (**D** and **E**, respectively). Correlations were determined by linear regression analysis. Open circles represent South Asian subjects, black circles white Caucasian subjects. BAT, brown adipose tissue.

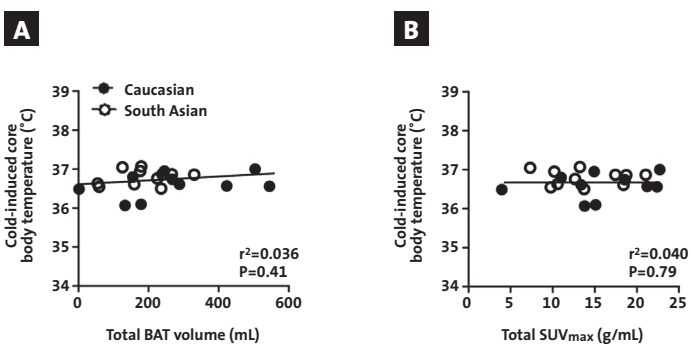

FIGURE 4 – Correlations between cold-induced core body temperature and ^{18}F-FDG uptake by brown adipose tissue in young, healthy male subjects. Cold-induced core body temperature in relation to total BAT volume **A** and total SUV_{max} **B**. Correlations were determined by linear regression analysis. Open circles represent South Asian subjects, black circles white Caucasian subjects. BAT, brown adipose tissue. SUV, standard uptake value.

Thermoregulation

Thermoregulation is shown in **TABLE 2.** Mean inlet water temperature of the cooling matresses at which shivering started was 9.9 ± 0.4 °C. Mean core body temperature was not affected by cold exposure. Mean total, proximal and distal skin temperature markedly decreased on cold stimulation. Consequently, core distal and core mean skin temperature gradients were significantly higher during cooling, indicating an insulative response. With respect to the clavicular region, supraclavicular skin temperature was significantly increased upon cold exposure (35.2 ± 0.1 *vs.* 35.5 ± 0.1 °C, p=0.001). Clavicular skin temperature was not affected and subclavicular skin temperature was significantly reduced.

Correlations thermoregulation and ^{18}F-FDG uptake by BAT

Linear regression analysis showed a clear positive correlation between SUV_{max} and total BAT volume (R^2=0.64, P<0.0001) **(FIGURE 2A;** this figure is modified from a previous publication [14]). Furthermore, a positive correlation was found between cold-induced supraclavicular skin temperature and total BAT volume (R^2=0.28, P=0.010) **(FIGURE 2B)** and SUV_{max} (R^2=0.32, P=0.005) **(FIGURE 2C)**. With respect to BAT that was located in the clavicular region only, again a clear positive correlation was found between SUVmax and BAT volume (R^2=0.52, P<0.0001) **(FIGURE 2D)**. Furthermore, cold-induced supraclavicular skin temperature correlated positively with clavicular BAT volume (R^2=0.20, P=0.030) **(FIGURE 2E)** and clavicular SUV_{max} (R^2=0.27, P=0.010) **(FIGURE 2F).** No correlations were found between cold-induced clavicular and subclavicular skin temperature and total and clavicular BAT volume **(FIGURE 3).** Furthermore, both total BAT volume and SUV_{max} did not correlate with cold-induced core body temperature (R^2=0.04, P=0.410, **FIGURE 4A;** R^2=0.004, P=0.790, **FIGURE 4B;** respectively). Finally, no correlations were found between delta (i.e. the change in temperature upon cooling) supraclavicular, clavicular and subclavicular skin temperature and total and clavicular BAT volume, respectively (data not shown).

DISCUSSION

BAT has emerged as a novel player in energy homeostasis in humans and is currently considered a potential new target for obesity and related diseases. The current 'gold standard' for quantification of BAT volume and activity in humans is the cold-induced ^{18}F-FDG uptake measured with PET-CT, which is, however, limited by cost and radiation exposure. Therefore, a less expensive and less burdensome alternative to determine BAT in human research is highly desirable. In the present study, we demonstrated that, while mean proximal and distal skin temperatures were markedly decreased upon cold exposure as expected, supraclavicular skin temperature was significantly increased. Furthermore, cold-induced supraclavicular skin temperature was positively correlated with both total and clavicular BAT volume and $SUV_{max,}$ suggesting that cold-induced supraclavicular skin temperature may have predictive value for BAT detection in humans. BAT is a thermogenic tissue with special importance in

neonates who are sensitive to develop hypothermia due to their large body surface area [1]. In this study, we detected BAT in 100% of the subjects with a corresponding thermogenic response, as indicated by a mean increase in energy expenditure of 16%. The strategic location of BAT, mainly in the interscapular region in neonates and in the neck area and along the great vessels in adults, results in efficient spreading of the produced heat throughout the body. Hence, an increase in temperature of the skin that overlies BAT, i.e. the supraclavicular region, upon BAT activation may be expected. Heat production by BAT is the direct result of uncoupling of ATP synthesis by the uncoupling protein UCP-1. The main stimulus for activation of this intracellular cascade is sympathetic activation with subsequent release of catecholamines, i.e. following cold induction [1]. Next to heat production, sympathetic activation may also result in alterations in BAT blood flow [2], aimed at spreading the heat throughout the body to maintain core body temperature and away from BAT. In addition, sympathetic activation induces peripheral cutaneous vasoconstriction [22], also facilitating maintenance of core body temperature. In the present study, blood pressure and core distal and core mean skin temperature gradients were significantly increased during cooling, suggesting cold-induced activation of the sympathetic nervous system.

We found that supraclavicular skin temperature significantly increased upon cold exposure. This is in line with a recent study in healthy human volunteers in which short-term (5 minutes) cooling of the hand resulted in a highly localized increase in supraclavicular skin temperature as measured by infrared thermal imaging [23]. However, in that study, changes in skin surface temperature had not been directly correlated with direct measurements of BAT activity. Rather, PET-CT images from a comparable group of age- and sex matched subjects were used. In the current study, we combined skin temperature measurements with ^{18}F-FDG PET-CT scans in the same subjects and found that cold-induced supraclavicular skin temperature significantly correlated with clavicular BAT volume and clavicular SUV_{max} though the R^2 was modest (up to 0.27 for clavicular SUV_{max}). Moreover, a comparable correlation was found with total BAT volume and SUV_{max} in the total BAT region. Thus, supraclavicular skin temperature may not only be indicative for activated BAT present in the clavicular region, but also for the total amount of BAT. Interestingly, Yoneshiro et al [5] previously showed that supraclavicular skin temperature as measured by means of small disc-type temperature data loggers was only decreased in subjects without detectable BAT during cold while in subjects with detectable BAT it remained equal. This difference may be attributable due to a difference in thermogenesis between BAT positive and BAT negative subjects. Our results are furthermore in accordance with a previous mouse study in which changes in BAT temperature as determined by thermal imaging highly correlated with increases in ^{18}F-FDG uptake within BAT [24]. Of note, we used iButtons to measure skin temperature instead of thermal imaging. iButtons have been shown to be a reliable, safe, cheap and extensively researched technique in both cold and warm conditions [19].

The rise in supraclavicular skin temperature may not solely be due to thermogenesis by activated BAT, but also due to short-term changes in BAT blood flow, as has been shown in rats [25] as well as in humans [2]. In line with this, cold acclimation in mice leads to increased mitochondrial density and increased sympathetic nerve fiber density together

with increased angiogenesis [26]. The physiological role of this increased blood flow is likely to spread the heat throughout the body to maintain core body temperature. Thus, the increased supraclavicular skin temperature is likely the consequence of a combination of increased BAT thermogenesis as well as increased BAT blood flow. However, since the underlying mechanism (i.e. increased sympathetic activation towards BAT) is the same, both provide a good measure of BAT activation and may thus be measured at the skin surface.

In our study, clavicular and subclavicular skin temperature did not correlate with BAT volume. This is likely explained by the fact that most of the clavicular BAT pool is located in the supraclavicular region ([23], and see **FIGURE 1)**. Furthermore, core body temperature did not correlate with total BAT volume nor with total SUV_{max}. In mice, core body temperature is commonly used as a measure for BAT activity [17], and core body temperature may transiently rise by as much as 1.5°C following BAT activation. However, as is evident from the current study as well as from a previous study [12], in human subjects core body temperature does not rise following BAT activation due to cold exposure but rather stays equal, likely as a consequence of BAT activation preventing a drop in core body temperature. The lack of a rise in core body temperature could be due to the fact that the relative amount of BAT in humans is lower as compared to mice. Accordingly, in mice housed at 5°C nutrient oxidation in BAT can account for over 60% of the total energy expenditure [27,28], as compared to 15-20% in humans [11], resulting in tremendous heat production and a subsequent rise in core body temperature. Thus, in humans, cold-induced core body temperature is likely no good measure of BAT volume.

A potential limitation of the current study is our cooling protocol. We used a personalized cooling protocol in which water-perfused cooling mattresses were used to cool subjects just above their shiver temperature. Though this cooling protocol results in maximal BAT activation under non-shivering conditions [11], the cooling mattresses do not cover all parts of the body, such as the head and feet. Furthermore, since the supraclavicular region is located at the upper region of the mattresses, we cannot exclude that this region may have been influenced by warmer airflows. However, temperature of the forehead, which was not cooled, significantly decreased upon the cooling protocol making influence of warmer airflows less likely. Furthermore, an extra bed sheet covered the upper cooling mattress in order to create a cold compartment. Lastly, in the study by Symonds et al [23], short-term cooling of a hand or foot also resulted in a rise in supraclavicular skin temperature, supporting the concept that a cold stimulus induces rapid BAT activation accompanied by supraclavicular heat production. Furthermore, an extra bed sheet covered the upper cooling mattress in order to create a cold compartment. Lastly, in the study by Symonds et al [23], short-term cooling of a hand or foot also resulted in a rise in supraclavicular skin temperature, supporting the concept that a cold stimulus induces rapid BAT activation accompanied by supraclavicular heat production. A strength of our study is that changes in supraclavicular skin temperature were correlated with measures of BAT activity as measured by 18F-FDG uptake in BAT. Furthermore, we measured BAT volume and SUVmax in both the total detectable BAT region and the clavicular region, in order to prevent confounding by localization.

In conclusion, supraclavicular skin temperature as measured by iButtons is a potential novel non-invasive tool that may have predictive value for BAT detection in adult humans.

This is highly desirable, since there is increasing interest in pharmacological interventions to stimulate BAT in human subjects given its role in energy homeostasis. Therefore, supraclavicular skin temperature may be a non-invasive method to monitor BAT activity in response to treatments.

ACKNOWLEDGEMENTS

This work was financed by the Dutch Diabetes Research Foundation (grant 2012.11.1500 to P.C.N.R. and M.R.B.). M.R.B. is supported by the Board of Directors of the Leiden University Medical Center (LUMC) and P.C.N.R. is Established Investigator of the Netherlands Heart Foundation (grant 2009T038). We also thank Roba Metals B. V. IJsselstein (Utrecht, The Netherlands) for financial support. The Blanketrol® III cooling device was kindly provided by FMH Medical (Veenendaal, The Netherlands). The authors thank Bram Sinon and Tjerk Lugthart (Rijnland Hospital, Leiderdorp, The Netherlands) for their excellent technical assistance.

CONFLICT OF INTEREST

The authors have no conflict of interest.

REFERENCES

1 Cannon B, Nedergaard J (2004) Brown adipose tissue: function and physiological significance. Physiol Rev 84: 277-359.

2 Orava J, Nuutila P, Lidell ME, Oikonen V, Noponen T, Viljanen T, Scheinin M, Taittonen M, Niemi T, Enerback S, Virtanen KA (2011) Different metabolic responses of human brown adipose tissue to activation by cold and insulin. Cell Metab 14: 272-279..

3 Ouellet V, Labbe SM, Blondin DP, Phoenix S, Guerin B, Haman F, Turcotte EE, Richard D, Carpentier AC (2012) Brown adipose tissue oxidative metabolism contributes to energy expenditure during acute cold exposure in humans. J Clin Invest 122: 545-552.

4 Vijgen GH, Bouvy ND, Teule GJ, Brans B, Schrauwen P, van Marken Lichtenbelt WD (2011) Brown adipose tissue in morbidly obese subjects. PLoS One 6: e17247.

5 Yoneshiro T, Aita S, Matsushita M, Kameya T, Nakada K, Kawai Y, Saito M (2011) Brown adipose tissue, whole-body energy expenditure, and thermogenesis in healthy adult men. Obesity (Silver Spring) 19: 13-16.

6 Cypess AM, Lehman S, Williams G, Tal I, Rodman D, Goldfine AB, Kuo FC, Palmer EL, Tseng YH, Doria A, Kolodny GM, Kahn CR (2009) Identification and importance of brown adipose tissue in adult humans. N Engl J Med 360: 1509-1517.

7 Bartelt A, Heeren J (2014) Adipose tissue browning and metabolic health. Nat Rev Endocrinol 10: 24-36.

8 Bartelt A, Bruns OT, Reimer R, Hohenberg H, Ittrich H, Peldschus K, Kaul MG, Tromsdorf UI, Weller H, Waurisch C, Eychmuller A, Gordts PL, Rinninger F, Bruegelmann K, Freund B, Nielsen P, Merkel M, Heeren J (2011) Brown adipose tissue activity controls triglyceride clearance. Nat Med 17: 200-205.

9 Stanford KI, Middelbeek RJ, Townsend KL, An D, Nygaard EB, Hitchcox KM, Markan KR, Nakano K, Hirshman MF, Tseng YH, Goodyear LJ (2013) Brown adipose tissue regulates glucose homeostasis and insulin sensitivity. J Clin Invest 123: 215-223.

10 Vosselman MJ, Brans B, van der Lans AA, Wierts R, van Baak MA, Mottaghy FM, Schrauwen P, van Marken Lichtenbelt WD (2013) Brown adipose tissue activity after a high-calorie meal in humans. Am J Clin Nutr 98: 57-64.

11 van Marken Lichtenbelt WD, Schrauwen P (2011) Implications of nonshivering thermogenesis for energy balance regulation in humans. Am J Physiol Regul Integr Comp Physiol 301: R285-R296.

12 van Marken Lichtenbelt WD, Vanhommerig JW, Smulders NM, Drossaerts JM, Kemerink GJ, Bouvy ND, Schrauwen P, Teule GJ (2009) Cold-activated brown adipose tissue in healthy men. N Engl J Med 360: 1500-1508.

13 Virtanen KA, Lidell ME, Orava J, Heglind M, Westergren R, Niemi T, Taittonen M, Laine J, Savisto NJ, Enerback S, Nuutila P (2009) Functional brown adipose tissue in healthy adults. N Engl J Med 360: 1518-1525.

14 Bakker LEH, Boon MR, Van der Linden RAD, Pereira Arias-Bouda L, Van Klinken JB, Smit F, Verberne HJ, Jukema JW, Tamsma JT, Havekes LM, van Marken Lichtenbelt WD, Jazet IM, Rensen PCN (2013) Brown adipose tissue volume in healthy lean south Asian adults compared with white Caucasians: a prospective, case-controlled observational study. The Lancet Diabetes & Endocrinology. In press.

15 Geerling JJ, Boon MR, van der Zon GC, van den Berg SA, van den Hoek AM, Lombes M, Princen HM, Havekes LM, Rensen PC, Guigas B (2014) Metformin lowers plasma triglycerides by promoting VLDL-triglyceride clearance by brown adipose tissue in mice. Diabetes. In press.

16 Vosselman MJ, Brans B, van der Lans AA, Wierts R, van Baak MA, Mottaghy FM, Schrauwen P, van Marken Lichtenbelt WD (2013) Brown adipose tissue activity after a high-calorie meal in humans. Am J Clin Nutr 98: 57-64.

17 Bajzer M, Olivieri M, Haas MK, Pfluger PT, Magrisso IJ, Foster MT, Tschop MH, Krawczewski-Carhuatanta KA, Cota D, Obici S (2011) Cannabinoid receptor 1 (CB1) antagonism enhances glucose utilisation and activates brown adipose tissue in diet-induced obese mice. Diabetologia 54: 3121-3131.

18 Kang HW, Ribich S, Kim BW, Hagen SJ, Bianco AC, Cohen DE (2009) Mice lacking Pctp /StarD2 exhibit increased adaptive thermogenesis and enlarged mitochondria in brown adipose tissue. J Lipid Res 50: 2212-2221.
19 van Marken Lichtenbelt WD, Daanen HA, Wouters L, Fronczek R, Raymann RJ, Severens NM, Van Someren EJ (2006) Evaluation of wireless determination of skin temperature using iButtons. Physiol Behav 88: 489-497.
20 Krauchi K, Cajochen C, Mori D, Graw P, Wirz-Justice A (1997) Early evening melatonin and S-20098 advance circadian phase and nocturnal regulation of core body temperature. Am J Physiol 272: R1178-R1188.
21 Hardy JD, Richards CH (1948) A new instrument for measuring the thermal radiation of the environment. Science 107: 461.
22 Charkoudian N (2003) Skin blood flow in adult human thermoregulation: how it works, when it does not, and why. Mayo Clin Proc 78: 603-612.
23 Symonds ME, Henderson K, Elvidge L, Bosman C, Sharkey D, Perkins AC, Budge H (2012) Thermal imaging to assess age-related changes of skin temperature within the supraclavicular region co-locating with brown adipose tissue in healthy children. J Pediatr 161: 892-898.
24 Carter EA, Bonab AA, Paul K, Yerxa J, Tompkins RG, Fischman AJ (2011) Association of heat production with 18F-FDG accumulation in murine brown adipose tissue after stress. J Nucl Med 52: 1616-1620.
25 Foster DO, Frydman ML (1978) Nonshivering thermogenesis in the rat. II. Measurements of blood flow with microspheres point to brown adipose tissue as the dominant site of the calorigenesis induced by noradrenaline. Can J Physiol Pharmacol 56: 110-122.
26 Murano I, Barbatelli G, Giordano A, Cinti S (2009) Noradrenergic parenchymal nerve fiber branching after cold acclimatisation correlates with brown adipocyte density in mouse adipose organ. J Anat 214: 171-178.
27 Cannon B, Nedergaard J (2011) Nonshivering thermogenesis and its adequate measurement in metabolic studies. J Exp Biol 214: 242-253.
28 Golozoubova V, Gullberg H, Matthias A, Cannon B, Vennstrom B, Nedergaard J (2004) Depressed thermogenesis but competent brown adipose tissue recruitment in mice devoid of all hormone-binding thyroid hormone receptors. Mol Endocrinol 18: 384-401.

PART 4

GENERAL DISCUSSION, SUMMARY AND CURRICULUM VITAE

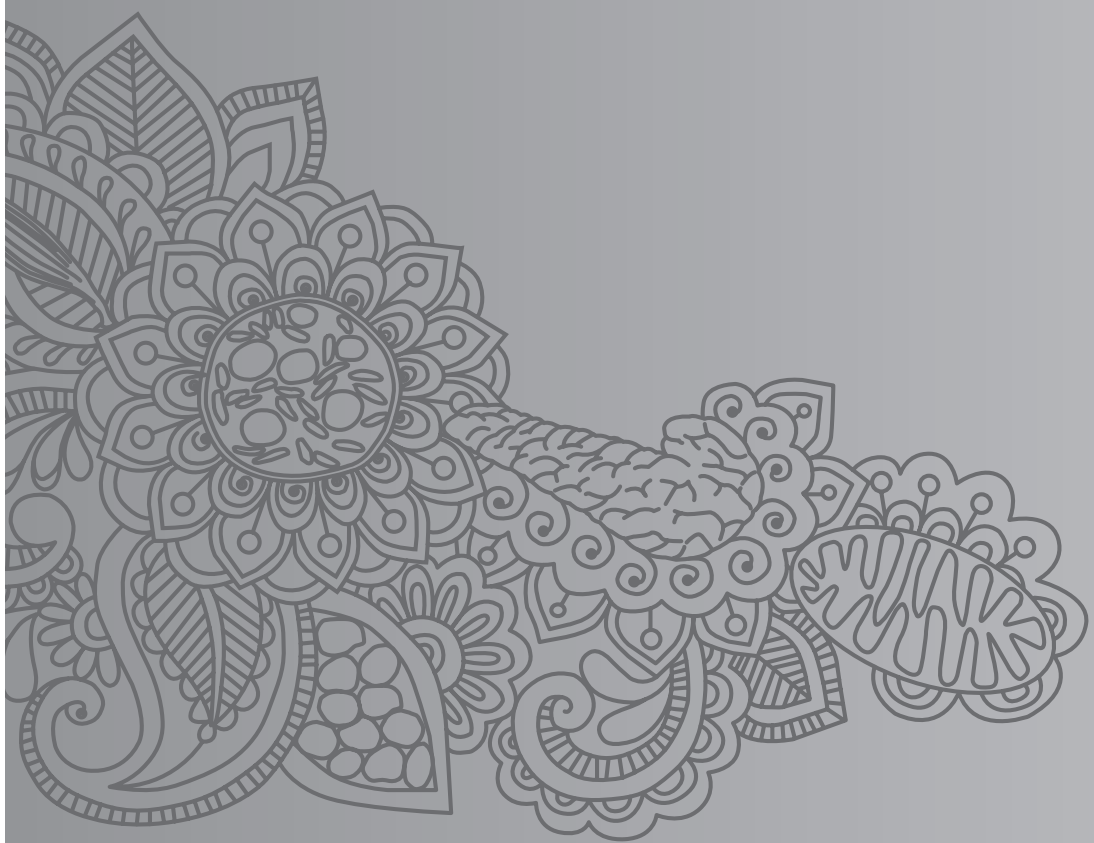

GENERAL DISCUSSION AND FUTURE PERSPECTIVES

15

The current 'diabesity' epidemic in Western society demands novel preventive and curative strategies to combat both obesity and its related morbidities, such as type 2 diabetes, cardiovascular disease (CVD) and cancer. The recent discovery of functional brown adipose tissue (BAT) in adult humans meant the beginning of an exciting new area in metabolic research. Potentially, everybody has its own tool to increase energy expenditure, and we now need to discover the right triggers to benefit from this tool. To enhance the understanding of BAT physiology, in this thesis we investigated the involvement of BAT in whole-body lipid metabolism as well as the role of the central melanocortin system in BAT function using well-established mouse models and *ex vivo* engineered radioactively labeled lipoprotein-mimicking particles. Furthermore, to identify novel targets that may activate BAT, we investigated the effect of several compounds *(e.g.* BMP7, metformin, a cannabinoid 1 receptor blocker and a ß3 adrenergic receptor agonist) on brown adipocyte activity *in vitro* and on BAT activity *in vivo*, as well as their effects on energy expenditure, lipid metabolism and atherosclerosis. In the last part of the thesis, we investigated the involvement of BAT in metabolism in humans by studying South Asians, a population with an unusually high risk to develop obesity, type 2 diabetes and CVD compared to white Caucasians. In addition, we studied additional factors that may contribute to their high CVD risk, such as endothelial dysfunction, inflammation and dysfunctional HDL. Lastly, in search for a non-invasive estimate of BAT activity, we studied whether supraclavicular skin temperature may be a novel tool to measure BAT volume and activity in humans.

From this thesis, various new insights on BAT have arisen which will be discussed and interpreted in this final chapter. In addition, possible clinical implications derived from this thesis and future directions of BAT in treating disease will be addressed.

SUBSTRATE UTILIZATION BY BROWN ADIPOSE TISSUE AND CONSEQUENCES FOR FUNCTIONAL IMAGING

Glucose uptake by brown adipose tissue

The presence of functional BAT in adult humans has been irrefutably proven in 2009, when cold-induced ^{18}F-fluorodeoxyglucose (^{18}F-FDG) positron emission tomography-computed tomography (PET-CT) scans showed high FDG uptake in regions that were histologically identified as being BAT (1-3). Importantly, BAT activity correlated positively with thermoneutral as well as cold-induced resting energy expenditure (REE) and lean subjects had more BAT compared to obese subjects, suggesting that BAT contributes substantially to energy metabolism in adult humans (2). The ^{18}F-FDG PET-CT scan, which is currently the gold standard to determine BAT volume and activity in humans, relies on the visualization and quantification of FDG, a glucose analogue that is taken up by metabolically active tissues without being metabolized. However, it may be questioned whether a glucose tracer is indeed the best method to visualize BAT and quantify BAT activity. First, it should be realized that metabolically active tissues such as the brain and heart show a high, but to some extent variable

uptake of FDG between individuals, which may affect the relative amount of radiolabel that can be taken up by BAT. Moreover, murine studies have repeatedly shown that the main fuel for BAT thermogenesis are fatty acids (FA) while glucose utilization for thermogenesis by BAT is considered low (~5-15%) (4). As described in **CHAPTER 1,** glucose is suggested to be mainly used for *de novo* lipogenesis in BAT. In addition, glucose is converted into lactate via anaerobic glycolysis to yield cytosolic ATP during thermogenesis (4). FA are likely also the dominant fuel for BAT in humans, as we found in **CHAPTER 11** that non-shivering thermogenesis (NST) following a personalized cooling protocol was exclusively due to an increase in FA oxidation (up to +46% in Caucasian subjects), while glucose oxidation was unaltered. Thus, this suggests that a tracer that monitors FA uptake by BAT, such as ^{18}F-fluoro-thiaheptadecanoic acid (^{18}F-FTHA), may be more reliable to estimate BAT activity with respect to combustion of FA as compared to ^{18}F-FDG.

Fatty acid uptake and combustion by brown adipose tissue

Ouellet et al (5) recently showed that two hours of cold exposure enhanced FTHA uptake by BAT as compared to muscle and WAT, though plasma triglyceride (TG) levels remained unaltered, which was likely due to the short time period of cold exposure. However, a drawback of use of a FA tracer as compared to a glucose tracer is that the uptake is rather non-specific since it is also largely taken up by other organs such as liver and intestine **(FIGURE 1)**. This may lower availability for uptake by BAT and thereby hamper its use as a tool to estimate BAT volume. Thus, the FA tracer needs to be optimized more before it can be used on a large scale.

Another important point of consideration is the mode of FA uptake by BAT. ^{18}F-FTHA traces the uptake of plasma free FA by BAT. However, as described in **CHAPTER 2,** a substantial part of FA taken up by BAT are derived from the TG-rich lipoproteins (TRLs) chylomicrons and very-low-density lipoproteins (VLDL) (6). In line with this, in **CHAPTER 4,** by performing kinetic studies using glycerol tri[^{3}H]oleate and [^{14}C]cholesteryl oleate double-labeled TRL-like emul-

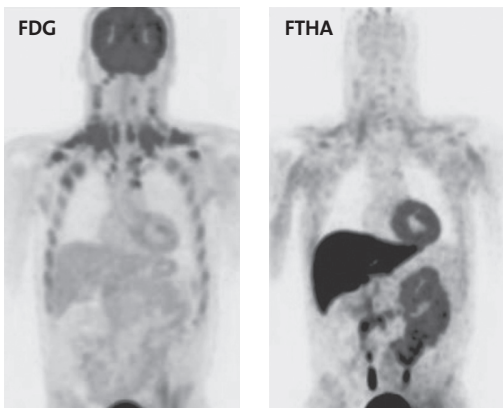

FIGURE 1 - Tissue glucose and fatty acid uptake. Postero-anterior projection of whole-body ^{18}F-FDG and ^{18}F-FTHA uptake during cold exposure.
Adapted from: Ouellet et al., JCI 2012

sion particles, we concluded that BAT delipidates TRL to selectively take up TG-derived FA released from the core of VLDL-mimicking particles. Just as in muscle and WAT, this process is likely dependent on lipoprotein lipase (LPL) that lipolyses the TG-rich particle to yield FA that are subsequently taken up by brown adipocytes via the FA transporter CD36 (7). Indeed, BAT activation has repeatedly been shown to massively increase LPL activity as well as CD36 expression (8,9). Additional evidence that the LPL/CD36 route is required for TRL-derived FA uptake by BAT emerged from a studies showing that inhibition of local LPL activity in BAT through injection of tetrahydrolipstatin abolished the uptake of [3H]oleate and that $CD36^{-/-}$ mice show cold intolerance due to inability of BAT to take up FA (8). It is likely that human BAT also utilizes FA from circulating lipoproteins, though this has not been investigated yet. Therefore, an interesting topic for future studies in human subjects would be to synthesize TRL-mimicking particles in which TG with radioactively labeled FA are incorporated, followed by visualization and quantification of uptake of the radiolabeled FA in BAT by PET-scan. This is likely a more specific way to visualize and quantify FA uptake by BAT, as it is restricted to LPL-mediated FA uptake. In addition, if TRL-derived FA are indeed the main substrate for human BAT, use of radiolabeled FA incorporated in TG will likely result in higher BAT uptake as compared to the ^{18}F-FTHA label which will enhance the sensitivity to estimate BAT volume and activity.

Measuring brown adipose tissue oxidative metabolism

In addition to a tracer that monitors uptake of substrates *(i.e.* glucose or fatty acid) by the tissue, a tracer that determines the metabolic capacity of BAT may also be used. Ouellet et al (5) determined oxidative metabolism in human BAT indirectly using ^{11}C-acetate PET imaging. ^{11}C-acetate is rapidly taken up by BAT and other tissues *(i.e.* myocardium, muscle) and metabolized to $^{11}CO_2$ and H_2O after intravenous injection. The rate of clearance of ^{11}C-acetate from the tissue reflects oxidative metabolism, with higher oxidative metabolism resulting in faster clearance from the tissue. Indeed, based on ^{11}C-acetate tissue kinetics, cold exposure markedly increased oxidative metabolism in BAT in all subjects (n=6). In a recent study, oxygen consumption was measured in BAT during cold exposure by means of dynamic oxygen (^{15}O) PET imaging, a possibly very adequate marker for BAT metabolism (10). Unfortunately, due to the limits of radiation exposure, both studies were unable to include the ^{18}F-FDG tracer in their study as it would be interesting to investigate whether oxygen consumption correlates with glucose uptake by BAT.

Measuring brown adipose tissue sympathetic activation

A tracer that has been shown to nicely correlate with ^{18}F-FDG uptake by BAT and furthermore identified the same anatomic regions as active BAT, is ^{123}I-metaiodobenzylguanidine (^{123}I-MIBG), an analog of noradrenalin, which thus monitors the sympathetic innervation of BAT (11). This tracer has not widely been used yet in the context of BAT studies, but may be a valuable tool, especially when used in combination with ^{18}F-FDG, to investigate whether compounds may enhance BAT activity by increasing sympathetic activation towards BAT, *i.e.* exert central effects.

Measuring brown adipose tissue heat production

The eventual product of BAT thermogenesis is heat. Therefore, methods could also be designed to determine BAT volume and activity by measuring the amount of heat produced by BAT. Indeed, in mice, in which most BAT is present in the interscapular region, 'interscapular temperature' is commonly used as a measure for BAT activity (12), as well as core body temperature (13). Since in humans a large part of BAT is located in the supraclavicular region **(FIGURE 2)** (1), recording cold-induced skin temperature in this specific area may be an attractive alternative for measuring BAT volume and/or activity instead of using radioactive tracers that are relatively expensive and pose a radiation burden on study subjects. Therefore, in **CHAPTER 12,** we performed a dedicated study in which we exposed healthy male subjects to a personalized cooling protocol and measured BAT volume and activity (by means of PET scan with ^{18}F-FDG) and supraclavicular skin temperature, in addition to core temperature.

Interestingly, we found that cold-induced supraclavicular skin temperature was positively correlated with both total and clavicular BAT volume and SUV_{max}, the latter being a measure of BAT activity. Curiously, we did not find a correlation between delta *(i.e.* the change in temperature upon cooling) supraclavicular skin temperature and total and clavicular BAT volume, which could be expected. However, we determined BAT volume and activity on the basis of FDG uptake. As mentioned above, glucose uptake may not be the optimal marker of BAT volume and activity. Therefore, it would be interesting to investigate the correlation between cold-induced delta skin temperature and BAT metabolism with use of a tracer that monitors BAT metabolism, such as ^{11}C-acetate. Anyhow, from **CHAPTER 12** it is evident that cold-induced supraclavicular skin temperature *per se,* rather than delta skin temperature, may be a qualitative marker of BAT activation in humans.

In the same study, core body temperature did not rise following BAT activation due to cold exposure but rather stayed equal, which is in accordance with a previous study (2). Likely heat produced by the activated BAT is just sufficient to prevent a drop in core body temperature. In mice, activation of BAT does generally result in a rise in core body temperature (13,14). The lack of a rise in core body temperature in humans could be due to the fact that

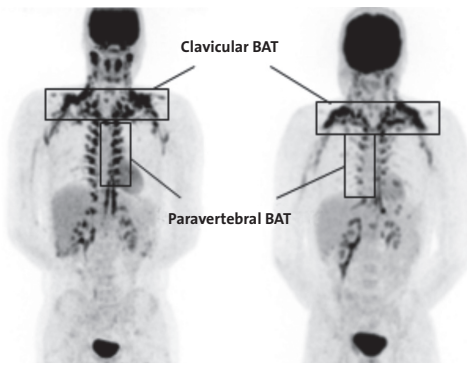

FIGURE 2 - Location of clavicular and paravertebral brown adipose tissue. Clavicular and paravertebral brown adipose tissue regions in young, healthy male subjects as assessed by PET-CT scan with ^{18}F-FDG.
Modified from Boon et al., *unpublished.*

the relative amount of BAT in humans is lower as compared to mice. Accordingly, in mice housed at 5°C, nutrient oxidation in BAT can account for over 60% of the total energy expenditure (15,16) as compared to 15-20% in humans (17,18) resulting in tremendous heat production and a subsequent rise in core body temperature. Thus, in contrast to mice, cold-induced core body temperature is likely not a reliable measure of BAT volume in humans.

In summary, BAT volume and activity in humans may be determined by use of a variety of radioactive tracers, followed by visualization and quantification by PET scan. Though the ^{18}F-FDG PET scan is currently the gold standard for BAT visualization in humans, tracers that monitor (TG-derived) FA uptake or BAT metabolism may be superior compared to ^{18}F-FDG, as glucose uptake by BAT is relatively low and (TG-derived) FA is the main substrate to be used for BAT thermogenesis. Furthermore, monitoring heat production by BAT may be a promising and noninvasive method to determine BAT volume and activity. Future studies should be directed at investigating and comparing these methods by performing prospective studies using adequate tracers and cooling methods.

BROWN ADIPOSE TISSUE AS A NOVEL TARGET TO COMBAT OBESITY AND RELATED DISEASES

Brown adipose tissue contributes to energy expenditure in humans

When considering BAT as a novel therapeutic tool to enhance energy expenditure thereby lowering obesity and related diseases in humans, it is highly relevant to assess the actual contribution of human BAT to total daily energy expenditure. Several assumptions can be made based on the results of this thesis and from previous studies. In **CHAPTER 11,** we found that healthy white Caucasian male subjects who were exposed to a personalized cooling protocol of approx. 2.5 h increased their REE with a mean increase of 20%, but up to a maximum increase of as much as 79%. As subjects did not shiver during the cooling protocol, the increase in REE upon cold exposure may equal NST, which is thought to exclusively arise from thermogenesis in BAT rather than uncoupling by muscle (19). This mean increase in NST of 20% is in line with previous studies (5,20-22). As REE accounts for 60-75% to the total daily energy expenditure (17), the contribution of BAT to total daily energy expenditure as calculated from our study could therefore be up to ~ 13% when the tissue is maximally stimulated by cold. As this will result in a sustained negative energy balance, this may thus significantly influence energy balance and body weight on the long term.

Additional evidence for the contribution of BAT in human energy expenditure appears from association and intervention studies by the research group of Masayuki Saito. They found that cold induction enhanced NST by 20% in BAT-positive subjects, while NST was enhanced by only 3% in BAT-negative subjects (23). Furthermore, BMI and body fat content were significantly lower in BAT-positive subjects (24). Intriguingly, these parameters increased with age in the BAT-negative group, while they remained unchanged from the twenties to fourties in the BAT-positive group (24). Importantly, a recent study by Yoneshiro

et al (25) recently inevitably showed that prolonged BAT activation by means of cold acclimation (2 h cold exposure at 17°C for 6 weeks) and capsinoids resulted in enhanced NST with concomitant decrease in body fat mass, which reached significance for cold exposure.

BAT has the potential to contribute even more to total daily energy expenditure when its mass and activity are enhanced due to catecholamine excess. This appears from patients with pheochromocytomas that are neuroendocrine tumors secreting excessive amounts of noradrenalin, an important stimulator of BAT activation and differentiation **(CHAPTER 2)** (4). ^{18}F-FDG-PET-CT-scans in patients with such tumors show an increased mass and activity of BAT (23,26), accompanied by increased energy expenditure up to two-fold in a recent case report (Sondergaard et al., unpublished). Thus, when further stimulated due to endogenous or exogenous factors, BAT has the potential to even more substantially contribute to total daily energy expenditure.

All together, these data unequivocally demonstrate that BAT contributes to NST in humans and that BAT activation is a promising novel therapeutic modality to combat obesity. Therefore, identification of novel therapeutic targets that may activate BAT is highly warranted. In this thesis, we have investigated the potential of several targets and compounds to activate BAT in mouse models, of which two *(i.e.* cannabinoid 1 receptor blockade and metformin) will be further discussed below.

Cannabinoid 1 receptor blockade as a tool to activate BAT

As described in **CHAPTER 2,** the cannabinoid 1 receptor (CB1R) inverse agonist rimonabant has been shown to induce long-term maintained weight loss and reduction of dyslipidemia in obese patients and was, therefore, regarded as one of the most promising therapeutic drugs to treat obesity (27-30). In **CHAPTER 7,** we showed that BAT likely plays a profound role in these beneficial effects. Systemic CB1R blockade by rimonabant led to massive BAT activation in diet-induced obese mice, resulting in increased energy expenditure and increased VLDL-TG clearance, caused by a increased uptake of VLDL-TG selectively by BAT. Since VLDL-TG production was not affected, we concluded that the TG-lowering effect of rimonabant was the consequence of increased BAT activity. BAT activation likely contributes to the anti-obesity and lipid lowering effects of rimonabant in humans as well, as a recent study showed that treatment of obese women with rimonabant for 12 weeks enhanced FA oxidation (31). This effect on energy expenditure was independent of the weight loss induced by the compound, as this was not found in the control group that lost equal amounts of weight through a hypocaloric diet.

Unfortunately, it is unlikely that rimonabant will be introduced on the market as a novel BAT activating drug, as central psychiatric side effects caused its removal from the market in 2008. However, several lines of evidence indicate that the effect of CB1R blockade was not restricted to a central mode of action, as the CB1R is also present on cells from peripheral tissues including hepatocytes (32), white adipocytes (33) and muscle cells (34). Therefore, strictly peripheral CB1R blockers have been developed and the results derived from these compounds in pre-clinical studies are promising. For instance, Tam et al (35) showed that the peripheral CB1R blocker AM6545 diminished obesity in diet-induced obese mice

and improved glucose metabolism, though the weight-reducing effect of the compound was somewhat less effective compared to rimonabant that also reduces food intake. Interestingly, in **CHAPTER 7,** we found that AM6545 is a very potent BAT activator *in vivo,* resulting in increased energy expenditure and TG-derived FA uptake by BAT. This suggests that the BAT activating effect of CB1R blockade is, at least in part, mediated via a direct peripheral mechanism. Indeed, we found that at thermoneutrality, in which sympathetic input towards BAT is largely diminished (4), rimonabant still activates BAT. Furthermore, we showed that the CB1R is highly expressed in BAT and that *in vitro* blockade of the CB1R in cultured brown adipocytes increases UCP-1 protein content and TG lipolysis, pointing to enhanced activity. Of note, CB1R blockade enhanced AMP-activated kinase (AMPK) phosphorylation in brown adipocytes, which has also been found in hepatocytes (36) and white adipocytes (37). It remains to be determined whether this is due to a direct effect of the compound on AMPK phosphorylation, or due to a secondary mechanism, *i.e.* following cAMP activation (38,39). Anyhow, AMPK may be a central player by which CB1R blockade results in BAT activation as well as by which it exerts its positive effects in other metabolic tissues. The possible role of AMPK in BAT function will be discussed further below.

Our data thus evidence that targeting the peripheral CB1R on BAT may be a promising method to increase energy expenditure and TG clearance by BAT. However, whether the CB1R is also present in human BAT and whether its blockade will enhance BAT activity in humans remains to be investigated. Furthermore, to the best of our knowledge, human trials aimed at investigating the metabolic effects of strictly peripheral CB1R blockers have not been conducted so far. Whether these blockers will be of benefit in humans should thus be investigated first.

Metformin as a tool to activate BAT

As discussed above, CB1R blockade may activate BAT, at least partly, via activating AMPK. Interestingly, the AMPK activator metformin is one of the most widely used glucose-lowering agents for the treatment of type 2 diabetes **(CHAPTER 2)** (40,41). In addition, metformin markedly reduces plasma TG levels in patients (42), of which the underlying mechanism(s) was unknown. In **CHAPTER 6,** we used APOE*3-Leiden (E3L).CETP transgenic mice, a well-established model for human-like lipoprotein metabolism (43,44), to unravel this mechanism. Metformin appeared to lower plasma TG due to activation of BAT, accompanied by increased uptake of TG-derived FA by BAT. The involvement of BAT in the TG-lowering effect of metformin in humans has not been studied yet. Several studies reported that metformin induces weight loss in obese diabetic patients (45-47). This may point to enhanced energy expenditure, possibly due to BAT activation. In fact, the weight loss induced by metformin is more pronounced in obese diabetic children (48-50), who also have more BAT than adults. Furthermore, in type 2 diabetes patients metformin decreases the respiratory exchange ratio without affecting energy expenditure, which is suggestive of increased fat oxidation, possibly due to BAT activation (51).

Our results in mice clearly showed that metformin directly activates BAT. Treatment of cultured brown adipocytes *in vitro* with metformin results in massive AMPK phosphorylation,

an effect that has previously been found for hepatocytes (52) and muscle cells (53,54). This was accompanied by massive intracellular lipolysis as evidenced by enhanced phosphorylation of hormone sensitive lipase (HSL) **(CHAPTER 1)** and glycerol release. In addition, metformin increases mitochondrial biogenesis in BAT in mice. This is likely a direct consequence of increased phosphorylation of AMPK, as activated AMPK is a potent inducer of mitochondrial biogenesis (55). Though we did not study central effects of metformin in our study, we cannot exclude that such effects may, at least in part, play a role. A recent study in rats has shown that metformin is able to cross the blood-brain barrier to reach the hypothalamus and change expression of orexigenic peptides (56), though we did not find effects on food intake in our study. Possibly, metformin may also enhance sympathetic outflow towards BAT from the hypothalamus, thereby increasing the activity of BAT. It would be interesting to investigate this aspect in more detail, for example by performing PET scans using ^{123}I-MIBG that monitors sympathetic outflow towards BAT.

AMPK: a central player in BAT activation?

The studies described in **CHAPTER 6** and **CHAPTER 7** demonstrate that both metformin and CB1R blockade by rimonabant enhance phosphorylation of AMPK in BAT. AMPK is a well-conserved energy sensing kinase that plays a crucial role in the regulation of catabolic versus anabolic pathways in cells (57,58). AMPK consists of a heterotrimeric complex containing a catalytic α subunit and two regulatory ß and γ subunits. The α1 subunit contains a threonine residue (Thr^{172}) whose phosphorylation by upstream kinases, such as the liver kinase B (LKB1), is required for AMPK activation. In addition, a decrease in cellular energy status (leading to high intracellular AMP and ADP levels) results in binding of AMP and/or ADP to the ß subunit and activation of AMPK (57,58). AMPK subsequently phosphorylates various downstream targets, resulting in inhibition of energy (ATP)-consuming processes *(i.e.* synthesis of glycogen, protein, and fatty acids) and stimulation of ATP-generating pathways *(i.e.* fatty acid oxidation) in order to restore energy balance (58).

The mechanism by which metformin activates AMPK in BAT is likely through phosphorylation of Thr^{172} within the α1 subunit. This is supported by our finding that metformin enhances Thr^{172} phosphorylation in BAT at equal AMP/ADP ratio **(CHAPTER 6),** and is consistent with previous observations in hepatocytes by others (59). Rimonabant may activate AMPK in BAT by activation of LKB1, which has been previously shown to occur in hepatocytes *in vitro* (36).

Apart from our pioneering studies, reports on the role of AMPK in BAT are so far limited. This is in sharp contrast to the extensive knowledge on the role of AMPK in liver, where activation leads to a reduction in lipogenesis and cholesterol synthesis and a simultaneous increase in FA oxidation resulting in decreased hepatic steatosis (60,61). AMPK protein amount and activity are two to threefold higher in BAT than in liver and chronic cold exposure of mice leads to a substantial increase in AMPK activity in BAT (62), while denervation reduces AMPK activity (63). These studies suggest a role for AMPK in BAT thermogenesis. Whole body AMPKα1$^{-/-}$ mice exhibit completely normal cold-induced thermogenesis, which is surprising at first glance, but this may be due to a compensatory upregulation of the

AMPKα2 subunit in BAT (64). Thus, future studies are needed to unravel the necessity of AMPK in BAT function, for instance by studying BAT thermogenesis also in AMPKα2$^{-/-}$ mice.

The intracellular pathways that are regulated by AMPK in BAT and that link AMPK with thermogenesis are not completely elucidated as yet. However, we found several intracellular mediators that were upregulated or phosphorylated upon metformin treatment in our *in vitro* and *in vivo* studies **(CHAPTER 6)** and literature exists on the intracellular pathways induced by AMPK in other cell types. Taken these data together, we speculate that AMPK activation, e.g. by metformin or CB1R blockade, increases phosphorylation of ATGL and HSL resulting in net increased lipolysis and breakdown/shrinking of intracellular lipid droplets and release of glycerol from the cells. The increased intracellular lipolysis results in release of FA and allosteric activation of UCP-1 in the inner membrane of the mitochondrion **(CHAPTER 1)** (4). Furthermore, we found that metformin enhances the phosphorylation of acetyl-CoA carboxylase (ACC). ACC was the first identified target of AMPK. ACC synthesizes malonyl-CoA from acetyl-CoA, and is, therefore, a key enzyme in the lipogenic pathway (65). Phosphorylation of ACC results in its inactivation; thereby the inhibition exerted by its product malonyl-CoA on CPT1α will be relieved, ultimately promoting mitochondrial FA transport and oxidation (58). Furthermore, we found that metformin enhances the phosphorylation of PGC-1α and eNOS, both of which are important regulators of mitochondrial biogenesis (66) and UCP-1 expression. The role of AMPK in eNOS phosphorylation is well-established in endothelial cells, resulting in enhanced NO production and vasodilation (67). Furthermore, NO itself may also enhance Pgc1α phosphorylation as has been shown in various cell types (68). Furthermore, AMPK has also been shown to directly enhance Pgc1α phosphorylation in muscle cells independent of NO (69).

In summary, as depicted in **FIGURE 3,** we postulate that AMPK is a cellular energy sensor that may enhance BAT thermogenesis by 1) increasing intracellular lipolysis and release of FA, thereby activating UCP1, 2) enhancing oxidation of FA by mitochondria, and 3) enhancing mitochondrial biogenesis. Taken together, this results in reduction of intracellular lipid droplet size and enhanced need for FA uptake from the plasma. The latter may also be mediated by AMPK, as AMPK has been shown to enhance LPL activity in muscle (70) as well as expression of the FA transporters CD36 and FAT (71), resulting in enhanced LPL-mediated FA uptake by BAT **(CHAPTER 6)**. This eventually results in lowering of plasma TG levels. It is interesting to note that, in contrast to other cell types such as hepatocytes and white adipocytes, AMPK in brown adipocytes does not merely stimulate generation of energy in the form of ATP, but rather induces dissipation of energy towards heat by promoting uncoupling. Thus, it may be questioned whether the term 'energy saver' for AMPK truly applies to BAT. Anyway, enhancing AMPK activation in BAT may thus be a very potent therapeutic strategy to increase energy expenditure, thereby lowering plasma lipid levels and diminishing obesity. It should be noted that the insight on the role of AMPK in BAT is still far from complete and assumptions are partly derived from the role of AMPK as found in other organs. Therefore, to gain more insight in the intracellular pathways in BAT evoked by AMPK, dedicated studies with AMPK modulators in BAT or brown adipocytes should be performed. Furthermore, the role of AMPK in regulating BAT activity in humans remains to be determined.

Effects of activation of BAT on other metabolic organs

As is evident from **CHAPTER 4** and previous literature (8), sympathetic activation of BAT results in increased uptake of FA towards BAT, a large part being derived from TRLs. However, this inevitably implies that FA are channeled away from other metabolic organs. Indeed, cold exposure enhances both hepatic VLDL-TG production (72) as well as WAT lipolysis (73) in mice. In line with this, in **CHAPTER 11,** we found a marked increase in plasma free FA levels in white Caucasian subjects after only approx. 2.5 h cold exposure, which suggests a marked increase in WAT lipolysis. The effects of cold exposure on hepatic VLDL-TG production in humans remain to be investigated.

We thus propose a model in which BAT activation results in enhanced uptake of TG-derived FA from VLDL in plasma. To fuel the increased need for FA by BAT, the liver enhances its VLDL-TG secretion in plasma, which in itself is fueled by an enhanced FA flux

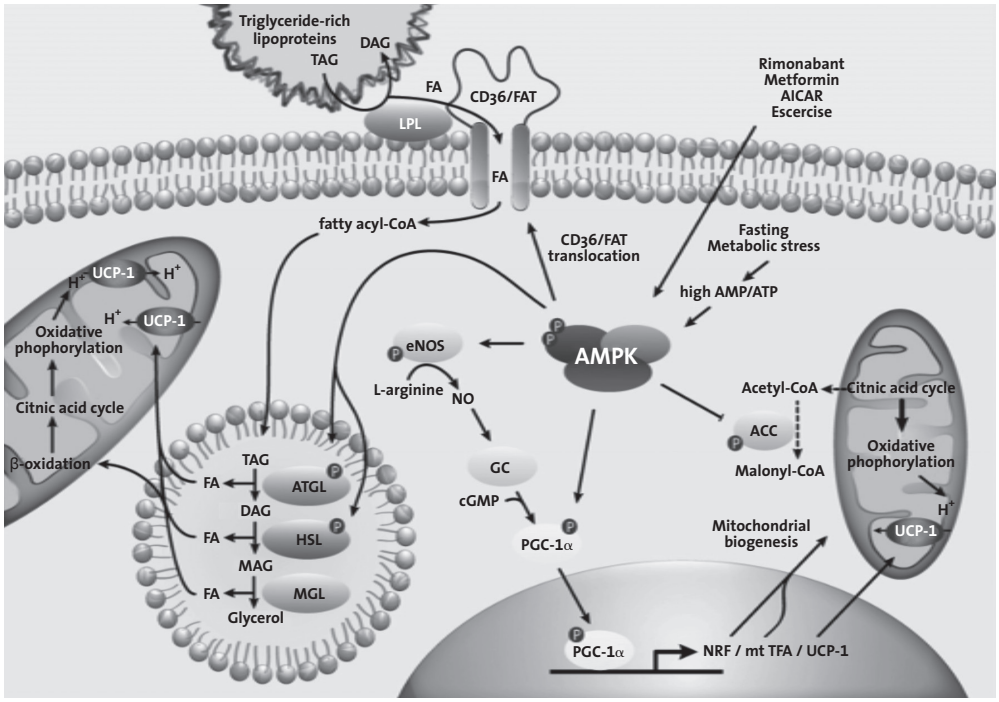

FIGURE 3 - Proposed effects of AMPK activation in the brown adipocyte. AMPK activation enhances the intracellular lipolytic capacity by increasing ATGL and HSL phosphorylation and activation, thereby enhancing FA release from TG stored in lipid droplets for oxidation. In addition, AMPK promotes FA oxidation in BAT by multiple (path)ways. First, AMPK phosphorylates and inactivates its downstream target ACC. This relieves the inhibition exerted by malonyl-CoA on CPT1α, ultimately promoting mitochondrial FA transport and oxidation. Second, AMPK increases mitochondrial biogenesis, likely through phosphorylation of eNOS and Pgc1α. Third, AMPK may enhance activation of LPL and translocation of CD36/FAT, resulting in enhanced FA uptake by the brown adipocyte for subsequent storage by the lipid droplet and ultimately combustion.
Kindly provided by Sander Kooijman.

derived from increased lipolysis by WAT (74). Thus, via this mechanism, shown in **FIGURE 4,** prolonged BAT activation will result in enhanced lipid fluxes from WAT and liver and consequently weight loss and diminished hepatic steatosis. Indeed, several compounds that were investigated in this thesis in **CHAPTER 5, CHAPTER 7** and **CHAPTER 9** *(i.e.* BMP7, rimonabant, and CL316243, respectively) resulted in both BAT activation and lowering of fat mass. In addition, BMP7 and rimonabant also massively lowered hepatic steatosis. Upon BAT activation, the sympathetic nervous system may, at least in part, mediate the enhanced lipid fluxes from WAT and liver towards BAT as activation of the sympathetic nervous system has been shown to enhance hepatic VLDL-TG production and WAT lipolysis (74). In addition, the compounds may also directly influence lipid homeostasis in WAT and liver, both of which express *e.g.* the CB1R (36,37).

Also in humans BAT activity may be linked to lipid storage in WAT and liver. Previous studies have shown that BAT activity negatively correlates with BMI and percentage of fat mass. As mentioned above, an exciting recent study provided direct evidence that activation of BAT by means of cold acclimation lowers fat mass in human subjects (25). In addition, a retrospective analysis of ^{18}F-FDG PET-CT-scans suggests an inverse relation between BAT

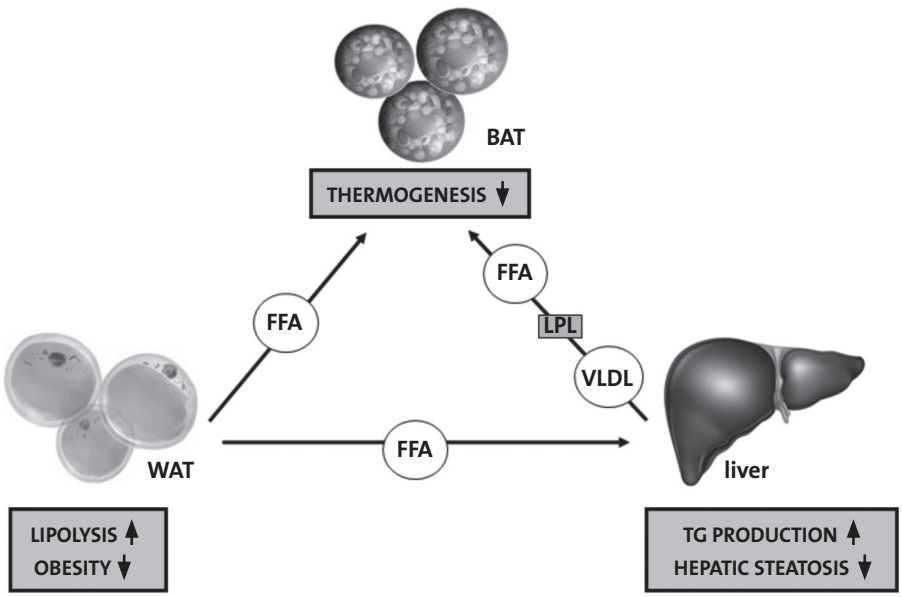

FIGURE 4 - Effects of BAT activation on FA fluxes. Activation of BAT results in combustion of FA to generate heat. Hepatic VLDL-TG production will be increased to fuel the enhanced FA demand by BAT. Lipolysis in WAT will also increase, resulting in release of FA that are transported to the liver to fuel the increased synthesis of VLDL-TG. In addition, FA may also be directly taken up as free FA from the plasma by BAT. The consequence of these processes is reduction of TG storage in WAT (i.e. obesity) and liver (i.e. hepatosteatosis). These processes may, at least in part, be modulated by enhanced sympathetic outflow towards the target organs.
Modified from Geerling and Boon et al. (75).

activity and hepatic steatosis (75), even after correction for several confounders such as BMI. Furthermore, genetic polymorphisms of UCP1 were also associated with hepatic steatosis (76).

POTENTIAL ROLE OF BROWN ADIPOSE TISSUE IN THE DISADVANTAGEOUS METABOLIC PHENOTYPE OF SOUTH ASIANS

As discussed in **CHAPTER 3,** in South Asians a disadvantageous metabolic profile that consists of central obesity, insulin resistance, and dyslipidemia, is highly prevalent. It is commonly assumed that an ethnic susceptibility towards a disturbed energy homeostasis *(e.g.* lower oxidation of glucose and FA by mitochondria) might underlie this phenotype (77). Indeed, in **CHAPTER 12,** we showed that thermoneutral REE was as much as 32% lower in healthy lean Dutch South Asian compared to Dutch white Caucasian adolescents. Intriguingly, we demonstrated by means of cold-induced ^{18}F-FDG PET-CT scans that the South Asian adolescents had 34% lower BAT volume compared to the Caucasians. Moreover, as reported previously (17,78), in white Caucasian subjects cold exposure resulted in increased serum free FA levels, lipid oxidation, and NST, the latter aiming at preventing a drop in core body temperature. In South Asians, all of these responses were lower. It is tempting to speculate that the lower BAT volume might underlie the smaller increase in NST in South Asians, although we could not find a significant correlation between BAT volume and NST, as has been shown previously (23,79), albeit not consistently (2,80).

It is interesting to speculate on potential mechanisms that could underlie the decreased BAT volume in South Asians. The fact that this is already found in healthy, lean adolescents, could point to an inborn defect in BAT development. This is further supported by our findings in **CHAPTER 9** in which we show that South Asians already express higher fat mass, dyslipidemia and hyperglycemia at birth. The fact that especially BAT volume and not the degree of ^{18}F-FDG uptake in BAT, as shown by SUV_{max} and SUV_{mean}, was significantly reduced in South Asians, could point to a defect in BAT differentiation resulting in lower total BAT volume. However, since ^{18}F-FDG uptake only represents glucose uptake by the tissue and not metabolism *per se,* a dysfunction in oxidative metabolism in the tissue cannot be excluded and should be further investigated, for example with an ^{11}C-acetate tracer as described above (5) or by studying BAT biopsies.

Several key molecules have been shown in rodent studies to be importantly involved in BAT differentiation, such as bone morphogenetic protein 7 (BMP7) as described in **CHAPTER 5** (81) and nitric oxide (NO). We have previously measured BMP7 levels in several cohorts of South Asian subjects including neonates, and we consistently found increased BMP7 levels compared to white Caucasians (Boon and Bakker et al., *unpublished).* Thus, decreased BAT volume in South Asians does not seem to be caused by decreased differentiation resulting from lower BMP7 availability. NO has been recently linked to BAT, as mice that lack the enzyme NO synthase, crucial for catalyzing the conversion of L-arginine to NO, have fewer

and smaller mitochondria in BAT and lower energy expenditure leading to obesity (82). Recently, healthy South Asian adolescents were shown to have lower flow-mediated vasodilation compared to matched Caucasians (83), which points to lower bioavailability of NO. Thus, an inborn reduction in NO bioavailability might underlie the lower BAT volume and activity in South Asians and is an interesting subject for future studies. In addition, cold acclimation has been recently shown to recruit BAT in healthy subjects (84) and may thus also be of interest in the South Asian population as a tool to enhance their BAT volume with the eventual aim to improve their metabolic phenotype and lower their risk to develop type 2 diabetes and cardiovascular disease.

CONCLUDING REMARKS AND FUTURE DIRECTIONS

Since its rediscovery in 2009, many studies have focused on investigating the physiology and therapeutic relevance of BAT for combating obesity. Murine studies, including those described in this thesis, have shown that activation of BAT markedly enhances energy expenditure resulting in attenuation of obesity, dyslipidemia, and even atherosclerosis. Thus, BAT may be regarded the 'holy grail' of metabolic disease as everybody can potentially benefit from this tool. Indeed, we found a marked increase in NST in healthy white Caucasian subjects upon cold exposure, suggesting that BAT may contribute to total energy expenditure when stimulated. Intriguingly, cold acclimation of healthy subjects has been recently shown to enhance NST and lower fat mass pointing towards a direct role for BAT in energy balance (25). The next few years will likely be as exciting as the past few years for metabolic research as we will now start investigating whether targeting BAT in obese subjects can be used to treat obesity and related diseases such as type 2 diabetes and even atherosclerosis.

Several promising therapeutic strategies to enhance BAT activation have arisen from the present thesis, and now is the time to investigate their efficacy in humans. Among the most promising candidates are peripheral CB1R antagonists **(CHAPTER 7)** although it is crucial to first assess whether the CB1R is also present in human BAT. However, the pharmaceutical industry may be hesitant to develop novel CB1R blockers, even those that would only act peripherally, because of the previous failure of rimonabant. Another promising candidates to activate BAT are MC4R agonists, that currently receive a lot of positive attention. In **CHAPTER 8,** we showed that inhibition of the central MC3/4R impaired BAT function accompanied by reduced energy expenditure. This suggests that enhancing MC3/4R signaling promotes BAT activation and may induce weight loss. Indeed, a recent phase 2 trial in 12 obese, insulin resistant monkeys showed that only 4 weeks of treatment with a MC4R agonist resulted in 13% lower body weight, improvement of insulin sensitivity and enhancement of energy expenditure, which may point to higher BAT activation (Van der Ploeg et al., *unpublished).* Phase 2 trials in humans are currently being performed, and are needed to demonstrate whether MC4R agonists are novel therapeutics to treat obesity and associated disorders, and whether their effects are exerted via activating BAT.

Of note, several mouse studies (85,86), including our study described in **CHAPTER 5,** have shown that enhancing BAT thermogenesis results in a compensatory increase in food intake. This is likely a counteracting mechanism to restore energy balance and may be mediated by several neuronal factors such as NPY. Therefore, energy intake is an important factor to take into account when considering BAT activation as a therapeutic strategy, as people can only benefit from BAT activation when they do not increase their energy intake to compensate for increased expenditure. We, therefore, speculate that in the coming years, studies will also focus on investigating the efficacy of combining BAT activation with other treatment strategies, such as those that lower energy intake *(i.e.* dietary interventions or appetite-suppressing compounds). A promising group of compounds in this respect are GLP-1 analogs or GLP-1 receptor agonists, such as exendin-4. GLP-1 is an incretin hormone produced by intestinal L cells and its endogenous action is to enhance insulin secretion by pancreatic ß cells (87). Therefore, it is currently used in the clinic for treatment of type 2 diabetes. Of note, besides beneficial effects on glucose metabolism, GLP-1 analogs also induce weight loss (88). At least part of the mechanism involves lowering of caloric intake (89), and whether it also affects energy expenditure remains to be determined. Interestingly, central administration of GLP-1 in mice activates BAT (90), making GLP-1 analogs a class of drugs that could potentially target both sides of the energy balance. Future studies should elucidate whether GLP-1 analogs also activate BAT in humans. In order to lower dyslipidemia, combining BAT activation with well-established lipid-lowering strategies may also prove to be very beneficial.

As described in **CHAPTER 9,** BAT activation results in increased delipidation of TRLs in BAT and subsequent hepatic clearance of the remnants, which is crucial to induce lowering of plasma cholesterol and atherosclerosis development. Therefore, combining BAT activation with a treatment strategy that enhances hepatic remnant clearance, *i.e.* statins or PCSK9 inhibitors, may be very promising in lowering dyslipidemia and atherosclerosis development. Future studies are needed to investigate this further.

Finally, a striking finding from the present thesis is that South Asians have lower BAT volume compared to Caucasian subjects. Therefore, a next step would be to investigate the metabolic effects of BAT-directed strategies specifically in the South Asian population, which may result in marked improvement of their disadvantageous metabolic phenotype and prevention of development of type 2 diabetes and cardiovascular disease. Whether a BAT directed strategy is even more effective in South Asians as compared to white Caucasians also remains to be determined.

REFERENCES

1 Cypess AM, Lehman S, Williams G, et al. Identification and importance of brown adipose tissue in adult humans. N Engl J Med 2009; 360: 1509-1517.

2 van Marken Lichtenbelt WD, Vanhommerig JW, Smulders NM, et al. Cold-activated brown adipose tissue in healthy men. N Engl J Med 2009; 360: 1500-1508.

3 Virtanen KA, Lidell ME, Orava J, et al. Functional brown adipose tissue in healthy adults. N Engl J Med 2009; 360: 1518-1525.

4 Cannon B, Nedergaard J: Brown adipose tissue: function and physiological significance. Physiol Rev 2004; 84: 277-359.

5 Ouellet V, Labbe SM, Blondin DP, et al. Brown adipose tissue oxidative metabolism contributes to energy expenditure during acute cold exposure in humans. J Clin Invest 2012; 122: 545-552.

6 Festuccia WT, Blanchard PG, Deshaies Y: Control of Brown Adipose Tissue Glucose and Lipid Metabolism by PPARgamma. Front Endocrinol (Lausanne) 2011; 2: 84.

7 Glatz JF, Luiken JJ, Bonen A: Membrane fatty acid transporters as regulators of lipid metabolism: implications for metabolic disease. Physiol Rev 2010; 90: 367-417.

8 Bartelt A, Bruns OT, Reimer R, et al. Brown adipose tissue activity controls triglyceride clearance. Nat Med 2011; 17: 200-205.

9 Laplante M, Festuccia WT, Soucy G, et al. Tissue-specific postprandial clearance is the major determinant of PPARgamma-induced triglyceride lowering in the rat. Am J Physiol Regul Integr Comp Physiol 2009; 296: R57-R66.

10 Muzik O, Mangner TJ, Leonard WR, et al. 15O PET measurement of blood flow and oxygen consumption in cold-activated human brown fat. J Nucl Med 2013; 54: 523-531.

11 Admiraal WM, Holleman F, Bahler L, et al. Combining 123I-metaiodobenzylguanidine SPECT/CT and 18F-FDG PET/CT for the assessment of brown adipose tissue activity in humans during cold exposure. J Nucl Med 2013; 54: 208-212.

12 Bajzer M, Olivieri M, Haas MK, et al. Cannabinoid receptor 1 (CB1) antagonism enhances glucose utilisation and activates brown adipose tissue in diet-induced obese mice. Diabetologia 2011; 54: 3121-3131.

13 Kang HW, Ribich S, Kim BW, et al. Mice lacking Pctp /StarD2 exhibit increased adaptive thermogenesis and enlarged mitochondria in brown adipose tissue. J Lipid Res 2009; 50: 2212-2221.

14 Gao Z, Yin J, Zhang J, et al. Butyrate improves insulin sensitivity and increases energy expenditure in mice. Diabetes 2009; 58: 1509-1517.

15 Cannon B, Nedergaard J: Nonshivering thermogenesis and its adequate measurement in metabolic studies. J Exp Biol 2011; 214: 242-253.

16 Golozoubova V, Gullberg H, Matthias A, et al. Depressed thermogenesis but competent brown adipose tissue recruitment in mice devoid of all hormone-binding thyroid hormone receptors. Mol Endocrinol 2004; 18: 384-401.

17 van Marken Lichtenbelt WD, Schrauwen P: Implications of nonshivering thermogenesis for energy balance regulation in humans. Am J Physiol Regul Integr Comp Physiol 2011; 301: R285-R296.

18 Bakker LEH, Boon MR, Van der Linden RAD, et al. Brown adipose tissue volume in healthy lean south Asian adults compared with white Caucasians: a prospective, case-controlled observational study. The Lancet Diabetes & Endocrinology 2014; in press.

19 van der Lans AA, Hoeks J, Brans B, et al. Cold acclimation recruits human brown fat and increases nonshivering thermogenesis. J Clin Invest 2013; 123: 3395-3403.

20 Celi FS, Brychta RJ, Linderman JD, et al. Minimal changes in environmental temperature result in a significant increase in energy expenditure and changes in the hormonal homeostasis in healthy adults. Eur J Endocrinol 2010; 163: 863-872.

21 Claessens-van Ooijen AM, Westerterp KR, Wouters L, et al. Heat production and body temperature during cooling and rewarming in overweight and lean men. Obesity (Silver Spring) 2006; 14: 1914-1920.
22 Wijers SL, Saris WH, van Marken Lichtenbelt WD: Cold-induced adaptive thermogenesis in lean and obese. Obesity (Silver Spring) 2010; 18: 1092-1099.
23 Yoneshiro T, Aita S, Matsushita M, et al. Brown adipose tissue, whole-body energy expenditure, and thermogenesis in healthy adult men. Obesity (Silver Spring) 2011; 19: 13-16.
24 Yoneshiro T, Aita S, Matsushita M, et al. Age-related decrease in cold-activated brown adipose tissue and accumulation of body fat in healthy humans. Obesity (Silver Spring) 2011; 19: 1755-1760.
25 Yoneshiro T, Aita S, Matsushita M, et al. Recruited brown adipose tissue as an antiobesity agent in humans. J Clin Invest 2013; 123: 3404-3408.
26 Dong A, Wang Y, Lu J, et al. Hypermetabolic Mesenteric Brown Adipose Tissue on Dual-Time Point FDG PET/CT in a Patient With Benign Retroperitoneal Pheochromocytoma. Clin Nucl Med 2014; 39: e229-e232
27 Addy C, Wright H, Van LK, et al. The acyclic CB1R inverse agonist taranabant mediates weight loss by increasing energy expenditure and decreasing caloric intake. Cell Metab 2008; 7: 68-78.
28 Despres JP, Golay A, Sjostrom L: Effects of rimonabant on metabolic risk factors in overweight patients with dyslipidemia. N Engl J Med 2005; 353: 2121-2134.
29 Pi-Sunyer FX, Aronne LJ, Heshmati HM, et al. Effect of rimonabant, a cannabinoid-1 receptor blocker, on weight and cardiometabolic risk factors in overweight or obese patients: RIO-North America: a randomized controlled trial. JAMA 2006; 295: 761-775.
30 Van Gaal LF, Rissanen AM, Scheen AJ, et al. Effects of the cannabinoid-1 receptor blocker rimonabant on weight reduction and cardiovascular risk factors in overweight patients: 1-year experience from the RIO-Europe study. Lancet 2005; 365: 1389-1397.
31 Backhouse K, Sarac I, Shojaee-Moradie F, et al. Fatty acid flux and oxidation are increased by rimonabant in obese women. Metabolism 2012; 61: 1220-1223.
32 Osei-Hyiaman D, DePetrillo M, Pacher P, et al. Endocannabinoid activation at hepatic CB1 receptors stimulates fatty acid synthesis and contributes to diet-induced obesity. J Clin Invest 2005; 115: 1298-1305.
33 Eckardt K, Sell H, Taube A, et al. Cannabinoid type 1 receptors in human skeletal muscle cells participate in the negative crosstalk between fat and muscle. Diabetologia 2009; 52: 664-674.
34 Cota D, Marsicano G, Tschop M, et al. The endogenous cannabinoid system affects energy balance via central orexigenic drive and peripheral lipogenesis. J Clin Invest 2003; 112: 423-431.
35 Tam J, Vemuri VK, Liu J, et al. Peripheral CB1 cannabinoid receptor blockade improves cardiometabolic risk in mouse models of obesity. J Clin Invest 2010; 120: 2953-2966.
36 Wu HM, Yang YM, Kim SG: Rimonabant, a cannabinoid receptor type 1 inverse agonist, inhibits hepatocyte lipogenesis by activating liver kinase B1 and AMP-activated protein kinase axis downstream of Galpha i/o inhibition. Mol Pharmacol 2011; 80: 859-869.
37 Tedesco L, Valerio A, Cervino C, et al. Cannabinoid type 1 receptor blockade promotes mitochondrial biogenesis through endothelial nitric oxide synthase expression in white adipocytes. Diabetes 2008; 57: 2028-2036.
38 Omar B, Zmuda-Trzebiatowska E, Manganiello V, et al. Regulation of AMP-activated protein kinase by cAMP in adipocytes: roles for phosphodiesterases, protein kinase B, protein kinase A, Epac and lipolysis. Cell Signal 2009; 21: 760-766.

39 Felder CC, Joyce KE, Briley EM, et al. LY320135, a novel cannabinoid CB1 receptor antagonist, unmasks coupling of the CB1 receptor to stimulation of cAMP accumulation. J Pharmacol Exp Ther 1998; 284: 291-297.
40 Goodarzi MO, Bryer-Ash M: Metformin revisited: re-evaluation of its properties and role in the pharmacopoeia of modern antidiabetic agents. Diabetes Obes Metab 2005; 7: 654-665.
41 Nathan DM, Buse JB, Davidson MB, et al. Medical management of hyperglycaemia in type 2 diabetes mellitus: a consensus algorithm for the initiation and adjustment of therapy: a consensus statement from the American Diabetes Association and the European Association for the Study of Diabetes. Diabetologia 2009; 52: 17-30.
42 Salpeter SR, Buckley NS, Kahn JA, et al. Meta-analysis: metformin treatment in persons at risk for diabetes mellitus. Am J Med 2008; 121: 149-157.
43 Bijland S, Pieterman EJ, Maas AC, et al. Fenofibrate increases very low density lipoprotein triglyceride production despite reducing plasma triglyceride levels in APOE*3-Leiden.CETP mice. J Biol Chem 2010; 285: 25168-25175.
44 de HW, van der Hoogt CC, Westerterp M, et al. Atorvastatin increases HDL cholesterol by reducing CETP expression in cholesterol-fed APOE*3-Leiden.CETP mice. Atherosclerosis 2008; 197: 57-63.
45 Golay A: Metformin and body weight. Int J Obes (Lond) 2008; 32: 61-72.
46 Kahn SE, Haffner SM, Heise MA, et al. Glycemic durability of rosiglitazone, metformin, or glyburide monotherapy. N Engl J Med 2006; 355: 2427-2443.
47 Yamanouchi T, Sakai T, Igarashi K, et al. Comparison of metabolic effects of pioglitazone, metformin, and glimepiride over 1 year in Japanese patients with newly diagnosed Type 2 diabetes. Diabet Med 2005; 22: 980-985.
48 Freemark M, Bursey D: The effects of metformin on body mass index and glucose tolerance in obese adolescents with fasting hyperinsulinemia and a family history of type 2 diabetes. Pediatrics 2001; 107: E55.
49 Gottschalk M, Danne T, Vlajnic A, et al. Glimepiride versus metformin as monotherapy in pediatric patients with type 2 diabetes: a randomized, single-blind comparative study. Diabetes Care 2007; 30: 790-794.
50 Srinivasan S, Ambler GR, Baur LA, et al. Randomized, controlled trial of metformin for obesity and insulin resistance in children and adolescents: improvement in body composition and fasting insulin. J Clin Endocrinol Metab 2006; 91: 2074-2080.
51 Boule NG, Robert C, Bell GJ, et al. Metformin and exercise in type 2 diabetes: examining treatment modality interactions. Diabetes Care 2011; 34: 1469-1474.
52 Stephenne X, Foretz M, Taleux N, et al. Metformin activates AMP-activated protein kinase in primary human hepatocytes by decreasing cellular energy status. Diabetologia 2011; 54: 3101-3110.
53 Musi N, Hirshman MF, Nygren J, et al. Metformin increases AMP-activated protein kinase activity in skeletal muscle of subjects with type 2 diabetes. Diabetes 2002; 51: 2074-2081.
54 Turban S, Stretton C, Drouin O, et al. Defining the contribution of AMP-activated protein kinase (AMPK) and protein kinase C (PKC) in regulation of glucose uptake by metformin in skeletal muscle cells. J Biol Chem 2012; 287: 20088-20099.
55 Shan T, Liang X, Bi P, et al. Myostatin knockout drives browning of white adipose tissue through activating the AMPK-PGC1alpha-Fndc5 pathway in muscle. FASEB J 2013; 27: 1981-1989.
56 Lv WS, Wen JP, Li L, et al. The effect of metformin on food intake and its potential role in hypothalamic regulation in obese diabetic rats. Brain Res 2012; 1444: 11-19.
57 Carling D, Thornton C, Woods A, et al. AMP-activated protein kinase: new regulation, new roles? Biochem J 2012; 445: 11-27.

58 Hardie DG, Ross FA, Hawley SA: AMPK: a nutrient and energy sensor that maintains energy homeostasis. Nat Rev Mol Cell Biol 2012; 13: 251-262.
59 Hawley SA, Gadalla AE, Olsen GS, et al. The antidiabetic drug metformin activates the AMP-activated protein kinase cascade via an adenine nucleotide-independent mechanism. Diabetes 2002; 51: 2420-2425.
60 Hardie DG: AMPK: a key regulator of energy balance in the single cell and the whole organism. Int J Obes (Lond) 2008; Suppl 4: S7-12.
61 Zhang BB, Zhou G, Li C: AMPK: an emerging drug target for diabetes and the metabolic syndrome. Cell Metab 2009; 9: 407-416.
62 Mulligan JD, Gonzalez AA, Stewart AM, et al. Upregulation of AMPK during cold exposure occurs via distinct mechanisms in brown and white adipose tissue of the mouse. J Physiol 2007; 580: 677-684.
63 Pulinilkunnil T, He H, Kong D, et al. Adrenergic regulation of AMP-activated protein kinase in brown adipose tissue in vivo. J Biol Chem 2011; 286: 8798-8809.
64 Bauwens JD, Schmuck EG, Lindholm CR, et al. Cold tolerance, cold-induced hyperphagia, and nonshivering thermogenesis are normal in alpha(1)-AMPK-/- mice. Am J Physiol Regul Integr Comp Physiol 2011; 301: R473-R483.
65 Sim AT, Hardie DG: The low activity of acetyl-CoA carboxylase in basal and glucagon-stimulated hepatocytes is due to phosphorylation by the AMP-activated protein kinase and not cyclic AMP-dependent protein kinase. FEBS Lett 1988; 233: 294-298.
66 Jornayvaz FR, Shulman GI: Regulation of mitochondrial biogenesis. Essays Biochem 2010; 47: 69-84.
67 Thors B, Halldorsson H, Thorgeirsson G: eNOS activation mediated by AMPK after stimulation of endothelial cells with histamine or thrombin is dependent on LKB1. Biochim Biophys Acta 2011; 1813: 322-331.
68 Nisoli E, Carruba MO: Nitric oxide and mitochondrial biogenesis. J Cell Sci 2006; 119: 2855-2862.
69 Jager S, Handschin C, St-Pierre J, et al. AMP-activated protein kinase (AMPK) action in skeletal muscle via direct phosphorylation of PGC-1alpha. Proc Natl Acad Sci U S A 2007; 104: 12017-12022.
70 Ohira M, Miyashita Y, Murano T, et al. Metformin promotes induction of lipoprotein lipase in skeletal muscle through activation of adenosine monophosphate-activated protein kinase. Metabolism 2009; 58: 1408-1414.
71 Jeppesen J, Albers PH, Rose AJ, et al. Contraction-induced skeletal muscle FAT/CD36 trafficking and FA uptake is AMPK independent. J Lipid Res 2011; 52: 699-711.
72 Mantha L, Deshaies Y: beta-Adrenergic modulation of triglyceridemia under increased energy expenditure. Am J Physiol 1998; 274: R1769-R1776.
73 Dong M, Yang X, Lim S, et al. Cold exposure promotes atherosclerotic plaque growth and instability via UCP1-dependent lipolysis. Cell Metab 2013; 18: 118-129.
74 Geerling JJ, Boon MR, Kooijman S, et al. Sympathetic nervous system control of triglyceride metabolism: novel concepts derived from recent studies. J Lipid Res 2014; 55: 180-189.
75 Yilmaz Y, Ones T, Purnak T, et al. Association between the presence of brown adipose tissue and non-alcoholic fatty liver disease in adult humans. Aliment Pharmacol Ther 2011; 34: 318-323.
76 Labruna G, Pasanisi F, Nardelli C, et al. UCP1 -3826 AG+GG genotypes, adiponectin, and leptin/adiponectin ratio in severe obesity. J Endocrinol Invest 2009; 32: 525-529.
77 Hall LM, Moran CN, Milne GR, et al. Fat oxidation, fitness and skeletal muscle expression of oxidative/lipid metabolism genes in South Asians: implications for insulin resistance? PLoS One 2010; 5: e14197.
78 Vosselman MJ, Brans B, van der Lans AA, et al. Brown adipose tissue activity after a high-calorie meal in humans. Am J Clin Nutr 2013; 98: 57-64.
79 Vijgen GH, Bouvy ND, Teule GJ, et al. Brown adipose tissue in morbidly obese subjects. PLoS One 2011; 6: e17247.

80 Vosselman MJ, van der Lans AA, Brans B, et al. Systemic beta-adrenergic stimulation of thermogenesis is not accompanied by brown adipose tissue activity in humans. Diabetes 2012; 61: 3106-3113.
81 Tseng YH, Kokkotou E, Schulz TJ, et al. New role of bone morphogenetic protein 7 in brown adipogenesis and energy expenditure. Nature 2008; 454: 1000-1004.
82 Nisoli E, Clementi E, Paolucci C, et al. Mitochondrial biogenesis in mammals: the role of endogenous nitric oxide. Science 2003; 299: 896-899.
83 Cubbon RM, Murgatroyd SR, Ferguson C, et al. Human exercise-induced circulating progenitor cell mobilization is nitric oxide-dependent and is blunted in South Asian men. Arterioscler Thromb Vasc Biol 2010; 30: 878-884.
84 van der Lans AA, Hoeks J, Brans B, et al. Cold acclimation recruits human brown fat and increases nonshivering thermogenesis. J Clin Invest 2013; 123: 3395-3403.
85 Plaisance EP, Henagan TM, Echlin H, et al. Role of beta-adrenergic receptors in the hyperphagic and hypermetabolic responses to dietary methionine restriction. Am J Physiol Regul Integr Comp Physiol 2010; 299: R740-R750.
86 Ravussin Y, Xiao C, Gavrilova O, et al. Effect of intermittent cold exposure on brown fat activation, obesity, and energy homeostasis in mice. PLoS One 2014; 9: e85876.
87 Phillips LK, Prins JB: Update on incretin hormones. Ann N Y Acad Sci 2011; 1243: E55-E74.
88 Boland CL, Degeeter M, Nuzum DS, et al. Evaluating second-line treatment options for type 2 diabetes: focus on secondary effects of GLP-1 agonists and DPP-4 inhibitors. Ann Pharmacother 2013; 47: 490-505.
89 Bradley DP, Kulstad R, Racine N, et al. Alterations in energy balance following exenatide administration. Appl Physiol Nutr Metab 2012; 37: 893-899.
90 Lockie SH, Heppner KM, Chaudhary N, et al. Direct control of brown adipose tissue thermogenesis by central nervous system glucagon-like peptide-1 receptor signaling. Diabetes 2012; 61: 2753-2762.

15

SUMMARY AND NEDERLANDSE SAMENVATTING

16

SUMMARY

In 1551, the Swiss naturalist Konrad Gessner first described brown adipose tissue (BAT) as being "neither fat, nor flesh *(nec pinguitudo, nec caro),* but something in between". Now, some 460 years later, we know that Gessner had guessed the origin of brown adipocytes correctly – they are not typical fat-storing cells or flesh (muscle cells), but rather have characteristics of both white adipocytes and muscle cells, as well as several characteristics unique to brown fat cells. A unique property of the brown adipocyte is its capacity to dissipate energy stored in triglycerides (TG) as heat, which is mediated via the uncoupling protein UCP1. The recent discovery that active BAT is present in human adults meant the beginning of an exciting new area in metabolic research. BAT is currently regarded as a potential target to combat obesity and related diseases by inducing a sustained increase in energy expenditure. Interestingly, South Asians have lower energy expenditure, which may thus theoretically be caused by a reduction in BAT activity. The studies of which the results are described in this thesis were aimed at 1) gaining more insight into the physiology of BAT, 2) identifying novel tools and targets that may activate BAT, and 3) investigating the involvement of BAT in metabolism in humans with a focus on potential differences between South Asians and white Caucasians.

CHAPTER 1, CHAPTER 2 and **CHAPTER 3** in the first part of the thesis serve as a general introduction to the physiology of BAT, its potential role in metabolic disease as well as an outline on the disadvantageous metabolic phenotype of the South Asian population.

In the second part of the thesis, we investigated the role of BAT in metabolism and obesity using mouse models. Fatty acids (FA) are the main fuel for thermogenesis in BAT and intracellular triglyceride (TG) stores are rapidly depleted upon BAT activation. Therefore, BAT is required to take up FA from the plasma in order to replenish its intracellular energy stores. In **CHAPTER 4,** we investigated the mechanism by which BAT takes up TG-derived FA from lipoproteins by performing kinetic studies using glycerol tri[^{3}H]oleate and [^{14}C]cholesteryl oleate double-labeled TG-rich lipoprotein -like emulsion particles. We showed that BAT takes up TG-derived FA by means of selective FA uptake, thereby generating remnant particles that are subsequently taken up by the liver. Large chylomicron-sized particles showed higher retention in BAT than small VLDL-sized particles, the mechanism of which is still unclear.

Next, we focused on compounds, receptors and intracellular pathways that may activate BAT, thereby enhancing energy expenditure and clearance of plasma TG, and the underlying mechanisms. Based on the discovery that BMP7 can activate BAT, in **CHAPTER 5,** we investigated the mechanism by which BMP7 activates BAT with special focus on the role of the sympathetic nervous system. Hereto, we treated high-fat diet fed lean mice and diet-induced obese mice with BMP7 at 21°C and 28°C, the latter being the thermoneutral temperature of mice at which sympathetic activation of BAT is largely diminished. We found that, at 21°C, BMP7 enhanced interscapular BAT volume and activity as well as energy expenditure, and reduced white adipose tissue (WAT) mass. Of note, all these effects were blunted at 28°C. Furthermore, BMP7 resulted in massive 'browning' *(i.e.* appearance of beige adipocytes) of the WAT depot, independent of environmental temperature. Furthermore,

treatment of diet-induced obese mice with BMP7 led to an improved metabolic phenotype, consisting of decreased fat mass, liver lipids and dyslipidemia. We concluded that 1) sympathetic activation of interscapular BAT is required for the effects of BMP7 on this BAT depot, suggesting at least in part a central mode of action of BMP7; 2) BMP7 has therapeutic potential to lower obesity and dyslipidemia by inducing recruitment and activation of interscapular BAT as well as browning.

In **CHAPTER 6,** the mechanism by which the anti-diabetic drug metformin lowers plasma TG was investigated in dyslipidemic APOE*3-Leiden.CETP transgenic mice, a well-established model for human-like lipoprotein metabolism. We showed that metformin did not affect liver lipids or hepatic VLDL-TG production. Rather, metformin enhanced plasma clearance of glycerol tri[^{3}H]oleate-labeled VLDL-like emulsion particles by inducing selectively enhanced uptake of [^{3}H]oleate by BAT. This was accompanied by enhanced activity of AMP-activated protein kinase (AMPK) α1 as well as higher HSL activity and decreased intracellular lipid droplet size in BAT. *In vitro* studies using T37i differentiated brown adipocytes showed that metformin exerts a direct effect on brown adipocytes by increasing AMPK and HSL activities and promoting lipolysis. Collectively, our results identified BAT as an important player in the TG-lowering effect of metformin and intracellular AMPK may be the crucial intracellular mediator of this effect.

Rimonabant is a systemic cannabinoid 1 receptor (CB1R) blocker that has been previously shown to induce sustained weight loss and lowering of plasma TG levels in obese patients. In **CHAPTER 7,** we investigated whether the TG-lowering effect of rimonabant was due to activation of BAT. To this end, we treated diet-induced obese APOE*3-Leiden.CETP transgenic mice with rimonabant and showed that, next to a massive lowering in body weight and plasma TG levels, rimonabant enhanced energy expenditure while only transiently decreasing food intake. Kinetic studies with glycerol tri[^{3}H]oleate-labeled VLDL-like emulsion particles showed that rimonabant selectively increased uptake of radiolabel by BAT, accompanied by decreased lipid droplet size in BAT, all pointing to increased BAT activity. Of note, the results could be fully recapitulated at thermoneutral temperature, suggesting that the mechanism involves peripheral rather than central activation of BAT. Indeed, we demonstrated that the CB1R is highly expressed in BAT and that *in vitro* blockade of the CB1R in cultured brown adipocytes increases UCP1 content and lipolysis. Furthermore, treatment of mice with the strictly peripheral CB1R antagonist AM6545 resulted in lowering of body weight and plasma VLDL-TG, together with enhanced BAT activation as evidenced by enhanced energy expenditure, uptake of VLDL-TG derived FA by BAT and UCP1 content in BAT. All together, we concluded that the TG-lowering effect of rimonabant is due to peripheral blockade of the CB1R on BAT.

Melanocortin 4 receptor (MC4R) deficiency is the most common monogenic cause of obesity. Therefore, in **CHAPTER 8,** we aimed to investigate the role of the melanocortin system in BAT function. We treated APOE*3-Leiden.CETP transgenic mice with the MC3/4R antagonist SHU9119 or vehicle for 2 weeks via continuous infusion into the lateral ventricle. We found that blockade of the central MC3/4R increases food intake and body weight and markedly diminishes fat oxidation, as well as impairs the uptake of [^{3}H]oleate from glycerol tri[^{3}H]

oleate-labeled VLDL-like emulsion particles by BAT. Furthermore, central MC3/4R blockade decreased UCP1 protein levels in BAT and induced large intracellular lipid droplets in the tissue, all pointing to lower BAT activity. All these effects were independent of the increased food intake induced by central MC3/4R blockade as mice that received SHU9119 while being pair-fed to the vehicle-treated group still exhibited these effects. We concluded that inhibition of central MC3/4R signaling impairs BAT function accompanied by reduced energy expenditure thereby promoting adiposity.

To investigate whether BAT activation could protect against atherosclerosis development, in **CHAPTER 9,** we treated dyslipidemic APOE*3-Leiden.CETP mice fed a Western-type diet with the ß3-adrenergic agonist CL316243. We found that CL316243 induces a massive increase in BAT activation, accompanied by increased energy expenditure, lower body fat mass and plasma TG levels, lower plasma cholesterol levels and reduced development of atherosclerosis. Kinetic studies showed that BAT activation enhanced the selective uptake of fatty acids from glycerol tri[^{3}H]oleate-labeled VLDL-like emulsion particles into BAT. Importantly, the cholesterol and atherosclerosis lowering effects of BAT activation were dependent on a functional hepatic apoE-LDLr clearance pathway, as BAT activation in *apoe*$^{-/-}$ and *ldlr*$^{-/-}$ mice, while lowering triglyceride levels, did not attenuate hypercholesterolemia and atherosclerosis. We concluded that activation of BAT is a novel tool to improve dyslipidemia and protect against atherosclerosis.

In the third part of the thesis, human studies on metabolism, obesity and BAT were performed. A well-known cause of obesity is long term high-fat feeding, which can result in development of insulin resistance and eventually type 2 diabetes. Recent studies have demonstrated elevated macrophage markers in skeletal muscle of obese subjects, which inversely related to insulin sensitivity. In **CHAPTER 10,** we aimed to investigate whether a short term high-fat high-calorie diet (HCD) diet already increases macrophage markers and affects glucose metabolism in skeletal muscle of healthy lean subjects. We found that 5 days of HCD markedly increases mRNA expression of several general macrophage markers as well as the M1 macrophage marker *MARCO* in muscle biopsies taken before and after the diet intervention. This was accompanied by downregulation of genes involved in uptake and storage of glucose, and elevation of plasma glucose and insulin levels together with HOMA-IR. We concluded that recruitment of macrophages into muscle may be an early event in development of insulin resistance in the course of obesity.

The South Asian population is especially prone to develop obesity and related disorders, such as type 2 diabetes and cardiovascular disease (CVD). In **CHAPTER 11,** we investigated whether the high CVD risk in the South Asian population may be due to an ethnic susceptibility to develop endothelial activation. To this end, we measured markers for endothelial activation (E-selectin, intercellular adhesion molecule 1 (ICAM-1), and vascular adhesion molecule 1 (VCAM-1)) in cord blood of South Asian and white Caucasian neonates. We found that plasma E-selectin levels are markedly higher in South Asian neonates, while levels of ICAM-1 and VCAM-1 do not differ from those in white Caucasian neonates. Strikingly, the South Asian neonates had hyperinsulinemia, dyslipidemia and higher C-reactive protein levels, the latter pointing to inflammation. Based on these data, we drew two important

conclusions: 1) in South Asian neonates, a sign for endothelial activation is already present in early life; 2) signs of the disadvantageous metabolic phenotype of South Asians are already present at birth.

Since endothelial activation may be the consequence of disturbed HDL function, in **CHAPTER 12** we investigated whether HDL dysfunction may be present in the South Asian population by measuring different measures of HDL functionality in 3 cohorts of South Asian subjects and matched white Caucasian subjects *(i.e.,* neonates, adolescents and adults). The cholesterol efflux capacity of HDL was comparable between groups. We found that the anti-oxidative capacity of HDL is lower in South Asian adults, while at younger ages this function is still comparable between both ethnicities suggesting that this function decreases over time. In contrast, the anti-inflammatory capacity of HDL was markedly lower in South Asian neonates, a difference that disappeared at adolescent and adult age. We concluded that South Asians exhibit disturbed HDL function compared to Caucasians, which may contribute to their endothelial activation and excess CVD risk.

The highly prevalent disadvantageous metabolic phenotype consisting of obesity, dyslipidemia and insulin resistance likely also underlies the high CVD risk in the South Asian population. Since an ethnic susceptibility towards a disturbed energy homeostasis may underlie this phenotype, we investigated in **CHAPTER 13** resting energy expenditure (REE) as well as BAT volume and activity by means of cold-induced ^{18}F-FDG PET-CT scans in healthy lean Dutch South Asian and matched white Caucasian subjects. We demonstrated that REE is a marked 32% lower in healthy lean Dutch South Asian compared to Dutch Caucasian adolescents. Furthermore, cold exposure significantly increased non-shivering thermogenesis (NST) in white Caucasians, but not in South Asians. Moreover, though SUV_{max} and SUV_{mean} did not differ, BAT volume was markedly lower in South Asians. Our study suggests that South Asians have lower REE and BAT volume as compared to matched Caucasians, which might underlie their high susceptibility to develop the disadvantageous metabolic phenotype at later age.

The ^{18}F-FDG PET-CT scan is currently the 'gold standard' to determine BAT volume and activity, but its use is limited by cost and radiation exposure. The eventual product of BAT thermogenesis is heat production. Therefore, in **CHAPTER 14** we investigated whether supraclavicular skin temperature as measured via iButtons or core body temperature as measured via a telemetric capsule may serve as a quantitative measure of ^{18}F-FDG uptake in human subjects. We found that cold-induced supraclavicular skin temperature positively correlates with both total and clavicular BAT volume and clavicular SUV_{max}, while core body temperature did not. Therefore, we concluded that supraclavicular skin temperature as measured by iButtons is a potential novel non-invasive tool for qualitative BAT detection in adult humans.

Taken together, the studies described in this thesis show that BAT is a promising target to combat obesity, dyslipidemia, and even atherosclerosis. We demonstrated that BAT is an important player in VLDL-TG metabolism by selective uptake of FA from plasma. Treatment of mice with BMP7, rimonabant, metformin or CL316243 enhances BAT activation, accompanied by reduction of fat mass and plasma TG levels. On the other hand, blockade of the

central MC3/4R causes BAT dysfunction and development of obesity. These findings suggest that pharmacological activation of BAT is feasible, possibly also in humans. We provided evidence that BAT may be of significance in adult humans by showing that South Asians, which are very prone to develop obesity, dyslipidemia and type 2 diabetes, exhibit a marked reduction in BAT volume together with lower NST and REE as compared to matched white Caucasians. The finding that supraclavicular skin temperature correlates with ^{18}F-FDG uptake in human subjects may be developed into a surrogate marker for BAT activity in the future. This is highly relevant as BAT is currently targeted as a novel strategy to comBAT obesity and related diseases such as type 2 diabetes and atherosclerosis.

NEDERLANDSE SAMENVATTING

In 1551 beschreef de Zwitserse naturalist Konrad Gessner bruin vet als "geen vet, en ook geen vlees *(nec pinguitudo, nec caro),* maar iets ertussenin". Nu, zo'n 460 jaar later, weten we dat Gessner de oorsprong van bruine vetcellen goed had geraden – het zijn geen typische opslagcellen voor vet of 'vlees' (spiercellen), maar hebben juist kenmerken van zowel witte vetcellen als spiercellen, evenals verscheidene kenmerken die uniek zijn voor bruine vetcellen. Eén van de unieke eigenschappen van bruin vet is de mogelijkheid om energie die opgeslagen is in vet ('triglyceriden', TG) te verbranden tot warmte, een proces waarvoor het ontkoppelingseiwit UCP1, dat specifiek in bruin vet voorkomt, mede verantwoordelijk is. De recente ontdekking dat bruin vet zowel aanwezig als actief is in volwassenen betekende het begin van een fascinerend nieuw onderzoeksgebied in het veld van metabolisme. Omdat bruin vet grote hoeveelheden vet letterlijk kan oplossen, en op die manier in belangrijke mate bijdraagt aan 'energieverbruik', wordt bruin vet momenteel beschouwd als een mogelijk aangrijpingspunt om obesitas en aan obesitas gerelateerde stoornissen in de stofwisseling tegen te gaan zoals type 2 diabetes en hart- en vaatziekten (HVZ). Interessant is dat Hindoestanen, een bevolkingsgroep die ten opzichte van blanke Kaukasiërs erg gevoelig is voor het ontwikkelen van type 2 diabetes en HVZ, een lager energieverbruik hebben wat in theorie dus veroorzaakt zou kunnen worden door een verlaagde activiteit van het bruin vet. De studies waarvan de resultaten in dit proefschrift beschreven staan hadden tot doel om 1) meer inzicht te verwerven in de fysiologie van bruin vet, 2) nieuwe methoden en aangrijpingspunten die bruin vet kunnen activeren te identificeren, en 3) te onderzoeken in hoeverre bruin vet betrokken is bij de stofwisseling in mensen, met name gericht op mogelijke verschillen tussen Hindoestanen en blanke Kaukasiërs.

HOOFDSTUK 1, HOOFDSTUK 2 en **HOOFDSTUK 3** fungeren als een algemene introductie op de fysiologie van bruin vet, de mogelijke rol van bruin vet in stofwisselingsziekten en geven tevens een overzicht van het ongunstige metabole fenotype van de Hindoestaanse bevolking.

In het tweede deel van het proefschrift onderzochten we de rol van bruin vet in de stofwisseling en obesitas in muismodellen. Vetzuren vormen de belangrijkste brandstof voor de warmteproductie ('thermogenese') in bruin vet en activatie van bruin vet leidt tot

snelle uitputting van intracellulair TG. Bruin vet moet daarom vetzuren opnemen uit het bloed om zijn energievoorraad aan te vullen. Het was al bekend dat bruin vet TG opneemt vanuit bolvormige deeltjes die vet door het bloed transporteren (zogenaamde 'lipoproteïnen'), maar het mechanisme was nog niet opgehelderd. In **HOOFDSTUK 4** onderzochten we het onderliggende mechanisme door gebruik te maken van emulsiedeeltjes die het biologisch gedrag vertonen van lipoproteïnen, en waarvan TG en cholesterolesters radioactief gemerkt kunnen worden met respectievelijk glycerol tri[^{3}H]oleaat en [^{14}C]cholesterololeaat. We toonden aan dat bruin vet veel meer [^{3}H]oleaat opneemt dan [^{14}C]cholesterololeaat, wat erop wijst dat bruin vet selectief vetzuren uit TG van lipoproteïnen onttrekt. Hierdoor ontstaan overblijfsels van lipoproteïnen (zogenaamde 'remnants') die vervolgens kunnen worden opgenomen door de lever.

Vervolgens bestudeerden we geneesmiddelen, receptoren en intracellulaire routes die bruin vet zouden kunnen activeren, als ook onderliggende mechanismen. Geïnspireerd door een eerdere ontdekking dat het eiwit BMP7 ('bone morphogenetic protein 7') bruin vet kan activeren, onderzochten we in **HOOFDSTUK 5** het mechanisme waarmee BMP7 bruin vet activeert waarbij we ons met name focusten op de rol van het sympathisch zenuwstelsel. Hiertoe behandelden we slanke muizen die een vetrijk dieet kregen en dikke muizen na een vetrijk dieet met BMP7. We toonden aan dat BMP7 het volume en de activiteit van het bruin vet tussen de schouderbladen ('interscapulair') verhoogde, evenals het energieverbruik, terwijl behandeling met BMP7 de hoeveelheid wit vet juist deed afnemen. Opvallend was dat deze effecten van BMP7 niet optraden als we de muizen huisvestten bij een omgevingstemperatuur van 28°C, de 'thermoneutrale' temperatuur waarbij de hersenen geen signaal meer sturen naar bruin vet door zogenaamde 'sympathische activatie' om de muis warm te houden. Tevens leidde behandeling met BMP7 tot aanzienlijke vorming van beige vetcellen in het witte vet (zogenaamde 'browning'), onafhankelijk van de omgevingstemperatuur. Ook verbeterde BMP7 het metabole fenotype van obese muizen; het verminderde de hoeveelheid vet in vetweefsel en in de lever en verlaagde de vetconcentratie in het bloed ('dyslipidemie'). We concludeerden daarom dat BMP7 bruin vet grotendeels activeert door sympathische activatie vanuit de hersenen. BMP7 kan dus mogelijk worden toegepast om obesitas en dyslipidemie te verminderen door vermeerdering en activatie van bruin vet en door vorming van beige vetcellen.

Metformine is een geneesmiddel dat in de kliniek wordt toegepast bij de behandeling van type 2 diabetes. Het verbetert de glucosestofwisseling maar verlaagt ook de TG concentratie in het bloed en veroorzaakt een geringe afname van het lichaamsgewicht. In **HOOFDSTUK 6** werd het onderliggende mechanisme onderzocht waardoor metformine TG verlaagt door gebruik te maken van dyslipidemische APOE*3-Leiden.CETP transgene muizen, een goed gevalideerd muismodel met een vetstofwisseling die sterk overeenkomt met die van de mens. We lieten zien dat metformine TG niet verlaagt door de productie van VLDL-TG door de lever te verminderen. In plaats daarvan verhoogde metformine selectief de opname van [^{3}H]oleaat vanuit glycerol tri[3H]oleaat-gelabelde VLDL-achtige emulsiedeeltjes door bruin vet. Dit ging gepaard met een verhoogde activiteit van zowel het AMP-geactiveerde proteïne kinase (AMPK) α1 als de activiteit van het hormoon-sensitieve lipase (HSL) in bruin

vet en het ontstaan van kleinere intracellulaire vetdruppels in het weefsel. *In vitro* studies met gedifferentieerde bruin vetcellen (zogenaamde 'T37i cellen') toonden aan dat metformine een direct effect op bruine vetcellen uitoefent door AMPK te activeren en daarmee de activiteit van HSL te verhogen en de afbraak van intracellulair TG ('lipolyse') te stimuleren. Al met al lieten onze resultaten zien dat bruin vet een belangrijke speler is in de effecten van metformine op TG en dat activatie van intracellulair AMPK daarbij een rol speelt.

Behandeling van obese patiënten met rimonabant, een remmer van de cannabinoid 1 receptor (CB1R), leidde tot langdurig gewichtsverlies en verbetering van hun dyslipidemie. Het werd echter in 2008 van de markt gehaald vanwege psychiatrische bijwerkingen. Om meer inzicht te krijgen hoe rimonabant zo'n groot en langdurig effect op obesitas kon hebben onderzochten we in **HOOFDSTUK 7** of rimonabant ook in staat zou zijn bruin vet te activeren. Hiertoe behandelden we dieet-geïnduceerde obese APOE*3-Leiden.CETP transgene muizen met rimonabant. We lieten zien dat rimonabant niet alleen leidde tot een behoorlijke verlaging in lichaamsgewicht en TG niveaus in het bloed, maar ook het energieverbruik verhoogde terwijl het slechts tijdelijk de voedselinname remde. Studies met glycerol tri[^{3}H] oleaat-gelabelde VLDL-achtige emulsiedeeltjes lieten zien dat rimonabant selectief de opname van [^{3}H]oleaat door bruin vet verhoogde en de vetdruppels in bruin vet verkleinde, wat allebei wijst op een verhoogde activiteit van het weefsel. Opvallend was dat we dezelfde resultaten verkregen bij thermoneutraliteit. Dit suggereert dat rimonabant waarschijnlijk niet de sympathische aansturing vanuit de hersenen moduleert maar direct aangrijpt op het bruin vet. Inderdaad konden we aantonen dat de CB1R in hoge mate tot expressie komt in bruin vet en dat *in vitro* remming van de CB1R in de T37i cellen leidde tot een verhoging van zowel de hoeveelheid UCP1 als de intracellulaire TG afbraak. Behandeling van muizen met de CB1R antagonist AM6545 die de hersenen dus niet kan bereiken ('strikt perifere antagonist') leidde ook tot verlaging van het lichaamsgewicht en TG, wat samenging met verhoogde bruin vet activatie. Dit laatste bleek uit een verhoogd energieverbruik, verhoogde opname van vetzuren vanuit VLDL-TG door bruin vet en tevens een verhoogde hoeveelheid UCP1. Samenvattend concludeerden we dat het effect van rimonabant op TG en lichaamsgewicht grotendeels toe te schrijven is aan directe remming van de CB1R in bruin vet.

Melanocortine 4 receptor (MC4R) deficiëntie is de meest voorkomende monogene oorzaak van obesitas. In **HOOFDSTUK 8** onderzochten we daarom de rol van het melanocortinesysteem in de functie van bruin vet. We behandelden APOE*3-Leiden.CETP transgene muizen met de MC3/4R antagonist SHU9119 of placebo gedurende 2 weken door middel van continue infusie in de laterale ventrikel in de hersenen omdat het melanocortinesysteem aldaar tot expressie komt. We toonden aan dat remming van de centrale MC3/4R leidde tot een verhoging van zowel de voedselinname als het lichaamsgewicht, een aanzienlijke verlaging in vetoxidatie, en een verlaagde opname van [^{3}H]oleaat vanuit glycerol tri[^{3}H]oleaat-gelabelde VLDL-achtige emulsiedeeltjes door bruin vet. Verder leidde remming van de centrale MC3/4R tot verlaagde UCP1 eiwit niveaus in bruin vet en leidde het tot de vorming van grote intracellulaire vetdruppels in het weefsel, beide wijzend op een verlaagde activiteit van het bruin vet. Al deze effecten waren onafhankelijk van de verhoogde voedselinname dat het gevolg was door centrale MC3/4R remming aangezien deze effecten nog steeds

optraden in muizen die behandeld werden met SHU9119 terwijl ze dezelfde hoeveelheid voedsel ontvingen als de controlemuizen. We concludeerden dat remming van centrale MC3/4R signalering de functie van bruin vet en het energieverbruik vermindert, wat leidt tot een toename van adipositas.

Om te onderzoeken of activatie van bruin vet zou kunnen beschermen tegen de ontwikkeling van atherosclerose, hebben we in **HOOFDSTUK 9** dyslipidemische APOE*3-Leiden.CETP muizen behandeld met CL316243, een agonist van de ß3-adrenerge receptor die normaalgesproken door stimulatie van het sympathische zenuwstelsel wordt geactiveerd. CL316243 leidde tot een opvallende activatie van het bruin vet en induceerde 'browning'. Tevens leidde CL316243 tot een toename van het energiegebruik, een verlaging van de hoeveelheid lichaamsvet en TG niveaus in het bloed, een verlaging van cholesterolniveaus in het bloed en beschermde het tegen de ontwikkeling van atherosclerose. Kinetische studies lieten zien dat activatie van de ß3-adrenerge receptor de selectieve opname van vetzuren vanuit glycerol tri[^{3}H]oleaat-gelabelde VLDL-achtige emulsiedeeltjes door het bruin vet verhoogde. Een belangrijke bevinding was tevens dat de verlaging van zowel cholesterol als atherosclerose ten gevolge van bruin vet activatie afhankelijk waren van de opname van gegenereerde lipoproteïnen remnants via het apolipoproteïne apoE door de LDL receptor op de lever. Activatie van bruin vet in muizen die het apoE of de LDL receptor niet tot expressie brengen leidde namelijk wel tot verlaging van TG niveaus maar niet tot vermindering van hypercholesterolemie en atherosclerose. Aangezien de APOE*3-Leiden.CETP transgene muis een beter model is voor de menselijke lipoproteïnenstofwisseling dan de apoE-deficiënte muis en de LDL receptor-deficiënte muis konden we concluderen dat activatie van bruin vet een veelbelovende nieuwe methode is om dyslipidemie te verbeteren en te beschermen tegen atherosclerose.

In het derde deel van het proefschrift werden studies uitgevoerd rondom de stofwisseling, obesitas en bruin vet in mensen. Het langdurig eten van voeding dat veel vet bevat is een bekende oorzaak van obesitas en kan leiden tot de ontwikkeling van insulineresistentie en uiteindelijk type 2 diabetes. Recente studies hebben laten zien dat in spierweefsel van obese mensen merkers van bepaalde ontstekingscellen ('macrofagen') in verhoogde mate voorkomen en dat deze omgekeerd gerelateerd zijn aan insulinegevoeligheid. In **HOOFDSTUK 10** onderzochten we of een kortdurend dieet dat rijk is aan vet en calorieën al zou leiden tot verhoging van macrofaagmerkers en effecten op de glucosestofwisseling in de skeletspier van gezonde slanke mensen. Door spierbiopten af te nemen voor en na de dieetinterventie konden we aantonen dat 5 dagen dieet al leidde tot een opvallende verhoging in de mRNA expressie van diverse algemene macrofaagmerkers waaronder de M1 macrofaagmerker *MARCO*. Tevens waren genen die betrokken zijn bij opname en opslag van glucose verlaagd, terwijl plasmaniveaus van glucose en insuline verhoogd waren. We concludeerden dat de vroege instroom van macrofagen in spieren een oorzaak zou kunnen zijn voor de latere ontwikkeling van insulineresistentie bij dieet-geïnduceerde obesitas.

De Hindoestaanse populatie is in het bijzonder gevoelig voor de ontwikkeling van obesitas en verwante stoornissen zoals type 2 diabetes en HVZ. In **HOOFDSTUK 11** onderzochten we of het hoge risico op HVZ in deze populatie verklaard kan worden door een etnische gevoelig-

heid voor het ontwikkelen van nadelige endotheelactivatie. Hiertoe maten we E-selectine, het intercellulaire adhesiemolecuul 1 (ICAM-1) en het vasculaire adhesiemolecuul 1 (VCAM-1) als merkers voor endotheelactivatie in navelstrengbloed van Hindoestaanse en blanke Kaukasische neonaten. We toonden aan dat plasmaniveaus van het E-selectine aanzienlijk verhoogd waren in de Hindoestaanse neonaten, terwijl de plasmaniveaus van ICAM-1 en VCAM-1 niet verschilden van die van blanke Kaukasische neonaten. Opvallend was dat Hindoestaanse neonaten zich al presenteerden met hyperinsulinemie, dyslipidemie en verhoogde plasmaniveaus van het C-reactieve proteïne (CRP), waarbij het laatste wijst op verhoogde ontsteking. Gebaseerd op deze data konden we concluderen dat Hindoestanen bij geboorte al tekenen vertonen van zowel endotheelactivatie als een ongunstige metabool fenotype.

Omdat activatie van endotheel het gevolg kan zijn van een verstoorde functie van het hoge-dichtheids lipoproteïne (HDL) onderzochten we in **HOOFDSTUK 12** de HDL functionaliteit van Hindoestanen. Hiertoe bepaalden we verschillende maten van HDL functionaliteit in neonaten, adolescenten en volwassenen van Hindoestaanse en blanke Kaukasische komaf. De functie van het HDL met betrekking tot het opnemen van cholesterol uit macrofagen was vergelijkbaar tussen de etniciteiten. De functie van het HDL om te beschermen tegen oxidatie was lager in Hindoestaanse ten opzichten van blanke Kaukasische volwassenen, terwijl deze functie op jongere leeftijden nog vergelijkbaar was tussen beide etniciteiten. Dit suggereert dat deze functie met de leeftijd vermindert. Aan de andere kant was de capaciteit van HDL om te beschermen tegen ontsteking opvallend lager in de Hindoestaanse ten opzichte van blanke Kaukasische neonaten, een verschil dat in de adolescenten en volwassenen niet meer aantoonbaar was. We concludeerden dat Hindoestanen een verstoorde HDL functie hebben in vergelijking met blanke Kaukasiërs, en dat dit zou kunnen bijdragen aan endotheelactivatie en hun verhoogde risico op HVZ.

Het is waarschijnlijk dat het zeer veel voorkomende ongunstige metabole fenotype van Hindoestanen bestaande uit obesitas, dyslipidemie en insulineresistentie ook bijdraagt aan hun hoge risico op HVZ. Aangezien een etnische gevoeligheid voor het ontwikkelen van een verstoord energiemetabolisme de onderliggende reden kan zijn van dit fenotype, onderzochten we in **HOOFDSTUK 13** het energieverbruik in rust ('resting energy expenditure', REE) evenals het volume en de activiteit van bruin vet door middel ^{18}F-fluorodeoxyglucose (FDG) PET-CT scans in gezonde slanke Nederlandse Hindoestanen en gematchte blanke Kaukasiërs, nadat we hun bruin vet maximaal activeerden door afkoeling tussen watergekoelde matten. We toonden aan dat REE maar liefst 32% lager was in de Hindoestanen vergeleken met de blanke Kaukasiërs. Verder leidde blootstelling aan kou tot een significante verhoging van 'non-shivering' thermogenese (NST) in blanke Kaukasiërs, maar niet in Hindoestanen. Bovendien was het bruin vet volume behoorlijk lager in Hindoestanen, terwijl er geen verschil was tussen de maximale opname (SUV_{max}) en gemiddelde opname (SUV_{mean}) van ^{18}F-FDG door het bruin vet tussen de etniciteiten. Wij konden concluderen dat Hindoestanen verlaagde REE en bruin vet volume hebben vergeleken met gematchte blanke Kaukasiërs en dat dit onderliggend zou kunnen zijn aan hun hoge gevoeligheid voor het ontwikkelen van een ongunstig metabool fenotype op latere leeftijd.

De ^{18}F-FDG PET-CT scan is momenteel de 'gouden standaard' voor het bepalen van het volume en de activiteit van bruin vet, maar het gebruik ervan wordt beperkt door hoge kosten en de stralingsbelasting voor de proefpersonen. Het uiteindelijke product van thermogenese is de productie van warmte. Daarom hebben we in **HOOFDSTUK 14** onderzocht of supraclaviculaire temperatuur van de huid en/of de kerntemperatuur van het lichaam, die we kunnen meten met respectievelijk iButtons en telemetrische capsules, een kwantitatieve maat zouden kunnen zijn voor de opname van ^{18}F-FDG in mensen. We vonden dat de koude-geinduceerde supraclaviculaire huidtemperatuur positief correleerde met zowel het totale bruin vet volume als het claviculaire bruin vet volume en claviculaire SUV_{max}, terwijl de koude-geinduceerde kerntemperatuur niet correleerde met deze variabelen. We concludeerden daarom dat de supraclaviculaire huidtemperatuur gemeten met iButtons een mogelijke nieuwe niet-invasieve methode is voor de kwalitatieve detectie van bruin vet in mensen.

De studies beschreven in dit proefschrift laten zien dat bruin vet een veelbelovend aangrijpingspunt kan zijn om obesitas en dyslipidemie tegen te gaan. We toonden aan dat bruin vet een belangrijke speler is in het metabolisme van TG-rijke lipoproteïnen doordat het selectief vetzuren uit deze lipoproteïnen onttrekt. Behandeling van muizen met BMP7, rimonabant, metformine en CL316243 leidde tot een verhoging van de activiteit van bruin vet en als een gevolg daarvan tot een vermindering in het lichaamsvet en plasmaniveaus van TG. Daarentegen leidde vermindering van de functie van bruin vet, door remming van het centrale melanocortinesyteem, tot de ontwikkeling van obesitas. Gezamenlijk geven deze bevindingen aan dat bruin vet farmacologisch geactiveerd kan worden, en mogelijk ook in mensen. Tevens toonden we aan dat bruin vet een belangrijke rol kan spelen in de stofwisseling van volwassenen, aangezien we hebben aangetoond dat Hindoestanen, die zeer gevoelig zijn voor het ontwikkelen van obesitas, dyslipidemie en type 2 diabetes, een sterke vermindering hebben van hun bruin vet volume evenals een verminderde NST en REE vergeleken met gematchte blanke Kaukasiërs. De bevinding dat de koude-geinduceerde supraclaviculaire huidtemperatuur correleert met ^{18}F-FDG opname in mensen kan in de toekomst mogelijk leiden tot de ontwikkeling van een surrogaat merker voor de activiteit van bruin vet. Dit is zeer relevant aangezien bruin vet inmiddels beschouwd kan worden als *de* nieuwe strategie om obesitas en aanverwante stoornissen zoals type 2 diabetes en atherosclerose te bestrijden.

LIST OF PUBLICATIONS (FULL PAPERS)

Boon MR, Van der Horst G, Van der Pluijm G, Tamsma JT, Smit JWA, Rensen PCN. Bone Morphogenetic Protein-7: a broad-spectrum growth factor with multiple target therapeutic potency. **Cytokine Growth Factor Rev 2011;** 22: 221-9

Boon MR, Karamali NS, De Groot CJM, Van Steijn L, Kanhai HH, Van der Bent C, Berbée JFP, Middelkoop B, Rensen PCN, Tamsma JT. E-selectin is elevated in cord blood of South Asian neonates compared with Caucasian neonates. **J Pediatr 2012;** 160: 844-8

Boon MR, Bakker LEH, Meinders AE, Van Marken Lichtenbelt W, Rensen PCN, Jazet IM. Bruin vet: een lichaamseigen mechanisme in de strijd tegen obesitas? **Ned Tijdschr Geneeskd 2013;** 157: A5502

Boon MR, Van den Berg SAA, Wang Y, van den Bossche J, Karkampouna S, Bauwens M, De Saint-Hubert M, van der Horst G, Vukicevic S, de Winther MP, Havekes LM, Jukema JW, Tamsma JT, Van der Pluijm G, Willems van Dijk K, Rensen PCN. BMP-7 activates brown adipose and reduces diet induced obesity only at subthermoneutrality. **PLoS One 2013;** 8: e74083

Widya RL, Hammer S, Boon MR, Van der Meer RW, Smit JWA, De Roos A, Rensen PCN, Lamb HJ. Effects of short-term nutritional interventions on right ventricle function in healthy men. **PloS One 2013;** 8: e76406

Auvinen HE, Coomans CP, Boon MR, Romijn JA, Biermasz NR, Meijer OC, Havekes LM, Smit JWA, Rensen PCN, Pereira AM. Glucocorticoid Excess induces long-lasting changes in body composition in male C57Bl/6J mice only with high-fat diet. **Physiol Rep 2013;** 1: e00103

Abdulrahman RM, Boon MR, Sips HC, Guigas B, Rensen PCN, Smit JW, Hovens GC. Impact of metformin and compound C on NIS expression and iodine uptake in vitro and in vivo: A role for CRE in AMPK modulation of thyroid function. **Thyroid 2014;** 24: 78-87

Boon MR*, Geerling JJ*, van der Zon GC, Van den Berg SAA, Van den Hoek AM, Lombès M, Princen HM, Havekes LM, Rensen PCN, Guigas B. Metformin lowers plasma triglycerides by promoting VLDL-triglyceride clearance by brown adipose tissue in mice. **Diabetes 2014;** 63: 1-12
[*Both authors contributed equally]

Boon MR*, Geerling JJ*, Kooijman S, Parlevliet ET, Havekes LM, Romijn JA, Meurs IM, Rensen PCN. Sympathetic nervous system control of triglyceride metabolism: novel concepts derived from recent studies. **J Lipid Res 2014;** 55: 180-9
[*Both authors contributed equally]

Boon MR*, Bakker LEH*, Van der Linden RAD, Pereira Arias-Bouda L, Van Klinken JB, Smit F, Verberne HJ, Jukema JW, Tamsma JT, Havekes LM, Van Marken Lichtenbelt WD, Jazet IM, Rensen PCN. Brown adipose tissue volume in healthy lean south Asian adults compared with white Caucasians: a prospective, case-controlled observational study. **The Lancet Diabetes & Endocrinology 2014;** 2: 210-217
[*Both authors contributed equally]

Heemskerk MM, van den Berg SAA, Pronk ACM, van Klinken JB, Boon MR, Havekes LM, Rensen PCN, Willems van Dijk K, van Harmelen V. Long term niacin treatment induces insulin resistance and adrenergic responsiveness in aqdipocytes by adaptive down-regulation of phophodiesterase 3B. **Am J Physiol Endocrinol Metab 2014;** 306: E808-813

Kooijman S, Boon MR, Parlevliet ET, Geerling JJ, van de Pol V, Romijn JA, Havekes LM, Meurs I, Rensen PCN. Inhibition of the central melanocortin system decreases brown adipose tissue activity. **J Lipid Res 2014;** *Conditionally accepted*

Boon MR, Bakker LEH, Haks MC, Quinten E, Van Beek L, Wang Y, Van Schinkel L, Van Harmelen V, Meinders AE, Ottenhoff THM, Willems van Dijk K, Guigas B, Jazet IM, Rensen PCN. Short-term high-fat diet increases macrophage markers in skeletal muscle accompanied by impaired insulin signaling in healthy male subjects. **Clin Sci 2014;** *Conditionally accepted*

Boon MR, Kooijman S, van Dam AD, Pelgrom LR, Berbée JFP, Visseren CAR, Van Aggele RC, van den Hoek AM, Sips HCM, Lombès M, Havekes LM, Tamsma JT, Guigas B, Meijer OC, Jukema JW, Rensen PCN. Cannabinoid 1 receptor blockade diminishes obesity and dyslipidemia via peripheral activation of brown adipose tissue. **FASEB J 2014;** *Revision invited*

Boon MR, Bakker LEH, Van der Linden RAD, Pereira Arias-Bouda L, Smit F, Verberne HJ, Van Marken Lichtenbelt WD, Jazet IM, Rensen PCN. Supraclavicular skin temperature as a measure of ^{18}F-fluorodeoxyglucose uptake by brown adipose tissue in human subjects. **PLoS One 2014;** *Revision invited*

Laurila P-P, Soronen J, Boon MR, Forsström S, van den Berg SAA, Coomans CP, Kaiharju E, Manninen T, Emtso J, Autio A, Silvennoinen R, Merikanto K, Isomi A, Tuomainen A, Tikka A, bin Ramadan O, Lee-Rueckert M, Mervaala E, Ehnholm C, Roivainen A, van Eck M, Ripatti S, Taskinen M-R, Peltonen L, Jalanko A, Olkkonen VM, Rensen PCN, Kovanen P, Suomalainen A, Jauhiainen M. Deficiency of *Usf1* Protects against obesity, insulin resistance, dyslipidemia, and atherosclerosis, and leads to increased energy expenditure and brown adipose tissue activity in mice. *Submitted*

Hillebrand S, Swenne CA, Maan AC, Boon MR, Biermasz N, de Koning EJP, de Roos A, Lamb HJ, Jukema JW, Rosendaal FR, den Heijer M, Rensen PCN, de Mutsert R. Sympathetic nervous system activation and lipid metabolism: the NEO study. *Submitted*

Boon MR*, Berbée JFP*, Khedoe PPSJ*, Bartelt A*, Schlein C, Worthmann A, Weigelt C, Jung C, Kooijman S, Vazirpanah N, Brouwers LPJ, Gordts PLSM, Esko JD, Hiemstra PS, Havekes LM, Scheja L, Heeren J, Rensen PCN. Central role for brown adipose tissue in dyslipidemia and atherosclerosis development. *Submitted*
[*Authors contributed equally]

Boon MR, Bakker LEH, Van der Linden RAD, Van Ouwekerk A, De Goeje PL, Counotte J, Jazet IM, Rensen PCN. High prevalence of cardiovascular disease in South Asians: central role for brown adipose tissue? *Submitted*

Boon MR*, Bakker LEH*, Annema W, Dikkers A, Jukema JW, Havekes LM, Meinders AE, Tietge UJF, Jazet IM, Rensen PCN. South Asians exhibit disturbed HDL functionality as compared to white Caucasians. *In preparation*
[*Both authors contributed equally]

Boon MR, Khedoe PPSJ, Hoeke G, Kooijman S, Dijk W, Kersten S, Havekes LM, Hiemstra P, Berbée JFP, Rensen PCN. Brown adipose tissue internalizes fatty acids by selective delipidation of lipoproteins rather than by uptake of lipoproteins. *In preparation*

16

CURRICULUM VITAE

Mariëtte Rebecca Boon werd op 17 oktober 1988 geboren te Alkmaar. Na het behalen van haar Gymnasium diploma *(cum laude)* aan het Bonhoeffer college te Castricum in 2006, begon zij in datzelfde jaar aan haar studie Geneeskunde aan de Universiteit Leiden. In 2007 behaalde ze haar propedeuse *(cum laude)* en ging zij verder voor haar doctoraal. In 2009 startte zij met de pre-master Biomedische Wetenschappen aan dezelfde universiteit die zij in 2011 succesvol afrondde. In datzelfde jaar behaalde ze ook haar doctoraal geneeskunde *(cum laude)* en startte ze met de master Biomedische Wetenschappen. Al vroeg in haar studie raakte zij gefascineerd door het ongunstige metabole fenotype van de Hindoestaanse bevolking. Zij sloot zich daarom als student aan bij de onderzoeksgroep van prof. Patrick Rensen van de afdeling Endocrinologie en Stofwisselingziekten van het LUMC, waar zij aantoonde dat een verstoorde stofwisseling en markers van endotheelschade in de Hindoestaanse bevolking al bij de geboorte aanwezig zijn. In januari 2011 startte zij haar afstudeeronderzoek voor Biomedische Wetenschappen bij de groep van prof. Rensen. Dat onderzoek richtte zich op het effect van de groeifactor BMP7 op de ontwikkeling van bruin vet, een recent ontdekte nieuwe speler in de stofwisseling, en de rol van sympathische innervatie van bruin vet hierin. Vervolgens verwierf zij een persoonsgebonden beurs van de Raad van Bestuur van het LUMC evenals een pilotstudiebeurs van het Diabetesfonds, en startte zij in augustus 2011 bij dezelfde groep haar promotieonderzoek, onder supervisie van prof. Patrick Rensen en dr. Ingrid Jazet. Voor presentaties over haar onderzoek ontving zij verscheidene prijzen, zowel op nationale (2^{e} Cardiovasculaire Conferentie Noordwijkerhout, 2012; 3^{e} Rembrandt Symposium Noordwijkerhout, 2012) als internationale (18th Annual Scandinavian Atherosclerosis Conference, 2012, Humlebaek, Denmark; 35th Annual European Lipoprotein Club Meeting, 2012, Tutzing, Germany, 20th Annual Scandinavian Atherosclerosis Conference, 2014, Humlebaek, Denmark) congressen. Verder ontving zij de 'beste jonge eerste auteur prijs' toegekend door het Nederlands Tijdschrift voor Geneeskunde voor haar artikel 'Bruin vet: een lichaamseigen middel in de strijd tegen obesitas?' (NTvG 2013). Het promotieonderzoek, waarvan de resultaten zijn beschreven in dit proefschrift, werd afgerond in januari 2014. Mariëtte is momenteel als postdoc onderzoeker verbonden aan zowel het LUMC, afdeling Endocrinologie, als de Universiteit Maastricht, afdeling Humane Biologie, op een persoonsgebonden Rubicon beurs toegekend door NWO.